Volume 25 - No. 1 - 2016
pp. 1 - 374

Fresenius Environmental Bulletin

Official Journal of:

- MESAEP - Mediterranean Scientific Association of Environmental Protection e.V.
- IAES - International Academy of Environmental Safety
- SECOTOX - Society of Ecotoxicology and Environmental Safety

ISSN 1018 - 46119

FEB-FRESENIUS ENVIRONMENTAL BULLETIN

Founded jointly by F.Korte and F.Coulston

Production by PSP-Vimy str 1e,85354 Freising,Germany in

cooperation with PRT-Parlar Research & Technology

Vimy Str 1e,85354 Freising

Printed in Germany-ISSN 1018-4619

Fresenius Environmental Bulletin is abstracted/indexed in:

Biology&Environmental Sciences,BIOSIS,CAB International,Cambridge Scientific abstracts,Chemical Abstracts,Chemical Abstracts,Current Awareness,Current Contents/Agriculture,CSA Civil Engineering Abstracts,CSA Mechanical&Transportation Engineering,IBIDS database,Information Ventures,NISC,research Alert,Science Citation Indey(SCI),Scisearch,Selected Water Resources Abstracts

CONTENTS

ORIGINAL PAPERS

© by PSP Volume 25 – No.1/ 2016, pages 4-13 Fresenius Environmental Bulletin

SORPTION OF AMMONIA NITROGEN ON SUSPENDED SEDIMENTS IN LANZHOU SECTION OF THE YELLOW RIVER, CHINA

Wu Fuping, Wang Yingchao, Xia Chuan, Huo Jinyan, Wei Bigui

(Engineering Research Center for Cold and Arid Regions Water Resource Comprehensive Utilization of Ministry of Education, School of Environmental and Municipal Engineering, Lanzhou Jiaotong University, Lanzhou, Gansu, 730070, China)

ABSTRACT

To explore the mechanism of water self-purification, the adsorption properties of ammonia nitrogen on the suspended sediment with different particle sizes in the Lanzhou section of the Yellow River, China were studied. The effects of sediment amount, concentration of ammonia nitrogen, sediment size and chemical components on the ammonia nitrogen adsorption, were analyzed. The results indicated that the Langmuir model provides a better description of equilibrium adsorption capacity of ammonia nitrogen, and the adsorption kinetics fits well to the pseudo-second-order kinetic model. Sediment amount has a significant effect on the adsorption of ammonia nitrogen, and both the adsorption capacity and equilibrium time have remarkable inverse relationships with the sediment amount. The initial concentration of ammonia nitrogen is positively correlated with ammonia nitrogen adsorption capacity and equilibrium time. In addition, the decrease of sediment size leads to increase in the ability to absorb ammonia, the adsorption capacity and the degree of reaction spontaneity. Moreover, the contents of organic matters, Fe_2O_3, Al_2O_3 and MgO in the sediment increase with the decrease in particle size, which has a positive effect on the maximum adsorption capacity of sediment. In summary, the sediment adsorption of ammonia has a positive effect on water self-purification in Lanzhou section of the Yellow River, China.

KEYWORDS:
the Yellow River; ammonia nitrogen; suspended sediment; adsorption; water self-purification; adsorption kinetics; Isothermal equilibrium

INTRODUCTION

The Lanzhou section of the Yellow River, China is wide and shallow with a high silt content, in which the purification of aqueous-phase pollutants mainly occurs through sediment adsorption or subsidence[1]. Development of the Yellow River coastal economy in recent years has led to increased sewage and wastewater emissions, resulting in heightened water pollution of the Yellow River Basin. Consequently, studying the influence of sediment on water quality of the Yellow River has become a priority for relevant departments. Ammonia is one of the prominent pollutants and an excess of ammonia can lead to phenomenon of eutrophication, as well as toxic effects on fish and other aquatic organisms [2, 3]. Since Lanzhou city using the Yellow River water as the main water source in industry and agriculture, as well as drinking water for people and livestock, studying ammonia adsorption to the sediment has important practical implications for understanding the water self-purification capacity of the Lanzhou section of the Yellow River [4, 5].

At present, there are few studies on sediment adsorption and ammonia degradation, and most of them are confined to the middle reaches of the Yellow River. These studies typically focus on the role of sediment particles in the ammonia nitrification and degradation processes [6-10], but research on adsorption of ammonia to the sediment itself has rarely been reported. Furthermore, results of such research have not given adequate consideration to issues such as the impact of ammonia adsorption, sediment classification, etc.

This paper assesses water quality of the Lanzhou section of the Yellow River through testing of silt content, sediment grain sizes and initial concentration of ammonia and other parameters. Detailed analysis revealed the role of sediment in ammonia adsorption and degradation processes in the Lanzhou section of the Yellow River, providing a basis for environmental assessment and water quality improvement of the Yellow River Basin.

MATERIAL AND METHODS

Materials. The test water and sediment were taken from the Silver Beach Bridge located in the Lanzhou section of the Yellow River. Samples were collected from the middle of the river under the

surface of flowing water by lowering a bucket down with rope. After adequate precipitation, the supernatant and the sediment were collected, respectively.

The collected water samples had a pH range of 7.7-8.3 and the ammonia concentration ranged from 0.12-0.38 mg/L. The water samples were filtered through a 0.45 μm filter membrane, sealed and stored in dark at room temperature.

The collected sediment was placed in a bucket, which was then filled with river water. The sediment was left to soak for two weeks and the water was changed twice daily. This process involved siphoning the water from the suspended sediment and stirring ensuring no silt remained at the bottom of the bucket. After the two weeks soaking period, the water was removed to allow the remaining sediment to dry. The effect of impurity on the sediment surface were eliminate by this procedure.

The sediment sample was obtained by dry-sieving through stainless steel sieves and then analyzed to determine the sediment particle size grading and major chemical composition. As shown in Fig. 1 and TABLE 1, the median particle diameter (D) values of the three sediment grades are 15.721, 43.660 and 67.188 μm.

TABLE 1
The main chemical composition of sediment in Lanzhou section of the Yellow River

Median particle diameter D(μm)	Organic matters	Fe_2O_3	SiO_2	Al_2O_3	MgO	CaO	Na_2O	K_2O
15.721	1.154	6.17	51.85	15.33	3.34	9.61	1.35	3.19
43.660	0.286	3.93	54.74	9.49	1.89	9.53	2.58	1.79
67.188	0.217	2.56	57.34	6.36	1.12	8.78	2.87	1.27

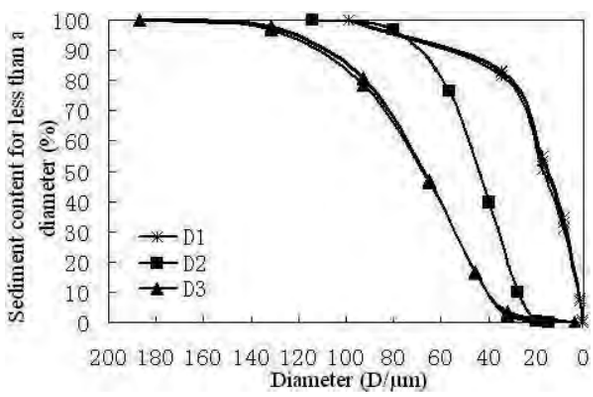

FIGURE 1
Grading curve of sediment particles in Lanzhou section of the Yellow River

TEST METHODS

The ammonia concentration was measured using Nessler's reagent spectrophotometry. The concentration and content of sediment organic matters ware determined by using potassium dichromate as digestion solution. The sediment particle size distribution was analyzed using the Mastersizer2000 Malvern automatic Zetasizer (Malvern Instruments Ltd, UK). The chemical composition of the sediment was analyzed using the MagixPW2403 X-ray fluorescence spectrometer (Dutch Philips, US).

Adsorption modelAdsorption model. The adsorption models used in this paper are described as follows:

(1) Pseudo first order kinetic equation expression

$$\frac{dq}{dt} = k_1(q_e - q) \quad (1)$$

Where: q is the adsorption amount at time t, mg/g; q_e is the equilibrium adsorption amount, mg/g; k_1 is the rate constant, h^{-1}; t is the adsorption time, h.

(2) Pseudo-second order kinetic equation expression

$$\frac{dq}{dt} = k_2(q_e - q)^2 \quad (2)$$

Where: k_2 is the rate constant, h^{-1}; other variables are the same as (1).

(3) Langmuir (L) isotherm expression:

$$q_e = \frac{S_m K_l C_e}{1 + K_l C_e} \quad (3)$$

Where S_m is the maximum sediment adsorption of pollutants, mg/g; K_l is the adsorption coefficient; q_e is the equilibrium adsorption amount, mg/g; C_e is the equilibrium concentration in the aqueous phase, mg/L.

(4) Freundlich (F) isotherm expression

$$q_e = K_f C_e^{\,n} \quad (4)$$

Where K_f represents the adsorption intensity; n is the absorption index.

Ammonia adsorption kinetics test. Samples were splited into two groups: 200 ml of sample water in Erlenmeyer flasks were (1) treated such that ammonia concentration in each sample was equal between samples and various sediment concentrations were used; (2) treated such that the sediment concentration in each sample was fixed and the initial ammonia concentration varied between samples. All the adsorption tests repeated in duplicate and the results are the mean values in this paper. To eliminate the effects of ammonia nitrogen adsorbed on original sediment sample, blank test corrections were performed to reach the final determined values. The water samples were placed into a temperature oscillation chamber with an oscillation speed of 200 ± 5 r/min and a water temperature of 20±0.5 ℃ for 24 h. Sampling occurred at various points within this time period and the supernatant was then collected after standing for 1 h and the ammonia concentrations were measured for each sample at every time point after filtration through a 0.45 μm filter membrane. The adsorption capacity of sediment for ammonia was calculated at each time point based on the initial concentration of ammonia and the concentration of sediment in the sample.

Ammonia isothermal equilibrium adsorption experiment. This test was carried out with three classes of sediment particle size, and each particle sizes was divided into several sediment concentrations and initial concentrations of ammonia. The preparation, measurement and calculation of the test water samples and the initial concentration of ammonia were performed in the same manner as in the ammonia adsorption kinetics tests. The only differences were the time spent in the temperature oscillation chamber and the time allowed to stay thermostatic before supernatant collection (48h and 2h, respectively).

RESULTS AND DISCUSSION

Influence of sediment concentration on the adsorption of ammonia

The rate of ammonia adsorption over time with an initial ammonia concentration of 1mg/L and different sediment concentrations (S) are shown in FIGURE 2. TABLE 2 list the fitting parameters for two adsorption kinetics equations.

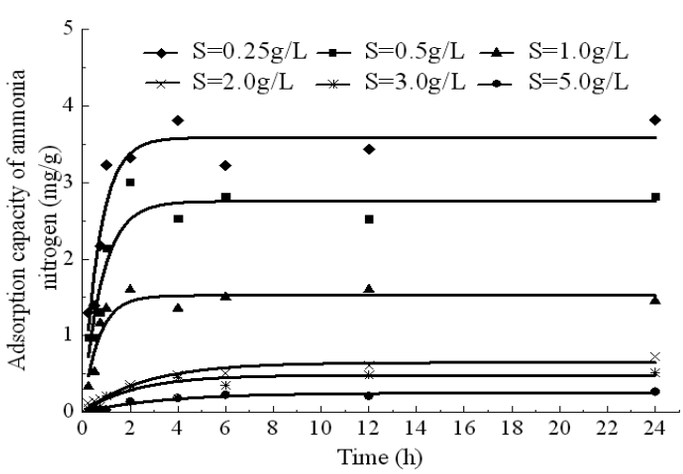

FIGURE 2
Effect of time on the adsorption capacity of ammonia nitrogen for various concentration of sediment

TABLE 2
Fitting parameters of adsorption kinetics for different sediment concentration

S (g/L)	quasi-one kinetic			quasi-two kinetic		
		k_1	R^2	q	k_2	R^2
0		1.429	0.8819	3.	0.453	0.9963
0		1.225	0.8620	2.	0.656	0.9959
1		1.482	0.8652	1.	2.331	0.9952
2		0.376	0.9440	0.	0.523	0.9932
3		0.450	0.9193	0.	0.598	0.9768
5		0.296	0.9340	0.	0.304	0.7894

FIGURE 2 shows that with increasing sediment concentration, the ammonia adsorption capacity decreased, and the adsorption rate is reduced accordingly. In contrast, higher sediment concentrations allowed for shorter equilibrium adsorption times.

Overall, ammonia adsorption equilibrium time, equilibrium adsorption capacity and adsorption rate decrease per unit of sediment mass as sediment concentration increases. These results are consistent with the findings of other researchers, domestic and abroad[11, 12]. This behavior can be explained by the surface area available for adsorption. When adsorbate (initial concentration of ammonia) is constant, the higher adsorbent (sediment) concentration provides more points for adsorption, hence the shorter equilibrium adsorption time. The higher sediment concentration also creates interference; sediment particles can interact with each other, thus reducing the effective surface area per unit mass of sediment. This interaction leads to the resultant decrease in equilibrium adsorption value of ammonia per unit mass of sediment (see TABLE 2), and the decreasing corresponding values qe-q. This in turn reduces the driving force for adsorption and the adsorption rate.

Table 2 shows the equilibrium adsorption capacity (qe) of the two kinetic models varies significantly. When sediment concentration increases from 0.25 g/L to 5.0 g/L, qe is reduced from 3.585 mg/g to 0.252 mg/g. This shows that the sediment concentration and ammonia adsorption capacity have a significantly negative correlation. The correlation coefficient of the pseudo-second order equation is significantly higher than that of pseudo first order dynamics, illustrating that the kinetics of the ammonia adsorption are more consistent with pseudo-second order kinetic equation parameters.

Ammonia adsorption capacity changes with the sediment concentration for three classes of sediment particles under the condition of different initial ammonia concentrations (C0) are presented in FIGURE 3. The fitting parameters of the two kinds of adsorption isotherm expressions under the corresponding conditions are also listed in TABLE 3.

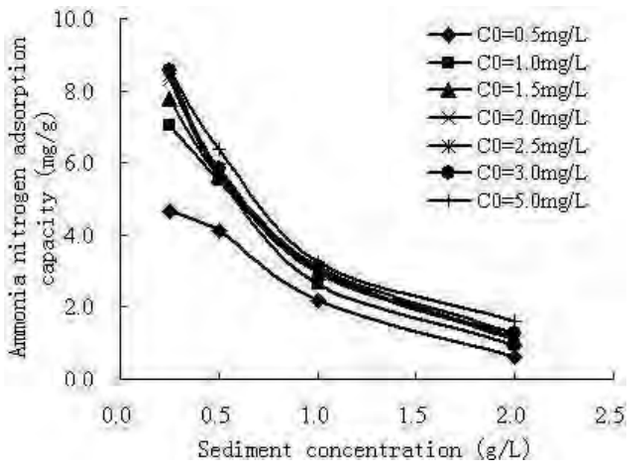

D=15.721μm

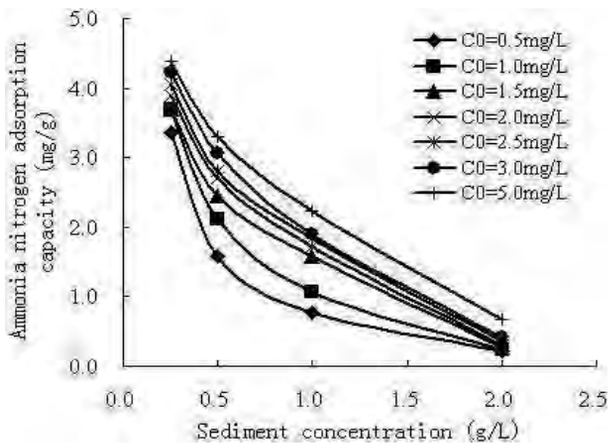

D=43.660μm

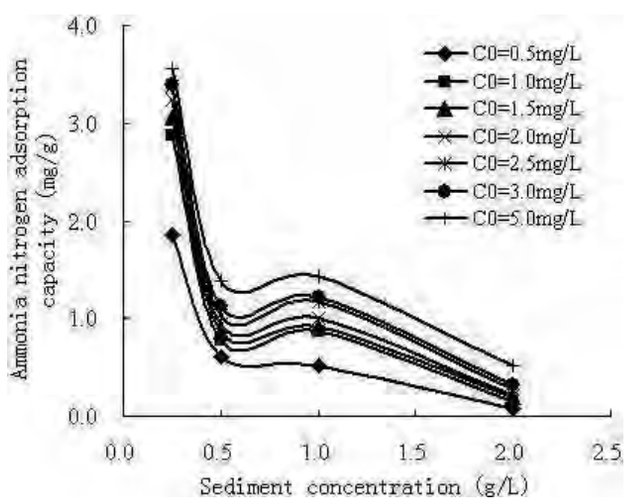

D=67.188μm

FIGURE 3
The effect of sediment concentration on the equilibrium adsorption capacity of ammonia nitrogen

TABLE 3
Fitting parameters of isothermal adsorption equation for ammonia nitrogen

S(g/L)	Fitting parameters of Langmuir								
	D =15.521μm			D =43.660μm			D =67.188μm		
	S_m	K_l	R^2	S_m	K_l	R^2	S_m	K_l	R^2
0.25	9.149	4.443	0.9980	4.581	4.297	0.9987	3.807	3.124	0.9990
0.5	6.485	5.863	0.9972	3.811	1.340	0.9984	1.566	1.097	0.9650
1.0	3.370	5.414	0.9996	3.011	0.670	0.9843	1.705	1.043	0.9786
2.0	1.804	1.218	0.9671	0.979	0.324	0.6923	0.872	0.236	0.7140
Average value	6.116	3.485	0.9905	3.096	1.658	0.9184	2.351	0.887	0.9142
S(g/L)	Fitting parameters of Freundlich								
	D=15.521μm			D=43.660μm			D =67.188μm		
	K_f	n	R^2	K_f	n	R^2	K_f	n	R^2
0.25	6.893	0.2282	0.7867	3.703	0.1165	0.9612	2.700	0.2383	0.8251
0.5	5.374	0.1264	0.8227	2.121	0.3276	0.9706	0.824	0.3039	0.9848
1.0	2.737	0.1501	0.8296	1.156	0.5205	0.9335	0.845	0.3701	0.9643
2.0	0.963	0.3411	0.9221	0.259	0.5053	0.8973	0.167	0.6636	0.9813
Average value	4.069	0.2389	0.8403	1.810	0.3675	0.9407	1.153	0.4186	0.9389

As shown in FIGURE 3, sediment concentration has a significant influence on the amount of ammonia adsorbed. Ammonia equilibrium adsorption capacity decreased with increasing sediment concentration. Sediment of different sizes display this same behavior. Sediment adsorption capacity is negatively correlated with sediment concentration. This conclusion coincides with the "unit mass of sediment adsorption capacity of ammonia decreases with the increase of sediment concentration". The dynamics expression emphasizes the impact of sediment concentration on the adsorption rate, while adsorption isotherm expression explains the impact of sediment concentration on the equilibrium adsorption capacity.

From TABLE 3 we can known that the maximum adsorption capacity S_m and adsorption intensity K_f both significantly decreased with the increase of sediment concentration. This proves, from the model itself, that sediment concentration has a negative correlation with S_m and K_f. Overall, there is little difference between the two isotherm models in terms of fits for sediment adsorption of ammonia, with the correlation coefficient > 0.9 for both. The L isotherm fits well at lower sediment concentrations, but the correlation decreases as the concentration increases, while the fit is not as obvious for the F isotherm.

Influence of initial ammonia concentration on the adsorption of ammonia. FIGURE 4 shows the change of ammonia adsorption capacity over time, with a different initial ammonia concentration (C_0) of ammonia nitrogen. Table 4 lists the fitting parameters of two adsorption kinetics equations.

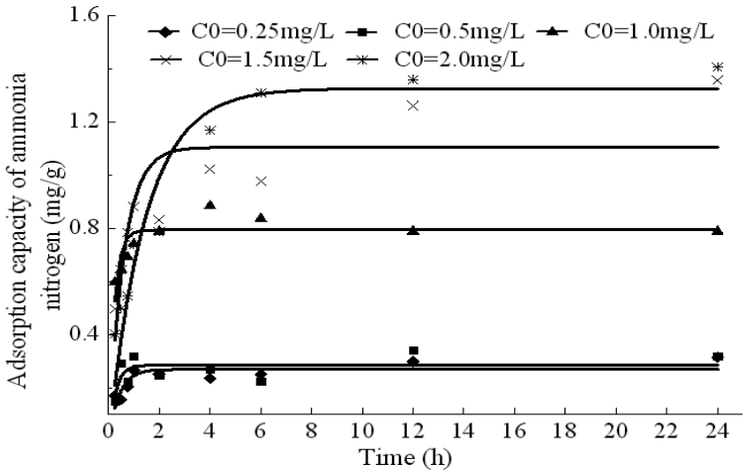

FIGURE 4
Effect of time on the adsorption capacity of ammonia nitrogen for various initial concentration of ammonia nitrogen

TABLE 4
Fitting parameters of adsorption kinetics for different initial concentration of ammonia nitrogen

C_0（mg/L）	quasi-two kinetic			quasi-two kinetic		
	q_e	k_1	R^2	q_e	k_2	R^2
0.25	0.269	2.455	0.5490	0.318	4.697	0.9956
0.5	0.285	3.897	0.3467	0.326	5.636	0.9863
1	0.793	4.351	0.5689	0.790	-38.540	0.9994
1.5	1.105	1.682	0.6582	1.385	0.711	0.9926
2	1.325	0.691	0.9012	1.471	0.640	0.9984

As seen in FIGURE 4, ammonia equilibrium adsorption capacity gradually increases with the higher initial ammonia concentration; the adsorption rate increased accordingly. Additionally, the low initial concentration of ammonia will more easily achieved equilibrium. Overall, per unit mass of sediment, ammonia adsorption equilibrium time, equilibrium adsorption capacity, and adsorption rate increase with increasing initial ammonia concentration. This occurs because the sediment adsorption process involves a constant fluctuation of contaminants between the aqueous and sediment phases. When there is a high ammonia concentration at a particular sediment concentration, a larger amount of the ammonia content in the aqueous phase must be distributed on the sediment surface in order to achieve equilibrium, hence the longer adsorption equilibrium time. Under the same conditions, the probability that there will be an interaction between the sediment surface and ammonia increases, which is a driving force behind the increased sediment adsorption of ammonia. This explains the increased equilibrium adsorption capacity of ammonia per unit mass sediment (listed in TABLE 4), the corresponding increased qe-q value, and the higher adsorption rate. Conversely, lower ammonia content with the same sediment concentration means a lower distribution of ammonia on the sediment surface, shorter adsorption equilibration time, decreased adsorption capacity, a lower qe-q value, and decreased adsorption rate.

TABLE 4 shows that: Equilibrium adsorption capacity qe of the two dynamic equations increases with higher initial ammonia concentrations; however, sediment concentration is a bigger factor in adsorption capacity than initial ammonia concentration. Furthermore, the correlation coefficient of the pseudo-second order kinetic equation was significantly better than pseudo-first order kinetic equation, illustrating that the different initial concentrations of ammonia adsorption kinetics are also consistent with pseudo-second order kinetic equation.

FIGURE 5 illustrates the changes of equilibrium adsorption capacity of ammonia on different sizes of sediment particles with varying initial ammonia concentration values.

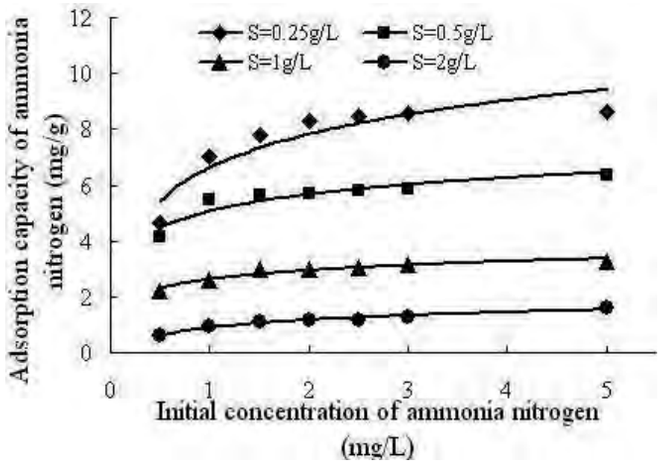

D=15.721μm

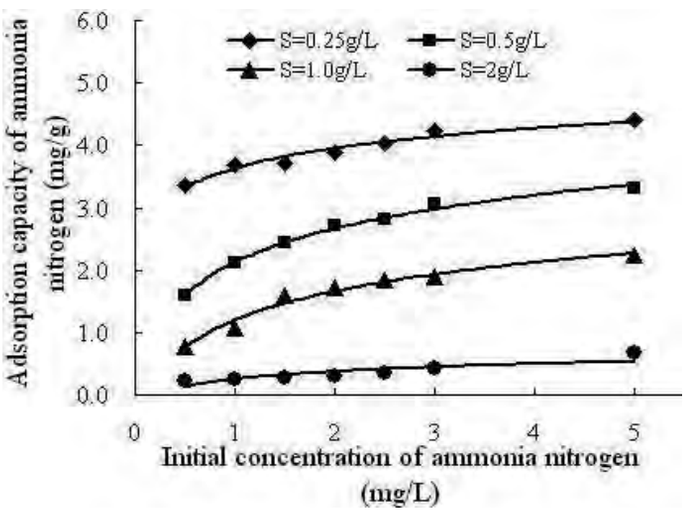

D=43.660μm

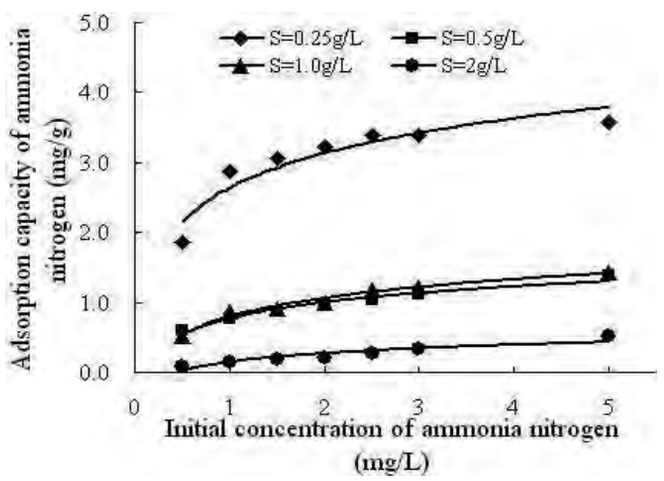

D=67.188μm

FIGURE 5
Effect of the initial concentration of ammonia nitrogen on the equilibrium adsorption capacity of ammonia nitrogen

FIGURE.5. shows that Ammonia adsorption to sediment increases with the increase of initial ammonia concentration. Different particle sizes of sediment have the same trend. The increase of equilibrium adsorption capacity of the low concentration region is more pronounced than that of the high concentration region. With the increases of initial concentration of ammonia, the ammonia adsorption amount reaches the system reaches maximum adsorption capacity. This occurs because sediment acts as a collector of ammonia nitrogen in the aqueous phase above the sediment surface, and when the ammonia concentration of the aqueous phase is too high, the sediment adsorption equilibrates after reaching its maximum capacity[13]. The higher the initial ammonia concentration, the higher the changing intervals of the equilibrium adsorption amount. As seen in Figure 2.2, changes in equilibrium adsorption amounts are more drastic as the initial ammonia concentration increases, with both curves demonstrating similar trends and relatively close values. These curves show that the initial concentration of ammonia has some impact on sediment adsorption, but sediment concentration has a bigger impact.

Effect of particle size on the adsorption of ammonia. Fig. 5 shows that ammonia adsorption capacity gradually decreases with increasing sediment particle size, where the adsorption capacity of the smallest particle size is twice that of the largest size. This indicates that sediment particle size also has large effects on ammonia adsorption capacity. Meanwhile, Table 3 shows that particle size has an inverse relationship with Sm and Kl values of L isotherm. Kl, the ratio of the adsorption rate and the desorption rate, is related to the binding energy on the surface, and the value reflects the degree of spontaneity of the adsorption reaction. The larger the Kl value the higher the degree of the spontaneity of the reaction, and the stronger of the adsorption capacity. Sm reacts the adsorption capacity of sediment to the pollutants. Therefore, it can be considered that, the finer of the sediment particles, the stronger of the adsorption capacity, and the higher the degree of spontaneous of the reaction. In the F isotherm equation, Kf also decreases with larger sediment particle sizes. Kf is an affinity coefficient that describes the adsorption of sorbents to adsorbents, and it changes with the parameter Sm in L isotherm. The larger the Kf value, the greater the adsorption capacity. The results showed that with the decreasing particle size, Kf value increases, indicating that the finer of the sediment particles, the greater of the adsorption capacity.

Finally, the chemical composition of the sediment is shown in Table 1The smaller sediment particles tend to have higher Fe2O3, Al2O3 and MgO content. However, the mineral types of the Yellow River sediment generally include montmorillonite, illite, kaolinite and quartz, whose main components are the metal oxides listed above. This indicates that the important metal oxides in sediment correlate to sediment adsorption capacity of ammonia; that is, these substances can directly affect the level of sediment adsorption of ammonia. Xiaoyun Wang[14, 15] also showed that there is a significant positive correlation between iron and aluminum content in the sediment and the maximum adsorption capacity. It shows that iron and aluminum have a relatively large influence on the adsorption capacity, and it can directly affect the amount of sediment adsorption of ammonia.

CONCLUSION

Sediment concentration has a significant impact on sediment adsorption of ammonia, and there is an inverse relationship between sediment concentration and adsorption capacity of ammonia. Ammonia adsorption capacity per unit mass of sediment and saturation time of ammonia adsorption decrease with the increase of sediment concentration, and ammonia adsorption kinetics of different sediment concentrations are more consistent with pseudo-second order kinetic equation. The Langmuir isotherm is better describes the relationship between the initial ammonia concentration in the aqueous phase and the equilibrium adsorption capacity of ammonia, for which there is a positive correlation. The equilibrium adsorption capacity value increases more at lower initial concentrations of ammonia than at higher concentrations. Ammonia nitrogen adsorption also reaches a maximum after reaching a certain level. Ammonia adsorption capacity per unit mass of sediment and equilibrium time of ammonia adsorption increase as the initial concentration rises. Adsorption kinetics of different initial concentrations of ammonia nitrogen follows the pseudo-second order kinetic equation. Generally, the finer the sediment particles are, the stronger the adsorption capacity, the higher the degree of spontaneity of the reaction, and the greater the adsorption capacity. Smaller sediment particle sizes also have higher metal oxide content in their chemical compositions, indicating a possible link between chemical composition and ammonia adsorption capacity. Sediment in Lanzhou section of the Yellow River allows for adsorption of aqueous phase ammonia. The finer the sediment particles are, the stronger the adsorption capacity of ammonia is; this and other data indicate that the sediment in the Yellow River has a certain role in promoting self-purification of the water.

ACKNOWLEDGEMENTS

The work was supported by the Natural Science Foundation of Gansu Province of China (No. 145RJZA209), the Young Scholars Science Foundation of Lanzhou Jiaotong University (No. 2012009), the Advanced Research Foundation of Jinchuan Group Co., Ltd. & Lanzhou Jiaotong University (No.JCYY2013011).

REFERENCES

[1] Xia X, Liu T, Yang Z, Zhang X, Yu Z. Dissolved organic nitrogen transformation in river water: Effects of suspended sediment and organic nitrogen concentration. Journal of Hydrology. 2013;484:96-104.

[2] Rabalais NN. Nitrogen in aquatic ecosystems. AMBIO: A Journal of the Human Environment. 2002;31:102-12.

[3] Seitzinger S, Sanders R. Contribution of dissolved organic nitrogen from rivers to estuarine eutrophication. Marine Ecology Progress Series. 1997;159:12.

[4] Cornell S, Jickells T, Cape J, Rowland A, Duce R. Organic nitrogen deposition on land and coastal environments: a review of methods and data. Atmospheric Environment. 2003;37:2173-91.

[5] Worsfold PJ, Monbet P, Tappin AD, Fitzsimons MF, Stiles DA, McKelvie ID. Characterisation and quantification of organic phosphorus and organic nitrogen components in aquatic systems: a review. Analytica Chimica Acta. 2008;624:37-58.

[6] Xia X, Li S, Shen Z. Effect of Nitrification on Nitrogen Flux Across Sediment-Water Interface. Water Environment Research. 2008;80:2175-82.

[7] Xia X, Yang Z, Huang G, Zhang X, Yu H, Rong X. Nitrification in natural waters with high suspended-solid content—A study for the Yellow River. Chemosphere. 2004;57:1017-29.

[8] Xia X, Yang Z, Huang GH, Maqsood I. Integrated evaluation of water quality and quantity of the Yellow River. Water international. 2004;29:423-31.

[9] Xia X, Yang Z, Zhang X. Effect of Suspended-Sediment Concentration on Nitrification in River Water: Importance of Suspended Sediment− Water Interface. Environmental science & technology. 2009;43:3681-7.

[10] Xia X, Zhou J, Yang Z. Nitrogen contamination in the Yellow River basin of China. Journal of Environmental Quality. 2002;31:917-25.

[11] Hou L, Liu M, Jiang H, Xu S, Ou D, Liu Q, et al. Ammonium adsorption by tidal flat surface sediments from the Yangtze Estuary. Environmental Geology. 2003;45:72-8.

[12] Sander M, Lu Y, Pignatello JJ. A thermodynamically based method to quantify true sorption hysteresis. Journal of environmental quality. 2005;34:1063-72.

[13] Holmboe N, Kristensen E. Ammonium adsorption in sediments of a tropical mangrove forest (Thailand) and a temperate Wadden Sea area (Denmark). Wetlands Ecology and Management. 2002;10:453-60.

[14] Wang X, Zhang L, Zhang H, Wu X, Mei D. Phosphorus adsorption characteristics at the sediment–water interface and relationship with sediment properties in FUSHI reservoir, China. Environmental Earth Sciences. 2012;67:15-22.

[15] Wang X-Y, Zhang L-P, Zhang H-S, Mei D-L. Kinetics of Phosphorous Sorption by Sediment in a Subtropical Reservoir. ASIAN JOURNAL OF CHEMISTRY. 2012;24:121-5.

Received: **02.10.2014**
Accepted: **07.12.2015**

CORRESPONDING AUTHOR

Wei Bigui
Lanzhou Jiaotong University
Engineering Research Center for Cold and Arid Regions Water Resource Comprehensive Utilization of Ministry of Education
School of Environmental and Municipal Engineering
Lanzhou, Gansu, 730070 – CHINA

email: weibg@mail.lzjtu.cn

© by PSP Volume 25 – No . 1/2016, pages 14-22 Fresenius Environmental Bulletin

GROWTH, MINERAL ACQUISITION AND ION UPTAKE RESPONSE OF COMMON BEAN (PHASEOLUS VULGARIS L.) TO INOCULATION WITH *RHIZOBIUM* UNDER DIFFERENT SALT

Ummuhan Karaca[1] Refik Uyanoz[1]

[1]Department of Soil Science and Plant Nutrition, Faculty of Agriculture, Selçuk University, 42031, Konya/TURKEY

ABSTRACT

This study was conducted in order to evaluate the symbiotic effectiveness of *Rhizobium Leguminosarum bv. phaseoli* strains isolated from common bean in comparison to standard bacterial culture under NaCl salinity stress conditions. The effect of seed *Rhizobium* inoculation and NaCI levels (control 0, 5 mM, 10 mM, 20 mM and 40 mM) on mineral accumulation of common bean (*Phaseolus vulgaris* L.) was studied under greenhouse condition. A commercial common bean cultivar (Akman 98) was inoculated with *R. tropici* strain CIAT899 and local *Rhizobium*. The results showed that the application of salt significantly decreased both concentration and the accumulation of most micro and macronutrients both in leaf and biomass. The bacterial inoculation had a significant effect on Ca^{++}, Fe accumulation and ion uptake (K^+ + P + Ca^{++}) + Na^+ and on P, Mg^{++}, Mn and Zn contents of leaf. However, the effect of inoculation on Na^+, K^+, Na^+/K^+, N and Cu contents of the leaf were insignificant. Significant interaction was detected between inoculation and salt concentration. Inoculation with *Rhizobium phaseoli* could work as a useful means for alleviating salinity stress in salt-sensitive plants.

KEYWORDS:
Common bean, macro and micronutrients, nodule, salinity, *rhizobium* associate

INTRODUCTION

Dry bean (*Phaseolus vulgaris* L.), also called common bean or kidney bean, is one of the major leguminous crops grown in the world. The legume seeds are widely consumed around the world and their acceptability depends on the climatic conditions in the planting area [1]. Salinity in arid and semi-arid regions of the world is a serious constraint to agriculture. Nearly 40 % of the world's land surface can be classified as endangered by salinity. Most such areas are in the tropics and in the Mediterranean region [2]. Production of grain legumes is severely reduced in salt-affected soils because their ability to form nitrogen-fixing nodules is impaired by both salinity and alkalinity [3].

Legumes can improve saline soil fertility and help reintroduce agriculture in nitrogen poor soils. Many legumes are very sensitive to salt levels by the increase in osmotic potential and by the toxic effect of high concentration of ions [4].

Identification of nutritional disorders in crops growing on saline soils may facilitate the development of breeding or agronomic practices that improve yields in saline areas. Salinity causes nutrient disturbances and reduces plant growth by affecting the availability, transport and partitioning of nutrients. Salinity causes nutrient deficiencies or imbalances, due to the competition of Na^+ and Cl^- with nutrients such as K^+, Ca^{+2}, and NO_3^-. In saline soils N is one of the most growth-limiting nutrients. Potassium uptake by plant can be affected by high salinity and the Na concentration in the soil solution [5].

Saline soils are characterized by the presence of extreme ratios of Na^+/Ca^{++}, Na^+/K^+, Ca^{++}, Mg^{++}, and Cl^-/NO_3^- [6] and high levels of neutral salts in the surface layers resulting from the capillary rise of water [7] excess of soluble salts in the soil leads to osmotic stress, which result in specific ion toxicity [8]. High salt (NaCl) uptake competes with the uptake of other nutrient ions, especially K^+, leading to K^+ deficiency [9].

In acid or alkaline soils, P always tightly binds with aluminum, iron, calcium and magnesium to form insoluble compounds or sparingly soluble phosphates, and unavailable for plant uptake [10]. In soil phosphorus reacts with iron, aluminum and calcium to form insoluble compounds [11]. Shoot and root growth of virtually all legume crops is increased with balanced phosphorus and potassium nutrition [12].

In this study, native *Rhizobium* was used as an inoculation material because it can better adapt to

the soil environment. In addition, the experiment was carried out under controlled conditions to determine the effect of *Rhizobium* strain. The effect of salt stress on the macro and micro-nutrient uptake of common bean cultivar inoculated by native *Rhizobium* was also investigated.

MATERIAL AND METHODS

Test plant**:** Common bean (*P. vulgaris* L. cv. Akman 98) was used in the inoculation experiments. Common bean seed was obtained from Anatolia Agricultural Research Institute, Eskişehir, Turkey.

Bacterial cultures**:** Rhizobial strain used in this study was *R. tropici* CIAT899, a widely used bean-nodulating strain [13]. Also, natural *Rhizobium* was isolated from the nodules of *P. vulgaris* plants which were grown in different locations of the Konya plain in Turkey. For this purpose 94 samples of plant root nodules were used. Rhizobial strains were isolated from the surface of sterilized nodules using the method described by Somasegaran et al. [14]. The strains were maintained at +4 ^{o}C on yeast extract mannitol agar (YMA). *P. vulgaris* was grown from seeds in Leonard jars (1 L) under greenhouse conditions for 8 weeks. Each jar contained three plants grown under supplemental lighting (14 h/10 h light/dark cycles), and the temperature was maintained at 24^{o}C/20^{o}C. Pure cultures were examined for nodulation [15]. The most effective single isolate was selected from the total 94 isolates and was used in the succeeding experiment.

Peat analyses**:** The pH and electrical conductivity (EC) were measured in an aqueous extract (1/2.5 w/v) of peat [16]. Available P was extracted with sodium bicarbonate [17]. Available K (extracted with ammonium acetate) was measured by flame photometry [18]. While total N was determined via the Kjeldahl method [19], lime content by Scheibler Calcimeter [20] and organic matter was extracted as described by Jackson [21]. In addition, Ca, Mg, Fe, Cu, Mn and Zn contents of the peat were determined using the samples treated with H_2SO_4 and H_2O_2 by ICP-AES [22]. The peat used in the experiments contained 83 % organic matter, 1.34 % total N, 0.11 % available P, 0.09 % available K. Its pH value was 6.10 while EC was 0.25 dS m^{-1}, Ca, Mg, Fe, Mn, Zn, and Cu content of experimental peat were found to be 4300, 5500, 2090, 10, 14 and 6 mg kg^{-1}, respectively.

Plant experiments**:** This study was conducted in 2012 growing season at the greenhouse of the Agricultural Faculty Selcuk University in Konya (Turkey). The experiment was carried out in a completely randomized block design involving 2 bacterial inoculations and 5 concentrations of NaCl (0, 5, 10, 20 and 40 mM) replicated three times. Seeds were surface-sterilized with sodium hypochlorite (0.5%), transferred aseptically to pots and inoculated with 1 mL (10^5–10^6 CFU mL^{-1}) of bacterial culture of *R. tropici* CIAT899 and local *Rhizobium* sp. Uninoculated plants were also included in each plant test. The plastic pots were filled up with 3 kg sterile peat. Peat was watered with N-free nutrient solution. Bacterial inoculation was done after salt application. All the plants were watered with distilled water every other day. The following mineral fertilizers were applied during planting: N, P, K at 12.5, 188.0, 157.0 mg per pot, respectively and Fe, Mn, Cu and Zn as sulphates at 170, 314, 14, 27 mg per pot respectively.

Plant measures (wet digestion and elemental analyses): Leaf samples were taken during flowering period and biomass (stem + leaf + flower) samples were taken after harvesting. The leaf and biomass were dried at 70 ^{o}C. Samples (0.3 g) were digested overnight at room temperature in 50 mL volumetric flasks with 2.5 mL of concentrated H_2SO_4 and subsequently heated on a hot plate at 180°C for 30 min. Analytical grade (30%) H_2O_2 was added drop-wise. Flasks were heated on a hot plate at 280°C for 10 min and cooled back to room temperature. This procedure was repeated until the flask content became colorless. The filtrate was analyzed for Na, K, Ca, Mg, Fe, Mn, Zn, and Cu on ICP–AES (Varian Vista Model) [22]. N content of plant leaf and biomass were determined using Kjeldahl method by Bremner [19].

Statistical Analysis: Data were analyzed as a factorial experiment in a completely randomized manner with three replication using the JMP statistical software, version 5.1 (SAS Institute INc., Cary, NC, USA). Sources of variation were treatments, incubation day and their interaction. Means were compared by Student's t-test at a significance level of 0.01 or 0.05.

RESULTS

In leaf, inoculation had a significant effect on the total ion uptake (K^+ + P + Ca^{++}) + Na^+, Mg, Fe, Mn and Zn (Table 1). The effect of salt concentration was also significant ($P<0.01$ and $P<0.05$) for all nutrients with the exception of Na^+ in the leaf. There were no significant ($P<0.05$) interactions between isolate and salt concentration in terms of Na^+/K^+, N, P and Mg. On the other hand, inoculation significantly ($P<0.05$) affected the concentrations of all the nutrients with the exception of (K^+ + P + Ca^{++}) + Na^+, N, P and Ca^{++} in the biomass. The effect of salt application was significant ($P<0.05$) for all micro and macro–nutrient contents. A similar result was observed for the effect of interaction between inoculation and salt concentration except for Zn.

TABLE 1
Computed F from the analysis of variance for the nutrient content in the leaf and biomass as a function of salt concentration and *Rhizobium* isolate (mean values)

	Shoot			Biomass		
	Source of variation					
	I	S	IxS	I	S	IxS
DF	1	4	4	1	4	4
Na^+	2.31ns	2.82ns	2.86*	5.97*	48.05**	3.91*
K^+	0.65ns	275.84**	9.90**	10.38**	457.06**	7.69**
Na^+/K^+	0.06ns	18.45**	2.02ns	7.69*	22.58**	7.12**
$(K^+ + P + Ca^{++}) + Na^+$	13.63**	147.03**	7.80**	0.89ns	188.02**	8.33**
N	0.72ns	3.68*	0.55ns	0.16ns	3.97*	3.93*
P	7.75*	22.58**	1.63ns	3.90ns	13.06**	5.55**
Ca	123.40**	18.71**	31.42**	2.83ns	20.32**	5.86**
Mg	4.34*	147.32**	2.70ns	8.49**	80.82**	17.57**
Fe	17.24**	63.05**	49.37**	5.49*	12.23**	4.11*
Cu	0.33ns	71.06**	24.45**	126.72**	23.0**	24.64**
Mn	4.61*	77.96**	15.24**	55.60**	1156.6**	372.69**
Zn	4.60*	40.50**	8.88**	6.15*	17.11**	1.60ns

I: Isolate S: Salt concentration
**; P <0.01; *; P<0.05; ns : not significant

Means within a nutrient followed by the same letter are not significantly different at the 5 % level of probability using LSD test

Changes in certain nutrients of the leaf and biomass are presented in Table 2. Na^+ and K^+ contents of common bean leaf increased as the level of salt increased regardless of the type of inoculation (Table 2). The highest Na^+ (0.28 %) content was observed in 40 m M salt application with CIAT899 inoculation. When the mean of the two inoculations was considered, a significant increase occurred with increasing salt levels in terms of K^+ content. The percentage of K^+ in leaves increased with salt levels, and the highest contents of K^+ were found in 20 mM salt application with both inoculations. The K^+ content of biomass was greater in increased salinity levels than in control applications. Salt stress increased the K^+ content of common bean leaves but resulted in significant differences between inoculations. Inoculation with *Rhizobium* CIAT899 significantly increased the K^+ uptake of common bean. A similar pattern was observed following inoculation with natural *Rhizobium*. Na^+ / K^+ and ion uptake $(K^+ + P + Ca^{++}) + Na^+$ % decreased with both inoculations and increasing salt levels. However, the lowest Na^+/K^+ rate was determined from 20 mM salt application with CIAT899 and local *Rhizobium* inoculations (0.03 and 0.02 %) respectively.

TABLE 2
Effects of different salt concentrations and *Rhizobium* inoculations on contents Na^+, K^+, total ion uptake ($K^+ + P + Ca^{++}$) + Na^+ of leaf and biomass concentration

		Salt concentration (mmol l^{-1})				
Leaf concentration (%)		0	5	10	20	40
Na	CIAT899	0.17b	0.18b	0.14b	0.20b	0.28a
	N isolate	0.17b	0.18b	0.18b	0.15b	0.18b
	Mean	0.17	0.18	0.16	0.18	0.23
K	CIAT899	1.83e	2.62d	2.15de	6.55a	4.46c
	N isolate	1.83e	2.16de	2.08de	6.10ab	5.88b
	Mean	1.83d	2.39c	2.12cd	6.33a	5.17b
Na/K	CIAT899	0.09	0.07	0.07	0.03	0.06
	N isolate	0.09	0.08	0.08	0.02	0.03
	Mean	0.09a	0.08a	0.08a	0.03c	0.05b
(K+P+Ca)+Na	CIAT899	4.64de	5.46c	5.03cd	9.48a	7.69b
	N isolate	4.64de	5.14cd	4.23e	7.63b	8.09b
	Mean	4.64d	5.3c	4.64d	8.55a	7.89b
		Salt concentration (mmol l^{-1})				
Biomass concentration (%)		0	5	10	20	40
Na	CIAT899	0.10d	0.08d	0.13cd	0.20c	0.47a
	N isolate	0.10d	0.09d	0.16cd	0.10d	0.33b
	Mean	0.10cd	0.09d	0.15bc	0.15bc	0.4a
K	CIAT899	2.27f	2.65f	3.60d	5.84c	6.37b
	N isolate	2.27f	3.04e	3.56d	5.70c	7.48a
	Mean	2.27e	2.85d	3.58c	5.77b	6.93a
Na/K	CIAT899	0.04bc	0.03cd	0.04bc	0.03cd	0.07a
	N isolate	0.04bc	0.03cd	0.04b	0.02d	0.04b
	Mean	0.04b	0.03c	0.04b	0.03c	0.06a
(K+P+Ca)+Na	CIAT899	5.35f	5.26f	6.76e	8.62c	9.49b
	N isolate	5.43f	5.40f	6.36e	7.92d	11.10a
	Mean	5.35d	5.33d	6.56c	8.27b	10.3a

N isolate : Natural isolate
Means within a nutrient followed by the same letter are not significantly different at the 5 % level of probability using LSD test

TABLE 3
Effects of different salt concentration and *Rhizobium* inoculations on contents N, P, Ca, Mg of leaf and biomass concentration

		Salt concentration (mmol l^{-1})				
Leaf concentration (%)		0	5	10	20	40
N	CIAT899	3.71	2.97	2.67	3.41	2.49
	N isolate	3.71	3.16	2.41	2.58	2.40
	Mean	3.71a	3.07ab	2.54b	2.99ab	2.45b
P	CIAT899	0.39	0.31	0.24	0.31	0.38
	N isolate	0.39	0.29	0.22	0.28	0.30
	Mean	0.39a	0.30c	0.23d	0.30c	0.34b
Ca	CIAT899	2.42c	2.53bc	2.64abc	2.62abc	2.85a
	N isolate	2.42c	2.69ab	1.93d	1.25e	1.91d
	Mean	2.42b	2.61a	2.29b	1.94c	2.38b
Mg	CIAT899	0.29	0.22	0.33	0.51	0.45
	N isolate	0.29	0.22	0.26	0.48	0.46
	Mean	0.29c	0.22d	0.30c	0.50a	0.46b
		Salt concentration (mmol l^{-1})				
Biomass concentration (%)		0	5	10	20	40
N	CIAT899	3.06ab	2.71ab	2.44abc	3.18a	1.74c
	N isolate	3.06ab	2.52ab	2.77ab	2.40bc	2.65ab
	Mean	3.06a	2.62ab	2.61ab	2.79a	2.20b
P	CIAT899	0.38a	0.31b	0.30b	0.36a	0.37a
	N isolate	0.38a	0.30b	0.31b	0.25c	0.39a
	Mean	0.38a	0.31b	0.31b	0.31b	0.38a
Ca	CIAT899	2.70bc	2.30de	2.86b	2.42cd	2.75bc
	N isolate	2.70bc	2.06e	2.49cd	1.97e	3.23a
	Mean	2.70b	2.18c	2.68b	2.20c	2.99a
Mg	CIAT899	0.34d	0.30e	0.33d	0.36c	0.37c
	N isolate	0.34d	0.29e	0.29e	0.41b	0.45a
	Mean	0.4c	0.30d	0.31d	0.39b	0.41a

Means within a nutrient followed by the same letter are not significantly different at the 5 % level of probability using LSD test

TABLE 4
Effects of different salt concentration and Rhizobium inoculations on micro elements contents (Fe, Cu, Mn, Zn) of leaf and biomass concentration

		Salt concentration (mmol l^{-1})				
Leaf concentration (mg kg^{-1})		0	5	10	20	40
Fe	CIAT899	124.75a	79.52c	79.10c	44.87c	104.47b
	N isolate	124.75a	80.56c	106.04b	101.99b	66.17d
	Mean	124.75a	80.04cd	92.57b	73.43d	85.32bc
Cu	CIAT899	3.83bc	2.51ef	2.22ef	6.54a	1.91f
	N isolate	3.83bc	2.67de	3.36c	4.28b	3.24cd
	Mean	3.83b	2.59c	2.79c	5.41a	2.58c
Mn	CIAT899	140.47bc	122.95c	136.23c	161.15a	52.79e
	N isolate	140.47c	159.12ab	127.00c	99.90d	44.27c
	Mean	140.47a	141.04a	131.61a	130.53a	48.53b
Zn	CIAT899	33.80cd	29.44de	30.07de	57.09a	33.83cd
	N isolate	33.80cd	31.27de	26.68e	41.72b	38.30bc
	Mean	33.80bc	30.36cd	28.38d	49.41a	36.07b
		Salt concentration (mmol l^{-1})				
Biomass concentration (mg kg^{-1})		0	5	10	20	40
Fe	CIAT899	60.89a	51.64ab	45.66b	42.02bc	42.33bc
	N isolate	60.89a	32.89c	33.60c	46.98b	42.63bc
	Mean	60.89a	42.27b	39.63b	44.50b	42.48b
Cu	CIAT899	4.62a	3.30b	2.82c	2.69c	3.57b
	N isolate	4.62a	3.44b	4.72a	4.72a	4.35a
	Mean	4.62a	3.37c	3.77b	3.71b	3.96b
Mn	CIAT899	60.20b	67.89a	47.88c	16.16g	11.88h
	N isolate	60.20b	29.44f	44.79d	35.80e	15.36g
	Mean	60.20a	48.67b	46.34c	25.98d	13.62e
Zn	CIAT899	38.53	30.63	34.11	34.17	45.94
	N isolate	38.53	33.81	42.34	33.43	53.76
	Mean	38.53b	32.22c	38.23b	33.80bc	49.85a

Means within a nutrient followed by the same letter are not significantly different at the 5 % level of probability using LSD test

On the other hand, N, P and Ca contents of common bean leaf significantly ($P<0.05$) decreased as the salt level increased ($P<0.05$) (Table 3). In contrast, the Mg contents of leaf increased with increasing salt levels.

The Fe content of common bean leaf was lower in control and 20 mM salt level compared with those in other salt concentrations (Table 4). The concentration of Cu changed in leaf in response to low salt treatment, and it significantly decreased in leaf ($P<0.05$) with an increase in soil salinity. The changes of Mn content in leaf were gradual under low salt treatment. There was not a significant reduction in the concentration of Zn in leaf in response to salt-stress. Similarly, Fe, Zn, Cu and Mn contents in leaf increased with inoculations, and these values were still much lower than those of control treatment (Table 4).

The results of biomass: There were significant increases in the Na^+ and K^+ uptake of common bean biomass compared with those of the control (Table 2). The highest increases were shown at 40 mM salt applications (0.4% and 6.93%) respectively. However, both CIAT899 and local *Rhizobium* had more effect at 20 mM salt level than at other salt levels ion uptake of common bean increased linearly with salt doses. These increases were significant ($P<0.05$). Salinity reduced the nitrogen contents of common bean in terms of biomass (Table 3). This reduction was found to be significant for *R. tropici* and local *Rhizobium* inoculations and salinity ($P<0.05$). Reduction of the negative effects of salt on total nitrogen contents was lower in natural inoculations than in CIAT899 inoculations. In terms of the means of inoculations, the highest nitrogen content was taken from the control application. Salinity reduced phosphate uptake and accumulation in crops grown in soils primarily by reducing phosphate availability but in solution cultures, ion imbalances might primarily result from competitive interactions. We determined that increasing salt levels and inoculations didn't have a significant effect on P concentration of biomass. Also, the highest P content was found in control (Table 3). Salinity generally increased the Ca uptake in common bean biomass under stressful conditions and inoculation treatment with CIAT899, yet decreased Ca content.

The average Mg content of biomass changed from 0.30% to 0.41%. The highest Mg content was determined in 40 mM salt application.

On the other hand, Fe, Cu, and Mn contents of biomass reduced with increasing salt concentration although the reverse is true for zinc.

DISCUSSION

Any environmental stress that affects plant growth is also likely to influence infection and nodulation [23]. Salinity reduces phosphate uptake and accumulation in crops grown in soils primarily by reducing phosphate availability but in solution cultures ion imbalances may primarily result from competitive interactions. In the present study, bean growth was not inhibited up to 40 mM salinity level, but after 40 mM plants gradually died because of the detrimental effect of salinity (data not shown), confirming that common bean (*Phaseolus vulgaris*) is more sensitive to saline conditions than other legumes. Macro and micro element content of leaf, shoots and biomass decreased under saline conditions. P uptake by plants can be affected by high salinity and the Na concentration in the soil solution. There is abundant evidence that Na and the Na/Ca ratio affects K uptake and accumulation within plant cells and organs and that salt tolerance is correlated with selectivity for K uptake over Na [5]. Giri et al. [24] indicated that accumulation of Na^+ was strongly influenced by storage of other cations, particularly K^+. Increased K^+ concentration under saline conditions may help to reduce Na^+ uptake, and this can indirectly sustain the chlorophyll content of the plant [25]. This study demonstrated that these results are consistent with previous studies. Uyanöz and Karaca [23] reported that application of salt with inoculation significantly reduced N, Na, Mg, K uptake of common bean leaf. The K^+ uptake in the common bean may illustrate the role of K in salt tolerance. The effect of inoculation on decreasing salt stress may partly be attributed to reduced Na^+ uptake by root and translocation-to-shoot tissues and low Na^+/K^+ ratio. Our results confirm previous findings that inoculated plants were not affected by salt stress conditions [26, 27]. Giri and Mukarji [25] reported that, in saline soil, higher absorption of P in inoculated plants may improve their growth rate and salt tolerance and suppress the adverse effect of salinity stress. Nyoki and Ndakidemi [27] disclosed that *B. japonicum* inoculants supplemented with phosphorus in cowpea improved the uptake of N, P, K, Mg, Ca and Na significantly relative to control. Makoi et al., [1] revealed that rhizobia inoculation significantly increased the uptake of P, K, Ca, and Mg in plant parts such as leaves, shoots, roots and pods of common beans (*Phaseolus vulgaris* L.). Factors, such as salinity, temperature, water supply, pH, mineral nutrition and combined nitrogen are of great importance to the symbiosis process [4].

In our experiments, the highest P accumulation of leaf and biomass was found in control treatments both in the CIAT899 and local *Rhizobium*. This shows that the bacterial inoculation can be important in reducing salt stress and overcoming the scarce P availability under saline conditions.

CONCLUSIONS

Overall, the macro and micro nutrition contents of leaf and biomass results indicated that salinity can cause severe damage to *P. vulgaris*. Rhizosphere environment is highly important for the interaction between root hairs and *Rhizobium*, as it encourages the healthy development of root hairs. Salts may inhibit plant growth and nutrient intake from plant because of the abnormally high intracellular solute concentration. Besides, as certain ions have direct effects on plant growth due to their inhibiting activity of essential enzymes, further researches should be conducted to evaluate such side effects of ions and salt, especially under field conditions.

REFERENCES

[1] Makoi, J.H., Bambara, S. and Ndakidemi, P.A. (2013) *Rhizobium* inoculation and the supply of molybdenum and lime affect the uptake of macro elements in common bean (*P. vulgaris L.*) plants. Australian Journal of Crop Science, 7, 784-793.

[2] Surange, S., Wollum, A.G., Kumar, N. and Natutiyal C.S. (1997) Characterizations of *Rhizobium* from root nodules of leguminous trees growing in alkaline soils, Can. J. Microbiol. 43, 891-894.

[3] Rao, D.L.N., Giller, K.E., Yeo, A.R. and Flowers, T.J. (2002) The effects of salinity and sodicity upon nodulation and nitrogen fixation in chickpea (*Cicer arietinum*), An. Of Botany 89(5), 563-570.

[4] Geeranjali, M. and Garg, N. (2008) Salinity and its effects on the functional biology of legumes, Acta Physiol Plant, 30, 595-618.

[5] Monica, N., Vidican, R., Rotar, I., Stoian, V., Pop, R. and Miclea, R. (2014) Plant nutrition affected by soil salinity and response of *Rhizobium* regarding the nutrients accumulation. ProEnvironment, 7, 71-75.

[6] Grattan, S. R. and Catherine, M. G. (1993) Mineral nutrient acquisition and response by plants grown in saline environments,

Handbook of Plant and Crop Stress, Marcel Dekker Inc, New York, 203-226.

[7] Al-Falih, A.M.K. (2002) Factors affecting the efficiency of symbiotic nitrogen fixation by *Rhizobium*, Pakistan Journal of Biological Sciences 5(11), 1277-1293.

[8] Agarwal, S. and Ahmad, Z. (2010) Contribution of the *Rhizobium* inoculation on plant growth and productivity of two cultivars of Berseem (*Trifolium alexandrinum L.*) in saline soil. Asian Journal of Plant Sciences, 9(6), 344-350.

[9] Parida A. K. and AnathBandhu, D. (2005) Salt tolerance and salinity effects on plants: a review, Ecotoxicology and Environmental Safety, 60, 324-349.

[10] Jian-Feng Li, S.Q, Zhang, P.H., Huo, S., Shi, L. and Miao, Y.Y. (2013) Effect of phosphate solubilizing *Rhizobium* and nitrogen fixing bacteria on growth of alfalfa seedlings under P and N deficient conditions, Pak.J. Bot., 45(5), 1557-1562.

[11] Fatima, Z., Zia M. and Chaudhary, M. F. (2006) Effect of *Rhizobium* strains and phosphorus on growth of soybean (Glycine max) and survival of *Rhizobium* and P solubilizing bacteria, Pak. J. Bot., 38(2), 459-464.

[12] Fageria, N.K., Baligar, V.C. and Jones, C.A. (2011) Growth and mineral nutrition of field crops. CRC Press, Boca Raton.

[13] Martinez-Romero, E., L., Segovia, F.M., Mercante Franco, A.A., Graham, P. and Pardo, M.A. (1991) *Rhizobium Tropici*, A novel species nodulating *Phaseolus vulgaris* L. beans and *Leucaena* sp. tress. Int. J. Syst. Bacteriol. 41, 417-426.

[14] Somasegaran, P. and Hoben, H.J. (1994) Handbook for rhizobia. Springer-verlag. New York USA.

[15] van Berkum, P.D., Beyene Bao, G., Campbell, T.A. and Eardly, B.D. (1998) *Rhizobium mongolense* sp. nov. is one of three rhizobial genotypes identified which nodulate and form nitrogen-fixing symbioses with Medicago ruthenica [(L.) Ledebour]. Int. J. Syst. Bacteriol. 48, 13-22.

[16] Anonymous, (1982) Methods of soil analysis (Ed. A.L. Page). Number 9, Part 2, Madison, Wisconsin, USA, 1159 pp.

[17] Olsen, S.R. and Sommers, L.E. (1982) Phosphorus. In: Page AL, et al (eds), Methods of soil analysis, Part 2, 2nd edn, Agron Monogr 9. ASA and ASSA, Madison WI, 403–430

[18] Knudsen, D.G., Peterson, A. and Pratt, P.F. (1982) Lithium, sodium and potassium. In: Page AL, Editor. Methods Soil Analysis, Part 2. Agronomy Monograph 9.Madison, WI, U.S.A. ASA and SSSA, 247-262.

[19] Bremner, J.M. (1982) Total nitrogen in methods of soil analysis, Part 2, ed Black, C.A., Evans, D.D., White, J.L., Ensminger, L.E., Clark, F.E. & Dinauer, R.C., 1149-1178. American Society of Agronomy, Inc., Madison, Wisconsin, USA. ISBN 0-89118-072-9.

[20] Soil Survey Staff (1993) Soil Survey Manual. USDA Handbook, Vol.18. Washington, USA.

[21] Jackson, M.C. (1962) Soil chemical analysis. Prentice Hall. Inc., Eng. Cliff., USA.

[22] Soltanpour, P.N. and Workman, S.M. (1981) Use of inductively-coupled plasma spectroscopy for the simultaneous determination of macro and micro nutrients in NH_4HCO_3-DTPA extracts of soils. Developments in atomic plasma analysis. In: Barnes RM (ed) USA, 673-680.

[23] Uyanöz, R. and Karaca, Ü. (2011) Effects of different salt concentrations and *Rhizobium* inoculation (native and *R. Tropici* CIAT899) on growth of dry bean (*P. vulgaris L.*) Eur. J. of Soil Biol. 47, 387-391.

[24] Giri, B., Kapoor, R. and Mukerji, K.G. (2003) Influence of Arbuscular Mycorrhizal fungi and salinity on growth, biomass, and mineral nutrition of *Acacia auriculiformis*. Biol. Fertil. Soils 38, 170–175.

[25] Giri, B. and Mukerji, K.G. (2004) Mycorrhizal inoculant alleviates salt stress in *Sesbania aegyptiaca* and *Sesbania grandiflora* under field conditions: Evidence for reduced sodium and improved magnesium uptake. Mycorrhiza 14, 307–312.

[26] Diouf, D., Duponnois, R., Tidiane, B.A., Neyra, M. and Lesueur, D. (2005) Symbiosis of *Acacia auriculiformis* and *Acacia mangium* with mycorrhizal fungi and *Bradyrhizobium* spp. improves salt tolerance in greenhouse conditions. Funct. Plant Biol. 32, 1143–1152.

[27] Nyoki, D. and Ndakidemi, P.A. (2014) Effects of *Bradyrhizobium japonicum* inoculation and supplementation with phosphorus on macronutrients uptake in cowpea (*Vigna unguiculata* (L.) Walp). American Journal of Plant Sciences, 5, 442-451.

Received: **06.10.2014**
Accepted: **07.01.2016**

CORRESPONDING AUTHOR

Ümmühan Karaca
Selçuk University
Faculty of Agriculture
Department of Soil Science and Plant Nutrition,
42031 Konya -TURKEY
email: ucetin@selcuk.edu.tr

DETERMINATION OF MAIN SOIL PROPERTIES USING SYNTHETIC APERTURE RADAR

M. Tolga Esetlili, Yusuf Kurucu
(Ege University, Faculty of Agriculture, Department of Soil Science and Plant Nutrition, 35100 Izmir/ TURKEY.)

ABSTRACT

The objective of this study was to examine the contribution of Synthetic Aperture Radar (SAR) images in determining and monitoring some of the main soil properties. In this research, seven SAR images (2 of RADARSAT-1 and 5 of ENVISAT ASAR) were gathered between April and October 2006. An ASTER image of May 2006 that belonged to the same area was also used as an ancillary data. Menemen (Izmir) Plain which covers about 400 km2 of the western part of the Gediz Basin in the west of Turkey was chosen as the area of study. The research was set out to investigate the relationships among some of the soil properties, such as, texture, organic matter, soil salinity, pH and lime content, which are believed to affect backscattering directly. The sigmanought and betanought values of RADARSAT-1 and ENVISAT-ASAR images were calculated in order determine the correlation between the soil properties and radar backscatter. The correlations between soil moisture content, soil texture and backscattering of all SAR images were found significant (r=0.85-0.91). However, no statistically significant relationships were found between backscatter values and organic matter, pH, salt and lime contents of the soils at the test points.

KEYWORDS:
Synthetic Aperture Radar, soil properties, texture, moisture, backscatter.

INTRODUCTION

Monitoring soil properties is very important for an effective soil management [1,2]. Besides, the use of microwave backscattering, spectral reflectance signatures taken in the optical spectrum are quite useful for some agricultural practices. For instance, a variety of information from optical and thermal sensors can be used in estimating soil moisture conditions [3]. However, the acquisition of optical sensor data is often hampered by unfavorable weather conditions which might significantly limit their capacity to provide helpful information.

Studies using remote sensing (RS) technique in the last ten years have put forth a strong correlation between soil moisture and Synthetic Aperture Radar (SAR) backscatter. Most of those studies were based on comparison of soils with the same properties involving images from one satellite, using different polarizations and angles. In some other studies, on the other hand, images from two different satellites were compared to see whether the soil moisture could be measured [4,5,6,7,8]. In this study, SAR data gathered through different polarizations, incidence angle and spatial resolution for the same area were used to estimate not only soil moisture, but also other important soil properties. Generally, smaller incident angles (<300) have been found to be valuable in soil moisture estimations, due to the decreased effects of roughness and vegetation attenuation. In general, the microwave backscatter value depends on sensor configurations, such as incident angle and polarization [9,10,11]. Soil moisture is also affected by soil and plant dielectric properties, and the topographic position of the earth's surface. It is suggested that important information on soil conditions could be provided by the combination of microwave signatures at different frequencies and/or polarizations [12,13,14,15].

Most of the relevant studies were oriented to detecting moisture levels by microwave RS technique. Limited number of studies used SAR images for soil texture and organic matter contents, despite the fact that these soil properties are as important as, and have a direct relation with soil moisture. Soil texture provides fundamental data for a range of academic fields, such as hydrology, ecology, meteorology, irrigation performance, crop pattern management and soil classification. Quite a number of studies alsoindicate that the dielectric coefficients of soils have a direct relation with soil texture and structure [16]. Therefore, investigations solely on the moisture levels will not be adequate for identifying the properties of soils because soil is a living entity with a complex structure resulting from many different types of reactions.

The objective of this study was to investigate the possibility of extracting information about some of the main properties of soils from two different satellite images. The investigated soils were with no

vegetation and the properties to be examined were soil moisture, texture, salinity, organic matter, pH, and CaCO3.

MATERIAL AND METHODS

Study Area. Menemen Plain which covers the western part of Gediz River Basin in the west of Turkey formed the study area of this investigation. The specified River Basin is situated in the most fertile soils of Ege region which has the second largest ground area among the four largest valleys in western Anatolia. Menemen Plain has the formation of both alluvial plains and delta geomorphology, and is situated at the point where 401 km long Gediz River reaches the sea. Inland of the plain has more fertile soils due to drainage and salinity problems particularly in the areas closer to the sea and due to saline and alkaline ground waters, which tend to rise seasonally, Menemen Plain has a very high risk of being affected by climate change. The plain covers an area of about 400 square kilometers and is located between 380 39' 30"/ 380 29' 30" North and 260 48' 09" / 270 04' 46" East (Fig. 1).

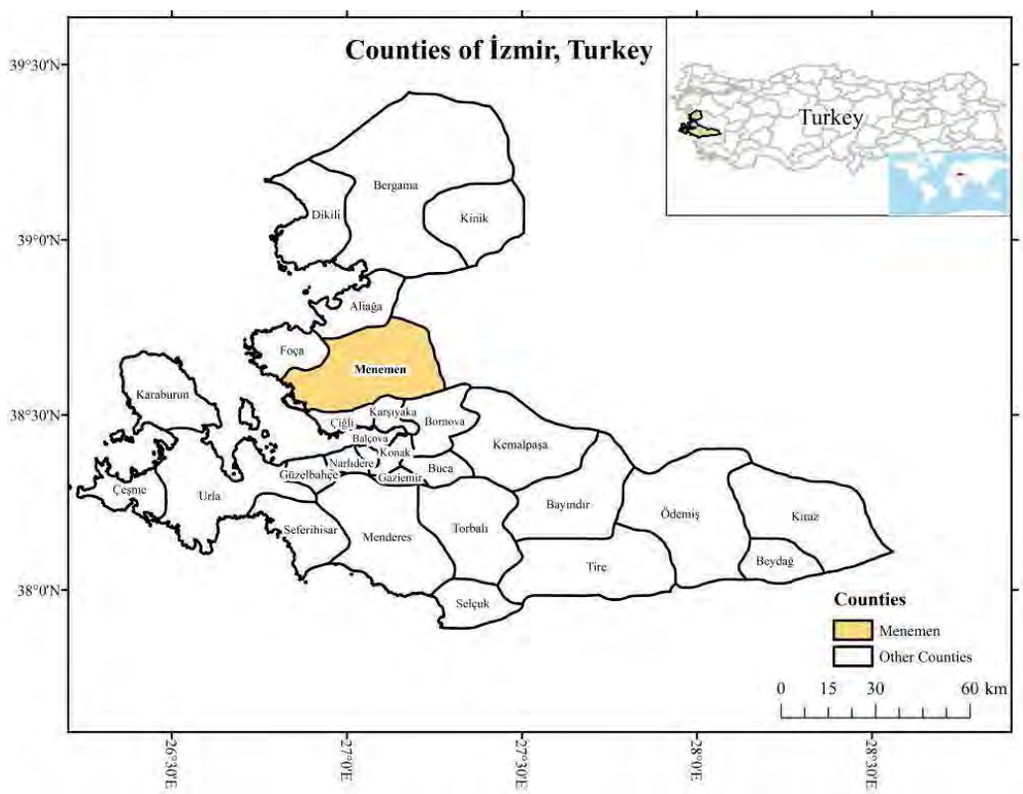

FIGURE 1
Study area.

Data set. In this study, 7 SAR images including two RADARSAT-1 and five ENVISAT-ASAR, were used. Both groups of images consisted of C band images with 5 cm wavelength intervals, but with different spatial resolutions and polarizations. The technical features of RADARSAT–1 and ENVISAT-ASAR images are given in Table 1. In order to monitor the natural moisture level of the soils, four of the SAR images were taken in spring, and three ENVISAT-ASAR images were taken later, in summer. Images were also used to detect the changes in moisture levels of the soil resulting from summer irrigation (Table 1, 2).

TABLE 1
Main characteristics of the RADARSAT-1 data set

Acquired Date	Sensor Mode	Orbit	Format	Pixel spacing	Polarization
04/05/'06	F1	Ascending	SGF	6.25 m x 6.25 m	H/H
28/05/'06	F1	Ascending	SGF	6.25 m x 6.25 m	H/H

TABLE 2
Main characteristics of the ENVISAT-ASAR data set.

Acquired Date	Sensor Mode	Orbit	Swat	Format	Pixel spacing	Polarization
23/05/'06	ASAR/IM	Ascending	I2	PRI ASA_IMP_1P	12.5 x 12.5 m	V/V
08/06/'06	ASAR/IM	Ascending	I1	PRI ASA_IMP_1P	12.5 x 12.5 m	V/V
11/06/'06	ASAR/IM	Ascending	I3	PRI ASA_IMP_1P	12.5 x 12.5 m	V/V
01/08/'06	ASAR/IM	Ascending	I2	PRI ASA_IMP_1P	12.5 x 12.5 m	V/V
17/08/'06	ASAR/IM	Ascending	I1	PRI ASA_IMP_1P	12.5 x 12.5 m	V/V

METHODS

Soil samples were taken from the pre-arranged test points in coordination with the acquisition of satellite images and the samples were tested for their moisture, texture, lime content, organic matter, soil reaction (pH) and salt contents. All soil samples were collected during the each SAR data acquired date. The final phases consisted of image processing, analysis of land surveys, physical and chemical analysis of soil samples and statistical assessments of findings. GIS software, GeoMedia Prof. 5.0. was used to carry out the digitalization of roads, settlements, canals, streams and other elements on a base map, which can be utilized for land surveys and geo-rectification of satellite images, and also on 1/5.000 scale cadastral maps.

In order to build correlations with backscatter values of SAR images and soil properties, geometric and radiometric corrections/calibrations were made prior to the processing and analyzing all SAR images. The radiometric calibration was involved in the procedure to convert the digital numbers into backscattering coefficient (0). The backscattering coefficients (0) were calculated for each RADARSAT-1 and ENVISAT-ASAR image using PCI Geomatics-v10 software. This procedure relies on SAR sensors and a particular data type [17,18]. All PRI (ENVISAT-ASAR) and SGF (RADARSAT-1) images were co-registered and rectified with reference to an ASTER panchromatic and false color composite image (15 May 2006), previously rectified from 1/5.000 scale cadastral maps (Fig. 2).

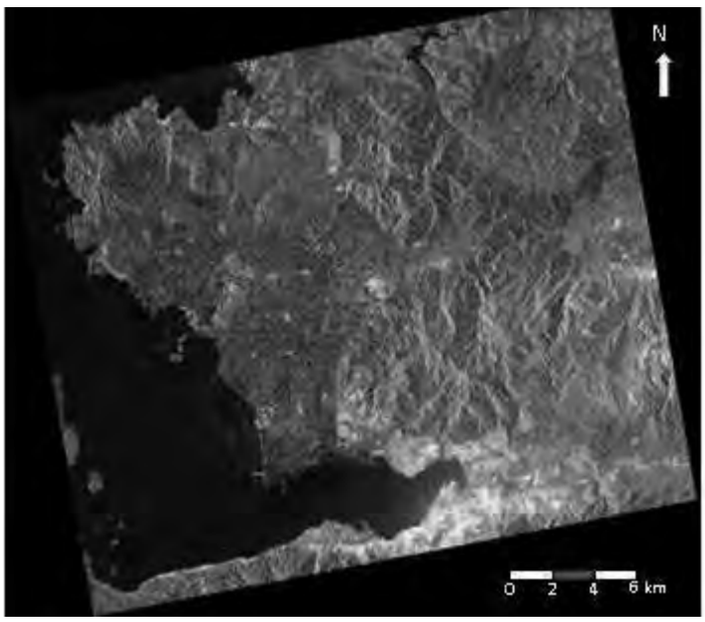

FIGURE 2
A geo-rectified SAR image (RADARSAT-1) by image to map method.

In order to be able to examine the relationships between SAR image backscatter values and soil characteristics, ground surveys were carried which synchronized with each of seven occasions of image capture. In this regard, totally 630 disturbed soil samples were taken (Fig 3). Most of the remotely sensed spectral observations still required site-specific calibrations using ground-sampling techniques [19].

Soil Analysis. At the field, soils were sampled (1.5-2 kg) from the surface (0-10 cm) to detect their moisture contents, and from deeper levels (0-30 cm) to determine their physical and chemical characteristics at each test point.

Excluding the samples for moisture determination, all of the soil samples were air-dried, ground, and sieved prior to analysis for their basic physical and chemical properties. Moisture, texture, soil organic matter, lime content (CaCO3), salinity and soil reactions (pH) [20,21,22,23,24,25] were assessed.

Gravimetric method was used to measure the surface soil moisture content. The method is based on removing soil moisture by oven-drying until the weight remains constant. Soil moisture content (%) is calculated from the sample weight before and after drying.

For other analysis, soil samples were sieved through a 12-mesh (approximately 2 mm). Table 3 shows the analytical methods used for each soil properties that were examined in this study.

TABLE 3
Analytical methods used for the soil properties

Soil properties	Protocols	References
Moisture	Gravimetric	[20]
Texture	Hydrometer	[21]
Organic matter	Wet digestion	[22]
Calcium carbonate	Scheibler	[23]
Water-soluble salts	Saturated paste	[24]
pH	Saturated paste	[25]

FIGURE 3
Soil sampling

For the measurement of soil moisture levels, flat and smooth fields with no vegetation were selected as test points to prevent possible deviations in SAR backscatter.

A GPS handset was used to determine the absolute location data necessary in marking the test points on the satellite image, and in locating them on the base map. Moisture level measurements was an important phase of the study; therefore, to be able to obtain the most accurate possible moisture readings, two techniques, time domain reflectometry (TDR) probe and gravimetric method, were applied in combination. Although TDR measurements are much more convenient and faster in delivering results compared to gravimetric method, it was determined that in areas with high salinity, its accuracy is lower; therefore, results obtained from the more accurate gravimetric method were used to determine the moisture level of soils.

It was observed that in the top 1-2 cm of soils, the moisture levels were relatively low due to wind and evaporation, and the values varied widely depending on the soil texture, whereas at depths deeper than 2 cm, moisture levels increased and changes were less dramatic. Taken into account that the energy, which forms the C band of SAR images, can penetrate approximately 10 cm, gravimetric soil moisture measurements were considered so that they symbolize 0-10 cm. On a clay loam soil, Bruckler et al. [26] found that the radar signal penetration depth decreases from about 5 cm with a soil moisture content of 10%, to 1 cm with a soil moisture content of 30%. The 5 cm soil moisture sampling depth is therefore in accordance with the penetration depth of a C-band radar signal [27]. Apart from moisture level measurements, soil samples were air-dried under laboratory conditions and passed through 2 mm sieves, before texture, pH, lime, water soluble salt, water soluble total salt and organic matter contents were determined.

Coordinates of test points were taken during soil sampling, and were transferred on to SAR images to enable the statistical investigation of SAR image backscatter values and also the results of soil analysis.

Backscatter values of test points were calculated after sigmanought and betanought conversions were made. After the calculation of the backscatter coefficient averages of 9 pixels taken around the central pixel corresponding to the test points, the obtained results were investigated in relation to the studied soil properties. In all image practices, PCI-Geomatics-10 software was used. This research revealed that dielectric coefficient of the water in the soil was one of the most important factors that affect the reflection of microwave energy. Wang [28] indicated the relationship between radar backscatter coefficient (sigmanought and betanought) and dielectric coefficient of soil and water, thus showing its very strong relationship with soil moisture.

RESULTS AND DISCUSSION

Backscatter and gravimetric soil moisture relationships. A significantly positive statistical relationship was determined between backscatter values of all SAR images used in the study and soil moisture (Fig. 4). During the study, the effects of both natural moisture levels and parcel based changing moisture levels depending on irrigation were investigated. A significant positive relationship was detected (r=0, 88; r2=0.79 and r=0, 90; r2=0.81) between soil moisture and backscatter values from RADARSAT-1 images with 6.25 m resolution, taken in May. Also there was an

investigation of the relationship between soil moisture and backscatter values of five ENVISAT-ASAR images with 12.5 m resolution, taken one in May, and four in the following summer months during the irrigation season. A positive relationship as in RADARSAT-1 was detected (r= 0, 85; r=0, 88; r= 0, 87; r=0, 89, r=0, 91), corresponding to the relationship between backscatter values of these five ENVISAT-ASAR images and soil moisture. The close relationships were due to the ongoing irrigation practices at the time of image captures, and therefore, some test points coincided with completely dry parcels, and others with well-irrigated wet parcels. The great differences in moisture levels between the different test points affected backscatter values as well (Table 3). The higher resolution of the RADARSAT-1 images is the reason for the significant statistical relationship between soil moisture levels and backscatter values of RADARSAT-1 images, which were taken in the pre-irrigation period when there were only natural moisture level differences. This result, which shows that the backscatter intensity of microwave energy increases in direct proportion with soil moisture, demonstrates the effectiveness of SAR images in monitoring soil moisture.

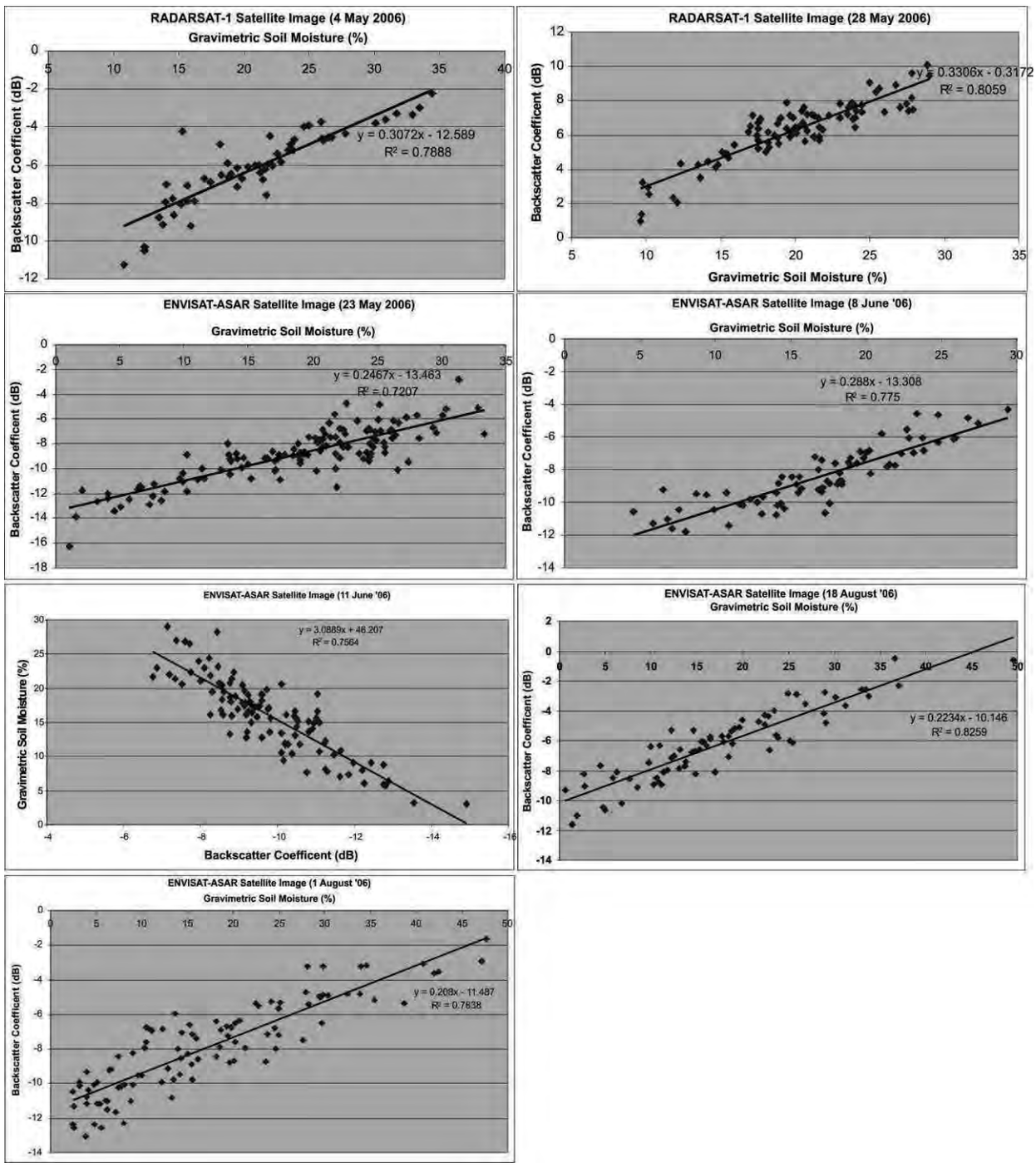

FIGURE 4
Relationship between gravimetric soil moisture and backscatter of RADARSAT-1 & ENVISAT-ASAR images

Backscatter and soil texture relationships. Also investigated were the statistical relationships between the backscatter values of SAR images, and soil texture, in other words, proportional composition of sand, silt and clay. In this regard, first, betanought and sigmanought conversions were made on RADARSAT-1 and ENVISAT-ASAR satellite images. Backscatter sigmanought averages for each central pixel, (corresponding to the test point) and the surrounding nine pixels were calculated and correlated to the soil texture distribution findings for each test point

When the statistical relationships between soil texture and backscatter values from SAR images were examined, a negative relationship with sand texture but a significantly positive relationship with clay texture was found.

Relationships between backscatter values of RADARSAT-1 images and soil texture. In relation to the backscatter values of RADARSAT-1 images and soil texture, land surveys consisting of soil moisture measurements and samplings were carried out at the time of each image capture. The sand, silt and clay ratios of the samples were determined.

For each image capturing period, the statistical relationships between soil texture fractions (%) and backscatter values were investigated. While there was a negative relationship between backscatter values of the image taken on 4 May, 2006 and the sand ratio in the soil texture (correlation coefficient: -0.5), a positive statistical relationship was found with clay ratio in the soil texture (correlation coefficient: 0.4; r2=0.13) (Fig. 5).

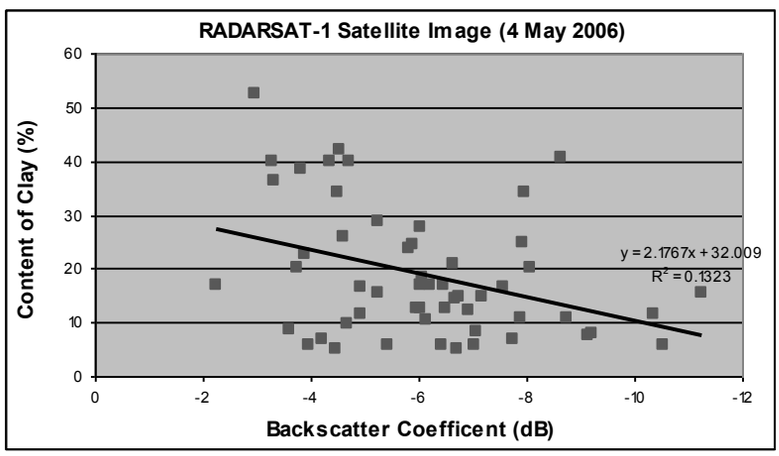

FIGURE 5
Statistical relationships between clay ratio in soil texture and backscatter of RADARSAT-1 image, 4 May, 2006

A strong negative relationship was determined between the backscatter values of the image taken on 28 May, 2006 and soil texture sand fraction (%) with a correlation coefficient of 0.73; however, with regard to clay ratio, a strong positive relationship was found (correlation coefficient: 0.63; r2=0.39) (Fig. 6).

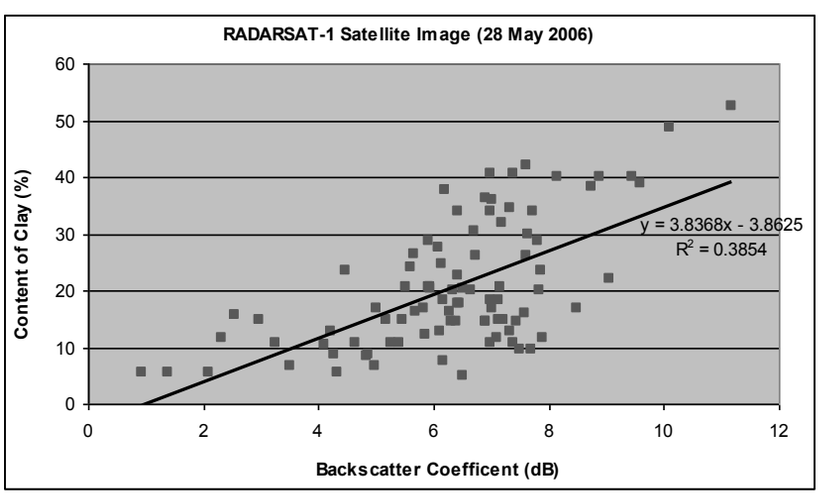

FIGURE 6
Statistical relationship between clay ratio in soil texture and backscatter of RADARSAT-1 image, 28 May, 2006.

Relationships between backscatter values of ENVISAT-ASAR images and soil texture. ENVISAT-ASAR images, used to investigate the relationship between soil texture and backscatter values, consisted of five images taken on 23 May, 08 June, 11 July, 01 August and 18 August respectively. The figure below shows the relationships between backscatter (sigmanought) values, and sand, silt and clay fractions (%) of soil texture, which were determined through the field surveys conducted at the image capture times.

A negative relationship (r=-0.5) was found to exist between the backscatter values of the ENVISAT-ASAR image taken on 23 May, 2006 and the sand fraction (%) of the soil texture recorded at the same time. The statistical relationship between backscatter values and the clay content (%) of the soil texture was found significantly linear and positive (r=0.5; r2=0.20) (Fig. 7).

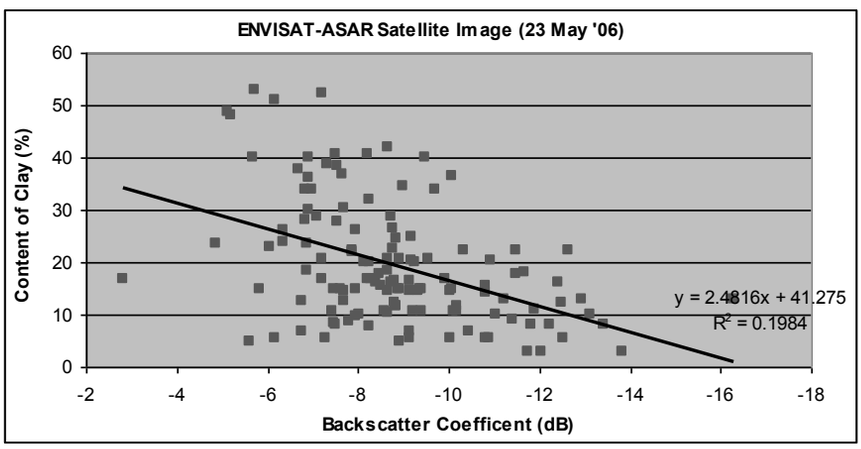

FIGURE 7
Statistical relationship between clay ratio in soil texture and backscatter of ENVISAT-ASAR image, 23 May, 2006.

A significant linear negative relationship (r=-0.58) was found between backscatter values of the ENVISAT-ASAR image taken on 08 June, 2006 and soil texture sand content (%) at this time. The statistical relationship of backscatter values with clay percentage of the soil texture was found significantly linear and positive (r=0.57; r2=0.33) (Fig. 8).

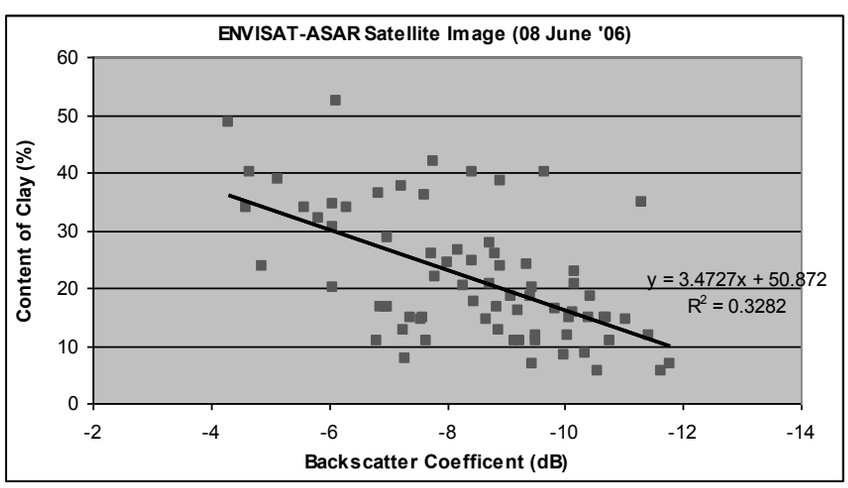

FIGURE 8
Statistical relationship between clay ratio in soil texture and backscatter of ENVISAT-ASAR image, 08 June, 2006.

On the ENVISAT-ASAR image taken on 11 June, 2006, a negative relationship (r=-0.42) between backscatter values and the soil texture sand ratio, and a positive relationship (r= 0.44; r2=0.19) between backscatter values and clay of soil texture were determined, but neither of the results were statistically significant (Fig. 9).

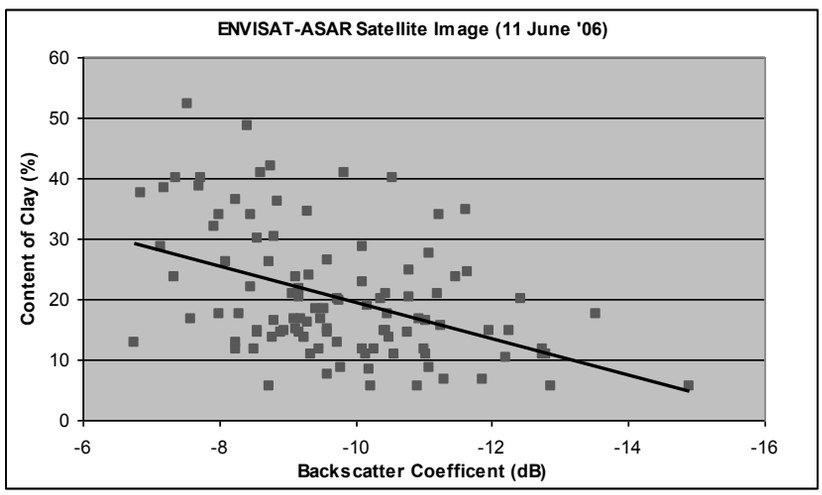

FIGURE 9
Statistical relationship between clay ratio in soil texture and backscatter of ENVISAT-ASAR image, 11 June, 2006.

On the ENVISAT-ASAR image taken on 01 August, 2006, the correlation coefficient was -0.22 for the relationship between backscatter values and soil texture sand content (%), but 0.27 for backscatter/clay relationship; however, no statistically significant relationship was determined in either case (Fig. 10).

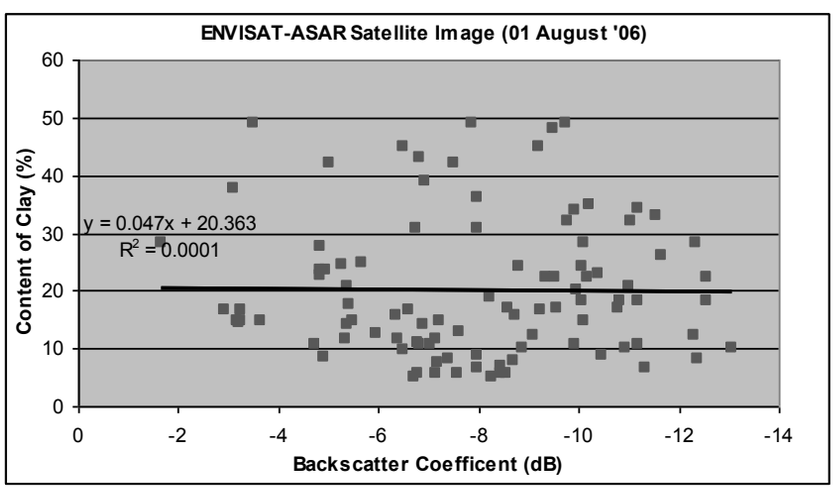

FIGURE 10
Statistical relationship between clay ratio in soil texture and backscatter of ENVISAT-ASAR image, 01 August, 2006.

On the ENVISAT-ASAR image for 18 August, 2006, the relationship was negative (correlation coefficient 0.22) between backscatter values and soil texture sand ratio, but positive (correlation coefficient: 0.27; r2=0.07) for the backscatter/clay relationship (Fig. 11).

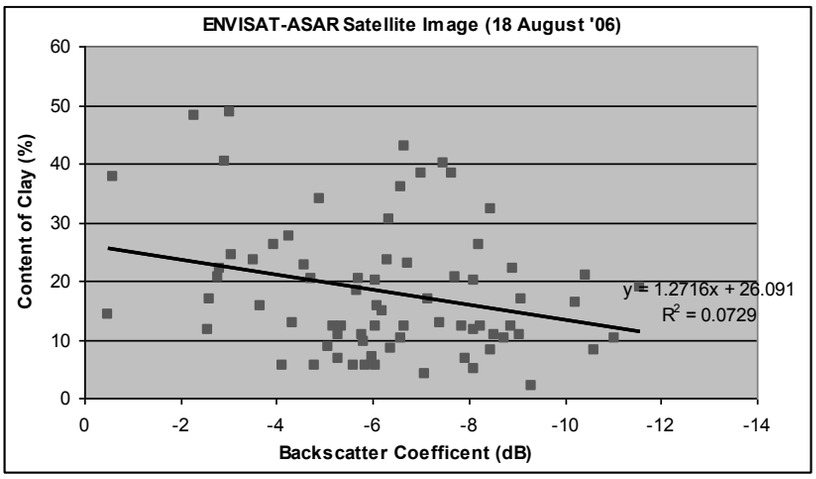

FIGURE 11
Statistical relationship between clay ratio in soil texture and backscatter of ENVISAT-ASAR image, 18 August, 2006.

Findings showed that statistically strong relationships existed between backscatter values for all RADARSAT-1 and ENVISAT-ASAR images and soil texture. The highlighted relationship is directly related to soil moisture, and thus, water holding capacity of the soils. Clearly, soil texture is the proportional expression of the fractions of sand, silt and clay in the soil. Therefore, the clay content of the soil directly affects both the water holding capacity and backscatter values. A statistically strong relationship between soil texture and backscatter values was found due to the fact that soil moisture was homogenously at natural levels because the irrigation of agricultural lands did not start until after the RADARSAT-1 images were taken. In addition, spatial resolution of RADARSAT-1 images was high. Correspondingly, for the ENVISAT-ASAR images taken on 23 May and 08 June, 2006, a strong statistical relationship between soil texture and backscatter values was found in this period before the start of irrigation; however, on the images taken after 10 June, after the beginning of an intense irrigation campaign on agricultural fields in the area, it was not possible to obtain a satisfactory significant relationship (Table 3). Another factor was the low spatial resolutions of ENVISAT-ASAR images.

Results were statistically correlated to determine the statistical relationships between backscatter values of all SAR images and organic matter, salinity, pH and lime contents of the soils in the study area. No statistically significant relationship was found between the organic matter, pH, salt and lime contents of the soils sampled from the test points and backscatter values (Table 4).

TABLE 4
Correlation coefficients of soil properties and backscatter of all SAR images

Satellite	Acquried Date	Gravimetric Soil Moisture (%)	Texture (%)		Salinity (%)	pH	$CaCO_3$ (%)	Organic Matter (%)
			Sand	Clay				
RADARSAT–1	04 May '06	0.88	-0.48	0.40	0.25	0.19	0.41	-0.06
	28 May '06	0.90	-0.73	0.62	0.25	0.17	0.35	0,07
ENVISAT-ASAR	23 May '06	0.85	-0.47	0.47	0.23	0.22	0.30	0.09
	08 June '06	0.88	-0.58	0.57	0.31	0.27	0.27	0.10
	11 June '06	0.87	-0.42	0.44	0.23	0.19	0.30	0.10
	01 August '06	0.89	-0.04	0.01	-0.07	0.1	0.25	0.09
	18 August '06	0.91	-0.22	0.29	0.27	0.38	0.20	0.08

CONCLUSIONS

The aim of this study was to investigate the possible assessment of some major soil characteristics enabled by the use of RADARSAT-1 and ENVISAT-ASAR images, taken on different dates in a one year. In this research, soil texture, lime, organic matter, salt contents and soil reaction (pH) were examined in relation to microwave backscatter.

In this regard, backscatter values of SAR images were obtained and the correlation analysis technique was applied to determine the statistical relationships among soil moisture, soil texture, organic matter, salinity, pH and lime contents of the soils. No statistically significant relationships were found between organic matter, salt, lime contents and pH of the soils sampled from the test points and backscatter values.

The investigation of the relationship between backscatter values and soil texture, one of the most important soil properties, was based on the parameters that form the texture. A positive linear relationship between the clay contents and the water-holding capacity of soils was found. In this study, texture analysis was conducted on the soil samples taken from the test points on which backscatter values were measured. According to the assessments of the statistical relationships between the obtained data and backscatter values on SAR images, there was a positive significant statistical relationship between soils with high clay content and backscatter values of four SAR images (2 RADARSAT-1 and 2 ENVISAT-ASAR) taken in May and early June, but, a negative significant statistical relationship in terms of backscatter values in soil with high sand content. The failure to determine a significant statistical relationship on the next three ENVISAT-ASAR images can be attributed to the likelihood of the externally affected changes in moisture content due to surface micro relief and drainage conditions. Furthermore, regardless of the soil texture, the moisture levels of fields increase during the irrigation season, affecting the backscatter values without having any effect on soil texture. Further studies are recommended in order to determine the effects on backscatter values of other parameters that are effective on moisture content.

REFERENCES

[1] Erturk, A., Alganci, U., Tanik, A., Seker, D. Z. (2012) Determination of land-use dynamics in a lagoon watershed by remotely sensed data. Fresenius Environmental Bulletin, 21 (10a), 3052–3058.

[2] Okatan, A., Aydin, M., Usta, A., Yilmaz, M. (2010) Effects of land use type on hydro-physical properties of soils in the Torul dam basin-Gumushane, Turkey. Fresenius Environmental Bulletin, 19 (12b), 3230–3241.

[3] Ghulam, A., Kusky, T.M., Teyip, T., Qin, Q. (2011) Sub-canopy soil moisture modeling in n-dimensional spectral feature space. Photogrammetric Engineering & Remote Sensing 77 (2), 149–156.

[4] J. Alvarez-Mozos, J., Casali, J., Gonzalez-Audicana, M., Verhoest, N.E.C. (2005) Correlation between ground measured soil moisture and RADARSAT-1 derived

backscattering coefficient over an agricultural catchments of Navvare (North of Spain). Biosystems Engineering 92 (1), 119-133.

[5] Holah, N., Baghdadi, N., Zribi, M. Bruand, A., King, C. (2005) Potential of ASAR/ENVISAT for the characterization of soil surface parameters over bare agricultural fields. Remote Sensing of Environment 96, 78-86.

[6] Kelly, R. E. J., Davie, T.J.A., Atkinson, P.M. (2003) Explaining temporal and spatial variation in soil moisture in a bare field using SAR imagery. International Journal of Remote Sensing 24 (15), 3059-3074.

[7] Crooks, W. T. S., Cheke, R. A. (2014) Soil moisture assessments for brown locust Locustana pardalina breeding potential using synthetic aperture radar. J. Appl. Remote Sens. 8 (1), 01-22.

[8] Ulaby, F. T., Dubois, P. C., and Van Zyl, J.J. (1996) Radar mapping of surface soil moisture. Journal of Hydrology, 184 (1-2): 57-84.

[9] Inoue, Y., Kurosu, T., Maeno H., Uratsuka, S., Kozu T., Dabrowska-Zielinska, K., Qi, J. (2002) Season-long daily measurements of multi-frequency (Ka, Ku, X, C and L) and full polarization backscatter signatures over paddy rice field and their relationship with biological variables. Remote Sensing Environment, 81, 194–204.

[10] Paloscia, S. (1998) An empirical approach to estimating leaf area index from multi-frequency SAR data. International Journal of Remote Sensing, 19 (2), 359–364.

[11] Vespe, M., Posada, M., Ferraro, G., Greidanus, H. (2011) Data fusion of SAR derived features and ancillary information for automatic oil spill detection. Fresenius Environmental Bulletin, 20 (1), 36-43.

[12] Bouman, B.A.M. and Uenk, D. (1992) Crop classification possibilities with radar in ERS–1 and JERS–1 configuration. Remote Sensing of Environment, 40, 1–13.

[13] Champion, I., (1996) Simple modelling of radar backscattering coefficient over a bare soil: variation with incidence angle, frequency and polarization. Int. Journal of Remote Sensing, 17 (4), 783–800.

[14] Moran, M.S., Vidal, A., Troufleau, D., Inoue, Y., Mitchell, T.A. (1998) Ku and C-band SAR for discriminating agricultural crop and soil conditions. IEEE Transactions on Geoscience and Remote Sensing, 36 (1), 265-272.

[15] Yang, Y., Yu, S., Li, Y., Lu, D. (2013) Integration of multidimensional parameters of polarimetric synthetic aperture radar images for land use and land cover classification. J. Appl. Remote Sens. 7 (1), 073472,

[16] Mironov, V.L. Dobson, M.C., Kaupp, V. H., Komarov, S.A., Kleshchenko, V.N. (2004) Generalized refractive mixing dielectric model for moist soils. IEEE Trans. Geosci. Remote Sens., 42 (4), 773–785.

[17] Laur, H., Bally, P., Meadows, P., Sanchez, J., Schaettler, B., Lopinto, E., Esteban, D. (1998) Derivation of the backscattering coefficients in ESA ERS SAR PRI products. ESA Document ES-TN-RS-PM-HL09, Issue 2, Rev. 5f.

[18] Srivastava, S., and Shepherd, N., (2000) Extraction of beta nought and sigma nought from RADARSAT CDPF products. Report No.: AS97-5001. Altrix Systems.

[19] Barnes, E.M., Sudduth, K. A., Hummel, J.W., Lesch, S.M., Corwin, D.L., Yang, C., Daughtry, C. S.T., Bausch W. C. (2003) Remote and ground-based sensor techniques to map soil properties. Photogrammetric Engineering & Remote Sensing, 69 (6), 619–630.

[20] Black, C.A. (1965) Methods of soil analysis: Part I-Physical and mineralogical properties, American Society of Agronomy, Inc., Publisher Madison, Wisconsin U.S.A.

[21] Bouyoucos, G.J. (1962) Hydrometer method improved for making particle size analysis of soils, Agron. J., 54:464-465.

[22] Schlichting, E., and Blume, H.P. (1966) Bodenkundliches Praktikum, Verlag, Paul Parey, Hamburg und Berlin, Germany.

[23]. Jackson, M. L. (1958) Soil chemical analysis-advanced course, Department of Soils, University of Wisconsin. Madison 6, Wisconsin, USA

[24]. Soil Survey Staff (1954) Soil Survey Manual, U.S. Department agriculture handbook, U.S. Government Print, Office, Washington, USA

[25] Jackson, M.L., (1967) Soil chemical analysis, Prentice Hall.Inc., Engle Wood Cliff, New Jersey, USA.

[26] BrucklerL., Witono, H., Stengel, P. (1988) Near surface moisture estimation from microwave measurements. Remote Sensing of Environment 26, 101–121.

[27] Ulaby, F. T., Moore, R. K., Fung, A. K. (1986) Microwave Remote Sensing, Active and Passive Volume III: from Theory to Applications. Artech House, Inc., USA.

[28] Wang, J.R. and Schmugge, T.J. (1980) An empirical model for the complex dielectric permittivity of soil as a function of water content. IEEE Trans. Geosci. Remote Sens., 18 (4), 288–295.

Received: **12.12.2014**
Accepted: **07.12.2015**

CORRESPONDING AUTHOR

Mustafa Tolga Esetlili
Ege University
Faculty of Agriculture
Department of Soil Science and Plant Nutrition
35100, Bornova, Izmir – TURKEY

e-mail: tolga.esetlili@ege.edu.tr
mustolga@gmail.com

by PSP Volume 25 – No. 1/ 2016, pages 37-42 Fresenius Environmental Bulletin

ANTIOXIDANT ENZYME ACTIVITIES AND LIPIDPEROXIDATION AMOUNT OF PEA VARIETIES (PISUM SATIVUM SP. ARVENSE L.) UNDER SALT STRESS

Fikret Yasar, Ozlem Uzal and Ozlem Yasar

Yüzüncü Yıl University, Faculty of Agriculture Department of Horticulture, 65080 Van, Turkey

ABSTRACT

This study examined the responses to salt stress of 5 pea genotypes, B-6, 110121, 1103220, 101917 and 10431 and two pea cultivars Winner and Karina under 75 mM NaCl salt treatment. Pea genotypes were selected from among cross-breed varieties of wild pea and white flowered pea growing different regions of Anatolia. While salinity reduced significantly fresh weight of BA, 110121, it did not cause a significant change fresh weight of the other pea varieties used in this study as compared to the control. Lipid peroxidation was increased by NaCI treatment in all varieties. This increase was more pronounced in BA and 11121 relatively to other pea varieties. On the basis of plant growth and MDA contents, B-6 and 110121 appeared as being more salt sensitive than other varieties

When compared to control, salt treatment increased antioxidant enzyme activities in all pea varieties used in this study. The increases were greater in salt tolerant 1103220, 101917 and 10431 pea varieties than salt sensitive BA and 110121 varieties. These results suggest that pea seedlings respond to salt-induced oxidative stress by increasing their antioxidant defense systems.

KEYWORDS:
Superoxide dismutase (SOD); catalase (CAT); ascorbate peroxidase (APX) ; Oxidative stress;

INTRODUCTION

The pea plant grows in temperate climates, with the largest sowing area found in Asia and the greatest production and yield found in Europe. Following bean, pea is the most widely sown plant crop globally. In Turkey, 1100 ha are devoted to pea cultivation, and the annual pea production is 2500 tons, giving an average yield of 2272 kg. ha-1 [1].

Salinity in soil or water is of importance to agriculture because it limits the distribution of plants in certain natural habitats and induces a wide range of adverse metabolic responses in higher plants. Although some crops are moderately tolerant of saline conditions, many crops are adversely affected by even low levels of salt [2]. Salinity stress affects the metabolism of plant cells leading to severe crop damage and loss of productivity [3].

Salt tolerance in higher plants is the result of a number of physiological responses. There is evidence that high salt concentrations cause an imbalance in cellular ions, resulting in ion toxicity and osmotic stress, leading to the generation of reactive oxygen species (ROS) which cause damage to of lipids, proteins, and nucleic acids [4]. To control the level of ROS and to protect the cells, plants possess a number of low molecular weight antioxidants (ascorbate, glutathione, phenolic compounds, tocopherols) and enzymes scavenging ROS and regenerating the active form of the antioxidants SOD, CAT, APX, GR. Under normal conditions, the production and scavenging of these activated oxygen species is regulated well. In this way, this enzyme system can eliminate the damaging effects of toxic oxygen species [5, 6, 7].

Many reports suggest that the extent of oxidative cellular damage in plants exposed to abiotic stress is controlled by the capacity of their antioxidant systems [8, 9,10]. The aim of this study was to determine the activities of some anti-oxidative stress enzymes (SOD, CAT and APX) and amount of MDA in some pea varieties grown in hydroponic culture under salt stress conditions.

MATERIAL AND METHODS

Material. Five pea genotypes (B-6, 110121, 1103220, 101917 and 10431) and two pea cultivars (Winner and Karina) from different region of Anatolia were used in the study.

Methods. Growing the plants: Pea seeds were germinated in a growth chamber at 20±2 Cº and 70% humidity with a 16-h photoperiod. Seeds were placed in plastic pots (40x25x5 cm) filled with pumice, and seedlings were irrigated with Hoagland nutrient solution following the emergence of the first true leaves. Following the emergence of the

second true leaf, seedlings were transplanted to plastic developing dishes (25x25x5 cm) for hydroponics culture using a Hoagland solution replaced at weekly intervals.

Seedlings were grown in control conditions until emergence of the fourth true leaf, at which time salt stress treatment was initiated. Salt treatment consisted of adding 25 mM NaCl daily until a concentration of 75 mM NaCl was attained. The experiment used a completely randomized design with three replications. Each experimental plot consists of 15 plants for each variety. Fourteen days after the initiation of salt treatment, six plants were randomly harvested from each replication for the fresh weights measurements

Enzymes extraction and assay: Fresh leaf samples were submersed for 5 min in liquid nitrogen. The frozen leaves were kept at -80o C for further analyses. Enzymes were extracted from 0.5 g leaf tissue using a mortar and pestle with 5 ml extraction buffer containing 50 mM potassium phosphate buffer pH 7.6 and 0.1 mM Na-EDTA. The homogenate was centrifuged at 15000 x g for 15 min and the supernatant fraction was used to assay for the various enzymes. All steps in the preparation of enzyme extracts were performed at 4 0C [11].

SOD was assayed according to Cakmak and Marschner[12] by monitoring the superoxide radical-induced nitro blue tetrazolium (NBT) reduction at 560 nm. One unit of SOD activity was defined as the amount of enzyme which causes 50% inhibition of the photochemical reduction of NBT [11].

Catalase activity was determined by monitoring the disappearance of H2O2 according to the method of Cakmak and Marschner[11].

APX activity was determined as described by Cakmak and Marschner [11], measuring ascorbate consumption at 290 nm. One unit of APX was defined as the amount of enzyme required to consume 1 μmol of ascorbate pe min.

Lipid peroxide content (MDA): Lipid peroxidation was measured as the amount of MDA determined by the thiobarbituric acid (TBA) reaction [12]. Frozen samples were homogenized in a pre-chilled mortar and pestle with two volumes of ice-cold 0.1% (w/v) tricloroacetic acid (TCA) and centrifuged for 15 min at 15000 x g. Assay mixture containing 1 ml aliquot of supernatant and 2 ml of 0.5 % (w/v) TBA in 20 % (w/v) tricloroacetic acid (TCA) was heated at 95 0C for 30 min and then rapidly cooled in an ice-bath. After centrifugation (10000 x g for 10 min at 4 0C), the supernatant absorbance (at 532 nm) was read and values corresponding to non-specific absorption (600 nm) were subtracted. Lipid peroxidation products were measured as the content of thiobarbituric acid-reactive substances. The MDA content was calculated according to the molar extinction coefficient of MDA (155 mM–1 cm–1).

All results reported were the means of three replicates. Data were analyzed by analyses of variance, the means separation was carried out by Duncan's multiple range test ($P<0.01$) using SAS [13] software.

RESULTS

When compared to control, NaCl treatment decreased significantly plant fresh weight in BA and 110121 pea varieties. Salt treatment caused slightly decrease in fresh weight of Winner pea too. This decrease was not found significant statistically. On the other hand, NaCl treatment did not cause a significant change in plant fresh weight of Karina, 1103220, 101917 and 10431 pea varieties relatively to control treatment. When considering plant growth, BA and 110121 appeared to be more sensitive to salt stress than Karina, 1103220, 101917 and 10431 pea varieties (Figure 1, A).

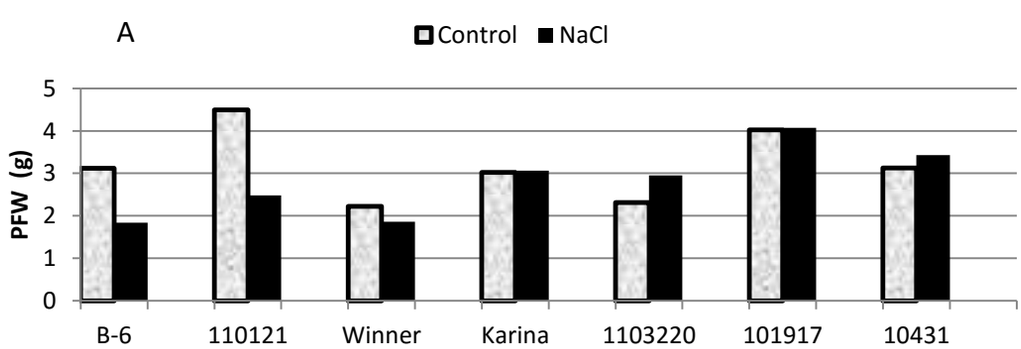

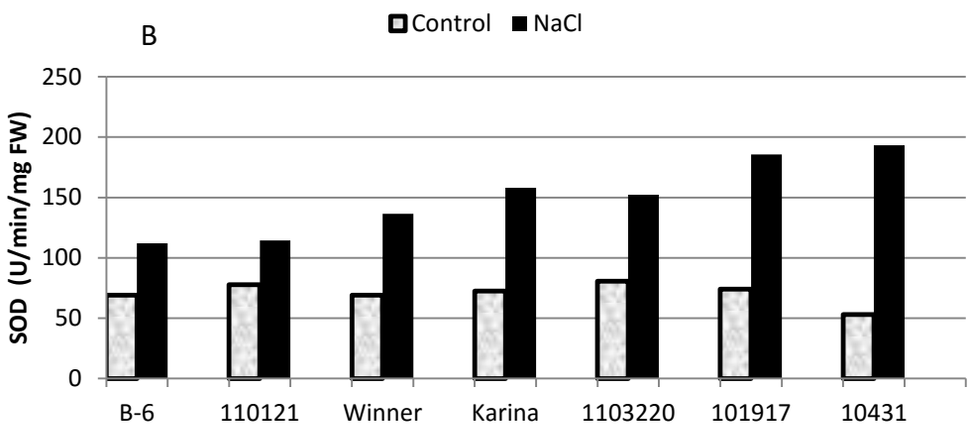
B
Control
NaCl
SOD (U/min/mg FW)
250
200
150
100
50
0
B-6
110121
Winner
Karina
1103220
101917
10431

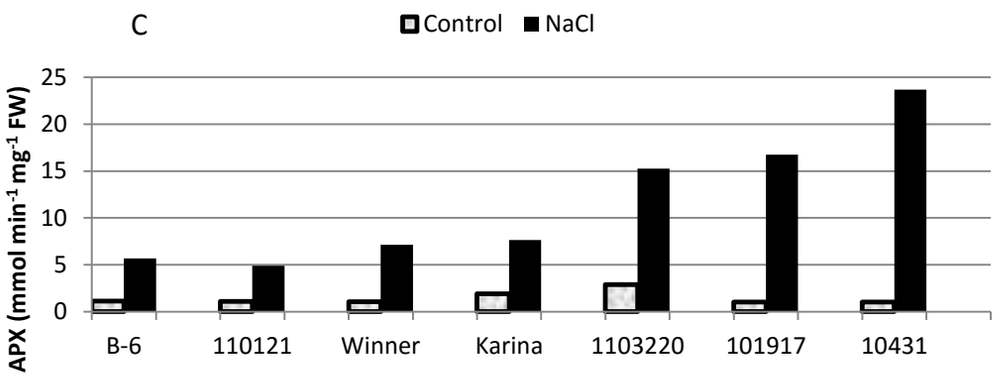
C
Control
NaCl
APX (mmol min-1 mg-1 FW)
25
20
15
10
5
0
B-6
110121
Winner
Karina
1103220
101917
10431

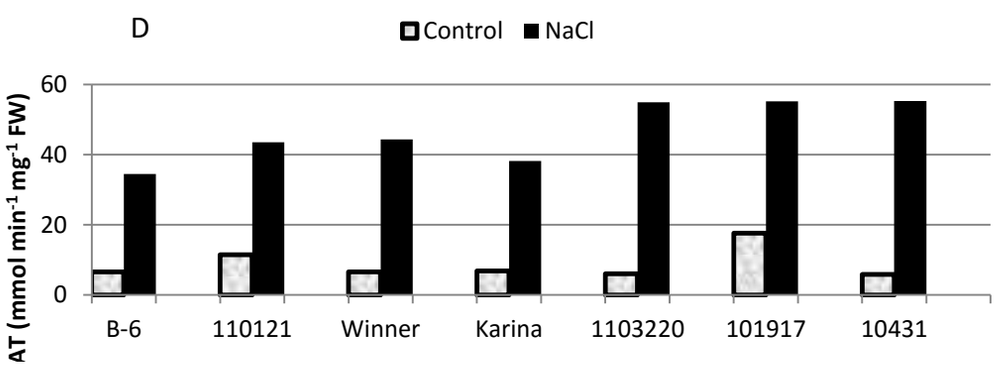
D
Control
NaCl
AT (mmol min-1 mg-1 FW)
60
40
20
0
B-6
110121
Winner
Karina
1103220
101917
10431

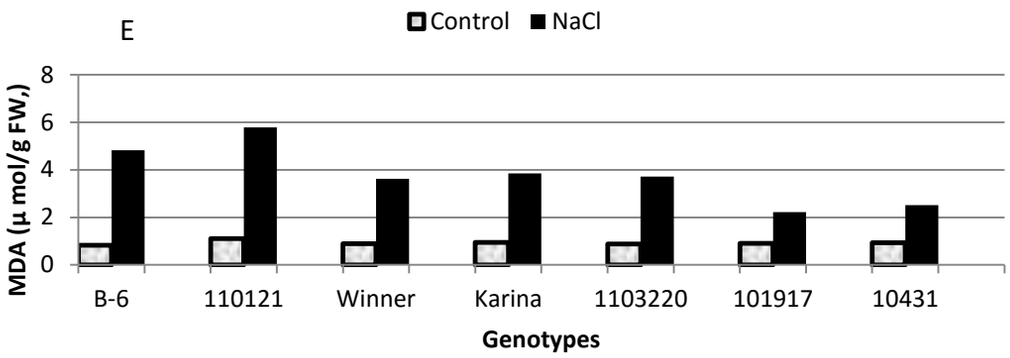

FIGURE 1
Comparison of control and NaCl treated pea varietie and cultures for fresh plant growth (PFW; Panel A), superoxide dismutase (SOD; Panel B) activitie, ascorbate peroxidase (APX ; Panel C) activitie, catalase (CAT; Panel D) activity and melondialdehide (MDA; Panel E) content Means followed by same latter are not significantly different at 0.05 probability level, based on DMR.

To determine the response of pea to salt-induced oxidative stress, SOD, CAT and APX activities, and MDA contents were measured in leaves of seedlings grown with or without elevated NaCl (75 mM).

NaCl treatment increased significantly activities of SOD, CAT and APX in all pea varieties. There were significant differences between varieties with regard to the amount of increase. Under salt stress, while BA and 110121 varieties had the lowest SOS activity, 10431 and 101917 varieties had the highest SOD activities among seven pea varieties used in this study. The increases in APX activities stemmed from NaCl application were much more pronounced in 10431, 101917 and 1103220 compared to other pea varieties. The increases in CAT activities with NaCl application were lowest in BA, followed by Karina and 110121, and highest in 10431 and 1103220. The increases in APX activities of Winner and 101917 varieties were intermediate among pea varieties MDA contents increased significantly in all pea varieties under salt stress relatively to control treatment. However the increases in MDA content of BA and 110121 pea varieties were significantly higher than the increases in MDA contents of the other pea varieties used in this study. Under salt-stress condition, the highest MDA content was measured in 110121 pea varieties, followed by BA and lowest in 101917 and 10431 pea varieties (Figure 1, B, C, D).

MDA contents increased significantly in all pea varieties under salt stress relatively to control treatment. However the increases in MDA content of BA and 110121 pea varieties were significantly higher than the increases in MDA contents of the other pea varieties used in this study. Under salt-stress condition, the highest MDA content was measured in 110121 pea varieties, followed by BA and lowest in 101917 and 10431 pea varieties (Figure 1, E).

DISCUSSION AND CONCLUSIONS

In this study, seven pea varieties differed in their susceptibility to salt stress. Considering plant growth measured on 15 day after salt application, it can be said that BA and 110121 appeared to be the most sensitive to salt stress than the other pea varieties. Under salt stress, the highest MDA content was found in sensitive BA and 110121 varieties. On the other hand the lowest MDA was measured in 101917 and 10431 varieties showing better growing under salt stress. These results are consistent with previous research results. It was reported that the genotypes with higher stress tolerance have less MDA and less lipid per oxidation, and those with higher lipid per oxidation are more precious to salt in study of Karanlik [14] on wheat, Fu and Huang [15] on grass, Aktas [16] on pepper, Turkan et al. [17] on bean. Similarly, MDA values of two green bean varieties grown under salt stress had been examined and it had been found that MDA amount increases depending on the increase of salt and MDA value of the more tolerant variety is less by 30% compared with the salt-sensitive variety [10].

Under normal growth conditions, the production of ROS in the cell is at low levels. However, under conditions of an abiotic stress such as high salinity, cellular homeostasis is disrupted and leads to the production of high levels of ROS. These radicals can damage vital cellular

macromolecules (e.g., via denaturation of proteins, mutation of DNA, and/or peroxidation of lipids). Free radical accumulation is normally controlled by free radical scavengers like SOD, CAT and APX. SOD is one of the ubiquitous enzymes in aerobic organisms and plays a key role in cellular defense mechanisms against ROS. [18, 19]. There have been reports of increased SOD activity in salt tolerant cultivars of pea [20], maize genotypes [21] and green bean genotypes [10] under salt stress. In this study, SOD activity increased in all pea cultivars under salt stress. But, there were significant differences between varieties in respect to the amount of increase. The increase in SOD activity was the highest in 101917 and 10431 varieties showing better growing under salt stress, and the lowest in sensitive BA and 110121 varieties. This result supports to the idea that SOD have important role in salt tolerant mechanism (10, 17, 22).

Protecting against salt stress damage, just as in previous studies on some plants [14, 10], could be a result of higher levels of APX, CAT anti oxidative enzyme systems. Shalata and Tal [23] studied changes in the anti-oxidant enzyme activities in wild tomato species and in cultured tomatoes under salt stress and reported that APX activity increased in salt-tolerant wild species and decreased in 'M82' which was a sensitive variety. In this study, salt application increased significantly APX and activities of all varieties and cultivars used in this study compared with control plants. On the other hand, salt-tolerant varieties (1103220, 101917 and 10431) showing a better growth in salted medium had higher APX activities than salt-sensitive varieties (BA and 110121) under salt stress. It was reported that APX enzyme activity became higher in the kind of strong against salt than sensitive type in green been (10), in pumpkin (24), in melon (25).

Yaşar (2003) reported that there were significant differences in catalase activity between species, and catalase activity increased in eggplant exposed to salt. Likewise, in present study, NaCl treatment increased CAT activities in all pea varieties. It was declared that CAT activity was higher in cotton and tomato genotipes having high resistant against salt than sensitive genotypes (6, 23). In this study, although CAT activities under salt stress was not a distinguishing feature as APX and SOD for salt sensitive and salt tolerant varieties, 1103220, 101917 and 10431 had higher CAT activities in relatively to the other pea varieties.

In conclusion, it is possible to say that anti-oxidative enzyme activities play a protective role against stress, and that the anti-oxidative defense mechanisms were considered to be effectively functioning to provide resistance to salt stress conditions in pea plants grown hydroponically.

REFERENCES

[1] Alan, M. N. (1984). Pea hand book. Ege Agricultural Research Institute Publications No:37 Menemen-İzmir, Turkey p:27

[2] Greenway, H., and Munns, R. (1980). Mechanisms of salt tolerance in non-halophytes. Annu. Rev. Plant Physiol, 31:149–190.

[3] Vaidyanathan, H., Sivakumar, P., Chakrabarty, R., and Thomas, G.(2003). Scavenging of reactive oxygen species in NaCl-stressed rice (Oryza sativa L.) differential response in salt-tolerant and sensitive varieties. Plant Science, 165:1411–1418.

[4] Laloi, C., Stachowiak, M., Pers-Kamczyc, E., Warzych, E., Murgia, I. and Apel, K. (2007). Cross-talk between singlet oxygen- and hydrogen peroxide-dependent signalling of stress responses in Arabidopsis thaliana. Proc Natl Acad Sci, 104: 672–677.

[5] Chen, G., and Asada, K. (1989). Ascorbate peroxidase in tea leaves: occurrence of two isozymes and differences in their enzymatic and molecular properties. Plant Cell Physiol., 30: 987-998.

[6] Meloni, D.A., Oliva, M.A., Martinez, C.A., and Cambraia, J.(2003). Photosynthesis and activity of superoxide dismutase, peroxidase and glutathione reductase in cotton under salt stress. Envir. and Exp.. Bot., 49: 69-79.

[7] Nunez, M., Mazzafera, P., Mazorra, L.M., Siquira, W.J., and Zullo, M.A.T.(2003). Influence of a brassinosteroid analogue on antioxidant enzymes in rice grown in culture medium with NaCl. Biol. Plant., 47: 67-70.

[8] Scandalio, L.M., Dalurzo, H.C., Gómez, M., Romero-Puertas, M.C. and Del Río, L.A. (2001). Cadmium-induced changes in the growth and oxidative metabolism of pea plants. Journal of Experimental Botany, 52: 2115–2126.

[9] Silvana, B.D., Gallego, S.M., Benavides, M.P. and Tomaro, M.L. (2003). Behaviour of antioxidant defense system in the adaptive response to salt stress in Helianthus annuus L. Cells. Plant Growth Regulation, 40: 81-88.

[10]Yasar, F., Ellialtioglu, S. and Yildiz, K. (2008). Effect of salt stress on antioxidant defense systems, lipid peroxidation, and chlorophyll content in green bean. Russian Journal of Plant Physiology 55(6): 782-786.

[11] Cakmak, I., and Marschner, H. (1992) Magnesium deficiency and highlight intensity enhance activities of superoxide dismutase, ascorbate peroxidase and glutathione

reductase in bean leaves. Plant Physiol. 98: 1222–1226.
[12] Heath, R.L. and Packer, L., Photoperoxidation in isolated chloroplasts. i. kinetics and stoichiometry of fatty acid peroxidation. Arch. Biochem. Biophys., 1968, vol. 125, pp. 189-198.
[13] Sas-Institue. 1985. Sas/State User's Guide 6.03 ed. SAS. Ins. Cary. N.C.
[14] Karanlik, S. (2001). Resistance to salinity in different wheat genotypes and physiological mechanisms involved in salt resistance. Ph. D. Thesis, Institute of Natural and Applied Science, University of Cukur Ova. Turkey, 122 p.(in Turkish).
[15] Fu, J. and Huang, B. (2001). Involvement of antioxidants and lipid peroxidation in the adaptation of two cool-season grasses to localized drought stress. Environ. Exp. Bot. 45: 105-114.
[16]. Aktas, H. (2002). Selection and physiological characterization of pepper for resistance to salinity stress. Ph. D. Thesis, Institute of Applied and Natural Science, University of Cukur Ova. Turkey, 105 p.(in Turkish).
[17] Türkan, İ., Bor, M., Özdemir, F. and Koca, H. (2005). Differential responses of lipid peroxidation and antioxidants in the leaves of drought-tolerant P. acutifolius Gray and drought-sensitive P. vulgaris L. subjected to polyethylene glycol mediated water stress. Plant Sci. 168: 223-231.
[18] Foyer, C.H. and Noctor, G. (2005). Oxidant and antioxidant signalling in plants: a re-evaluation of the concept of oxidative stress in a physiological context. Plant Cell Environment. 28: 1056–1071.
[19] Mittler, R. (2002). Oxidative stress, antioxidants and stress tolerance. Trends Plant Science. 7: 405-410.
[20] Hernandez, J.A. and Almansa, M.S. (2002). Short-term effects of salt stress on antioxidant systems and leaf water relations of pea lines. Physiologia Plantarum. 115: 853-862.
[21] Neto, A.D.de A., Prisco, J.T., Eneas-Filho, J., de Abreu, C.E.B. and Gomes-Filho, E. (2006). Effect of salt stress on antioxidative enzymes and lipid peroxidation in leaves and roots of salt-tolerant and salt-sensitive maize genotypes, Environmental and Experimental Botany, 56: 87–94.
[22] Yasar, F. (2003). Investigation of some antioxidant enzyme activities in eggplant genotypes grown under salt stress in vitro and in vivo. Ph. D. Thesis, Institute of Natural and Applied Science, University of Yuzuncu Yil. Turkey, 139 p.(in Turkish).
[23] Shalata, A. and Tal, M. (1998). The Effect of Salt Stress on Lipid Peroxidation avd Antioxidants in The Leaf of the Cultivated Tomato and Its Wild Salt-Tolerant Relative Lycopersicon pennellii. Physiology Plant, 104: 169-174.
[24] Yasar, F., Uzal, O., Kose, S, Yasar, O.and Ellialtioglu, S. (2014). Enzyme actıvıtıes of certaın pumpkın (cucurbıta spp) specıes under drought stress, Fresenius Environmental Bulletin, 23(4): 1093-1099
[25] Kusvuran S., Ellialtioglu, S., Yasar, F. and Abak, K.. (2012). Antioxidative enzyme activities in the leaves and callus tissues of salt-tolerant and salt-susceptible melon varieties under salinity, African Journal of Biotechnology, 11(3): 635–641

Received: **18.12.2014**
Accepted: **25.12.2015**

CORRESPONDING AUTHOR

Fikret YASAR
Yuzuncu Yıl University
Faculty of Agriculture
Department of Horticulture
Van – Turkey

e-mail: fyasar@yyu.edu.tr

by PSP Volume 25 – No. 1/ 2016, pages 43-54 Fresenius Environmental Bulletin

INFLUENCE OF TREATED SEWAGE SLUDGE APPLICATIONS ON CORN AND SECOND CROP WHEAT YIELD AND SOME SOIL PROPERTIES OF SANDY LOAM SOIL

Sezai Delibacak[1*] and Ali Rıza Ongun[1]

[1]Ege University, Faculty of Agriculture, Department of Soil Science and Plant Nutrition, 35100 Bornova İzmir Turkey

ABSTRACT

In this study, influence of treated sewage sludge (TSS) rates on corn and second crop wheat yield and some soil properties of sandy loam soil (Typic Xerofluvent) were investigated. The field study was conducted in 20 plots in a randomized-block design with four replications and five different applications including control, mineral fertilizer, treated sewage sludge 12.5 $Mg.ha^{-1}$, 25.0 $Mg.ha^{-1}$, 37.5 $Mg.ha^{-1}$ as dry matter during 2011-2012 in Menemen-İzmir, Turkey. Corn (*Zea mays*) and wheat (*Triticum vulgare*) were sown as the first and second crop respectively. During the experiment, soil samples were taken five times in two years. Increasing TSS applications to this soil resulted in significantly increased total biomass and grain yield of corn according to the control. Available nutrient concentrations in the soil decreased in the last periods. That's why grain yield of second crop wheat did not significantly change with increasing TSS applications. Increasing TSS aplications were significiantly increased total N, available P and K, pH, total salt and organic matter (OM) content of sandy loam soil. However, $CaCO_3$ and cation exchange capacity (CEC) values of soil did not change significantly when compared with the control. Due to decomposition of TSS in the soil, effect of TSS levels on soil properties decreased in the last periods. For this reason, it is recommended that 37.5 $Mg.ha^{-1}$ TSS as dry matter can be added once in 2 years for improving plant nutrients and soil properties of sandy loam soil, which are characterized by low OM content in Mediterranean region.

KEYWORDS:
Corn, Sandy loam soil, Sewage sludge, Soil properties, Wheat

INTRODUCTION

Agricultural recycling of organic wastes is an interesting solution since it enables a reduction of the quantities of mineral fertilizers applied and an improvement of organic matter (OM) content of soil. Treated Sewage Sludge (TSS) is an ultimate product of municipal wastewater treatment plant and highly enriched in OM. At present the major ways of disposing of sewage sludges are deposition, landfill and incineration, only a part of the sludges are used in agriculture. Where sludge is to be used on land, it is usually stabilised by mesophilic anaerobic digestion, or aerobic digestion and then treated with polymers and mechanically dewatered using filter presses, vacuum filters or centrifuges. Other treatment processes for sludge going to land include long-term storage, conditioning with lime, thermal drying and composting. As municipalities upgrade waste water treatment systems and public opinion and legislation discourages disposal of organic materials in landfills, TSS are projected to become increasingly available for agricultural use. Organic materials can differ considerably in terms of the extent to which they increase soil organic matter contents and alter soil physical and chemical properties [1]. Sewage sludge may contain significant amounts of N, P and trace elements. The use of sewage sludge has been recommended to improve the chemical and physical properties of soil [2, 3]. The beneficial effects of using sludge on agricultural soils have been proven by numerous researchers [2, 3, 4, 5, 6, 7, 8]. The use of sewage sludge as agricultural soil amendments and fertiliser replacements is also relatively well researched [9, 10, 11, 12] and fertiliser advice is available for these materials [13]. TSS contains macronutrients, trace elements and heavy metals. These attributes potentially make TSS an excellent fertilizer at very low cost for agricultural land in Turkey which is generally rich in lime, low in OM. However, special care should be taken with respect to micronutrients and heavy metals so as not to introduce excessive amounts of these elements, which could have an adverse effect on the environment, especially when soil is acidic [12, 14, 15, 16]. The purpose of this work has been to evaluate the effect of municipal TSS doses on the corn and second crop wheat yield and some soil

properties of sandy loam soil during five different periods in two years (1st, August 3, 2011-3 weeks after sowing of corn; 2nd, December 15, 2011-after corn harvest; 3rd, July 11, 2012-after wheat harvest; 4th, August 7, 2012-3 weeks after sowing of second year corn; 5th, November 23, 2012- after corn harvest of second year).

MATERIALS AND METHODS

Experimental. The experiment was conducted at the research field of Aegean Agricultural Research Institute in Menemen plain, Izmir, Turkey (38°56′87.96″-38°56′91.02″N; 27°03′57.52″-27°03′58.61″E). The experimental site is in the Western Anatolia region of Turkey (Figure 1), where the Mediterranean climate prevails with a long-term mean annual temperature of 16.8 °C. Long-term mean annual precipitation is 542 mm, representing about 75% of rainfalls during the winter and spring, and the mean relative humidity is 57%. Long-term mean annual potential evapotranspiration is 1,570 mm [17]. The investigated soil is characterized by sandy loam texture with slightly alkaline reaction and classified as a Typic Xerofluvent [18]. Some selected properties of experimental soil is given in Table 1 and some selected properties and total heavy metal concentrations in TSS used in the experiment is given in Table 2.

TABLE Fehler! Kein Text mit angegebener Formatvorlage im Dokument.
Some selected properties of experimental soil

Sand	(%)	55.84	pH	(Saturation paste)	7.61
Silt	(%)	31.44	Salt	(%)	0.085
Clay	(%)	12.72	$CaCO_3$	(%)	4.56
Texture		Sandy loam	OM*	(%)	1.80

*OM:organic matter

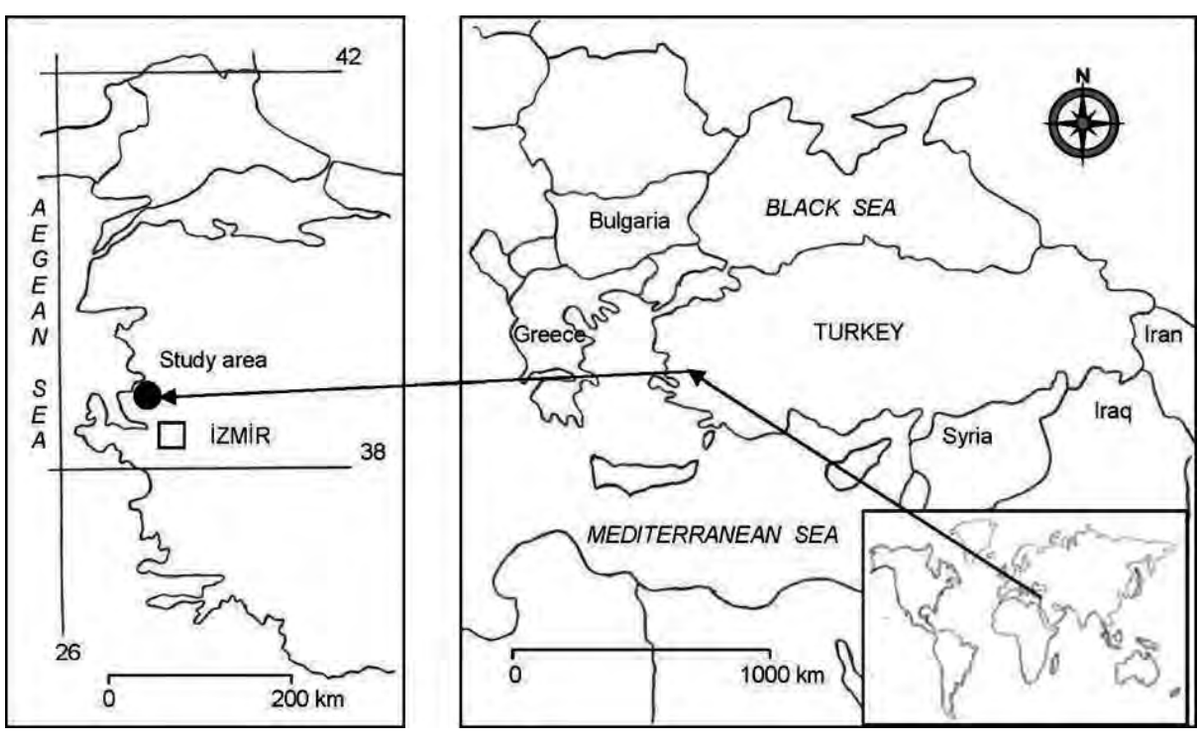

FIGURE 1
Location of study area

TABLE 2
Some selected properties and total heavy metal concentrations of treated sewage sludge used in the experiment

EC	dS/m	16,35	Fe	%	1,14
$CaCO_3$	(%)	10,24	Cu	mg/kg	268,8
Org. matter	(%)	70,32	Zn	mg/kg	1335
Org. C	(%)	40,79	Mn	mg/kg	298,6
N[1]	(%)	5,33	B	mg/kg	035,2
P[1]	(%)	1,33	Co	mg/kg	014,2
K[1]	(%)	0,68	Cd	mg/kg	004,1
Ca[1]	(%)	3,74	Cr	mg/kg	250,6
Mg[1]	(%)	0,68	Ni	mg/kg	115,4
Na[1]	(%)	0,59	Pb	mg/kg	199,4

[1]Total

Field experiment. The field study was conducted in 16 plots in a randomized-block design with four replications, during 2011-2012. The plot dimensions were 3 m width and 3 m length. The TSS used in the experiment was obtained from the wastewater treatment plant of Metropolitan Region, Izmir city. It may produce around 600 Mg (moist basis) sewage sludge per day. Calcium oxide was added to raise the efficiency of the dewatering process of sewage sludge. In addition, the SS produced presented a pH varying between 10 and 13, what increased the pathogen control and decreased the heavy metal availability by added calcium oxide. TSS was added to the soil under investigation at the rates of 12.5 $Mg.ha^{-1}$; 25.0 $Mg.ha^{-1}$; 37.5 $Mg.ha^{-1}$ as dry matter on July 8, 2011. Also 150 kg N, 150 kg P_2O_5, 150 kg K_2O ha^{-1} (1000 kg ha^{-1} 15.15.15. composed fertilizer) were applied to the only mineral fertilizer parcels at the same time and mixed with soil to 15 cm depth. Corn (*Zea mays*) seeds were sown with seeding machine on rows 18 cm and in rows 70 cm apart. Drop irrigation was provided when required. Harvest of corn was done by hands on December 15, 2011. Wheat (*Triticum vulgare*) seeds were sown with seeding machine on December 22, 2011 to 5 cm of soil depth as second crop. Also 80 kg N and 80 kg P_2O_5 ha^{-1} (400 kg ha^{-1}20.20.0. composed fertilizer) were applied to the only mineral fertilizer parcels at the same time and mixed with soil to 15 cm depth before wheat seeding. Wheat was harvested with machine on July 10, 2012. Second year, without applying any TSS (for determination of its second year effect), corn seeds were sown with seeding machine on July 18, 2012. Also 150 kg N, 150 kg P_2O_5, 150 kg K_2O ha^{-1} were applied to the only mineral fertilizer parcels at the same time and mixed with soil to 15 cm depth before corn seeding. Harvest of second year's corn was done by hands on November 23, 2012.

Soil sampling and analyses. During the experiment, soil samples were taken from the center of each plot in five different periods (1st, August 3, 2011-3 weeks after sowing of corn; 2nd, December 15, 2011-after corn harvest; 3rd, July 11, 2012-after wheat harvest; 4th, August 7, 2012-3 weeks after sowing of second year corn; 5th, November 23, 2012- after corn harvest of second year). The samples were air-dried and sieved using 2-mm sieve. All analysis were done in these sieved soils. Particle size distribution of experimental soil was determined by the Bouyoucos hydrometer method [19] . Total salt, OM concentration, $CaCO_3$, pH, total P, K, Ca, Mg, Na, Fe, Cu, Mn, Zn, Cd, Cr, Co, Ni, Pb and B concentrations of TSS were all determined according to Page et al. [20]. Some properties (total salt, OM concentration, $CaCO_3$, pH) of the soil were also determined according to Page et al. [20] . Cation exchange capacity (CEC) of experimental soil was determined according to Chapman [21] . Total N content of soil and TSS were determined using a modified Kjeldahl method [22]. Available P in soil was determined by the Mo blue method in $NaHCO_3$ extract [23]. Available K was analyzed with 1N NH_4OAc extract method [24].

Statistical analysis. Data were analyzed using the Statistical Package for the Social Sciences (SPSS) version 17 [25]. Analysis of variance was performed to determine influence of TSS rates on corn and second crop wheat yield and N, P, K content and some soil properties of sandy loam soil. Tukey test was used to find if differences in the treatments were significant at $P \leq 0.01$ or $P \leq 0.05$.

RESULTS AND DISCUSSION

Influence of TSS applications on yield of corn and second crop wheat grown in sandy loam soil. Influence of TSS applications on total biomass and grain yield of corn grown in sandy loam soil are given in Table 3 and Table 4, respectively. The increasing TSS rates significantly increased average of 1st and 2nd year total biomass and grain yield of corn in the experiment. Antolı´n et al. [26] stated that the yield of barley increased in sludge and mineral amended plots in comparison to unamended plots. This increased grain yield was primarily due to increased ear number per unit of area. The higher yields in sludge-treated crops are usually attributed to an improvement in the soil conditions, by the supply of additional C from the sludge [27, 28].

TABLE 3
Influence of treated sewage sludge (TSS) applications on total biomass yield of corn grown in sandy loam soil (Turkey: P≤ 0,01: P≤ 0,05)

Applications	Average of 1st and 2nd. year yield (Mg.ha^{-1})	1st year yield (Mg.ha^{-1})		2nd year yield (Mg.ha^{-1})		
Control	34.58 b[1]	40.68 a	A[2]	28.47 ab	B	**
Fertilizer	36.30 ab	42.14 a	A	30.47 ab	B	**
12.5 Mg.ha^{-1}TSS	33.79 b	42.45 a	A	25.14 b	B	**
25.0 Mg.ha^{-1}TSS	37.84 ab	44.44 a	A	31.24 ab	B	**
37.5 Mg.ha^{-1}TSS	42.09 a	47.78 a	A	36.40 a	B	**
	*			**		

Significant differences between treatments at ** P≤ 0,01 or * P≤ 0,05 level indicated by different letters. [1]Small letter in column for applications, [2]capital letter in row for years.

TABLE 4
Influence of treated sewage sludge (TSS) applications on grain yield of corn grown in sandy loam soil
(Turkey: P≤ 0,01: P≤ 0,05)

Applications	Average of 1st and 2nd. year yield (Mg.ha^{-1})	1st year yield (Mg.ha^{-1})		2nd year yield (Mg.ha^{-1})		
Control	7.47 c[1]	9.29 b	A[2]	5.65 ab	B	**
Fertilizer	9.25 abc	11.47 ab	A	7.04 ab	B	**
12.5 Mg.ha^{-1}TSS	8.44 bc	11.78 ab	A	5.10 b	B	**
25.0 Mg.ha^{-1}TSS	10.58 ab	13.50 a	A	7.65 ab	B	**
37.5 Mg.ha^{-1}TSS	12.00 a	14.93 a	A	9.08 a	B	**
	*	**		**		

Significant differences between treatments at ** P≤ 0,01 or * P≤ 0,05 level indicated by different letters. [1]Small letter in column for applications, [2]capital letter in row for years.

Influence of TSS applications on grain yield of second crop wheat grown in sandy loam soil are given in Table 5.

TABLE 5
Influence of treated sewage sludge (TSS) applications on grain yield of second crop wheat grown in sandy loam soil (Turkey: P≤ 0,05)

Applications	Control	Fertilizer	12.5 Mg.ha^{-1}TSS	25.0 Mg.ha^{-1}TSS	37.5 Mg.ha^{-1}TSS
Grain yield of second crop wheat (Mg.ha^{-1})	2.587 b[1]	4.366 a	2.773 b	3.452 ab	3.058 b

[1]Significant differences between treatments at * P≤ 0,05 level indicated by different letters.

The highest grain yield of wheat as second crop was found with commercial fertilizer application. It can be said that nutrient concentration in the soil decreased particularly for second crop wheat because of first crop corn plant uptake of nutrients that came from sewage sludge in soil. Hernandez et al. [29], Jamil et al. [30], Jamil et al. [31] and Tamrabet et al. [32] reported that sewage sludge increased the grain yield and straw production of wheat. They mentioned that the maximum yields in both grain and straw were obtained at 40 Mg ha^{-1} of sewage sludge application. Al-Mustafa et al. [33], Singh and Singh [34], Al Zoubi et al. [35] and Ailincăi et al. [36] also mentioned highest increase in the grain and straw yield of wheat treated with sewage sludge.

Influence of TSS applications on total N, plant available P and K content of sandy loam soil. Influence of TSS applications on total N content of sandy loam soil is given in Table 6.

TABLE 6
Influence of treated sewage sludge (TSS) applications on total N content of sandy loam soil, Total N (%)
(Turkey: P≤ 0,01)

Applications	**Average of 5 periods**	**Soil sampling periods**										
		1		**2**		**3**		**4**		**5**		
Control	0.076 b[1]	0.101 b	A[2]	0.083 b	AB	0.074 a	AB	0.080 a	AB	0.043 a	B	**
Fertilizer	0.096 ab	0.141 ab	A	0.104 ab	AB	0.080 a	BC	0.110 a	AB	0.043 a	C	**
12.5 Mg.ha^{-1}TSS	0.087 ab	0.129 ab	A	0.108 ab	A	0.076 a	AB	0.079 a	AB	0.041 a	B	**
25.0 Mg.ha^{-1}TSS	0.104 ab	0.158 a	A	0.125 ab	AB	0.085 a	BC	0.096 a	BC	0.055 a	C	**
37.5 Mg.ha^{-1}TSS	0.114 a	0.178 a	A	0.147 a	AB	0.113 a	BC	0.090 a	CD	0.043 a	D	**
	**	**		**								

Significant differences between treatments at ** P≤ 0,01 level indicated by different letters. [1]Small letter in column for applications, [2]capital letter in row for periods.

The increasing TSS rates significantly increased total N concentration of the average of 5 sampling periods of soil compared with the control. Total N concentration in the soil decreased particularly in the last periods because of the plant uptake of N in soil. Brofas et al. [37] stated that N concentration increased with sludge applications. Bozkurt and Cimrin [38] determined that sewage sludge applications increased the total N concentration about five-fold at the highest sludge rate. White et al. [39] found that N mineralization potentials were significantly higher at high sludge rates. Magdoff and Amadon [40] estimated that 55% of organic N in sludge incorporated in soil was mineralized during the first year. Under optimum laboratory conditions at a temperature of 35 °C, 55 to 95% of the organic N was mineralized in a 24-week period. The rate of mineralization is a function of the amount of the sludge added to soil. A good N balance is a critical factor in any land application program. Over application of N can result in groundwater contamination. Under application can lead to less than optimum crop yields and consequently to farmer dissatisfaction. It is important that sufficient sludge is applied to obtain optimum crop response without excessive NO_3-leaching. Further investigation is needed to develop more precise methods for balancing N

from different sludge types and for varying soil conditions.

Influence of TSS applications on plant available ($NaHCO_3$-extractable) P content of sandy loam soil is given in Table 7. Applications of increasing TSS rates significantly increased the plant available P concentrations of soil in 5 different soil sampling periods according to the control. In the course of time, depending on decomposition of OM and using of plant available P in soil by produced plants, the effect of TSS rates on plant available P concentrations in soil decreased especially in the last periods. White et al. [39] and Brofas et al. [37] also reported a remarkable increase in plant available P in soil after the application of sewage sludge. Another study showed that P concentrations increased more than six-fold from control to the highest application rate plots [41].

Influence of TSS applications on plant available K content of sandy loam soil is given in Table 8. Increasing TSS rates significantly increased available K concentration of the average of 5 sampling periods of soil compared with the control. In the last period (5), all available K concentrations of soil samples were nearly the same. Delibacak et al. [12] found that, plant available K increased with TSS rates from 340 mg kg^{-1} in the control plots to 419 mg kg^{-1} with the 90 Mg ha^{-1} application rate. On the other hand, Martı´nez et al. [42] noted that, plant available K concentrations in soil were low and did not increase significantly with sewage sludge treatments compared with the control.

TABLE 7
Influence of treated sewage sludge (TSS) applications on plant available ($NaHCO_3$-extractable) P content of sandy loam soil. Available P (mg.kg^{-1}) (Turkey:P≤ 0,01; P≤ 0,05)

Applications	Average of 5 periods	Soil sampling periods										
		1		2		3		4		5		
Control	100.05 b[1]	154.85 b	A[2]	107.69 c	B	85.05 b	B	72.53 b	B	80.14 b	B	**
Fertilizer	110.42 b	161.30 b	A	117.05 bc	B	100.83 ab	BC	79.91 ab	C	92.99 ab	BC	**
12.5 Mg.ha^{-1}TSS	107.09 b	161.40 b	A	114.78 bc	B	89.29 b	B	81.52 ab	B	88.47 ab	B	**
25.0 Mg.ha^{-1}TSS	139.91 a	214.40 b	A	150.75 b	B	112.96 ab	C	109.18 a	C	111.75 a	C	**
37.5 Mg.ha^{-1}TSS	154.66 a	214.93 a	A	192.30 a	A	132.97 a	B	115.50 a	B	113.70 a	B	**
	**	**		**		**		**		*		

Significant differences between treatments at ** P≤ 0,01 or * P≤ 0,05 level indicated by different letters. [1]Small letter in column for applications, [2]capital letter in row for periods.

TABLE 8
Influence of treated sewage sludge (TSS) applications on plant available (1N NH_4OAc- extractable) K content of sandy loam soil. Available K (mg.kg^{-1}) (Tukey:P≤ 0,01)

Applications	Average of 5 periods	Soil sampling periods										
		1		2		3		4		5		
Control	475.82 b[1]	514.49 b	A[2]	514.10 ab	AB	440.57 a	B	439.11 b	B	443.85 a	B	**
Fertilizer	515.72 ab	563.41 b	A	543.34 ab	A	453.89 a	B	559.41 a	A	458.57 a	B	**
12.5 Mg.ha^{-1}TSS	478.04 b	566.49 b	A	465.37 b	BC	406.68 a	C	496.17 ab	AB	455.49 a	BC	**
25.0 Mg.ha^{-1}TSS	505.75 ab	618.49 ab	A	501.91 ab	BC	429.94 a	C	522.93 a	B	455.16 a	BC	**
37.5 Mg.ha^{-1}TSS	529.13 a	648.08 a	A	548.21 a	B	449.84 a	D	532.66 a	BC	466.88 a	CD	**
	**	**		**				**				

Significant differences between treatments at ** P≤ 0,01 level indicated by different letters. [1]Small letter in column for applications, [2]capital letter in row for periods.

Influence of TSS applications on some properties of sandy loam soil. Influence of TSS applications on pH of sandy loam soil is given in Table 9. The increasing TSS rates significantly increased pH values of the average of 5 sampling periods and in the first period sampling of soil

compared with the control. It can be said that the reason of increasing pH value of soil is high pH values of sewage sludge treated with lime to eliminate the pathogens. In the last four periods, all pH values of soil samples were nearly the same. It is recommended that soil pH should be maintained above 6.5 for sludge amended soils [43]. Smith [44] noted that optimal pH value for growth of the majority of plants was between 6.5 and 7.0. The soil pH is also one of the major factors controlling the availability of heavy metals.Influence of TSS applications on total salt content of sandy loam soil is given in Table 10.

TABLE 9
Influence of treated sewage sludge (TSS) applications on pH of sandy loam soil (pH, Turkey:P≤ 0,01)

Applications	Average of 5 periods	Soil sampling periods										
		1		2		3		4		5		
Control	7.91 ab[1]	7.64 ab	B[2]	8.05 a	A	7.92 a	A	7.91 ab	A	8.05 a	A	**
Fertilizer	7.83 b	7.49 b	D	8.05 a	A	7.85 a	BC	7.73 b	C	8.02 a	AB	**
12.5 Mg.ha^{-1}TSS	7.93 ab	7.67 ab	B	8.04 a	A	7.94 a	A	7.92 a	A	8.11 a	A	**
25.0 Mg.ha^{-1}TSS	7.93 ab	7.65 ab	C	8.09 a	A	7.95 a	AB	7.88 ab	B	8.08 a	A	**
37.5 Mg.ha^{-1}TSS	7.95 a	7.73 a	C	8.05 a	AB	7.99 a	AB	7.87 ab	BC	8.11 a	A	**
	**	**						**				

Significant differences between treatments at ** P≤ 0,01 level indicated by different letters. [1]Small letter in column for applications, [2]capital letter in row for periods.

TABLE 10
Influence of treated sewage sludge (TSS) applications on total salt content of sandy loam soil (Total salt (%), Turkey:P≤ 0,01)

Applications	Average of 5 periods	Soil sampling periods										
		1		2		3		4		5		
Control	0,057 b[1]	0,084 c	A[2]	0,036 a	AB	0,026 a	B	0,076 a	AB	0,064 a	AB	**
Fertilizer	0,065 ab	0,104 c	A	0,041 a	B	0,026 a	B	0,075 a	AB	0,080 a	AB	**
12.5 Mg.ha^{-1}TSS	0,066 ab	0,116 bc	A	0,064 a	AB	0,025 a	B	0,056 a	B	0,068 a	AB	**
25.0 Mg.ha^{-1}TSS	0,079 ab	0,168 ab	A	0,066 a	B	0,030 a	B	0,065 a	B	0,067 a	B	**
37.5 Mg.ha^{-1}TSS	0,094 a	0,199 a	A	0,081 a	B	0,035 a	B	0,071 a	B	0,084 a	B	**
	**	**										

Significant differences between treatments at ** P≤ 0,01 level indicated by different letters. [1]Small letter in column for applications, [2]capital letter in row for periods.

It was found that, there is no statistical relationship between TSS levels and salt content of soil in all periods, except for first period. Total salt content of soil was significantly increased by increasing TSS levels in soil samples of 1st period. The highest total salt was 0.199% with 37.5 Mg.ha^{-1}TSS level. This was followed by 25.0 (0.168%) and 12.5 (0.116%) Mg.ha^{-1}TSS levels, respectively (Table 10). In the last four periods, all salt contents of soil samples were nearly same. It can be said that irrigation and precipitation caused this situation.

Influence of TSS applications on $CaCO_3$ content of sandy loam soil is given in Table 11.

TABLE 11
Influence of treated sewage sludge (TSS) applications on $CaCO_3$ content of sandy loam soil ($CaCO_3$ (%) Turkey:P≤ 0,01; P≤ 0,05)

Applications	Average of 5 periods	Soil sampling periods										
		1		2		3		4		5		
Control	4.87 a[1]	4.47 a	B[2]	4.76 b	B	5.53 a	A	4.49 a	B	5.11 a	AB	**
Fertilizer	4.91 a	4.46 a	B	4.88 ab	AB	5.27 a	A	4.75 a	AB	5.17 a	AB	**
12.5 Mg.ha^{-1}TSS	5.13 a	4.78 a	B	5.15 ab	AB	5.55 a	A	4.77 a	B	5.41 a	AB	**
25.0 Mg.ha^{-1}TSS	5.11 a	4.80 a	AB	5.17 ab	AB	5.47 a	A	4.64 a	B	5.45 a	A	**
37.5 Mg.ha^{-1}TSS	5.20 a	4.93 a	AB	5.45 a	A	5.47 a	A	4.82 a	B	5.34 a	AB	*
				*								

Significant differences between treatments at ** P≤ 0,01 or * P≤ 0,05 level indicated by different letters. [1]Small letter in column for applications, [2]capital letter in row for periods.

The increasing TSS rates were not significantly increased $CaCO_3$ content of the average of 5 sampling periods of soil compared with the control. Also Delibacak et al. [45] determined that $CaCO_3$ content were not significantly affected by the TSS levels in their research.Influence of TSS applications on cation exchange capasity (CEC) of sandy loam soil is given in Table 12.

TABLE 12
Influence of treated sewage sludge (TSS) applications on cation exchange capacity (CEC) of sandy loam soil (CEC (meq/100g) Turkey:P≤ 0,01)

Applications	Average of 5 periods	Soil sampling periods										
		1		2		3		4		5		
Control	12.48 a[1]	10.96 a	B[2]	11.32 a	B	10.23 a	B	16.67 a	A	13.23 a	B	**
Fertilizer	12.36 a	10.50 a	BC	11.86 a	BC	9.96 a	C	16.10 a	A	13.40 a	AB	**
12.5 Mg.ha^{-1}TSS	12.78 a	10.96 a	BC	11.05 a	BC	10.23 a	C	17.77 a	A	13.90 a	B	**
25.0 Mg.ha^{-1}TSS	13.25 a	11.14 a	B	11.59 a	B	11.05 a	B	18.50 a	A	13.98 a	B	**
37.5 Mg.ha^{-1}TSS	13.31 a	11.32 a	BC	11.59 a	BC	10.96 a	C	18.52 a	A	14.15 a	B	**

Significant differences between treatments at ** P≤ 0,01 level indicated by different letters. [1]Small letter in column for applications, [2]capital letter in row for periods.

It was found that, there is no statistical relationship between TSS levels and CEC of soil in all periods. Ahmed et al. [46] determined that use of sewage sludge in soil showed higher nitrogen and phosphorus contents than the control soil, but a similar content of cation exchange capacity (CEC). On the other hand, Alcantara et al. [47] observed that the concentrations of phosphorus, nitrogen, sulfate, and CEC, organic carbon were positively correlated with sewage sludge dose applied to the soil.

Influence of TSS applications on organic matter content of sandy loam soil is given in Table 13.

TABLE 13
Influence of treated sewage sludge (TSS) applications on organic matter (OM) content of sandy loam soil
OM (%) Turkey:P≤ 0,01

Applications	Average of 5 periods	Soil sampling periods										
		1		2		3		4		5		
Control	1.50 b[1]	1.84 b	A[2]	1.40 b	A	1.47 a	A	1.40 a	A	1.37 a	A	
Fertilizer	1.58 b	2.27 ab	A	1.46 ab	B	1.41 a	B	1.43 a	B	1.33 a	B	**
12.5 Mg.ha^{-1}TSS	1.67 ab	2.45 a	A	1.51 ab	B	1.55 a	B	1.45 a	B	1.39 a	B	**
25.0 Mg.ha^{-1}TSS	1.95 a	2.81 a	A	2.01 a	B	1.83 a	B	1.64 a	B	1.45 a	B	**
37.5 Mg.ha^{-1}TSS	1.95 a	2.82 a	A	2.02 a	B	1.83 a	B	1.59 a	B	1.46 a	B	**
	**	**		**								

Significant differences between treatments at ** P≤ 0,01 level indicated by different letters. [1]Small letter in column for applications, [2]capital letter in row for periods.

Treatments of increasing TSS levels significantly increased OM content of soil samples in the first and second periods and average of 5 periods. In the course of time, depending on decomposition of OM in soil, the effect of TSS levels on OM concentration in soil decreased especially in the last 3 periods. Analogously to our study, Delibacak et al. [45] found out an increase in the concentrations of OM in soil caused by increasing doses of sewage sludge introduced to soil.

CONCLUSION

Increasing TSS applications to sandy loam soil resulted in significantly increased total biomass and grain yield of corn according to the control. However, grain yield of second crop wheat did not significantly change with increasing TSS applications. It can be said that available nutrient concentrations in the soil decreased particularly for second crop wheat because of plant uptake of nutrients from the applied TSS in first vegetation period. On the other hand, increasing treated sewage sludge aplications were significiantly increased total N, plant available P and K, pH, total salt and organic matter content of sandy loam soil as average of 5 sampling periods . However, $CaCO_3$ and CEC values of soil did not change significantly as average of 5 sampling periods when compared with the control. In the course of time, effect of TSS levels on soil properties decreased particularly in the last periods due to decomposition of TSS in soil. For this reason, it is recommended that 37.5 Mg.ha^{-1} TSS as dry matter can be added once in 2 years for improving plant nutrients and soil properties of sandy loam soil under Mediterranean climate, which are characterized by low OM content and high pH. Sewage sludge application to agricultural land has been a widely accepted practice during recent years. Its use in agricultural land is promoted because it is considered that it will solve not only the problem of disposal but also will increase productivity in agriculture. Further investigations are necessary to quantify the fertiliser replacement value of plant nutrients. In particular, accurately characterising the P fertiliser replacement value of sewage sludge will become an increasingly important issue for effective P recycling in agricultural production and food security in future as geological P reserves are depleted and P fertiliser costs increase. At levels above the agronomic recommended rate, however, the potential for negative externalities may be quite substantial. Monitoring the soil periodically for nutrient levels would be prudent to avoid any excess levels on N or other plant nutrient. More continuous long-term experiments are needed to improve the understanding of the effects of sewage sludge on soil fertility and crop yield to contribute to the development of sustainable agricultural practices. However, negative effects of sewage sludge such as elevated heavy metal levels resulting from the usage of sewage sludge must also be taken into consideration [48]. Sewage sludge containing pathogenic organisms should be handled and applied in a proper manner to reduce the risks to human and animal health. Finally, the application of TSS to soil must obey the limited regulations. After the analysis of sewage sludge and soil, a governmental permission is needed to apply them to agricultural lands in Turkey.

ACKNOWLEDGEMENTS

We thank the Scientific and Technical Research Council of Turkey (TUBITAK) for financial support (Project no: 108G167).

The authors have declared no conflict of interest.

REFERENCES

[1] Barker, A.V., Stratton, M.L. and Rechcigl, J.E. (2000) Soil and by-product characteristics that impact the beneficial use of byproducts. Pages 169-213 in W. A. Dick et al. eds. Land application of Agricultural, Industrial, and Municipal by-products. SSSA, Madison, WI.

[2] Wong, J.W. and Su, D.C. (1997) The growth of Agropyron elongatum in an artificial soil mix from coal fly ash and sewage sludge. Bioresource Technology, 59(1), 57–62.

[3] Debosz, K., Petersen, S.O., Kure, L.K. and Ambus, P. (2002) Evaluating effects of sewage sludge and household compost on soil physical, chemical and microbiological properties. Applied Soil Ecology, 19(3), 237–248.

[4] Aggelides, S.M. and Londra, P.A. (2000) Effect of compost produced from town wastes and sewage sludge on the physical properties of a loamy and a clay soil. Bioresource Technology, 71, 253–259.

[5] Benitez, E., Romero, M., Gomez, M., Gallardolaro, F. and Nogales, F. (2001) Biosolid and biosolid ash as sources of heavy metals in plant–soil system. Water, Air and Soil Pollution, 132, 75–87.

[6] Selivanovskaya, S.Y., Latypova, V.Z., Kiyamova, S.N. and Alimova, F.K. (2001) Use of microbial parameters to access treatment methods of municipal sewage sludge applied to grey forest soils of Tatarstan. Agriculture, Ecosystem and Environment, 86, 145–153.

[7] Dede, G., Özdemir, S., Dede, Ö. H., Altundağ, H., Dündar, M. Ş., Kızıloğlu, F. T., 2015. Effects of sewage sludge nutrient availability for kiwi fruits under high pH conditions. Fresenius Environmental Bulletin. Volume:5a.

[8] Niewiadomska, A., Sulewska, H., Wolna-Maruwka, A., Szymanska, G., 2015. The effect of fertilisation of sewage sludge on soil activity in the year of application and in succesive years following its introduction in maize grown for grain. Fresenius Environmental Bulletin Volume:5.

[9] Cogger, C.G., Bary, A.I., Sullivan, D.M. and Myhre, E.A. (2004) Biosolids processing effects on first and second year available nitrogen. Soil Sci Soc Am J. 68:162–167.

[10] Correˆa, R.S. (2004) Efficiency of five biosolids to supply nitrogen and phosphorus to ryegrass. Pesq. Agropec. Bras., 39:1133-1139, 2004.

[11] Tarraso´n, D., Ojeda, G., Ortiz, O., Alcan˜iz, J.M. (2008) Differences on nitrogen availability in a soil amended with fresh, composted and thermally-dried sewage sludge. Bioresource Technology 99, 252–259.

[12] Delibacak, S., Okur, B. and Ongun, A.R. (2009a) Influence of treated sewage sludge applications on temporal variations of plant nutrients and heavy metals in a Typic Xerofluvent soil. Nutr. Cycl. Agroecosyst., 83: 249-257.

[13] Defra, (2010) Policy narrative on global food security and sustainable agriculture, London: DEFRA

[14] Mercik, S., Stêpieñ, W. and Gêbski, M. (2003) Uptake by plants and solubility of Cu,Zn,Pb and Cd in different extraction solutions depending on soil acidity. Zesz. Probl. Post. Nauk Rol., 493: 913-921.

[15] Pascual, I., Antolín, M.C., García, C., Polo, A., Sánchez-Díaz, M. (2004) Plant availability of heavy metals in a soil amended with a high dose of sewage sludge under drought conditions. Biol. Fertil. Soils, 40: 291-299.

[16] Inglezakis, V. J., Zorpas, A. A., Karagiannidis, A., Samaras, P., Voukkali, I., Sklari, S., 2014. European Union legislation on sewage sludge management. Fresenius Environmental Bulletin 23(2a):635-639.

[17] IARTC (2012) Weather Station Climate Datas of International Agricultural Research and Traning Center. Menemen, İzmir.

[18] Soil Survey Staff, (2006) Keys to soil taxonomy. 10th ed. Washington DC, USA: US Government Printing Office.

[19] Bouyoucos, G.J. (1962) Hydrometer method improved for making particle size analysis of soil. Agronomy Journal, 54(5), 464–465.

[20] Page, A.L., Miller, R.H. and Keeney, D.R. (Eds.), (1982) In:Methods of soil analysis. Part 2. Chemical and microbiological properties, 2nd ed. Agron. Monogr. 9. ASA-SSA, Madison, USA.

[21] Chapman, H.D. (1965) Cation-exchange capacity. In: C.A. Black (ed.). Methods of soil analysis - Chemical and microbiological properties. Agronomy 9:891-901.

[22] Bremner, J.M. (1965) 'Total Nitrogen', in C. A. Black (Ed.). Methods of Soil Analysis. Part 2, American Society of Agronomy Inc., Madison, Wisconsin, USA. 1149-1178.

[23] Olsen, S.R., Cole, C.V., Watanabe, F.S. and Dean, L.A. (1954) Estimation of available phosphorus in soil by extraction with sodium bicarbonate. U.S. Dep. Agric.Circ.939, USDA Washington, DC.

[24] Kacar, B. (1994) Chemical analysis of plant and soil: III soil analysis. Ankara University, Faculty of Agriculture, Education Res. and Extension Found. Publications: 3 Ankara (in Turkish)

[25] SPSS 17.0, (2008) SPSS 17.0 for Windows. Chicago, IL, SPSS Inc.

[26] Antolı´n, M.C., Pascual, I., Garcıa, C., Polo, A., Sanchez-Diaz, M. (2005) Growth, yield and solute content of barley in soils treated with sewage sludge under semiarid Mediterranean conditions. Field Crops Research 94, 224-237.

[27] Navas, A., Bermu´dez, F., Machı´n, J., (1998) Influence of sewage sludge application on physical and chemical properties of Gypsisols. Geoderma 87, 123–135.

[28] Christie, P., Easson, D.L., Picton, J.R. and Love, S.C.P. (2001) Agronomic value of alkaline-stabilized sewage biosolids for spring barley. Agron. J. 93, 144–151.

[29] Hernandez, T., Moreno, J.I. and Costa F. (1991) Influence of sewage sludge application on crop yields and heavy metal availability. Soil Science and Plant Nutrition 37, 201-210.

[30] Jamil, M., Qasim, M., Umar, M. and Rehman K. (2004) Impact of organic wastes (sewage sludge) on the yield of wheat (*Triticum aestivum* L.) in a calcareous soil. International Journal of Agriculture and Biology 6(3), 465-467.

[31] Jamil, M., Qacim, M. and Umar, M. (2006) Utilization of sewage sludge as organic fertilizer in sustainable agriculture. Journal of Applied Science 6, 531-535.

[32] Tamrabet, L., Bouzerzour, H., Kribaa, M. and Makhlouf, M. (2009) The effect of sewage sludge application on durum wheat (*Triticum durum*). Inernational Journal of Agriculture and Biology 11, 741–745.

[33] Al-Mustafa, W.A., El-Shall, A.A., Abdallah, A.E. and Modaihsh, A.S. (1995) Response of wheat to sewage sludge applied under two different moisture regimes. Experimental Agriculture 31, 355-9.

[34] Singh, C.P.J. and Singh, S.S. (1999) Effect of urea and sludge based compost application on the yield of wheat (*Triticum aestivum* L.). Madras Agricultural Journal 86, 511-3.

[35] Al Zoubi, M.M., Arslan, A., Abdelgawad, G., Pejon, N., Tabbaa, M. and Jouzdan, O. (2008) The effect of sewage sludge on productivity of a crop rotation of wheat, maize and vetch) and heavy metals accumulation in soil and plant in Aleppo governorate. American-Eurasian Journal of Agriculture and Environmental Sciences 3(4), 618-625.

[36] Ailincăi, C., Jităreanu, G., Ailincăi, D. and Balan, A. (2010). Influence of some organic residues on wheat and maize yield and eroded soil fertility. Cercetări agronomice in Moldova Vol. XLIII, No. 1 (141).

[37] Brofas, G., Michopoulos, P. and Alifragis, D. (2000) Sewage sludge as an amendment for calcareous bauxite mine spoils reclamation. J Environ Qual 29:811–816.

[38] Bozkurt, M.,A. and Cimrin, K.M. (2003) The Effects of Sewage Sludge Applications on Nutrient And Heavy Metal Concentration in a Calcareous Soil. FEB/ Vol 12/ No 11/ 2003-pages 1354-1360.

[39] White, C.S., Loftin, S.R., Aguilar, R. (1997) Application of biosolids to degraded semiarid rangeland: nine-year response. J. Environ. Qual. 26:1663–1671.

[40] Magdoff, F.R. and Amadon, J.F. (1980) Nitrogen availability from sewage sludge. J Environ Qual 9:451–455

[41] Sullivan, T.S., Stromberger, M.E., Paschke, M.W. and Ippolito, J.A. (2006) Long-term impacts of infrequent biosolids applications on chemical and microbial properties of a semi-arid rangeland soil. Biol Fertil Soils 42: 258–266. DOI 10.1007/s00374-005-0023-z

[42] Martı´nez, F., Cuevas, G., Calvo, R. and Walter, I. (2003) Biowaste effects on soil and native plants in a semiarid ecosystem. J Environ Qual 32:472–479.

[43] Henning, B.J., Snyman, H.G. and Aveling, T.A.S. (2001) Plant-soil interactions of sludge-borne heavy metals and the effect on maize (*Zea mays* L.) seedling growth. Water SA 27(1):71–78.

[44] Smith, S.R. (1994) Effect of soil pH on availability to crops of metals in sewage sludge-created soils. I. Nickel, copper and zinc uptake and toxicity to ryegrass. Environ Pollut 85(3):321–327. doi:10.1016/0269-7491(94)90054-X

[45] Delibacak, S., Okur, B. and Ongun, R.A. (2009b) Effects of treated sewage sludge levels on temporal variations of some soil properties of a Typic Xerofluvent soil in Menemen Plain, Western Anatolia, Turkey. Environmental Monitoring and Assessment, 148: 85-95.

[46] Ahmed, H.K., Fawy, H.A. and Abdel-Hady, E.S. (2010) Study of sewage sludge use in agriculture and its effect on plant and soil. Agric. Biol. J. N. Am., 1(5): 1044-1049.

[47] Alcantara, S., Pérez, D.V., Almeida, R.A., Silva, G.M., Polidoro, J.C. and Bettiol, W. (2009) Chemical changes and heavy metal partitioning in an oxisol cultivated with maize (*Zea mays* L.) after 5 years disposal of a domestic and an Industrial sewage sludge. Water, Air, and Soil Pollution 203, 3-16.
[48] Smith, S.R. (1996) Agricultural recycling of sewage sludge and the environment. p. 155–206. In Nutrients. CAB Int., Wallingford, UK.

Received: **27.08.2015**
Accepted: **05.12.2015**

CORRESPONDING AUTHOR

Sezai Delibacak
Ege University
Faculty of Agriculture
Department of Soil Science and Plant Nutrition
35100 Bornova, İzmir – Turkey

e-mail 1: sezai.delibacak@ege.edu.tr
e-mail 2: sezai.delibacak@gmail.com

© by PSP Volume 25 – No. 1/2016, pages 55-66 Fresenius Environmental Bulletin

CONCENTRATION OF HEAVY METALS AND INVESTIGATION OF BACTERIAL TOXIC METAL RESISTANCE IN COSTAL CITY SEDIMENTS (EASTERN AEGEAN SEA)

Asli Kacar[1], Ali Kocyigit[2] and Esin Uluturhan [1]

[1]DEU, Institute of Marine Sciences and Technology, Baku Bul. No:100, 35340, Inciralti/ Izmir, Turkey
[2]Ege University, Faculty of Science, Basic and Industrial Microbiology Section, 35040, Bornova/ Izmir, Turkey

ABSTRACT

Izmir is located on the Eastern Coast of the Aegean Sea in Turkey. In this study, it was aimed to determine the toxic metal resistance of bacterial isolates from coastal city sediments. Twenty-six isolates (*Bacillus, Marinibacillus, Halobacillus*) were identified and these strains were investigated in respect of the minimum inhibitory concentrations of metals, susceptibility of some antibiotics (Ampicillin, Tetracycline, Chloramphenicol, Tobramycin). The MICs of metals were different for each strain but the general order of resistance to the metals was found to be as Ni>Pb>Cu>Cr>Cd>Hg and the toxic effects of these metals increased with increasing concentration. Bacterial isolates were highly resistant to Ni (13 mM), Pb (6 mM). Additionally, it was found that the

strains were resistant to Ampicillin. The highest concentrations of metals were found in the sediments of the inner part of the Bay, which is intensely industrialized compared to the middle and outer parts of the Bay. This study and several other studies suggest that sediment bacteria in an area polluted with heavy metal can be biological indicators.

KEYWORDS:
Heavy metals**,** toxicity, bioindicators, metal resistance, *Bacillus*, Aegean Sea

INTRODUCTION

Various human activities such as industrial and domestic wastes and agricultural inputs cause contaminants enter aquatic environments. These contaminants disrupting the natural balance are industrial wastes, petrol derivatives, pesticides, artificial agricultural chemicals, detergents, radioactive substances, inorganic salts, organic substances etc. Heavy metals in industrial wastes and some pesticides may become a threat to the ecological balance. Entrance of metals to aquatic environments may occur by natural or human resources. These inputs result from atmospheric transport, mining applications, usage of fossil fuel, veterinary drugs, discharge of urban and industrial wastes, and vessel applications. Heavy metals in marine environments may be found in dissolved (free ions, compound ions etc.) or solid phase (colloid form, adsorbed on particle surfaces, in mineral matrix), inorganic or organic forms [1, 2, 3, 4]. Metals might be accumulated by aquatic organisms and be highly toxic even at low levels. Metal pollution has toxic effects on organisms at biochemical, cellular, population and community levels. Sediment is a significant accumulation area for heavy metals and therefore, it is used to determine the level of metal pollution in aquatic environments [5]. However, sediment is also a significant living and feeding ground for various organisms. Heavy metals lead to problems by accumulating in sediments instead of water colon. Thus, bacteria in sediment adapt to the environment in terms of survival and transfer characteristics and gain resistance. In other words, they are able to tolerate high concentration of heavy metals. If there are heavy metals in the sediment, microorganisms affect the catabolism of organic chemicals and ecology of the environment. As a result, microorganisms develop various mechanisms in order to tolerate the metals. These mechanisms include converting into volatile form, extracellular precipitation, adsorbing cell surface, and

intercellular accumulation. Also, bacteria perform chemical transformations of these metals. Heavy metal resistant microorganisms may be used in genetic transfer studies of the heavy metal resistance mechanism [6]. They may also be used as indicators of potential toxicity for other viable forms [7]. Heavy metals have a significant role as selective agents in the evolution of microbial communities [8]. Briefly, microorganisms have a significant role in biogeochemical cycles of metals and they can be used for bio-regeneration in polluted environments [9, 10]. However, correlation is frequently observed in antibiotic resistance besides metal resistance because resistance genes in chromosome or plasmid are close to each other. Increases in antibiotic resistance lead to problems in the treatment of infectious diseases worldwide. Therefore, it is needed to be careful when pesticides, antimicrobials containing metals and antibiotics entering the environment are used [11, 12]. Thus, biological accumulation and bioavailability potentials of heavy metals in aquatic environments are becoming a matter of concern globally. Screening of heavy metal resistance patterns of bacteria and heavy metal contamination in areas with industrial input such as bay are important for the identification of metal effects on the location of flora and fauna in that area and their survival [8].

In this study, heavy metal resistant bacteria species in sediment samples collected from the harbor and other areas of Izmir Bay which were intensely polluted were investigated and heavy metals in the sediment were measured.

MATERIALS AND METHODS

Study Area. Izmir Bay is one of the biggest bays in the Mediterranean Sea with totally 200 km^2 areas and 11.5 billion m^3 water capacity profoundly inserted to Anatolia coasts of Aegean Sea. Izmir, a significant city of commerce, industry and harbor, is the biggest residential area with approximately 88000 ha areas surrounding the bay. Izmir Bay has been polluted since 1960 due to the disemboguement of unrefined domestic and industrial waste waters directly to the bay as a result of increases in population and the number of industrial foundations. This pollution became worse in early 2000s. Especially intensive harbor activities inside the bay and pollution due to domestic and industrial wastes became rampant and ecological balance was disrupted difficult to fix. Pollution was taken under control by Cigli Waste Water Treatment Plant becoming a part of activity in 2000 and recovering in the bay has been observed until now. Izmir Bay is divided into 3 main groups as inner, middle and outer bay due to its hydrological and ecological features. The outer bay is the area between Karaburun peninsula and Gediz delta which extends in the northwest-southeast direction and has the larger and deeper part is. The length of the external gulf is 45 km while its width is about 24 km. The depth of the external bay ranges between 45m and 70m. The middle bay starts from the southeast part of the external bay, extends in the west-east direction to the inner bay. The total length of this area is 38 km while its width is 20 km in west and becomes narrower to east [13, 14].

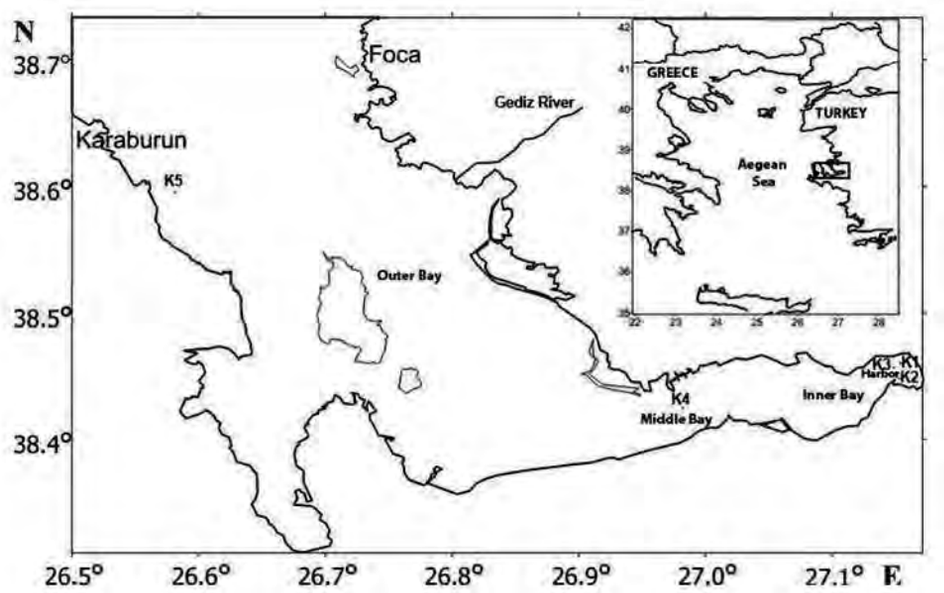

FIGURE 1
Sampling station of Izmir Bay

Analysis of Heavy Metals in Surface Sediments. The surface sediment samples were collected using by Van-Veen grab for heavy metals from 5 sampling stations as part of a cruise of the R/V K. Piri Reis in 2011 (Fig. 1). Immediately after their collection, the samples were placed in acid cleaned polyethylene bottles and were kept frozen at –20ºC until analysis. Samples of the surface sediment were freeze-dried then sieved to pass a 63 µm sieve and homogenized. Later, triplicate samples were digested in a microwave digestion system (Milestone 1200) with acid mixture solutions [15, 16, 17, 18]. A Varian Spectra Model AA280FS and AA280 Zeeman atomic absorption spectrophotometer (AAS) were used for the analysis of heavy metals. The Hg measurements were performed by using cold vapour atomic absorption technique. The concentrations of Pb, Cr, Cu, Mn, Ni, Zn and Fe in the sediment were measured by flame atomization (air-acetylene flame). Also, Cd levels were detected by graphite furnace with AAS. The detection limits for heavy metals are Hg: 0.05 μgkg^{-1}, Cd: 0.10 μgkg^{-1}, Pb: 0.10 $mgkg^{-1}$, Cr: 0.06 $mgkg^{-1}$, Cu: 0.03 mg kg^{-1}, Zn: 0.01 mg kg^{-1}, Mn: 0.02 $mgkg^{-1}$, Ni:0.10 $mgkg^{-1}$, Fe: 0.06 $mgkg^{-1}$. Intercalibration sediment (IAEA-433) samples (from the International Laboratory of Marine Radioactivity, IAEA) were used as a control for the analytical methods. The values obtained (in mg kg^{-1} dry wt) for the analysis of six replicates of this sample (certified: observed values in mg kg^{-1} dry weight ± standard deviation) were as follows: Hg, 0.168 ± 0.017: 0.168 ± 0.00; Cd, 0.153 ± 0.033: 0.140 ± 0.025; Pb, 26.0 ± 2.7: 27.0 ± 3.1; Cr, 136 ± 10.0: 136.7 ± 2.0; Cu, 30.8 ± 2.6: 30.8 ± 2.3; Zn, 101 ± 8.0: 101.1 ± 1.9; Ni:39.4±3.1; 39.4±0.27.

Bacteriological Analysis of Surface Sediments. Surface sediment samples obtained from five various points by Van-Veen grab (Fig. 1) were transferred to the laboratory at +4ºC in sterile falcon tubes, and isolation and identification of the microorganisms were performed for microbiological analyses. Sediment samples were diluted to 10^{-7} and inoculated onto the plates containing Zobell Marine Agar by the spread plate method and incubated at 26ºC for 3-4 days. Approximately 50 bacterial colonies were selected but 26 of these colonies were stored by inoculating pure colonies for further identification. 16S rDNA based molecular analyses were performed to identify bacteria species. For this purpose, genomic DNAs of bacteria were obtained by Genomic DNA Isolation Kit (Zymo Research, USA) and their 16S rRNAs were amplified by PCR using conventional bacterial primers (27F and 1522R). For this test, the Fast Start Taq DNA Polymerase dNTPack Kit (Roche, Germany) was used. Primers were 0.2M and template DNA was 10 ng, and the PCR protocol was performed 30 cycles (first cycle at 95ºC for 5

min, denaturation at 95ºC for 55 s, annealing at 52ºC for 40 s, elongation at 72ºC for 1.5 min, and final elongation step at 72ºC for 7 min) [6, 17, 18]. The DNA sequence analyses of purified PCR products were performed using automatic sequencer ABI Prism 3100 from REFGEN Biotechnology (Turkey).After the sequence results were checked by Chimera program, accession numbers to gene bank numbers were taken by comparing data base in which genes are found (http://www.ncbi.nlm.nih.gov) by Blast program. Phylogenetic tree of the species were generated by using the MEGA 6 program [21, 22].

The minimum Inhibition Concentration (MIC) analysis was performed in order to determine the resistance that the bacterial isolates whose species were identified showed to heavy metals. Thus, heavy metals such as Hg, Cr, Cu, Ni, Pb, Cd were tested. Stock solution of the metals were sterilized by 0.2 µm membrane filtering and then added into Mueller Hinton Agar (Difco, USA) medium at various concentrations ranging between 0.01 and 15.0 (mM). After the bacteria were inoculated into the mediums containing heavy metals, the plates were incubated at 26ºC for 24-48 hours and minimum concentration in which no growth was observed was determined [19, 23].Besides heavy metal resistance analyses, antibiotic resistance of the bacteria was also determined by the disc diffusion method using Mueller Hinton Agar medium. In this analysis, 4 different antibiotics were used: Ampicillin (AM, 10 µg), Chloramphenicol (C, 30 µg), Tetracycline (TE, 30 µg) and Tobramysine (TM, 10 µg) (Bioanalyse, Turkey). After the bacteria were cultured for 24h, 0.1 ml was inoculated into Mueller Hinton Agar. After 1 h incubation at 26ºC, the antibiotic discs were placed on the agar and the plates were incubated again at 26ºC for 24-48 hours. The results were evaluated as resistant or sensitive according to inhibition zone diameter measurements [12, 19, 23].

TABLE 1
The mean ± SD values of metals in sediments from Izmir Bay (mg kg^{-1} dry wt.) and background values.

Station	Hg	Cd	Pb	Cr	Cu	Zn	Mn	Ni	Fe
K1	0.59± 0.06	0.17± 0.01	47.9± 0.43	116± 1.66	46.8± 0.71	159± 3.78	456± 0.89	76.4± 1.08	16190± 839
K2	7.04± 0.15	0.21± 0.01	52.3± 1.70	168± 1.52	72.3± 0.60	278± 1.71	442± 0.84	65.8± 3.49	31922± 1015
K3	0.40± 0.01	0.18± 0.002	50.4± 1.40	114± 3.13	54.4± 0.39	193± 1.91	481± 4.33	125± 0.55	40133± 14.1
K4	0.19± 0.014	0.07± 0.01	20.3± 1.29	140± 6.00	23.4± 0.56	101± 1.53	314± 5.04	74.2± 1.08	29035± 609
K5	0.28± 0.01	0.13± 0.01	13.3± 0.88	122± 5.16	22.6± 0.29	77.4± 2.15	649± 11.5	98.2± 0.13	35698± 419
Backgr. values(a)	**0.40**	**0.30**	**20**	**90**	**45**	**95**	**850**	**68**	**47000**
Mediter Backgrd[b]	**0.34**	**0.10-2.3**	**25**	**15**	**15**	**50**			

a Turekian and Wedepohl[36] b UNEP [37], Whitehead et al.[38] and MAP [39]

TABLE 2
The enrichment factors of heavy metals in sediments from Izmir Bay

Station	Hg	Cd	Pb	Cr	Cu	Zn	Mn	Ni
K 1	4.29± 0.39	1.60± 0.14	6.97± 0.45	3.74± 0.13	3.04± 0.21	4.89± 0.41	1.56± 0.09	3.29± 0.18
K 2	26.0± 0.39	0.98± 0.04	3.91± 0.02	2.73± 0.07	2.38± 0.09	4.31± 0.17	0.77± 0.02	1.42± 0.06
K 3	1.16± 0.04	0.72± 0.01	2.99± 0.07	1.47± 0.05	1.42± 0.01	2.37± 0.02	0.66± 0.01	2.16± 0.04
K 4	0.75± 0.07	0.32± 0.07	1.59± 0.12	2.48± 0.17	0.85± 0.01	1.74± 0.03	0.60± 0.00	1.78± 0.04
K 5	0.91± 0.01	0.41± 0.00	1.16± 0.07	1.67± 0.05	0.28± 0.01	0.64± 0.03	0.52± 0.01	1.45± 0.03

RESULTS AND DISCUSSION

Concentrations of Heavy Metals in Surface Sediments. The means of heavy metals concentrations in sediment from Izmir Bay and background levels were presented in Table 1. The comparison of the metal concentrations with background values revealed that the stations K1, K2 and K3 (Harbour) in the Inner Bay were polluted with Hg, Pb and Cu. Additionally, Cu levels at K4 and K5 were higher than these background levels. The values of Cr and Ni were generally higher than those for background levels in all sampling stations (except K2 for Ni). Although the concentrations of Zn in sampling stations (except the station K5) were detected to be higher than those at background levels, this metal level detected at K5 was higher than those in the Mediterranean. On the contrary, Cd, Mn and Fe concentrations were lower than these values (Table 1). The metal enrichment factor (EF) is utilized as an index to evaluate anthropogenic influences of metals in sediments. The EF is generally defined that ratio of the observed metal to conservative elements (Fe or Al). Al and Fe are the main components of the elements in sediments, and they are not affected by contaminants. The mean heavy metal enrichment factors of the sediments in Izmir Bay are given in Table 2. While EF values between 0.5 and 1.5 indicate that the heavy metals originate from the earth's crust, EF values > 1.5 indicate that the heavy metals have anthropogenic pollution origin [24]. According to the enrichment index, enrichment values of Cd and Mn were less than 1.5 in all the stations except for the station K1. Pb, Cr and Ni enrichment values were greater than 1.5 in all the stations. Conversely, the maximum enrichment of Hg, Pb, Cu and Zn existed at stations K1, K2 and K3 in the Inner Bay. Besides, Hg, Pb, Cr, Zn and Ni were generally enriched. It means that a significant portion of Hg, Cr, Zn, Ni and Pb were provided by anthropogenic sources.The comparison of bibliographical data on metal concentrations of sediments from various regions of the Mediterranean and Aegean Sea was given in Table 3.In this study, the concentrations of Cd were found relatively higher than those found in other studies except the conducted on Venice [25], Izmit [26] and Izmir Bay [27, 28], while Hg values were higher than those determined in all the other areas. Generally, the Pb, Cr and Mn contents of the sediments were lower compared to those obtained in other areas (Table 2). The Pb, Cr, and Zn pollution at all the sampling areas and Hg, Pb, Cr, Cu, Ni and Zn pollution at K1, K2 and K3 are anthropogenic sources. In the past various studies were conducted measure the heavy metals pollution in the sediments of Izmir Bay (Table 3). The highest Cd, Pb, Cr and Cu values were determined as 0.82, 119, 316 and 109 mg $kg^{-}1$, respectively [27]. In another study by Bergin et al. [29] in Izmir Bay, the highest Ni concentration was found as 157 mg kg^{-1}. The Gediz River usually transports high concentrations of

metals due to the inputs of textile, pigment, metal plating, beverage and paper factories and domestic wastes to the bay. The Inner Bay generally was polluted by beer industries, antifouling paints, iron, paper, chlorine–alkali plants, cement factories, and intense harbor activities.In addition, the streams and hundreds of small domestic discharge outlets flow into the Inner Bay. Until the municipal treatment system was introduced in 2000, domestic and industrial wastes were discharged into the Izmir Bay without treatment. Consequently, in the Izmir Bay, the sediment which was continuously in contact with water was intensely polluted.

TABLE 3
Metal concentrations (mg kg^{-1}, dry weight) in surface sediments in various coastal ecosystems

	Hg	Cd	Pb	Cr	Cu	Mn	Ni	Zn	Reference
This study	**0.17-7.21**	**0.05-0.22**	**17.0-54.0**	**110-169**	**8.26-72.8**	**309-485**	**62-126**	**45-280**	
Izmir Bay	0.05-1.3	0.01-0.82	3.10-119	19-316	2.2-109	14-412	-	-	[14]
Izmir Bay	-	0.13-0.42	5.0-62.0	64-300	12-70	74-586	29-148	23-260	[28]
Izmir Bay	0.05-0.39	0.01-0.14	14.0-69.0	40-165	2.6-50	227-777	25-157	20-249	[29]
Saros Gulf	0.07-0.19	0.01-0.04	3.9-48.2	18.8-216	12-42	351-4718	47-152	49-117	[40]
Gökova Gulf	0.07-0.17	0.01-0.05	10-21.8	63-332	10-41.1	399-963	283-426	48-91	[40]
Marmara Sea	0.04-3.0	-	10-85	11-654	3.0-107	100-2610	8.0-1731	33-410	[41]
Izmit Bay	-	3.3-8.9	24-178	58-116	61-139	-	38-71	510-1190	[26]
Aeagean Sea	0.01-0.08	0.003-0.05	1.75-51	22-163	3.2-32	-	-	8.9-84	[42]
Taranto Bay	0.09-0.41	-	44.74.8	77.1-102.8	42.4-52.3	552-2826	47.9-61	87-129	[43]
Northern Aeagean Sea	-	-	10-218	7-172	19-165	-	-	74-358	[44]
Northern Aeagean Sea	-	-	131-2233	213-364	51-206	-	-	159-927	[45]
Venice	0.7-1.6	0.59-3.1	19-56	28-107	12-51	222-379	11-50	71-433	[25]

Heavy Metal Resistant-Bacteria. Of the isolates obtained from surface sediments of five sampling stations (K1, K2, K3, K4 and K5) in Izmir Bay, 26 were identified. Phylogenetic analysis using 16S rDNA indicated that the 26 sediment strains belong to genus *Bacillus, Halobacillus* and *Marinibacillus* (*Bacillus aquimaris* K3-5, *B. baekryungensis* K1-7, *B. cereus* K3-4, *Bacillus endophyticus* K4-12, *B. firmus* K3-12, *B. halmapalus* K4-2, *B. indicus* K1-5, *B. marisflavi* K4-4, *B. megaterium* K3-11, *B. pumilus* K4-5, *B. safensis* K4-13, *B. simplex* strain K2-6, *B. simplex* K3-7, *B. simplex* K1-4, *B. simplex* K1-6, *B. simplex* K2-2, *B. simplex* K3-2, *B. simplex* K5-2, *B. simplex* K5-3, *Bacillus* sp. K4-10, *Bacillus* sp. K1-8, *B. subtilis* K3-9, *B. subtilis* K4-7, *B. subtilis* K4-11, *Halobacillus campisialis* K5-5, *Marinibacillus campisalis* K4-3) reported in this article were submitted to GenBank and assigned the accession numbers KJ161398 - KJ161424, respectively. Minimum inhibitory concentrations of heavy metals are shown in Table 4.

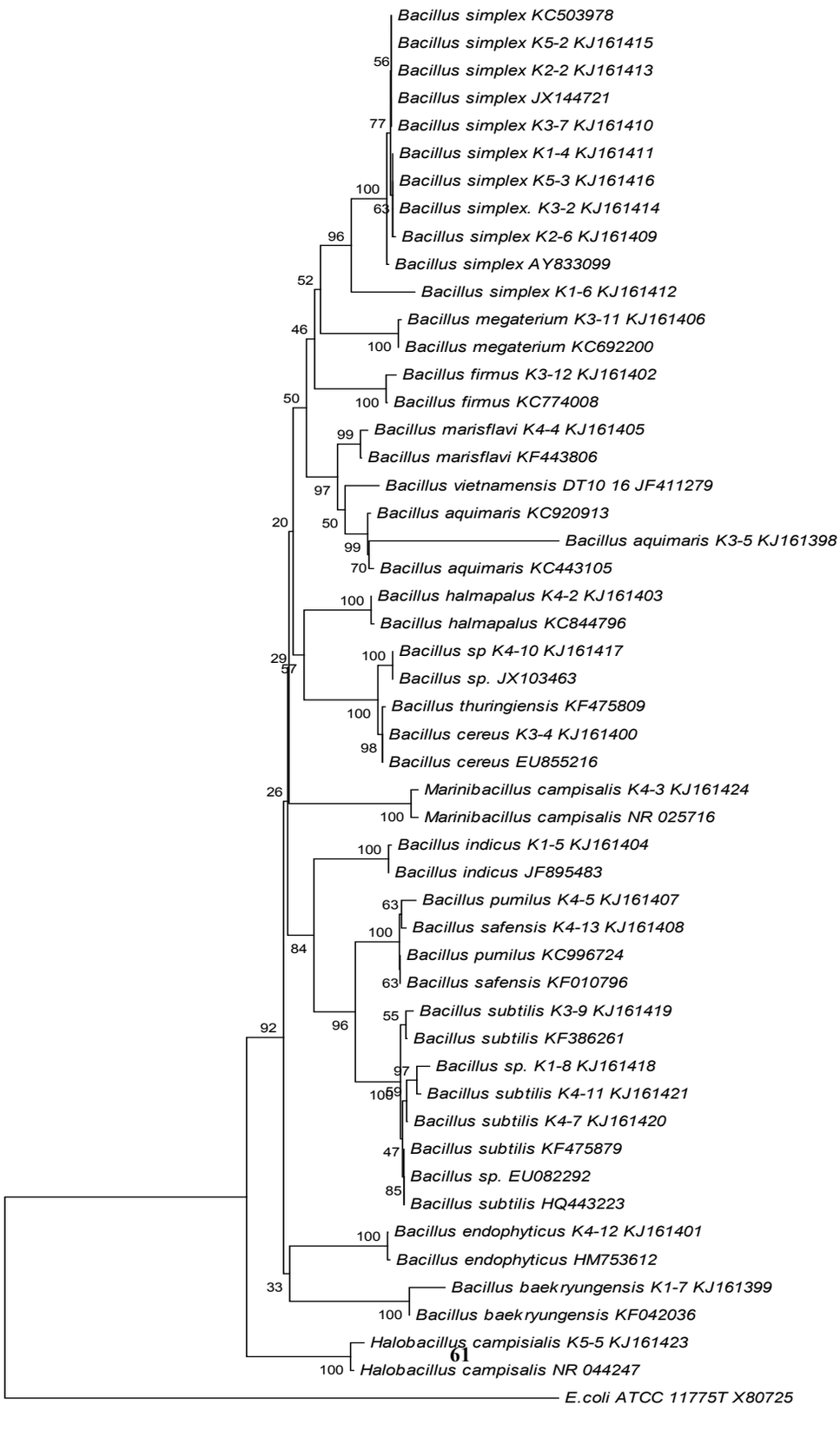
Bacillus simplex KC503978
Bacillus simplex K5-2 KJ161415
Bacillus simplex K2-2 KJ161413
Bacillus simplex JX144721
Bacillus simplex K3-7 KJ161410
Bacillus simplex K1-4 KJ161411
Bacillus simplex K5-3 KJ161416
Bacillus simplex. K3-2 KJ161414
Bacillus simplex K2-6 KJ161409
Bacillus simplex AY833099
Bacillus simplex K1-6 KJ161412
Bacillus megaterium K3-11 KJ161406
Bacillus megaterium KC692200
Bacillus firmus K3-12 KJ161402
Bacillus firmus KC774008
Bacillus marisflavi K4-4 KJ161405
Bacillus marisflavi KF443806
Bacillus vietnamensis DT10 16 JF411279
Bacillus aquimaris KC920913
Bacillus aquimaris K3-5 KJ161398
Bacillus aquimaris KC443105
Bacillus halmapalus K4-2 KJ161403
Bacillus halmapalus KC844796
Bacillus sp K4-10 KJ161417
Bacillus sp. JX103463
Bacillus thuringiensis KF475809
Bacillus cereus K3-4 KJ161400
Bacillus cereus EU855216
Marinibacillus campisalis K4-3 KJ161424
Marinibacillus campisalis NR 025716
Bacillus indicus K1-5 KJ161404
Bacillus indicus JF895483
Bacillus pumilus K4-5 KJ161407
Bacillus safensis K4-13 KJ161408
Bacillus pumilus KC996724
Bacillus safensis KF010796
Bacillus subtilis K3-9 KJ161419
Bacillus subtilis KF386261
Bacillus sp. K1-8 KJ161418
Bacillus subtilis K4-11 KJ161421
Bacillus subtilis K4-7 KJ161420
Bacillus subtilis KF475879
Bacillus sp. EU082292
Bacillus subtilis HQ443223
Bacillus endophyticus K4-12 KJ161401
Bacillus endophyticus HM753612
Bacillus baekryungensis K1-7 KJ161399
Bacillus baekryungensis KF042036
Halobacillus campisialis K5-5 KJ161423
Halobacillus campisalis NR 044247
E.coli ATCC 11775T X80725
0.02

FIGURE2
The dendogram of isolates based on 16s rRNA genes

TABLE 4
MIC concentrations of sediment isolates against heavy metals

Isolates	Heavy Metals (mM)					
	Hg	Cd	Ni	Cr	Cu	Pb
Marinibacillus campisalis K4-3	0.01	0.6	4	0.8	1	4
B. simplex K1-6	0.01	0.2	11	2	2	2
B. megaterium K3-11	0.01	0.2	8	2	2	2
B. halmapalus K4-2	0.01	0.4	4	0.8	0.8	2
Bacillus sp. K4-10	0.02	1.0	8	2	2	6
B. marisflavi K4-4	0.01	0.2	6	2	2	4
Bacillus sp. K1-8	0.01	0.2	13	2	2	4
B. simplex K3-2	0.01	0.08	10	0.8	2	4
B. pumilus K4-5	0.01	0.1	10	2	2	6
B. indicus K1-5	0.01	0.2	2	2	2	2
B. simplex K2-2	0.01	0.08	8	0.8	2	2
B. subtilis K4-11	0.01	0.04	8	2	2	4
B. aquimaris K3-5	0.04	2.0	10	2	2	4
B. firmus K3-12	0.01	0.04	2	2	2	2
B. simplex K2-6	0.01	0.06	6	2	2	4
B. simplex K5-2	0.01	0.2	10	0.8	2	2
B. subtilis K4-7	0.01	0.2	13	2	2	4
B. safensis K4-13	0.01	1.0	2	2	2	4
B. simplex K1-4	0.01	0.2	10	2	2	4
B. simplex K3-7	0.01	0.2	6	2	2	2
B. subtilis K3-9	0.01	0.1	6	2	2	4
B. endophyticus K4-12	0.01	0.1	8	2	2	6
Halobacillus campisialis K5-5	0.01	0.2	4	2	2	4
B. simplex K5-3	0.01	0.1	10	2	2	2
B. cereus K3-4	0.01	0.4	10	0.4	2	4
B. baekryungensis K1-7	0.01	0.2	8	2	2	2

Sediment isolates showed higher tolerance to Ni and Pb. The highest resistance to nickel was in *Bacillus sp*. K1-8 and *B. subtilis* K4-7 isolates with 13 mM concentration. Resistance to lead was found in *Bacillus sp. K4-10, B. pumilus K4-5, B. endophyticus K4-12* with concentration of 6 mM. The highest resistance values for copper, chrome and cadmium were determined as 2 mM. Mercury was the most toxic metal for all of the isolates and it had the lowest inhibition concentration. Among the antibiotic resistance analyses working by the same mechanism as heavy metal resistance, the highest resistance was commonly detected to Ampicillin (Table 5).

TABLE 5
Antibiotic resistance of sediments isolated (mm)

Isolates	Antibiotics			
	Chloramphenicol (30µg)	Tetracycline (30µg)	Ampicillin (10µg)	Tobramycin (10µg)
Marinibacillus campisalis K4-3	24	22	16	-
B. simplex K1-6	22	18	10	24
B. megaterium K3-11	34	22	16	20
B. halmapalus K4-2	30	22	20	10
Bacillus sp. K4-10	20	8	14	13
B. marisflavi K4-4	40	18	22	18
Bacillus sp. K1-8	35	18	18	26
B. simplex K3-2	22	18	8	26
B. pumilus K4-5	23	16	8	20
B. indicus K1-5	32	22	14	18
B. simplex K2-2	16	18	10	22
B. subtilis K4-11	18	20	-	18
B. aquimaris K3-5	32	20	22	20
B. firmus K3-12	38	24	12	28
B. simplex K2-6	22	20	-	22
B. simplex K5-2	18	20	8	25
B. subtilis K4-7	36	20	20	26
B. safensis K4-13	-	16	8	18
B. simplex K1-4	20	20	12	22
B. simplex K3-7	18	20	8	24
B. subtilis K3-9	30	-	13	26
B. endophyticus K4-12	16	21	18	28
Halobacillus campisialis K5-5	38	26	30	22
B. simplex K5-3	18	22	10	22
B. cereus K3-4	36	22	22	24
B. baekryungensis K1-7	32	20	13	19

Most of the bacterial isolates were determined to be sensitive to Chloramphenicol.

According to the similar studies, the areas taking various anthropogenic inputs have a natural reservoir role for bacterial strains with poly-resistance. The most common bacteria in areas polluted with heavy metals were the members of heterotrophic *Bacillus* genus [8, 30, 31]. Zolgharnein et al. [32] determined that bacteria isolated from aquatic environments near industrial areas live in 0.5-1.0 mM metal concentrations (i.e; Zn, Cu, Pb ve Cd). In another study, it was shown that heavy metal and antibiotic resistance were related to each other [23, 30, 31]. In a study by Nithya et al. [8] in India Palk Gulf, it was determined that Co, Cd, Pb, Hg, As and Se resistant bacteria were *B. arsenicus, B. pumilus, B. indicus, B. clausii* after molecular analysis and it was revealed that these sediment bacteria might be biological indicators of heavy metal contamination. Kamala-Kaanan and Lee [31] identified that *Bacillus* species isolated from sediments in Sunchan Bay (South Korea) showed maximum resistance to Mn and Ampicillin, Tetracycline, Kanamycin and Streptomycin. In a study performed in Izmit Bay in Turkey Gul-Seker and Mater [30] identified that bacteria species resistant to Cu, Cd, Cr, Chloramphenicol and Ampicillin were the members of *Acinetobacter* and *Bacillus* genus. Another study in Turkey was performed in Iskenderun Bay which was industrially polluted. In that study, metal toxicity of the isolates was determined as Cd>Cu>Cr>Pb>Mn and that they reported to have high resistance to Ampicillin, Streptomycin and Cefazolin [23]. Bacteria can adapt to the environment by developing tolerance mechanism to heavy metals due to lateral gene transfer between bacterial populations and plasmid resources [33, 34]. Aquatic environments are of interest to all stakeholders in terms of their users and their contribution to socioeconomic development. These areas are under pressure

regarding coastal infrastructures, pollution, direct exploitation, biological resources and marine biodiversity [35]. Therefore, biological accumulation of heavy metals in aquatic environments and their bioavailibility potential are becoming a matter of concern globally [8, 31]. The identification of species with poly-resistance to especially heavy metals and antibiotics may indicate that these coastal areas may have problems, which may pose a risk for humans and animals. Thus, further investigations are needed.

CONCLUSION

When the average threshold values were compared to Mediterranean background levels, Hg, Pb and Cu concentrations were high in sediments in the Harbor area stations. Besides, Cr and Ni levels were higher than these levels in all of the stations. According to the enrichment index, Pb, Cr, Ni enrichments were observed in all of the stations. However, Hg, Cu and Zn enrichment was determined in the Harbor area stations. According to this information, Pb, Cr and Ni pollution in all of the Bay area and Hg, Cu and Zn pollution in the Harbor area were anthropogenic. In this study, the members of *Bacillus* genus were shown to be dominant among the bacteria isolated from Izmir Bay sediments. When we consider Pb, Cr and Ni enrichment, each isolate was resistant at different concentrations due to their heavy metal resistance but it was determined that generally resistance was as Ni>Pb>Cu>Cr>Cd>Hg. It was determined that the most toxic metal for bacteria was Hg. In this study, it was observed that the highest resistance was to Ampicillin as in most of the studies considering heavy metal and antibiotic resistance mechanisms are similar. These results showed that the identified bacteria are able to survive in sediments polluted by heavy metals. While most of the bacteria are sensitive to even low concentrations of metals under specific conditions, they can adapt to their environment quickly and develop resistance to metals. For this reason, it is considered that these bacteria may be suitable indicators for the identification of heavy metal potential toxicity in coastal areas polluted with metal and they can be also designed for bioremediation applications by further investigations.

ACKNOWLEDGEMENTS

Financial support by Scientific Research Projects Coordination Unit of Dokuz Eylul University (Project number: 2012.KB.FEN.022) for this work is gratefully appreciated.

REFERENCES

[1] Kucuksezgin F., Kontas A., Altay O., Uluturhan E., Darilmaz E. (2006) Assessment of marine pollution in Izmir Bay: nutrient, heavy metal and total hydrocarbon concentrations. Environ Int 32:41–51

[2] Kennish M.J. (1998) Pollution in Estuarine and Marine Environments, Pollution Impacts on Marine Biotic Communities. Institute of Marine and Coastal Sciences, Rutgers University, New Jersey

[3] Ozden S., Tuncer, S. (2015) Heavy metal concentrations in *Mytilus galloprovincialis* from Çanakkale Strait, NW Turkey. Fresen Environ Bull 24(9):2725-2731

[4] Baydan E., Kaya S., Cagirhan H., Yildirim E., Altintas L., Yurdakok B., Ekici H., Aydin F. G., Kucukosmanoglu A.G. (2014) Determination of veterinary drug residues in sea water, sediment and natural fish in the Aegean Sea. Fresen Environ Bull 23(10a):2602-2609

[5] Salamons W. Long-term strategies for handling contaminated sites and large-scale areas. In: SalamonsW, Stigliani W, editors. Biogeodynamics of pollutants and sediments. Berlin' Springer-Verlag; 1995

[6] De Rore H., Top E., Houwen F., Mergeay M., Verstraete W. (1994) Evolution of heavy metal resistant transconjugants in a soil environment with a concomitant selective pressure. FEMS Microbiol Ecol14:263-273

[7] Jansen E., Michels M., Til M., Doelman P. (1994) Effects of heavy metals in soil on microbial diversity and activity as shown by the sensitivity-resistance index, an ecologically relevant parameter. Biol Fert Soils 17:177-184

[8] Nithya C., Gnanalakshmi B., Pandian S.K. (2011) Assessment and characterization of heavy metal resistance bacteria in Palk Bay sediment. Mar Environ Res 7(1):283-294

[9] Balkis N., Altug G. (2009) Levels of some toxic elements and frequency of bacterial heavy metal resistance in sediment and sea water. Environ Monit Assess 149:61–69

[10] Unaldi-Coral M.N., Korkmaz H., Arikan B., Coral G. (2005) Plasmid mediated heavy metal resistances in *Enterobacter spp*. isolated from Sofulu landfill, in Adana, Turkey. Ann Microbiol 55(3):175-179

[11] Samanta A., Bera P., Khatun M., Sinha C., Pal P., Lalee A., Mandal A. (2012) An

investigation on heavy metal tolerance and antibiotic resistance properties of bacterial strain *Bacillus sp*. isolated from municipal waste. J Microbiol Biotech Res 2(1):178-189

[12] Li K., Ramakrishna W. (2011) Effect of multiple metal resistant bacteria from contaminated lake sediments on metal accumulation and plant growth. J Hazard Mater 189:531–539

[13] IZSU. (2011) http://www.izsu.gov.tr/pages/standartPage.aspx?id=199

[14] Kucuksezgin F., Kacar A., Kucuksezgin G., Uluturhan E. (2010) Monitoring metal contamination levels and fecal pollution in clam (*Tapes decussatus*) collected from Izmir Bay (Turkey). Environ Monit Assess 162:407–415

[15] UNEP. (1985a) Determination of total Hg in marine sediments and suspended solids by cold vapour AAS. Reference Methods for Marine Pollution Studies 26

[16] UNEP. (1985b) Determination of total cadmium in marine sediments by flameless AAS. Reference Methods for Marine Pollution Studies 27

[17] UNEP. (1985c) Determination of total chromium in marine sediments by flameless AAS. Reference Methods for Marine Pollution Studies 31

[18] UNEP. (1985d) Determination of total lead in marine sediments by flameless AAS. Reference Methods for Marine Pollution Studies 34

[19] Kacar A., Kocyigit A. (2013) Characterization of Heavy Metal and Antibiotic Resistant Bacteria Isolated from Aliaga Ship Dismantling Zone, Eastern Aegean Sea, Turkey. Int J Environ Res 7(4):895-902

[20] Nithya C., Pandian S.K. (2009) Isolation of heterotrophic bacteria from Palk Bay sediments showing heavy metal tolerance and antibiotic production. Microbiol Res 65:578-593

[21] Altschul S.F., Madden T.L., Schaffer A.A., Zhang J., Zhang Z., Miller W., Lipman D. (1997) Gapped BLAST and PSIBLAST: a new generation of protein database search programs. Nucleic Acids Res 25:3389-3402

[22] Thompson J.D., Higgins D.G., Gibson T.J. (1994) Clustal W: Improving the sensitivity of progressive multiple sequence alignment through sequence weighting position specific gap penalties and weight matrix choice. Nucleic Acids Res 22:4673-4680

[23] Matyar F., Kaya A., Dincer S. (2008) Antibacterial agents and heavy metal resistance in Gram-negative bacteria isolated from seawater, shrimp and sediment in Iskenderun Bay, Turkey. Sci Total Environ 407:279–285

[24] Zhang L., Ye X., Feng H., Jing Y., Ouyang T., Yu X. (2007) Heavy metal contamination in western Xiamen Bay sediments and its vicinity. China. Mar Pollut Bull 54:974–982

[25] Bernardello M., Secco T., Pellizzato F., Chinellato M., Sfriso A., Pavoni B. (2006) The changing state of contamination in the Lagoon of Venice. Part 2: Heavy metals. Chemosphere 64:1334–1345

[26] Pekey H. (2006) Heavy metal pollution assessment in sediments of the Izmit Bay, Turkey. Environ Monit Assess 123:219–231

[27] Kucuksezgin F., Kontas A., Uluturhan E. (2011) Evaluations of heavy metal pollution in sediment and Mullus barbatus from the Izmir Bay (Eastern Aegean) during 1997–2009. Mar Pollut Bull 62(7):1562-1571

[28] Atgin R.S., Omar E., Zararsız A., Kocatas A., Parlak H., Tuncel G. (2000) Investigation of the sedimentpollution in Izmir Bay: trace elements. Spectrochim Acta Part B 55:1151–1164

[29] Bergin F., Kucuksezgin F., Uluturhan E., Barut I.F., Meric E., Avsar N., Nazik A. (2006) The response of benthic foraminifera and ostracoda to heavy metal pollution in Gulf of Izmir (Eastern Aegean Sea). Estuar Coast Shelf Sci 66:368-386

[30] Gul-Seker M., Mater Y. (2009) Assessment of metal and antibiotic-resistance in marine bacteria isolated from Izmit Bay and Bosphorus entrance of Marmara and Black Sea, Turkey. Fresen Environ Bull 18(11):2192-2202

[31] Kamala-Kaanan S., Lee K.J. (2008) Metal Tolerance and Antibiotic Resistance of Bacillus species Isolated from Snchon Bay Sediments, South Korea. Biotechnology 7(1):149-152

[32] Zolgharnein H., Azmi M., Saad M.Z., Mutalib A.R., Mohamed C.A.R. (2007) Detection of plasmids in heavy metal resistance bacteria isolated from the Persian Gulf and enclosed industrial areas. Iranian J Biotechnol 5(4): 232- 239

[33] Hoostal M.J., Bidart-Bouzat M.G., Bouzat J.L. (2008) Local adaptation of microbial communities to heavy metal stress in polluted sediments of Lake Erie. FEMS Microbiol Ecol 65:156-168

[34] Martinez R.J., Wang Y., Raimondo M.A., Coombs J.M., Barkay T., Sobecky P.A. (2006) Horizontal gene transfer of PIB-type ATPases among bacteria isolated from radionuclide-

and metal-contaminated subsurface soils. Appl Environ Microbiol 72:3111-3118

[35] Bianchi C.N., Morri C. (2000) Marine biodiversity of the Mediterranean sea: situation, problems and prospects for future research. Mar Pollut Bull 40:367-376

[36] Turekian K.K., Wedepohl K.H. (1961) Distribution of the elements in some major units of the earth's crust. Geol Soc Am Bull 72:175–192

[37] UNEP. (1978) Preliminary report on the state of pollution of the Mediterranean Sea. Ingovermental review Meeting of Mediterranean Coastal States on the Mediterranean Action Plan UNEP/IG.11/INF 4

[38] Whitehead N.E., Oregioni B., Fukai R. (1985) Background levels of trace metals in Mediterranean sediments. J Etud Pollut 7:233–240

[39] MAP. (1987) Assessment of the state of pollution of the Mediterranean Sea by mercury and mercury compounds. Tech Rep Series 18 UNEP, Athens

[40] Uluturhan E. (2010) Heavy metal concentrations in surface sediments from two regions (Saros and Gökova Gulf) of the Eastern Aegean Sea. Environ Monit Assess 165:675–684

[41] Algan O., Balkis N., Cagatay M.N., Sari E. (2004) The sources of metal contents in the shelf sediments from the Marmara Sea, Turkey. Environ Geol 46: 932–950

[42] Akcali I., Kucuksezgin F. (2011) A biomonitoring study: heavy metals in macroalgae from eastern Aegean coastal areas. Mar Pollut Bull 62:637–645

[43] Buccolieri A., Buccolieri G., Cardellicchio N., Dell'Atti A., Di Leo A., Maci A. (2006) Heavy metals in marine sediments of Taranto Gulf (Ionian Sea, Southern Italy). Mar Chem 99: 227-235

[44] Chistophoridis C., Dedepsidis D., Fytianos K. (2009) Occurrence and distribution of selected heavy metals of Thermaikos Gulf, N. Greece, assessment using pollution indicators. J Hazard Mater 168:1082-1091

[45] Stamatis N., Ioannidou D., Christoforidis A., Koutrakis E. (2002) Sediment pollution by heavy metals in the Strymonikos and Ierissos Gulf, North Aegean Sea, Greece. Environ Monit Assess 80:33–49

Received: **06.01.2015**
Accepted: **04.12.2015**

CORRESPONDING AUTHOR

Asli Kacar
DEU - Institute of Marine Sciences and Technology
Baku Bul. No: 100
35340, Inciralti, Izmir – Turkey

e-mail: asli.kacar@deu.edu.tr

by PSP Volume 25 – No. 1/ 2016, pages 67-77 Fresenius Environmental Bulletin

AN ANOXIC/OXIC MEBRANE BIOREACTOR FOR THE TREATMENT OF CONCENTRATED COLD-ROLLING WASTEWATER FROM REVERSE OSMOSIS PROCESS

Enchao Li[1,2] Xuewen Jin[2] Sheng Wu[2] Shuguang Lu[1]

[1]State Environmental Protection Key Laboratory of Environmental Risk Assessment and Control on Chemical Process, East China University of Science and Technology, Shanghai 200237, China;
[2]Research Institute, Baoshan Iron & Steel Co., Ltd., Shanghai 201900, China

ABSTRACT

An anoxic/oxic membrane bioreactor (MBR) system was developed and operated for 8 runs during 236 days operation for concentrated cold-rolling wastewater (CRW) from reverse osmosis (RO) process in a steel manufacturing company. The trans-membrane pressure (TMP) variation demonstrated that MBR was feasible for RO concentrated water treatment. Total nitrogen (TN) removal efficiency of 97.7 % and chemical oxygen demand (COD) removal efficiency of 96.0 % were obtained. Mixed liquor suspended solids (MLSS), mixed liquor volatile suspended solids (MLVSS) and sludge particle size distribution showed that high salinity in CRW could decrease the ratio of MLVSS and MLSS, and reduce the particle size of activated sludge. The results of high-throughput 454 pyrosequencing indicated that microbial communities in MBR system for RO concentrated water treatment were significantly distinct. *Thauera* was the dominant genus in MBR system and it could be able to degrade aromatic matters which are commonly found in steel industrial wastewater.

KEYWORDS:
Membrane bioreactor (MBR); cold-rolling wastewater (CRW); reverse osmosis (RO) concentrated water; industrial wastewater treatment; activated sludge

INTRODUCTION

Steel manufacture is a water requirement industry, and at the same time a large amount of wastewater is discharged [1]. Cold rolling wastewater (CRW) generated from cold rolling process is very difficult for treatment. In the conventional treatment process, the most widely used methods are ultrafiltration (UF), gas-energy-management (GEM) and membrane bioreactor (MBR) [2-4]. Nevertheless, a large amount of wastewater can be regarded as the secondary water resource to recycle water, especially for water scarcity area. Reverse osmosis (RO) technology has been successfully used in seawater desalination [5]. RO membrane can allow water to pass through and simultaneously reject dissolved salts. By applying a pressure difference across the membrane, which is higher than the osmotic pressure of the feed water, fresh water is forced to permeate through the membrane [6]. Therefore, RO can achieve a high quality effluent. It was also applied for the treatment of wastewater from stainless steel manufacture due to its higher quality effluent [7, 8].

However, the reverse osmosis technology can generate a portion of concentrated water, which contains salts and retained compounds, in which the concentrations are much higher than those in feed water [9]. Therefore, the reverse osmosis concentrated wastewater needs a suitable and environmentally friendly management strategy. Conventional biological treatment is strongly inhibited by salts [10]. MBR, as one of the most promising biological technologies, has a high sludge concentration and a strong ability to resist shock loads [11-14], which might facilitate the degradation of recalcitrant organic substances in concentrated CRW under high salt concentrations. For instance, MBR has been applied for leachate treatment which also contains lots of inorganic salts [15]. Under these circumstances, the use of MBR might offer a potential solution for the treatment of concentrated CRW from steel manufacturing company.

This study developed an anoxic/oxic MBR system for CRW treatment from cold rolling process in a steel manufacturing company. The system performance and sludge characteristics were investigated under various operational conditions. High-throughput 454 pyrosequencing was carried out to characterize the microbial communities in the system.

MATERIALS AND METHODS

Characteristics of RO concentrated water. The RO concentrated water was collected from the reverse osmosis reactor that was used to treat CRW in a steel manufacturing company in Shanghai, China. The main ions and their concentrations in RO concentrated water are shown in Table 1. The concentrations of metal ions were determined by an inductively coupled plasma spectrometer (720ES, Agilent, America), while anions

were determined using an ion chromatograph (ICS-5000, ThermoFisher, America).

TABLE 1
The main ions concentrations in RO concentrated water (*n=5*)

Ions	Concentrations (mg/L)	Ions	Concentrations (mg/L)
Cl^-	4640 ± 451	Mg	504 ± 62.7
SO_4^{2-}	1070 ± 126	Al	24.3 ± 5.2
Na	2470 ± 261	Fe	5.2 ± 0.3
Ca	2080 ± 190	Zn	11.4 ± 0.4

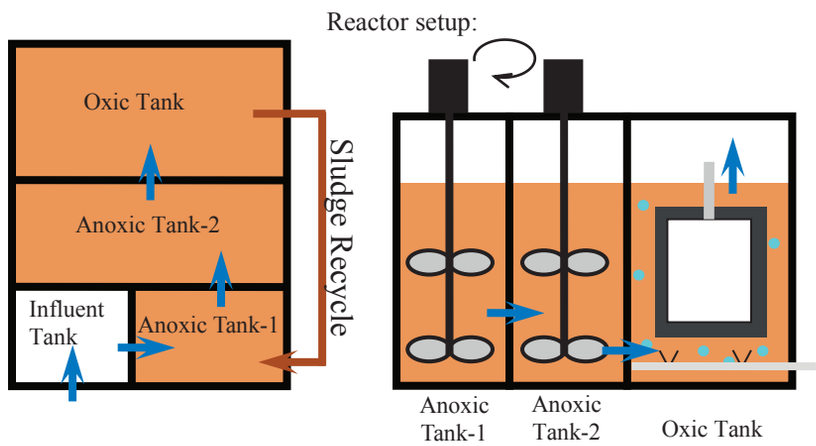

FIGURE 1
The schematic diagram of the reactor

An anoxic/oxic-MBR reactor was used in this study and its schematic diagram is shown in Fig. 1. The effective size of anoxic tank-1, anoxic tank-2 and oxic tank were 12× 11 × 25, 13.5 × 20 × 25 and 20 × 14 × 25 cm, respectively. Each anoxic tank was assembled with a blender to maintain the sludge mixture uniformity. Two microfiltration flat sheet membrane modules with a mean pore size of 0.2 μm were installed in oxic tank. The membrane module with an effective area of 8 × 10 cm^2 was purchased from Zizheng Co. Shanghai. Two perforated Plexiglas tubes were mounted below the membrane modules to supply oxygen for microbes and to maintain a cross-flow velocity (CFV) along membrane surfaces.

Inoculation and operation conditions. The A/O-MBR system was inoculated with activated sludge from Quyang municipal wastewater treatment plant in Shanghai, China. The initial mixed liquor suspended solids (MLSS) concentration was 4.8 g/L and the mixed liquor volatile suspended solids (MLVSS) concentration was 3.1g/L.After inoculation, wastewater was continuously pumped into the influent tank using a peristaltic pump (LangeCo., Baoding, China). Then the wastewater continuously passed through a non-return valve and flew into the anoxic tank and oxic tank, and was finally discharged through the membrane filtration using a peristaltic pump. An overflow tube was installed in the influent tank to control the water level of the reactor. Eight stages were carried out in this study and the conditions of all stages are summarized in Table 2. In order to maintain the sludge concentration of anoxic tank, about 300% of sludge recirculation ratio was adopted. The trans-membrane pressure (TMP) was monitored by a pressure gauge to indicate the anti-fouling performance of membranes. The water temperature was monitored by a temperature gauge.

TABLE 2
The flowchart of land use / land cover classification methodology.

Runs	Time (d)	HRT_O (h)	HRT_A (h)	SRT (d)	Flux (L/(m^2·h))	COD : TN
1	0~35	8.8	12.5	70	10	4:1
2	36~49	8.8	12.5	70	10	5:1
3	50~70	8.8	12.5	70	10	7:1
4	71~101	8.8	12.5	70	10	5:1
5	102~129	12.4	17.6	70	7	5:1
6	130~141	12.4	17.6	70	7	6:1
7	142~200	12.4	17.6	70	7	6:1
8	201~237	12.4	17.6	47	7	6:1

Analytical methods. Centrifugation-ultrasonication method was used to extract soluble microbial products (SMP) and extracellular polymeric substances (EPS) [16, 17]. Then the three-dimensional excitation-emission matrix (EEM) fluorescence spectroscopy of SMP and EPS were measured using a luminescence spectrometry (F-4500 FL spectrophotometer, Hitachi, Japan) according to a previous study [18]. A scanning electron microscopy (SEM, XL-30, Philips, Netherlands) was used to characterize the morphology of initial and fouled membrane surface. The SEM coupled an energy-diffusive X-ray (EDX) analyzer (Phoenix, EDAX Incorporated, USA) was employed to determine the inorganic components on the fouled membrane surface. In order to characterize the sludge in different stages, particle size distribution (PSD) analysis was performed using a PSD analyzer (MS3000h, Malvern, English). Chemical oxygen demand (COD) and total nitrogen (TN) were assayed using APHA standard methods [19]. High-throughput 454 pyrosequencing was carried out to characterize the microbial communities of system according to the methods described previously [20, 21]. The microbial samples were collected at the operation time of 200 day.

The membrane filtration resistance can be expressed by Eq. (1) according to Darcy's law.

$$R_t = R_m + R_c + R_P = \frac{TMP}{\mu J} \times 3600 \qquad (1)$$

where R_t is the total membrane resistance (m^{-1}), R_m is the intrinsic resistance of membrane (m^{-1}), R_C is the cake layer resistance (m^{-1}), R_P is the pore-clogging resistance (m^{-1}), J is the instantaneous flux ($m^3/(m^2 \cdot h)$), TMP is the trans-membrane pressure (Pa) and μ is the dynamic viscosity of permeate water (Pa·s). The method was also described in other previous studies [22, 23].

RESULTS AND DISCUSSION

Membrane performance. The variations of TMP and water temperature in A/O-MBR system under different operational conditions are shown in Fig. 2. At the initial stage (0 ~ 35 d), the TMP increased rapidly, indicating that the membrane fouling was severe. The possible reason is that inoculation sludge collected from municipal wastewater treatment plant has not adapted to the RO concentrated water treatment. Temmerman also reported that upon salt addition, an increase in supernatant proteins and polysaccharides was observed as well as an increase in irreversible membrane fouling rate [24]. SMP and EPS are often considered important contributors to membrane fouling in MBR [25, 26]. Elevated salt concentrations may deteriorate sludge quality through deflocculation by disturbing the multivalent cation bridging among EPS [27, 28]. A decrease in sludge quality resulting from increased salt concentration leads to the worse sludge filterability and increased membrane fouling caused by the EPS that released into the bulk liquid [24]. However, after acclimation, membrane fouling rate significantly decreased, especially when the flux decreased (after run 4, Table 2), the duration of an operational cycle was further extended. After 185 days running, the time span of the operational cycle decreased, which might be resulted from the water temperature decrease. Lower water temperature leads to the increase of EPS, soluble chemical oxygen demand, polysaccharides and proteins in the supernatants, which can lead to the increase of membrane fouling rate [29].

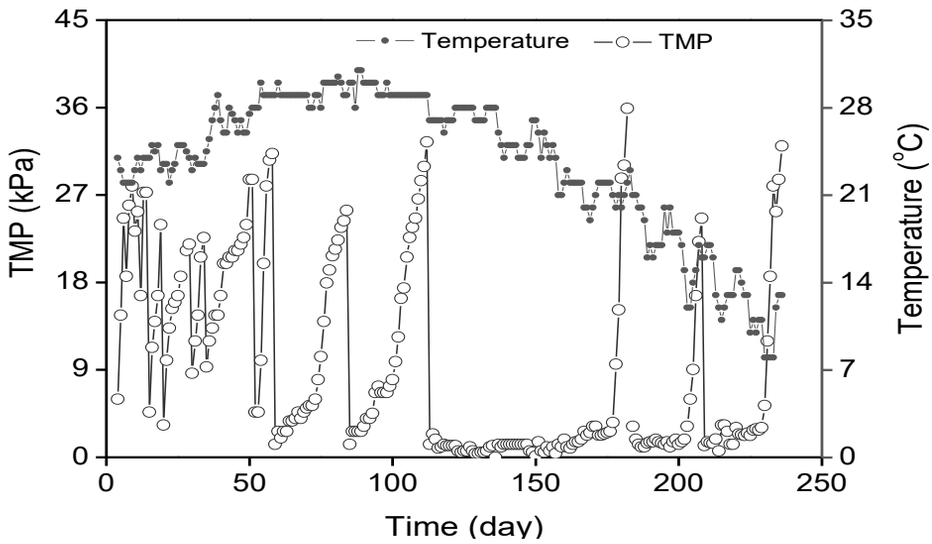

FIGURE 2
Variation of TMP and water temperature in system under different operational conditions

In order to examine the membrane fouling for RO concentrated water treatment, the SEM analyses of virgin and fouled membrane were carried out. Fig. 3 represents the SEM images of the virgin membrane (Fig. 3A) and the fouled membrane (Fig. 3B), respectively. As shown in Fig. 3, the virgin membrane surface was smooth, and no membrane fouling pollutants attached on it, while the fouled membrane surface was covered with an apparent fouling layer. Fig. 3B also exhibits that mineral crystal layer has attached on the membrane surface. Element analysis was further performed on the surface layer in order to identify the chemical components of the fouling layer by EDX analysis. The results showed that Ca and Mg were the main metal elements, which was consistent to the relatively high concentrations of Ca and Mg in RO concentrated water (Table 2). The biopolymers contain anion groups such as SO_4^{2-}, CO_3^{2-}, PO_4^{3-} and OH^-, and thus the cations such as Ca^{2+} and Mg^{2+} could be easily precipitated with these negative ions [26, 30].

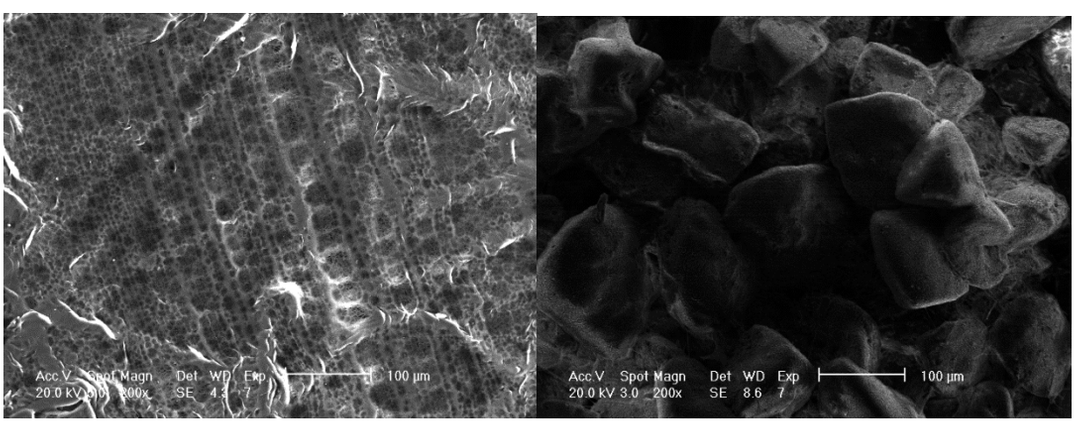

FIGURE 3
Representative SEM images of (A - left) the virgin membrane and (B - right) fouled membrane

The resistance distribution in membrane filtration demonstrated that R_C and R_P accounted for 50.8% and 33.1% of total filtration resistance, respectively. This indicated that the inorganic fouling layer caused severely irreversible membrane fouling. Furthermore, once the fouling layer was developed, it would become difficult to remove the layer from membrane surface by routine aeration or physical cleaning in this test. On the other

hand, the inorganic precipitation could couple the organic foulants to enhance the formation of fouling layer in MBR [26, 31]. Therefore, in order to reduce the membrane fouling caused by organic coupled inorganic fouling layer, the countermeasures for membrane cleaning should be developed, for instance, metal chelating agents and acid cleaning should be used in combination with oxidant cleaning [32, 33].

Pollutants removal performance. COD and TN removals in the system were thoroughly investigated and the results are shown in Fig. 4. After run 1, the average effluent COD concentrations of run 2 and run3 were 28.2 ± 21.2 and 37.0 ± 19.8 mg/L, respectively (Fig. 4A). When the influent COD concentration increased, the average effluent COD concentration slightly increased to 51.5 ± 25.5, as shown in run 4. Then, the average effluent COD concentrations reduced to less than 50 mg/L due to the extending of HRT in run 5, 6 and 7. Even when the influent COD was around 1190 ± 198 mg/L and the temperature was 12.8 ± 2.7 ºC, the average effluent COD concentration maintained at 86.0 ± 48.0 mg/L in run 8. These indicated that the MBR system showed a good COD removal performance for RO concentrated water treatment.

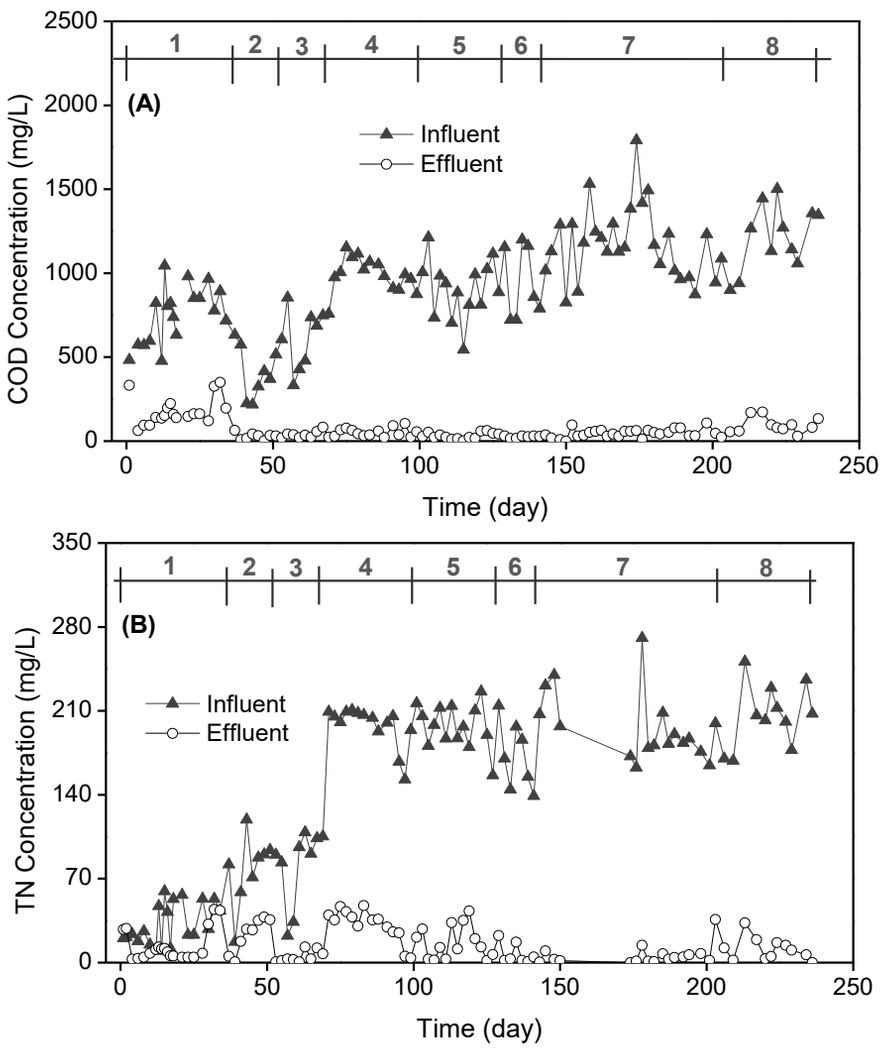

FIGURE 4
COD (A) and TN (B) removals in the system

It is noted that after acclimation, when the ratio of COD and TN increased from 5:1 to 7:1, the average effluent TN concentration reduced to 8.0 ± 10.8 mg/L from run 2 to run 3 (Fig. 4B). Under the ratio of COD and TN of 6:1, the effluent TN concentration reduced to 16.8 ± 13.8 mg/L from 30.8 ± 13.1 mg/L due to the extended HRT from run 4 to run 5. Then, when the ratio of COD and TN increased to 6:1, the effluent TN concentration

decreased to 4.9 ± 6.1 mg/L despite the influent TN concentration as high as 165 ± 23.1 mg/L in run 6. These demonstrated that the concentrated water did not inhibit the denitrification, which was also confirmed by Catarina that salinity did not regulate denitrification after acclimation [34].

Sludge characteristics. The MLSS, MLVSS and MLVSS/MLSS under different stages are illustrated in Fig. 5. The average value of MLSS was 3.72 g/L in run 1, indicating that the biomass growth was probably not occurring. After acclimation, the values of MLSS increased due to the increase of influent COD from run 2 to run 4. At the same HRT and SRT conditions, the higher influent COD concentration could lead to a higher volume loading rate (VLR) for system, which in turn resulted in a higher biomass growth rate. A slightly lower MLSS (15.57 ± 3.87 g/L) was observed under a longer HRT in run 5 compared with 18.54 ± 4.32 g/L in run 4. However, at the same VLR, the MLSS was significantly increased to 31.16 g/L in run 6. It was interesting that MLVSS was only increased to 8.98 g/L in run 6 from 6.15 g/L in run 5. This probably indicated that a longer SRT was conductive to accumulation of inorganic matters during the long-term operation.

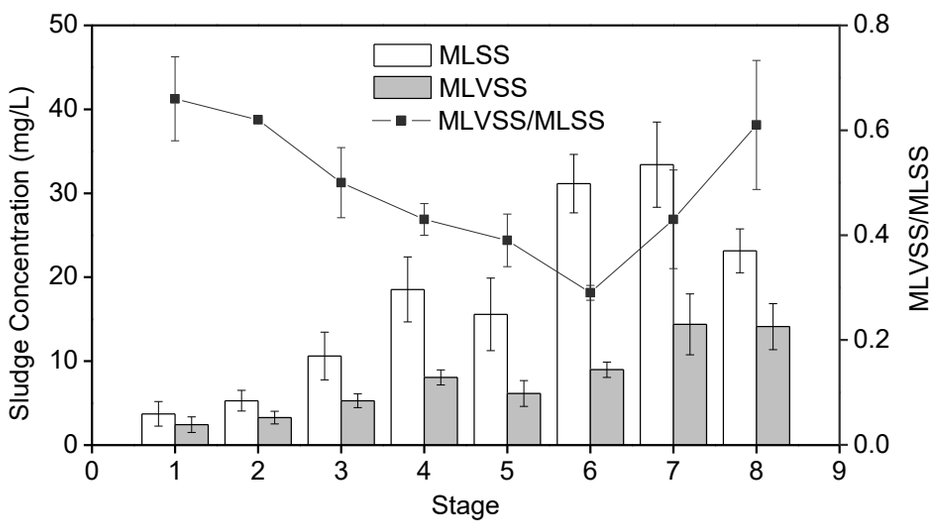

FIGURE 5
MLSS, MLVSS and MLVSS/MLSS evolution profiles under different stages

It is worth noting that the ratio of MLVSS and MLSS was continuously declined from run 1 (0.66 ± 0.08) to run 6 (0.29 ± 0.01). This probably attributed to the high salinity of RO concentrated water. The metal ions of Ca^{2+}, Mg^{2+}, Fe^{3+}/Fe^{2+} and Al^{3+} contained in CRW could be easily precipitated with negative ions of SO_4^{2-}, CO_3^{2-}, PO_4^{3-} and OH^- contained in biopolymers, which could result in the accumulation of these metal ions in suspended liquor [29,33]. When the influent COD concentration was further increased in run 7, the MLSS, MLVSS and the ratio of MLVSS and MLSS were also increased. From run 7 to run 8, the SRT was decreased to 47 from 70 d, and the MLSS was decreased to 23.13 g/L. However, the values of MLVSS were remained in the same level in run 7 and run 8. This demonstrated that a shorter SRT could alleviate the accumulation of inorganic matters in mixed liquor.

The particle size distributions of the sludge at the startup and sludge obtained in run 4 and run 7 are shown in Fig. 6. The mean particle size was evaluated on the basis of volume of particles. As shown in Fig. 6, it is evident that the sludge particle size decreased obviously along with the operation time. The mean particle size of sludge at start-up was 87.1 μm, while this value was dropped to 75.7 μm in run 4 and to 46.2 μm in run 7, after operation time of 94 and 164 days, respectively. The possible reason was that deflocculation behavior caused by high salt concentrations could destroy the bioflocs, which resulted in the particle size reduction. Three-dimensional EEM fluorescence spectra of SMP and EPS in MBR system are illustrated in Fig. 7.

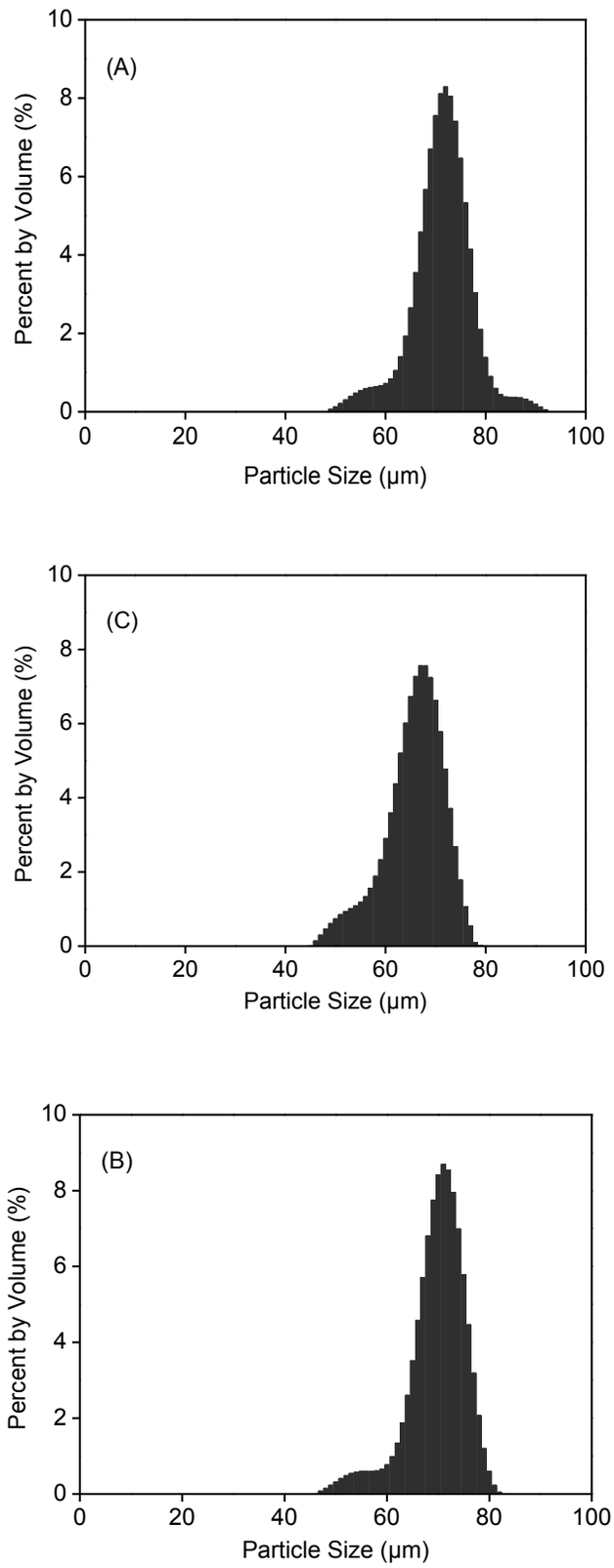

FIGURE 6

Particle size distribution of (A) sludge at start-up, (B) sludge in run 4 and (C) sludge in run

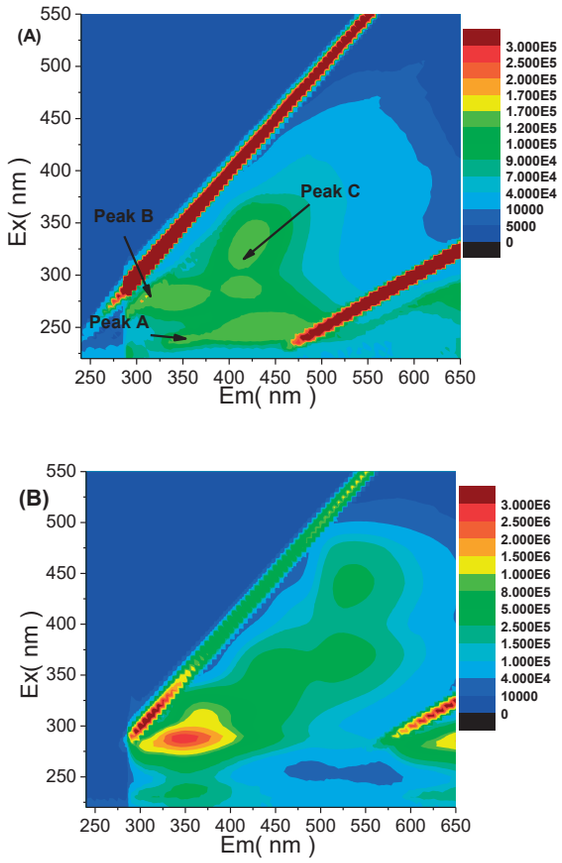

FIGURE 7

EEM fluorescence spectra of (A) SMP and (B) EPS in MBR system

The information about the chemical composition of SMP and EPS samples is displayed in EEM spectra in Fig. 7. According to the previous study, three main peaks could be identified from the fluorescence spectra including Peak A located at the excitation/emission wavelengths (Ex/Em) of 235-240/340-355nm,PeakB(Ex/Em:280-285/320-335 nm) and Peak C (Ex/Em: 305-315/405-415 nm) [18]. Peak A and peak B have been reported to be associated with the aromatic protein-like substances and typtophan protein-like substances, respectively, while the fluorescence of peak C is related to humic acids and fulvic acids [18]. As shown in Fig. 7, all three peaks were observed in both SMP and EPS, indicating that protein-like substances and humic acids were the main substances in SMP and EPS. Specifically, in Fig.7B, the fluorescence intensity of peak B was much stronger compared with peak A and peak C, which demonstrated that typtophan protein-like substances were the major substances in EPS. These organic substances could cause irreversible fouling in particular in the presence of metal ions. Microbial community structure in MBR system**:**In order to understand the microbial community structure and composition in MBR system for RO concentrated water treatment, 454 high-throughput pyrosequencing was applied to analyze the 16S rRNA gene of bacteria.

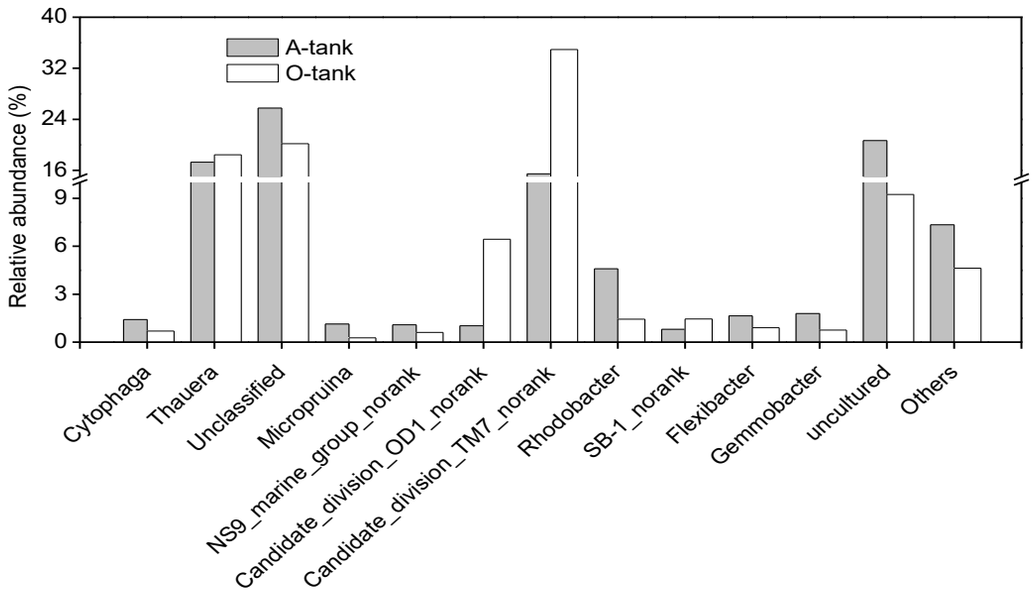

FIGURE 8

Relative abundance of microbial groups at genus level (Relative abundance is defined as the number of sequences affiliated with that taxon divided by the total number of sequences per sample (%). Genera of which relative abundance is less than 1.0 % in both samples are defined as "others")

The relative abundance of microbial groups obtained at anoxia tank (A-tank) and oxic tank (O-tank) at genus level is illustrated in Fig. 8. In total, 74 identified genera were observed in A-tank, while 72 genera were obtained in O-tank. The genera accounted for about 61.9 % for A-tank and 64.4 % for O-tank were not identified at genus level. As shown in Fig. 8, *Thauera* was the dominant genus in both A-tank and O-tank, and its relative abundances were 17.3 and 18.5 %, respectively. However, the relative abundance of *Thauera* was only 2.7 % in a MBR with same inoculation for artificial wastewater treatment [20]. This demonstrated that microbial communities in MBR for RO concentrated water treatment from CRW were significantly distinct from the artificial wastewater treatment [20]. *Thauera* is commonly found in activated sludge for industrial wastewater treatment due to its ability in degradation of aromatic matters. For example, Mao isolated three *Thauera* strains from a coking wastewater treatment bioreactor that could degrade phenol, methylphenol and indole [35]. Liu found that *Thauera* might play an important role for quinoline removal [36]. *Thauera* have been reported to be able to use 3,4-dihydroxybenzoic acid, 4-hydroxycinnamic acid (*p*-coumaric acid), 4-hydroxy-3-methoxycinnamic acid (ferulic acid), 3,4-dimethoxybenzoic acid (veratric acid), and 3,4,5-trihydroxybenzoic acid (gallic acid), which are commonly found in industrial wastewater as the carbon source in liquid cultures [37-39].

CONCLUSIONS

In summary, this study introduced an MBR system for RO concentrated water treatment from CRW, which was collected from a cold rolling process in a steel manufacturing company. The TMP variation demonstrated its feasibility of using MBR for CRW treatment. In addition, the MBR also exhibited high COD and TN removal efficiencies under different operational conditions, which indicated that this MBR system had a strong ability to resist shock loading. High salinity in original CRW can affect the ratio of MLVSS and MLSS, and particle size distribution. The results of high-throughput 454 pyrosequencing showed microbial communities in MBR system for RO concentrated water treatment from CRW were significantly distinct from those regarding artificial wastewater treatment. *Thauera* was the dominant genus in MBR system and it could be able to degrade aromatic matters which are commonly found in industrial wastewater.

REFERENCES

[1] B. Chakrabarty, A.K. Ghoshal, M.K. Purkait, Ultrafiltration of stable oil-in-water emulsion by polysulfone membrane, Journal of Membrane Science, 325 (2008) 427-437.

[2] H. Song, S. Li, X. Min, Study On the Treatment of Cold Rolling Wastewater by Using Bio-fluidized Bed, in: H. Li, Q.J. Xu, D. Zhang (Eds.) Progress in Environmental Science and Engineering, 2012, pp. 78-82.

[3] M.M. Amin, B. Bina, Y. Hajizadeh, A. Ebrahimi, R. Ghanbari, Feasibility of lab-scale vacuum-driven submerged hollow fiber anaerobic membrane bioreactor (sanmbr) for the treatment of synthetic acidified wastewater, Fresenius Environmental Bulletin, 24(2015) 2220-2231.

[4] B. Zhao, W. Li, Y. Zhang, F. Ma, O.D. Nartey, Effect of tween 80 on removal of chromate using ultrafiltration enhanced by cetylpyridinium chloride, Fresenius Environmental Bulletin, 22(2013) 3718-3724.

[5] L. Henthome, B. Boysen, State-of-the-art of reverse osmosis desalination pretreatment, Desalination, 356 (2015) 129-139.

[6] R. Valladares Linares, Z. Li, S. Sarp, S.S. Bucs, G. Amy, J.S. Vrouwenvelder, Forward osmosis niches in seawater desalination and wastewater reuse, Water Research, 66 (2014) 122-139.

[7] Y.J. Jung, Y. Kiso, T. Yamada, T. Shibata, T.G. Lee, Chemical cleaning of reverse osmosis membranes used for treating wastewater from a rolling mill process, Desalination, 190 (2006) 181-188.

[8] Y.H. Kim, E.D. Hwang, W.S. Shin, J.H. Choi, T.W. Ha, S.J. Choi, Treatments of stainless steel wastewater containing a high concentration of nitrate using reverse osmosis and nanomembranes, Desalination, 202 (2007) 286-292.

[9] P. Chelme-Ayala, D.W. Smith, M.G. El-Din, Membrane concentrate management options: a comprehensive critical review, Canadian Journal of Civil Engineering, 36 (2009) 1107-1119.

[10] O. Lefebvre, R. Moletta, Treatment of organic pollution in industrial saline wastewater: A literature review, Water Research, 40 (2006) 3671-3682.

[11] Z. Wang, Z. Wu, J. Hua, X. Wang, X. Du, H. Hua, Application of flat-sheet membrane to thickening and digestion of waste activated sludge (WAS), Journal of Hazardous Materials, 154 (2008) 535-542.

[12] Q. Wang, Z. Wang, Z. Wu, X. Han, Sludge reduction and process performance in a submerged membrane bioreactor with aquatic worms, Chemical Engineering Journal, 172 (2011) 929-935.

[13] Z. Wang, P. Wang, Q. Wang, Z. Wu, Q. Zhou, D. Yang, Effective control of membrane fouling by filamentous bacteria in a submerged membrane bioreactor, Chemical Engineering Journal, 158 (2010) 608-615.

[14] H. Zhao, L. Wang, B. Xia, S. Tan, Y. Liu, Q. Liao, Treatment of water containing unsymmetrical dimethylhydrazine using electrolyzed oxidizing water combined with a membrane bioreactor, Fresenius Environmental Bulletin, 22(2013) 3577-3583.

[15] G. Wang, Z. Fan, D. Wu, L. Qin, G. Zhang, C. Gao, Q. Meng, Anoxic/aerobic granular active carbon assisted MBR integrated with nanofiltration and reverse osmosis for advanced treatment of municipal landfill leachate, Desalination, 349 (2014) 136-144.

[16] X. Han, Z. Wang, C. Zhu, Z. Wu, Effect of ultrasonic power density on extracting loosely bound and tightly bound extracellular polymeric substances, Desalination, 329 (2013) 35-40.

[17] J. Huang, Z. Wang, J. Zhang, X. Zhang, J. Ma, Z. Wu, A novel composite conductive microfiltration membrane and its anti-fouling performance with an external electric field in membrane bioreactors, Scientific reports, 5 (2015) e9268.

[18] Z. Wang, Z. Wu, S. Tang, Characterization of dissolved organic matter in a submerged membrane bioreactor by using three-dimensional excitation and emission matrix fluorescence spectroscopy, Water Research, 43 (2009) 1533-1540.

[19] Y.K. Wang, G.P. Sheng, B.J. Shi, W.W. Li, H.Q. Yu, A Novel Electrochemical Membrane Bioreactor as a Potential Net Energy Producer for Sustainable Wastewater Treatment, Scientific reports, 3 (2013).

[20] J. Huang, Z. Wang, C. Zhu, J. Ma, X. Zhang, Z. Wu, Identification of Microbial Communities in Open and Closed Circuit Bioelectrochemical MBRs by High-Throughput 454 Pyrosequencing, Plos One, 9 (2014).

[21] J. Ma, Z. Wang, Y. Yang, X. Mei, Z. Wu, Correlating microbial community structure and composition with aeration intensity in submerged membrane bioreactors by 454 high-throughput pyrosequencing, Water Research, 47 (2013) 859-869.

[22] X. Zhang, Z. Wang, Z. Wu, F. Lu, J. Tong, L. Zang, Formation of dynamic membrane in an anaerobic membrane bioreactor for municipal wastewater treatment, Chemical Engineering Journal, 165 (2010) 175-183.

[23] Q. Wang, Z. Wang, Z. Wu, J. Ma, Z. Jiang, Insights into membrane fouling of submerged

membrane bioreactors by characterizing different fouling layers formed on membrane surfaces, Chemical Engineering Journal, 179 (2012) 169-177.
[24] L. De Temmerman, T. Maere, H. Temmink, A. Zwijnenburg, I. Nopens, Salt stress in a membrane bioreactor: Dynamics of sludge properties, membrane fouling and remediation through powdered activated carbon dosing, Water Research, 63 (2014) 112-124.
[25] Z. Wang, X. Mei, Z. Wu, S. Ye, D. Yang, Effects of biopolymer discharge from MBR mixture on sludge characteristics and membrane fouling, Chemical Engineering Journal, 193 (2012) 77-87.
[26] Z. Wang, Z. Wu, X. Yin, L. Tian, Membrane fouling in a submerged membrane bioreactor (MBR) under sub-critical flux operation: Membrane foulant and gel layer characterization, Journal of Membrane Science, 325 (2008) 238-244.
[27] C.A. Biggs, A.M. Ford, P.A. Lant, Activated sludge flocculation: direct determination of the effect of calcium ions, Water Science and Technology, 43 (2001) 75-82.
[28] R. Van den Broeck, J. Van Dierdonck, B. Caerts, I. Bisson, B. Kregersman, P. Nijskens, C. Dotremont, J.F. Van Impe, I.Y. Smets, The impact of deflocculation-reflocculation on fouling in membrane bioreactors, Separation and Purification Technology, 71 (2010) 279-284.
[29] Z. Wang, Z. Wu, S. Tang, Impact of temperature seasonal change on sludge characteristics and membrane fouling in a submerged membrane bioreactor, Separation Science and Technology, 45 (2010) 920-927.
[30] A. Seidel, M. Elimelech, Coupling between chemical and physical interactions in natural organic matter (NOM) fouling of nanofiltration membranes: implications for fouling control, Journal of Membrane Science, 203 (2002) 245-255.
[31] B. Ma, W. Yu, H. Liu, J. Qu, Effect of low dosage of coagulant on the ultrafiltration membrane performance in feedwater treatment, Water Research, 51 (2014) 277-283.
[32] Z. Wang, J. Ma, C.Y. Tang, K. Kimura, Q. Wang, X. Han, Membrane cleaning in membrane bioreactors: a review, Journal of Membrane Science, 468 (2014) 276-307.
[33] P. Wang, Z. Wang, Z. Wu, Q. Zhou, D.H. Yang, Effect of hypochlorite cleaning on the physiochemical characteristics of polyvinylidene fluoride membranes, Chemical Engineering Journal, 162(2010) 1050-1056.
[34] C.M. Magalhaes, S.B. Joye, R.M. Moreira, W.J. Wiebe, A.A. Bordalo, Effect of salinity and inorganic nitrogen concentrations on nitrification and denitrification rates in intertidal sediments and rocky biofilms of the Douro River estuary, Portugal, Water Research, 39 (2005) 1783-1794.
[35] Y. Mao, X. Zhang, X. Xia, H. Zhong, L. Zhao, Versatile aromatic compound-degrading capacity and microdiversity of Thauera strains isolated from a coking wastewater treatment bioreactor, Journal of Industrial Microbiology & Biotechnology, 37 (2010) 927-934.
[36] B.B. Liu, F. Zhang, X.X. Feng, Y.D. Liu, X. Yan, X.J. Zhang, L.H. Wang, L.P. Zhao, Thauera and Azoarcus as functionally important genera in a denitrifying quinoline-removal bioreactor as revealed by microbial community structure comparison, Fems Microbiology Ecology, 55 (2006) 274-286.
[37] A. Dibenedetto, R.M. Lo Noce, M. Narracci, M. Aresta, Structure-biodegradation correlation of polyphenols for Thauera aromatica in anaerobic conditions, Chemistry and Ecology, 22 (2006) 133-143.
[38] K. Schuhle, G. Fuchs, Phenylphosphate carboxylase: a new C-C lyase involved in anaerobic in phenol metabolism in Thauera aromatica, Journal of Bacteriology, 186 (2004) 4556-4567.
[39] Y. Shinoda, Y. Sakai, H. Uenishi, Y. Uchihashi, A. Hiraishi, H. Yukawa, H. Yurimoto, N. Kato, Aerobic and anaerobic toluene degradation by a newly isolated denitrifying bacterium, Thauera sp strain DNT-1, Applied and Environmental Microbiology, 70 (2004) 1385-1392.

Received: **06.03.2015**
Accepted: **05.12.2015**

CORRESPONDING AUTHOR

Shuguang Lu
East China University of Science and Technology
State Environmental Protection Key Laboratory of Environmental Risk Assessment and Control on Chemical Process
Shanghai 200237 – CHINA

e-mail: lvshuguang@ecust.edu.cn

by PSP Volume 25 – No. 1/ 2016, pages 78-88 Fresenius Environmental Bulletin

SORPTION OF TRIOCTYL AMINE TO KAOLINITE

Francis Moyo[1], Roman Tandlich[1*], Phindile Madikizela[1], Ethel Chifunda[1] and Gary M. Watkins[2]

[1] Environmental Health and Biotechnology Research Group, Division of Pharmaceutical Chemistry, Faculty of Pharmacy, Rhodes University, P. O. Box 94, Grahamstown, 6140, South Africa.
[2] Department of Chemistry, Faculty of Science, Rhodes University, P. O. Box 94, Grahamstown, 6140, South Africa

ABSTRACT

Sorption of trioctyl amine onto kaolinite from kerosene was studied using a sorbent with the specific surface area of 18.2 ± 0.8 m^2 g^{-1} and the loss on ignition of 0.009 ± 0.004 % (w/w). The kaolinite particles were hexagonal in shape and this was not affected by the trioctyl amine sorption. All the major XRD peaks of kaolinite were detected in the region of 1.5405 Å regardless of their exposure to kerosene and trioctyl amine. Trioctyl amine sorbed onto the kaolinite surface. This was concluded from the presence of signals from C-H stretching and C-H bending vibrations of trioctyl amine molecules in the infra-red spectra of kaolinite exposed to the trioctyl amine solution in kerosene. Sorption equilibrium for trioctyl amine was reached after 144-168 hours. The equilibrium removal efficiencies of trioctyl amine ranged from 17.5 to 35.8 %, depending on the initial trioctyl amine concentration, its particle size and the solid-liquid ratio. The relevant equilibrium sorption capacities for trioctyl amine ranged from 0.88 to 0.93 g/g. The linearised Freundlich isotherms had an R^2 between 0.9719 and 0.9795 and the optimised values of n and K_f ranged from 1.077 to 1.086; and from 2.622 to 2.843, respectively.

KEYWORDS:
Freundlichisotherm,siloxane,trioctylamine, EGME/$CaCl_2$.

AIM

This article is aimed at addressing a knowledge gap on the sorption of trioctyl amine onto mineral surfaces or soil minerals from non-aqueous phase liquids which are modelled by kerosene.

INTRODUCTION

In metal refinery operations, amines have also been used as extractants in solvent extraction for metal recovery [1-4]. In the environment, amines can be toxic and corrosive to aquatic organisms [5]. Trioctyl amine (TOA) has been reported to be an efficient extractant in processes such as the production of lactic acid where it was toxic against the lactic-acid producing microorganisms [6]. It has been used and studied extensively in the extraction of platinum group metals [7]. Even though most of the South African and global metal refineries are run on the zero-discharge principle, widespread use of amines as extractants and their relevant diluents on an industrial scale poses potential environmental dangers. These originate from accidental spillages and seepage of the extractants; and their solutions in various diluents into the groundwater [8,9]. Spillage like these can result in formation of the non-aqueous phase liquids (NAPLs) [10,11], prolonging duration of the contamination [10].

NAPLs are long-term sources of environmental contamination by serving depots of the spilled extractant such as TOA. Contamination of soil and groundwater occurs by partitioning of the dissolved organic compounds between the NAPLs and the surrounding environmental compartments [12]. In this context, several research questions about the fate of TOA remain unanswered. One such important question is the extent of TOA sorption onto soil particulate matter. To partially fill this knowledge gap, the current study focused on the sorption of TOA onto kaolinite which is a clay mineral. Kaolinite has been studied as sorption medium for barium ions [13], as have been the clay minerals for metal recovery with addition of trioctyl amine [14]. However, no detailed study on the interaction of the trioctyl amine and the kaolinite surfaces has been conducted to date. The model NAPL is kerosene and the experiments were performed using the batch-equilibration technique. The sorption of TOA onto kaolinite was presented in the context of the properties of the solid phase/sorbent.

MATERIAL AND METHODS

TOA, $CaCl_2$, ethanol, crystal violet and kerosene were purchased from Sigma Aldrich

(Johannesburg, South Africa). The titrant of for the TOA quantification was the 0.1 N $HClO_4$ in CH_3COOH which along with potassium hydrogen phthalate (KHP), sulphuric acid and ethylene glycol mono-ethyl ether (EGME) were purchased from Merck (Pty.) Ltd (Johannesburg/Cape Town, South Africa). All masses were measured using a PA1214 analytical balance (Pioneer™, Ohaus Corporation, Johannesburg, South Africa). All glassware and 15 mL crucibles were purchased from Sigma-Aldrich (Johannesburg, South Africa). Kaolinite was obtained from a mining company in Grahamstown (South Africa). Dry weight and the loss on ignition of kaolinite samples were determined on approximately 5 g of kaolinite sample which was weighed out analytically. Dry weight was determined in triplicate by drying the kaolinite samples in the UFE 700 oven (Memmert, Schwabach, Germany) at 105 °C for 24 hours. Loss on ignition of the dried samples (LOI) was then determined in triplicate by heating at 400 °C until constant weight of the kaolinite samples was reached. The ignition was performed in the App 9B 4152 SP Muffle Furnace (Gallenkamp, Leicestershire, United Kingdom). The specific surface area of kaolinite was determined using the modified EGME/$CaCl_2$ method [12,15].

For sorption kinetics, 1.021 g of TOA was weighed out and dissolved quantitatively in 95 ml of kerosene. The solution was transferred into a 100 ml volumetric flask and mixed by vigorous hand-shaking. Then the volume was made up to the mark with kerosene to get a solution of TOA with the concentration of 10.21 g/l (m/v). Ten grams of kaolinite was weighed out into a 250 mL Erlenmeyer flask and 50 ml of 10.21 g/l of TOA in kerosene was added. Thus this experiment was conducted as the solid-liquid ratio (referred to as SL in further text) of 0.2. The flasks were closed with aluminium foil and Parafilm$^{(TM)}$ and agitated using the Chiltern orbital shaker SS70 (Slough, Berkshire, Chiltern Scientific, United Kingdom) at 100 rpm and 21 ± 2 ˚C. Twenty five millilitres aliquots were removed with a glass pipette in triplicate after time periods ranging from 30 minutes to 168 hours of incubation. One replicate Erlenmeyer flask was used per determination. The solid particles were removed from the Erlenmeyer subsample flasks by centrifugation at 3000 rpm for 10 minutes on the Allegra X-15 benchtop centrifuge (Beckman Coulter, Johannesburg, South Africa). The supernatant was analysed for the TOA content using the non-aqueous acidimetric titration technique (see below).

Experiments were also re-run with 20 g/L of the initial concentration of TOA, i.e. SL of 0.4. The TOA concentration was determined using the titrimetric method of Kar [16]. The titrant was the approximately 0.1 N solution of $HClO_4$ in CH_3COOH and the point of equivalence was determined using the 0.5 % solution of crystal violet in ethanol as the indicator. Colour change of the indicator was from purple to lime green at point of equivalence. Control samples indicated that the precision of the titration was 15 % or better and the accuracy of the trioctylamine quantification was 120 % of the target. All results were corrected for these values. Volume of the titrant was not affected by the temperature changes during the sorption experiments of the TOA quantification. The titrant was standardised against KHP. Sorption isotherms were run under the same conditions as the sorption kinetics, but the initial concentrations of TOA ranged from 0 to 50 g/L in kerosene and the incubation period was kept constant at 168 hours.

The sorption kinetics data was used to determine the time required for the TOA sorption to reach apparent sorption equilibrium. For this, the removal efficiency of TOA, i.e. the percentage of the initial TOA concentration that was removed after a given period of incubation/sorption was calculated. The particular values of removal efficiency were calculated as shown in equation (1).

$$Removal\ efficiency = M0 - MfMO \times 100 \quad (1)$$

In equation 1, M_0 is the initial concentration of TOA in kerosene before sorption and M_f is the final concentration of TOA (both properties have the unit of g/L). Quantification of TOA continued done until the removal efficiency of TOA became constant, i.e. an indication that the apparent sorption equilibrium for TOA was reached. This is when the experiments were then terminated. To check the mass balance and the evaporative losses of TOA, control experiments were done by incubating solutions of TOA under the same conditions as the sorption experiments. The same initial concentrations of TOA as in the sorption experiments were used, but with no kaolinite added to the Erlenmeyer flasks. The mass balance of TOA was always 90 % or better and so the physical losses were assumed not to affect the sorption results.

The maximum amount of TOA sorbed to kaolinite at equilibrium was estimated by calculating the sorption capacity which is equal to the maximum sorbed concentration of TOA at equilibrium. It is calculated using equation (2) and

its unit is identical to that of the sorbed TOA concentration (g TOA/g kaolinite).

$$Sorption\ capacity = \frac{equilibrium\ amount\ of\ TOA\ sorbed}{mass\ of\ sorbent} \quad (2)$$

Once the period of apparent sorption equilibrium was determined, the sorption isotherms were measured. The data was then modelled using the linearised form of Freundlich isotherm as shown in equation (3).

$$lnqe = lnkf + 1nlnCe \quad (3)$$

In equation (3), qe is the sorbed TOA concentration in the kaolinite (g TOA/g kaolinite), while Ce is the equilibrium dissolved TOA concentration (g/L), and Kf and n are isotherm constants indicating the capacity and intensity of the adsorption, respectively. All sorbed TOA concentrations were calculated per dry weight of the kaolinite sorbent. The Freundlich isotherm assumes adsorption takes place on heterogeneous surfaces [17]. Thus if this model is used to quantitatively evaluate the sorption of TOA onto kaolinite, then the degree of surface heterogeneity can be ascertained. Under these sorption conditions, the ratio of the amount of solute adsorbed onto a given mass of the adsorbent to the amount of concentration of the solute in solution is not constant at different solution concentrations [18]. The sorption isotherm was only measured for the SL value of 0.4.

To detect any changes to the structure of the kaolinite crystal lattice, as well as to verify the presence of the TOA molecules on the kaolinite surface, several techniques were used. Firstly, the IR spectra of kaolinite samples were measured using the KBr method on a Perkin-Elmer® Precisely FT-IR spectrometer Spectrum 100 (Perkin-Elmer® Pty Ltd, Beaconsfield, England). Scans were performed in a range of 4000-500 cm^{-1}. Samples analysed include raw kaolinite and the kaolinite exposed to the TOA solutions in kerosene. The latter samples were collected from the sorption experiments after the apparent sorption equilibrium was reached. Subsamples from the kaolinite samples that were analysed by IR spectroscopy where also subjected to scanning electron microscopy (SEM) and the X-Ray diffraction analysis (XRD).

The SEM was performed using the Tescan scanning electron microscope (VEGA LMU, Brno, Czech Republic). For this, the kaolinite samples were placed on a double-sized carbon stub which was then placed on a disc carrier of 3 mm height and 10 mm diameter. This was gold coated under a vacuum (0.25 Torr) and the coated samples were imaged using a 20kV electron beam. XRD patterns of the kaolinite samples were recorded using a Bruker D8 Discover machine (Bruker, Johannesburg, South Africa) equipped with the PSD Lynx Eye detector, using Cu-K radiation (λ = 1.5405 Å, nickel filter). Samples were placed on the zero background (511) silicon wafer embedded in a generic sample holder and data recorded within the range $2\theta = 10^{\circ}$ to 100°, scanning at 1° min^{-1} with a filter time constant of 2.0 s per step at room temperature. A slit width of 6.0 mm was used in the measurements. The data was fitted using evaluation (Eva) curve fitting software.

RESULTS AND DISCUSSION

Average LOI (%) of kaolin samples was 0.009 ± 0.004 %. The LOI was higher than the value of 0.001 % reported by Tandlich and Baláž [15]. The LOI values measure the concentration of soil organic matter in the kaolinite samples. Such concentrations need to be higher than 0.01-0.2 % (w/w) in order for the soil organic matter to play an important role in the sorption uptake of TOA to kaolinite [19,20]. The LOI value measured in the current study was not significantly different from 0.01 % (w/w) at 5 % level of significance (p-value > 0.10), but it was lower than 0.2 %. Therefore the sorption of TOA onto kaolinite will mainly be governed by the amine molecule interaction with the clay mineral matrix. The EGME/$CaCl_2$ specific surface area of kaolinite was measured at 18.2 ± 0.8 m^2 g^{-1}, which is comparable to the literature values of that have been reported to range from 5.9 to 25.5 m^2g^{-1} [21-23]. Thus sorption characteristics of the Grahamstown kaolinite are comparable with kaolinite matrices studied by other authors.

Kaolinite is a natural occurring inorganic polymer. It consists of siloxane and gibbsite layers; and its chemical formula is $Al_2[Si_2O_5](OH)_4$ and Its crystal lattice contains a 1:1 arrangement of octahedral alumosilicate sheet with aluminium cations bonded and tetrahedral sheets with silicon cations [24,25]. These sheets are stacked on top of each other and the adjoining layers form van der Waals forces and hydrogen bonds because of the availability of an OH group and an oxygen atom in the two adjacent layers [25]. The hydroxyl functional groups on kaolinite are the most reactive [25,26]. They may take part in various chemical reactions including ion exchange processing. The kaolinite crystal lattice lacks the ability to expand due to hydrogen bonds between the siloxane and

gibbsite layers [15]. This means that the internal surface area of kaolinite is negligible in size and the specific surface area measured in this study is completely accounted for by the external surface area of kaolinite particles [27]. The TOA sorption will take place on the outer surface of kaolinite only [28].

Figure 1 shows the SEM micrographs of kaolinite samples, which indicate that the kaolinite particles adhere to each other and form clusters. The surfaces of the kaolinite flakes show that they are a composite of particles greater than 20 µm. This behaviour has been reported for the bulk kaolin [29] and kaolinite from Chile [30]. This may reduce the surface area available for the TOA sorption. It can also be seen that the shape of the kaolinite particles is hexagonal, which agrees with the findings purported by other studies [31]. The SEM images agree well with the general structure of kaolinite particles reported in literature. The SEM images also indicate that the particle properties were not affected by the exposure to kerosene. Figure 2 show the XRD spectra of the kaolinite particles.

From the XRD spectrum, using an XRD background of 2θ = 10˚ to 100˚, it can be seen that the crystal lattice of kaolinite was not altered by the presence of kerosene and the TOA amine during the duration of the batch equilibration experiments.

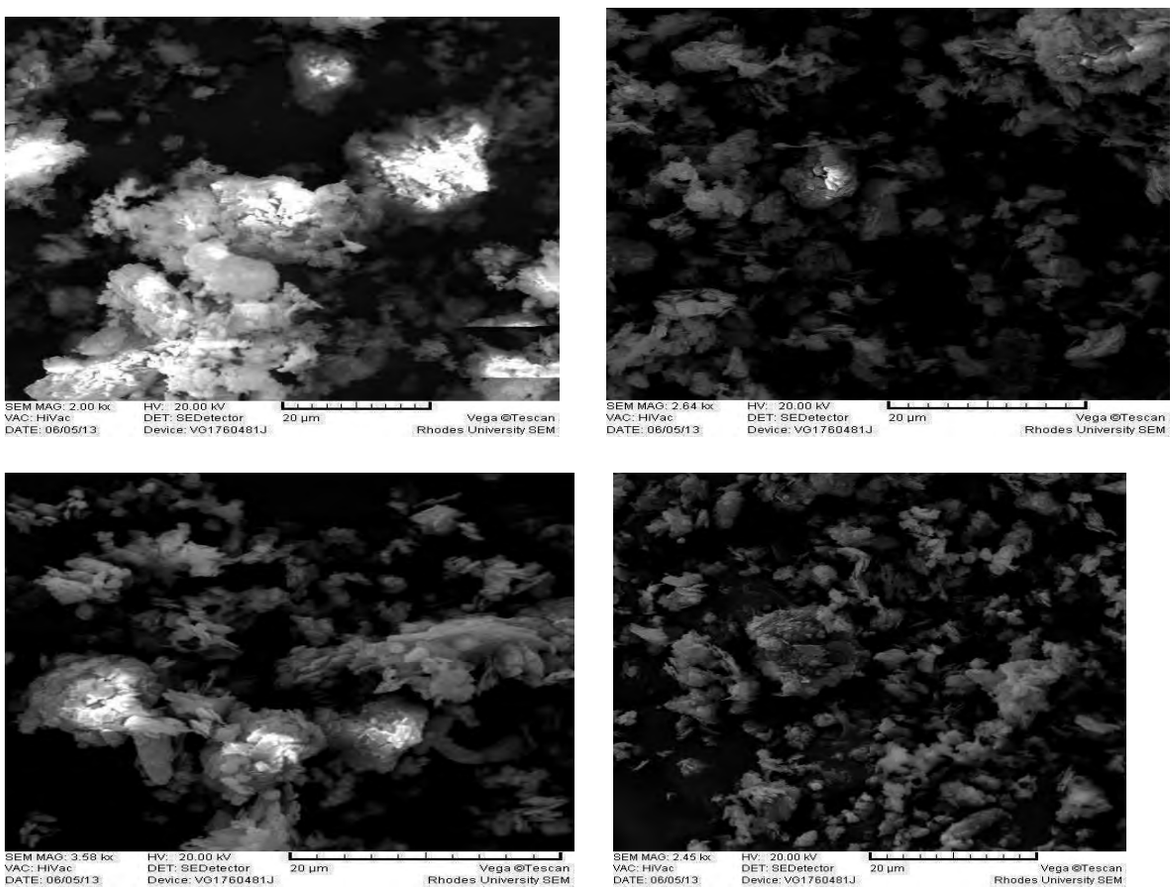

FIGURE 1
SEM images of kaolinite at different time intervals during batch equilibration: left,above:control sample of kaolinite which was not exposed to kerosene or TOA; right,above: the kaolinite images after exposure for the TOA solution in kerosene for 24h; left,below: for 72h ;right,below: for 168 hour

All the major diffraction peaks of kaolinite in the region of 1.5405 Å were observed for the control sample and in the sample after 168 hours of exposure to kerosene and TOA during batch equilibration sorption experiments. The intensity of the largest peak at 2θ = 27˚ increased after 24 hours and reduced after 72 hours and 168 hours. The XRD spectrums show that the position of the major

peaks conforms to previous literature data reported by Kakali et al. [32] and He et al. [33]. Figure 3 depicts the IR spectrum of the raw kaolinite sample, TOA and the kaolinite exposed to kerosene solution of TOA. Bands with wavenumbers 3700-3620 cm^{-1} correspond to the well-crystallized structure of kaolinite [33].

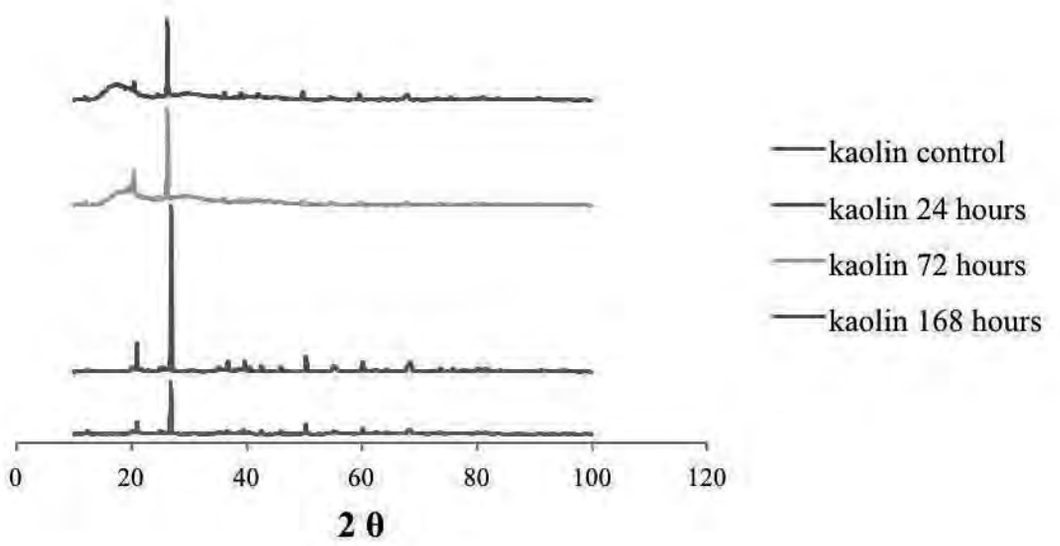

FIGURE 2
XRD patterns of kaolinite at different time intervals (24 hours, 72 hours and 168 hours) during batch equilibration. The control sample was not exposed to kerosene or TOA. The term kaolin and kaolinite are interchangeable here.

The bands at 937 and 914 cm^{-1} correspond to the Si-OH bending vibrations, while those at 983 and 1035 cm^{-1} can be attributed to the Si–O–Si in-plane vibrations [34]. Signals recorded at wavenumbers from 3 693 to 3 620 cm^{-1} were observed for kaolinite before and after the batch equilibration experiments (see Figure 3). They originate from the inner surface -OH stretching vibration that can be found inside the kaolinite crystal structure. Signal at wavenumbers from 1 027 to 1 002 cm^{-1} were also seen for the original sample (D), corresponding to O-Si-O bending vibrations. For spectra (B) and (C), these were shifted to 999 cm^{-1} and 995 cm^{-1}, i.e. indicating a potential interaction between TOA and the Si-O bonds. Bands at wavenumbers of 911 cm^{-1} (D), 908 cm^{-1} (C) and 910 cm^{-1} (B) were observed and most likely originate from the Al-OH bending vibrations. Signals at 796 cm^{-1} and 692 cm^{-1} corresponded to Si-O-Al compounded vibrations and Si-O stretching vibration, respectively. These bands were found in the kaolinite IR spectra after the sorption experiment and the kaolinite exposure to kerosene and TOA (see Figures 3B and 3C)..

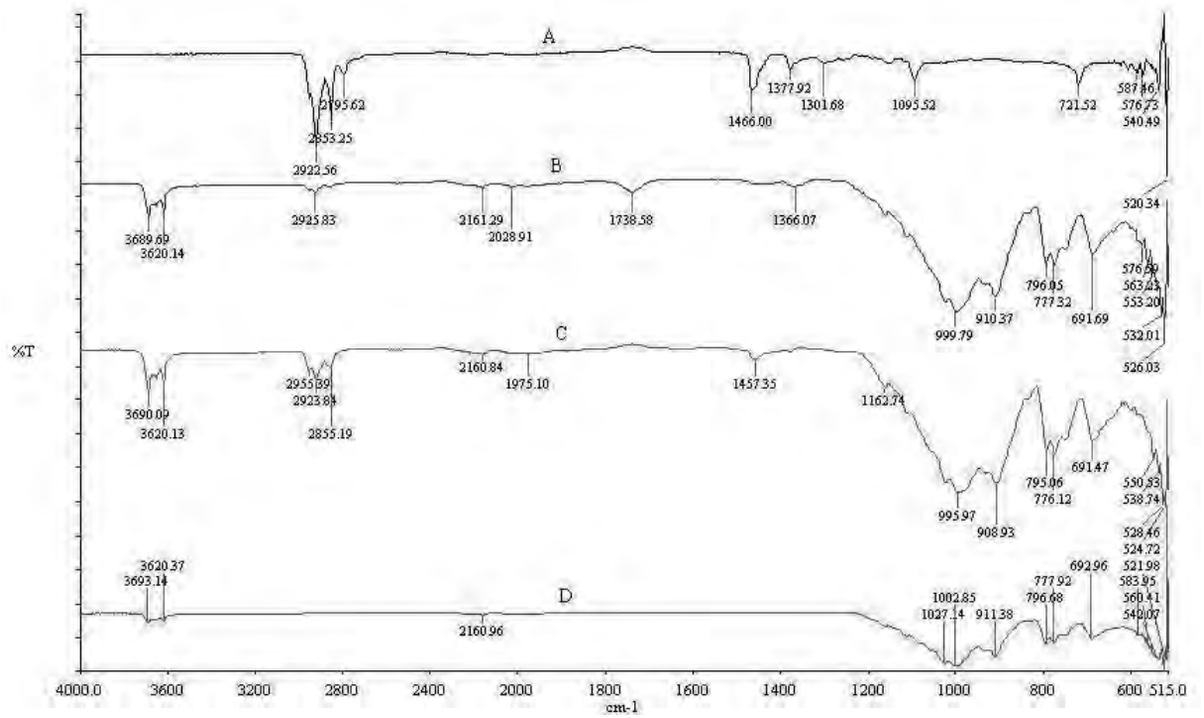

FIGURE 3

The reference infrared spectrum of TOA is depicted in figure (A). Figure (B) depicts the infrared spectrum of air-dried kaolinite after 168 of the batch equilibration with a TOA solution in kerosene. Figure (C) contains the infrared spectra of kaolinite after 168 hours of batch equilibration, but before air-drying. Finally, Figure (D) depicts the infrared spectrum of the control kaolinite sample with no exposure to any TOA solution in kerosene.

The bands from the TOA IR spectrum, namely 2 922 cm-1, 2 955 cm-1, 1 457 cm-1 and 1 366 cm-1, were observed in spectra (B) and (C). Thus traces amounts of TOA were detected on the kaolinite particle surface soon after batch experiments and after the kaolinite had been dried. This is based on the presence of signals from C-H stretching and C-H bending vibrations and it proves that TOA sorbed to kaolinite. It can be seen from the original sample of kaolinite that these bands did not exist before introduction of TOA. The IR spectral results also show that the sorption of TOA had some influence on the kaolinite crystal lattice. Sorption of butyl amine onto kaolinite has been reported to take place on acidic sites on the surface of kaolinite [35]. Lloyd and Conley [29] found that the sorption of amines can take place on the basal SiO and AlOH groups or on the same functional groups located on the external surface of kaolinite particles. This data supports the findings of the TOA presence on the surface of the kaolinite in this study.

Example of the sorption kinetics of TOA at the SL of 0.4 is shown in Figure 4. The removal efficiency is plotted as percentage of the initial concentration removed after a given period of sorption experiment. As it can be seen the apparent sorption equilibrium was reached after 144-168 hours of incubation. The same time period was required to achieve sorption equilibrium for both particle diameters at the SL of 0.2. There are no reference data on the sorption of the TOA onto mineral surfaces and so the apparent equilibrium periods are new in literature. The estimated hydrophobicity of TOA, measured by the logarithm of the 1-octanol/water partition coefficient, is around 10.5 [36]. Studies on the sorption of such highly hydrophobic organic pollutants onto the mineral surfaces are scarce in literature. Murphy et al. [37] reported that the apparent sorption equilibrium of carbazole, anthracene and dibenzothiophene onto kaolinite from the aqueous solutions of the compounds was established after 8-10 hours of incubation [35]. Sorption of asphaltenes onto kaolin from the compound's solution in toluene were assumed to reached apparent equilibrium after 24 hours, but no kinetic studies were conducted [38]. Zhang et al. [39] reported that tumbling of a kaolin suspension with octadecyl amine for 24 hours or more is required to reach sorption equilibrium. Thus time periods required for the establishment of the apparent sorption equilibrium of TOA onto the Grahamstown kaolinite from kerosene was longer than the comparable data from the literature. The removal efficiencies for TOA after the apparent equilibrium was established are shown in Table 1. The

equilibrium removal efficiency of TOA at SL of 0.2 and the kaolinite particle size 65-100 µm and 101-400 µm was equal to 18.1 % and 17.5 %, respectively (see Table 1). The respective sorption capacities for TOA were 0.92 g/g and 0.88 g/g. At the SL of 0.4, the TOA removal efficiency was 35.8 % for the 65-100 µm kaolinite particle range and 33.2 % for the 101-400 µm kaolinite particle range. The relevant sorption capacities for TOA were 0.93 g/g and 0.87 g/g.

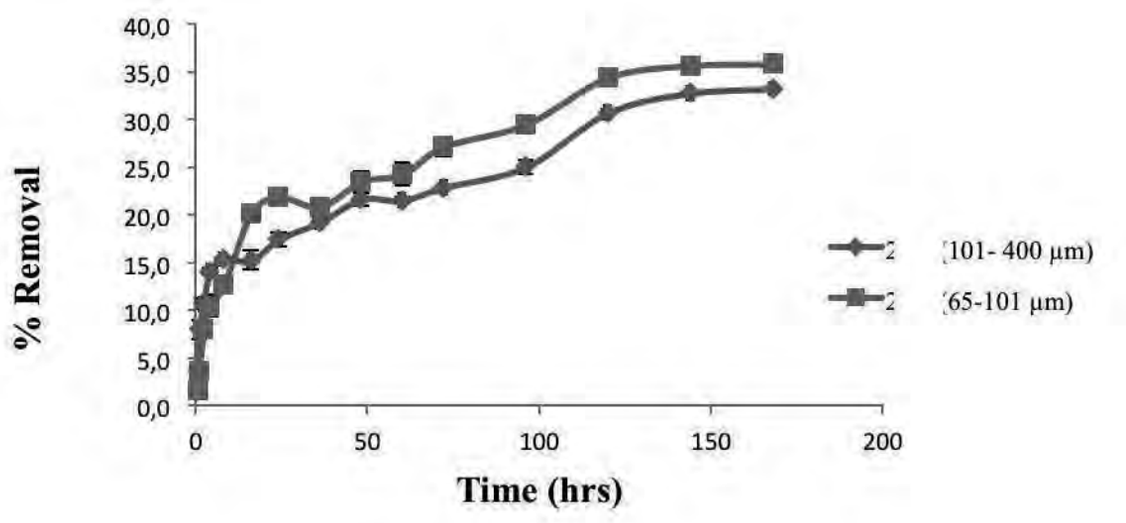

FIGURE 4
Sorption of TOA onto the kaolinite sorbent with particle diameters of 65-100 µm and 101- 400 µm. Both sorption kinetics were measured at the SL value of 0.4.

TABLE 1
The equilibrium TOA removal efficiencies and sorption capacities.

SL (g)	Particle size (µm)	Removal efficiency (%)	Sorption capacity (g/g)
0.2	65-100	18.1	0.92
	101-400	17.5	0.88
0.4	65-100	35.8	0.93
	101-400	33.3	0.87

The equilibrium removal efficiency is directly proportional to the SL. Therefore the removal efficiency is directly proportional to the interfacial area of kaolinite that is available for the sorption of TOA. An apparent contradiction with this statement appears to originate from the lack of dependence of the equilibrium removal efficiency on the particle diameter of the kaolinite sorbent at a constant SL value (see Table 1 for details). The apparent sorption capacity of kaolinite for TOA follows an analogical trend as the removal efficiency. The possible explanation for both observations could be that the majority of the particles in the 65-100 µm fraction of kaolinite had an average diameter very close to 100 µm. On the other hand, the majority of the particles in the 101-400 µm fraction of kaolinite probably had a particle diameter which was close to the lower end of the particle diameter interval. Further studies on the particle size of the kaolinite use will have to be required to ascertain the nature of this assumption. Findings from Table 1 seem to be in contradiction with the data of Zhou et al. [40] and Wang and Keller [41].

Parameters of the Freundlich isotherm are shown in Table 2. The Freundlich exponent values are very close to 1.0, i.e. the optimisation of the Freundlich isotherm parameters by Microsoft Excel (Microsoft Inc., Johannesburg, South Africa), almost linear. The respective values are equal to 1.077 for the 65-100 μm particle diameter range and to 1.086 for the 101-400 μm range. This mean that the sorption surface available for TOA uptake by kaolinite particle is very close to homogeneity, i.e. the TOA sorption probably took place evenly throughout the kaolinite particle surface. The Freundlich sorption coefficient increased as the particle diameter of kaolinite decrease, i.e. 2.843 (L/g)1.077 for the 65-100 μm particle diameter range and to 2.622 (L/g)1.086 for the 101-400 μm range. Results from the sorption experiments indicate that the kaolinite surface is wetted by kerosene and it can remove substantial amounts of TOA from the NAPL-type solutions. These findings indicate that the kaolinite surface must be in part at least hydrophobic in nature and these are the sites of the sorption of highly hydrophobic compounds such as TOA. The possible explanations for these observations are provided below.

TABLE 2
Optimised values of the adjustable parameters of the TOA Freundlich sorption isotherm onto kaolinite.

Particle size range (μm)	K_f **(L/g)^n**	***N***	R^2
Particle size range (μm)	**Kf (L/g)n**	**N**	R2
65 - 100	2.843	1.077	0.9719
101 - 400	2.622	1.086	0.9795

Saada et al. [42] examined the hydrophilicity and hydrophobicity of the kaolinite surfaces. They reported only 25 % of the kaolinite surface to be hydrophilic and the remaining part is either neutral or hydrophobic in nature [42]. They stated that the surface of kaolinite is more oleophilic and is hence easily wetted by oils [42]. Therefore this could explain the wetting of kaolinite used in this study by kerosene. As the extent of kaolinite wetting with kerosene becomes increases, the kaolinite surfaces would become even more hydrophobic. This in turn would make it an excellent site for the TOA sorption to kaolinite. Hydrophobic moieties in the crystal lattice of kaolinite are the hydrophobic siloxane groups which have been reported by various authors in the crystal lattice of clay minerals [27, 43]. Their hydrophobic nature is supported by the report that during the adsorption of poly(ethylene oxide) on smectites, the hydrophobic part of poly(ethylene oxide) had a high affinity for the siloxane groups in the smectite crystal lattice soils [44]. Similar sorption mechanism could be used to explain the uptake of TOA onto kaolinite. Furthermore, kaolinite has a higher affinity for organic compounds compared to other clay surfaces, especially illite [42, 45]. This explains why the kaolinite surface would be more hydrophobic in kerosene.

CONCLUSION

Hydrophobicity of the tertiary amine and organic carbon content of kaolinite, the structure of kaolinite and the presence of hydrophobic siloxane bonds play a crucial role in its adsorption. In this study, the organic carbon content was negligible and the sorption of the tertiary amine was not attributed to the carbon content. The hydrophobic medium, kerosene, also has an effect on the structure of kaolinite. The hydrophobic nature of a large portion of the sorption surface area of kaolinite makes it easily wetted by organic chemicals, such as kerosene. This increases its hydrophobicity. It is also concluded that the hydrophobicity of the tertiary amine affected its sorption to kaolinite. Smaller sized particles proved to have the highest adsorption capacity and better removal efficiency. This suggests that Kaolinite carries a potential for being used in the remediation of metal processing wastewaters containing hydrophobic extractants.

ACKNOWLEDGEMENTS

The authors are grateful to the Rhodes Research Council Fund for funding the first authors Masters of Science degree during which the study was conducted. The authors would further like to acknowledge the Water Commission of South Africa (Grant number K5/2011/3) for financial support of the experimental part of the study. The Nanotechnology Innovation Centre and department of Chemistry at Rhodes University are acknowledged for providing support with kaolinite sorbent characterisation.

REFERENCES

[1] J. Y. Lee, B. Raju, B. N. Kumar, J. R. Kumar, H. K. Park, B. R. Reddy: Solvent extraction separation and recovery of palladium and platinum from chloride leach liquors of spent automobile catalyst. Separation and Purification Technology, 73 (2), 213 (2010).

[2] C. Yin, A. N. Nikoloski, M. Wang: Microfluidic solvent extraction of platinum and palladium from a chloride leach solution using Alamine 336. Minerals Engineering, 45, 18 (2013).

[3] M. K. Jha, D. Gupta, J. Lee, V. Kumar, J. Jeong: Solvent extraction of platinum using amine based extractants in different solutions: A review. Hydrometallurgy, 142, 60 (2014).

[4] H. Shoji, H. Kobayashi: Method for scrubbing an amine type extractant after stripping. US Patent Application no. CA 2674490. Available at: http://www.google.com/patents/CA2674490C?cl=en (website accessed on 2nd June 2015) (2015).

[5] A. C. Araujo, P. R. M. Viana, A. E. C. Peres: Reagents in iron ores flotation. Minerals Engineering, 18(2 SPEC. ISS.): 219 (2005).

[6] B. Choudhury, A. Basha, T. Swaminathan: Study of lactic acid extraction with higher molecular weight aliphatic amines. J. of Chemical Technology and Biotechnology, 72 (2), 111 (1998).

[7] F. Moyo, R. Tandlich: Daphnia Pulex Toxicity Testing of Ethylenediaminetetraacetic Acid Tetrasodium Salt Dihydrate and the Wastewater Effluent from Extraction of Rhodium using Emulsion Liquid Membranes. International J. of Environmental Research, 8 (4), 1019 (2014).

[8] T. Kistemann, J. Hundhausen, S. Herbst, T. Claßen, H. Färber: Assessment of a groundwater contamination with vinyl chloride (VC) and precursor volatile organic compounds (VOC) by use of a geographical information system (GIS). International Journal of Hygiene and Environmental Health, 211 (3-4), 308 (2008).

[9] L. V. C. Bonaparte, A. T. P. Neto, L. G. S. Vasconcelos, R. P. Brito, J. J. N. Alves: Remediation procedure used for contaminated soil and underground water: A case study from the chemical industry. Process Safety and Environmental Protection, 88 (5), 372 (2010).

[10] L. Goldstein, S. O. Prasher, S. Ghoshal: Three-dimensional visualization and quantification of non-aqueous phase liquid volumes in natural porous media using a medical X-ray computed tomography scanner. J. of Contaminant Hydrology, 93 (1-4), 96, (2007).

[11] Z. Yang, A. Niemi, F. Fagerlund, T. Illangasekare, R. L. Detwiler: Dissolution of dense non-aqueous phase liquids in vertical fractures: Effect of finger residuals and dead-end pools. J. of Contaminant Hydrology, 149, 88 (2013).

[12] R. Tandlich: PCB biodegradation and binding to soil components. PhD thesis, North Dakota State University, Fargo, ND, USA, 2004.

[13] D. Jaremko, D. Kalembasa: Application of adsorption isotherms for describing the sorption of barium by kaolinite. Fresenius Environmental Bulletin, 22 (11 A), 3352 (2013).

[14] Y. K. Aktaş, H. Ibar: Sorption and preconcentration of cadmium, iron and antimony on bentonite modified with trioctylamine. Fresenius Environmental Bulletin, 14 (11), 983 (2005).

[15] R. Tandlich, Š. Baláž: Biphenyl sorption to different soil clay minerals. African Journal of Agricultural Research, 6 (10), 2321 (2011).

[16] A. Kar: Pharmaceutical Drug Analysis. New Age International Publishers, New Delhi, India, 2005.

[17] M. Arami, N. Y. Limaee, N. M. Mahmoodi, N. S. Tabrizi: Equilibrium and kinetics studies for the adsorption of direct and acid dyes from aqueous solution by soy meal hull. J. of Hazardous Materials, 135 (1-3), 171 (2006).

[18] I. D. Mall, V. C. Srivastava, N. K.Agarwal: Removal of orange-G and methyl violet dyes by adsorption onto bagasse fly ash-kinetic study and equilibrium isotherm analyses. Dyes and Pigments, 69 (3), 210 (2006).

[19] I. V. Perminova, N. Y. Grechishcheva, V. S. Petrosyan: Relationships between structure and binding affinity of humic substances for polycyclic aromatic hydrocarbons: Relevance of molecular descriptors. Environmental Science & Technology, 33 (21) 3781 (1999).

[20] W. Huang, P. Peng, Z. Yu, J. Fu: Effects of organic matter heterogeneity on sorption and desorption of organic contaminants by soils and sediments. Applied Geochemistry, 18 (7), 955 (2003).

[21] G. Churchman, C. Burke, R. Parfitt: Comparison of various methods for the determination of specific surfaces of sub soils. J. of Soil Science, 42 (3), 449 (1991).

[22] A. B. Cerato, A. J. Luteneggerl: Determination of surface area of fine-grained soils by the ethylene glycol monoethyl ether. Geotechnical Testing Journal, 25 (3), 315 (2002).

[23] Y. Yukselen, A. Kaya: Comparison of methods for determining specific surface area of soils. J. of Geotechnical and

Geoenvironmental Engineering, 132 (7), 931 (2006).
[24] T. A. Elbokl, C. Detellier: Intercalation of cyclic imides in kaolinite. J. of Colloid and Interface Science, 323 (2), 338 (2008).
[25] H. Cheng, Q. Liu, J. Yang, S. Ma, R. L. Frost: The thermal behavior of kaolinite intercalation complexes-A review. Thermochimica Acta, 545, 1 (2012).
[26] S. Letaief, T. Diaco, W. Pell, S. I. Gorelsky, C. Detellier: Ionic conductivity of nanostructured hybrid materials designed from imidazolium ionic liquids and kaolinite. Chemistry of Materials, 20 (22), 7136 (2008).
[27] W. Jaynes, S. Boyd: Hydrophobicity of siloxane surfaces in smectites as revealed by aromatic hydrocarbon adsorption from water. Clays and Clay Minerals, 39 (4), 428 (1991).
[28] V. Gianotti, M. Benzi, G. Croce, P. Frascarolo, F. Gosetti, E. Mazzucco, M. Bottaro, M. C. Gennaro: The use of clays to sequestrate organic pollutants - leaching experiments. Chemosphere, 73 (11), 1731 (2008).
[29] M. K. Lloyd, R. F. Conley: Adsorption studies on kaolinites. Clays and Clay Minerals, 18, 37 (1970).
[30] R. A. R. Da Silva, D. J. L. Guerra: Use of natural and modified kaolinite/ilite as adsorbent for removal methylene blue dye from aqueous solution. J. of the Chilean Chemical Society, 58 (1), 1517 (2013).
[31] H. Xu, J. S. J. van Deventer: Microstructural characterisation of geopolymers synthesised from kaolinite/stilbite mixtures using XRD, MAS-NMR, SEM/EDX, TEM/EDX, and HREM. Cement and Concrete Research, 32 (11), 1705 (2002).
[32] G. Kakali, T. Perraki, S. Tsivilis, E. Badogiannis: Thermal treatment of kaolin: The effect of mineralogy on the pozzolanic activity. Applied Clay Science, 20 (1-2), 73 (2001).
[33] C. He, E. Makovicky, B. Osbæck: Thermal stability and pozzolanic activity of calcined kaolin. Applied Clay Science, 9, 165 (1994).
[34] H. Cheng, J. Yang, R. L. Frost, Q. Liu, Z. Zhang: Thermal analysis and infrared emission spectroscopic study of kaolinite–potassium acetate intercalate complex. J. of Thermal Analysis and Calorimetry, 103 (2), 507 (2011).
[35] H. A. Benesi: Acidity of Catalyst Surfaces. II. Amine Titration Using Hammett Indicators. J. of Physical Chemistry, 61(7), 970 (1957).
[36] Pubchem (2015). Chemical and physical properties of trioctyl amine. Available at: http://pubchem.ncbi.nlm.nih.gov/compound/Trioctylamine#section=Chemical-and-Physical-Properties (website accessed on 3rd June 2015).
[37] E. M. Murphy, J. M. Zachara, S. C. Smith: Influence of mineral-bound humic substances on the sorption of hydrophobic organic compounds. Environmental Science & Technology, 24 (10), 1507 (1990).
[38] A. W. Marczewski, M. Szymula: Adsorption of asphaltenes from toluene on mineral surface. Colloids and Surfaces A: Physicochemical and Engineering Aspects, 208 (1-3), 259 (2002).
[39] Y. Zhang, D. I. Gittins, D. Skuse, T. Cosgrove, J. S. van Duijneveldt: Nonaqueous suspensions of surface-modified kaolin. Langmuir, 23 (6), 3424 (2007).
[40] Y. Zhou, R. Liu, H. Tang: Sorption interaction of phenanthrene with soil and sediment of different particle sizes and in various $CaCl_2$ solutions. J of Colloid and Interface Science, 270 (1), 37 (2004).
[41] P. Wang, A. A. Keller: Particle-size dependent sorption and desorption of pesticides within a water-soil-nonionic surfactant system. Environmental Science & Technology, 42 (9), 3381 (2008).
[42] A. Saada, B. Siffert, E. Papirer: Comparison of the hydrophilicity/hydrophobicity of illites and kaolinites. J. of Colloid and Interface Science, 174 (1), 185 (1995).
[43] H. Cheng, Q. Liu, J. Yang, Q. Zhang, R. L. Frost: Thermal behavior and decomposition of kaolinite–potassium acetate intercalation composite. Thermochimica Acta, 503-504, 16 (2010).
[44] C. C. Su, Y. H. Shen: Adsorption of poly (ethylene oxide) on smectite: Effect of layer charge. J. of Colloid and Interface Science, 332 (1), 11 (2009).
[45] J. L. Bantignies, C. Cartier Dit Moulin, H. Dexpert: Wettability contrasts in kaolinite and illite clays: Characterization by infrared and X-ray absorption spectroscopies. Clay and Clay Minerals, 45 (2), 184 (1997).

Received: **09.06.2015**
Accepted: **26.11.2015**

CORRESPONDING AUTHOR

Roman Tandlich
Rhodes University
Faculty of Pharmacy
Division of Pharmaceutical Chemistry
Environmental Health and Biotechnology Research Group
P. O. Box 94
Grahamstown, 6140 – South Africa

e-mail: roman.tandlich@gmail.com

by PSP Volume 25 – No. 1/ 2016, pages 89-102 Fresenius Environmental Bulletin

SEASONAL AND ANNUAL PRECIPITATION TREND PREDICTION IN XIN'ANJIANG CHINA

Muhammad Zaman, Guohua Fang *,Muhammad Saifullah,Qaiser Javed

College of Water Conservancy and Hydropower engineering, Hohai University, Nanjing, 210098,China

ABSTRACT

This study emphasized the predication of future precipitation trend at Xin'anjiang-Fuchunjiangwatershed and its comparison with that of the base (past) years. Possible beginning of change in precipitation trend has also been studied in order to get an idea about future water resources. CMIP5 data has been downscaled to the observed metrological stations using change factor downscaling method according to local conditions of watershed. In order to remove the serial effect of data, non-parametric pre-whitening technique was used. Non-parametric Mann Kendall (MK), Spearman's rho (SP/SR), Theil Sen's (TSA) and Sequential Mann Kendall (SQMK) techniques were applied on two different base (1960-2010) and future (2011-2060) precipitation data series. Mann Kendall and Spearman's rho have been applied to detect any significant trend within a data series, whereas TSA have been used to get the magnitude of the trend. The SQMK non parametric technique has applied in order to get an idea about the beginning of a potential change in precipitation trend. Results revealed that there is no significant change in annual precipitation trend for either base or future data series, meanwhile, an increasing trend was evident during winter and autumn seasons while summer and spring seasons exhibited a decreasing one. Same changes in precipitation trend were observed in the study area during 2020-2030 decade.

KEYWORDS:
Non-parametric, change factor, future precipitation, Xin'anjiang, CMIP5

INTRODUCTION

In recent decades, global warming is increasingly bringing attentions toward climate changes Besides the increase in temperature of the globe, a significant change in precipitation has been also noticed[1]. Temporal and spatial expansions of precipitation patterns are much important for water resources [2]. Global warming affects the precipitation patterns ultimately affecting the water resources and hydrology [3]. Studies found that average precipitation pattern is spatially expanding throughout the world [4-6] but such an expansion occurs at different ratios over various locations [7, 8]. IPCC has also detected expansion in precipitation patterns spatially in the east of northern and southern America and several parts of northern and central Asia and Europe whereas Sahel, various parts of Africa and South Asia and the Mediterranean presented a decrease in the precipitation tendency through 1900-2005 [9]. Tropical areas display non-significant precipitation change, however significant increase in the precipitation amount has been observed in northern hemisphere between (30-60^0 N) during (1901-2008) identified by IPCC 2013.[10]

Xin'anjiang watershed lies in the eastern part of China. Several researchers have tried to determine the precipitation trend in China. Ding et al. found that there is no significant annually averaged precipitation trend in the country while there is an interdecadel trend with its variability found at regional basis [11, 12]. Wang and Zhou have found a decreasing trend in mean annual precipitation during 1961-2001 in the northeast, north and central China, whereas a significant increasing trend has been found in southwest east and northwest China [13]. Studies have shown an adjustment of precipitation trend in eastern China after 1970. [14-16]. Researchers indicated that southern China and Yangtze River basin have suffered from heavier precipitation and severe flooding events over this area, while northeast and north China experienced a lot of severe droughts.[11, 12, 17-19]

Researchers worked to estimate the precipitation amount around the globe. Anli (2015) worked to estimate the precipitation amount on regional and point bases[20]. Previous studies found that the precipitation distribution is uneven and extremely varied, spatially and temporally, in different regions [21]. Several studies have been conducted to determine the precipitation trend at local scale in China. Wang et al. used precipitation data from Jinshajiang River basin during 1961-2008 and found an insignificant increasing trend [22]. However, Zhong and Li (2009) detected a decreasing trend in annual precipitation in Mianyang basin of Sichuan province, China [23]. Xu et al. (2010) have observed an increase in precipitation in Tarim River basin during 1960-2007 [24]. Many researchers tried to find the precipitation trend at large scale in the country [25-31] but not much work have done to determine the precipitation trend over medium watersheds such as Xin'anjiang-Fuchunjiangwatershed.

Future assessment of hydrology and water resources is gaining much more attention from city planners and water allocation and utilization organizations [32, 33]. General Circulation Model (GCMs) and regional climate models have been proved to be one of the best tools to analysis the climate scenarios and to predict future scenarios [34, 35]. Many researchers have tried to downscale GCMs to predict the future hydrology in their relevant study areas [36-40]. Different results can be obtained by applying different downscaling techniques showing that a small change in precipitation results influence a significant effect at the hydrology of the area.[41, 42]

Many statistical techniques have been developed and used for trend detection in the past, among which non-parametric technique is more powerful and reliable as compared to parametric method [43]. Mann Kendall [44, 45] and Theil Sen's [46, 47] non parametric approaches have developed by Mann Kendall and Sen are commonly used to detect the trend and its magnitude, respectively. Researchers often used MK and Sen Slope to determine the trend and its magnitude in most of hydrological studies [48-58]. Topaloglu used non

parametric Mann Kendall approach to detect the precipitation trends in turkey [59]. Spearman's rho is also an important statistical technique that was not only used for the determination of hydro metrological data trend [60] but also employed to be compared with Mann Kendall test in many studies [60-64]. In the past, it was very common to use an advance form of Mann Kendall method, namely Sequential Mann Kendall technique, in order to determine the start of a possi

MATERIALS AND METHODS

STUDY AREA AND DATA COLLECTION

The study area, namely Xin'anjiang-Fuchunjiang watershed, is located upstream of Xin'anjiang and Fuchunjiang hydropower station on the Xin'an River.

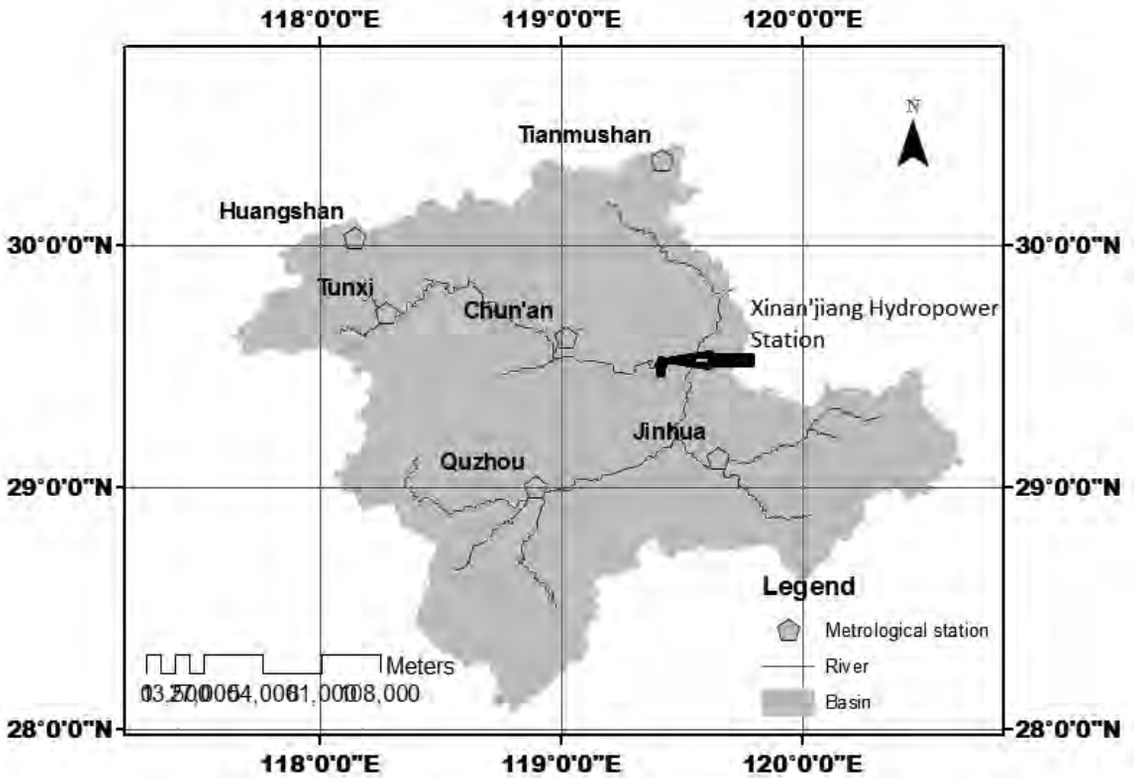

FIGURE 1
Study area indicating the locations of metrological stations

It is located between longitudes of 117^0 45′-120^0 15' and latitudes of 28^0 15′-30^0 15′N having 35620.2 km^2 area, as is shown in Figure 1. The study area embraces Xin'anjiang reservoir with a capacity of 22 billion m^3 upstream of the Xin'anjiang hydropower station.

The observed meteorological data was collected from the Chinese meteorological department and the data for future prediction were collected from CMIP5 project of a CCSM4 model in order to determine the trend of precipitation over next 50 years. The precipitation data series have divided into base year(1960-2010) and future (2011-2060) data series.

METHODOLOGY

Change Factor (CF) downscaling method: The Change Factor downscaling method [68, 69] is a bias correction technique used to minimize the bias between the observed data and GCMs outputs. In this method, observed data regarding daily variables (precipitation) are modified by adding mean values of monthly changes between the base and future years. Modified precipitation data for future years are obtained by multiplying observed daily precipitation for the base year by the following ratio in Equation (1).

$$\mathbf{P_{adj;fur;d}} = (\mathbf{P_{obs;d\_x}} \sum_{i=1}^{k} \boldsymbol{P_i} \left(\boldsymbol{P_{GCM,fut.m}} / \boldsymbol{P_{GCM.ref.m}}\right) \quad \textbf{(1)}$$

where $\mathbf{P_{adj;fur;d}}$ is adjusted daily precipitation for a future year, while $\mathbf{P_{obs;d\_}}$ is observed daily precipitation for the base year. $\boldsymbol{P_{GCM,fut.m}}$ and $\boldsymbol{P_{GCM.ref.m}}$ are future and reference (base) years' monthly precipitation of GCM output

while $\boldsymbol{P_I}$ is the weight of every grid cell and k is the number of grid cells

Pre whitening of data: Data employed for non-parametric tests, should not be correlated. In order to determine the correlation effect on the data, a two tailed test has been applied at a confidence interval of 5% to determine correlation coefficient r_i as shown in Equation (2)

$$r_i = \frac{\sum_{i=1}^{n=1}(x_i-\overline{x})(x_{i+1}-\overline{x})}{\sum_{i=1}^{n}(x_i-\overline{x})^2} \quad \textbf{(2)}$$

While value of r_i was determined at 95% null hypothesis as given in Equation (3):

$$r_i = \frac{-1 \pm 1.96\sqrt{n-2}}{n-1} \quad \textbf{(3)}$$

If r_i value is between the upper and lower limit of 95% confidence interval, that means that data is serially correlated and we need to apply trend free pre-whitening technique [70] in order to remove the

correlation effect from the data, as is done by many researchers [64, 71-73].

Mann Kendall trend test: The non-parametric Mann Kendall [44, 45] trend test has been applied to the observed and future data in order to determine the possible trend within the data. The mathematical equations used in MK test are given below (where S is MK test statistics):

$$\mathbf{S}=\sum_{i=1}^{n-1}\ \sum_{j=i+1}^{n} \boldsymbol{sgn}(x_j - x_i) \quad (4)$$

$$\mathbf{sgn}(x_j - x_i) = \begin{cases} +1, if\ (x_j - x_i) > 0 \\ 0, if\ (x_j - x_i) = 0 \\ -1, if\ (x_j - x_i) < 0 \end{cases} \quad (5)$$

Where variance is given by equation 6

$$\mathbf{V(S)} = \frac{n(n-1)(2n+5)-\sum_{k=1}^{m} t_k(t_k-1)(2t_k+5)}{18} \quad (6)$$

If more than 10 data points existed, then MK statistics Z_s is calculated as:

$$Z_s = \begin{cases} \frac{S-1}{\sqrt{V(S)}} & if\ S > 0 \\ 0 & if\ S = 0 \\ \frac{S+1}{\sqrt{V(S)}} & if\ S < 0 \end{cases} \quad (7)$$

where $x_j\ and\ x_i$ are time series data in chronological order with j>I, and n is the number of data points. t_k is the number of data ties point with an extent of k and m is the number of tied groups.

Positive values of Z_s correspond to an upward (increasing) trend, while negative values are associated with downward (decreasing) trends. The null hypothesis, Ho, in this method is defined as "no trend in the data", while alternate H_1 represents the presence of a trend within the data. If $|Z|>Z_{1-\frac{\alpha}{2}}$, then Ho is rejected and the data will certainly following a trend. $Z_{1-\frac{\alpha}{2}}$ values for p values of 0.05, 0.01 and 0.001 are 1.96, 2.57 and 3.2, respectively, given in the standard normal table.

Spearman's rho Test: Spearman's rho is a [74, 75] rank based non-parametric test used for trend detection and comparison with MK trend test. In this test, Ho null hypothesis, Ho, indicates no trend while alternative hypothesis, H_1, indicates the presence of the a trend and with changes in data represented by exhibits with changes in i [70]. The test R_{sp} and standard Z_{sp} statistics are given by below relations:

$$\mathbf{R_{sp}} = 1 - \frac{6\sum_{i=1}^{n}(D_i - i)^2}{n(n^2-1)} \quad (8)$$

$$\mathbf{Z_{sp}} = \mathbf{R_{sp}}\sqrt{\frac{n-2}{1-R_{sp}^2}} \quad (9)$$

where D_i is rank of ith data point with i being the chronological order number, while n is total length of time series. Z_{sp} in Equation (9) is the student's t value with (n-2) degree of freedom. An increasing trend is detected if Z_{sp} is found to be positive whereas its negative value indicates the presence of a decreasing trend within the data. The critical value of t is defined as $\boldsymbol{t}_{(n-2,1-\frac{\alpha}{2})}$ at a significance level of 0.05 [76]. A significant trend exists within the data if $\mathbf{Z_{sp}} > \boldsymbol{t}_{(n-2,1-\frac{\alpha}{2})}$.

Theil Sen's slope: Sen's slope technique has been applied in this study in order to get the magnitude of the trend as follows:

$$\boldsymbol{Q_k} = \frac{(x_j - x_i)}{j-i} \text{ for k=1….N} \quad (10)$$

where x_j and x_i are data values of jth and ith data series, respectively.

$$\boldsymbol{Q_{med}} = \begin{cases} \boldsymbol{Q}_{(N+1)/2} & if\ N is\ odd \\ \boldsymbol{Q}_{\frac{N}{2}} + \boldsymbol{Q}_{(N+2)/2} & if\ N\ is\ even \end{cases} \quad (11)$$

Where N=n (n-1)/2. Negative value of Q_{med} represents a decreasing slope while a positive value is associated with an increasing slope.

Abrupt change detection: Sequential Mann Kendall (SQMK) rank based test has been used in many studies to determine the beginning of the trend along with potential abrupt changes over the course of the trend [77, 78].Step by step test statistics are given below

i. Rank values are used instead of the original values. n_i is the number of cases found having $x_i > x_j$ statistices ,where x_i(i=1,2,3,…i) and x_j (j=2,3,4,…i-1) are sequential values of time series.

ii. Then magnitudes of ranks are compared. The test statistic is given below.

$$\boldsymbol{t_i} = \sum_{i=1}^{j} \boldsymbol{n_i} \quad (12)$$

iii. The mean value of test statistics is given by:

$$\mathbf{E}\ (\boldsymbol{t_i}) = \frac{i(i-1)}{4} \quad (13)$$

Moreover, the variance is equal to:

$$\mathbf{Var}\ (\boldsymbol{t_i}) = \frac{i(i-1)(2i+5)}{72}. \quad (14)$$

iv. Finally, the SQMK value was calculated as

$$\mathbf{u}\ (\boldsymbol{t_i}) = \frac{t_i - \mathrm{E(t)}}{\sqrt{Var(t_i)}} \quad (15)$$

Forward $u(t_i)$ is obtained from original time series while data series is reversed and resorted before being used as backward statistics $u'(t_i)$ with the trend change starting at the intersection point of both series.

RESULTS AND DISCUSSION

Primarily statistical results:

Statistical techniques were applied on both the observed (base) and downscaled (future) data before employing any other test and the results are presented in Table 1. Results revealed that mean annual precipitation of future data series is more than that of base data series, indicating an increase in the precipitation in future. In base data series, the maximum precipitation have been observed in the east of the watershed decreasing towards west with the minimum precipitation observed in the northwest of the watershed. The maximum precipitation obtained for the base data series was 674mm/year, whereas it was found to be about 700mm/year for the future data series.

Coefficient of variation varies within the range of 0.1 to 0.2, whereas the standard deviation ranges from 48 to 65. As is shown in Table 1, the coefficient of skewness ranges from -0.6 to 1.1, whereas the coefficient of kurtoses belongs to -0.9 to 1-1.2 interval for both the base and future data series. Since coefficients of skewness and kurtosis are not equal to 0 and 3, respectively, data is not positively distribute

TABLE 1
Preliminary Statistical analysis

Stations Name	Longitude	Latitude	Mean (mm)		Standard Deviation		Cs		Ck		Cv	
			Base	Future	Base	Future	Base	Future	Base	Future	Base	Future
Huangshan	118.15	30.03	674	699	46.1	46.1	-0.6	-0.6	0.5	0.5	0.1	0.1
Tianmushan	119.42	30.35	421	435	63.0	64.2	-0.6	-0.6	0.0	0.0	0.1	0.1
Tunxi	118.28	29.72	430	441	64.8	69.3	1.1	1.0	1.2	1.0	0.2	0.2
Jinhua	119.65	29.12	419	421	44.8	46.9	-0.4	-0.5	-0.7	-0.6	0.1	0.1
Chunan	119.02	29.62	448	455	50.7	52.0	0.2	0.0	-0.9	-0.9	0.1	0.1
Quzhou	118.9	29	478	486	64.0	64.4	0.5	0.3	-0.8	-0.9	0.1	0.1

Monthly base and future trends: As it can be seen from Figure 2 (a, b, c, d, e, f), there is not much difference in Mann Kendall (MK) and Spearman's rho (SR) significance values. Results revealed that future data series showed a little bigger values of significance than those of base data series.

Huangshan station: Results of monthly future and base data using Mann Kendall and Spearman's rho are shown in Figure 2a. It can be seen that there is no much difference between MK and SP significance levels. Results showed that at Huangshan station February and December have significantly increasing trend while October has significantly decreasing trend at 99% significance level. Other months of the years did not exhibit a significantly increasing or decreasing trend for neither the base nor the future data series, as is shown in Figure 2a.

Tianmushan station: As shown in Figure 2b, future and base data series corresponding to Junes, Julys and Augusts exhibit significantly increasing trend while those corresponding to Novembers have a decreasing significant trend at 99% confidence level. Other months did not exhibit a significantly increasing or decreasing trend.

Tunxi station: Results of statistical MK and SR for Tunxi station indicate that only Decembers have significantly increasing trend at 99% confidence level for the base and future data series. Furthermore, base data series also showed an increasing trend during the months of July, at 99% significance level, while no trend is evident within the future data series corresponding to this month. Other monthly data series did not exhibit a significant trend, as can be seen from Figure 2c.

Jinhua station: An increasing trend has been observed for monthly data series corresponding to Januarys, Februarys, Octobers, Novembers and Decembers at 99% significance level. In contrast, Aprils and Mays exhibited a decreasing trend for Jinhua station as illustrated in Figure 2d. Other monthly data series did not exhibit any significant trend.

Quzhou station: January, October, November and December series of base and future data of Quzhou station revealed a significance increasing trend at 99% significance level, whereas March, April and May series showed significantly decreasing trend, as is given in Figure 2e.

Chun'an station: At Chun'an, significant positive trends were detected for both the base and future data series corresponding to Januarys, Octobers, Novembers, and Decembers, while significant negative trends found for March, April and May months, as is shown in Figure 2f.

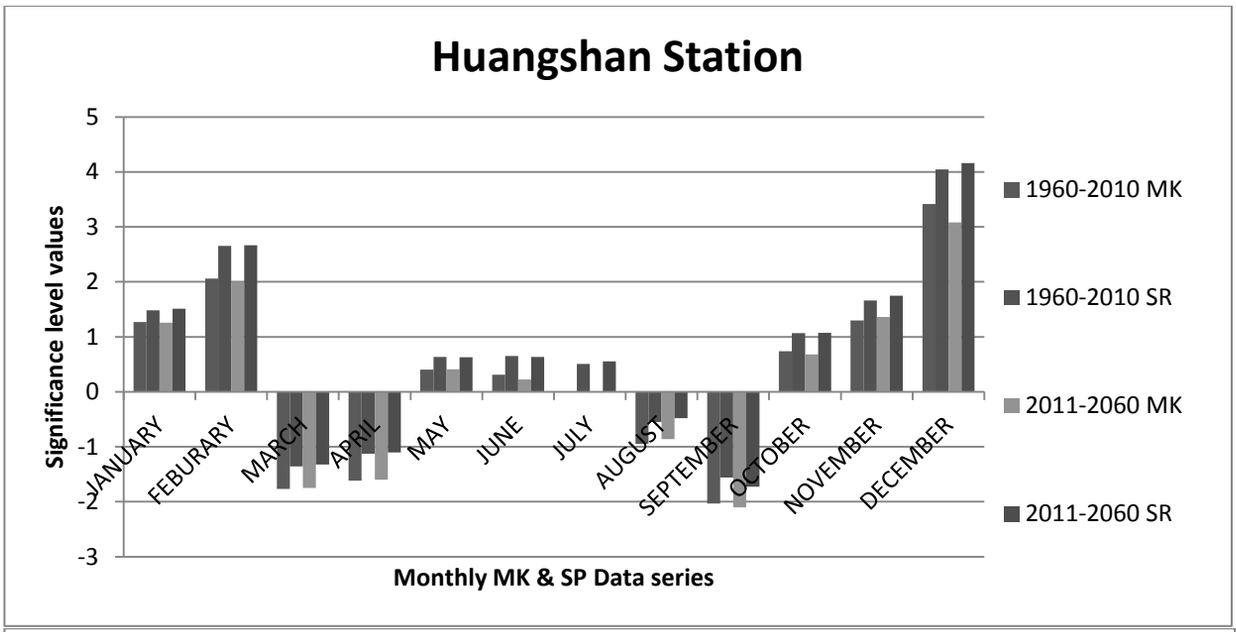
Huangshan Station
Significance level values
5
4
3
2
1
0
-1
-2
-3
JANUARY
FEBURARY
MARCH
APRIL
MAY
JUNE
JULY
AUGUST
SEPTEMBER
OCTOBER
NOVEMBER
DECEMBER
Monthly MK & SP Data series
1960-2010 MK
1960-2010 SR
2011-2060 MK
2011-2060 SR

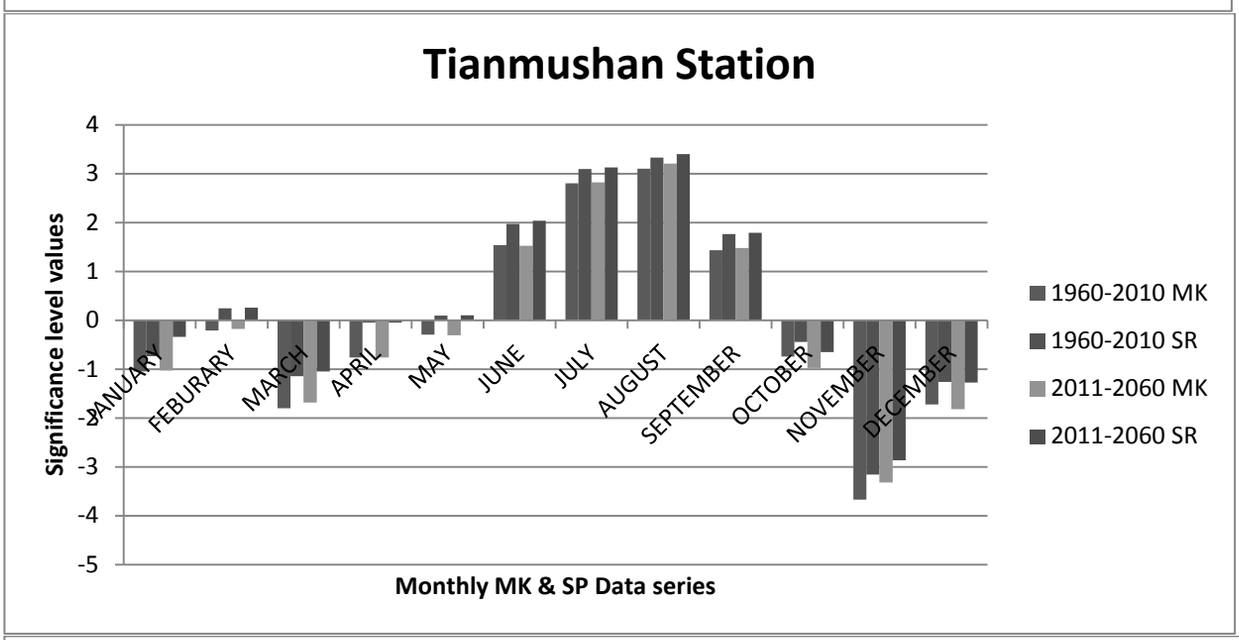
Tianmushan Station
Significance level values
4
3
2
1
0
-1
-2
-3
-4
-5
JANUARY
FEBURARY
MARCH
APRIL
MAY
JUNE
JULY
AUGUST
SEPTEMBER
OCTOBER
NOVEMBER
DECEMBER
Monthly MK & SP Data series
1960-2010 MK
1960-2010 SR
2011-2060 MK
2011-2060 SR

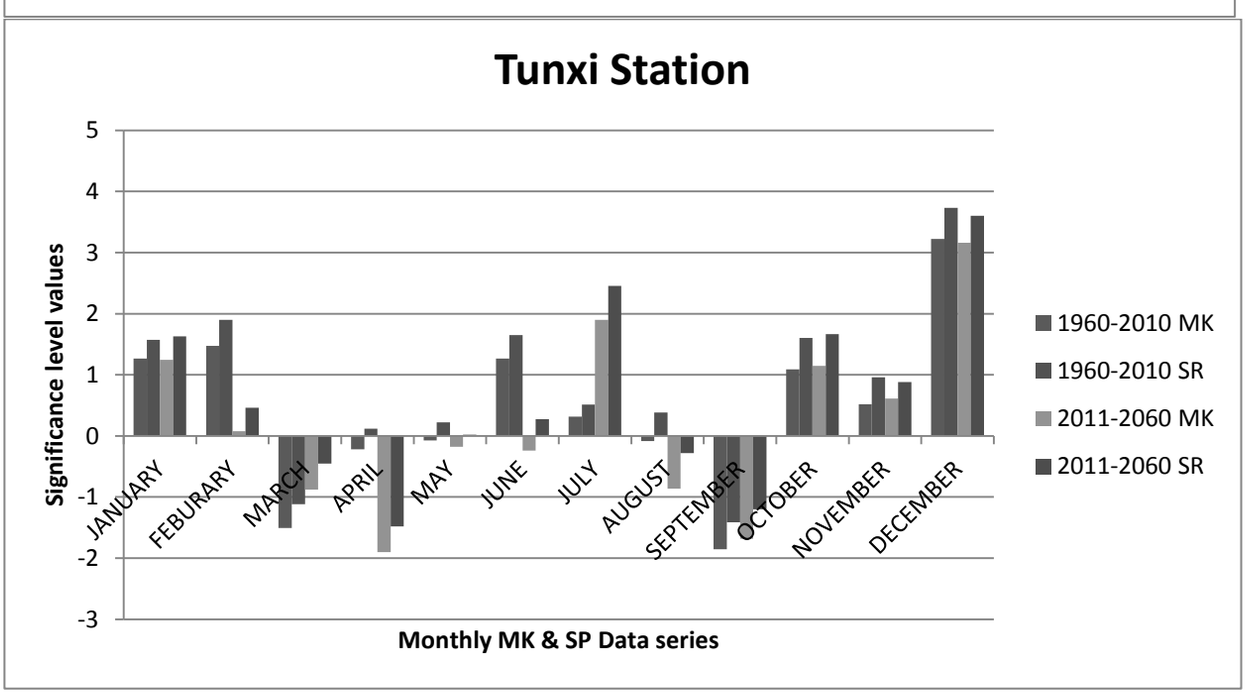
Tunxi Station
Significance level values
5
4
3
2
1
0
-1
-2
-3
JANUARY
FEBURARY
MARCH
APRIL
MAY
JUNE
JULY
AUGUST
SEPTEMBER
OCTOBER
NOVEMBER
DECEMBER
Monthly MK & SP Data series
1960-2010 MK
1960-2010 SR
2011-2060 MK
2011-2060 SR

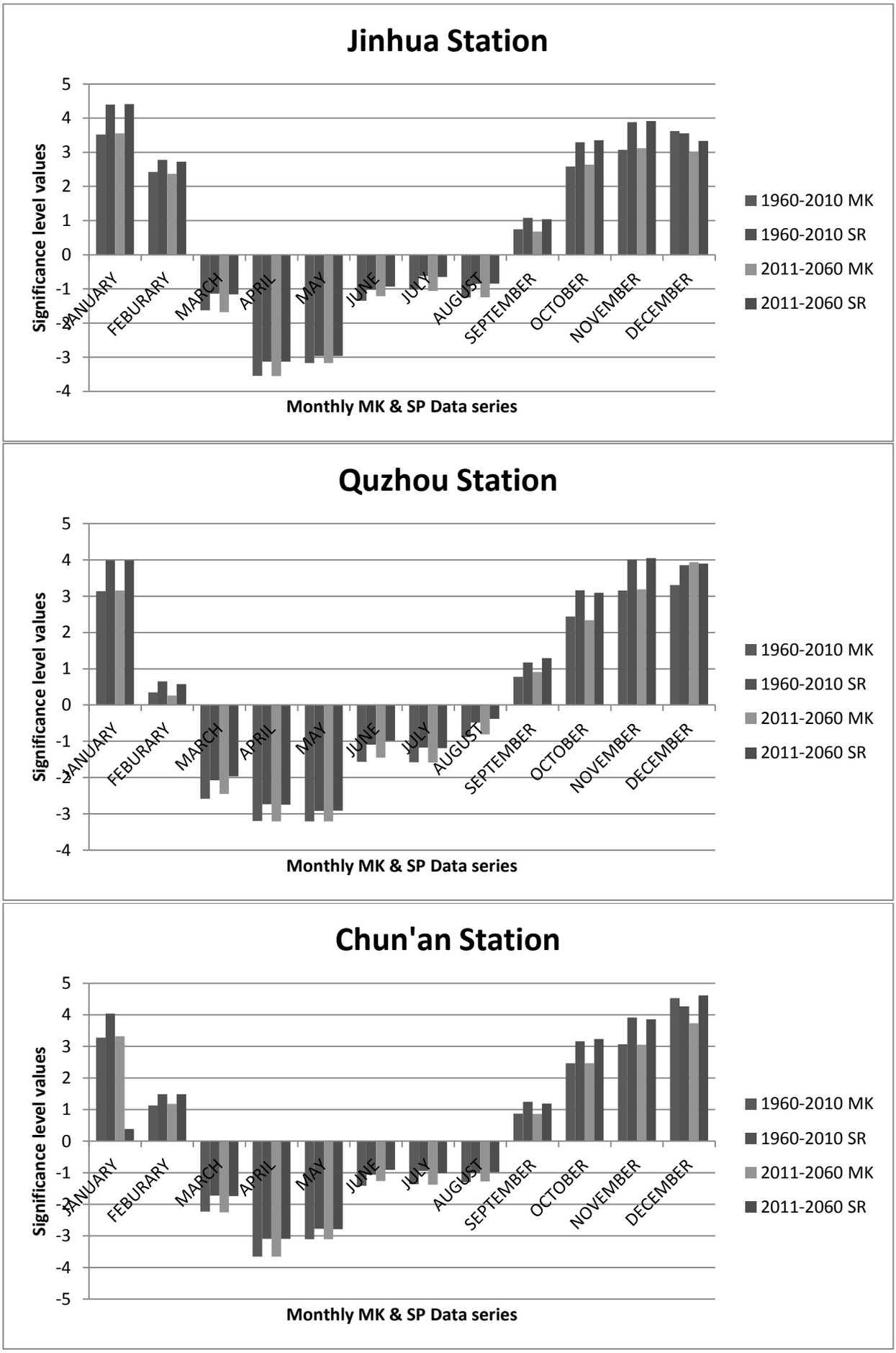

FIGURE 2
Monthly Mann Kendall & Spearman's rho results for the base and future precipitation of (a) Huangshan, (b) Tianmushan, (c) Tunxi, (d) Jinhua, (e) Quzhou, and (f) Chun'an stations.

stations have shown insignificant positive trends for the past and future data series. The Results also revealed that there is not much difference between Mann Kendall (MK) and Spearman's rho (SP) trend magnitudes. TSA non-parametric results showed that Tianmushan station fall in the region where precipitation decreases at a rate of -0.06 to -0.03 mm/year, whereas other stations exhibit an increase of 0.01 to 0.06 mm/year in precipitation for the past data series, as is shown in Figure 8a. TSA results showed that precipitation at Tianmushan station decreased at a rate of -0.07 to -0.04 mm/year, while it was increased at all other stations at a rate ranging from 0.013 to 0.1 mm/year for the future precipitation time data series, as is shown in Figure.

Winter data series: Non-parametric MK, SP and TSA results of the base and future winter data series are shown in Figure 3. It can be seen from the figure that all stations have increasing significant trends except for Tianmushan station which shows an insignificant negative trend for both the base and future winter data series. Bar chart of both figures show that there is not much difference between MK and SP results. TSA results, presented into Figure, show that precipitation at Tianmushan station decreases at a rate of 0.014 to 0.14 mm/year, whereas Huangshan and Tunxi stations exhibit an increasing trend at a rate of 0.014 to 0.21 mm/year and Chun'an, Quzhou and Jinhua station have also increasing trends at a rate of 0.62-0.76 mm/year for the base data series. It can be seen that Tianmushan station has a decreasing trend in precipitation at a rate of 0.15 to 0.02 mm/year, whereas all other stations have an increasing trend at a rate of 0.02-0.86 mm/year for future data series. Results showed that there is not much difference between the base and future data series within all extents.

Spring data series: Non-parametric MK, SP and TSA results of the base and future data series are shown in Figures 3. Results revealed that all stations within the watershed showed decreasing precipitation trends for both the base and future data series. Jinhua, Quzhou and Chun'an stations showed significant decreasing trends while Huangshan, Tianmushan and Tunxi stations showed insignificant decreasing trends for both the base and future data series. TSA results of the base data series revealed that precipitation at Huangshan and Tunxi stations have been decreased at a rate of 0.03 to 0.21 mm/year, whereas it is decreased at a rate of 0.39 to 1.2 mm/year at Tianmushan, Chun'an and Quzhou stations. Obtained data for Huangshan and Tunxi stations showed a decreasing trend at a rate of 0.031 to 0.21 mm/year, while Tianmushan, Chun'an and Quzhou stations exhibited a decrease in precipitation at a rate of 0.38 to 1.08 mm/year for the future data series, as shown in Figure 5b.

Summer trends: MK and Sp non parametric results for the base and future summer data series are shown in Figures 3. The Results indicated that Tianmushan station has an increasing significant trend at a rate of 0.25-0.40 mm/year, whereas Chun'an, Quzhou and Jinhua stations have significant decreasing trends at a rate of 0.31-0.45 mm/year for both the base and future precipitation data series, as is shown in Figures. Results revealed that the base and future data series of precipitation exhibits the similar trends with a little difference.

Autumn data series: Non-parametric test results revealed that Chun'an, Quzhou and Jinhua stations have significantly increasing trends of precipitation at a rate of 0.31-0.50 mm/year, whereas Tianmushan station exhibits a significant decreasing trend at a rate of 0.05 to 0.15 mm/year for the base and future precipitation data series, as is shown in Figure3. Other stations did not exhibit any significant trend.

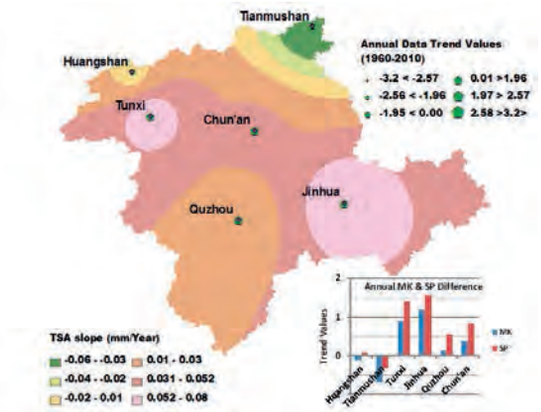
Tianmushan
Huangshan
Tunxi
Chun'an
Jinhua
Quzhou
Annual Data Trend Values (1960-2010)
-3.2 < -2.57
-2.56 < -1.96
-1.95 < 0.00
0.01 >1.96
1.97 > 2.57
2.58 >3.2>
TSA slope (mm/Year)
-0.06 - -0.03
-0.04 - -0.02
-0.02 - 0.01
0.01 - 0.03
0.031 - 0.052
0.052 - 0.08
Annual MK & SP Difference
Trend Values
MK
SP

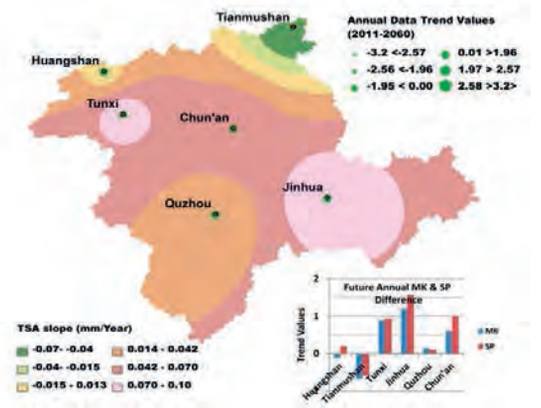
Tianmushan
Huangshan
Tunxi
Chun'an
Jinhua
Quzhou
Annual Data Trend Values (2011-2060)
-3.2 <-2.57
-2.56 <-1.96
-1.95 < 0.00
0.01 >1.96
1.97 > 2.57
2.58 >3.2>
TSA slope (mm/Year)
-0.07- -0.04
-0.04- -0.015
-0.015 - 0.013
0.014 - 0.042
0.042 - 0.070
0.070 - 0.10
Future Annual MK & SP Difference
Trend Values
MK
SP

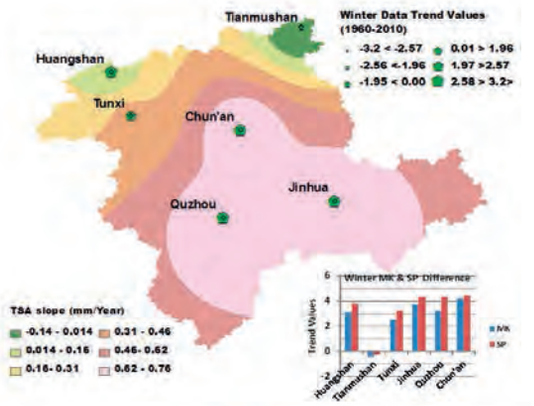
Tianmushan
Huangshan
Tunxi
Chun'an
Jinhua
Quzhou
Winter Data Trend Values (1960-2010)
-3.2 < -2.57
-2.56 <-1.96
-1.95 < 0.00
0.01 > 1.96
1.97 >2.57
2.58 > 3.2>
TSA slope (mm/Year)
-0.14 - 0.014
0.014 - 0.16
0.16- 0.31
0.31 - 0.46
0.46- 0.62
0.62 - 0.76
Winter MK & SP Difference
Trend Values
MK
SP

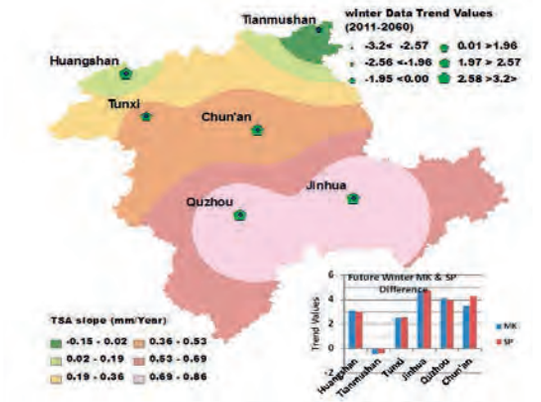
Tianmushan
Huangshan
Tunxi
Chun'an
Jinhua
Quzhou
winter Data Trend Values (2011-2060)
-3.2< -2.57
-2.56 <-1.96
-1.95 <0.00
0.01 >1.96
1.97 > 2.57
2.58 >3.2>
TSA slope (mm/Year)
-0.15 - 0.02
0.02 - 0.19
0.19 - 0.36
0.36 - 0.53
0.53 - 0.69
0.69 - 0.86
Future Winter MK & SP Difference
Trend Values
MK
SP

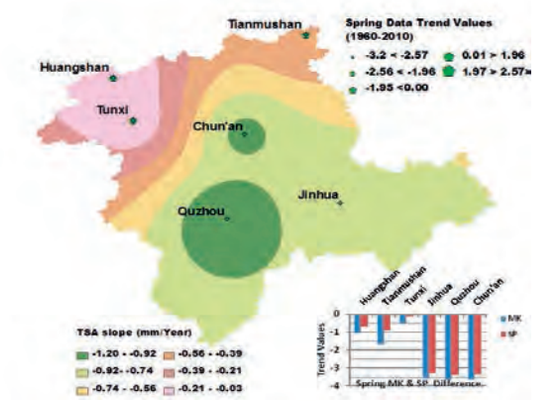
Tianmushan
Huangshan
Tunxi
Chun'an
Jinhua
Quzhou
Spring Data Trend Values (1960-2010)
-3.2 < -2.57
-2.56 < -1.96
-1.95 <0.00
0.01 > 1.96
1.97 > 2.57>
TSA slope (mm/Year)
-1.20 - -0.92
-0.92 - -0.74
-0.74 - -0.56
-0.56 - -0.39
-0.39 - -0.21
-0.21 - -0.03
Spring MK & SP Difference
Trend Values
MK
SP

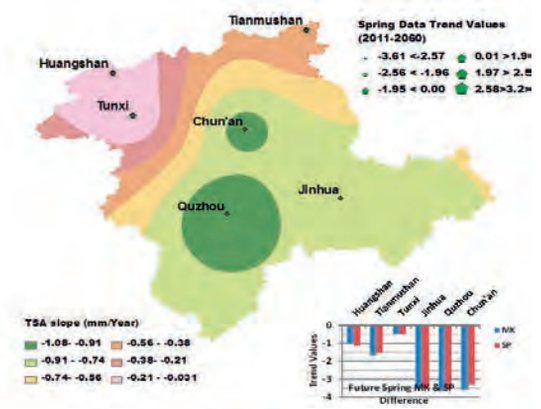
Tianmushan
Huangshan
Tunxi
Chun'an
Jinhua
Quzhou
Spring Data Trend Values (2011-2060)
-3.61 <-2.57
-2.56 < -1.96
-1.95 < 0.00
0.01 >1.9
1.97 > 2.5
2.58>3.2>
TSA slope (mm/Year)
-1.08- -0.91
-0.91 - -0.74
-0.74- -0.56
-0.56 - -0.38
-0.38- -0.21
-0.21 - -0.031
Future Spring MK & SP Difference
Trend Values
MK
SP

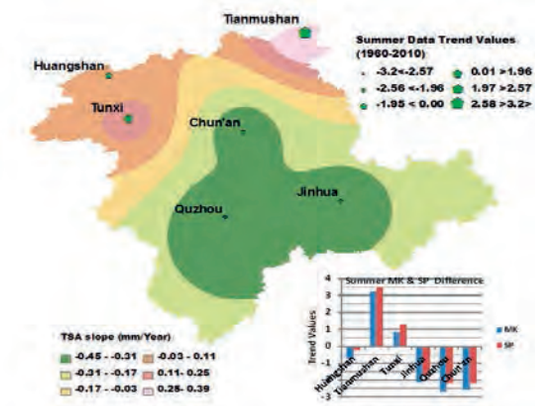
Tianmushan
Huangshan
Tunxi
Chun'an
Jinhua
Quzhou
Summer Data Trend Values (1960-2010)
-3.2<-2.57
-2.56 <-1.96
-1.95 < 0.00
0.01 >1.96
1.97 >2.57
2.58 >3.2>
TSA slope (mm/Year)
-0.45 - -0.31
-0.31 - -0.17
-0.17 - -0.03
-0.03 - 0.11
0.11- 0.25
0.25- 0.39
Summer MK & SP Difference
Trend Values
MK
SP

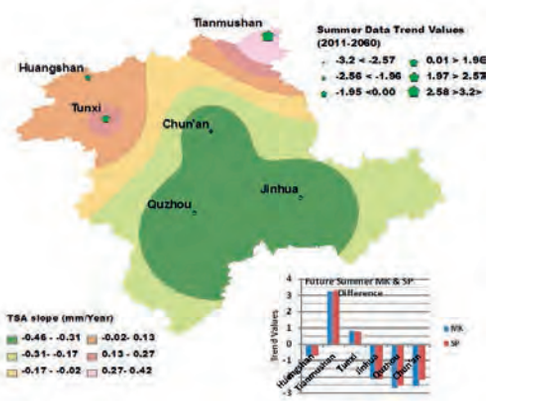
Tianmushan
Huangshan
Tunxi
Chun'an
Jinhua
Quzhou
Summer Data Trend Values (2011-2060)
-3.2 < -2.57
-2.56 < -1.96
-1.95 <0.00
0.01 > 1.96
1.97 > 2.57
2.58 >3.2>
TSA slope (mm/Year)
-0.46 - -0.31
-0.31- -0.17
-0.17 - -0.02
-0.02- 0.13
0.13 - 0.27
0.27- 0.42
Future Summer MK & SP Difference
Trend Values
MK
SP

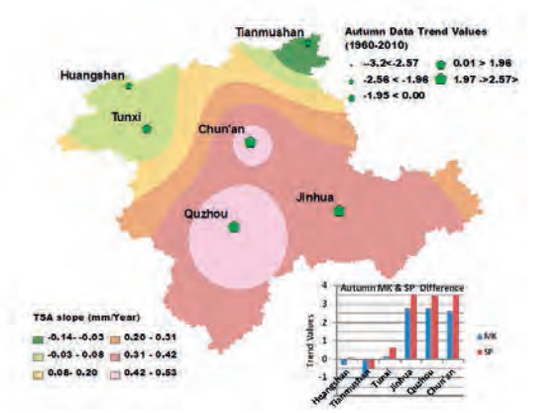
Tianmushan
Huangshan
Tunxi
Chun'an
Jinhua
Quzhou
Autumn Data Trend Values (1960-2010)
-3.2<-2.57
-2.56 < -1.96
-1.95 < 0.00
0.01 > 1.96
1.97 >2.57>
TSA slope (mm/Year)
-0.14- -0.03
-0.03 - 0.08
0.08- 0.20
0.20 - 0.31
0.31 - 0.42
0.42 - 0.53
Autumn MK & SP Difference
Trend Values
MK
SP

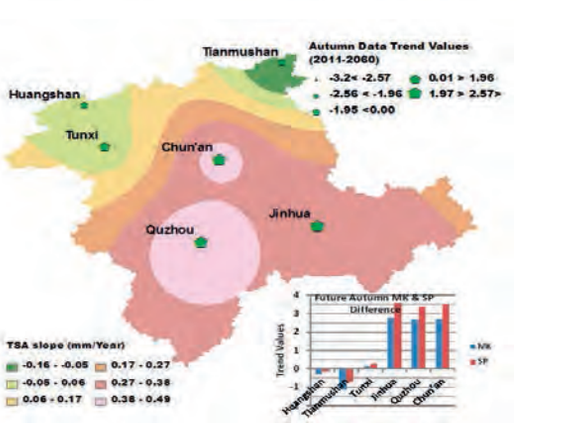
Tianmushan
Huangshan
Tunxi
Chun'an
Jinhua
Quzhou
Autumn Data Trend Values (2011-2060)
-3.2< -2.57
-2.56 < -1.96
-1.95 <0.00
0.01 > 1.96
1.97 > 2.57>
TSA slope (mm/Year)
-0.16 - -0.05
-0.05 - 0.06
0.06 - 0.17
0.17 - 0.27
0.27 - 0.38
0.38 - 0.49
Future Autumn MK & SP Difference
Trend Values
MK
SP

FIGURE 3
MK, SP, and TSA results of annual and seasonal precipitation for the base (1960-2010) and future (2011-2060) data

Abrupt change detection: Results of Sequential Mann Kendall (SQMK) for the base and future data series are given in Table 2, while some stations results are shown in Figure 4.

Base data series results: Results of Sequential Mann Kendall (SQMK) of base and future data series are given in Table 2. Summer data series of Tianmushan and Quzhou stations with significant increasing and decreasing precipitation trends are shown in Figures 4a and 4b, respectively. Results revealed that the base annual precipitation data did not include any significant trend. Winter data series of the base years indicated there is no significant trend for Tianmushan station, whereas a significant increasing trend has been started in 1970s and become significant within 1990s. Base data series of Huangshan, Tianmushan and Tunxi stations did not exhibit any trend, while a significant decreasing trend has been started sometime between 1970-1975 for Chun'an, Jinhua and Quzhou stations and became significant between 1977-1982. There was no significant trend for summer data series of Huangshan and Tunxi stations, whereas an increasing significant trend has been started in 1979 and became significant in 1998. In addition, a significant decreasing trend was evident for Chun'an, Jinhua and Quzhou stations which was started in 1975-1980 and became significant during 1985-1992. No trend was found for Huangshan, Tianmushan and Tunxi stations within autumn data series, whereas a positive increasing trend was obtained for Chun'an, Jinhua and Quzhou stations, which started during 1974-1975 and became significant in 2008.

Future data series: It is really important to know about a possible abrupt start of a trend in the future, so as to prepare for planning and installation of water resources and hydrology projects. There was no significant trend founded for annual future and Huangshan winter data series. In Huangshan, Tunxi, Chun'an, Jinhua and Quzhou stations, a significant increasing trend was started during 2025-2030 and became significant during 2040s. A significant decreasing trend started in 2023-2026 and became significant in 2028 and 2038-2048 was detected for spring and summer data series of Chun'an, Jinhua and Quzhou, respectively, as is given in Table 2. For Tianmushan station, an increasing trend for future summer was found in 2029 and became significant in 2048. Results showed that an increasing significant trend will be started in 2025-2026 and become significant in 2056-2057 for the future autumn's data series, as is given in Table 2.

TABLE 2
SQMK results for base and future

Station name	Year	Annual		Winter		Spring		Summer		Autumn	
	Time series	Base	Future	Base	Future	Base	Future	Base	Future	Base	Future
Huangshan	Start Year			+1974	+2029						
	Significant			+1992	+2042						
Tianmushan	Start Year							+1979	+2029		
	Significant							+1998	+2048		
Tunxi	Start Year			+1974	+2028						
	Significant			+1994	+2042						
Chun'an	Start Year			+1975	+2025	-1973	-2023	-1980	-2026	+1975	+2025
	Significant			+1999	+2049	-1977	-2028	-1988	-2038	+2008	+2056
Jinhua	Start Year			+1974	+2024	-1974	-2024	-1976	-2026	+1974	+2026
	Significant			+1999	+2048	-1982	-2031	-1985	-2038	+2008	+2057
Quzhou	Start Year			+1976	+2026	-1973	-2024	-1975	-2026	+1974	+2026
	Significant			+1999	+2048	-1978	-2028	-1992	-2048	+2008	+2057

(+ sign indicates an increasing trend, while – sign indicates a decreasing one)

Overall watershed trends: Results of MK and TSA showed that monthly data series of January, February, October, November and December exhibit a significantly increasing trend at a rate of 0.22-0.50 mm/year, whereas March, April and May showed significantly decreasing trends ranging from 0.39 to 0.68 mm/year for the whole watershed considering the base data series, as is given in Table 3. Results revealed that winter and autumn seasons are associated with significantly increasing trends of 0.21-0.43 mm/year, whereas spring season precipitation decreased significantly to 0.48 mm/year.

Results of future monthly data series showed that there is a significant increase of 0.14 to 0.25 mm/year in January, October and December months, whereas a significant decreasing trend of 0.24 to 0.33 mm/year was evident in April and May months for future data series, as is given in Table 3. Winter and autumn seasons revealed a significant increase trend at 0.10-0.20 mm/year, whereas spring precipitation significantly decreased to 0.26 mm/year. No significant trend was evident within other data series.

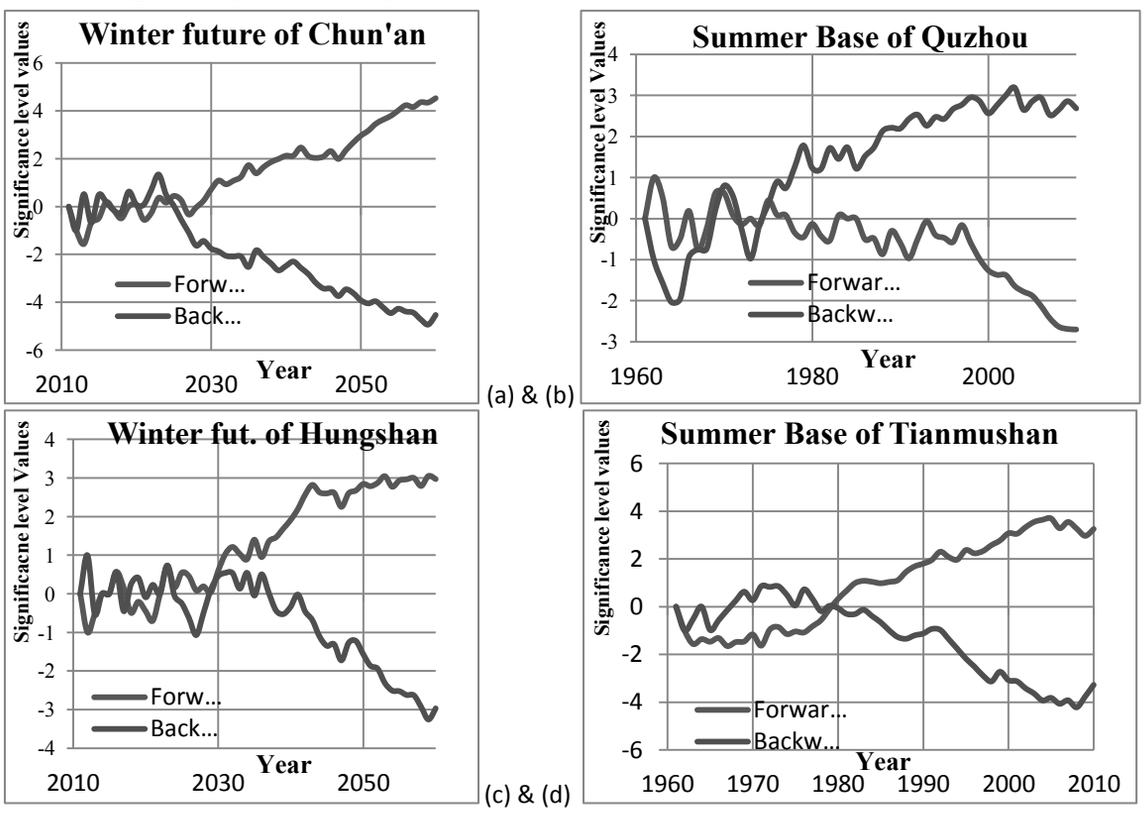

FIGURE 4
SQMK results of summer base of Tianmushan (d),Quzhou (b) and future winter of Chun'an(a) and Huangshan(c) stations

TABLE 3
Overall Watershed Mann Kendall and TSA results

	1960-2010		2011-2060	
Data Series	Z	TSA	Z	TSA
JAN	2.97	0.44	3.00	0.25
FEB	2.10	0.33	1.56	0.12
MAR	-2.23	-0.39	-2.45	-0.20
APR	-2.79	-0.45	-3.22	-0.24
MAY	-2.67	-0.68	-2.97	-0.33
JUN	-0.09	-0.03	-1.08	-0.10
JUL	-0.18	-0.02	-0.61	-0.03
AUG	-0.49	-0.05	-0.64	-0.04
SEP	0.59	0.08	1.10	0.04
OCT	2.57	0.30	2.74	0.14
NOV	2.05	0.22	2.23	0.09
DEC	3.75	0.50	3.58	0.25
Annual	0.28	0.02	0.03	0.00
Winter	4.32	0.43	4.22	0.20
Spring	-3.24	-0.48	-3.37	-0.26
Summer	-1.08	-0.11	-1.90	-0.08
Autumn	2.56	0.21	2.74	0.10

CONCLUSION

The presented study emphasized the predication of precipitation trend at Xin'anjiang-Fuchunjiang watershed and its comparison with the base year's trend. Possible beginning of changes in precipitation trend has also been studied in order to get an idea about future water resources. CMIP5 data has been downscaled using change factor downscaling technique according to local conditions of the watershed. To remove the serial effect of data, non-parametric pre-whitening technique has been employed. Non-parametric Mann Kendall (MK), Spearman's rho (SP/SR), Theil Sen's (TSA) and Sequential Mann Kendall (SQMK) techniques have applied to two different precipitation data series (1960-2010 and 2011-2060). Mann Kendall and Spearman's rho have been applied to detect any significant trend within a data series, whereas TSA was used to get the magnitude of the detected trend. The SQMK non-parametric technique has been applied in order to get an idea about the beginning of a possible change in precipitation trend.

Results revealed that the precipitation trend at the northern most part of the study area is totally opposite to that in other part of the study region. Monthly results of the base and future data series revealed that October, November, December and January have positive increasing trends, whereas significant negative trends were found in March, April, May data series for most of the stations in the study area, except for Tianmushan station where a totally different trend was obtained. Results revealed that there is no significant change in annual precipitation trend for the base and future data series, whereaswinter and autumn exhibit up to 0.5 mm/year increase and summer and spring indicate up to 0.45 mm/year decrease in precipitation.

During 1970s, a positive change in precipitation trend started in winter and summer seasons, whereas a negative change in precipitation trend in the summer and autumn seasons has been observed for the base data series at the majority of stations in the study area. The increasing trend in the future winter and autumn data series began during 2020s, whereas summer and spring precipitation decrease started during the same decade in majority of stations within the study area.

This study will be fruitful for the hydrology and water resource planners who plan for water allocation within the study area. This will also be helpful for those engineers working on flood control in the study area and power generation at the Xinan'jiang hydropower station. Further study using different CMIP5 and hydrological models is needed to predict the exact flow of water in the study region.

ACKNOWLEDGMENT

The author thanks to the Priority Academic Program Development of Jiangsu Higher Education Institutions （PAPD） for the funding of this research project.

REFERENCES

[1] Chou C, CW Lan. Changes in the annual range of precipitation under global warming. J Climate. 25 (2011) 222–35, doi: 10.1175/JCLI-D-11-00097.1.

[2] Campling P, A Gobin, J Feyen. Temporal and spatial rainfall analysis across a humid tropical catchment. Hydol Process. 15 (2001.) 359–75.

[3] Maragatham RS. Trend analysis of rainfall data: a comparative study of existing methods. Int J Phys Math Sci. 2 (2011) 13–8.

[4] Allen MR, WJ Ingram. Constraints on future changes in climate and the hydrologic cycle. Nature. (2002) 224–32.

[5] Meehl GA, TF Stocker, WD Collins, P Frienlingstein, AT Gaye, JM Gregory, et al. Global climate projections, in: Climate Change: The Physical Science Basis, Contribution of Working Group I to the Fourth Assessment Report of the Intergovernmental Panel of Climate Change,edited by: Solomon, S., Qin, D., Manning, M., Chen, Z., Marquis, M., Averyt, K. B., Tignor, M., and Miller, H. L. Cambridge University, Cambridge University Press,Cambridge, UK and New York, NY, USA,, 2007. pp. 747–845.

[6] Trenberth KE, PD Jones, P Ambenje, R Bojariu, D Easterling, A Klein Tank, et al. Observations: surface and atmospheric climate change, in: Climate Change 2007.The Physical Science Basis, Contribution of Working Group I to the Fourth Assessment Report of the Intergovernmental Panel on Climate Change, edited by: Solomon, S., Qin, D., Manning, M., Chen, Z., Marquis, M., Averyt, K. B., Tignor, M., and Miller H. L. Cambridge, UK and New York, NY, USA, Cambridge University Press, 2007. pp. 235–336, .

[7] Fu G, J Yu, X Yu, R Ouyang, Y Zhang, P Wang, et al. Temporal variation of extreme rainfall events in China, 1961–2009. Journal of Hydrology. 487 (2013) 48-59.

[8] Chen F, W Huang, L Jin, J Chen, J Wang. Spatiotemporal precipitation variations in the arid Central Asia in the context of global warming. Science China Earth Sciences. 54 (2011) 1812-21, doi: 10.1007/s11430-011-4333-8.

[9] IPCC. Climate Change 2007: The Physical Science Basis,Contribution of Working Group I to the Fourth Assessment Report of the Intergovernmental Panel of Climate Change. Cambridge University Press,, Cambridge and New York, , 2007. pp. 7–258.

[10] IPCC. Climate Change 2013: The Physical Science Basis, Contribution of Working Group I to the Fifth Assessment Report of the Intergovernmental Panel of Climate Change. Cambridge University Press,Cambridge, UK,5-204, 2013.

[11] Ding Y, Y Sun, Z Wang, Y Zhu, Y Song. Inter-decadal variation of the summer precipitation in China and its association with decreasing Asian summer monsoon Part II: Possible causes. International Journal of Climatology. 29 (2009) 1926-44, doi: 10.1002/joc.1759.

[12] Ding Y, Z Wang, Y Sun. Inter-decadal variation of the summer precipitation in East China and its association with decreasing Asian summer monsoon.Part I: Observed evidences. International Journal of Climatology. 28 (2008) 1139-61, doi: 10.1002/joc.1615.

[13] Wang YQ, L Zhou. Observed trends in extreme precipitation events in China during 1961–2001 and the associated changes in large-scale

circulation. Geophysical Research Letters. 32 (2005), doi: 10.1029/2005gl022574.
[14] Chen L, R Wu. Interannual and Decadal Variations of Snow Cover over Qinghai-Xizang Plateau and Their Relationships to Summer Monsoon Rainfall in China. Adv Atmos Sci. (2000) 8–30.
[15] Ho CH, JH Kim, KM Lau, KM Kim, DY Gong, YB Lee. Interdecadal changes in heavy rainfall in China during the northern summer,. Terr Atmos Ocean Sci. 16 (2005) 1163–76,.
[16] Wang HJ. The weakening of the Asian monsoon circulation after the end of 1970s, . Adv Atmos Sci. 18 (2001) 376-86.
[17] Hu Z-Z, S Yang, R Wu. Long-term climate variations in China and global warming signals. Journal of Geophysical Research. 108 (2003), doi: 10.1029/2003jd003651.
[18] Yang F, KM Lau. Trend and variability of China precipitation in spring and summer: linkage to sea-surface temperatures. International Journal of Climatology. 24 (2004) 1625-44, doi: 10.1002/joc.1094.
[19] Zhou T, D Gong, J Li, B Li. Detecting and understanding the multi-decadal variability of the East Asian Summer Monsoon – Recent progress and state of affairs. Meteorologische Zeitschrift. 18 (2009) 455-67, doi: 10.1127/0941-2948/2009/0396.
[20] Anli AS. REGIONAL AND POINT PRECIPITATION ESTIMATION FOR 1975-2010 PERIOD OVER SEMI-ARID CENTRAL ANATOLIA REGION OF TURKEY. Fresenius Environmental Bulletin. 24 (2015) 632-43.
[21] Manish KG. Statistical analysis of long term trends of rainfall during 1901–2002 at Assam, India, . Water Resour Manag. 28 (2014) 1501–15, doi: 10.1007/s11269-014-0529-y.
[22] Wang SJ, XL Zhang, ZG Liu, DM Wang. Trend analysis of precipitation in the Jinsha River Basin in China. J Hydrometeorol. 14 (2013) 290–303, doi: 10.1175/JHM-D-12-033.1.
[23] Zhong AH, YQ Li. Spatial and temporal distribution characteristics and variation tendency of precipitation in Mianyang, Sichuan Province, . Plateau Mountain Meteor Res. 29 (2009) 63–9.
[24] Xu ZX, ZF Liu, GB Fu, YN Chen. Trends of major hydroclimatic variables in the Tarim River basin during the past 50 years. J Arid Environ. 74 (2010) 256–67, doi: 10.1016/j.jaridenv.2009.08.014.
[25] Xu C, J Li, J Zhao, S Gao, Y Chen. Climate variations in northern Xinjiang of China over the past 50 years under global warming. Quaternary International. 358 (2015) 83-92, doi: 10.1016/j.quaint.2014.10.025.
[26] Gong ZS, M He. Relationship between summer rainfall in Changjiang River valley and SSTA of various seasons, Meteor. . Mon. 32 (2006) 56–61.
[27] Su BD, G Marco, T Jiang, GY Ren. Probability distribution of precipitation extremes over the Yangtze River Basin during 1960–2005. Adv Climate Change Res. 3 (2007) 208–13.
[28] Su BD, T Jiang. Distribution feature of time series of extreme precipitation over the Yangtze River Basin, . J Lake Sci, . 20 (2008) 123–8.
[29] Xu ZX, JY Li, CM Liu. Long-term trend analysis for major climate variables in the Yellow River basin, . Hydrol Process. 21 (2007) 1935-48, doi: doi:10.1002/hyp.6405.
[30] Zhang YL, QZ Gao, YG Ding, T Jiang. Analysis of time-spatial characteristics and evolutional trends of summer precipitation in the Yangtze River catchment. J Trop Meteorol. 22 (2006) 161-8.
[31] Zhang Y, XR Du. Analysis of temperature and precipitation change over last 50 years in Leshan City. Plateau Mountain Meteor Res,. 28, (2008) 68-71.
[32] Gleick P. Climate change, hydrology, and water resources. Rev Geophys 27 (1989) 329-44.
[33] Kiely G. Climate change in Ireland from precipitation and streamflow observations. . Adv Water Resour. 23 (1999) 141-51.
[34] Xu. C. Climate change and hydrologic models: a review of existing gaps and recent research developments. . Water Resour Manag 13 (1999) 369-82.
[35] Sen B, R Kilinc, B Sen, E Sonuc. VALIDATION OF DAILY PRECIPITATION ESTIMATES OF THE REGIONAL CLIMATE MODEL REGCM4 OVER THE DOMAINS IN TURKEY WITH NWP VERIFICATION TECHNIQUES. Fresenius Environmental Bulletin. 23 (2014) 1892-903.
[36] Christensen NS, Wood AW, Voisin N, Lettenmaier DP, P RN. The effects of climate change on the hydrology and water resources of the Colorado river basin. . Clim Chang. 62 (2004) 337-63.
[37] Charlton R, Fealy R, Moore S, Sweeney J, M C. Assessing the impact of climate change on water supply and flood hazard in Ireland using statistical downscaling and hydrological modelling techniques. Clim Chang 74 (2006) 475-91.
[38] Steele-Dunne S, P Lynch, R McGrath, T Semmler, S Wang, J Hanafin, et al. The impacts of climate change on hydrology in Ireland. Journal of Hydrology. 356 (2008) 28-45, doi: 10.1016/j.jhydrol.2008.03.025.
[39] Ludwig R, May I, Turcotte R, Vescovi L, Braun M, Cyr J-F, et al. The role of hydrological model complexity and uncertainty in climate change impact assessment. Adv Geosci 21 (2009) 63-71.
[40] Bastola S, Murphy C, S J. The role of hydrological modelling uncertainties in climate change impact assessments of Irish river catchments. . Adv Water Resour 34 (2011) 562-76.
[41] Risbey JS, E D. Observed Sacramento Basin streamflow response to precipitation and temperature changes and its relevance to climate impact studies. . J Hydrol. 184 (1996) 209-23.
[42] Whitfield PH, Cannon AJ. Recent variations in climate and hydrology in Canada. . Can Water Resour J 25: (2000) 19-65.
[43] Sonali P, KD Nagesh. Review of trend detection methods and their application to detect temperature changes in India. JHydrol 476 (2013) 212-27.
[44] Mann HB. Non-parametric tests against trend. . Econometrica. 13 (1945) 245-59.
[45] Kendall MG. Rank Correlation Measures. Charles Griffin, London, 1975.
[46] Theil H. A rank-invariant method of linear and polynomial regression analysis. Proc K Ned Akad Wet. A53 (1950) 386-92.
[47] Sen PK. Estimates of the regression coefficient based on Kendall's tau. J Am Stat Assoc. 63 (324) (1968) 1379-89.

[48] Nalley D, J Adamowski, K B., Ozga-Zielinski. Trend detection in surface air temperature in Ontario and Quebec, Canada during 1967-2006 using the discrete wavelet transform. Atmospheric Research 132-133 (2013) 375-98.

[49] Ying GUa, Jin LINa, X-L WANG, X-J ZHANG. Trend of Annual Runoff for Major Rivers in China under Climate Change. 2012 International Conference on Modern Hydraulic Engineering2012.

[50] Karaburun A, A Demirci, F Kara. Analysis of spatially distributed annual, seasonal and monthly temperatures in Istanbul from 1975 to 2006. World Applied Sciences Journal , . 12 (10) (2011) 1662-75.

[51] Ceppi P, SC Scherrer, AM Fischer, C Appenzeller. Revisiting Swiss temperature trends 1959-2008. International Journal of Climatology 32 (2) (2012) 203-13.

[52] Fan X-H, M-B Wang. Change trends of air temperature and precipitation over Shanxi Province, China. Theor Appl Climatol 103 (3-4) (2011) 519-31.

[53] Jiang Y, Y Luo, Z Zhao, S Tao. Changes in wind speed over China during 1956-2004. Theoretical and Applied Climatology 99 (3-4) (2010) 421-30.

[54] ElNesr MN, MM Abu-Zreig, AA Alazba. Temperature trends and distribution in the Arabian Peninsula. American Journal of Environmental Sciences. 6 (2010) 191-203.

[55] Longobardi A, P Villani. Trend analysis of annual and seasonal rainfall time series in the Mediterranean area. International Journal of Climatology, . 30 (2010) 1538–46.

[56] Yanming Z, W. Jun, W Xinhua. Study on the change trend of precipitation and temperature in Kunming city based on Mann-Kendall analysis. Future Computer, Communication, Control and Automation. vol 119 (2011) of Advances in Intelligent and Soft Computing, pp. 505-13.

[57] Z. F. Yang, Y. Yan, Q. Liu. The relationship of streamflowprecipitation- temperature in the Yellow River Basin of China during 1961-2000. Procedia Environmental Sciences, . vol. 13 (2012) pp. 2336–45.

[58] Q.-X. Wang, X.-H. Fan, Z.-D. Qin, M-B Wang. Change trends of temperature and precipitation in the Loess Plateau Region of China, 1961-2010. Global and Planetary Change. 92-93 (2012.) 138-47.

[59] Topaloglu F, M Oezfidaner. REGIONAL TRENDS OF PRECIPITATION IN TURKEY. Fresenius Environmental Bulletin. 21 (2012) 2908-15.

[60] S. Yue P, Pilon, G Cavadias. Power of the Mann-Kendall and Spearman's rho tests for detecting monotonic trends in hydrological series. Journal of Hydrology. 259 (2002) 254-71.

[61] Kahya E, S Kalaycı. Trend analysis of streamflow in Turkey. Journal of Hydrology. 289 (2004) 128-44.

[62] Z. L. Li, Z. X. Xu, J. Y. Li, Z. J. Li. Shift trend and step changes for runoff time series in the Shiyang River Basin, Northwest China,. Hydrological Processes. 22 (2008) 4639-46.

[63] C. Yaning, X. Changchun, HXe al. Fifty-year climate change and its effect on annual runoff in the TarimRiver Basin, China,. Quaternary International. 208 (2009) 53-61.

[64] M.Shadmani, S.Marofi, M.Roknian. Trendanalysis inreference evapotranspiration usingMann-Kendall and Spearman's Rho tests in arid regions of Iran. Water ResourcesManagement. 26, (2012) 211-24.

[65] Partal T, E Kahya. Trend analysis in Turkish precipitation data. Hydrol Process. 20 (2006) 2011-26.

[66] Some'e BS, A Ezani, H Tabari. Spatiotemporal trends and change point of precipitation in Iran. Atmos Res. 113 (2012) 1-12.

[67] Sonali P, KD Nagesh. Review of trend detection methods and their application to detect temperature changes in India. JHydrol. 476 (2013) 212-27.

[68] Diaz-Nieto J, Wilby R. A comparison of statistical downscaling and climate change factor methods: impacts on low flows in the River Thames, United Kingdom. . Clim Chang 69 (2005) 245-68.

[69] Hay LE, Wilby RL, LG . A comparison of delta change and downscaled GCM scenarios for three mountainous basins in the United States. JAWRA J Am Water Resour Assoc. 36 (2000) 387-97.

[70] S. Yue, P. Pilon, G. Cavadias. Power of the Mann-Kendall and Spearman's rho tests for detecting monotonic trends in hydrological series. Journal of Hydrology. 259 (2002) 254-71.

[71] On¨oz B, M. Bayazit. Block bootstrap for Mann-Kendall trend test of serially dependent data. Hydrological Processes. 26 (2012) 3552-60.

[72] M. Yaseen, T. Rientjes, G. Nabi, H. ur-Rehman, M. Latif. Assessment of recent temperature trends inMangla watershed,. Journal of Himalayan Earth Sciences,. 47 (2014) 107-21.

[73] Gocic M, S Trajkovic. Analysis of changes in meteorological variables using Mann-Kendall and Sen's slope estimator statistical tests in Serbia. Global and Planetary Change. 100 (2013) 172-82, doi: 10.1016/j.gloplacha.2012.10.014.

[74] Lehmann EL. Nonparametrics, Statistical Methods Based on Ranks. Holden-Day, San Francisco,Calif, USA, 1975.

[75] R. Sneyers. On the statistical analysis of series of observations. Technical Note 143,WMO no 415,World Meteorological Organization1990.

[76] Dahmen ER, M. J. Hall, , . Screening of Hydrological Data:Tests for Stationarity and Relative Consistency. Publication #49,ILRI,Wageningen, The Netherlands, 1990.

[77] Tabari H, P Hosseinzadeh Talaee. Analysis of trends in temperature data in arid and semi-arid regions of Iran. Global and Planetary Change. 79 (1-2) (2011) 1-10.

[78] Tabari H, P Hosseinzadeh Talaee. Temporal variability of precipitation over Iran: 1966-2005. Journal of Hydrology. 396 (3-4) (2011) 313-20.

Received: **06.10.2015**
Accepted: **20.12.2015**

CORRESPONDING AUTHOR

Guohua Fang
Hohai University

College of Water Conservancy and Hydropower engineering
Nanjing, 210098 - CHINA

e-mail:hhufgh@126.com

by PSP Volume 25 – No. 1/ 2016, pages 103-112 Fresenius Environmental Bulletin

APPLICATION OF HEAVY METALS IN STREET DUST IN THE MONITORING OF CHANGES IN ENVIRONMENT

Wojciech Kwasowski[1], Teresa Kozanecka[1], Ewa Beata Górska[2], Dariusz Gozdowski[3], Pawel Kowalczyk[4]*

[1]Department of Environmental Soil Sciences, Warsaw University of Life Sciences-SGGW, Nowoursynowska 166, 02-787 Warsaw, Poland,
[2]Department of Microbial Biology, Faculty of Agriculture and Biology, Warsaw University of Life Sciences-SGGW, Nowoursynowska 166, 02-787 Warsaw, Poland,
[3]Department of Experimental Statistics and Bioinformatics, Faculty of Agriculture and Biology, Warsaw University of Life Sciences-SGGW,
[4]Bionicum LTD, Chełmska 21, 00-724, Warsaw, Poland.

ABSTRACT

The presented investigations were focused on the content of heavy metals (Zn, Cu, Pb, Cd) in street dust from localities in Central Poland with variable urban, industrial and transportation development. Forms soluble in 20% HCl were subject to the analysis. It has been concluded that the content of Zn, Cu, Pb and Cd in street dust did not depend on the agglomeration size but usually on the degree of urbanization and industrial development. The content of Zn and Cd in street dust was significantly influenced by transportation. In Central Poland the pattern of heavy metals in street dust is according to the following series of decreasing values: Zn>Cu>Pb>Cd or Zn>Pb>Cu>Cd.

KEYWORDS:
Heavy metals, street dust, soil, urban development

INTRODUCTION

Development of human civilization influences the increase of heavy metal content in soil, atmosphere and water, which may cause irreversible harmful effects in these environmental elements. One of the sources of heavy metals in the environment may also be street dust deposited on the margins and surfaces of roads and streets [1, 2 , 3, 4, 5, 6,7].

The sources of heavy metals in street dust include for instance the components of exhaust fumes, rubbed off road pavements, car tires and metal elements of car engines. The dust comprises also airborne soil particles as well as atmospheric rain of industrial and urban dusts. Existing literature [3,7] clearly indicates gradual pollution by trace elements of agricultural and forest soils lying adjacent to transportation routes.

The excessive content of heavy metals in the environment influences the biological properties of soils and groundwater, and causes pollution of the food chain [6, 8, 9, 10]. At present, heavy metals can be found almost everywhere, in soil and in food. The presence of street dust with heavy metals causes that they are accumulated in human bodies and thus become health hazards [8, 11, 12]. The aim of the investigations was testing the content of heavy metals in street dust from areas with diverse urban, industrial and transportation development, located in Central Poland.

MATERIAL AND METHODS

The investigations were conducted in Central Poland (Fig. 1). Four objects differing in the degree of urban, industrial and transportation development were selected:

FIGURE 1
Localization of investigate place

Object 1 – Warsaw city with the highest degree of urban and transportation development from among the selected objects, inhabited by about 2 million resident and migrant population. The investigations were conducted in 8 sites along roads located in the Warszawa-Ursynów district with intense traffic comprising motor cars and urban transportation. Worth noting is the fact that the localities along the margins of the investigated roads were subject to frequent sweeping and washing;

Object 2 – Wiązowna village with a low population density of 91 pop./km^2 (average population in Poland: 124 pop./km^2), situated about 50 km from Warsaw; an agglomeration with recreational–service–housing functions;

Object 3 – Karczew town situated about 40 km from Warsaw, characterized by a larger number of enterprises than Wiązowna: foodstuffs, meat, poultry, and dairy produce, production of plastics and cables, wrapping, as well as printing, chemical and iron-work enterprises;

Object 4 – Lipsko town situated about 150 km from Warsaw, a town with high industrial development (production of sandwich panels, fruit and vegetable production, dairy and meat produce, metal industry), surrounded by farmlands and forests.

Three regions with low (nos. 1, 2, 3, 10, 11, 12, 19, 20, 21), medium (nos. 4, 5, 6, 13, 14, 15, 22, 23, 24) and high (nos. 7, 8, 9, 16, 17, 18, 25, 26, 27) traffic density were selected in each of the objects (except Warsaw) (Table 1).

TABLE 1
Content of heavy metals in street dust in localities outside Warsaw (mg·kg $^{-1}$).

Object no.	Locality	Zn	Cu	Pb	Cd
1	Wiązowna	17.0	16.5	4.5	0.25
2		27.0	81.6	5.0	0.30
3		25.0	6.9	5.0	0.10
4		30.0	9.4	12.5	0.25
5		48.5	12.6	15.5	0.80
6		53.5	8.1	28.0	0.70
7		113.0	25.7	15.0	0.50
8		83.5	49.5	14.0	0.25
9		37.5	12.1	10.5	0.40
10	Karczew	30.0	9.35	12.5	0.40
11		74.0	48.8	8.0	0.28
12		89.0	62.6	233.2	0.32
13		44.0	112.9	28.0	0.36
14		63.0	137.7	28.0	0.29
15		94.0	49.8	15.6	0.40
16		95.0	22.6	12.0	0.56
17		132.0	67.0	93.6	0.68
18		52.0	52.6	9.2	0.42
19	Lipsko	44.4	8.6	9.4	0.28
20		88.8	15.0	37.8	0.66
21		71.6	20.2	24.6	0.38
22		91.6	22.0	21.0	0.44
23		95.4	20.9	34.0	0.54
24		101.2	36.0	30.8	0.54
25		182.0	32.2	34.4	1.1
26		211.0	30.1	42.2	0.8
27		253.6	31.2	42.8	0.9
Cv (%)	68.7	87.7	81.67	49.0	

Regions with low traffic density included roads running through forests, fields and housing zones, entrance road to the municipal waste dump, transportation stops, roads running through remote areas and roads with small enterprises located along them. Roads with medium traffic density were located in the centres of the analyzed objects in sites with medium density, including entrance roads to certain objects and state roads. Most sites with high traffic density were located along the main entrance roads in the analyzed objects, characterized by everyday intense traffic density of both motor cars and public transportation, with numerous enterprises, warehouses and housing objects.

Samples of street dust were collected to plastic bags from the road margins, from three points along 10 m of the selected sites.

The dust samples were dried, sieved through a perlon sieve with mesh size of 1 mm, and ground in an agate mortar. In this material the pH value in KCl was measured electrometrically, and after mineralization in dry conditions in 480^{o}C the material was dissolved in 20% HCl in an Ethos Plus Melestone microwave digester. As a result, solutions of Zn, Cu, Pb and Cd forms soluble in 20% HCl were obtained. The content of the investigated elements was determined using atomic adsorption spectrophotometry (AAS). Certified reference material EnviroMAT SS-2 was used for each series of analyses.

The concordance of the obtained results with reference material was at the level of 100%. Assessment of the content of the elements in street dust was made by comparing the obtained results with the heavy metal content in soils considered as the geochemical background for soils in Poland [13], as well as by comparison to norms of the Ministry of the Environment [14] Regulation of the Minister of the Environment of 9th September 2001 on the soil quality standards and ground quality standards, Journal of Laws, no. 165, pos. 1359 of 4th October 2002) for soils, because ranges for

street dust have not been established. Range correlation analysis was used to assess the relationships between particular heavy metals. The analyses were conducted using Statgraphics 4.1 software.

RESULTS

The pH values in the samples of street dust were approximately the same in the analyzed objects; they varied between 7.3 and 8.9. Zn, Cu, Pb and Cd contents in street dust collected from the road margins of the analyzed objects were variable; the mean contents of heavy metals for the entire analyzed area were: 85.8 mg·kg^{-1} for Zn, 35.55 mg·kg^{-1} for Cu, 21.9 mg·kg^{-1} for Pb and 0.76 mg·kg^{-1} for Cd (Tables 1 and 2).

TABLE 2
Mean contents of heavy metals in street dust in particular studied objects (mg·kg^{-1})

Element	Locality	Range	Mean value	Mean for the entire area	Geochemical background
Zn	Warszawa	70.70-126.0	93.5	17.0-253.6	5.0-59.0
	Wiązowna	17.0-113.0	48.3		
	Karczew	30.0-132.0	74.8	85.8	30.0
	Lipsko	44.0-253.6	126.6		
Cu	Warszawa	12.8-39.3	30.9	6.9-137.7	0.4-23.5
	Wiązowna	6.9-81.6	24.7		
	Karczew	9.4-137.7	62.6	35.6	7.1
	Lipsko	8.6-32.2	24.0		
Pb	Warszawa	13.5-29.8	20.3	4.5-233.2	0.5-21.0
	Wiązowna	4.5-28.0	12.2		
	Karczew	8.0-93.6 (8.0-233.2)*	24.2 (48.9)*	21.9 (28.1)*	9.8
	Lipsko	9.40-42.80	30.80		
Cd	Warszawa	0.45-1.95	1.60	0.10-1.95	0.03-1.00
	Wiązowna	0.10-0.80	0.39	0.76	0.18
	Karczew	0.28-0.68	0.41		
	Lipsko	0.28-1.10	0.64		

Explanations: * calculated for mean value

In Warsaw, the content of zinc in street dust collected from the margins of the streets near bus-stops varied between 70.7 and 126.0 mg·kg^{-1}, and attained averagely 93.5 mg·kg^{-1}. The content of zinc in Warsaw insignificantly varied among the analyzed sites (Tables 2 and 3). The variability coefficient was 21.6%. Higher amounts of zinc in Warsaw were noted in sites where street dust was not swept away frequently (sites 4, 5). The average content of Zn in the street dust from Warsaw exceeded three times the geochemical background estimated for the soils of Poland [15] and exceeded the average value obtained for all objects.

In turn, in areas outside the Warsaw agglomeration, the highest contents of zinc were noted in street dust in Lipsko town located at the largest distance from Warsaw (Tables 1 and 2). In Lipsko the content of Zn in street dust averagely exceeded four times the geochemical background for soils of Poland and in some localities (sites 25, 26, 27) along which were situated industrial enterprises and transportation routes – even 7 and 8 times (Tables 1 and 2). In Wiązowna and Karczew the street dust contained averagely less Zn than the street dust from Lipsko and Warsaw.

In areas outside Warsaw in some localities (sites 7, 17, 24, 25, 26, 27), the Zn content in street dust exceeded the admissible concentrations of this element in natural and protected soils >100 mg·kg^{-1} announced in the Journal of Laws by the Ministry of the Environment in 2002 (tab.7). These sites include transportation routes with high density of motorcars and urban transportation, near which occurred services and production enterprises. The variability coefficient for zinc in street dust collected from areas outside Warsaw was significantly higher and reached 68.7% (Table 1) in comparison to the data from Warsaw (Table 3).

TABLE 3
Heavy metal content in street dust collected from selected sites in Warsaw (mg·kg^{-1})

No.	Sites	Zn	Cu	Pb	Cd
1.	At exit road from Warsaw	77.5	12.8	16.5	1.90
2.	Bus-stop on Nowoursynowska Str.	70.7	25.2	14.2	0.45
3.	Bus-stop on Nowoursynowska Str.	94.0	37.1	13.5	1.90
4.	Corner of Ciszewskiego and Anody streets	121.1	23.0	17.5	1.57
5.	Entrance road to parking lot	126.0	32.5	29.8	1.40
6.	Klinika bus-stop	94.5	39.3	22.5	1.85
7.	Stary Ursynów bus-stop	81.5	16.1	19.1	1.75
8.	Old campus near Economical Building	82.5	25.1	26.5	1.95
	Range	70.7 -126.0	12.8-39.3	13.5-29.8	0.45-1.95
	Mean	**(93.5)**	**(30.9)**	**(20.3)**	**(1.60)**
	Cv (%)	21.6	35.8	29.3	31.3

Comparison of the obtained Zn content with the values given in literature reports from the last 10 years (Table 4) allows to conclude that the Zn content in Central Poland again reveals an uptrend. This increase may be caused by the appearance of new zinc sources in the environment or the increase of values from existing sources such as rise of transportation density and poor condition of the vehicles, road quality, increased number of housing and small enterprises.

Copper in street dust varied in the investigated areas between 6.9 and 137.7 mg·kg^{-1} and clearly differed between the sampling localities (Tables 1, 2, 3). In Warsaw, Wiązowna and Lipsko, the average values of Cu in street dust were similar and lower than the average for the entire analyzed area. Only in Karczew situated 40 km from Warsaw, averagely higher values of Cu were noted in street dust in comparison to the average for the entire analyzed area. Higher Cu contents were observed in street dust collected from roads along which were situated shops, industrial enterprises (e.g. poultry–meat produce or cable manufactory), along the entrance road to the municipal waste dump and roads to other localities (sites: 2, 8, 11, 12, 13, 14, 17, 18). In comparison to studies conducted in 1998–2007 in Central Poland, the content of copper in street dust shows an uptrend (Table 4). The presented studies indicate that in 30% of the analyzed sites, street dust collected outside Warsaw exceeded the norms for copper for type A soils given in the appendix to the Regulation of the Minister of the Environment from 2002 on the quality of soils and grounds reaching < 30 mg·kg-^{1} Cu for unpolluted soils (group A), (tab.7).

The mean values of lead in street dust from Warsaw, Wiązowna, Karczew and Lipsko varied insignificantly and reached: 12.23; 20.30; 24.16; 30.8 mg·kg^{-1}, respectively (Table 2). The highest content of lead in street dust (233.2 mg·kg^{-1}) was noted in Karczew (site 12) in a sample collected from the entrance road to the municipal waste dump as well as in street dust collected from the main exit road from this town surrounded on both sides by houses (site 17), and in Lipsko in street dust from roads adjacent to industrial enterprises (sites 25, 26, 27). The variability coefficient of lead in street dust from the area outside Warsaw was 81.67% and higher than in Warsaw (Tables 1, 2, 3). In Warsaw the content of lead in street dust was rather invariable, which may be explained by a similar traffic density, good quality of vehicles, similar urban conditions as well as frequent road sweeping. These measures largely caused decrease of the content of lead and other heavy metals in street dust. In Warsaw there is a lowest variability coefficient for lead in street dust (29.3%), which suggests that the main source of lead pollution in Warsaw is traffic (Table 2).

The content of lead in street dust in Warsaw was about twice higher than the geochemical background. The mean contents of Pb in street dust from Warsaw were similar to the content of lead in areas outside Warsaw (Table 2). In street dust collected in sites 12 and 17, lead content (50 mg·kg-^{1}) exceeded values given by the Ministry of the Environment for soils in natural and protected areas (group A) tab.7.

Comparison of the obtained results with earlier studies of street dust from Central Poland shows that from 2003 the content of lead in the environment is maintained at a similar level (Table 4).

The highest content of cadmium – averagely 1.60 mg·kg^{-1} – was noted in street dust from

Warsaw. The mean content of cadmium in street dust from Warsaw exceeded the geochemical background of this element (0.18 mg·kg^{-1}) almost 10 times and showed low variability among the particular sites (Tables 2 and 3). In turn, the content of cadmium in street dust from areas outside Warsaw was about 3 to 4 times lower than the content of cadmium in Warsaw (Tables 1 and 2). Usually, higher contents of cadmium in areas outside Warsaw were noted in the vicinity of various industrial enterprises (sites 25, 26, 27), as well as in street dust collected from roads in housing zones (sites 5 and 6). The variability coefficient for cadmium in areas outside Warsaw was 49.0% and similar to the variability coefficient of street dust from Warsaw (31.3%) (Tables 1 and 3). As evidenced by the obtained results, the largest source of cadmium in the environment was traffic as well as various industries.

Earlier investigations [2, 16, 17] and the presented analyses of street dust indicate that the mean content of cadmium in the environment in the study area is maintained at a similar level for the last 10 years (Table 4).

TABLE 4
Changes in the heavy metal content in street dust in Warsaw and outside Warsaw during the last 10 years based on the results of various authors and the soil geochemical background (mg·kg^{-1})

Year	Zn	Cu	Pb	Cd
1998 *	**230.9** (61-460)	**57.4** (11-156)	**79.9** (24-282)	**0.95** (0.2-2.6)
2003 **	**63.6** (13-173)	**30.6** (3-84)	**33.8** (12-124)	**0.67** (0.48-2.16)
2007***	**65** (22-133)	**20.5** (6-62)	**20.1** (8-72)	**0.80** (0.46 - 1.34)
2012****	**85.8** (17.0-253.6)	**35.6** (6.9-137.7)	**21.9** (4.5-233.2) **28.1***	**0.76** (0.1-1.95)
Background	**30.0** (5.0-59.0)	**7.1** (0.4-23.5)	**9.8** (0.5-21.0)	**0.18** (0.03-1.0)

* Czarnowska K., Bednarz I. (2000)
** Kozanecka T., Czarnowska K., Jaworska A. (2003)
*** Kozanecka T., Czarnowska K., Łaszczyk K. (2007
**** this report

The calculated range coefficients between the content of particular heavy metals in street dust from areas outside the Warsaw agglomeration have shown positive relationships between Zn and Pb, Zn and Cd as well as Pb and Cd (Table 5). The increase of zinc content in street dust has significantly influenced the increased content of cadmium and lead. This causes that in these areas the increased supply of one of these elements at the same time contributed to the increase of the content of each of these elements in street dust.

TABLE 5
Rank correlation coefficients between the content of particular heavy metals in street dust from outside Warsaw

	Zn	Cu	Pb	Cd
Zn	1.000	0.347	0.725*	0.689*
Cu	0.347	1.000	0.290	0.008
Pb	0.725*	0.290	1.000	0.630*
Cd	0.689*	0.008	0.630*	1.000

* statistically significant correlations at the level P=0.05

TABLE 6
Mean values reflected as average and median values (in parentheses) of the heavy metal content in street dust from sites with variable traffic density outside Warsaw (mg·kg^{-1})*

Traffic density	Zn	Cu	Pb	Cd
low	51.87 (44.4)a	29.95 (16.5)a	37.78 (9.4)a	0.33 (0.30)a
medium	69.02 (63.0)a	45.49 (22.0)a	23.71 (28.0)a	0.48 (0.44)a
high	128.84 (113.0)b	35.89 (31.2)a	30.41 (15.0)a	0.62 (0.56)a

*The different letters refer to statistically significant differences between various levels of traffic density (statistically significant differences were noted only for Zn).

It has also been observed that the traffic density in a given area variously influenced the heavy metal content in street dust (Table 6). The content of Zn in street dust was significantly higher in sites with high traffic density in comparison to objects with low or medium traffic density. In turn, the development of urbanization and traffic did not significantly influence the increase of the Cu, Pb and Cd contents. It should be emphasized than in the case of cadmium, its content rises with the development of traffic and industry.

DISCUSSION

The presented investigations show that the heavy metal content in street dust from Central Poland was variable and did not depend on the agglomeration size. A lower content of Zn was usually observed in Warsaw, which is the largest agglomeration, with a high degree of urban and traffic development and in small localities, located close to Warsaw, whereas higher contents of Zn were noted in Lipsko, which is located at the largest distance from the Warsaw agglomeration. These results can be explained by the differences in the quality of the technical condition of the vehicles, industrial enterprises and better road pavements in Warsaw in comparison to areas outside Warsaw. As indicated by the investigations of Al-Khashmann [3], significant Zn sources in Jordan in the Industrial Centre at Karak were transportation and car services, quality of car carburettors, iron-works, steelworks, heaters, aluminium industry and housing. These anthropogenic factors influenced also the high correlation between the content of Zn and Pb, which is evidenced also by the results of this report. The maximal contents of Zn (253.6 mg·kg^{-1}) in street dust in our investigations are similar to those obtained in Jordan (123 mg·kg^{-1}) [3], and Accra in Ghana (213.0; 371.0 mg·kg^{-1}) [5]. In turn the mean content of Zn (85.50 mg·kg^{-1}) in Central Poland is similar to the mean value in an industrial town in China [18]. The high variability coefficient for Zn indicates that the content of Zn in street dust is influenced by many factors, such as e.g. technical quality of vehicles, quality of petrol, technical condition of the machines, equipment and chimney channels, road quality and other local factors.

The variability of these factors has impact on the increase of zinc in the environment, as evidenced by the presented investigations. In the study area, the content of copper is lower than the content of zinc in comparison to data from other countries [19]. The maximal content of copper (137.7 mg·kg^{-1}) in street dust noted in the area with the waste dump was close to the values obtained in Madrid (188 mg·kg^{-1}) [20] (167 mg·kg^{-1}) [21], and was 10 times lower than in Istanbul (1385 mg·kg^{-1}) [3]. The mean contents of Cu in street dust from Central Poland are close to those noted in Accra, Ghana (29–76 mg·kg^{-1}) [5].

Despite a high variability coefficient, the content of Cu in street dust from Central Poland is maintained at a similar level for the last 10 years with a slight uptrend.

Lead is not an element that is indispensable for the physiological functions of organisms and its values exceeding the geochemical background pose a hazard to the environment. The presented investigations have shown similar contents of these elements in street dust in the studied areas. The maximal content of Pb in street dust (233.2 mg·kg^{-1}) from the entrance road to the waste dump is a hazard for the environment and the population. In most sites of the study areas, the content of lead in street dust has almost twice exceeded the background for soils in Poland. Similar relationships were noted by Atiemo [5] in Accra, Ghana. A low variability coefficient for lead in Warsaw suggests that the main factor influencing lead content in street dust is the quality of vehicles and the applied petrol. It is worth noting that sweeping of dust from the street margins significantly influences the decrease of Pb in the

environment. These studies show that the development and intensification of traffic did not increase the content of lead in street dust during the last 10 years in the studied sites in Central Poland.

The obtained results show that the development of transportation and heavy industry (steelworks, electric industry, urbanization, etc.) significantly influences the zinc content and statistically insignificantly influences the content of Cd in street dust, which is also confirmed by the results of other authors [3,4].

The investigations show that the content of cadmium in street dust in the study area depended on the agglomeration size. In comparison to the geochemical background, the increase of cadmium in Warsaw was the highest, almost 10 times higher, whereas in towns located at the largest distances from Warsaw, this increase varied from 2 to 5 times. These data indicate that the circulation of cadmium in the environment is influenced mainly by the development of urbanization, industry and traffic. The content of Cd in street dust from Warsaw in comparison to other reports is similar to the content in other European cities, e.g. 1.4 $mg \cdot kg^{-1}$Cd were noted in Oslo [20].

The content of heavy metals in street dust in the study area followed a pattern according to the decreasing values (mean values in $mg \cdot kg^{-1}$): Zn (85.8) > Cu (35.5) > Pb (21.9) > Cd (0.76). Such pattern of heavy metals in street dust was characteristic for the Warsaw agglomeration as well as smaller localities such as Wiązowna and Karczew.

The only exception was the area of Lipsko, located at the largest distance from Warsaw, where the heavy metals from street dust followed a pattern according to the decreasing quantities (mean values in $mg \cdot kg^{-1}$): Zn (126.6) > Pb (30.8) > Cu (24.0) > Cd (0.64). This series of heavy metals in street dust is similar to the series of metals occurring in arable soils situated close to communication routes and subject to strong anthropopression, and in street dust from Warsaw.(Table 7) [1, 22].

TABLE 7
Regulation of the Minister of the Environment of 9 September 2001 on the soil quality standards and ground quality standards. Journal of Laws, no. 165, pos. 1359 of 4 October 2002

Heavy metals	Allowable concentrations of heavy metals in soils Regulation of the Minister of the Environment of 9 October 2002 ($mgkg^{-1}$)		
	Group A	Group B	Group C
		Depth in m; C in ppt	
		0-0,3	**0-2**
As	20	20	60
Ba	200	200	1000
Cr	50	150	500
Sn	20	20	350
Zn	100	300	1000
Cd	1	4	15
Co	20	20	200
Cu	30	150	600
Mo	10	10	250
Ni	35	100	300
Pb	50	100	600
Hg	0,5	2	30

• A- land in an area subjected protection, B-land classified as agricultural land except land under ponds and ditches, woodlands and urban and built-up (without the industrial areas of arable lands fossil and communication), C industrial areas, utilities and fossil sites

CONCLUSIONS

Street dust may be a good indicator to assess changes occurring in various urban and rural environments, areas with a variable degree of industrialization and different traffic density. The content of Zn, Cu, Pb, and Cd in street dust usually did not depend on the agglomeration size but on the degree of urbanization and industrialization as well as traffic density. The type, technical condition and number of vehicles significantly influenced the content of Zn and Cd in street dust. Likewise, frequent road sweeping contribute to the decrease of the heavy metal content in street dust. In Central Poland the content of the analyzed heavy metals is according to the following patterns of decreasing values: Zn (85.8) > Cu (35.5) > Pb (21.9) > Cd (0.76) or Zn (126.6) > Pb (30.8) > Cu (24.0) > Cd (0.64).

REFERENCES

[1] Czarnowska K., Bednarz I. 2000. Heavy metals in street dust from Warsaw, 51: 29-36.

[2] Kozanecka T., Czarnowska K., Jaworska A. 2003. Content of heavy metals in road coarse dust of Warsaw environs. Soil science yearbooks, 54: (3): 73-78.

[3] Al-Kashman O. 2000. Heavy metal distribution in dust, street dust and soils from the work place in Karak Industrial Estate, Jordan. Atmospheric Environment, 38: 6803-6812.

[4] Shi Xingmin, Chen L., Wang J. 2013. Multivariate analysis of heavy metal pollution in street dusts of Xianyang city, NW China. Environ. Earth Sci. 69, 1973-1979.

[5] Atiemo M.S., Ofosu G.F, Kuranchie-Mensah H., Tutu A.O, Palm N.D.M., Blankson A. 2011. Contamination assessment of heavy metals in road dust from selected roads in Accra, Ghana. Research Journal of Environmental and Earth Sciences, 3; (5): 473-480.

[6] Yap C.K., Chew W.Y., Tan S.G. 2012, Heavy metal concentrations in Ceilling Fan and Roadside car park dust collected from residential colleges in university Putra Malaysia, Serdang, Selangor. Pertanika J. Trop. Agric. Sci. 35: (1): 75-83.

[7] Zhang B., Luo B., Jiang T., Mei Z. 2014, Concentration of nutrients in street dusts of mega-city, chengdu, Southwest China. Fresen.Environ.Bull. 23: 2239-224.
Wang S.M., Li Q., Wang Z.D., Gao X. 2013, Concentration distribution and composition of heavy metals in street dust from small towns in Yongchuan, Chongqing. Fresen Environ Bull.22, 556-560.

[9] Wei N, Yang L. 2010, A review of heavy metal contaminations in urban soils, urban road dusts and agricultural soils from China, Microchemical Journal, 94: 99-107.

[10] Marazioti C., Maramathas C., Marazioti P.,Maraziotis E. 2009, Multi-element composition of airborne particulate matter in the patras urban area, Greece. Fresen Environ Bull.18, 960-967

[11] Papas D., Efstathiou G.A., Zoumakis N.M., Koutroubelis S., Apostolos G. Kelessis A.G., Petrakakis M.J. 2010, Modelling of traffic pollution at an urban site using a microscale CFD dispersion model. Fresen Environ Bull.19,1997-2001

[12] Wyszkowska J., Borowik A., Kucharski M. , Kucharski J. 2013, Effect of cadmium, copper, and zinc on plants, Soil microorganisms and soil enzymes. J. Elem.769–796

[13] Kwasowski W., Kozanecka T. 2010. Evaluation of the content of zinc and lead in selected vegetative organs of potatoes (Solanum tuberosum) growing in the vicinity of the Warszawa- Poznań speedway. Fresen Environ Bull, 19, 378-382

[14] Kozanecka T., Kazem-Bek A., Czarnowska K., Kwasowski W. 2010. Application of algae and lichens in the monitoring of changes in the natural environment. Fresen Environ Bull, 19, 553-557.

[15] Plum L.M, Rink L., Haase H. 2010. The essential toxin: impact of zinc on human health, Int. J. Environ. Res. Public Health 7, 1342-1365

[16] Xue Xu, Xinwei Lu, Xiufeng Han, Ni Zhao. 2015. Ecological and health risk assessment of metal in resuspended particles of urban street dust from an industrial city in China. CURRENT SCIENCE, 108. 72: (1):72-79.

[17] Czarnowska K. 1996. Total content of heavy metals in bedrocks as the geochemical background of soils. Soil Science Yearbooks 57, 43-50.

[18] Regulation of the Minister of the Environment of 9 September 2001 on the soil quality standards and ground quality standards. Journal of Laws, no. 165, pos. 1359 of 4 October 2002.

[19] Wyszkowska J., Kucharski J., Lajszner W. 2006. The effects of copper on soil biochemical properties and its interaction with other heavy metals. Polish J. of Environ. Stud. 15: (6): 927-934.

[20] Xue Xu, Xinwei Lu, Xiufeng Han, Ni Zhao. Ecological and health risk assessment of metal in resuspended particles of urban street dust from an industrial city in China. 2015, CURRENT SCIENCE, 108. 72 1, (2015), p.72-79;
[21] Kozanecka T., Czarnowska K., Łaszczyk K. 2007. Content of trace elements in street dust from the Zegrze–Mrągowo road. Soil science yearbooks 32: (1): 140-144.
[22] Wang G., Oldfield F., Xia D., Zhang W. 2012. Magnetic properties and correlation with heavy metals in urban street dust. A case study from the city of Lanzhou, China, Atmospheric Environment, 46: 289-298
[23] Yongming H, Peixuan D, Jungi C, Posmentier E. S. 2006. Multivariate analysis of heavy metal contamination in urban dusts of Xi'an, Central China. Sci Total Environ, 355: 176-186.
[24] Miguel D.E., Llamas J.F., Cghacon E., Berg T., Larssen S., Royset O., Vadset M. 1997, Origin and patterns of distribution of trace elements in street dust: unleaded petrol and urban lead. Atmospheric Environment. 31: 2733-2740.
[25] Sutherland T.A., Tolosa C., 2000. Multi-element analysis of road deposited sediment in urban drainage basin, Honolulu, Hawaii. Environ. Pollution. 110: 483-495.
[26] Czarnowska K., Chlibiuk M., Kozanecka T. 2002. Trace elements in arable soils along roads around Warsaw. Soil Science Yearbooks 53, 67-74.

Received: **10.06.2015**
Accepted: **26.11.2015**

CORRESPONDING AUTHOR

Pawel Kowalczyk
Bionicum LTD
Chełmska 21
00-724 Warsaw – POLAND

e-mail:pawel.kowalczyk@bionicum.com.pl

by PSP Volume 25 – No. 1/ 2016, pages 113-120 Fresenius Environmental Bulletin

BIODEGRADATION OF SIMAZINE BY *RHODOCOCCUS RHODOCHROUS*: KINETIC MODELING

Serkan Eker*, Ceyda Ceren Uyar

Department of Environmental Engineering, Dokuz Eylul University, Buca, Izmir, Turkey

ABSTRACT

Biodegradation of simazine by pure culture of *Rhodococcus rhodochrous* (DSM 43241) was studied in batch culture. Biodegradation experiments were carried out at different initial simazine concentrations between 0.886 and 4.967 mgL^{-1} in the presence of basal salts medium containing glucose. A significant decrease in the percent removal of simazine was observed with increasing initial simazine concentrations due to toxic effects of simazine. Degradation rate of simazine increased with the initial simazine concentration up to 2.7 mg L^{-1} and decreased with further increases. A non-competitive inhibition model was used to correlate the experimental data and to determine the kinetic constants which were found to be k = 0.055 mg-simazine $gX^{-1}h^{-1}$, K_S = 5.50 mgL^{-1} and K_{SI} = 3.6 mgL^{-1}. R*hodococcus rhodochrous* was found to be very effective for biodegradation of simazine with potential use in biological treatment of pesticide containing wastewaters.

KEYWORDS:
Biodegradation; inhibition; kinetic model; *Rhodococcus rhodochrous*; simazine; micropollutants

INTRODUCTION

Pesticides are used extensively in agriculture to prevent harmful organisms. One of the most commonly used pesticide in agricultural areas are herbicides. Extensive use of herbicides causes serious environmental pollution problems in surface and drinking waters. The priority substances containing pesticides and other pollutants are specified by Water Framework Directive (WFD) 2000/60/EC (Annex X) and Directive 2013/39EU to protect the aquatic environment from adverse effects of pollutants under the Water Framework Directive (WFD) [1,2]. Surface runoff from agricultural areas is the main source of pesticide contaminations. Pesticides are also present frequently in wastewater treatment plant effluents because of non-agricultural uses in urban areas [3,4] Simazine (6-chloro-N,N′-diethyl-1,3,5-triazine-2,4-diamine) is one of the substances listed in Priority Substances (WFD Annex X). It is a synthetic chemical with low solubility of 6.2 mgL^{-1} and is widely used as a preferred herbicide to control the growth of weeds in agricultural areas [2,5,6].

Different physical, chemical and biological methods such as adsorption, chemical oxidation and biological degradation were used for removal of pesticides from water [7-12]. Microbial or chemical degradation of pesticides are required for effective removal from water sources. Chemical degradation may cause formation of undesirable and even more toxic end products. Microbial degradation is more specific; however, it is relatively slow[13]. Toxic substances are difficult to remove by conventional bio-treatment systems. Effective degradation of pesticides can be achieved by using special bacterial species, which can use the pesticides as a sole carbon and nitrogen source [13]. The pesticides alone are not sufficient for growth of bacteria in the absence of a carbon and energy source [14]. Bacterial growth must be stimulated by addition of a carbon and energy source into the medium for effective degradation of pesticides [5,15,16]. *Rhodococcus* strains have been used for biodegradation of complex organic compounds including herbicides such as propazine, simazine, and cyanazine [17]. Some toxic compounds such as pesticides can be effectively removed from wastewater by using activated sludge containing *Rhodococcus* strains [5,17-26]. Degradation rate of simazine in soil was also investigated at different temperature and moisture at laboratory conditions [27].

Limited number of studies was reported in literature on biodegradation of pesticides by the *Rhodococcus* strains. Biodegradation kinetics of simazine by *Rhodococcus rhodocrous* was not studied and reported in literature. The major objective of this study is to investigate biodegradation of simazine by *R. rhodocrous* in batch culture. A kinetic model was developed and the kinetic constants were determined by using the experimental data.

MATERIALS AND METHODS

Experimental system. Biodegradation experiments were carried out at 30 ºC by using a gyratory incubator shaker. The experiments were performed in 500 ml baffled shake flasks. The flasks were charged with 100 mL of the nutrient media and simazine was added to the flasks in desired concentrations between 0.886 and 4.967 mgL^{-1}. The initial pH of the medium was adjusted to 6.8 for optimal growth of *Rhodococcus rhodochrous*. pH was controlled at 6.8 ± 0.2 by addition of a few drops 0.2 N NaOH during experiments. Sterilized flasks were inoculated with 10 mL culture and were incubated in a controlled environment shaker at 150 rpm and 30 ºC for 7 days (168 hours). A control flask containing simazine and nutrient medium without *Rhodococcus rhodochrous* (DSMZ 43241) was used to determine the non-biological degradation of simazine. Shake flasks including the controls were prepared in duplicates. The samples were withdrawn in every 24 hours.

Nutrient medium composition. One litre the synthetic media used in the experimental studies had the following composition: 5 g glucose, 1.5 g $(NH_4)_2SO_4$, 0.2 g K_2HPO_4, 0.1 g $MgSO_4.7H_2O$, 0.05 g $CaCl_2$. $2H_2O$ at pH=6.8. The liquid media was sterilized by autoclaving at 121°C for 15 minutes. Initial simazine concentration in the flasks was adjusted to desired concentrations between 0.886 mgL^{-1} and 4.967 mg l^{-1}. Two control flasks were used to quantify non-biological degradation of simazine and adsorption of simazine onto organism in duplicates. The first control flask, containing 0.8 mg-simazineL^{-1} was free of microorganisms. The second control flask contained 0.8 mg-simazine L^{-1} and sterilized dead organisms.

Organisms. Pure culture of *Rhodococcus rhodochrous* (DSMZ 43241) was obtained from Deutsche Sammlung von Mikroorganismen und Zellkulturen GmbH, Braunschweig, Germany to be used in the experimental studies. The culture was cultivated on a shaker at 30°C and 150 rpm under aseptic conditions by using a nutrient medium containing 0.2 mgL^{-1} simazine, 5 g glucose, 1.5 g $(NH_4)_2SO_4$, 0.1 g $MgSO_4.7H_2O$, 0.2 g K_2HPO_4, 0.05 g $CaCl_2$. $2H_2O$ and 1 g yeast extract in one liter of water (Pamukoglu and Kargi, 2008). The cultivated cells were centrifuged and washed with sterile water before inoculation. The same amounts of concentrated cell suspensions were used for inoculation of the experimental flasks. The initial concentration of the microorganisms in the flasks was 887±30 mgL^{-1}.

Chemicals. All chemicals were analytical grade and used without any further purification. Simazine was supplied by Dr Ehrenstorfer GmbH, Germany. Chromatographic grade acetonitrile, analytical grade H_2SO_4 (98–99%) and NaOH were purchased from Merck, Germany. The water used for solutions and mobile phase were purified using a Mili-Q system (milipore filtration).

Analytical methods. Simazine was analyzed using an HPLC (Agilent 1100 model), equipped with a UV-detector and a C18 column. The mobile phase composition was H_2O/Acetonitrile with a ratio of 40/60. The UV-detection was operated at 214 nm. The flow rate was 1 mL min^{-1} and the injection volume was 20 µL. The retention time for simazine was 4 min (Catalkaya and Kargi, 2009a). Simazine calibration curve was prepared for concentrations between 0.002 and 5 mgL^{-1} with a correlation coefficient of R^2= 0.9998. A pH meter (WTW, Germany) was used to monitor pH. Samples were withdrawn from the flasks every day and centrifuged at 8000 g for 15 minutes to remove biomass from the liquid phase. Biomass concentration was determined at the beginning of the experiments by filtering the samples through 0.45 µm Millipore filter and drying in an oven at 105°C to constant weight. Samples were analyzed in triplicates and the standard deviations were less than 3% of the average.

RESULTS AND DISCUSSION

Variations of simazine concentrations with time during experiments are shown in Figure 1 for different simazine concentrations. Simazine concentration in the control flask did not change during the experimental period indicating no adsorption and no biodegradation. Simazine concentration in the experimental flasks decreased considerably for the first 72 hours and then remained constant especially for high simazine concentrations.

Variations of final simazine concentrations and percent simazine removals with the initial simazine concentrations are shown in Figure 2. Final simazine concentrations increased and percent simazine removals decreased with increasing initial simazine due to toxic effects of simazine on *Rhodococcus rhodochrous*. Percent simazine degradation was 64.2 % at the end of 168 h with the

initial simazine concentration of 0.886 mgL^{-1} which decreased to 58.8 % for the initial simazine concentration of 1.851 mgL^{-1}, and further to 20.5% for the initial simazine of 4.967 mgL^{-1}.

Figure 3 depicts variation of initial degradation rate of simazine with the initial simazine concentration. The rate of degradation increased with initial simazine concentration up to 2.7 $mg\ L^{-1}$ and then decreased for higher concentrations, indicating inhibitory effects of simazine on *Rhodococcus rhodochrous* for concentrations above 2.7 mgL^{-1}.

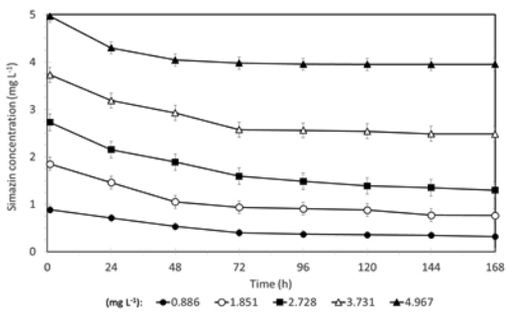

FIGURE 1
Variation of simazine concentration with time for different initial simazine concentrations

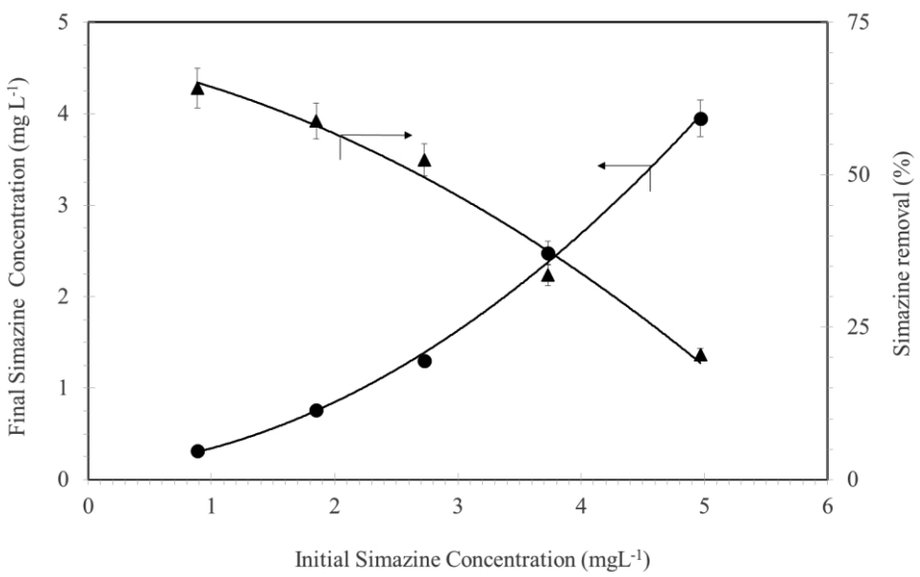

FIGURE 2
Variation of final simazine concentrations and percent simazine removals with the initial simazine concentrations.

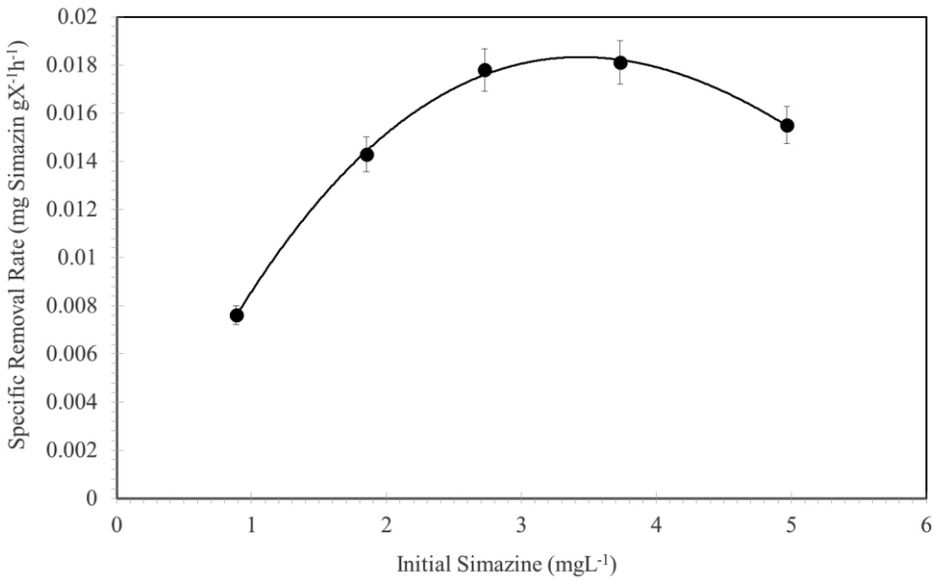

FIGURE 3
Variation of initial degradation rate of simazine with initial simazine concentration.

The data presented in Figure 3 indicates typical substrate inhibition kinetics. The following rate equation was suggested for non-competitive substrate inhibition kinetics.

$$Rso = \frac{k.Xo.So}{Ks+So}\frac{Ksı}{Ksı+So} = \frac{k.Xo}{(1+{Ks}/{So})(1+{So}/{Ksı})} \quad (1)$$

or

$$Rxo = \frac{Rso}{Xo} = \frac{k.So}{Ks+So}\frac{Ksı}{Ksı+So} \quad (1a)$$

where R_{So} is the initial rate of simazine degradation ($mgL^{-1}h^{-1}$); S_o is the initial simazine concentration (mg L^{-1}); K_S is the saturation constant (mgL^{-1}), X_o is the initial biomass concentration (gXL^{-1}), k is the biodegradation rate constant for simazine (h^{-1}) and K_{SI} is the inhibition constant for simazine (mgL^{-1}). R_{so} is determined by using the initial simazine degradation rate as $R_{so} = \Delta S/\Delta t$, where ΔS is ($S_o - S$) and Δt is 72 hours. R_{xo} is the specific rate of simazine degradation (mg-simazine $gX^{-1}h^{-1}$) and is determined as R_s/X_o where X_o is 0.887 gL^{-1}. The first term in equation 1 represents biodegradation rate of simazine by the bacteria in form of Monod rate expression. The second terms represents non-competitive substrate inhibition by simazine.

The inhibition term can be neglected at simazine concentrations below 2.7 mgL^{-1} ($S_o << K_{SI}$) and initial rate equation can be written as

$$Rso = \frac{k.Xo.So}{Ks+So} = \frac{Rmo.So}{Ks+So} \quad (2)$$

or

$$Rxo = \frac{Rso}{Xo} = \frac{k.So}{Ks+So} \quad (2a)$$

where $R_{mo} = k\ X_o$ is the maximum initial rate of simazin biodegradation ($mgL^{-1}h^{-1}$). In reciprocal form, equation 2a can be written as follows:

$$\frac{1}{Rxo} = \frac{1}{k} + \frac{Ks}{k}\frac{1}{So} \quad (3)$$

A plot of $1/R_{xo}$ versus $1/S_o$ results in a line with a slope of K_S/k and intercept of 1/ k.

For high initial simazine concentrations of above 2.7 mgL^{-1}, the first term in equation 1 may be neglected ($S >> K_S$) and the inhibition term becomes the rate determining factor. Therefore, for high initial simazine concentrations, the rate expression takes the following form:

$$Rso = k.Xo\ \frac{Ksı}{Ksı+So} \quad (4)$$

or

$$Rxo = \frac{Rso}{Xo} = \frac{k.Ksı}{Ksı+So} \quad (4a)$$

In reciprocal form, equation 4a can be written as follows:

$$\frac{1}{Rxo} = \frac{1}{k} + \frac{1}{k.Ksı}\ So \quad (5)$$

A plot of $1/R_{xo}$ versus S_o for high simazine concentrations results in a line with a slope of

1/ k K_{SI} and intercept of 1/k. Experimental data presented in Figure 3 were used to determine the kinetic constants. Plots of $1/R_{xo}$ versus $1/S_o$ at low initial concentrations of simazine and $1/R_{xo}$ versus S_o at high initial concentrations of simazine were shown in Figure 4 and 5, respectively. The kinetic constants were calculated from the slope and intercept of the best-fit line.

Kinetic constants were also determined by using regression analysis. Quasi-Newton method in Statistica v10 software was used to estimate the kinetic constants by using the experimental data. The kinetic constants determined from the graphical and regression methods are listed in Table 1.

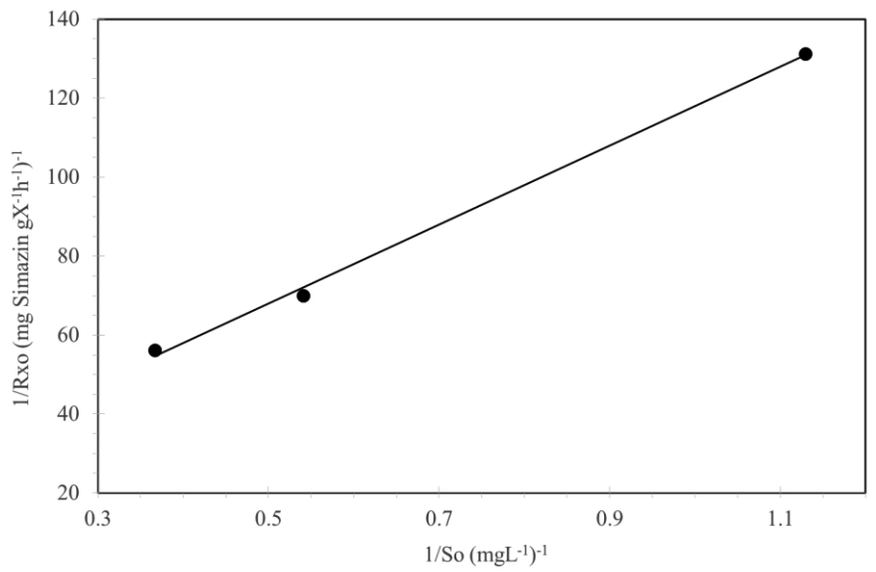

FIGURE 4
Double reciprocal plot of $1/R_{xo}$ versus $1/S_o$ at low simazine concentrations.

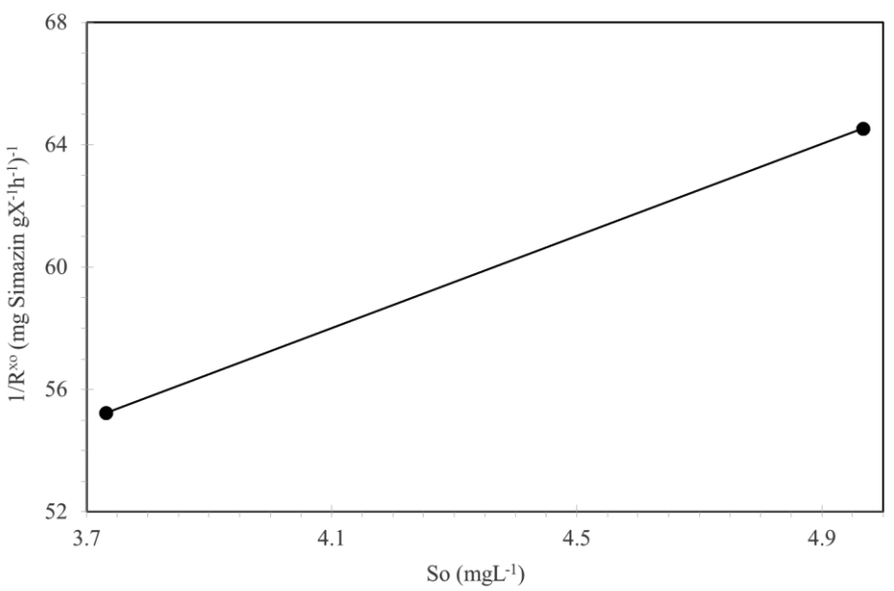

FIGURE 5
A plot of $1/R_{xo}$ versus initial simazine (S_o) at high simazine concentrations.

TABLE 1
Estimated kinetic constants using the experimental data

	k (mg-simazine $gX^{-1}h^{-1}$)	Ks (mgL^{-1})	K_{SI} (mgL^{-1})	R^2
Graphical method (Model Prediction 1)	0.055	5.50	3.60	0.99
Regression Method (Model Prediction 2)	0.069	4.62	4.62	0.86

High regression coefficients (R^2) indicated good agreement between the model predictions and the experimental data. Experimental data and model predictions are compared in Figure 6. The graphical method resulted in better fit to the experimental data. Therefore, a non-competitive substrate inhibition model was found to be suitable for biodegradation of simazine by *R. rhodocrous*. Simazine concentrations above 2.7 mg L^{-1} were inhibitory since the rate of simazine degradation decreased for concentrations above this level. Low K_I value for simazine inhibition indicated high level of simazine inhibition. In other words the rate decreases to one-half of the maximum level when simazine is 3.6 mg l^{-1}.

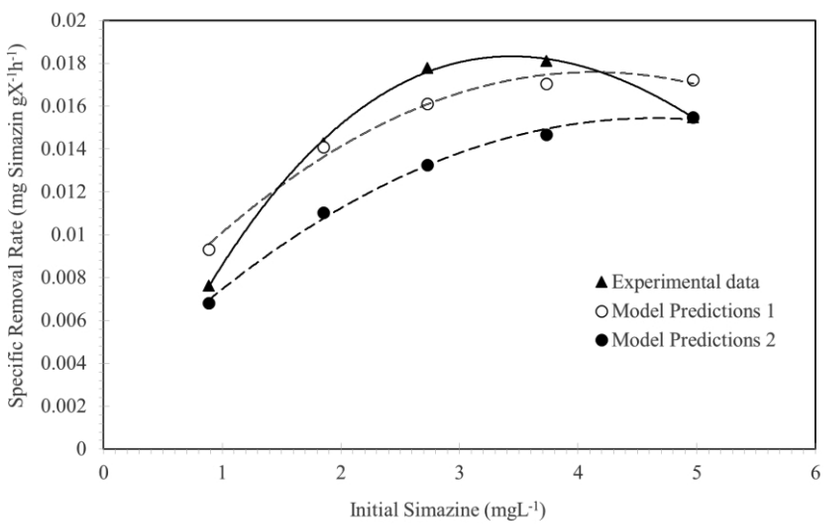

FIGURE 6
Comparison of experimental results with the kinetic model predictions

CONCLUSIONS

Biodegradation of simazine by the pure culture of *Rhodococcus rhodochrous* (DSMZ 43241) was investigated at different initial simazine concentrations between 0.886 and 4.957 mgL^{-1}. Percent simazine removal was 64.2% for 0.886 mgL^{-1} initial simazine concentration which dropped to 20.5% for the initial simazine of 4.967 mgL^{-1}. The rate of biodegradation increased with simazine concentration up to 2.7 mgL^{-1} and decreased for higher concentrations due to toxic effects of simazine. Monod kinetics with a non-competitive substrate inhibition was proposed to describe inhibitory effects of high simazine concentrations. The kinetic model was correlated with the experimental data to determine the kinetic constants. The inhibition/saturation constant ratio (K_I/Ks) was low, indicating strong inhibition effects at high concentrations of simazine for *Rhodococcus rhodochrous*. This study indicated that *Rhodococcus rhodochrous* was effective in biodegradation of simazine and may be used in activated sludge systems for removal of simazine and possibly other pesticides from wastewater.

REFERENCES

[1] Vorkamp K, Bossi R, Bester K, Bollmann UE, Boutrup S (2014) New priority substances of the European Water Framework Directive: Biocides, pesticides and brominated flame retardants in the aquatic environment of Denmark. Sci Total Environ 470, 459-468.

[2] Catalkaya EC, Kargi F (2009) Degradation and Mineralization of Simazine in Aqueous Solution by Ozone/Hydrogen Peroxide Advanced Oxidation. J Environ Eng-Asce 135, 1357-1364.

[3] Belgiorno V, Rizzo L, Fatta D, Della Rocca C, Lofrano G, et al. (2007) Review on endocrine disrupting-emerging compounds in urban wastewater: occurrence and removal by photocatalysis and ultrasonic irradiation for wastewater reuse. Desalination 215, 166-176.

[4] Kock-Schulmeyer M, Villagrasa M, de Alda ML, Cespedes-Sanchez R, Ventura F, et al. (2013) Occurrence and behavior of pesticides in wastewater treatment plants and their environmental impact. Sci Total Environ 458, 466-476.

[5] Kodama T, Ding LX, Yoshida M, Yajima M (2001) Biodegradation of an s-triazine herbicide, simazine. J Mol Catal B-Enzym 11, 1073-1078.

[6] Galindez-Najera SP, Ramos-Monroy O, Ruiz-Ordaz N, Salmeron-Alcocer A, Juarez-Ramirez C, et al. (2011) Simultaneous degradation of atrazine and simazine by a binary culture of Stenotrophomonas maltophilia and Arthrobacter sp in a two-stage biofilm reactor. J Chem Technol Biot 86, 554-561.

[7] Catalkaya EC, Kargi F (2009) Dehalogenation, degradation and mineralization of diuron by peroxone (peroxide/ozone) treatment. J Environ Sci Heal A 44, 630-638.

[8] Mosteo R, Gumy D, Pulgarin C (2008) Coupled photo-Fenton-biological system: effect of the Fenton parameters such as residual H(2)O(2), Fe(2+) and pH on the efficiency of biological process. Water Sci Technol 58, 1679-1685.

[9] Torres RA, Mosteo R, Petrier C, Pulgarin C (2009) Experimental design approach to the optimization of ultrasonic degradation of alachlor and enhancement of treated water biodegradability. Ultrason Sonochem 16, 425-430.

[10] Sanches S, Penetra A, Rodrigues A, Ferreira E, Cardoso VV, et al. (2012) Nanofiltration of hormones and pesticides in different real drinking water sources. Sep Purif Technol 94, 44-53.

[11] Feakin SJ, Gubbins B, Mcghee I, Shaw LJ, Burns RG (1995) Inoculation of Granular Activated Carbon with S-Triazine-Degrading Bacteria for Water-Treatment at Pilot-Scale. Water Res 29, 1681-1688.

[12] Gebrekidan A, Nicolai H, Vincken L, Teferi M, Asmelash T, et al. (2013) Pesticides Removal by Filtration over Cactus Pear Leaves: A Cheap and Natural Method for Small-Scale Water Purification in Semi-Arid Regions. Clean-Soil Air Water 41, 235-243.

[13] Gunasekara AS, Troiano J, Goh KS, Tjeerdema RS (2007) Chemistry and fate of simazine. Rev Environ Contam T 189, 1-23.

[14] Robertson BK, Alexander M (1994) Growth-Linked and Cometabolic Biodegradation - Possible Reason for Occurrence or Absence of Accelerated Pesticide Biodegradation. Pestic Sci 41, 311-318.

[15] Kargi F, Eker S (2005) Kinetics of 2,4-dichlorophenol degradation by Pseudomonas putida CP1 in batch culture. Int Biodeter Biodegr 55, 25-28.

[16] Kargi F, Eker S (2004) Toxicity and batch biodegradation kinetics of 2,4 dichlorophenol by pure Pseudomonas putida culture. Enzyme Microb Tech 35, 424-428.

[17] Behki R, Topp E, Dick W, Germon P (1993) Metabolism of the Herbicide Atrazine by Rhodococcus Strains. Appl Environ Microb 59, 1955-1959.

[18] Pamukoglu MY, Kargi F (2008) Biodegradation kinetics of 2,4,6-trichlorophenol by Rhodococcus rhodochrous in batch culture. Enzyme Microb Tech 43, 43-47.

[19] Nalli S, Cooper DG, Nicell JA (2006) Interaction of metabolites with R-rhodochrous during the biodegradation of di-ester plasticizers. Chemosphere 65, 1510-1517.

[20] Nalli S, Cooper DG, Nicell JA (2002) Biodegradation of plasticizers by Rhodococcus rhodochrous. Biodegradation 13, 343-352.

[21] DeWever H, DeCort S, Noots I, Verachtert H (1997) Isolation and characterization of Rhodococcus rhodochrous for the degradation of the wastewater component 2-hydroxybenzothiazole. Appl Microbiol Biot 47, 458-461.

[22] Martinkova L, Uhnakova B, Patek M, Nesvera J, Kren V (2009) Biodegradation potential of the genus Rhodococcus. Environ Int 35, 162-177.

[23] Chand D, Kumar H, Sankhian UD, Kumar D, Vitzthum F, et al. (2004) Treatment of simulated wastewater containing toxic amides by immobilized Rhodococcus rhodochrous NHB-2 using a highly compact 5-stage plug flow reactor. World J Microb Biot 20, 679-686.
[24] Jones LR, Owen SA, Horrell P, Burns RG (1998) Bacterial inoculation of granular activated carbon filters for the removal of atrazine from surface water. Water Res 32, 2542-2549.
[25] Herrera-Gonzalez VE, Ruiz-Ordaz N, Galindez-Mayer J, Juarez-Ramirez C, Santoyo-Tepole F, et al. (2013) Biodegradation of the herbicide propanil, and its 3,4-dichloroaniline by-product in a continuously operated biofilm reactor. World J Microb Biot 29, 467-474.
[26] Verma K, Agrawal N, Farooq M, Misra RB, Hans RK (2006) Endosulfan degradation by a Rhodococcus strain isolated from earthworm gut. Ecotox Environ Safe 64, 377-381.
[27] Fernandez MD, Perez RA, Sanchez-Brunete C, Tadeo JL (2001) Persistence of simazine and hexazinone in soil. Fresenius Environmental Bulletin 5,10, 490-494

Received: **06.12.2015**
Accepted: **07.12.2015**

CORRESPONDING AUTHOR

Serkan Eker
Dokuz Eylul University
Department of Environmental Engineering,
Buca, Izmir – TURKEY

e-mail: serkan.eker@deu.edu.tr

by PSP Volume 25 – No. 1/ 2016, pages 121-129 Fresenius Environmental Bulletin

EFFECTS OF *ORIGANUM VULGARE* OIL ON OXIDATIVE STRESS IN PENTACHLOROPHENOL-INTOXICATED RATS*

Mehmet Akıllı[1] and Gökhan Eraslan[2]**

[1]. Erciyes University, Collage of Health Science, Department of Pharmacology and Toxicology, Kayseri, Turkey
[2]. Erciyes University, Faculty of Veterinary Medicine, Department of Pharmacology and Toxicology, Kayseri, Turkey.

ABSTRACT

Effects of *Origanum vulgare* oil on oxidant-antioxidant system in pentachlorophenol-given rat were investigated. Total thirty-two Wistar Albino race male rats were used. Rats were divided into four even groups. Group 1 was assigned control. Groups 2, 3, and 4 were given *Origanum vulgare* oil at the dose of 1.5 ml/kg.bw/day, pentachlorophenol at the dose of 60 mg/kg.bw/day and *Origanum vulgare* oil at the dose of 1.5 ml/kg.bw/day plus pentachlorophenol at the dose of 60 mg/kg.bw/day into the stomach directly, respectively, for 21 days. At the end of the 21th day, tissues (liver, kidney, brain) and blood samples of all groups were taken. Malondialdehyde (MDA) and nitric oxide (NO) levels and superoxide dismutase (SOD), catalase (CAT) and glutathione peroxidase (GSH-Px) activities were measured in the all samples. As a result, while pentachlorophenol exposure caused oxidative damage to erythrocytes and some tissue of rats at different rates, *Origanum vulgare* oil alleviated the severity of pentachlorophenol-induced oxidative stress. *Origanum vulgare* oil alone also has not any negative effects. In conclusion, *Origanum vulgare* oil can be applied as a therapeutic agent or food additive for prophylaxis against exposure to pentachlorophenol.

KEYWORDS:
Pentachlorophenol, *Origanum vulgare* oil, exposure, oxidative stress, rats

INTRODUCTION

Pentachlorophenol is a chlorinated aromatic compound in solid crystalline form and with a colour varying from white to brown.Owing to its chemical structure, this compound is referred to as penta,2,3,4,5,6pentachlorophenol and chlorophene. When heated, it has a strong phenolic odour. It is neither inflammable nor corrosive. While its solubility is limited in water, pentachlorophenol is highly soluble in alcohol [1-6]. Pentachlorophenol disrupts the intracellular energy metabolism by altering intracellular Na^+-K^+ ATPase activity [2]. Generally, this compound is used as a wood preservative and fungicides [3]. Although it can also be used for in the textile and leather industries [4], and as an herbicide and biocide [5], its use for these purposes is on the decrease. In most countries its use has either been highly restricted or completely abandoned. On the other hand, this particular compound continues to be a major pesticide for several developing countries [6]. The environmental persistence of pentachlorophenol is at medium level and highly depends on the change of environmental conditions (organic material, oxygen, heat, etc.) [7-11]. Across the world, Origanum species hold an important place among medicinal plants. Of these, *Origanum vulgare* subspecies display the richest variety. Oregano (*Origanum vulgare*) has been used both as a medicinal plant and as a food spice. Origanum oil is known to have antioxidant effects. The primary phenolic compounds found in origanum oil are thymol, carvacrol, p-cymene, β-fenchyl alcohol and γ-terpinene [12-15].As a result of its widespread use, pentachlorophenol is among one of the primary environmental contaminants. The accumulation of this compound in the environment (soil, water and air) also brings about the risk of toxicity. This study, carried out in rats, was aimed at the demonstration of the protective effect of *Origanum vulgare* oil against subacute intoxication with pentachlorophenol, which has common use in different areas and is highly toxic for experimental animals and mammals. Also, mentioned research provides a detailed investigation of the antioxidant effects of *Origanum vulgare* oil.

MATERIALS AND METHODS

Animal Material: The study was performed in 32 male Wistar Albino rats weighing 200-250 g. Rats were divided into 4 even groups, comprising one control and three experimental. The animals consisting of groups 2, 3 and 4 were administered: *Origanum vulgare* oil at the dose of 1.5 ml/kg.bw/day (Solgar®), pentachlorophenol (pentachlorophenol sodium salt 80%, Fluka) at the dose of 60 mg/kg.bw/day and pentachlorophenol at

the dose of 60 mg/kg.bw/day plus *Origanum vulgare* oil at the dose of 1.5 ml/kg.bw/day into the stomach via gavage for 21 days, respectively. Pentachlorophenol was dissolved in deionized water as vehicle. The animals were maintained at a fixed temperature of 20-22 ºC and were grown on a light regime of 12 h light/12 h dark. They were provided with standard laboratory rodent feed pellet (3,100 kcal/kg metabolic energy, 23% raw protein and 7% crude cellulose) and drinking water ad libitum in the experimental period. Pentachlorophenol was given in the early morning, whilst *Origanum vulgare* oil was given 6 h after the pentachlorophenol treatment performed that day. The study protocol was approved by the Animal Ethics Committee, University of Erciyes.

Collection and Preparation of Blood Samples and tissues for Analysis: Blood samples were taken from all animals into heparinised tubes under light ether anaesthesia. All tubes were centrifuged for the separation of plasma and blood cells. Following the separation of plasma, the erythrocyte layer was washed and haemolysed [16]. The tissues extracted after their death were homogenized and centrifuged. The supernatant was transferred into eppendorf tubes.

Analysis of Biochemical Parameters: Following homogenization of tissues (liver, kidney, brain), tissue malondialdehyde (MDA) levels were measured according to the method described by Ohkawa et al. [17], and tissue protein levels were determined as described by Lowry et al. [18] and modified by Miller [19]. Plasma MDA levels were performed in accordance with the method defined by Yoshioka et al [20]. Nitric oxide (NO) levels were determined as described by Tracey et al. [21]. Haemoglobin levels in the haemolysate were done by the method described by Fairbanks and Klee [22]. Catalase (CAT) activity measurement was done as described by Luck [23]. Superoxide dismutase (SOD) activity analyses were performed in accordance with the method described by Sun et al. [24]. The method described by Paglia and Valentine [25] was used for glutathione peroxidase (GSH-Px) analyses.

Statistical Analysis: Statistical calculations were performed by using ‘’the SPSS 13.0 for Windows’’ software package programme. Data was implied in arithmetical mean and standard deviations. Meaningful significant differences between the groups were determined by means of one-way analysis of variance (ANOVA) and Tukey post-hoc test.

RESULTS

Origanum vulgare oil: When compared to the control group, in the group administered with *Origanum vulgare* oil alone, no significant change was observed in the MDA levels of the samples analysed. Likewise, no significant difference was determined between the groups (groups 1 and 2) for tissue and erythrocyte SOD activity. CAT activity was ascertained to have significantly decreased in the renal and hepatic tissues, in comparison to the control group. No significant change was detected in the CAT activity of the cerebral tissue and erythrocytes. The controls and the group administered with *Origanum vulgare* oil alone did not display any statistically significant difference for GSH-Px activity, excluding the values measured in the renal tissue. While the NO levels were determined to have significantly decreased in the renal tissue, no statistically significant difference was detected in the other biological samples analysed (Tables 1-4).

TABLE 1
Effects of *Origanum vulgare* oil and pentachlorophenol on liver oxidative stress markers in rats

Parameters	Groups*			
	Group 1	Group 2	Group 3	Group 4
MDA (nmol/mg-protein)	0.80±0.09^{a}	0.78±0.12^{a}	3.17±0.63^{b}	2.37±0.73^{c}
SOD (U/mg-protein)	3.83±0.59^{a}	3.56±0.81^{ab}	2.57±0.55^{b}	5.43±1.29^{c}
CAT (k/g-protein)	91.29±17.43^{a}	55.19±18.72^{b}	49.04±14.65^{b}	105.15±13.12^{a}
GSH-Px (U/g-protein)	305.96±65.82^{a}	276.59±22.57^{a}	184.30±43.17^{b}	274.55±56.77^{a}
NO (µmol/mg-protein)	7.00±1.39^{a}	7.05±1.93^{a}	19.83±5.89^{b}	5.66±1.86^{a}

^{a,b,c}. Means not sharing a common superscript letters differ significantly at $p<0.05$.

* Group 1 control; Group 2 *Origanum vulgare* oil; Group 3 Pentachlorophenol; Group 4 *Origanum vulgare* oil plus Pentachlorophenol

Pentachlorophenol: When compared to the control group, in the group administered with pentachlorophenol alone, MDA levels were observed to have significantlyincreased in the hepatic, renal and cerebral tissues as well as in the erythrocytes. On the other hand, SOD activity was ascertained to have significantly decreased in the hepatic, renal and cerebral tissues and erythrocytes, in comparison to the control group. While CAT activity was determined to have significantly decreased in the hepatic and renal tissues and erythrocytes, it was observed to have significantly increased in the cerebral tissue. Furthermore, GSH-Px activity had significantly decreased in the liver, kidneys, brain and erythrocytes. Compared to the controls, NO levels had significantly increased in all of the samples analysed (Tables 1-4).

TABLE 2
Effects of *Origanum vulgare* oil and pentachlorophenol on kidney oxidative stress markers in rats

Parameters	Groups*			
	Group 1	Group 2	Group 3	Group 4
MDA (nmol/mg-protein)	1.32±0.19^{a}	1.39±0.34^{a}	3.11±0.68^{b}	1.51±0.33^{a}
SOD (U/mg-protein)	4.23±0.73^{a}	4.08±0.69^{ab}	3.28±0.43^{b}	5.19±0.81^{c}
CAT (k/g-protein)	128.87±19.16^{a}	98.02±15.66^{b}	90.33±9.89^{b}	137.39±25.07^{a}
GSH-Px (U/g-protein)	157.09±30.18^{a}	126.39±12.77^{bc}	106.55±15.18^{c}	149.90±22.08^{ab}
NO (µmol/mg-protein)	6.09±1.42^{a}	4.15±1.00^{b}	9.66±0.61^{c}	7.59±1.94^{a}

^{a,b,c}. Means not sharing a common superscript letters differ significantly at $p<0.05$
* Group 1 control; Group 2 *Origanum vulgare* oil; Group 3 Pentachlorophenol; Group 4 *Origanum vulgare* oil plus Pentachlorophenol

Pentachlorophenol and Origanum vulgare oil: In general, the values measured in the group administered with a combination of pentachlorophenol and *Origanum vulgare* oil were determined to have drawn closer to those of the control group. However, the statistically significant difference determined between the group administered with pentachlorophenol alone and the controls was determined not to have completely disappeared in the group administered with both pentachlorophenol and *Origanum vulgare* oil. When compared to the control group, MDA levels were determined to have significantly increased in the hepatic tissue. SOD activity had significantly increased in the hepatic and renal tissues. GSH-Px activity had decreased in the cerebral tissue. Plasma NO levels had significantly increased (Tables 1-4)

TABLE 3
Effects of *Origanum vulgare* oil and pentachlorophenol on brain oxidative stress markers in rats

Parameters	Groups*			
	Group 1	Group 2	Group 3	Group 4
MDA (nmol/mg-protein)	0.44±0.16^{a}	0.43±0.24^{a}	1.32±0.37^{b}	0.62±0.23^{a}
SOD (U/mg-protein)	3.56±1.38^{a}	3.52±1.36^{a}	1.55±0.38^{b}	2.53±0.87^{ab}
CAT (k/g-protein)	29.93±11.07^{ab}	20.62±6.57^{a}	70.37±11.25^{c}	40.20±10.21^{b}
GSH-Px (U/g-protein)	101.92±18.01^{a}	89.71±11.68^{ab}	53.18±14.64^{c}	78.09±11.30^{b}
NO (µmol/mg-protein)	6.75±0.80^{a}	6.01±1.38^{a}	8.80±1.54^{b}	6.44±1.19^{a}

^{a,b,c}. Means not sharing a common superscript letters differ significantly at $p<0.05$.
*. Group 1, control; Group 2, *Origanum vulgare* oil; Group 3, Pentachlorophenol; Group 4, *Origanum vulgare* oil plus Pentachlorophenol.

When compared to the group administered with pentachlorophenol alone, MDA levels had significantly decreased in all of the samples analysed. SOD activity had significantly increased in the hepatic and renal tissues. While CAT activity was determined to have significantly increased in the hepatic and renal tissues and erythrocytes, a significant decrease was detected in the cerebral

tissue. While GSH-Px activity was ascertained to have significantly increased in the hepatic, renal and cerebral tissues and erythrocytes, NO levels were determined to have significantly decreased in the hepatic, renal and cerebral tissues (Tables 1-4).

TABLE 4
Effects of *Origanum vulgare* oil and penthachlorophenol on erythrocytes/plasma oxidative stress markers in rats (arithmetic mean±standart deviation).

Parameters	Groups*			
	Group 1	Group 2	Group 3	Group 4
MDA (nmol/mgHb)	0.33±0.09[a]	0.35±0.20[a]	0.64±0.16[b]	0.38±0.20[a]
SOD (U/mgHb)	1.25±0.23[a]	1.19±0.33[ab]	0.87±0.13[b]	1.19±0.23[ab]
CAT (k/gHb)	93.75±15.36[a]	77.85±13.18[ab]	59.50±10.87[b]	87.78±14.03[a]
GSH-Px (U/gHb)	68.71±17.35[a]	54.98±10.27[ab]	43.04±7.32[b]	62.70±14.77[a]
NO (µmol/ml plasma)	88.88±18.25[a]	94.75±22.66[ab]	132.75±18.29[c]	116.61±14.37[bc]

[a,b]. Means not sharing a common superscript letters differ significantly at $p<0.05$.
*. Group 1, control; Group 2, *Origanum vulgare* oil; Group 3, pentachlorophenol; Group 4, *Origanum vulgare* oil plus pentachlorophenol.

DISCUSSIONS

Xenobiotics such as pesticides and other compounds are known to induce oxidative stress [26-28]. Pentachlorophenol is a compound, which is known to induce oxidative stress, as both the primary compound itself and its intermediate metabolites resulting from hepatic metabolism cause the generation of free radicals [29-31].

Free radicals are highly reactive products. The generation of free radicals, at levels exceeding the physiological limits, has adverse effects on both the cytoplasmic membrane and the intracellular organelles (in particular the lysosome, endoplasmic reticulum and mitochondria) as well as on the nuclear DNA. The peroxidation of the membrane, as a result of the adverse effects of these products on this structure which is rich in lipids, brings about major changes in the structural components and selective permeability of the biological membrane. Furthermore, the changes in the intracellular and extracellular ion concentrations (increase in the intracellular calcium level and changes in the Na/K levels) and the functions of the transport proteins (e.g. Na-K ATPase)/receptors found in the membrane also trigger several adverse effects [32-38]. The increased severity of these effects causes both tissue damage and a disruption of organ functions [39-42]. Enzymatic antioxidant mechanisms play an essential role in the prevention of oxidative stress. Of the antioxidant enzymes, SOD converts the superoxide radicals into the less harmful hydrogen peroxide (H_2O_2). Superoxide radicals are also involved in the generation of other free radicals. Therefore, both the level of the superoxide radical in the organism and the rendering of this radical harmless, are of great concern for the development and severity of lipid peroxidation. Another antioxidant enzyme is the CAT. The CAT converts H_2O_2 into the non-toxic metabolites, water and oxygen. A third antioxidant enzyme, GSH-Px is found in the cell cytosol and mitochondria, and converts H_2O_2 into water [34, 36, 38, 43]. For the determination of the presence of lipid peroxidation and oxidative stress, it is required to perform measurements for the intermediate and final products of lipid peroxidation and antioxidant enzymes in biological materials. One of the methods used most commonly for this purpose is the assessment of MDA and NO levels and SOD, CAT and GSH-Px activities in biological materials [36-38, 44-48].

Owing to their low toxicity, essential oils are considered as an alternative to conventional pharmaceuticals in both human and veterinary medicine [12, 13]. In the group administered with *Origanum vulgare* oil alone, in particular the MDA and NO levels not having increased demonstrated that this compound did not cause oxidative stress. Similar conditions having been detected for most of the antioxidant enzyme activities in the biological materials analysed, was in support of the results obtained for MDA and NO levels. The significant decrease detected in the NO levels and CAT and GSH-Px activities in some samples was attributed to *Origanum vulgare* oil strengthening the antioxidant system (most probably by binding to the free radicals generated under physiological conditions). Previous research conducted on *Origanum vulgare* oil also suggests this compound to have no adverse effect on lipid peroxidation [49, 50].

Pentachlorophenol is a compound that has found use at an industrial scale in several fields. Although its use has been restricted due to major adverse effects, it is still in use in some developing countries [1-6, 9]. Several physiological systems are affected by exposure to pentachlorophenol, and the

most severely affected organs are firstly the liver and secondly the kidneys. After being absorbed, pentachlorophenol is rapidly distributed to most of the tissues and organs (liver, lungs, kidneys, blood, adipose tissue and brain). Since it passes through the enterohepatic circulation, its residence time in the body is rather long. It accumulates in the hepatic and renal tissues at a higher level and at lower concentrations in the adipose, cerebral and muscle tissues. Pentachlorophenol is eliminated, to a large extent, from the kidneys. When ingested, pentachlorophenol causes severe damage to the liver and kidneys, and some biochemical changes in the erythrocytes [1-4, 31, 51, 52].

In the present study, when compared to the control group, in the group administered with pentachlorophenol alone, the MDA and NO levels in the liver, kidneys, brain and erythrocytes/plasma having been determined to have significantly increased, suggests that this particular compound is capable of inducing lipid peroxidation alone. This demonstrates that pentachlorophenol leads to the generation of free radicals at a high level. The free radicals generated, result in the peroxidation of the lipid membrane, which significantly increases NO and MDA levels. On the other hand, in the group administered with pentachlorophenol alone, SOD activity was determined to have significantly decreased in the hepatic, renal and cerebral tissues and erythrocytes, in comparison to the control group. While CAT activity was observed to have significantly decreased in the hepatic and renal tissues and erythrocytes, it was ascertained to have significantly increased in the brain. Furthermore, GSH-Px activity had significantly decreased in all of the samples analysed. These results obtained for antioxidant enzyme activity demonstrated that pentachlorophenol caused bidirectional changes in the parameters investigated. The changes observed in the form of inhibition can be interpreted as the consumption of the enzymes either individually or as a result of it converting the free radicals resulting from its metabolism into less harmful or harmless products. On the other hand, the changes observed in the form of enzyme induction can be interpreted as the cellular defense system increasing enzyme synthesis with an aim to protect the cell from the attack of free radicals. However, both mechanisms having failed in maintaining the generation of free radicals within physiological limits and lipid peroxidation having developed at cellular level can be explained with the increase detected in the MDA and NO levels. It is considered that these results are related to the dose of pentachlorophenol administered to the animals, as well as to the length of exposure of the animals to this compound. Previous researches also suggest that pentachlorophenol induces the generation of free radicals and leads to significant changes in the intermediate and final products of lipid peroxidation [29-31, 53-55].

Origanum vulgare oil contains several components. Of these components, those that have a phenolic structure are known to be primarily responsible for the antioxidant effect. These components show antioxidant effect by means of different mechanisms, one which is the direct binding of free radicals [13-15,56-60].Thereby, under physiological conditions, the cellular antioxidant system suffices in preventing the development of lipid peroxidation and oxidative stress. Another underlying mechanism of the antioxidant effect of the phenolic components is the chelation of some metals (iron, copper, manganese, etc.) required for the reactions involved in the generation of free radicals [60, 61]. A third mechanism is the direct inhibition of some enzymes (i.e. cyclooxygenase, lipoxygenase and xanthine oxidase) involved in the generation of free radicals and peroxide [61, 62]. The most common phenolic compounds found in *Origanum vulgare* oil are thymol, carvacrol, p-cymene, β-fenchyl alcohol and γ-terpinene as mentioned before [12-15, 56].

In the present study, the analysis of the values measured in the group administered with both pentachlorophenol and *Origanum vulgare* oil demonstrated that, in general, these values had drawn closer to the values of the control group. However, it was also determined that these changes were not in the form of a complete reverse in all of the biological materials analysed. Therefore, it can be suggested that *Origanum vulgare* oil did not completely eliminate the oxidative stress caused by pentachlorophenol. On the other hand, it is considered that the antioxidant mechanisms explained above played a major role in the alleviation of oxidative stress. Therefore, it is possible that the generation of free radicals may have been reduced, in association with the prevention of the lipid peroxidation reactions by means of a high level of irreversible binding of the free radicals already generated. Finally, it may have been possible that the phenolic components of *Origanum vulgare* oil inhibited the enzymes involved in the generation of free radicals, and thereby, reduced the level of free radicals generated. Similar results have been reported in previous research on the efficacy of *Origanum vulgare* oil [49, 50].

CONCLUSION

In conclusion, when administered at the ingested dose for the indicated time period, pentachlorophenol was determined to have caused oxidative stress. The administration of *Origanum vulgare* oil was ascertained to have significantly alleviated this effect. Therefore, the demonstration of the possible use of *Origanum vulgare* oil as a supportive agent in intoxication cases bears significance for the assessment of new treatment options for pentachlorophenol intoxication. Similarly, depending on the dose of pentachlorophenol ingested in the diet and the length of exposure, it is possible that *Origanum vulgare* oil could be used as a protective agent against risk of pentachlorophenol exposure.

ACKNOWLEDGEMENT

This research (project code: TSY-11-3463) was supported by the Research Fund of Erciyes University.

REFERENCES

[1] EPA. (2009). Toxicological review of pentachlorophenol, In support of summary information on the integrated risk information system (IRIS). US Environmental Protection Agency Washington, DC, CAS No. 87-86-5.

[2] Gupta, P.K. and Aggrawal, M. (2012). Toxicity of Fungicides, In: Gupta, RC (Eds), Veterinary Toxicology: Basic and Clinical Principle. 2nd Ed. Academic Press, USA; pp 653-670.

[3] Williams, P.L. (1982). Pentachlorophenol, an assessment of the occupational hazard. *American Industrial Hygiene Association Journal*, 43: 799-810.

[4] Exon, J.H. (1984). A review of chlorinated phenols. *Veterinary and Human Toxicology*, 26: 508-520.

[5] McLellan, I., Carvalho, M., Silva Pereira, C., Hursthouse, A., Morrison, C., Tatner, P., Martins, I., San Romão, M.V. and Leitão, M. (2007). The environmental behaviour of polychlorinated phenols and its relevance to cork forest ecosystems: a review. *Journal of Environmental Monitoring*, 9: 1055-1063.

[6] WHO. (1998). Pentachlorophenol in Drinking-water. Background document for development of WHO guidelines for drinking-water Quality. Guidelines for drinking-water quality, 2nd Ed. 2: 1-13.

[7] Demir, G., Barlas, H. and Bayat, C. (2002). The toxic effect of solvent on the biological degradation of pentachlorophenol and pentachloronitrobenzene by white rot fungus. *Fresen Environ Bull*, 11: 880-884.

[8] Sevcik, P., Cik, G. and Sersen, F. (2009). Inhibition of toxic effects of chlorophenols on the growth of Chlorella vulgaris by modified tio(2) photocatalyst. *Fresen Environ Bull*, 18: 2165-2169.

[9] Crosby, D.G., Beynon, K.I., Greve, P.A., Korte, F., Still, G.G. and Vonk,.J.W. (1981). Environmental chemistry of pentachlorophenol. Pure and Applied Chemistry, 53: 1051-1080.

[10] Seiler, J.P. (1991). Pentachlorophenol. *Mutation Research*, 257: 27-47.

[11]Proudfoot,A.T.(2003).Pentachlorophenol poisoning. *Toxicological Reviews*, 22: 3-11.

[12] Radusiene, J. and Janulis, V. (2004). Improvement of diversity, trade and conservation of medicinal and aromatic plants. *Medicina (Kaunas)*, 40: 705-709.

[13] Nakatani, N. (2000). Phenolic antioxidants from herbs and spices. *Biofactors*, 13: 141-146.

[14] Faleiro, L., Miguel, G., Gomes, S., Costa, L., Venâncio, F., Teixeira, A., Figueiredo, A.C., Barroso, J.G. and Pedro, L.G. (2005). Antibacterial and antioxidant activities of essential oils isolated from Thymbra capitata L. (Cav.) and Origanum vulgare L. *Journal of Agricultural and Food Chemistry*, 53: 8162-8168.

[15] Teixeira, B., Marques, A., Ramos, C., Serrano, C., Matos, O., Neng, N.R., Nogueira, J.M., Saraiva, J.A. and Nunes, M.L. (2013). Chemical composition and bioactivity of different oregano (Origanum vulgare) extracts and essential oil. *Journal of The Science of Food and Agriculture*, 93: 2707-2714.

[16] Witterbourn, C.C., Hawkins, R.E., Brian, M. and Carrel,R W. (1975). The estimation of red cell superoxide dismutase activity. *Journal of Laboratory and Clinical Medicine*, 85: 337-341.

[17] Ohkawa, H., Ohishi, N. and Yagi, K. (1978). Reaction of linoleic acid hydroperoxide with thiobarbutiric acid. *Journal of Lipid Research*, 19: 1053-1057.

[18] Lowry, O.H., Rosebrough,.N.J., Farr, A.L. and Randall, R.J. (1951). Protein measurement with the folin phenol reagent. *Journal of Biological Chemistry*, 193: 265-275.

[19] Miller, G.L. (1959). Protein determination for large numbers of samples. *Analytical Chemistry*, 31: 964.

[20] Yoshioka, T., Kawada, K., Shimada, T. and Mori, M. (1979). Lipid peroxidation in maternal and cord blood and protective mechanism against activated-oxygen toxicity in the blood. *American Journal of Obstetics and Gynecology*, 135: 372-376.

[21] Tracey, W.R., Tse, J. and Carter, G. (1995). Lipopolysaccharide-induced changes in plasma nitrite and nitrate concentrations in rats and mice: pharmacological evaluation of nitric oxide synthase inhibitors. *Journal of Pharmacology and Experimental Therapeutics*, 272: 1011-1015.

[22] Fairbanks, V.F. and Klee, G.G. (1987). Biochemical aspect of haematology. In: Tietz NW (Ed), Fundamentals of Clinical Chemistry, WB Saunders, 3rd edn. Philadelphia; pp 803-804.

[23] Luck, H. (1965). Catalase. In: Bergmeyer H.U. (Ed). Methods of Enzymatic Analysis. Academic Press, London, pp 885-894.

[24] Sun, Y., Oberley, L.W. and Li, Y. (1988). Simple for clinical assay of superoxide dismutase. *Clinical Chemistry*, 34: 497-500.

[25] Paglie, D.E. and Valentie, W.N. (1967). Studies on the quanlitative and quantitative characterization of erytrocyte glutathione peroxidase. *Journal of Laboratory Medicine*, 70: 158-169.

[26] Uzun, F.G., Kalender, S., Durak, D., Demir, F. and Kalender, Y. (2009). Malathion-induced testicular toxicity in male rats and the protective effect of vitamins C and E. *Food and Chemical Toxicology*, 47: 1903-1908.

[27] Henkler, F., Brinkmann, J. and Luch, A. (2010). The role of oxidative stress in carcinogenesis induced by metals and xenobiotics. *Cancers (Basel)*, 2: 376-396.

[28] Kalender, Y., Kaya, S., Durak, D., Uzun, F.G. and Demir, F. (2012). Protective effects of catechin and quercetin on antioxidant status, lipid peroxidation and testis-histoarchitecture induced by chlorpyrifos in male rats. *Environmental Toxicology and Pharmacology*, 33: 141-148.

[29] Wang, Y.J., Lee, C.C., Chang, W.C., Liou, H.B. and Ho, Y.S. (2001). Oxidative stress and liver toxicity in rats and human hepatoma cell line induced by pentachlorophenol and its major metabolite tetrachlorohydroquinone. *Toxicology Letters*, 122: 157-169.

[30] Dong, Y.L., Zhou, P.J., Jiang, S.Y., Pan, X.W. and Zhao, X.H. (2009). Induction of oxidative stress and apoptosis by pentachlorophenol in primary cultures of Carassius carassius hepatocytes. *Comparative Biochemistry and Physiology C-Toxicology&Pharmacology*, 150: 179-185.

[31] Pietsch, C., Hollender, J., Dorusch, F. and Burkhardt-Holm, P. (2014). Cytotoxic effects of pentachlorophenol (PCP) and its metabolite tetrachlorohydroquinone (TCHQ) on liver cells are modulated by antioxidants. *Cell Biology and Toxicology*, 30: 233-252.

[32] Piotrowska, A. and Bartnik, E. (2014). The role of reactive oxygen species and mitochondria in aging. *Postepy Biochemii*, 60: 240-247.

[33] Kulbacka, J., Saczko, J. and Chwiłkowska, A. (2009). Oxidative stress in cells damage processes. *Polski Merkuriusz Lekarski*, 27: 44-47.

[34] Halliwell, B. (2007). Biochemistry of oxidative stress. *Biochemical Society Transactions*, 35: 1147-1150.

[35] Halliwell, B. (2009). The wanderings of a free radical. *Free Radical Biology and Medicine*, 46: 531-542.

[36] Halliwell, B. (2012). Free radicals and antioxidants: updating a personal view. *Nutrition Reviews*, 70: 257-265.

[37] Ayala, A., Muñoz, M.F. and Argüelles, S. (2014). Lipid peroxidation: production, metabolism, and signaling mechanisms of malondialdehyde and 4-hydroxy-2-nonenal. *Oxidative Medicine and Cellular Longevity*, 360438. doi: 10.1155/2014/360438.

[38] Rahal, A., Kumar, A., Singh, V., Yadav, B., Tiwari, R., Chakraborty, S. and Dhama, K. (2014). Oxidative stress, prooxidants, and antioxidants: the interplay. *BioMed Research International* 761264. doi: 10.1155/2014/761264.

[39] Oliveira, B.F., Nogueira-Machado, J.A. and Chaves, M.M. (2010). The role of oxidative stress in the aging process. *ScientificWorldJournal*, 10: 1121-1128.

[40] Birben, E., Sahiner, U.M., Sackesen, C., Erzurum, S. and Kalayci, O. (2012). Oxidative stress and antioxidant defense. *World Allergy Organ Journal*, 5: 9-19.

[41] Kmiecik, B., Skotny, A., Batycka, M., Wawrzaszek, R. and Rybak, Z. (2013). Influence of oxidative stress on tissue regeneration. *Polimery w Medycynie*, 43: 191-197.

[42] Ogura, S. and Shimosawa, T. (2014). Oxidative stress and organ damages. *Current Hypertension Reports*, 16: 1-5.

[43] Evans, P. and Halliwell, B. (2001). Micronutrients: oxidant/antioxidant status. *British Journal of Nutrition*, 85: 67-74.
[44] Hageman, J.J., Bast, A. and Vermeulen, N.P. (1992). Monitoring of oxidative free radical damage in vivo: analytical aspects. *Chemico-Biological Interactions*, 82: 243-293.
[45] Somogyi, A., Rosta, K., Pusztai, P., Tulassay, Z. and Nagy, G. (2007). Antioxidant measurements. *Physiological Measurement*, 28: 41-55.
[46] Nam, T.G. (2011). Lipid peroxidation and its toxicological implications. *Toxicology Research*, 27: 1-6.
[47] Csonka, C., Páli, T., Bencsik, P., Görbe, A., Ferdinandy, P. and Csont, T. (2015). Measurement of NO in biological samples. *British Journal of Pharmacology*, 172: 1620-1632.
[48] Niki, E. (2014). Biomarkers of lipid peroxidation in clinical material. *Biochimica et Biophysica Acta-General Subjects*, 1840: 809-817.
[49] Srihari, T., Sengottuvelan, M. and Nalini, N. (2008). Dose-dependent effect of oregano (Origanum vulgare L.) on lipid peroxidation and antioxidant status in 1,2-dimethylhydrazine-induced rat colon carcinogenesis. *Journal of Pharmacy and Pharmacology*, 60: 787-794.
[50] Sikander, M., Malik, S., Parveen, K., Ahmad, M., Yadav, D., Hafeez, Z.B. and Bansal, M. (2013). Hepatoprotective effect of Origanum vulgare in Wistar rats against carbon tetrachloride-induced hepatotoxicity. *Protoplasma*, 250: 483-493.
[51] Coussement, W. (1996). Gastro-intestinal toxicology: structure, function and enterohepatic circulation. In: Niesink RJM, Vries J, Hollinger MA (Eds), Toxicology: principles and applications, CRC Press, New York, pp 606-636.
[52] Cheng, L. (2004). Assesment report on pentachlorophenol for developing anbient air quality objectives. Alberta Environment, Prepared for Alberta Environment by WBK & Associates Inc, pp 1-64.
[53] Sai-Kato, K., Umemura, T., Takagi, A., Hasegawa, R., Tanimura, A. and Kurokawa, Y. (1995). Pentachlorophenol-induced oxidative DNA damage in mouse liver and protective effect of antioxidants. *Food and Chemical Toxicology*, 33: 877-882.
[54] Klobucar, G.I., Lajtner, J. and Erben, R. (1997). Lipid peroxidation and histopathological changes in the digestive gland of a freshwater snail Planorbarius corneus L. (Gastropoda, Pulmonata) exposed to chronic and sub-chronic concentrations of PCP. *Bulletin of Environmental Contamination and Toxicology*, 58: 128-134.
[55] Michałowicz, J. (2010). Pentachlorophenol and its derivatives induce oxidative damage and morphological changes in human lymphocytes (in vitro). *Archives of Toxicology,* 84: 379-387.
[56] Wojdyło, A., Oszmianski, J. and Czemerys, R. (2007). Antioxidant activity and phenolic compounds in 32 selected herbs. *Food Chemistry*, 105: 940-949.
[57] Dambolena, J.S., Zunino, M.P., Lucini, E.I., Olmedo, R., Banchio, E., Bima, P.J. and Zygadlo, J.A. (2010). Total phenolic content, radical scavenging properties, and essential oil composition of Origanum species from different populations. *Journal of Agricultural and Food Chemistry*, 58: 1115-1120.
[58] Saleh, M.A., Clark, S., Woodard, B. and Deolu-Sobogun, S.A. (2010). Antioxidant and free radical scavenging activities of essential oils. *Ethnicity&Disease*, 20: 78-82.
[59] Karakaya, S., El, S.N., Karagözlü, N. and Sahin, S. (2011). Antioxidant and antimicrobial activities of essential oils obtained from oregano (Origanum vulgare ssp. hirtum) by using different extraction methods. *Journal of Medicinal Food*, 14: 645-652.
[60] Majid, R., Ahmad, L. and Zargar, M.A. (2012). Antioxidant screening of ethanolic and aqueous extracts of Organum vulgare L. in-vitro. *African Journal of Biochemistry Research*, 6: 165-171.
[61] Miguel, M.G. (2010). Antioxidant and anti-inflammatory activities of essential oils: A short review. *Molecules*, 15: 9252-9287.
[62] Bustanji, Y., Hudaib, M., Tawaha, K., Mohammad, M.K., Almasri, I., Hamed, S., and Oran, S. (2011). In vitro xanthine oxidase inhibition by selected jordanian medicinal plants. *Jordan Journal of Pharmaceutical Sciences*, 4: 49-56.

*This study is the MSc thesis of Mehmet Akıllı.

Received: **13.06.2015**
Accepted: **07.01.2016**

CORRESPONDING AUTHOR

e-mail: geraslan38@hotmail.com

**Prof. Dr. Gökhan Eraslan
Erciyes Üniversitesi
Veteriner Fakültesi
Farmakoloji ve Toksikoloji Anabilim Dalı
Melikgazi, Kayseri – TURKEY

by PSP Volume 25 – No. 1/ 2016, pages 130-141 Fresenius Environmental Bulletin

AN INVESTIGATION INTO THE EFFICIENCY OF NEW TYPE ORGANIC COMMERCIAL COAGULANTS IN THE PRETREATMENT OF ACRYLIC MANUFACTURING WASTEWATERS

Edip Avsar[a]

[a]Bitlis Eren University Engineering and Architecture Faculty, Engineering Department, Rahva Campus, 13000 Center Bitlis TURKEY.

ABSTRACT

The aim of this study was to investigate the efficiency of several new types of commercial coagulants in the pretreatment of acrylic manufacturing process wastewaters. This new type of coagulant basicly differs from the convantional Al, Fe based inorganic ones in their organic structure and biodegrability. In the study, the effects of these coagulants on COD, turbidity, color (actual and apparent), pH, and the TSS removal of acrylic manufacturing wastewater are determined. It is stated by the manufacturer that the new type of commercial coagulants used in this study are capable of removing COD with a percentage of around 40, and the TSS around 95%. Also, significant color removal can also be achieved in textile wastewaters by applying these coagulants. Therefore, coagulation with these coagulants may be used as an alternative pretreatment instead of advanced oxidation processes. The optimum working pH values are determinated experimentally, and the treatment efficiencies are determinated for 5 new types of commercial coagulants. It was concluded that the COD removal efficiency of the new type cogulants was higher than the classical inorganic coagulants by approximately 10% when using approximately 3 times lower dosages. However, the treatment cost is 2 or 3 times higher than that of the ferrous coagulants. The maximum COD removal efficiency of the coagulants was determined as 31%. The TSS removal is determined to be closer to the efficiency given by the manufacturer, but inefficient color removal is observed.

KEYWORDS: Acrylic manufacturing wastewaters, organic coagulants, pretreatment, COD removal

INTRODUCTION

The fibres that are used in the textile industry are generally classified as both natural and man-made (synthetic). Synthetic fibres encompass both purely synthetic materials of petrochemical origin, and regenerative cellulosic materials manufactured from wood fibres [1]. It has important advantages over natural fibers in terms of its durability, resistance to chemicals and cotton-like texture, and these features put this sector in a prominent position on the global manmade market [2]. This industry is over 50 years old, has rapidly progressed over recent decades, and has four major product types: nylon, polyester, acrylic and polypropylene. The first acrylic fiber to be made on a commercial scale was orlon [3,4].

Polyacrylonitrile (PAN) fiber is one of the forms of acrylic fiber. These produced fibers are composed of at least 85% by weight of acrylonitrile units [5], and are obtained by radical polymerisation of acrylonitrile in aqueous emulsion, or in solvent. If the obtained polymer is composed of 100 % acrylonitrile (also called PAN), these fibres posses insufficient dye-binding capabilities, due to the high glass transition temperature (> 100 ºC). In this case this polymer is no longer used in the textile industry. Acrylic fibres (PAC), commonly available today, are anionic copolymers, which contain 85 – 89 % of acrylonitrile, 4 – 10 % of a non-ionic comonomer (vinyl chloride, vinyl acetate, methyl acrylate), and 0.5 – 1 % of ionic comonomers containing sulphonic or sulphate groups [1].

Synthetic fibres are typically extruded into continuous filaments. The continuous filaments can then be used directly (in general, following further shaping or texturing), cut into a staple length, and then spun in a process resembling the one used for wool or cotton. The three main methods are available in terms of continuous filaments production (primary spinning): these methods are; melt, dry and wet spinning [1].

Wet spinning is the oldest process. In this process the polymer that is used for fiber-forming has been dissolved in a solvent. The spinnerets are submerged in a chemical bath, and as the filaments emerge they precipitate from a solution and thus, solidify. Because the solution is extruded directly into the precipitating liquid, this process for making the fibers is called wet spinning. Acrylic, rayon, aramid, modacrylic, and spandex, can be produced by this process [6]. For the dry spinning process, the polymer is used as dissolved in dimethylformamide (DMF). If the fibre is manufactured through the wet spinning, besides the DMF, dimethylacetamide, dimethylsulphoxide, ethyl carbonate and aqueous solutions of inorganic salts, or acids, are also used. Residues of these solvents (0.2 - 2 % of the weight of the fibre) are found in the wastewater from the pre-treatment [1].
The main environmental issues arising from the activities in the textile industry are the refractory COD and color [7-9]. In terms of wastewater treatment, acrylic fiber manufacturing companies typically adopted a conventional biological treatment system followed by the physicochemical methods of neutralization, coagulation, and sedimentation [10]. The membrane processes (ultrafiltration and reverse osmosis) were also employed too. In addition, a combined three-stage process of thermophilic anaerobic/anoxic denitrification/aerobic nitrification, fluidized bed reactor, and the advanced oxidation processes were used to treat acrylic fiber manufacturing wastewater [10]. Due to the high organic load, toxicity, and presence of biorefractory compounds, the biological processes were not efficient in terms of acrylic fiber manufacturing wastewater treatment [10].

The aim of this study is to investigate the pre-treatment efficiency of the five new type organic coagulants in acrylic fiber manufacturing wastewaters.

MATERIALS AND METHODS

SAMPLE USED

The wastewater used in this research was taken from an acrylic polymer manufacturing factory where the manufacturing process was based on the application of both wet spinning and dying processes. The 24 hour composite wastewater sample was collected, and all the experiments were conducted with this sample.

TREATABILITY EXPERIMENTS

5 new types of coagulant and 1 flocculant (anionic type, 1g/L concentration), which are commercially avalilable were obtained. The high biodegrability and organic structure are the basic differences between these coagulants and the Al-Fe based conventional ones. The information about the coagulants used in this study is given in Table 1 below.

TABLE 1
Specifications of the coagulants used in this research [11]

No	Content	Physical condition	pH	Density (g/cm^3)	Ecological info	Dilution prepared mL/100mL	Dilution pH
1	Cationic dicyandiamide formaldehyde	liquid, colorless	4-5	1.05-1.10	organic %100 biodegrable	1	5.05
2	Polyaluminiumchloride hydroxidesulphate	liquid, clear	2-3	1.30-1.33	organic %100 biodegrable	1	4.06
3	Mixture of Polydiallydimetil Amonium chloride and cationic emulsion polymer	liquid, white	4-5	1.30-1.33	organic %100 biodegrable	1	4.71
4	Mixture of Poliquarternaryamin and cross-link cationic emulsion polymer	liquid, reddish	6-7	1.02-1.06	organic %100 biodegrable	1	4.64
5	Mixture of polydially dimethyl ammonium chloride and solvent	liquid, yellowish	2.5-3	1.30-1.33	organic %100 biodegrable	1	3.97

The methodology utilized for the jar test experiments are summarized in Table 2 below [12].

TABLE 2
Experimental methodology

Step	Processes
pH maintenance	pH maintenance was carried according to further details on 500 mL of wastewater sample
Coagulation	Coagulants added to sample according to further details given at the first and second step of the experimentthen Sample was stirred for 5 min at 120 rpm
Flocculation	2 mL of anionic polyelectrolyte was added to sample and stirred for 30 min at 10 rpm after coagulation
Settling	The sample was allowed to slowly settle for 30 min after flocculation

0.01 N NaOH and 0.01 N HCl was used for pH adjustment. At the end of the jar test procedure; the TSS, COD (total and soluble), color, and turbidity (apperant and true) measurements were conducted for every samples' supernatant phase.

ANALYTICAL PROCEDURE

The parameters and methods which were used in this research are given in Table 3 below. For a better understanding of the color removal mechanisim, 2 different color measurement methods were used. The true color measurement is the method that was utilized for the sample after the filtration of the particles that caused turbidity. The apperant color measurement is the method that was utilized for the sample without any pretreatment step.

TABLE 3
Parameters and methods [13]

Parameter	Method
TSS	Gravimetric Method, SM 2540:D
COD	Open Reflux Method, SM 5220:B
Color	Spektrophotometric Method, SM 2120:C
Tubidity	Spektrophotometric Method, SM 2130:B

RESULTS AND DISCUSSION

WASTEWATER CHARACTERISTIC

The wastewater characteristics are shown in Table 4 below.

As seen from Table 4, the important part of the COD was composed of dissolved COD.

In this context, the COD portion that can be removed by chemical treatment was limited with the suspended part that corresponds to 36.2 % of the COD, and practically, the chemical treatment efficiency cannot exceed this portion.

TABLE 4
Wastewater characterictics of the investigated wastewater

Sample Name	TSS (mg/L)	Real color (Pt-Co)	Apparent color (Pt-Co)	COD (mg/L)	Particulate COD (mg/L)	Soluble COD (mg/L)	Turbidity (NTU)	pH
Acrylic manufacturing	290	855	6218	1892	696	1196	48	6.76

According to the Table, the real color of the sample was determined as 855 Pt-Co, but the apparent color was determined as 6218 Pt-Co. This difference came from the membrane filtration (0.45 μm) process that was utilized for the real color determination as a pre-treatment, but in the apparent color determination, there was no pre-treatment step, and the determination was conducted with the raw sample.

When the characterization of the wastewater was compared with the literature, it was found that it was indeed, compatible with the literature. The literature data shows that wastewater characterization can differ according to either the main process used or the different additional processes. The results of the wastewater characterization obtained from the literature are given in Table 5.

TABLE 5
Characterization of various acrylic fiber manufacturing wastewaters

Parameter	Literature			
	[14]	[15]	[10]	[16]
COD	1091	800-1000	4378-4611	921
pH	6.56	7.0	3.0-3.8	5.7
TSS	N.A*	50	N.A*	N.A*

*N.A: not available in the text.

The characterization adopted from [10] was quite complicated because the process which was investigated in this study included an acrylonitrile unit, a vinyl acetate unit, and the wastewater also included also oligomers, DMAc, EDTA, and sulfate.

TREATABILITY EXPERIMENTS

Optimum pH Determinations. At the first stage of the experiments, the optimum pH values of the 5 different coagulants were determined with the aid of an anionic polyelectrolyte. For this purpose, the settling efficiency of the coagulants were determined at the fixed coagulant dosage at five different pH values. The pH value interval was determined between the 6.5-8.5 range (6.5, 7.0, 7.5, 8.0, 8.5) considering the pH of the wastewater was close to a neutral pH, the wastewater was able to enter the other treatment step following the pre-treament step, and the greater amounts of chemicals for the pH adjustment would increase the operating cost.

In the context of the optimum pH determination study including the 5 pH values, the coagulant dosage was utilized as 4 mL for all of the 5 coagulants, and the anionic polyelectrolyte dosage was 2 mL. After the coagulation-flocculation process, the turbidity measurement was conducted for every sample at different pH values, and then the optimum pH was determined for each of the 5 coagulants. The achieved results are shown in Figure 1 below.

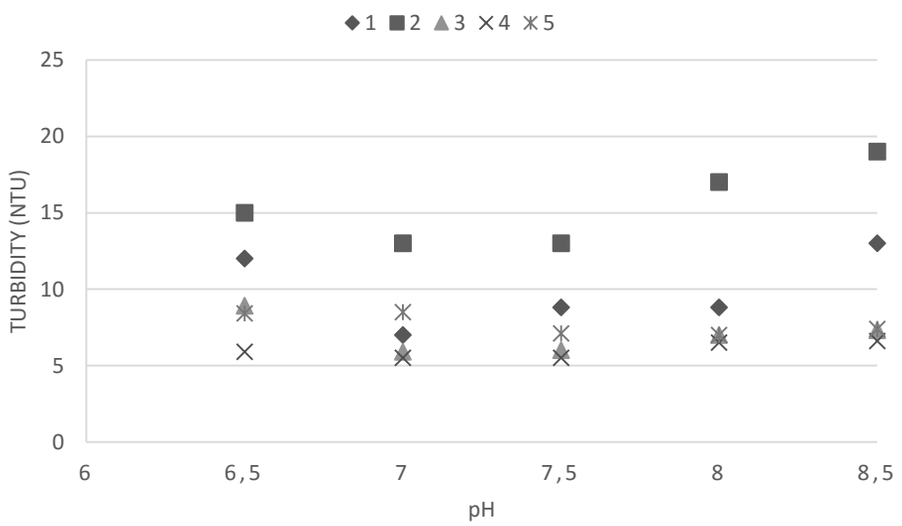

FIGURE 1
Optimum pH determinations of the coagulants at the fixed dosage

According to Figure 1, it can be seen that results were close for all of the coagulants. The lowest turbidity results were obtained for the coagulant 1 and 2 (7 and 5.9 NTU respectively) when the pH value was 7. In terms of coagulant 2 and 4 (13 and 5.5 NTU respectively), the same lowest results were obtained with both pH values being 7 and 7.5. It was understood that the pH variation between 7-7.5 values did not impact on the efficiency of the chemicals. The optimum pH value was determined as 8 in terms of the turbidity removal (7 NTU) for the coagulant 5.

When the optimum pH of the chemical treatment process was compared with the fenton oxidation and ferrous combined systems for acrylic fiber manufacturing wastewaters, it was determined that the pH value had a decisive effect on the oxidation potential. When the pH value was 3.0, a peak was obtained both for the overall COD removal and the COD removal by oxidation [10]. These results indicated that working at a neutral pH for the investigated coagulants was suitable, and in this way, the requirement of the pH adjustment like the fenton process is minimized.

Treatment efficiencies. In the second stage of the study, the optimum contaminant removal dosages were determined for the aforementioned coagulants according to the optimum pH values determined in the first stage of the work. In this case the jar test was repeated for each of the 5 coagulants at four different dosages (2-4-6-8 mL) with the aid of an anionic polyelectrolyte. In this context, the chemical concentrations calculated for each dosage are given in Table 6 below.

TABLE 6
Chemical concentration calculations of 4 different dosages utilized for jar tests

Chemical dosage (mL)	Chemical concentration (ppm/mL dosage)	Concentration in the sample ppm/500mL
2	20000	40
4	40000	80
6	60000	120
8	80000	160

According to the results, the parameter based removal efficiencies and optimum contaminant removal dosages of the coagulants were determined Within the context of the study, the turbidity removal efficiency of 5 different coagulants was investigated with the aid of anionic polyelectrolide. The experimental results are given in Figure 2. According to Figure 2, it was determined from that the treatment efficiency increased with the increased coagulant dosages.

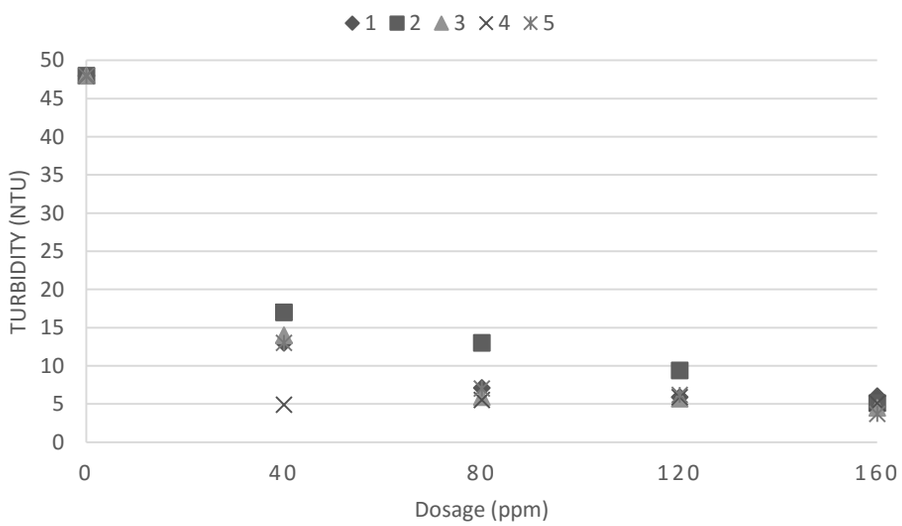

FIGURE 2
Turbidity removal efficiency of the coagulants at different dosages

However, in the case of coagulant 4, the highest turbidity removal efficiency was determined for the lowest (40 ppm) dosage; the removal effiency decreased along with the increased dosage and, at the highest dosage (160 ppm) it was found to increase again. The highest turbidity removal efficiency was obtained for coagulant 4 at a 160 ppm dosage (yield 92.3%). The lowest removal efficiency was achieved for coagulant 2 for the 40 ppm dosage (64.6%). When all trials had been considered, the average removal efficiency was identified as 83.6% in terms of turbidity removal.

TSS removal efficiency of the acrylic fiber manufacturing wastewater was investigated for the same dosages conducted for turbidity removal experiments. The result is given in Figure 3.

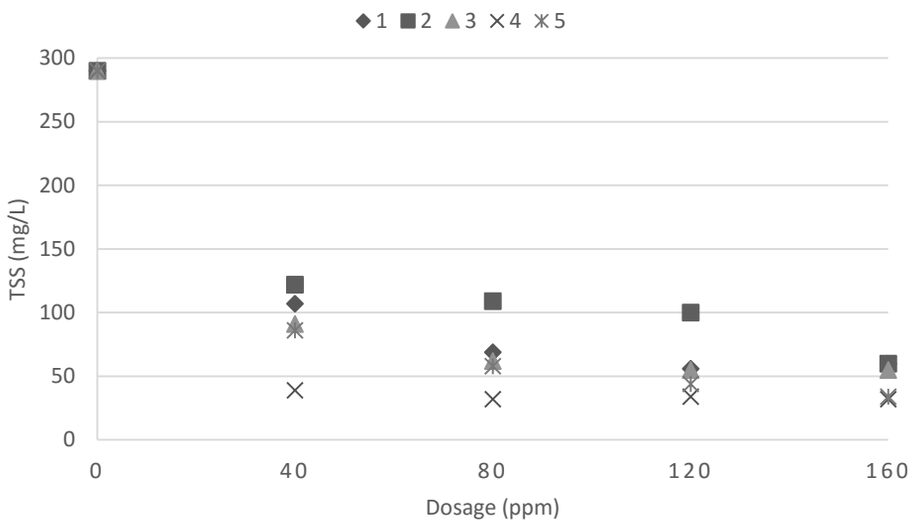

FIGURE 3
TSS removal efficiency of the 5 coagulants at 4 different dosages

It can be seen from Figure 3, that in general, the removal effiency increased with the increasing coagulant dosages as obtained for the turbidity. This is especially true in terms of the findings from the coagulants 2 and 5 experiments as they fully fitted in with this trend. However, the removal efficiency of the coagulants 1, 3, 4, increased with the dosages up to 80 ppm, and a significant increase in the removal efficiency was not observed for any dosages higher than 80 ppm.

The TSS and turbidity removal figures which were similar to each other indicated that, the TSS was the most important turbidity source for the wastewater, and significant levels of turbidiy removal was achieved by means of the TSS removal. The maximum TSS removal efficincy was obtained as 89 % by using 80 ppm of the coagulant 4. The average removal efficiency of the coagulants was determined as 77.5%.

The true color and apperant color were determined as 855 and 6218 Pt-Co respectively, for the raw wastewater.

The true color removal efficiencies for the 5 different coagulant for the 4 different dosages are given in Figure 4 below.

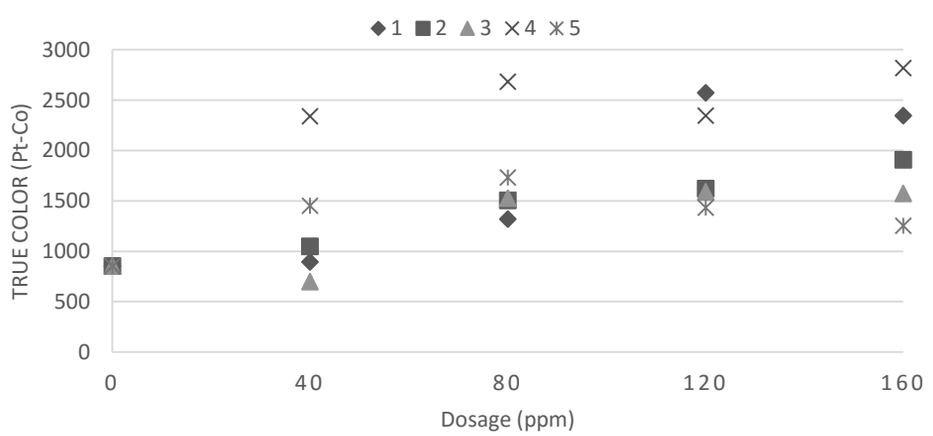

FIGURE 4
True Color removal efficiency of the 5 coagulants at 4 different dosages

According to Figure 4, apart from coagulant 3, the true color increased along with the increased coagulant dosage. This fact indicated that the coagulants elevated the true color of the wastewater. Only an 18% true color treatment efficiency was achieved for coagulant 3 at a 40 ppm dosage.

The apparent color measurement results are given in Figure 5.

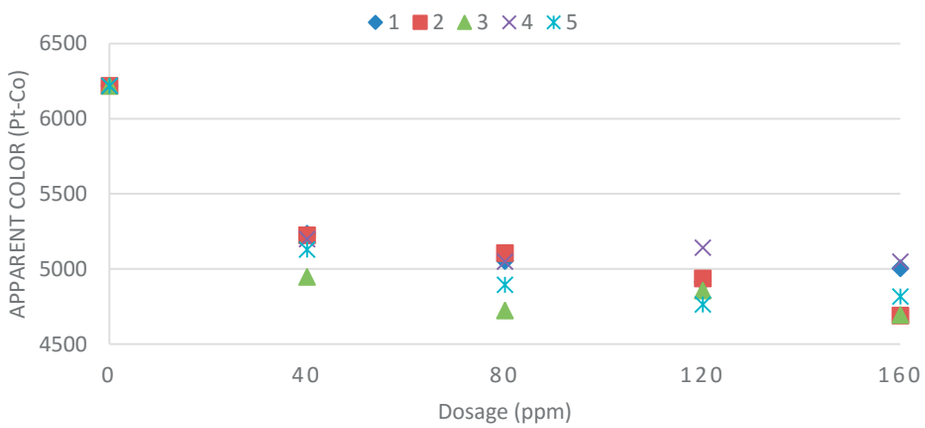

FIGURE 5
Apparent Color removal efficiency of the 5 coagulants at 4 different dosages

According to Figure 5, the removal efficiency of coagulant 2 increased with the increased dosage, and a maximum removal efficiency was determined as 24.6% for the 160 ppm dosage. In terms of coagulants 4 and 3, the removal efficiency increased up to a 120 ppm dosage. At a 120 ppm dosage, the efficiency decreased to the same level of the 40 ppm dosage. At the 160 ppm dosage, the efficiency increased to the same level as the 80 ppm dosage. The maximum removal efficiencies of coagulants 4 and 3 were observed at 18.8% and 24.5% respectively. In terms of coagulants 1 and 5, the removal efficiency increased up to a 160 ppm dosage. At a 160 ppm dosage, the efficiency decreased to the same level as the 80 ppm dosage. The maximum removal efficiencies of coagulants 1 and 5 were observed as 21% and 23.4% respectively.

The true and apperant color measurement results indicated that, an important part of the TSS was removed by the coagulants, but its effect on color removal was limited because dissolved solids were the main color source of the wastewater. The true color, turbidity, and TSS removal figures, which were seen to fit each other also indicated that this was the case.

The color of the wastewater sample mainly came from the dying process. According to the literature, chemical coagulation is not effective in the removal of dissolved reactive dyestuffs as there is no single process capable of color removal because the effluents of the dying process are complex in nature [17,18]. Because of this, in practice, a combination of different processes are often used to achieve the desired treatment efficiency, and in the most economical way. According to the literature, these systems consist mainly of a combination of adsorption-biological treatment systems in order to both improve the biodegradation of the dyestuffs, and minimize sludge production [17,18]. In this study, the obtained color removal efficiencies were confirmed from the literature findings.

The COD was another parameter where removal efficiency was investigated. For a better understanding of the coagulants COD removal efficiency, their measurements were conducted both for the particulate and the soluble phase, and then the removal efficiency was determinated for both of them. In the context of the study, the total COD removal efficiency of the five coagulants at 4 different dosages are given in Figure 6 below.

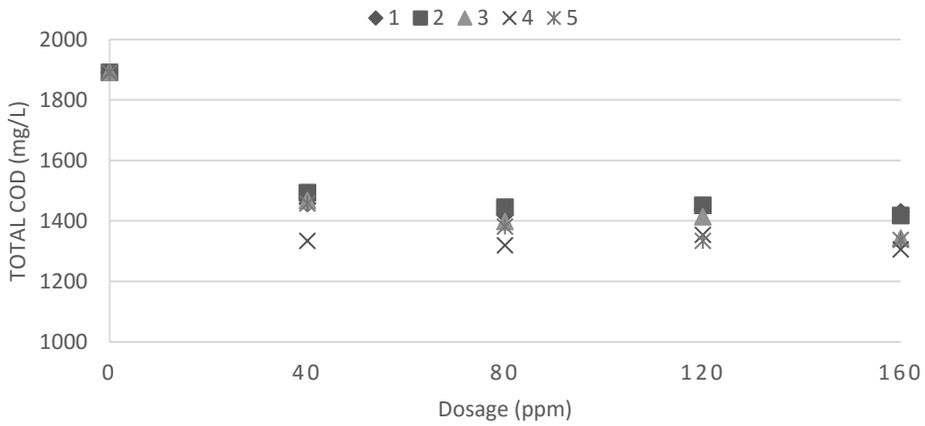

FIGURE 6
Total COD removal efficiency of the coagulants at different dosages

In terms of total COD removal, 80 ppm was the optimum dosage for all of the coagulants, and increasing the dosage had no effect on the removal efficiency. In terms of the total COD, both the maximum and average removal efficiencies were determined as 31% and 26% respectively. According to [16] the effluent of the acrylic fiber manufacturing factory was subjected to coagulation via poly aluminum chloride (PAC). According to the results, the PAC removed most of the low polymers, and the removal efficiency was determined as 21.4%. These results indicated that the new type of coagulants had a better total COD removal when compared to the PAC.

In the context of the study, the particulate COD removal efficiencies of the 5 coagulants are given in Figure 7 below.

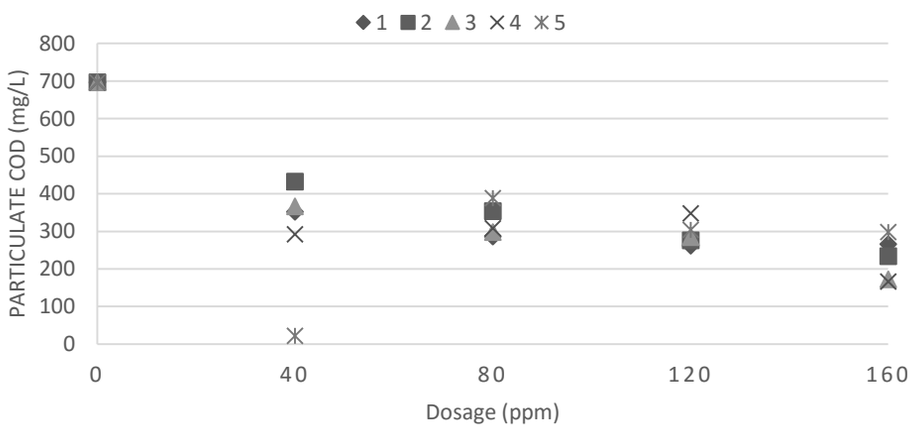

FIGURE 7
Particulate COD removal efficiency of the coagulants at 4 different dosages

According to Figure 7, it was concluded that the particulate COD removal and the total COD removal efficiencies were similar to each other. This case indicated that the particulate phase of the total COD was usually removed by the coagulants used in this research. The maximum particulate COD removal efficiency was determined as 99.6% for coagulant 5 at a 40 ppm dosage. For this coagulant, the efficiency decreased for dosages higher than 40 ppm. In terms of coagulants 2 and 3, the removal efficiency increased along with the increased dosage. However, the removal efficiency decreased for the coagulants coded 4 up to a 160 ppm dosage but the maximum removal efficiency was achieved for the 160 ppm dosage. For the coagulant 1, the removal efficiency increased up to a 160 ppm dosage. The average and minimum particulate COD removal efficiency was observed as 59% and 37.9% respectively. The correspondancy of the Particulate COD, the turbidity, and the TSS removal figures, indicated

that the turbidity and particulate COD decreased along with the TSS removal.

The soluble COD removal efficiences of the 5 coagulants are given in Figure 8 below. It is obvious from the the Figure that the soluble COD removal was considerably limited. The maximum soluble COD removal was determined as 16.9% for the coagulant 5 at 80 ppm dosage. In this case, it was determined that the important part of the total COD removal efficiency was constituted by the particulated COD removal, and in terms of soluble part, there was no remarkable removal efficiency.

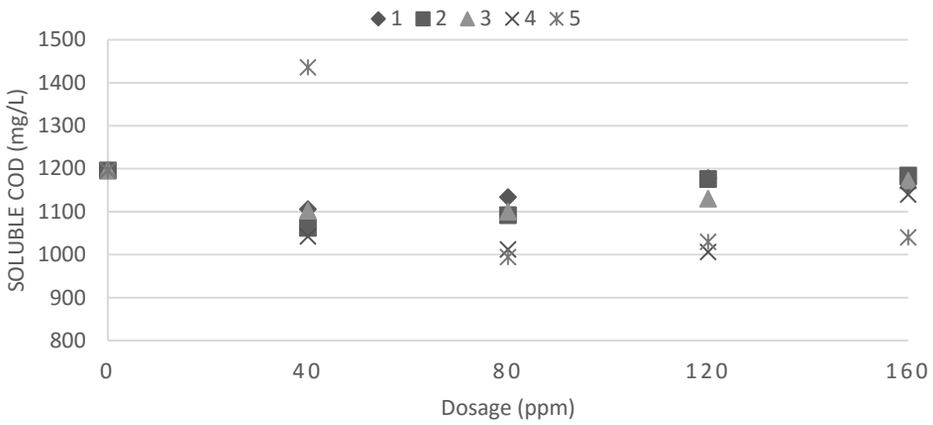

FIGURE 8
Soluble COD removal efficiency of the coagulants at different dosages

Li et al, 2012, used the fenton process combined with the coagulation by ferrous to pre-treat the acrylic fiber manufacturing wastewaters. The COD removal by coagulation was approx 10% when the ferrous dosage was 100 ppm. An approximate 20% COD removal was obtained when the dosage was increased to 300 ppm. When the ferrous was combined with the fenton (500 ppm), the total removal was increased to 62%. When the research results were compared with the aforementioned literature that dealt with ferrous, it was clear that the new type of coagulants provided a higher removal efficiency with lower dosages. However, when conventional coagulants were combined with the oxidation process, the removal efficiency increased twice as much as with the new type coagulants.

According to the Turkish Water Pollution Control Regulation Table 10.7 [19], COD and color limit values are enforced as 300 mg/L and 260 Pt-Co respectively. To meet these limit values, 77% COD and 63% color removals are required. Methods such as biological oxidation or activated carbon adsorption can be used as consequtive treatment steps for achieving the limit values [17].

The average removal efficiencies of the coagulants on the basis of the parameters are given in Figure 9 below.

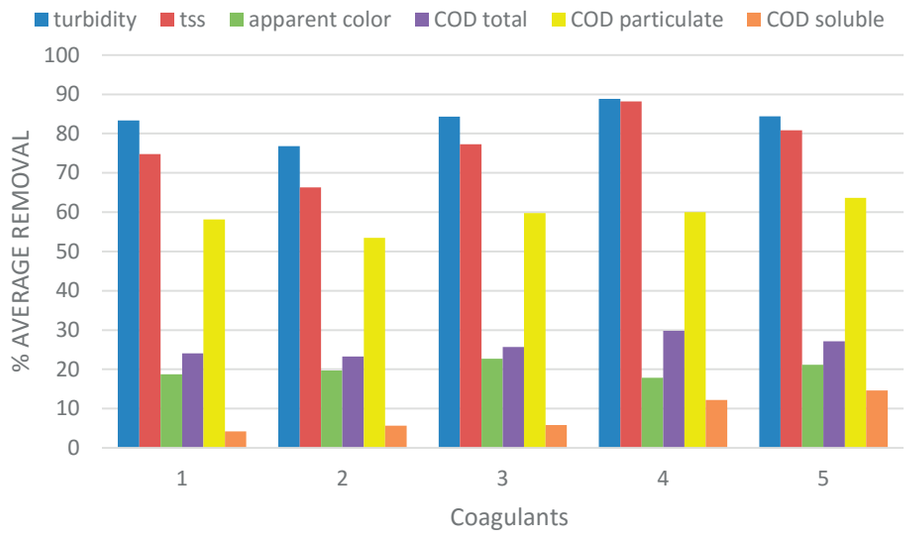

Average removal efficiencies of coagulants on the basis of parameters

According to the Figure; in terms of color removal, the most effective is coagulant 3, for the turbidity, TSS, and the total COD, the most effective is coagulant 4, and for the particulate and soluble COD, coagulant 5 is the most effective.

Treatment cost. The cost analysis based on the maximum COD removal efficiency. The cost of 1 L of coagulant is approximately 0.50 euro [20], and 1kg of anionic polyelektrolite is approximately 4.96 euro [21]. For the optimum dosage of 80 ppm and 1 ton of wastewater treatment, the total cost was estimated to be approximately 0.05 euro or 50 euro for 1000 tons of wastewater on the basis of the chemical cost. In the case of the ferrous coagulants, the cost of 1 kg coagulant is between 0.046 - 0.092 euro. For the 300 ppm dosage given in the literature, 1 ton of the wastewater treatment total cost was estimated to be approximately 0.014 - 0.028 euro or 14- 28 euro for 1000 tons of wastewater on the basis of the chemical cost [22]. As a result, the new type of organic coagulants with better treatment efficiencies cost 2 or 3 times more.

CONCLUSION

In the context of this study, the pretreatment of acrylic fiber manufacturing wastewaters originating from wet spinning and dying processes via 5 different new type coagulants were investigated. According to the results; a true color removal efficiency (18%) was only achieved via coagulant 3, at a 40 ppm dosage, and true color removal could not be achieved in any of the other coagulants. Also, the true color of the wastewater sample was increased by the coagulants.

The COD results indicated that the colloidal and suspended parts of the COD were removed effectively, but as expected, a considerably limited removal efficiency was obtained in terms of the soluble part of the total COD. When the parameter based removal efficiencies of the coagulants were examined, the coagulant that gave the maximum removal efficiency for each parameter seemed to be different. The maximum true color removal efficiency of 18% was achieved by using coagulant 3, the maximum total COD and TSS removal efficiencies of 31% and 89% respectively were achieved by using chemical coded 4, and in terms of the TSS, a maximum removal efficiency of 89% was achieved by using chemical coded 4. In terms of cost analysis based on COD removal, a higher removal was achieved at lower dosages, but the cost was 2 to 3 times higher when compared to conventional ferrous coagulants.

The application of the new type coagulants was more effective than the conventional ones in terms of COD and TSS removal, but coagulation-flocculation alone was not adequate in achieving the discharge limits, and also was more expensive than conventional coagulants. Therefore, treatment units such as activated sludge, must be used after the coagulation-flocculation process.

REFERENCES

[1] Integrated Pollution Prevention and Control (IPPC) Reference Document on Best Available Techniques for the Textiles Industry Europen Comission, July 2003

[2] B. Ray, A. Lamsam, A.P. Annachhatre, Treatment and management of wastewater

from an acrylic fiber ındustry, GMSARN International Conference on Sustainable Development: Issues and Prospects for GMS, 2006.
[3] J.C. Masson, Acrylic Fiber Technology and Applications, Marcel Dekker Inc, 1995, ISBN 0-8247-8977-6.
[4] J. Wei, Y. Song, X. Tu, L. Zhao, E. Zhi, Pretreatment of dry-spun acrylic fiber manufacturing wastewater by Fenton process: optimization, kinetics and mechanisms, Chemical Engineering Journal 218 (2013) 319–326.
[5] A. Sedghi, R.E. Farsani, A. Shokuhfar, The effect of commercial polyacrylonitrile fibers characterizations on the produced carbon fibers properties, Journal of Materials Processing Technology 198 (2008) 60–67.
[6] (http://www.fibersource.com/f-tutor/techpag.htm), Last Access on 31.03.2015.
[7] I. A. Alaton,G. Eremektar, F. G. Babuna, H. Selcuk, D. Orhon, Chemical pre-treatment of textile dye carriers with ozone: effects on acute toxicity and activated sludge inhibition, PSP Volume 13 (2004) – No 10.
[8] I.A. Alaton, G. Insel, G. Eremektar, F.G. Babuna, D. Orhon, Effect of textile auxiliaries on the biodegradation of dyehouse effluent in activated sludge, Chemosphere 62 (2006) 1549–1557.
[9] S. Koyunluoglu, I.A. Alaton, G. Eremektar, F.G. Babuna, Pre-ozonation of commercial textile tannins: Effects on Biodegradability and Toxicity, Journal of Environmental Science and Health Part A, 41 (2006) 1873–1886.
[10] J. Li, Z. Luan, L. Yu, Z. Ji, Pretreatment of acrylic fiber manufacturing wastewater by the Fenton process, Desalination 284 (2012) 62–65.
[11] Kemira Water solutions B.V. 2015. MSDS No: KEMIRA-TR 0005836, KEMIRA-TR 0005836, KEMIRA-TR 0005836, KEMIRA-TR 0005826, KEMIRA-TR 0005840, Botlekveg 175. Haven 4501 Holland.
[12] ASTM D2035-13, 2013. Standard Practice for Coagulation-Flocculation Jar Test of Water, West Conshohocken, PA 19428-2959. United States
[13] Standard Methods for the Examination of Water & Wastewater, 2005. (21st edition)American Public Health Association, Washington, DC.
[14] J. Wei, Y. Song, X. Tu, L. Zhao, E. Zhi, Pretreatment of dry-spun acrylic fiber manufacturing wastewater by Fenton process: Optimization, kinetics and mechanisms, Chemical Engineering Journal 218 (2013) 319–326.
[15] Y.S. Na, C. H. Lee, T.K. Lee, S.W Lee, Y.S. Park, Y.K. Oh, S.H. Park, S.K. Song, Photocatalytic decomposition of nonbiodegradable substances in wastewater from an acrylic fibre manufacturing process, Korean J. Chem. Eng., 22(2), 246-249 (2005).
[16] Zhang C., Wang L., Zhoub H., Fua D., Gua Z., 2011. Anodic treatment of acrylic fiber manufacturing wastewater with boron-doped diamond electrode: A statistical approach, Chemical Engineering Journal 161 (2010) 93–98
[17] O.T. Can, M. Kobya, E. Demirbas, M. Bayramoglu, Treatment of the textile wastewater by combined electrocoagulation, Chemosphere 62 (2006) 181–187.
[18] G. Crini, Non-conventional low-cost adsorbents for dye removal: A review, Bioresource Technology 97 (2006) 1061–1085.
[19] Turkish Water Pollution Control Regulation (Official Gazette dated 31.12.2004 – No. 25687
[20] (http://www.trakyacevre.com/aritma-dosyasi.pdf), Last Access on 31.03.2015.
[21] (http://www.aritmasepeti.com/HYDROFLOC-A-3605-SA-ANYONIK-POLIELEKTROLIT,PR-363.html), Last Access on 31.03.2015.
[22] (http://turkish.alibaba.com/product-gs/price-ferrous-sulphate-60016098189.html), Last Access on 31.03.2015.

Received: **17.06.2015**
Accepted: **12.01.2016**

CORRESPONDING AUTHOR

Edip Avsar
Bitlis Eren University
Engineering and Architecture Faculty
Engineering Department
Rahva Campus
13000 Center Bitlis – TURKEY

email: eavsar@beu.edu.tr

by PSP Volume 25 – No. 1/ 2016, pages 142-152 Fresenius Environmental Bulletin

THE EFFECT OF EXOGENOUS SELENIUM ON THE GROWTH AND PHOTOSYNTHETIC PIGMENTS CONTENT OF CUCUMBER SEEDLINGS

Weronika Jóźwiak[1], Mirosław Mleczek[2], Barbara Politycka[1]

[1]Department of Plant Physiology, Poznań University of Life Sciences, Wołyńska 35, 60-637 Poznań, Poland
[2]Department of Chemistry, Poznań University of Life Sciences, Wojska Polskiego 75, 60-625 Poznań, Poland

ABSTRACT

The aim of the study was to verify whether exogenous selenium (Se) influences the growth and photosynthetic pigments content in cucumber (*Cucumis sativus* L.) seedlings. Seedlings were grown on Hoagland's nutrient solution with sodium selenite (1, 5 or 10 μM) or without it (control). Exogenous Se caused a marked increase in the accumulation of endogenous Se in roots and cotyledons of cucumber seedlings. The highest content of Se in tissues was noted at 10 μM Se; the levels of Se in roots and cotyledons were higher than before supply of Se, by 66% and 50%, respectively. Seedlings growing on a medium with sodium selenite exhibited a growth reduction in relation to the control. Se at the highest concentration (10 μM) decreased fresh weight of roots and cotyledons by about 20% and 40%, respectively. An increase in dry weight/fresh weight ratios of cotyledons exposed to 5 and 10 μM Se was found. Increasing concentrations of Se in the nutrient solution resulted in a linear increase in chlorophyll *a* and *b* as well as carotenoids contents. Chlorophyll *a/b* ratio was enhanced with increasing Se concentrations. These results indicate that exogenous Se at higher concentration (5 and 10 μM) limited the growth of plants but did not inhibit the content of photosynthetic pigments.

KEYWORDS: *Cucumis sativus* L., photosynthetic pigments, plant growth, selenium, toxicity

INTRODUCTION

The biological significance of selenium (Se) in human and animal metabolism is well documented [1, 2]. In contrast, there are still many questions about the role of Se in higher plants. However, over the last two decades Se has been shown to affect many physiological processes in plants, including the growth [3, 4]. Se is known as the "double-edged sword element" for its dual toxic and beneficial activity depending on the dosage; thus some data show its positive effects on plant species at low concentrations, and negative at higher. Much attention has been focused on studies of Se influence on plants under various stress conditions [5, 6, 7, 8]. It has been demonstrated that exogenous Se can promote the growth of plants subjected to high-energy radiation by enhancing their antioxidative capacity [9, 10]. In contrast, Se at high concentrations can act as a prooxidant reducing yield [11, 12]. At concentrations of 10-30 μM Se exerted an adverse effect on antioxidant enzymes activities and growth of sorrel seedlings [13]. An inhibitory effect of Se on growth has also been reported for ryegrass (above 10 mg kg^{-1} soil) and lettuce (1.0 mg kg^{-1} soil) [14].

The different plant responses to the same Se dose may be partly explained by the form in which Se is supplied to the roots. In aerobic soils the predominant inorganic Se forms are selenate (SeO_4^{-2}) and selenite (SeO_3^{-2}), depending on the redox potential and pH. Selenate was found to be more easily distributed from the roots to shoots than selenite. Moreover, the uptake, further translocation and accumulation of Se within the plant are determined also by its concentration in growth medium [15, 16].

The aim of the study was to examine whether exogenous Se at different concentrations in the nutrient medium affects the growth of cucumber (*Cucumis sativus* L.) seedlings and photosynthetic pigments content.

MATERIALS AND METHODS

Plant material and growth conditions. The hydroponic experiments were carried out in a controlled-environment growth chamber with the following conditions: a 14-h light period day with a light intensity of 140 W m^{-2} (Philips lamps), at 27/23 °C day/night temperatures and relative humidity of about 50%. Cucumber (*C. sativus* L. cv. Dar) seeds were surface-sterilized in 0.25% (v/v) sodium hypochlorite (NaOCl) for 5 min and rinsed with double-distilled water. Seeds were

germinated on plates with moist filter paper for 7 days. The uniform and best-developed seedlings were then transferred into a modified 1/5 strength aerated Hoagland nutrient solution (Table 1) for the next 4 days.

TABLE 1
Composition of the modified 1/5 strength Hoagland nutrient solution used in the experiments

Hoagland solution			
Macronutrient salts	Concentration (mM)	Micronutrient salts	Concentration (μM)
KH_2PO_4	0.1	H_3BO_3	3.0
KNO_3	1.0	$MnCl_2 \cdot 4H_2O$	1.0
$Ca(NO_3)_2 \cdot 4H_2O$	1.0	$ZnSO_4 \cdot 7H_2O$	1.0
$MgSO_4 \cdot 7H_2O$	0.457	$CuSO_4 \cdot 5H_2O$	1.0
Fe(III)-EDTA	0.06	$(NH_4)_6Mo_7O_{24}$	1.0

It was added to the Hoagland's medium as sodium selenite ($Na_2SeO_3 \cdot 5H_2O$) at concentrations of 1, 5 and 10 μM. Each treatment had three replicates. Cucumber seedlings were grown on the Hoagland's medium with sodium selenite for 96 h. Samples were collected after 96 h of culture. Analyses of photosynthetic pigments content were performed on fresh sample material, while to determine Se concentration samples were dried.

Growth indices. The growth of cucumber seedlings was determined by measuring the fresh weight (FW) and dry weight (DW) of cotyledons and the root system as well as the area of cotyledons per seedling. DWs were recorded after oven-drying at 65°C to a constant weight. DigiShape software (Cortex Nova, Poland) was used to estimate the area of cotyledons.

Photosynthetic pigments. Total chlorophyll (Chl) and carotenoids (Car) were extracted by dimethylsulfoxide (DMSO) according to the method of [17]. Samples (0.05 g) of cotyledons were placed in glass tubes containing 5 cm^3 DMSO. Samples were incubated in a water bath at 65°C for one hour, in the dark. Absorbance was measured spectrophotometrically (Jasco V-530, Tokyo, Japan) at 480, 649 and 665 nm, relative to a DMSO blank. Chlorophyll *a* (Chl *a*) and *b* (Chl *b*) as well as total carotenoids (Car) contents were calculated following the equations proposed in [18].

Determination of total Se. Collected samples were washed with deionized water, dried in an electric drier at 105±5ºC for 96 hours, and then ground for 2 min in a laboratory Cutting Boll Mill PM 200 by RETSCH. The material was mineralized with 65% HNO_3 (Fluka) and 30% H_2O_2 (POCH) in a CEM Mars 5 Xpress microwave mineralization system (*CEM*, Matthews, NC), according to a microwave program composed of three stages: first stage – temperature 120ºC, 6 min at power 800 W; second stage – temperature 150ºC, 10 min at power 1600 W; third stage – temperature 200ºC, 10 min at power 1600 W. After digestion and filtration through 45-mm filters (Qualitative Filter Papers Whatman, Grade 595: 4–7 μm), the supernatant was diluted with deionized water [Milli-Q Academic System (non-TOC)] to a final volume of 50 cm^3.

Se concentration was analyzed with hydride generation atomic absorption spectrometry (HGAAS) using a Varian SpectrAA Duo-AA280FS/AA280Z spectrometer (Varian Inc., Mulgrave, Victoria, Australia) equipped with a Varian hollow-cathode lamp (HCL). Calibration curves were prepared before the analysis with five replicates per Se concentration out of stock solution of 1 g dm^{-3} (Fluka). Solutions of individual Se concentrations were prepared from analytical grade nitrate (V) standard solutions (Merck KGaA, Darmstadt, Germany) dissolved in deionized water. The characteristics of analytical parameters of the applied technique are presented in Table 2.

TABLE 2
Experimental conditions of used technique and statistical parameters of the calibration curve

Parameter	Unit	Se
Technique		HGAAS
Wavelength	Nm	196.0
Slit width	Nm	0.5R
Lamp current	mA	---
Model	Quadratic – provides a second order least squares line forced through zero	
Sensitivity	B(x)	0.06
Limit of detection	mg kg^{-1}	0.17
Minimum concentration	C_{min}/mg kg^{-1}	0.11
Maximum concentration	C_{max}/mg kg^{-1}	0.71
Correlation coefficient	R	0.9991

To verify quality of analytical results, three certified reference materials were used: Leaves of Poplar (NCS DC 73350), Bush Branches and Leaves (NCS DC 73348) and Pine Needles (NIST SRM 1575a), which were analyzed in every tenth measuring set. The characteristics of obtained results are presented in Table 3.

TABLE 3
Comparison of selected results in own results (OR) with reference values of selenium concentration (mg kg^{-1} DW) in particular CRMs of plants

CRM	Reference value	Own result
NCS DC 73348	0.310±0.030	0.320±0.040
NCS DC 73350	0.069±0.007	0.071±0.008
NIST SRM 1575a	0.099±0.004	0.096±0.003

Statistical analysis. The statistical analyses were carried out using Statistica 9.0 software package (StatSoft, Tulsa, USA). A one-way analysis of variance (one-way ANOVA) was performed on the data. All data represent the means from three independent experiments. Results are presented as means calculated with three replicates. Individual treatment means were compared with Duncan's test to determine their statistical significance at the 0.05 probability level. Statistically significant differences were indicated by different letters reported in figures. Similar letters indicate no significant differences between mean values. Pearson correlation coefficients with alpha level fixed at 5% were calculated for the relationships between Se accumulation and measured parameters.

RESULTS AND DISCUSSION

Effects of Se supply on growth indices. The growth of cucumber seedlings was different depending on Se concentration in nutrient solution (Table 4).

TABLE 4
The effect of Se addition (as $Na_2SeO_3 \cdot 5H_2O$) on selected growth parameters of cucumber seedlings

Concentration of Se (μM)	Root			Cotyledons			
	FW (mg/plant)	DW (mg/plant)	DW/FW ratio	FW (mg/plant)	DW (mg/plant)	DW/FW ratio	Area of cotyledons (cm^2/plant)
0	102.632a	4.265a	0.0416a	139.973a	8.913a	0.0637b	6.779a
1	98.776ab	4.084a	0.0413a	133.126a	8.607ab	0.0647b	6.360a
5	93.676b	3.968a	0.0423a	105.096b	7.713bc	0.0737ab	4.636b
10	82.550c	3.788a	0.0459a	82.322c	6.866c	0.0840a	4.102c

The means in each column followed by the same letter do not differ at $p \leq 0.05$ (one-way ANOVA/Duncan range test).

In the presence of 5 and 10 μM Se a significant reduction in FW and DW of roots and cotyledons was found. At the highest concentration of Se (10 μM) the FW of roots and cotyledons decreased by about 20% and 40%, respectively, as compared to the control. However, the negative effect of Se on roots DW was small (about 11%). The lowest Se concentration (1 μM) did not generally affect either FW or DW of roots and cotyledons. The DW/FW ratio of cotyledons showed an increase in seedlings exposed to 5 and 10 μM Se. Moreover, Se addition affected the surface area of cotyledons and after introducing 10 μM Se into the nutrient solution it was about 40% smaller than the control.

In recent years research concerning the role of Se in plants has been extensively discussed. Although there is still no proof that this chemical element is essential in plant cells, some studies have reported beneficial effects of low Se concentration on plant growth. Se at the concentrations of 1–5 μM tends to promote the growth and activities of antioxidant enzymes (superoxide dismutase and peroxidase) of sorrel seedlings subjected to salinity, indicating that this effect of Se may be related to its antioxidative function [13]. Se concentrations such as 5–10 μM Se enhanced the growth of cucumber seedlings subjected to salt stress [19].

In the present study a growth-promoting effect of Se was not observed in the young seedlings of cucumber. The growth of roots and cotyledons was unaffected at the lowest Se concentration (1 μM Se), while higher Se concentration significantly decreased both FW and DW of cotyledons. FWs of cotyledons were 1.33 and 1.70 times lower whereas DWs were 1.15 and 1.30 times lower for 5 μM and 10 μM, respectively, as compared to the control.

The reduction of FW and DW of seedlings cultured on medium with Se is a symptom of the Se-evoked stress. Perhaps it is related to the disturbance of mineral balance of plants [20, 21]. According to numerous authors the range of Se concentrations causing a significant growth reduction varies among different plant species. Alterations of growth parameters in the leaves of coffee seedlings at 1000 μM Na_2SeO_3 were observed [22]. Treatments with 1, 2 and 3 mg Se kg^{-1} soil promoted biomass accumulation of wheat seedlings exposed to enhanced UV-B radiation [23]. In turn, in the presence of 1 and 2.5 mg Na_2SeO_3 kg^{-1} soil no significant differences of FW and DW production of Indian mustard plants were detected [24]. Similar results were obtained in lettuce seedlings, in which the lower Se additions (0.1–1.0 mg kg^{-1}) did not affect either FW or DW of the younger plants despite an increase in total chlorophyll, but did stimulate the growth of senescing seedlings [25].

In addition, in this study the DW/FW ratios for cotyledons of seedlings exposed at 5 and 10 μM Se were 1.16- and 1.32-fold higher, respectively, than for the control. This may be related to a reduction in water content as a consequence of disorder in water uptake and translocation through the plant. It was observed, water content in dicotyledonous plants decreased very rapidly with increasing Se (IV) concentrations, primarily in the shoots, while it did not change significantly in the roots [26].

Effects of Se supply on photosynthetic pigments content. The amount of chlorophylls (*a* and *b*) and total carotenoids (Car) in the cotyledons of cucumber seedlings changed in the presence of Se as compared to the control (Fig. 1).

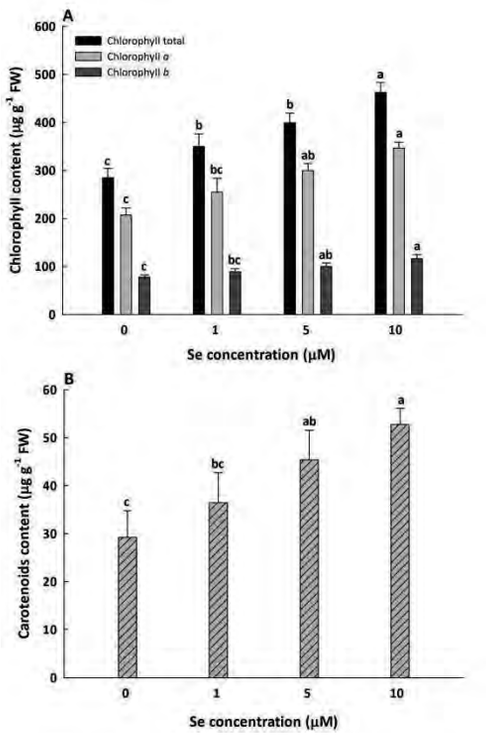

FIGURE 1
The effect of exogenous Se (as $Na_2SeO_3 \cdot 5H_2O$) on chlorophylls (A) and carotenoids (B) contents in cotyledons of cucumber seedlings. The means followed by the same letter do not differ at $p \leq 0.05$ (one-way ANOVA/Duncan range test)

The level of total chlorophyll content at 1, 5 and 10 μM Se increased by 23%, 40% and 62%, respectively. It should be emphasized that the highest increase in the total chlorophyll content, including chlorophyll *b*, was observed at concentration of 10 μM Se. Carotenoids (Car) content changed significantly only at 5 and 10 μM Se. The highest Se concentration caused an increase of Car accumulation by about 80%. The determined pigment ratios are presented in Fig. 2.

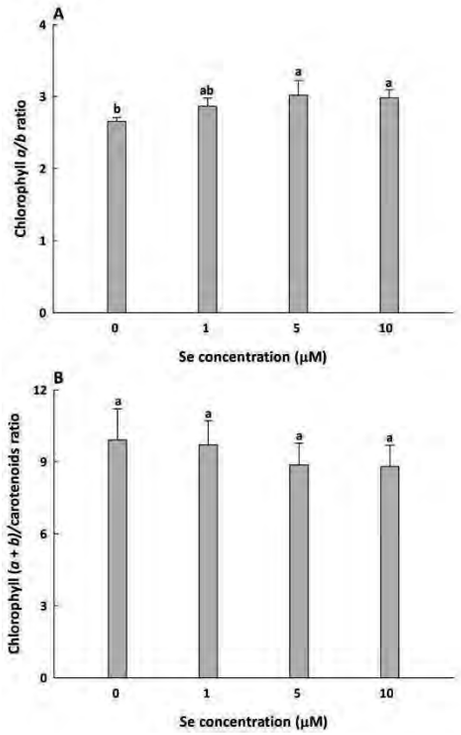

FIGURE 2
The effect of exogenous Se (as $Na_2SeO_3 \cdot 5H_2O$) on chlorophyll a/b ratio (A) and chlorophyll (a+b)/carotenoids ratio (B) in cotyledons of cucumber seedlings. The means followed by the same letter do not differ at p≤0.05 (one-way ANOVA/Duncan range test)

Chl *a*/*b* ratio increased slightly by 12% at the concentrations of 5 and 10 µM Se, indicating significant differences in the content of both these pigments. On the other hand, Se addition had no significant effect on Chl *a*+*b*/Car ratio in comparison with the control.

We demonstrated that increasing concentrations of Se in the nutrient solution resulted in a linear increase in photosynthetic pigments content in cucumber cotyledons. In the presence of 5 and 10 µM Se a significant increase Chl *a* and Chl *b* contents and consequently in total chlorophyll was detected. Obtained results are consistent with findings on wheat [27, 28]. Se is believed to improve stability of membranes and chlorophyll as well as influencing synthesis of pigments by protection of chloroplast enzymes or stimulation of plastids to chloroplast development [29, 30]. However, the results of the present study indicate that Se at the concentrations of 5 and 10 µM could cause mild water stress, as mentioned, which increased protoplasm concentration and enhanced chlorophyll content because of cotyledon growth reduction. This is supported that the loss of cell water content increases chlorophyll concentration in leaves and the effect on chlorophyll content is misleading as well as dependent on environmental conditions [31]. Moreover, it is noteworthy that chlorophyll *a/b* ratio, which is used as a stress indicator, increased slightly with increasing Se concentrations in our study. Increasing values for the Chl *a*/Chl *b* ratio indicate changes in the PS II/PS I ratio in stressed leaves [32]. Obtained data could suggest the toxicity of Se at the concentration of 5 and 10 µM to cucumber seedling. These results are consistent with previous findings by other authors who have reported an increase in chlorophyll *a/b* ratio under the influence of such stress factors as heavy metals and salinity [26, 33]. In addition, an increase of Car at 5 and 10 µM Se concentrations may be related to a defence strategy of the plant to reduce stress. Carotenoids are well-known non-enzymatic antioxidants that play an important role in the protection of chlorophyll pigments under stress [34]

Effects of Se supply on Se accumulation in tissues. The addition of Se to the nutrient solution resulted in an increase of Se content in tissues of cucumber seedlings (Fig. 3).

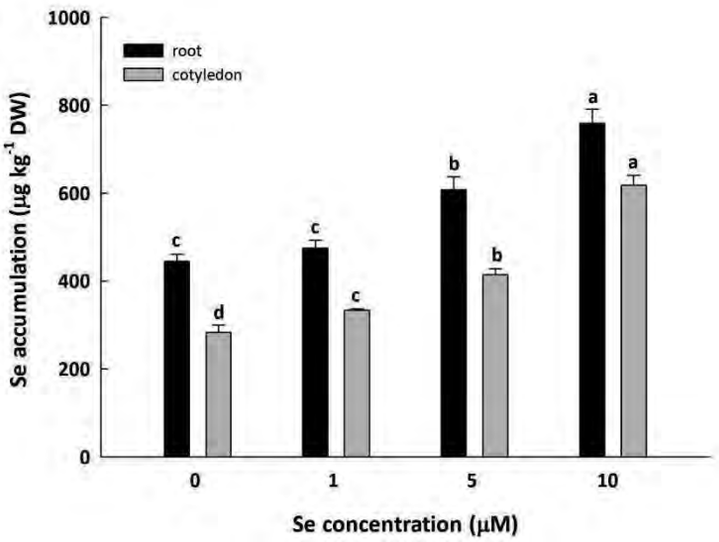

FIGURE 3
The effect of exogenous Se (as $Na_2SeO_3 \cdot 5H_2O$) on Se accumulation in roots and cotyledons of 11-day-old cucumber seedlings. The means followed by the same letter do not differ at p≤0.05 (one-way ANOVA/Duncan range test)

It is evident that the total Se content in tissues was Se-dosage dependent. A greater amount of Se was found in roots than in cotyledons. The maximum Se accumulation was 759.44±32 µg kg^{-1} DW in roots of seedlings treated with the highest Se concentration (10 µM Se). The treatment with 1 µM Se slightly but significantly increased the accumulation of Se (by 18%) only in cotyledons. In the case of 5 and 10 µM Se, content of Se increased in both roots and cotyledons 1.36- and 1.47-fold (5 µM) and 1.71- and 2.19-fold (10 µM), respectively, as compared to control seedlings.

In the present study, the accumulation of total Se increased with elevation of its concentrations in the nutrient solution. It is noteworthy that the addition of Se in form of selenite resulted in a higher Se content in roots than in cotyledons. The Se levels reached 618.22±23 µg g^{-1} DM and 759.44±32 µg g^{-1} DM for cotyledons and roots, respectively, with the application of the highest Se concentration (10 µM). Our findings are supported by other research which showed that this difference in Se accumulation depends on the form of Se applied to the plants. It should be stressed that selenite is a chemical form that can be easily taken up by plants. It was revealed that total Se accumulation in roots of Indian mustard, broccoli, rice and sugar beet plants, supplied with 20 µM Se as selenite, was much greater than in shoots [35]. Maximum Se levels were 230-690 µg kg^{-1} for roots and 78-169 µg kg^{-1} for shoots. In another study, it was also found that selenite application at the rate of 1, 2, 4 mg kg^{-1} soil increased Se concentration in roots of rapeseed 1.4–2 times more than shoots [36].

The reason why most of the selenite taken up by plants remained in the roots could possibly be attributed to its poor translocation to shoots due to rapid reduction to selenium-containing amino acids, which are not removed [37, 38]. This may be an explanation of the detrimental effect of Se on cucumber seedlings' growth. In fact, we obtained highly significant negative linear correlations between both root and cotyledon Se accumulation and fresh weight. Surprisingly, Se concentration in roots and cotyledons from control plants were higher than we expected (445.11 and 282.78 µg kg^{-1} DW, respectively); thus the difference between the maximum Se accumulation at the highest Se concentration was not so marked. These results may be related to plant species and age. A greater leaf surface area contributes to a higher transpiration rate and increases transport of Se to transpiring organs [39]. Our data support these findings. Firstly, during our research very young seedlings (11 days old) were analyzed, and secondly, the area of cotyledons was highly reduced with increasing endogenous level of Se.

Correlations between examined parameters and Se accumulation. The determined relationships are presented in Figs. 4 and 5.

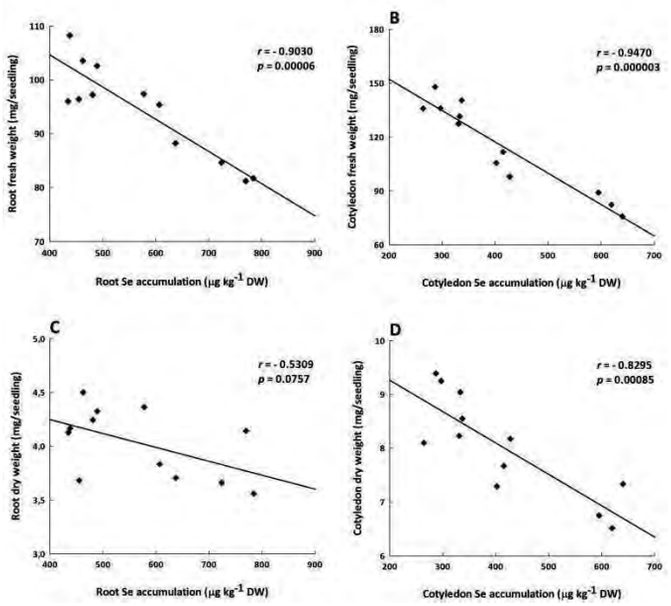

FIGURE 4
Correlation (Pearson's r) between Se accumulation and growth indices: root FW (A), cotyledon FW (B), root DW (C), and cotyledon DW (D) in cucumber seedlings affected by Se addition (as $Na_2SeO_3 \cdot 5H_2O$)

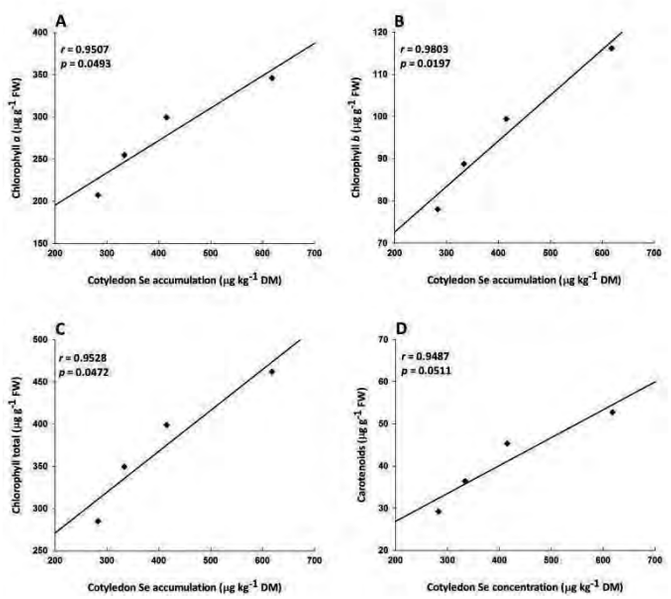

FIGURE 5
Correlation (Pearson's r) between Se accumulation and photosynthetic pigments content: chlorophyll a (A), chlorophyll b (B), total chlorophyll (C), and carotenoids (D) in cucumber seedlings affected by Se addition (as $Na_2SeO_3 \cdot 5H_2O$). Each value is the mean of three replicates.

There were significantly negative linear correlations between Se accumulation by cotyledons and both FW (r=−0.9470, p=0.000003) and DW (r=−0.8295, p=0.00085). A high Pearson correlation coefficient was also obtained for root FW (r=−0.9030, p=0.00006), whereas no significant correlation was detected between root Se accumulation and root DW (r=−0.5309,

p=0.07570). The content of chlorophyll a+b was positively linearly correlated with the rate of Se accumulation. The highest coefficient of correlation was recorded for Chl b (r=0.9803, p=0.01966). On the other hand, the correlation between Car and cotyledon Se accumulation was non-significant (r=−0.5309, p=0.05114).

The accumulation of Se in plant tissues at which they begin to show symptoms of toxicity is variable among crops. It was reported a reduction in total DW of rice above 2 mg kg^{-1} Se and in white clover at Se content of 330 mg kg^{-1} [38]. The decrease in yield was found to be 18.9 µg g^{-1} in wheat, 41.5 µg g^{-1} in rice and 76.9 µg g^{-1} in maize [41]. Different reaction to various Se accumulation may be a result of the individual species' ability to manage this element on a cellular level. Numerous reports have shown that plants commonly replace the sulfur atom in the amino acids cysteine and methionine with a Se ion, although a Se atom is slightly larger (the radius of Se^{2+}=0.5 Å) than a S atom (S^{2+}=0.37 Å). Seleno-amino acids may then be incorporated specifically into selenoproteins or nonspecifically into other molecules [40]. Actually, most studies have shown that selenite is more phytotoxic than selenate. It was found selenite toxicity to lettuce plants from the concentration of 10 µM, when the shoot biomass was almost 2 times lower than the control [43]. In contrast, when selenate was applied, the shoot biomass increased up to a concentration of 20 µM, while it decreased at the concentration of 120 µM.

CONCLUSION

This study provides important information concerning the relationship between the endogenous level of Se in plants and its impacts on growth and photosynthetic pigments content. The results confirm the fact that Se interaction with plants depends on its form and concentration in the growth medium. The addition of more than 5 µM of sodium selenite ($Na_2SeO_3 \cdot 5H_2O$) to the nutrient medium caused a significant reduction in plant growth. Se application at higher concentrations (5 and 10 µM) limited the growth of plants but does not inhibit the content of photosynthetic pigments.

ACKNOWLEDGEMENTS

The study was supported by the Ministry of Science and Higher Education through the Faculty of Horticulture and Landscape Architecture, Poznań University of Life Sciences.

REFERENCES

[1] Brown, K.M. and Arthur, J.R. (2001). Selenium, selenoproteins and human health: a review. Publ. Health Nutr. 4(2B), 593-599.

[2] Lyons, M.P., Papazyan, T.T. and Surai, P.F. (2007). Selenium in food chain and animal nutrition: Lessons from nature. Asian-Aust. J. Anim. Sci. 20(7), 1135-1155.

[3] Germ, M., Kreft, I., and Osvald, J. (2005). Influence of UV-B exclusion and selenium treatment on photochemical efficiency of photosystem II, yield and respiratory potential in pumpkins (Cucurbita pepo L.). Plant Physiol. Biochem. 43, 445-448.

[4] Ning, C.J., Ding, N., Wu, G.L., Meng, H.J., Wang, Y.N. and Wang, Q.H. (2013). Proteomics research on the effects of applying selenium to apple leaves on photosynthesis. Plant Physiol. Biochem. 70, 1-6.

[5] Hanson, B., Lindblom, S.D., Loeffler, M.L. and Pilon-Smits, E.A.H. (2004). Selenium protects plants from phloem feeding aphids due to both deterrence and toxicity. New Phytologist 162, 655-662.

[6] Fargašová, A., Pastierová, J. and Svetková, K. (2006). Effect of Se-metal pair combinations (Cd, Zn, Cu, Pb) on photosynthetic pigments production and metal accumulation in Sinapis alba L. seedlings. Plant Soil Environ. 52(1), 8-15.

[7] Malik, J.A., Goel, S., Kaur, N., Sharma, S., Singh, I. and Nayyar, H. (2012). Selenium antagonises the toxic effects of arsenic on mungbean (Phaseolus aureus Roxb.) plants by restricting its uptake and enhancing the antioxidative and detoxification mechanisms. Environ. Exp. Bot. 77, 242-248.

[8] Yigit, E., Akbulut, G.B., Gok, Y. and Bayram D. (2012). The effects of organic selenium on some physiological and biochemical parameters in Hordeum vulgare L. and Triticum aestivum L. exposed to salt stress. Fresen Environ Bull. 21(3), 743-747.

[9] Hartikainen, H. and Xue, T.L. (1999). The promotive effect of selenium on plant growth as triggered by ultraviolet irradiation. J. Environ. Qual. 28, 1372-1375.

[10] Cartes, P., Gianfera, L. and Mora, M.L. (2005). Uptake of selenium and its antioxidative activity in ryegrass when applied as selenate and selenite forms. Plant Soil 276, 359-367.

[11] Lyons, G.H., Stangoulis, J.C.R. and Graham, R.D. (2005). Tolerance of wheat (Triticum aestivum L.) to high soil and solution selenium levels. Plant Soil 270, 179-188.

[12] Zhao, C., Ren, J., Xue, C. and Lin, E. (2005). Study on the relationship between soil selenium and plant selenium uptake. Plant Soil 277, 197-206.
[13] Kong, L., Wang, M. and Bi, D. (2005). Selenium modulates the activities of antioxidant enzymes, osmotic homeostasis and promotes the growth of sorrel seedlings under salt stress. Plant Growth Regul. 45, 155-163.
[14] Hartikainen, H., Xue, T. and Piironen, V. (2000). Selenium as an anti-oxidant and pro-oxidant in ryegrass. Plant Soil 225, 193-200.
[15] Zhang, L.H., Ackley, A.R. and Pilon-Smits, E. (2007). Variation in selenium tolerance and accumulation among 19 Arabidopsis thaliana accessions. J. Plant Physiol. 164(3), 327-336.
[16] Qatatsheh, A. (2011) Selenium in soils and plants of the Ma'an district – Jordan. Adv. Food Sci. 33(2), 104-108.
[17] Hiscox, J.D. and Israelstam, G.F. (1979). A method for the extraction of chlorophyll from leaf tissue without maceration. Can. J. Bot. 57, 1332-1334.
[18] Wellburn, A.R. (1994). The spectral determination of chlorophylls a and b, as well as total carotenoids, using various solvents with spectrophotometers of different resolution. J. Plant Physiol. 144, 307-313.
[19] Hawrylak-Nowak, B. (2009). Beneficial effects of exogenous selenium in cucumber seedlings subjected to salt stress. Biol. Trace Elem. Res. 132(1), 259-269.
[20] Hawrylak-Nowak, B. (2008). Effect of selenium on selected macronutrients in maize plants. J. Elementol. 13(4), 513-519.
[21] Zembala, M., Filek, M., Walas, S., Mrowiec, H., Kornaś, A., Miszalski, Z. and Hartikainen, H. (2010). Effect of selenium on macro- and microelement distribution and physiological parameters of rape and wheat seedlings exposed to cadmium stress. Plant Soil 329(1-2), 457-468.
[22] Mazzafera, P. (1998). Growth and biochemical alterations in coffee due to selenite toxicity. Plant Soil 201, 189-196.
[23] Yao, X., Chu, J. and Wang, G. (2009). Effects of selenium on wheat seedlings under drought stress. Biol. Trace Elem. Res. 130, 283-290.
[24] Di Gregorio, S., Lampis, S., Malorgio, F., Petuzzelli, G., Pezzarossa, B. and Vallini, G. (2006). Brassica juncea can improve selenite and selenate abatement in selenium contaminated soils through the aid of its rhizospheric bacterial population. Plant Soil 285, 233-244.
[25] Xue, T., Hartikainen, H. and Piironen, V. (2001). Antioxidative and growth-promoting effect of selenium in senescing lettuce. Plant Soil 27, 55-61.
[26] Molnárová, M., and Fargašová, A. (2009). Se (IV) phytotoxicity for monocotyledonae cereals (Hordeum vulgare L., Triticum aestivum L.) and dicotyledonae crops (Sinapis alba L., Brassica napus L.). J. Hazard. Mater.172(2-3), 854-861.
[27] Wang, C.Q. (2011). Water-stress mitigation by selenium in Trifolium repens L. J. Plant Nutr. Soil Sci. 174(2), 276-282.
[28] Chu, J., Yao, X., Yue, Z., Li, J., and Zhao, J. (2013). The effects of selenium on physiological traits, grain selenium content and yield of winter wheat at different development stages. Biol. Trace Elem. Res. 151(3), 434-440.
[29] Filek, M., Gzyl-Malcher, B., Zembala, M., Bednarska, E., Laggner, P., and Kriechbaum, M. (2010). Effect of selenium on characteristics of rape chloroplasts modified by cadmium. J. Plant Physiol. 167(1), 28-33.
[30] Yao, X., Chu, J., He, X. and Ba, C. (2011). Protective role of selenium in wheat seedlings subjected to enhanced UV-B radiation. Rus. J. Plant Physiol. 58(2), 283-289.
[31] Ward, K., Scarth, R., Daun, J. and McVetty, P.B.E. (1992). Effects of genotype and environment on seed chlorophyll degradation during ripening in four cultivars of oilseed rape (Brassica napus). Can. J. Plant Sci. 72, 643-649.
[32] Anderson, J.M. (1986). Photoregulation of the composition, function, and structure of thylakoid membranes. Annu. Rev. Plant Physiol. 37, 93-136.
[33] Delfine, S., Alvino, A., Villiani, M.C. and Loreta, F. (1999). Restrictions to carbon dioxide conductance and photosynthesis in spinach leaves recovering from salt stress. J. Plant Physiol. 119, 1101-1106.
[34] Lefsrud, M.G., Kopsell, D.A., Kopsell, D.E. and Curran-Celentano, J. (2006). Irradiance levels affect growth parameters and carotenoid pigments in kale and spinach grown in a controlled environment. Physiol. Plant. 127, 624-631.
[35] Zayed, A., Lytle, C.M., and Terry, N. (1998). Accumulation and volatilization of different chemical species of selenium by plants. Planta 206, 284-292.
[36] Sharma, S., Bansal, A., Dhillon, S.K. and Dhillon, K.S. (2010). Comparative effects of selenite and selenite on growth and biochemical composition of rapeseed (Brassica napus L.). Plant Soil 329(1-2), 339-348.
[37] de Souza, M.P., Pilon-Smits, E.A.H., Lytle, C.M., Hwang, S., Tai, J., Honma, T.S.U., Yeh,

L.T. and Terry, N. (1998). Rate-limiting steps in selenium assimilation and volatilization by Indian mustard. Plant Physiol. 117, 1487-1494.
[38] Li, H.F., McGrath, S.P. and Zhao, F.J. (2008). Selenium uptake, translocation and speciation in wheat supplied with selenate or selenite. New Phytologist 178, 92-102.
[39] Banuelos, G.S., Ajwa, H.A., Wu, L., Xun Guo, Akohoue, S. and Zambrzuski, S. (1997). Selenium-induced growth reduction in Brassica land races considered for phytoremediation. Ecotoxicol. Environ. Saf. 36, 282-287.
[40] Mikkelsen, R.L., Haghnia, G.H., and Page, A.L. (1989). Factors affecting selenium accumulation by crop plants. In: Jacobs LW [ed.], Selenium in Agriculture and the Environment, 65-93, Soil Science Society of America and American Society of Agronomy, Madison, WI.
[41] Rani, N., Dhillon, K.S. and Dhillon, S.K. (2005). Critical levels of selenium in different crops grown in an alkaline silty loam soil treated with selenite-Se. Plant Soil 277, 367-374.
[42] Garifullina, G.F., Owen, J.D., Lindblom, S., Tufan, H., Pilon, M. and Pilon-Smits, E.A.H. (2003). Expression of a mouse selenocysteine lyase in Brassica juncea chloroplasts affects selenium tolerance and accumulation. Physiol. Plant. 118(4), 538-544.
[43] Ríos, J.J., Blasco, B., Cervilla, L.M., Rubio-Wilhelmi, M.M., Ruiz, J.M. and Romero, L. (2008). Regulation of sulphur assimilation in lettuce plants in the presence of selenium. Plant Growth Regul. 56, 43-51.

Received: **23.06.2015**
Accepted: **06.01.2016**

CORRESPONDING AUTHOR

Barbara Politycka
Poznań University of Life Sciences
Department of Plant Physiology
Wołyńska 35
60-637 Poznań – POLAND

e-mail: barpolit@yahoo.pl

by PSP Volume 25 – No. 1/ 2016, pages 153-162 Fresenius Environmental Bulletin

FIRST DETAILED MEASUREMENTS OF ENVIRONMENTAL RADIOACTIVITY AND RADIATION HAZARD ASSESSMENT FOR GERZE-TURKEY

Aslı Kurnaz

Department of Physics, Faculty of Arts and Sciences, Kastamonu University, 37100 Kastamonu, Turkey

ABSTRACT

A gamma spectrometric study of distribution of natural and artificial radionuclides in soil samples collected from the terrestrial environment of Gerze counties of Sinop Province in Turkey was performed using a NaI(Tl) γ-ray spectrometer with the aim of estimating the radiation hazard as well as establishing a database for radioactivity levels of the tourist area. The concentrations of primordial (^{238}U, ^{232}Th and ^{40}K) and the fission product (^{137}Cs) radionuclides were determined. The mean activity concentrations of ^{238}U, ^{232}Th, ^{40}K and ^{137}Cs were determined as 63.87±1.09, 72.66±1.70, 609.65±5.92 and 13.58±0.48 Bqkg^{-1} for soil samples, respectively. Based on the measured concentrations of these radionuclides, the mean absorbed gamma dose in air and the annual effective dose due to terrestrial gamma radiation were calculated. The contribution to the total absorbed gamma dose rate in air in the decreasing order was due to the presence of ^{232}Th (44%), followed by ^{238}U (30%), ^{40}K (25.6%) and ^{137}Cs (0.4%) in Gerze soils. In situ measurements of the gamma dose rate in air were performed in the same 60 locations, soil samples were collected from, using a portable G-M tube and the mean gamma dose rate and the annual effective dose were ascertained.

KEYWORDS:
Environmental Radioactivity, Radiological Hazards, Statistical Analysis

INTRODUCTION

The exposure to ionising radiation from natural sources is a continuing and inescapable feature of life on earth. The main contributor to natural radiation exposure is radioactive nuclides (^{238}U, ^{232}Th and their decay products and ^{40}K) that originated in the earth's crust and are present everywhere. These radioactive nuclides that are found in air, soil and water naturally are called the background radiation [1]. In addition, man-made sources such as nuclear events, reactor accidents, nuclear tests and the use of technological products also affect the level of background radiation in a region and also, the level of natural background radiation varies depending on location [2].The background radioactivity studies were done all over the world and still, researchers worldwide routinely carry out environmental radioactivity measurements in order to determine the nationwide background radiation levels. However, there is not enough number of studies done in Turkey, especially in the most part of the rural areas. This research area have been selected because, the region is a touristic area. And also it is planned to establish a thermal power plants in this region. Therefore, the main aim of this study is to identify and determine natural (^{238}U, ^{232}Th and ^{40}K) and artificial (^{137}Cs) radioactivity concentrations in soil samples collected from 60 locations around Gerze County of Sinop/Turkey and to evaluate the health risks. In addition, the gamma dose rate at 1 m in air, coming from terrestrial and cosmic radionuclides, was investigated in the studied area. Up to now, there has been no survey reported on the background radiation levels in Gerze/Sinop. Also, the data presented will be useful as baseline data for future estimations of exposure of a population.

MATERIALS AND METHODS

Survey Area. Gerze is a county of Sinop Province in the Black Sea region of Turkey. It has a population of 21517 of which 12734 live in Gerze city centre and the region covers an area of 594 km^2. The study area lies between 41°80′ N and 35°19′ E (peak elevation: 900 m, elevation: 50 m average height above sea level for the entire province). In the study area, main geological units are carbonate, sand, clay rocks and line Stones [3].

Radioactivity in Surface Soil. Sixty soil samples were collected from study area in the spring of 2014. After clearing the ground surface of stones, pebbles, vegetation and roots, about 1 kg of

material from the first 15 cm of top soil samples reflecting the geological characteristics of the region were placed in labeled polythene bags and then transferred to Kastamonu University, Department of Physics, Nuclear Physics Laboratory. The samples were dried and pulverized. About 160 g of each sample was packed in gas tight, radon impermeable, plastic cylindrical polyethylene containers. To reach secular equilibrium, each sample was sealed for at least 4 weeks before counting. All results here in are based on dry weight (DW) masses. In addition, the coordinates of each sampling locations were determined using a GPS device.

The natural radioactivity in soil of region has been measured by gamma ray spectrometry using ORTEC 905-4 Series, 3-inch x 3-inch NaI(Tl) Scintillation detector. The best resolution achievable is typically 8% for the 662 keV gamma rays from ^{137}Cs. The detector was housed in a cylindrical lead shield of about 22 cm diameters, 56 cm in overall height and 7 cm thickness. The pulse processing and data analysis system matched to a computer and the spectral analysis was performed using ScintiVision computer software obtained from ORTEC. The efficiency and energy calibration of the spectrometer were carried out using The IAEA gamma-ray spectrometry reference materials RGU-1, RGTh-1 and RGK-1. The quality assurance of measurements was carried out by periodical calibrations using calibration sources that contained ^{133}Ba, ^{109}Cd, ^{57}Co, ^{22}Na, ^{137}Cs, ^{54}Mn and ^{60}Co and generated photon emission peaks in the energy range between 80 and 1400 keV and repeating sample measurements. The samples were counted for 50000 s with background measurements made under the same conditions [4].

In this study, the 1.76MeV and 1.12 MeV peaks of ^{214}Bi, the 2.62MeV peak of ^{208}Tl, the 1.46MeV peak of ^{40}K and 0.66 MeV peak of ^{137}Cs were used for quantitative determination of uranium, thorium, potassium and cesium, respectively.

Ambient gamma dose. An outdoor ambient gamma dose rate measurement has been performed in the study area. The level of dose rate in air was ascertained at 60 locations using a dose rate meter (G-M tube). The measurement points were in the same locations as the soil samples were collected. At each spot, a reading was taken in air for 600 s at 1 m above ground level. Six reading were taken at each sampling region and the average was calculated. The results, including both terrestrial and cosmic ray components of gamma radiation, were recorded in units of μR h^{-1}. The measured values were converted into nGy h^{-1} using the conversion factor of 8.7 nGy μR^{-1} (from the definition of Roentgen).

RESULTS AND DISCUSSIONS

Gamma spectrometry results

The activity concentration results of the natural radionuclides ^{238}U, ^{232}Th and ^{40}K and artificial radionuclide ^{137}Cs (from the Chernobyl accident and other nuclear activities) for 60 soil samples collected from the study area were determined (Table 1) and plotted (Fig. 1). The ± values of radioactivity concentrations shown in Tables are because of the 1σ variation due to counting uncertainties.

TABLE 1
Distribution of the soil radioactivity concentrations (in units of Bq kg^{-1}).

	^{238}U	^{232}Th	^{40}K	^{137}Cs
Range (±uncertainity)	27.20±5.09-111.40±8.13	38.20±4.20-121.90±6.70	379.10±36.90-821.10±42.70	11.0±0.90-21.50±2.50
Mean (±SD)	63.87±1.09	72.66±1.70	609.65±5.92	13.58±0.48
Median	60.23	70.70	612.95	13.15
Standard Deviation	22.03	16.82	118.27	2.16

For all of the soil samples, the mean activity concentrations of ^{238}U, ^{232}Th and ^{40}K were ascertained as 63.87±1.09, 72.66±1.70 and 609.65±5.92 Bq kg^{-1}, respectively. World's mean activity concentrations of these nuclides are 35, 30 and 400 Bq kg^{-1}, respectively [5]. The results obtained from this research show that the mean activity concentration values of ^{238}U, ^{232}Th and ^{40}K for soil samples are 1.8, 2.4 and 1.5 times higher than the world mean values.

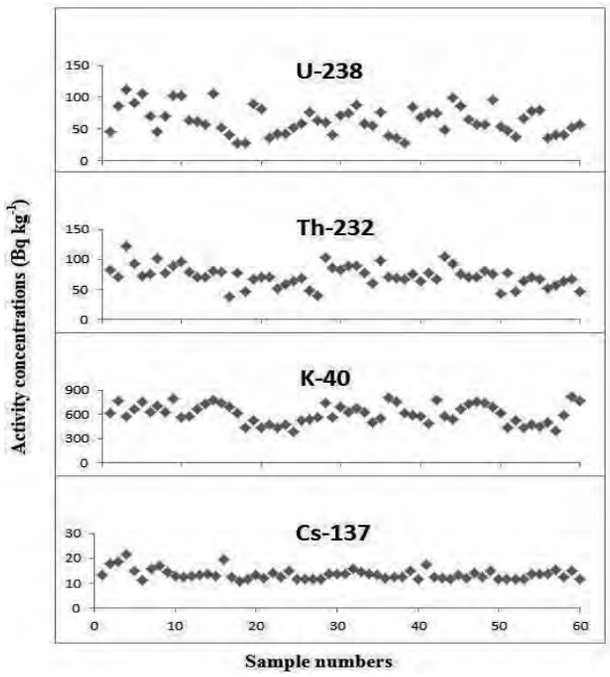

FIGURE 1
The activity distributions of ^{238}U, ^{232}Th, ^{40}K and ^{137}Cs in the soil samples.

The artificial radionuclide ^{137}Cs was seen in all soil samples. The specific activity concentrations of ^{137}Cs was determined in the ranges 11 Bq kg^{-1} to 22 Bq kg^{-1} with corresponding mean value of 13.58±0.48 Bq kg^{-1}, (Table 1). This artificial radionuclide may have different origins, such as Chernobyl accident, nuclear weapons and bomb tests. Although the lack of data related to ^{137}Cs activity concentrations in this region before the Chernobyl accident, it is thought that Chernobyl accident is the most likely candidate responsible for the results [6].

The main objective of natural radioactivity research was to estimate the radiation exposure of the human. Radiation exposure can be defined with many parameters. The contribution of radionuclides to the absorbed dose rate in air (ADRA) depends on the activity concentration of ^{238}U, ^{232}Th, ^{40}K and ^{137}Cs. The total absorbed dose rate ADRA (nGy h^{-1}) in air at1 m above ground level due to the presence of radionuclides in the soil samples was estimated using the following formula [4,5]:

$$ADRA\ (nGy\ h^{-1}) = 0.462\ A_U + 0.604\ A_{Th} + 0.0417\ A_K + 0.030\ A_{Cs} \quad (1)$$

where A_U, A_{Th}, A_K and A_{Cs} are the activity concentrations of ^{238}U, ^{232}Th, ^{40}K and ^{137}Cs, respectively, in the soil samples. The absorbed dose rates in air at study area for soil samples varied from 58.78 to 149.90 nGy h^{-1} and the mean value was calculated to be 99.23 nGy h^{-1} (the second column of Table 2). According to UNSCEAR [5] report, the dose rate in air outdoors from terrestrial gamma-rays in normal circumstances is about 57 nGy h^{-1}. It can be seen that our mean value is exceed the normal level. The mean contributions of the uranium decay series, thorium decay series, non-series nuclide ^{40}K and artificial radionuclide ^{137}Cs to the absorbed dose rate in air were 30%, 44%, 25.6% and 0.4%, respectively.

The annual effective dose equivalent was calculated from following equation:

$$AEDE\ (\mu Sv\ y^{-1}) = ADRA(nGy\ h^{-1}) \times 8760\ (h\ y^{-1}) \times 0.2 \times 0.7\ (Sv\ Gy^{-1}) \times 10^{-3} \quad (2)$$

where, 0.2 is the outdoor occupancy factor, 0.7 Sv Gy^{-1} is the conversion coefficient from absorbed dose in air to effective dose received by adults [5]. The results of the calculation were given in the fourth column of Table 2. The annual effective dose rates varied from 72.08 to 183.83 μSv y^{-1} and the mean annual effective dose based on all soil samples is 121.69 μSv y^{-1} which is about 1.7 times higher than the world population weighted mean value of 72 μSv y^{-1} [5], and is below the permissible limit 1mSv y^{-1} [7]. Even the maximum value of 183.83 μSv y^{-1} is about five times lower than the permissible limit.

TABLE 2
The absorbed dose rates in air (ADRA) and annual effective dose equivalent (AEDE) in Gerze/Sinop.

	Absorbed gamma dose rate in air (nGy h^{-1})		Annual effective dose equivalent (μSv y^{-1})	
	Terrestrial	Terrestrial+cosmic	Terrestrial	Terrestrial+cosmic
Range	58.78-149.90	69.6-182.7	72.08-183.83	85.36-224.06
Mean	99.23	125.1	121.69	153.4
Median	99.61	124.0	122.16	152.0
Standard Deviation	19.14	28.0	23.47	34.3

The results were evaluated in terms of the radiation hazard by means of the Radium equivalent activity (Raeq) and external hazard index (Hex). Radium equivalent activity (Ra_{eq}), is a widely used hazard index and it is calculated through the relation given by Beretka and Mathew [8].

$$\mathbf{Ra_{eq}(Bq\ kg^{-1}) = A_{Ra} + 1.43A_{Th} + 0.077A_K} \quad (3)$$

where, A_{Ra}, A_{Th} and A_K are the activity concentration of ^{226}Ra, ^{232}Th and ^{40}K in Bq kg^{-1}, respectively. The values of Ra_{eq} varied from 126.41 to 330.49 Bqkg^{-1} and the mean value was found to be 214.72 Bq kg^{-1} (Table 3). The estimated average values of Raeq in the present work are 1.7 times lower than the recommended maximum value of 370 Bq kg^{-1}[8].

The external hazard index Hex was calculated for all samples using the model proposed by Krieger [9]. It is assumed that 370 Bq kg^{-1} of ^{226}Ra, 259 Bq $kg^{-1}$of ^{232}Th and 4810 Bq kg^{-1} of ^{40}K produce the same gamma-ray dose rate. The external hazard index is given by,

$$\mathbf{Hex = A_{Ra}/370 + A_{Th}/259 + A_K/4810 \leq 1} \quad (4)$$

where, A_{Ra}, A_{Th} and A_K are the activity concentration of ^{226}Ra, ^{232}Th and ^{40}K in Bqkg^{-1}, respectively. The results range from 0.34 to 0.89 and mean value was found to be 0.58 (Table 3). There is no value calculated higher than the radiation dose to permissible limit of 1 mSv y^{-1} [7] in this research.

The representative level index (Iγr), is used to estimate the level of gamma radiation hazard associated with the natural radionuclides [10,11] is given as,

$$\mathbf{I\gamma r\ (Bq\ kg^{-1}) = A_{Ra}/150 + A_{Th}/100 + A_K/1500} \quad (5)$$

where, A_{Ra} A_{Th}, and A_K are the mean activity concentrations of ^{226}Ra ^{232}Th, and ^{40}K in Bq kg^{-1}, respectively. The mean representative level index was calculated as 1.56 Bq kg^{-1} (min: 0.93 Bq kg^{-1}; max: 2.35 Bq kg^{-1}) (Table 3). The mean Iγr value of soil samples is higher than the internationally accepted values 1 Bq kg^{-1} [12]. Even, only, the minimum value of 0.93 Bq kg^{-1} is lower than the permissible limit. Other values are about 1.5 times higher than the permissible limit.

The excess lifetime cancer risk (ELCR) was calculated by using the equation,

$$\mathbf{ELCR = AEDE\ x\ DL\ x\ RF} \quad (6)$$

where DL is the duration of life (70 y) and RF is the risk factor (Sv^{-1}), fatal cancer risk per Sievert. For stochastic effects, ICRP uses value of 0.057 [13] for the public. The excess lifetime cancer risk (ELCR) was calculated using the annual effective dose for soil samples. The mean ELCR was found as 0.00049 % according to ICRP [13] for soil samples

TABLE 3
Radium equivalent activity (Raeq), external hazard index (Hex), representative level index (Iγr) and excess lifetime cancer risk (ELCR) in Gerze/Sinop.

	Ra_{eq} (Bq kg^{-1})	H_{ex} ≤1 mSv y^{-1}	Iγr (Bq kg^{-1})	ELCR (%)
Range	126.41-330.49	0.34-0.89	0.93-2.35	$2.88x10^{-4}$-$7.34x10^{-4}$
Mean	214.72	0.58	1.56	$4.86x10^{-4}$
Median	216.03	0.58	1.57	$4.87x10^{-4}$
Standard deviation	**42.39**	**0.11**	**0.30**	**$0.94x10^{-4}$**

The comparison of the radioactivity levels (Table 4) in soil samples of studying area with those reported from other parts of Turkey is given. As shown in Table 4, among the mean ^{238}U, ^{232}Th activity concentrations, our values are higher than the others except Çanakkale (granite area) [14]. It can be said that among the mean ^{40}K activity concentrations, our value is higher than the other except Balıkesir [15], Kırklareli [16] and Çanakkale [14]. If, ^{137} Cs activity concentrations were compared, our mean value is nearly similar to Batman [17], Kayseri [18], is lower than Artvin [19], Çanakkale [14], İstanbul [20], Trabzon[4] and is higher than the others.

TABLE 4
Radioactivity concentrations in soil from different parts of Turkey.

Province	^{238}U (Bq kg^{-1})	^{232}Th (Bq kg^{-1})	^{40}K (Bq kg^{-1})	^{137}Cs (Bq kg^{-1})
Trabzon [4]	41	38	443	21
Çanakkale [14]	95	110	1273	19
Balıkesir [15]	38	55	675	3
Kırklareli [16]	28	40	667	8
Batman [17]	35	25	274	12
Kayseri [18]	36	37	430	12
Artvin [19]	22	19	358	54
İstanbul [20]	21	37	342	18
Adana [21]	18	21	298	-
Bayburt [22]	41	37	615	9
Çankırı [23]	18	22	357	4
Gaziantep [24]	25	24	289	8
Kastamonu [25]	33	27	431	8
Kütahya [26]	33	32	225	-
Elazığ [27]	23	29	281	-
Şanlıurfa [28]	21	25	299	9
Gerze/Sinop*	**64**	**73**	**610**	**14**

* present study

The basic statistics were used to describe the statistical characteristics of radionuclides. Pearson correlation analysis were carried out using the statistics software package SPSS in order to clarify

the relationship among the distribution of natural and artificial radionuclides and the radiation hazard parameters (Table 5). Correlation is significant at the 0.05 level (two-tailed).

TABLE 5
Pearson correlation coefficients among the radionuclide levels and radiation hazard parameters in soil samples.

Variables	^{238}U	^{232}Th	^{40}K	^{137}Cs	ADRA	AEDE	Ra_{eq}	H_{ex}	Iγr	ELCR
^{238}U	1									
^{232}Th	0.45	1								
^{40}K	0.19	0.23	1							
^{137}Cs	0.30	0.24	0.14	1						
ADRA	0.82	0.83	0.48	0.33	1					
AEDE	0.82	0.83	0.48	0.33	1	1				
Ra_{eq}	0.81	0.85	0.45	0.32	1	1	1			
H_{ex}	0.81	0.85	0.45	0.32	1	1	1	1		
Iγr	0.80	0.85	0.49	0.32	1	1	1	1	1	
ELCR	0.82	0.83	0.48	0.33	1	1	1	1	1	1

The positive correlation coefficient was absorbed between ^{238}U and ^{232}Th because uranium and thorium decay series occurs together in nature [29]. As shown in Table 5, very weak correlation was observed between ^{238}U-^{232}Th and ^{40}K-^{137}Cs since ^{40}K and ^{137}Cs origins are in different from ^{238}U-^{232}Th series. Also, these results show that the radiation hazard parameters have high good positive correlation coefficients with ^{238}U and ^{232}Th, so, it can be said very strong relationship between these radionuclides in soil samples and radiological parameters. Already, these parameters were calculated using the specific activity concentration of ^{238}U and ^{232}Th because of this reason, the results met our expectations. This strong relationship implies that these radionuclides contribute to the emission of gamma radiation in study area.

The frequency distributions of all radionuclides were analyzed, and the histograms are given in Figs. 2 and 3. The frequency distribution graphs of ^{238}U, ^{232}Th ^{40}K and ^{137}Cs show that these radionuclides have a normal (bell-shape) distribution.

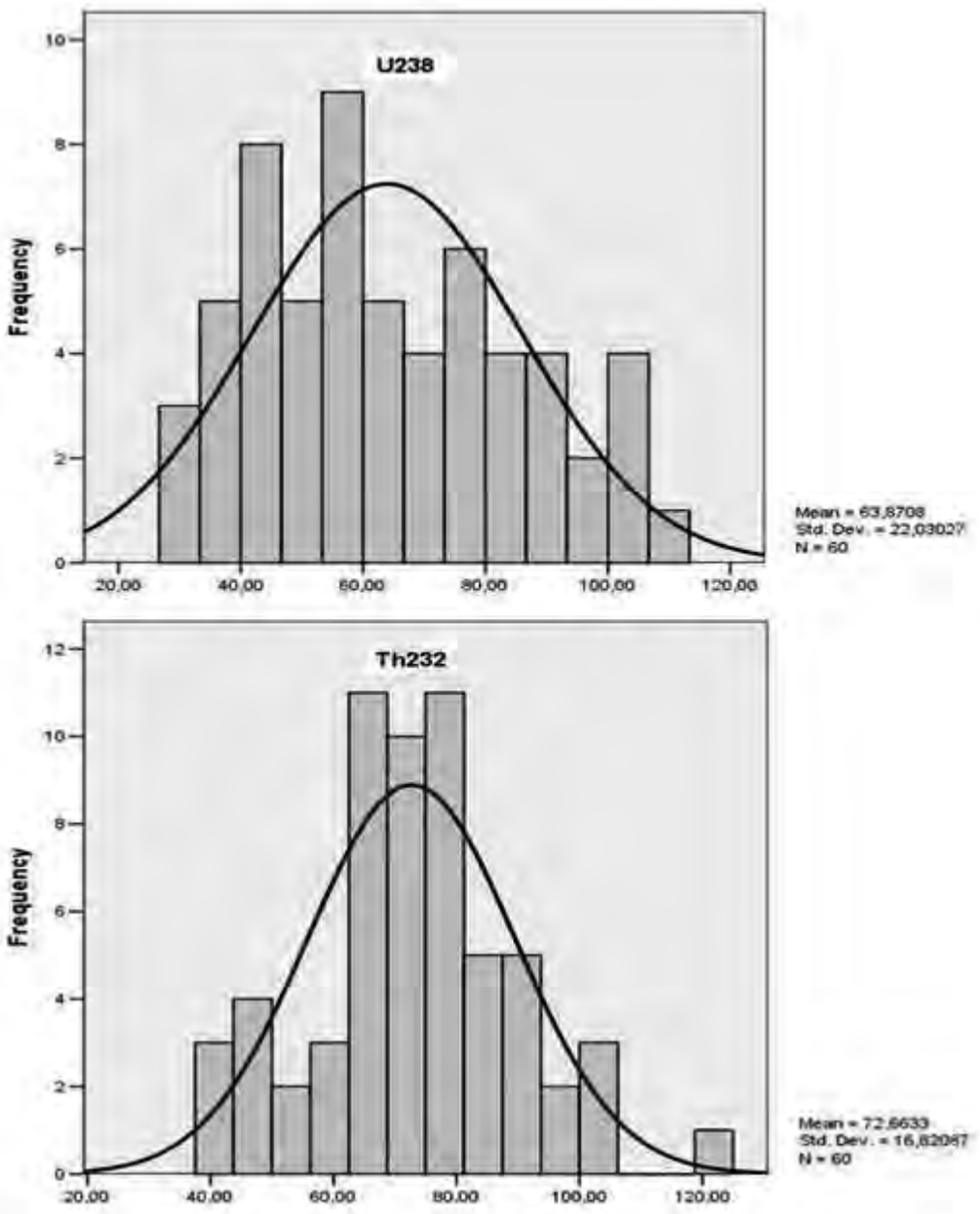

FIGURE 2
The frequency distribution of ^{238}U and ^{232}Th.

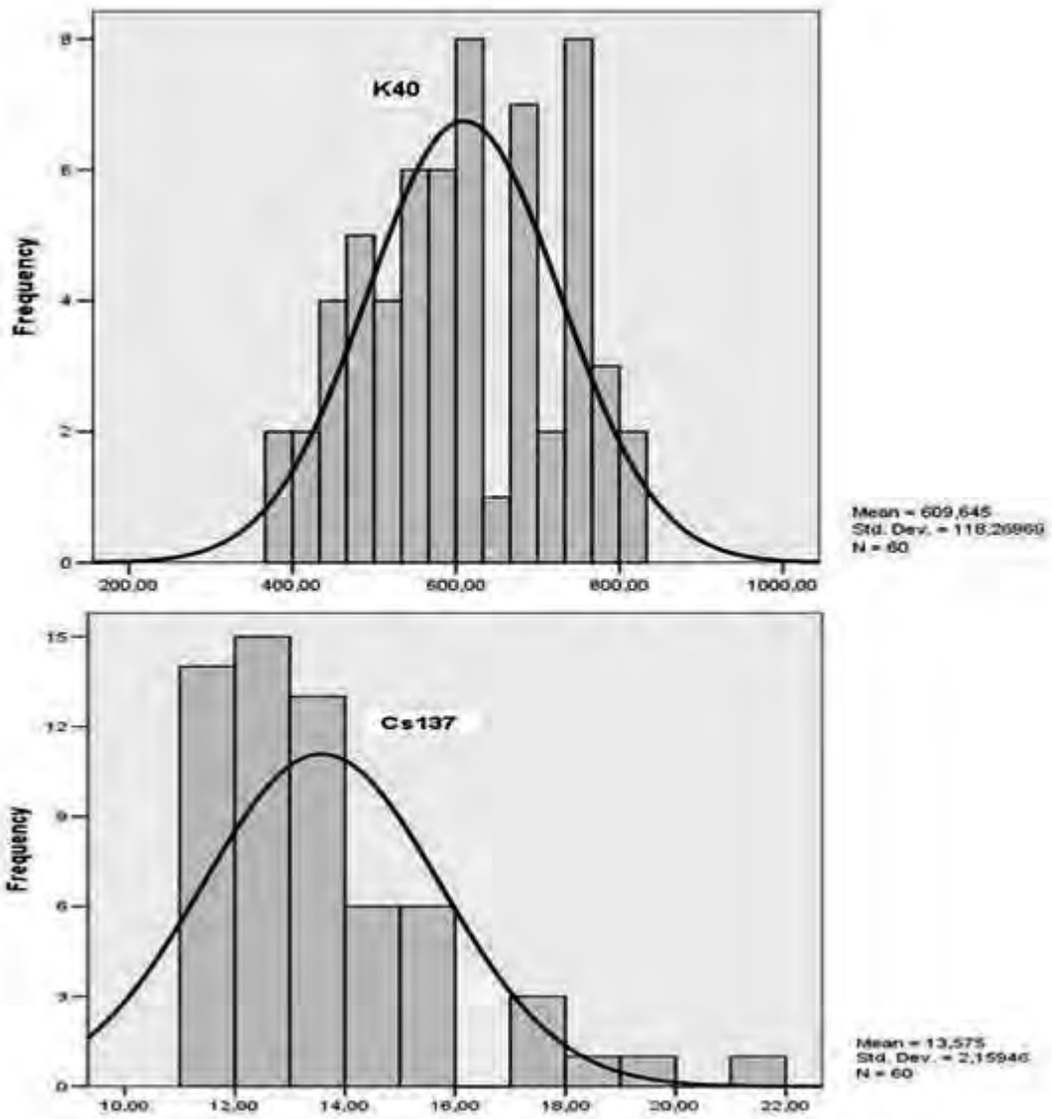

FIGURE 3
The frequency distribution of ^{40}K and ^{137}Cs

Gamma absorbed dose in air. In this research, the outdoor gamma absorbed doses in air (ADRA) measured using a Geiger-Muller tube and the annual effective dose equivalent (AEDE) calculated from these are given in the third and fifth columns of Table 2, respectively. The outdoor gamma absorbed dose values ranged from 69.6 to 182.7 nGy h^{-1} and the mean (60 measurements) was determined as 125.1 nGy h^{-1}. Using the same conversion coefficient and occupancy factor as above, the calculated values of annual effective dose equivalent varied from 85.36 to 224.06 μSv y^{-1} and the mean value was calculated as 153.4 μSv y^{-1}. In this research, the mean annual effective dose equivalent was ascertained is about two times higher than the world mean value of 72 μSv y^{-1} [5]. There is a good agreement between the absorbed gamma dose rate measured by the G-M tube and the one calculated from the radionuclides determined from the soil samples for outdoor environments.

CONCLUSION

In this research, the activity concentrations of the natural and artificial radionuclides in 60 soil samples collected across the Gerze/Sinop were determined by the gamma ray spectroscopy. Using these results, the absorbed gamma dose and annual effective dose were calculated. According to these

values obtained, the radiation hazard parameters such as Radium equivalent activity (Raeq), external hazard index (Hex), representative level index (Iγr) and excess lifetime cancer risks (ELCR) were determined. In addition, the outdoor gamma doses were measured at the same sites as soil samples were collected using a portable G-M tube and from that, the annual effective doses were ascertained. The best part of this study; this is the first detailed study of radioactivity concentrations in Gerze. The results of the present study useful in assessment of the exposures of radiation doses and will be valuable database for future estimations of the impact of radioactive pollution.

ACKNOWLEDGMENT

The author is thankful to Prof. Dr. M. Atıf ÇETİNER and Kastamonu University Scientific Research Project Commission (KUBAP-01/2013-14) for support and cooperation.

REFERENCES

[1] Rizzo, S., Tomarchio, E. and Vella G. (2010) Environmental radioactivity measurements in the Mediterranean area. Fresenius Environmental Bulletin 19, 2433-2443.

[2] Aytekin, H. and Baldık, R. (2011) Radioactivity measurement and dose assessment from surface soils around the Catalagzi coal-fired power plant, Turkey. Fresenius Environmental Bulletin 20, 7.

[3] Çellek, S. (2007) Gerze (Sinop) Yöresindeki Aktif Heyelan Alanlarının Mühendislik Jeolojisi Açısından İncelenmesi, Karadeniz Teknik Üniversitesi Fen Bilimleri Enstitüsü, Jeoloji Mühendisliği Anabilim Dalı, Yüksek Lisans Tezi, (in Turkish).

[4] Kurnaz, A., Küçükömeroğlu, B., Damla, N. and Cevik, U. (2011) Radiological maps for Trabzon, Turkey. Journal of Environmental Radioactivity 102, 393-399.

[5] UNSCEAR (United Nations Scientific Committee on the Effect of Atomic Radiation) (2000) Sources and effects of ionizing radiation United Nations Scientific Committee on the Effects of Atomic Radiation. Report to the General Assembly with scientific annexes, New York, USA, 111-125.

[6] TAEK (Turkish Atomic Energy Authority) (2007) 7. yılında Çernobil, Türkiye Büyük Millet Meclisi Araştırma Komisyonu Raporu (in Turkish).

[7] ICRP 60 (1990) Recommendations of the International Commission on Radiological protection. ICRP Publication 60. Annals of the ICRP. Pergamon Press, Oxford, UK.

[8] Beretka, J. and Mathew, P.J. (1985) Natural radioactivity of Australian building materials, industrial wastes and by-products. Health Physics 48, 87-95.

[9] Krieger, R. (1981) Radioactivity of construction materials. Betonwerk Fertigteil Technik 47, 68.

[10] NEA/OECD (Nuclear Energy Agency) (1979) Exposure to radiation from natural radioactivity in building materials. Report by NEA Group of Experts, OECD, Paris.

[11] Isinkaye, M.O. (2008) Radiometric assessment of natural radioactivity levels of bituminous soil inAgbabu, southwest Nigeria. Radiation Measurements 43, 125-128.

[12] Lu, X., Wang, F., Jia, X. and Wang, L (2007)Radioactive Analysis and Radiological Hazards of Lime and Cement Fabricated in China. IEEE Transactions Nuclear Science 54, 2.

[13] ICRP (International Commission on Radiological Protection) (2007) Annals of the ICRP, The 2007 Recommendations of the International Commission on Radiological Protection. ICRP Publication 103. Ann. ICRP 37, 2-4.

[14] Kam, E., Bozkurt, A. and Ilgar, R. (2010) A study of background radioactivity level for Canakkale, Turkey. Environmental Monitoring and Assessment 168, 1-4, 685-90.

[15] Kapdan, E., Varinlioglu, A. and Karahan, G. (2012) Outdoor radioactivity and health risks in Balıkesir, northwestern Turkey. Radiation Protection Dosimetry 148, 301-309.

[16] Taşkın, H., Karavus, M., Ay, P., TopuzA., Hıdıroğlu, S. and Karahan, G. (2009) Radionuclide concentrations in soil and lifetime cancer risk due to gamma radioactivity in Kırklareli, Turkey. Journal of Environmental Radioactivity 100, 49-53.

[17] Damla, N., Cevik, U., Kobya, A. I., Ataksor, B. and Isık, U. (2010) Assessment of environmental radioactivity for Batman, Turkey. Environmental Monitoring and Assessment 160, 401-412.

[18] Otansev, P., Karahan, G., Kam, E., Barut, I. and Taskın, H. (2012) Assessment of naturalradioactivity concentrations and gamma dose rate levels in Kayseri, Turkey. Radiation Protection Dosimetry 148, 227-236.

[19] Küçükömeroğlu, B., Yeşilbağ, Y.Ö., Kurnaz, A., Çelik, N., Çevik, U. and Çelebi, N. (2011) Radiological characterisation of Artvin and

Ardahan provinces of Turkey. Radiation Protection Dosimetry 145, 389-394.
[20] Karahan, G. and Bayülken, A. (2000) Assessment of gamma dose rates around Istanbul, Turkey. Journal of Environmental Radioactivity 47, 213-22.
[21] Değerlier, M., Karahan, G. and Özger, G. (2008) Radioactivity concentrations and dose assessment for soil samples around Adana, Turkey. Journal of Environmental Radioactivity 99, 7, 1018-1025.
[22] Küçükömeroğlu, B., Kurnaz, A., Damla, N., Çevik, U., Çelebi, N., Ataksor, B. and Taşkın, H. (2009) Environmental radioactivity assessment for Bayburt, Turkey. Journal of Radiological Protection 29, 417-428.
[23] Kapdan, E., Taşkın, H., Kam, E., Osmanlıoğlu, A. E., Karahan, G. and Bozkurt, A. (2012) A Study of Environmental Radioactivity Measurements for Çankırı, Turkey. Radiation Protection Dosimetry 150, 398-404.
[24] Osmanlıoğlu, A. E., Kam, E. and Bozkurt, A. (2007) Assessment of background radioactivity level for Gaziantep region of southeastern Turkey. Radiation Protection Dosimetry 124, 407-410.
[25] Kam, E. and Bozkurt, A. (2007) Environmental radioactivity measurements in Kastamonu region of northern Turkey. Applied Radiation and Isotopes 65, 440-444.
[26] Şahin, L. and Cavas, M. (2008) Natural radioactivity measurements in soil samples of central Kutahya (Turkey). Radiation Protection Dosimetry 131, 526-530.
[27] Canbazoğlu, C. and Doğru, M. (2013) A preliminary study on determination of radiological parameters of soil samples collected from central Elazig, Turkey. Fresenius Environmental Bulletin, 22, 3377-3382.
[28] Bozkurt, A., Yorulmaz, N., Kam, E., Karahan, G. and Osmanlıoğlu, A.E. (2007) Assessment of environmental radioactivity for Sanliurfa region of southeastern Turkey. Radiation Measurements 42 8, 1387-1391.
[29] Tanaskovic, I., Golobocanin, D. and Miljevic, N. (2012) Multivariate statistical analysis of hydrochemical and radiological data of Serbian spa waters. Journal of Geochemical Exploration 112, 226-234.

Received: **19.06.2015**
Accepted: **06.01.2016**

CORRESPONDING AUTHOR

Aslı Kurnaz
Kastamonu University
Faculty of Arts and Sciences
Department of Physics
37100 Kastamonu, Turkey

e-mail: akurnaz@kastamonu.edu.tr

by PSP Volume 25 – No. 1/ 2016, pages 163-173 Fresenius Environmental Bulletin

CONCENTRATION, SPECIATION AND BIOACCESSIBILITY OF CADMIUM IN DUSTFALL FROM COAL MINE AREAS: CASE STUDY IN NORTHERN ANHUI PROVINCE, CHINA

Q. Li[1, 2], Y. F. Han[1], and S. L. Huang[1]

[1]School of Environment and Surveying Engineering, Suzhou University, Suzhou 234000, China
[2]State Engineering & Technological Research Center for Coal Mine Water Disaster Prevention, Suzhou University, Suzhou 234000, China

ABSTRACT

An investigation of 23 samples which have been collected from five coal mining areas in the south-eastern of Suzhou was performed to study the concentration, speciation distribution and bioaccessibility of cadmium in dustfalls. From the results of atomic absorption spectrophotometer, higher concentration of Cd was found compared to the soil environmental background values of Anhui province (BVA) and the Secondary Environmental Quality Standard for Soils in China (EQS). Besides, four chemical fractions were extracted using the three-step BCR sequential extraction procedure and decreased in the order of acid soluble > reducible > residual > oxidizable, implying high migratory ability and potential toxicity of Cd in dustfalls. Findings from in vitro digestion method showed that average Cd bioaccessibilities were >50% in the gastric phase, while only 21%-28% in the intestinal phase. Furthermore, correlation analysis indicated that pH and organic matter content (OM) were the important factors in distribution of chemical fractions, and decrease of particle diameter can improved Cd bioaccessibility in dustfall. A very significant correlation between the gastro-intestinal phase and acid soluble fraction was also identified, suggesting that the latter was the main source of the extracted Cd in in vitro digestion process.

KEYWORDS:
Cadmium, Chemical fraction, Bioaccessibility, In vitro digestion, Dustfall, Coal mining area

INTRODUCTION

Dustfall is a type of airborne particulate matters with fine size which naturally settle on the surface of houses, doors, windows, and other solid objects. As a carrier and transporter for many pollutants, the dustfall particles can attract the heavy metal ions to its surface and then thus lead to potential biological activities [1]. Previous studies have confirmed that the mobility and toxicity of trace metals strongly depend on their specific chemical speciation distributions [2]. For this reason, several methods of fraction separation and extraction were developed and applied to predict long-term behavior of metals in contaminated solid materials. In the above-mentioned methods, BCR sequential extraction procedure, which divides the total metal content into four fractions of acid soluble, reducible, oxidizable and residual, is more widely used by environmental researchers because of its simple operating processes and outstanding reproducibility[3,4]. Along with that more and more scientists paid attention to health hazard of toxic metals, the concept of bioaccessibility, which represents the amount of a contaminant that is liberated into an aqueous from within the gastro-intestinal tract and probably absorbed into human body [5], was introduced. Currently, the commonest determination approach of bioaccessibility is the physiologically based extraction test (PBET) [6], an in vitro digestion procedure with the simulated conditions similar to those in gastro-intestinal tract.

The metal cadmium (Cd) is a global contaminant and commonly exists in various environmental media with low concentrations. Exposure to Cd, mainly by inhalation and ingestion, can significantly increase the risk of human carcinogenesis[7]. It also has ecotoxic effects on microorganisms, plants, animals and humans, while these toxicities are variable and closely related to the chemical speciation, especially to concentration of the soluble Cd ion. Many studies have discussed the speciation distribution and bioaccessibility of Cd in soils[8,9], sediments[10,11], and even in medicine[12], but the similar research on dustfalls is rarely reported.

Suzhou coal mining area, located in the northern part of Anhui province, has been intensively exploited for twenty years. The long-term mining activities have produced large amounts of coal gangue which contains high Cd and are usually piled around mines (such as Taoyuan, Qinan, et al.). Under the effect of

meteorological factor, these gangue can be gradually weathered and become a significant source of atmospheric dust particles, causing serious environmental problems in the mining area. The aims of this work are as follows: (1) to investigate the pollution status of Cd in dustfalls from coal mining areas; (2) to analyse speciation distribution and bioaccessibility of Cd in dustfalls, using BCR sequential extraction procedure and in vitro digestion test; and (3) to identify the correlations between physicochemical parameters, total Cd concentration, chemical fractions and the gastro-intestinal phase.

MATERIALS AND METHODS

STUDY AREA

Suzhou City is located in the northern part of Anhui Province of China, between latitude 33°18'N~34°38'N and longitude 116°09'E~118°10'E, with an area of 9,785 sq km. The climate is characterized by warm and semi--humid monsoons, with a wide variation in temperature ranging from 32℃ in summer to -2℃ in winter. The annual average rainfall ranges between 770 and 990 mm with maximum rainfall during May-September. Intensively coal exploiting activities in Suzhou started from 1990s, and more than fifteen million tons of coal can be produced since 2011. The long-term mining activities has resulted in serious environmental pollution, such as excessive accumulation of metal elements in soil and crops[13]. The mining area is concentrated in the south-eastern of Suzhou, and five coal mines distributed in the area were selected for this study (Fig.1).

Zhuxianzhuang (ZXZ) coal mine is situated in the east of urban area, while Luling (LL) coal mine lies in the southeast, and the last three coal mines named Taoyuan (TY), Qinan (QN) and Qidong (QD) are located in the south.

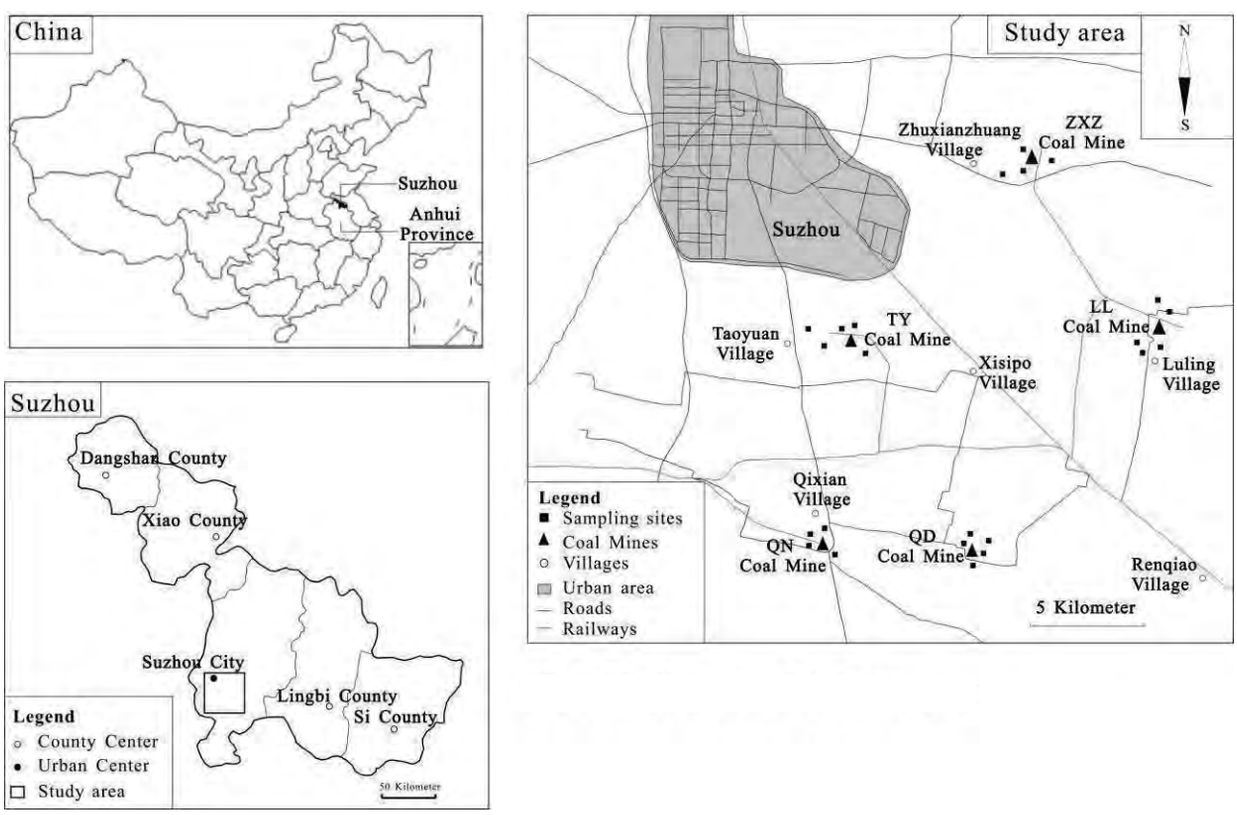

FIGURE 1
Study area and sampling sites.

SAMPLE COLLECTION AND PRETREATMENT

Around each coal mine, 4 to 5 sampling sites were randomly selected at villages and settlements. A total of 23 dustfall samples were collected from the surfaces of wooden doors and glass windows, and brushed into clean sample bags in early March 2015, using a rabbit hair brush and a plastic spade. Each sample was about 25~50 g. All samples were transported to the laboratory of *State Engineering & Technological Research Center for Coal Mine Water Disaster Prevention* immediately, and air-dried for 2 to 3 days at room temperature. Than we sieved them by a 100-mesh sieve to collect the particle size faction <150 μm. The sieved samples were stored in sealed plastic bags.

Sample digestion. A portion (0.15 g) of each dust sample was weighed and placed in a 50 ml teflon digestion tank, and then 8 ml HNO_3 and 2 ml $HClO_4$ was added into tank. After initial reaction, each tank was covered with lid and allowed to stand overnight. The tanks were placed in a graphite digester (SH230N, Hanon Instruments Co., LTD, China) and heated at 110℃ for 2 h. The solutions were allowed to cool for 10 min until the volume reduced to 2~3 ml, and then 5 ml HNO_3 and 3 ml HF was slowly added into each tank. The mixture was heated again at 180℃ for thermal decomposition until the digestion solution was near dryness, the remaining digests were transferred to volumetric flask after cooling to room temperature and diluted to 50 ml using MilliQ water.

BCR sequential extraction method. The three-step BCR sequential extraction procedure[14] was performed to determine the chemical fractions of Cd in dustfalls from the investigated area. Each fraction was defined as follows:

Step 1 (acid soluble fraction): 1.0 g of dustfall sample was placed into a polyethylene centrifuge tube and extracted with 40 ml 0.11 M acetic acid for 16 h at a room temperature of 22.0±0.5℃ with continuous shaking of 180 rpm. After extraction, the extracted liquid was separated from the solid residue by centrifugation at 4000 rpm for 20 min. The supernatant liquid was filtered through 0.45 μm filter membrane to 50 ml polyethylene volumetric flask for analysis. Then, 20 ml of MilliQ water was added into the tube for washing the solid phase, by continuous shaking for 15 min and centrifugation for 20 min. The supernatant was decanted and discharged carefully to avoid loss of the solid residues.

Step 2 (reducible fraction): 40 ml of 0.5 M hydroxylamine hydrochloride (pH of 1.5) was added to the solid residues from step 1 in the centrifuge tube. The extraction was carried out for 16 h at a room temperature of 22.0±0.5℃ with continuous shaking of 180 rpm. Then, the separation of the extracts, filtration and collection of the supernatant, washing of the solid residues were the same as described for step 1 before proceeding to step 3.

Step 3 (oxidizable fraction): 10 ml of 8.8 M hydrogen peroxide (pH of 2-3) was added to the solid residues from step 2 in the centrifuge tube. Initially, the mixture was digested at room temperature for 1 h, with loosely cover and occasional manual shaking, and then the sample was heated to 85±1℃ in a water-bath for further digestion, until the volume reduced to 2~3 ml. After cooling, an addition 10 ml of 8.8 M hydrogen peroxide (pH of 2-3) was added into the tube. Heating was performed again at 85±1℃ until the volume reduced to 2~3 ml. Finally, 50 ml of 1.0 M ammonium acetate (pH of 2) was added to the cool residues. The mixture was shaken for 16 h at 22.0±0.5℃, and then centrifuged for 20 min at 4000 rpm. The filtration, collection and washing processes that had been performed at the end of the step 1 were repeated for this step as well.

Residue (residual fraction): After the above extraction procedure, the solid residue in the centrifuge tube was transferred to a pre-cleaned beaker containing 15 ml of aqua regia solution. The digestion was performed for 2 h on a hot plate, until the solution was transparent. Later, we transferred the digest into volumetric flask and diluted it to 50 ml with MilliQ water.

In vitro digestion procedure. In order to assess the bioaccessibility of Cd in dustfalls, the PBET method[6] was adopted to determine the in vitro digestibility of Cd from the investigated samples, under the simulated gastric and small-intestinal regimes. In brief, synthetic gastric solution was prepared by dissolving 0.5 g sodium citrate, 0.5 g malate, 1.25 g pepsin, 420 μl lactic acid and 500 μl acetic acid into 1 l MilliQ water, and acidifying to pH of 2.5 using HCl (12 M). 0.4 g of each dustfall sample was extracted with 40 ml prepared gastric solution for 1 h in a polyethylene centrifuge tube, at a body temperature of 37℃ and a shaking speed of 100 rpm. After extraction, the extract was centrifuged for 15 min at 4000 rpm, then 5 ml of supernatant was collected using a syringe, filtered through 0.45 μm filter membrane and preserved under refrigeration as an analytic sample of gastric phase. To compensate for the removed 5 ml supernatant, the same

volume of original gastric solution was added into the tube. Subsequently, pH of the extracted solution was adjusted to 7.0 for simulating small-intestinal condition followed by the addition of 70 mg bile salts and 20 mg pancreatin to each tube. A four hour extraction was performed and pH was measured and adjusted at 15 min intervals, to ensure that pH of 7.0 in the extraction solution was maintaining. Then, the centrifugation of the extracts, filtration and preservation of the supernatant were the same as described for gastric phase.

SAMPLE ANALYSIS AND QUALITY CONTROL

pH of dustfall samples were determined in the mixture solution (dust-water ratio=1:2.5, w/v) by a pH meter[15], while the organic matter content (OM) and mechanical composition (MC) were tested using potassium dichromate oxidation-colorimetric method and laser particle size analyzer (2008A, Jinan Winner Particle Instruments Co., LTD, China), respectively. All of the analytic samples prepared in the above digestion and extraction procedures were analyzed for cadmium (Cd) using atomic absorption spectrophotometer (Model TAS-990FG, Purkinje General Instrument, Beijing, China).

To improve the accuracy of results, all chemicals used in the experiment were of analytical grade, and all the glassware and centrifuge tubes were soaked in dilute nitric acid for 24 h followed by rinsed with MilliQ water three times before use. During each digestion and extraction procedure, reagent blanks were prepared for correcting blank and eliminating analytical bias. Each sample was determined with three replicates to test the reproducibility, and relative standard deviation was less than 10%.

BIOACCESSIBILITY OF Cd

On the basis of in vitro results, bioaccessibility of Cd was calculated as the radio of extracted Cd concentration in the gastric or intestinal phase to the total Cd concentration in the corresponding dustfall sample[8], the formula is given as follows:

$$in\ vitro\ Cd\ bioaccessibility = \frac{in\ vitro\ Cd}{total\ Cd} \times 100$$

Where, *in vitro Cd* ($mg \cdot kg^{-1}$) is the extracted quantity of Cd in a particular in vitro simulated digestion and *total Cd* ($mg \cdot kg^{-1}$) is the total concentration of Cd in the corresponding dustfall sample.

DATA ANALYSIS

Data analyses were performed by Excel 2003 and SPSS 13.0 for windows, and all figures in this article were drawn by CorelDRAW 12.0. Correlation coefficients of the observed variables in dustfalls were calculated to identify the relationships between physicochemical parameters, total Cd concentration, chemical fractions and the gastro-intestinal phase.

RESULTS AND DISCUSSION

PHYSICAL-CHEMICAL PARAMETERS AND TOTAL Cd CONCENTRATION IN DUSTFALL

The main physical-chemical properties and total concentration of Cd in dustfall samples collected from the investigated area are listed in Table 1.

TABLE 1.
Physical-chemical properties and total Cd concentration of dustfall samples from the investigated areas

Site (Sample number)	Index	pH (1:2.5)	OM ($g \cdot kg^{-1}$)	MC (%) Clay	Silt	Sand	Total Cd ($mg \cdot kg^{-1}$)
LL (5)	Range	6.16-9.02	8.0-59.0	4.47-10.54	56.83-79.14	13.14-38.70	0.735-1.082
	Mean±SD	7.60±1.09	36.9±19.2	7.40±2.28	68.56±8.48	24.04±9.99	0.829±0.149
QD (5)	Range	6.14-9.43	14.3-87.0	5.94-7.13	53.77-77.38	16.17-39.53	0.582-0.866
	Mean±SD	7.88±1.24	54.5±36.6	6.49±0.46	65.41±8.52	28.10±8.46	0.695±0.117
QN (4)	Range	7.45-8.40	41.6-108.4	5.05-5.75	54.55-66.90	28.05-40.27	0.560-0.930
	Mean±SD	7.97±0.41	78.7±28.2	5.28±0.32	60.70±6.03	34.02±5.85	0.779±0.176
TY (5)	Range	5.68-8.03	30.9-85.4	4.91-11.81	61.48-79.42	12.55-32.47	0.680-0.844
	Mean±SD	7.22±1.01	53.6±21.7	7.58±2.64	66.67±7.46	25.74±8.65	0.745±0.071
ZXZ (4)	Range	6.68-8.83	8.4-59.6	3.92-9.94	62.07-77.49	13.64-33.03	0.698-1.048
	Mean±SD	7.69±0.96	30.3±23.0	6.91±2.94	69.74±6.53	23.35±7.95	0.808±0.163
Average	Mean±SD	7.66±0.95	50.5±29.0	6.79±2.03	66.30±7.51	26.91±8.49	0.769±0.133
BVA (the soil environmental background values of Anhui province)							0.097
EQS (the Secondary Environmental Quality Standard for Soils of China)							0.6

There were no statistically significant difference for the arithmetic means and ranges of pH between dustfalls from the five sampling areas, and the pH of all dustfall samples were varied between 5.68 and 9.43 with an average pH of 7.66, which suggests that most dustfall samples are weakly alkalic. The organic matter content of the sampled dustfalls varied considerably within each coal mine area and ranged across the five mines from 8.0 to 108.4 $g \cdot kg^{-1}$ with an average value of 50.5 $g \cdot kg^{-1}$. Mechanical composition of dustfalls showed a medium-size distribution pattern, and the clay, silt and sand contents averaged 6.79±2.03%, 66.30±7.51% and 26.91±8.49%, respectively.

The concentrations of Cd in all dustfall samples ranged from 0.560 to 1.082 $mg \cdot kg^{-1}$, with average value of 0.766 $mg \cdot kg^{-1}$. Among the five coal mines investigated, the highest and lowest Cd concentrations were found in LL (0.829±0.149 $mg \cdot kg^{-1}$) and QD (0.695±0.117 $mg \cdot kg^{-1}$) coal mine area, which were both much higher than the soil environmental background values of Anhui province (BVA) and had slightly exceeded the Secondary Environmental Quality Standard for Soils of China (EQS) by 1.38- and 1.16-fold. Meanwhile, they were also higher than Cd concentration of soils in the same investigated areas (0.33-0.38 $mg \cdot kg^{-1}$)[16], but lower than those in dustfalls from vanadium-titanium magnetite mining area in Panzhihua (1.7-7.7 $mg \cdot kg^{-1}$)[17], and from large cities in china such as Nanjing (5.8 $mg \cdot kg^{-1}$)[18] and Hangzhou (15.6 $mg \cdot kg^{-1}$)[19].

CHEMICAL FRACTIONS OF Cd IN DUSTFALL

The descriptive statistics of Cd fraction contents and percentages in dustfall samples from the different coal mine areas are shown in Fig.2.

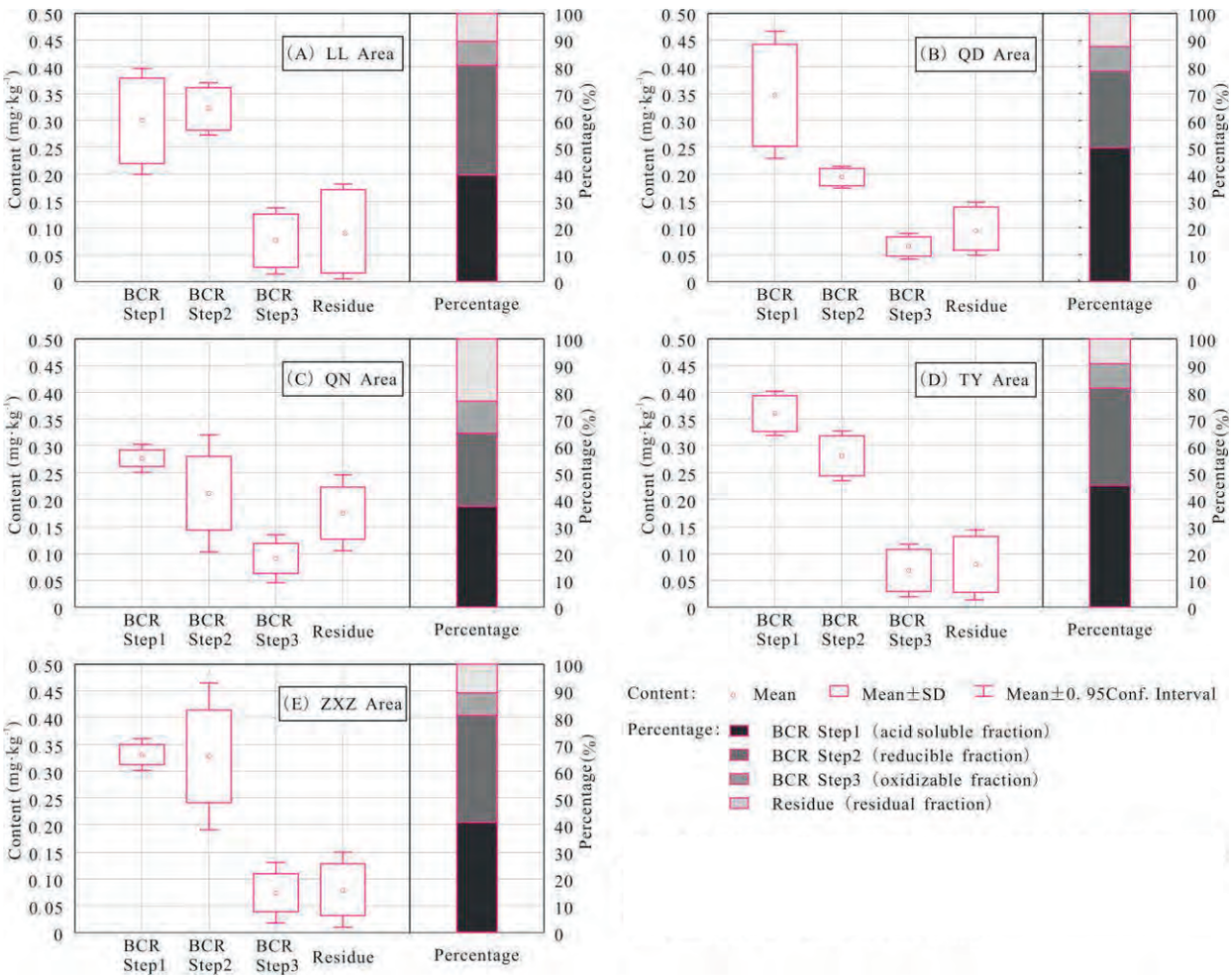

FIGURE 2.
Content and percentage of extraction of Cadmium obtained by BCR sequential extraction procedure in the dustfall samples from the mining areas Luling (LL), Qidong (QD), Qinan (QN), Taoyuan (TY) and Zhuxianzhuang (ZXZ).

In each investigated coal mine area, the sum of the four Cd fraction contents (mean values, Fig.2) agreed well with the total Cd concentrations determined by the mixture acid digestion method (Table 1), indicating that an effective experiment quality control and good mass balance were achieved. Previous studies have reported that element behaviors (solubility, transferability and etc.) are mainly affected by the distribution pattern of metal fraction[2]. For Cd in the investigated dustfall samples, the average contents associated with the different fractions was generally in the order of acid soluble > reducible > residual > oxidizable, with an exception appeared to the samples from LL area where the reducible fraction was slightly higher than the acid soluble fraction. Percentage of the dominant fraction (acid soluble) ranged from 36.94% to 49.08% in the five mine areas implying high migratory ability and potential toxicity of Cd, while reducible, oxidizable and residual fractions accounted for 27.71-40.73%, 8.67-12.07%, 9.96-23.28% of total Cd, respectively.

Compared with the studies conducted in Baotou[20] and Huangshi city[21] (Table 2, both of the two cities in china are characterized by typical mining industry, B is in Neimenggu province and H is in Hubei province), similar speciation distribution of Cd in agreement with this article were observed.

TABLE 2.
Comparison of Cd speciation distributions in dustfalls from some typical cities in China

Regions	Percentage of each fractions in total Cd content (%)				References
	Acid soluble	Reducible	Oxidizable	Residual	
Baotou City	69.2	23.0	3.9	3.9	Pan et al. (2010)
Huangshi City	51.6	24.9	9.1	14.4	Liu et al. (2014)
Xi'an City	4.6	-	10.6	84.8	Mei et al. (2011)
Chengdu City	15.3	3.4	2.4	78.9	Zhou et al. (2006)
This work (average value of all 23 samples)	42.42	34.93	9.67	12.97	

Whereas, opposite results that highest content existed in the residual fraction were also reported in Xi'an city by Mei[22] and in Chengdu city by Zhou[23]. That distinction can be explained by diverse sources of Cd concentrated in dustfalls between the above regions. Wang[24] found that Cd additions due to interior source pollution inherited from soil parent materials was mainly presented in stable fraction, while the exterior source pollution caused by anthropogenic activities was just the reverse. Considering the structure of energy consumption and industrial economy in the coal mine areas, such observation points to that Cd addition in the dustfall is an ongoing procedure due to emissions from coal combustion and mining activities.

BIOACCESIBILITY OF Cd IN DUSTFALL

The bioaccessibility is an important index for assessing the potential adverse effects of Cd in dustfalls to humans, and it can be described by determining the soluble Cd species presented in simulated gastrointestinal solutions. Table 3 lists extracted Cd contents in the gastric and intestinal phases and their corresponding percentage bioaccessibility for the dustfall samples, showing inapparent variation among the different coal mine areas.

TABLE 3.
Extracted contents and bioaccessibilities of Cd in the gastric and intestinal phases by in vitro digestion

Area	Gastric phase		Intestinal phase	
	Content ($mg \cdot kg^{-1}$)	Bioaccessibility (%)	Content ($mg \cdot kg^{-1}$)	Bioaccessibility (%)
LL	0.501±0.032	61.59±9.17	0.188±0.030	22.77±2.02
QD	0.469±0.046	69.48±15.05	0.165±0.052	24.30±9.06
QN	0.440±0.024	59.02±15.18	0.156±0.040	21.16±8.90
TY	0.510±0.025	69.25±9.35	0.204±0.037	27.52±5.43
ZXZ	0.487±0.041	61.41±7.96	0.198±0.045	24.66±4.33

In gastric phase, the average quantities of Cd extracted within the simulated environment of human stomach ranged from 0.440 mg to 0.510 mg per kilogram of dustfalls from the five mine areas, with the highest bioaccessibility of 69.48% in QD and the lowest bioaccessibility of 59.02% in QN. While in intestinal phase, the quantities of extracted Cd were varied between 0.156 mg and 0.204 mg per kilogram of dustfalls, with the highest bioaccessibility of 27.52% in TY and the lowest bioaccessibility of 21.16% in QN.

It is obviously that average bioaccessibilities in gastric phase were about 2-3 times higher than the intestinal phase, revealing that Cd bioaccessibility largely depended on their solubility in human stomach. That is coinciding with the results observed in nine contaminated soils from Balikesir region of Turkey

using PBET by Karadas C and Kara D[8]. pH of simulated solutions may act on an important part to the occurrence of distinction between gastric and intestinal phase, because it can change the surface charge of dustfall particles and the enzymatic activity in digestion system[25]. When pH rises from gastric phase into intestinal phase, Cd solubility decreased as a result of more negative charge at the particle surface and weaker enzymatic activity, thus causing the relatively decline of Cd bioaccessibility in intestinal phase.

CORRELATION ANALYSIS

In order to obtain an intensive understanding of the relationships between physicochemical parameters, total Cd concentration, chemical fractions and the gastro-intestinal phase of dustfalls, correlation analysis was performed on the experimental datum from the 23 samples collected from the five mining areas, and the results were given in Table 4.

TABLE 4.
Correlation analysis between physicochemical parameters, total Cd, chemical fractions and the gastro-intestinal phase in dustfalls (n=23)

	Total Cd	BCR Step1	BCR Step2	BCR Step3	BCR Step4	Gastric phase	Intestinal phase	pH	OM	Clay	Silt	Sand
Toal Cd	1											
BCR Step1	0.122	1										
BCR Step2	**0.459***	0.177	1									
BCR Step3	0.203	-0.088	0.175	1								
BCR Step4	0.38	-0.075	-0.331	0.132	1							
Gastric phase	0.042	**0.735****	**0.486***	0.020	-0.221	1						
Intestinal phase	0.256	**0.678****	0.366	0.144	-0.121	**0.618****	1					
pH	-0.177	**-0.485***	-0.101	0.003	-0.035	**-0.422***	-0.306	1				
OM	-0.093	**-0.478***	-0.280	**0.429***	0.139	-0.346	-0.366	0.320	1			
Clay	0.245	**0.486***	0.179	-0.087	-0.124	**0.514***	**0.458***	-0.352	-0.327	1		
Silt	-0.1	0.161	0.328	-0.035	-0.267	0.387	**0.429***	0.336	-0.033	0.38	1	
Sand	0.03	-0.258	-0.333	0.052	0.266	**-0.465***	**-0.489***	-0.213	0.108	**-0.575****	**-0.975****	1

* Correlation is significant at the 0.05 level (two-tailed)
** Correlation is significant at the 0.01 level (two-tailed)
BCR Step1-Step4 represent different chemical fractions and have given in Fig.2

For the relationship of physicochemical parameters and chemical fractions, pH showed a significant negative correlation (-0.485, $p<0.05$) with acid soluble fraction, indicating that it maybe the prime determinant of Cd reactivity in BCR step 1. When in the acidic environment, Cd is likely to exist in the form of the free ions rather than to bind with the anion of the mineral acid as insoluble salt, so the solubility of Cd is enhanced. Similar to pH values, OM was negatively correlated with acid soluble fraction as well (-0.478, $p<0.05$), and furtherly had an added positive correlation with oxidizable fraction (0.429, $p<0.05$), that is mainly caused by the complexation between organic matter and Cd ions. Due to the effect, higher OM values can promote the transfer ability of partial Cd ions from acid soluble fraction to oxidizable fraction. However, in oxidation condition, these ions will be released again to the original fraction as a result of organics degradation. Despite clay content had a high correlation with acid soluble fraction (0.486, $p<0.01$), suggesting most of the soluble Cd were present in ultrafine particles, there was no obvious relationship between the other particle sizes and each fraction, and presumably it was caused by the complex components and multi-sources of dustfall samples.

The Cd quantities extracted from the gastric and intestinal phase had negative correlations with pH values (gastric:-0.422, $p<0.05$; intestinal:-0.306, insignificant), and low correlations with OM values, which might be relative to the less oxidizable fraction of Cd in dustfalls. Significant correlations between the gastro-intestinal phase and mechanical composition of dustfalls were observed, with exceptions of inapparent coefficients between gastric phase and silt (0.387), showing that Cd bioaccessibility can be improved with decrease of particle diameter. This is similar to the result reported by Smith et al., who found that arsenic bioaccessibility increased from 25±16% in the <250-microm soil particle fraction to 42±23% in the <10-microm soil particle fraction[26].

Stronger significant positive correlations were found between the gastro-intestinal phase and acid soluble fracton (gastric:0.735, $p<0.01$; intestinal:0.678, $p<0.01$), it means that the Cd extracts in the in vitro digestion test were mainly supplied from the most active fraction. Reducible fraction had an obvious positive correlation with gastric phase (0.486, $p<0.05$), but displayed an inapparent relationship with intestinal phase (0.366). That might be attributed to high pH in intestinal extracted solution which has inhibiting effect on release of Cd ions from the binding sites, such as Fe/Mn oxides. In recent years, in vitro digestion model has been widely applied in bioaccessibility determination of heavy metals in various environmental media, but uncommon in comparison with the BCR sequential extraction phases. One of the few publications was conducted in Turkey soils by Karadas C[27], finding the highest correlation between the gastro-intestinal phase and reducible fraction, rather than acid soluble fraction, which is not coincident with the result in our work and probably due to the different speciation distribution. Cd in the investigated samples from Turkey mostly occurred in the reducible fraction, while in our work showed the highest affinity for the acid soluble fraction. Additionally, considering to the weak relationships between the gastro-intestinal phase and total Cd (gastric phase: 0.042; intestinal: 0.256), or between the acid soluble fraction and total Cd (0.122), it also should be noted that results of in vitro digestion test, as well as the acid soluble fraction, could be as effective indicators for assessing the potential biological toxicity of Cd in dustfall, rather than those based on total Cd.

CONCLUSIONS

According to the study on the five mining areas, high concentrations of Cd in dustfalls were observed with an average value of 0.766 $mg \cdot kg^{-1}$, much higher than BVA and slightly exceeded EQS. BCR sequential extraction results showed that >40% of Cd was mainly in the acid soluble fraction, posing a stronger migratory ability and a greater potential toxicity to the acid environment. Due to the difference of pH values in the simulated gastro-intestinal solutions, bioaccessibilities of Cd in gastric phase (59.02%-69.48%) were obviously higher than those in intestinal phase (21.16%-27.52%), revealing that Cd bioaccessibility largely depended on their solubility in human stomach. Correlation analysis suggested that physicochemical parameters (pH, OM and mechanical composition) have important influences on the speciation distribution of Cd in dustfalls, as well as on the gastro-intestinal phase. Most Cd quantities extracted in the gastro-intestinal phase were mainly supplied from acid soluble fraction. Both of the results of in vitro digestion test and the acid soluble fraction, more effective than the total Cd, were proposed for representing the potential biological toxicity of Cd in dustfall.

ACKNOWLEDGEMENTS

This work was financially supported by the National Natural Science Foundation of China (No.41302274), the Natural Science Foundation of Anhui Education Department (KJ2014A251) and the Opened Foundation of Anhui Engineering & Technological Research Center for Coal Exploration (no.2013YKF05)

REFERENCES

[1] Al-Khashman O (2004) Heavy metal distribution in dust, street dust and soils from the work place in Karak Industrial Estate, Jordan. Atmos Environ 38(39):6803-6812

[2] Pénilla S, Bordas F and Bollinger JC (2005) Sequential heavy metals extraction from polluted solids: Influence of sulphate overconcentration. J Colloid Interface Sci 292:20-28

[3] Francisco R, Rafael B, Fernando F, Manuel A (2008) Comparison of three sequential extraction procedures for trace element partitioning in three contaminated Mediterranean soils. Environ Geochem Health 30(2):171-175

[4] Oyeyiola AO, Olayinka KO, Alo BI (2011) Comparison of three sequential extraction protocols for the fractionation of potentially toxic metals in coastal sediments. Environ Monit Assess 172(1-4):319–327
[5] Jack C, Albert J, Euan S, Ravi N (2015) Assessing the bioavailability and bioaccessibility of metals and metalloids. Environ Sci Pollut Res 22(12):8802-8825
[6] Ruby MV, Davis A, Schoof R, Eberle S, Sellstone CM (1996) Estimation of lead and arsenic bioavailability using a physiologically based extraction test. Environ Sci Technol 30:422-430
[7] Bettina J, Alicja W, Laura DT, Agneta AK (2013) Exposure to cadmium from food and risk of cardiovascular disease in men: a population-based prospective cohort study. Eur J Epidemiol 28(10):837–840
[8] Karadaş C, Kara D (2011) In-vitro gastro-intestinal method for the assessment of metal bioavailability in contaminated soils. Environ Sci Pollut Res 18(4):620–628
[9] Li B, Wang QQ, Yan H, Yang LM, Huang BL (2003) Chromatographic behavior of cadmium in an ion-pair reversed-phase micro HPLC system and its application to the determination of bio-available cadmium in soil samples. Anal Bioanal Chem 376(6):923-927
[10] Krzysztof L, Danuta W (2002) Speciation of Cadmium in the Bottom Sediment of Rybnik Reservoir. Water, Air, and Soil Pollution 141(1-4):73-89
[11] C. Carapeto, D. Purchase (2000) Use of Sequential Extraction Procedures for the Analysis of Cadmium and Lead in Sediment Samples from a Constructed Wetland. Bull Environ Contam Toxicol 64(1):51-58
[12] Yang DH, Lee YJ (2009) Determination of cadmium bioaccessibility in herbal medicines and safety assessment by in vitro dissolution and ICP-AES. Microchim Acta 167(1-2):117-122
[13] Li Q, Han YF, Xu DS, Gao Y (2014) Enrichment Characteristics and Pollution Assessment of Three Food Crops around Gangue Dump. Journal of Safety and Environment 14(5):321-326 (In Chinese)
[14] Ure AM, Quevauviller PH, Muntau H, Griepink B (1993) Speciation of heavy metals in soils and sediments-an account of the improvement and harmonization of extraction techniques undertaken under the auspices of the BCR of the Commission-of-the-European-Communities. Int J Environ Anal Chem 51:135-151
[15] Luo J, Zhang H, Zhao FJ, Davison W (2010) Distinguishing diffusional and plant control of Cd and Ni uptake by hyperaccumulator and nonhyperaccumulator plants. Environ Sci Technol 44:6636-6641
[16] Yuan XT, Zhang CL, Sun Q, Wu YC. (2011) Characteristices of heavy metal concentrations in soil around coal mining area in Suzhou City 30(8): 1451-1455 (In Chinese)
[17] Jiang S, Zhang CJ, Xu ZQ, Xu JY (2009) Distribution characteristices of heavy metals in dustfall from Panzhihua mining area. Acta Mineralogica Sinica z1:400-401 (In Chinese)
[18] Huang SS, Hua M, Jin Y, Wu XM, Liao QL, Zhu BW, Pan YM (2008) Concentrations and sources of heavymetal in atmospheric dustfall in the Nanjing city, East China. Earth Science Frontiers, 15(5):161-166 (In Chinese)
[19] Jiao L, Shen JD, Yao L, Yang L (2013) Pollution characteristics and sources of heavy metals in atmospheric dustfall of Hangzhou. Environmental Pollution and Control 35(1):73-80 (In Chinese)
[20] Pan HJ, Liu JT, Zhao SZ, Zhong R, Liu YB, Zhao JZ (2010) Speciation analysis of Cadmium in dustfall in Baotou city. Journal of Inner Mongolia Agricultural University 31(4):105-109 (In Chinese)
[21] Liu WL, Xiao WS, Zhang JQ, Fu GZ, Zhan CL, Hong M, Yao HD (2014) Research on Pollution and Speciation Characteristics of Heavy Metals in Atmospheric Dustfall of Huangshi. Journal of Hubei Polytechnic University 30(2):32-37 (In Chinese)
[22] Mei FM, Xu CY, Zhou L (2011) Chemical species and bioavailability of Cu, Pb, Zn, Ni and Cd of dustfall from Xi'an park in China. Environmental Chemistry 30(7):1284-1290 (In Chinese)
[23] Zhou L, Zeng Y, Ni SJ, Zhang CJ (2006) Research about Cd Species of Dustfall in Chengdu Region. Guangdong Trace Elements Science 13(2):44-48 (In Chinese)
[24] Wang LP, Zhang MK (2007) Release behaviors of heavy metals from pollued soils with heavy metals of different sources. Research of Environmental Sciences 20(4):134-138 (In Chinese)
[25] Ren JH, Williams PN, Luo J, Ma HR, Wang XR (2015) Sediment metal bioavailability in Lake Taihu, China: evaluation of sequential extraction, DGT, and PBET techniques. Environ Sci Pollut Res (Published online)
[26] Smith E, Weber J, Juhasz A L (2009) Arsenic distribution and bioaccessibility across particle fractions in historically contaminated soils.

Environmental geochemistry and health, 31(1):85-92.
[27] Karadaş C, Kara D (2012) Chemometric evaluation for the relation of BCR sequential extraction method and in vitro gastro-intestinal method for the assessment of metal bioavailability in contaminated soils in Turkey. Environ Sci Pollut Res 19(4):1280-1295.

Received: **05.07.2015**
Accepted: **26.12.2015**

CORRESPONDING AUTHOR

Q. Li
Suzhou University
School of Environment and Surveying Engineering
Suzhou 234000 – CHINA

e-mail: liqi821113@163.com

by PSP Volume 25 – No. 1/ 2016, pages 174-182 Fresenius Environmental Bulletin

LEACHING TOXICITY ANALYSIS AND ECOLOGICAL RISK ASSESSMENT OF HEAVY METALS IN SPENT ACRYLONITRILE CATALYSTS

Jian Liu, Zhaofu Qiu*, Ji Yang, Shuguang Lu, Limei Cao, Wei Zhang

State Environmental Protection Key Laboratory of Environmental Risk Assessment and Control on Chemical Process, East China University of Science and Technology, Shanghai 200237, China

ABSTRACT

The contents of heavy metals in spent acrylonitrile catalyst were analyzed along with the leaching toxicity characteristics under different landfill conditions. The BCR (European Communities Bureau of Reference) sequential extraction procedure and Hakanson's potential ecological risk index method were used to assess the morphological features of the spent acrylonitrile catalyst and the potential ecological risks of heavy metals, respectively. The spent acrylonitrile catalyst contained the heavy metals Ni, Cu, Zn, Cr, Pb, As and Hg, and the contents of Ni were more than 7.2%. Using the sulfuric acid and nitric acid leaching method, leaching toxicity analysis showed that the Ni and As concentrations exceeded the leaching toxicity identification standard by more than 10 times and that the Hg concentration exceeded the standard value by 5 times. These results indicate that spent acrylonitrile catalyst should be identified as hazardous waste. The BCR analysis illustrated that the heavy metals in the spent catalyst primarily (more than 85%) existed in oxidizable form or reducible form and that the contents of the acid exchangeable form were commonly higher than those of the residual form. Therefore, we predict that the heavy metals in spent acrylonitrile catalyst have a high probability of leaching and considerable environmental availability. According to the potential ecological risk index values, the order of potential ecological risk for the individual heavy metals was As>Ni>Hg>Cr>Cu>Zn, and the general potential ecological risks were 382.43 and 382.07 in the two samples, which indicates severe potential ecological risk.

KEYWORDS:
Spent acrylonitrile catalyst; heavy metals; BCR sequential extraction; leaching toxicity analysis; ecological risk assessment

INTRODUCTION

Acrylonitrile is an important chemical raw material used mainly for the synthesis of polyacrylonitrile fiber, ABS/SAN resin, adiponitrile, acrylamide, and carbon fiber. In 2013, the world acrylonitrile yield was approximately 5.55 million tons[1], and the Merchant Research & Consulting Company predicted that global acrylonitrile production would reach 7 million tons in 2017. Almost all of the acrylonitrile production processes in the world presently involve propylene ammonia oxidation because of its advantages such as cheap raw material, low production cost, and simple production processes. The catalyst is the core of this method, and approximately 90% of propylene ammonia oxidation processes use a Mo catalyst [2,3]. A large number of acrylonitrile catalysts are scrapped every year that often contain poisonous elements such as Ni (the active catalyst component) and other poisonous elements such as As, Pb, Cr, and Hg[4]. These elements may come from raw materials, reagents, equipment materials, and other components used in the actual production process.

In many of the developing countries, spent catalysts are dumped in open areas as solid wastes regardless of any eco-sanitary concern[5]. Landfill is one of the most important anthropogenic sources of trace as well as heavy metals [6]. Spent acrylonitrile catalyst poses a direct risk of exposure to the natural environment: the poisonous and harmful components may be leached out by rain[7, 8] or garbage leachate[9] and subsequently pollute soil and water[10]. Therefore, it presents a potential ecological risk under inappropriate treatment or disposal conditions.

Recently, an increasing number of researches [11-16] on the exposure pathways, transportation and transformation behavior and risk assessment of heavy metals in different solid wastes were on the account of frequent incidents of heavy metals contamination. It is of great suspicion that spent acrylonitrile catalysts were hazardous wastes, and the hazardous waste identification and risk assessment are of great significance. The aims of this work were to determine the contents and morphological features of heavy metals in spent acrylonitrile catalysts, to identify the leaching toxicity characteristics, and to assess the potential ecological risk.

MATERIALS AND METHODS

CHEMICALS AND REAGENTS

The two spent catalyst samples used in this study were obtained from a petrochemical corporation in northeastern China. The samples had been generated in different periods of the propylene-ammoxidation process. All of the chemicals and reagents used in the analyses were produced by the Shanghai Lingfeng Chemical Reagent Co., Ltd. Standards for H_2SO_4, HNO_3, HCl, and CH_3COOH were guaranteed reagent and standards for CH_3COONH_4, H_2O_2, and $HONH_3Cl$ were analytical pure.

APPARATUS

The main apparatus used in this study are shown in Table 1.

TABLE 1
Location map of the study area.

apparatus	model	manufacturer
Energy Dispersal X-ray Spectroscopy	Falion 60S	EDAX, Inc.
Inductively Coupled Plasma Atomic Emission Spectrometry	Agilent 725ES	Agilent Technologies Inc.
Microwave Extraction Apparatus	ETHOS A	Shenzhen Kwachung Technologies Co., Ltd.
Table-top, Large Capacity, Low Speed Centrifuge	RJ-TDL-40B	Shanghai Baidiantech Instrument Co., Ltd.
Automated Surface Area and Pore Size Analyzer	TriStar Ⅱ 30	Micromeritics Instrument Co., Ltd.
Gas Bath Thermostatic Oscillator	THZ-82	Jintan Jincheng Guosheng instrument plant

SAMPLE CHARACTERISTICS

The BET specific surface area of Sample 1 was 35.24 m^2/g, and the average particle size was 170.26 nm, whereas the corresponding data for Sample 2 were 36.32 m^2/g and 165.21 nm. The analysis results of EDS (energy dispersal x-ray spectroscopy) and XRD (X-ray diffraction) are presented in Table 2 and Fig. 1, respectively. XRD patterns were analyzed by identification and quantification software (Jade 6.0). The existence of heavy metals in the samples was determined through the PDF card index method using the card PDF-2004. Combined with the data provided in Table 2 and Fig. 1, this method revealed that the main metal elements of the two samples were Mo, Ni and Fe and that the samples were typical Mo catalysts for propylene ammoxidation to acrylonitrile.

TABLE 2
Results of the EDS analysis (mass fraction, %).

element	C	O	Mg	Si	Mo	Fe	Ni
Sample 1	2.35	34.39	0.87	30.72	20.18	2.86	8.64
Sample 2	3.40	33.53	1.01	30.18	20.13	2.99	9.38

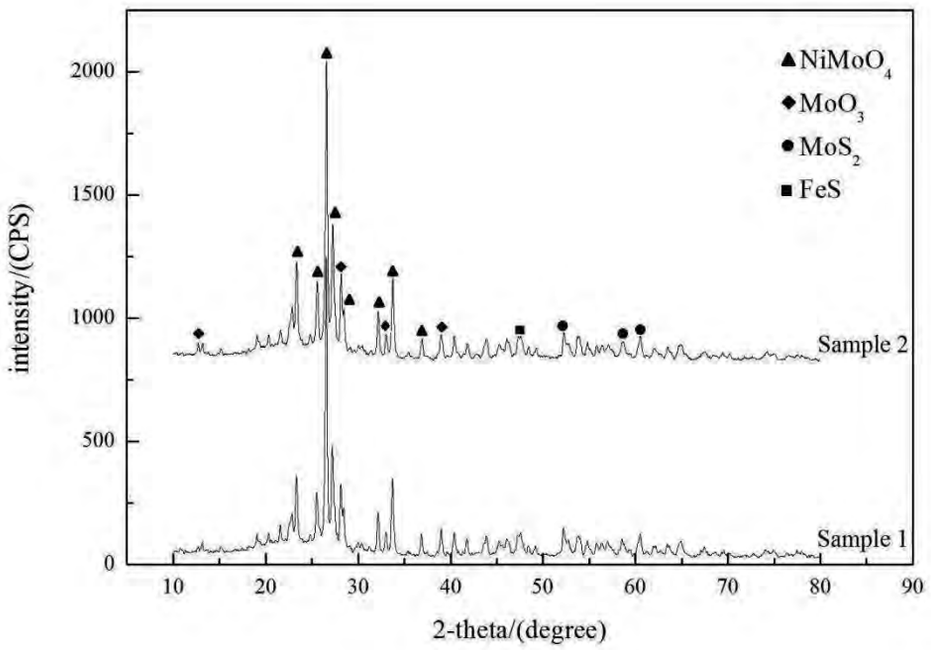

FIGURE 1
XRD patterns of two spent acrylonitrile catalyst samples

ANALYTICAL METHODS

Heavy metals in the aqueous phase were measured by inductively coupled plasma atomic emission spectroscopy (ICP-AES). Each analysis was conducted three times, and the final result was the average of the three testing values, and blank analyses were carried out during the entire procedure.

Heavy metal content test. A total of 8 mL of sulfuric acid and 2 mL of hydrochloric acid were added to 0.2000-0.3000 g of spent acrylonitrile catalyst in a digestion tank, and the digestion tank was placed into a microwave extraction apparatus. The temperature procedure was set as follows: heat to 175°C over 20 min, maintain at this temperature for 30 min, and then cool to room temperature. After cooling, the liquors in the digestion tank were transferred to a 50 mL colorimetric tube, diluted with deionized water to volume and stored at 4°C for analysis.

Leaching toxicity analysis. During disposal, the heavy metals in the spent acrylonitrile catalyst may be leached out, potentially migrating into the environment, transforming and subsequently polluting the environment; therefore, leaching toxicity analysis is necessary. Two situations were simulated in this study. Situation 1: The spent acrylonitrile catalysts were buried in non-standard industrial solid-waste landfill sites. Situation 2: The spent acrylonitrile catalysts were buried in sanitary landfills in which 15% of the industrial waste was merged with 85% of municipal garbage.

In Situation 1, the leach liquor could be rain, surface water or groundwater. Rain is the most common source of leach liquor, and there is greater potential for heavy metals to be leached out under acid rain conditions. Procedures were therefore conducted according to the standard (Solid waste. Extraction procedure for leaching toxicity. Sulphuric acid & nitric acid method. HJ/T 299-2007) to simulate Situation 1. In Situation 2, the leach liquor was primarily landfill leachate, and acetic acid is a typical low molecular weight organic acid in landfill leachate [17, 18]. Therefore, procedures were conducted according to the standard (Solid waste. Extraction procedure for leaching toxicity. Acetic acid buffer solution method. HJ/T 300-2007) to simulate Situation 2.

Sequential extraction procedure. A three-step extraction procedure was used to analyze the effective combination forms of heavy metals in the spent acrylonitrile catalyst. This procedure was first proposed by the Community Bureau Reference and is known as BCR [12, 19].

Step 1: Twenty milliliters of acetic acid (0.11 mol/L) was added to 0.5000 g of spent acrylonitrile catalyst in a 50 mL centrifuge tube. The centrifuge tube was shaken in an oscillator at 25°C for 16 h; during the oscillation process, the sample was maintained in a state of

suspension. The extract was separated from the solid residue by centrifuging (5000 r/min) for 30 min, decanted into a polyethylene container and stored at 4°C for analysis. The residue was washed with 10 mL of distilled water by shaking for 60 min and then centrifuged, and the washings were discarded.

Step 2：The residue from Step 1 was slurried with 20 mL of hydroxyammonium chloride (0.1 mol/L), adjusted to pH 2 with nitric acid), transferred quantitatively back to the centrifuge tube and shaken in the centrifuge tube artificially to fully scatter the sample. The extraction procedure was then performed as in Step 1.

Step 3: Five milliliters of hydrogen peroxide (8.8 mol/L, adjusted to pH 2 with nitric acid) was added to the residue from Step 2. The centrifuge tube was covered with a tube cap, and the contents were digested at room temperature for 1 h with manual shaking (once every 15 minutes). Digestion was continued by heating the tube to 85°C in a water bath for 2 h. The tube cap was removed, and the tube contents were evaporated to a small volume (1±0.5 mL). A second addition of 5 mL of hydrogen peroxide (8.8 mol/L, adjusted to pH 2 with nitric acid) was added, and the digestion procedure was repeated. Twenty-five milliliters of ammonium acetate (1.0 mol/L, adjusted to pH 2 with nitric acid) was then added to the centrifuge tube. The extraction procedure was then performed as in Step 1.

Step 4: The solid residue was retained for microwave digestion and analyzed by ICP-AES.

POTENTIAL ECOLOGICAL RISK INDEX METHOD

The potential ecological risk index method[20, 21] proposed by the Swedish scientist Hakanson is one of the most common methods used to evaluate heavy metal pollution[22, 23]. The contamination factor (F_i) of a single heavy metal was used to evaluate the pollution level of the single heavy metal in the spent acrylonitrile catalyst samples. The formula for the calculation of F_i is as follows:

$F_i=C_i/C_e$ (1)

Where F_i is the contamination factor for a single heavy metal, C_i is the measured value of the heavy metal in the samples, and C_e is the parameter for calculation with reference to the Grade III standard of environmental quality for soil (National Quality Standard for Soil Environment GB15618-2008) (Table 3). The potential ecological risk factor and the potential toxicity response index of elements were estimated as proposed by Hakanson[24-26] (Table 4).

The potential ecological risk factor (E_i) of a single heavy metal is calculated by the following formula:

$E_i= T_i \cdot F_i$ (2)

where T_i is the Hakanson toxicity coefficient of heavy metals for a given heavy metal. The formula of the potential toxicity index is as follows:

$R=\sum E_i$ (3)

The assessment results of all of the evaluation criteria of the potential ecological risk of metals are presented in Table 5.

TABLE 3
Grade III standard of environmental quality for soil (mg/kg)

element	Ni	Cu	Zn	Cr	Pb	As	Hg
standard value	200	400	500	300	400	40	1.5

TABLE 4
Hakanson toxicity coefficients of heavy metals

element	Ni	Cu	Zn	Cr	Pb	As	Hg
toxicity coefficient	5	5	1	2	5	10	40

TABLE 5
Grading standards of potential ecological risk of heavy metals

scope of potential ecological risk index (E_i)	ecological risk of single-factor pollution	scope of potential toxicity index (R)	general level of potential ecological risk
E_i <40	Low	R<150	Low grade
40≤E_i<80	Moderate	150≤R<300	Moderate
80≤E_i<160	Higher	300≤R<600	Severe
160≤E_i<320	High	600≤R	Serious
320≤E_i	Serious		

RESULTS AND DISCUSSION

CONTENTS OF HEAVY METALS

The contents of heavy metals in the two spent acrylonitrile catalyst samples analyzed by ICP-AES are summarized in Table 6. Ni, As, Pb, Cr, Cu, Zn and Hg were the elements detected in the two samples. The content of Ni was greater than 7.2%, which was the highest content recorded. The contents of As and Pb were also high; Cd was undetected. The components and contents of heavy metals were similar between the two samples, and the total contents of heavy metals were 7.36% and 7.55%. The two spent acrylonitrile catalysts had similar heavy metal components and contents and were constant under the same production process. Due to the generally high contents of heavy metals, the environmental risks of spent acrylonitrile catalyst should not be ignored.

TABLE 6
Contents of heavy metals in spent acrylonitrile catalyst (mass fraction, %)

element	Ni	Cu	Zn	Cr	Pb	Cd	As	Hg	total amount
Sample 1	7.2320	0.0010	0.0010	0.0016	0.0104	nd	0.1104	0.0002	7.3566
Sample 2	7.4174	0.0010	0.0012	0.0014	0.0130	nd	0.1160	0.0002	7.5502

LEACHING TOXICITY ANALYSIS

The results of the leaching toxicity analysis are shown in Table 7. There was a large difference in the leaching rates of heavy metals between the two different leaching methods. The leaching rates were generally higher using the sulfuric acid and nitric acid method, which indicates that the spent acrylonitrile catalyst presented higher toxicity and environmental risk in Situation 1. Using the sulfuric and nitric acid leaching method, the concentrations of Ni and As exceeded the leaching toxicity identification standard by more than 10 times, and the concentration of Hg exceeded the standard by 5 times. Considering As as an example, the concentration of As exceeded the leaching toxicity identification standard by more than 10 times using the sulfuric and nitric acid leaching method, but the concentration was lower than the toxicity identification standard using the acetic acid buffer solution method. We therefore conclude that As poses a greater environmental risk in Situation 1. In conclusion, spent acrylonitrile catalyst can be considered a hazardous waste based on its leaching toxicity characteristics according to the Identification Standard for Extraction Procedure Toxicity of Solid Waste (GB5085.3-2007), and we recommend that it be included in the National Hazardous Waste List of China.

TABLE 7
Leaching toxicity of spent acrylonitrile catalyst

element		Ni	Cu	Zn	Cr	Pb	As	Hg
identification standards for hazardous waste (mg/L)		5	100	100	5 (Cr^{6+})	5	5	0.1
Sample 1	sulfuric acid and nitric acid method (mg/L)	75	<0.050	0.40	0.11	1.2	53	0.51
	Leaching rate (%)	0.21%	nd	8.00%	1.38%	2.31%	9.60%	51.00%
	acetic acid buffer solution method (mg/L)	8.0	<0.050	0.27	<0.050	<0.050	3.2	0.50
	Leaching rate (%)	0.02%	nd	5.40%	nd	nd	0.58%	50.00%
Sample 2	sulfuric acid and nitric acid method (mg/L)	58	<0.050	0.5	0.09	1.3	55	0.50
	Leaching rate (%)	0.16%	nd	8.33%	1.29%	2.00%	9.48%	50.00%
	acetic acid buffer solution method (mg/L)	6.9	<0.050	0.39	<0.050	<0.050	3.3	0.48
	Leaching rate (%)	0.02%	nd	6.50%	nd	nd	0.57%	48.00%

Note: The underlined data exceed the identification standards for hazardous waste.

MORPHOLOGICAL FEATURES ANALYSIS

The results obtained by the BCR three-step sequential extraction procedure are shown in Table 8，Fig. 2 and Fig. 3. In general, most of the heavy metals (greater than 85% of the total) in the spent acrylonitrile catalyst existed in oxidizable form or reducible form, and the contents of the acid exchangeable form were commonly greater than those of the residual form. The high contents of the acid exchangeable form indicate that the heavy metals are highly susceptible to leaching and that their environmental availability is high. The results for S1 (the acid exchangeable form) show that the concentrations of As, Cr and Zn are higher in the acid exchangeable form than in the other states, which indicates that the exchangeable fractions of these metals can be easily distributed in the environment. The residual form fraction of Pb was the highest residual form fraction recorded (more than 42%), indicating that Pb was inactive and presented less environmental risk than the other heavy metals.

TABLE 8
Morphological features of heavy metals in spent acrylonitrile catalyst (mg/kg).

sample	state	Ni	Cu	Zn	Cr	Pb	As	Hg	total amount
1	S1	7000	2.10	4.20	5.80	nd	700.00	1.20	7713.30
	S2	27200	2.48	2.88	2.40	0.26	208.00	2.64	27418.66
	S3	36056	4.30	3.50	4.28	74.63	132.86	0.16	36275.85
	S4	3041	1.12	0.00	2.55	55.04	73.08	0.00	3172.92
2	S1	6600	2.10	4.50	4.70	nd	750.00	1.12	7362.42
	S2	25600	2.48	2.88	2.40	0.28	224.00	2.64	25834.68
	S3	39081	4.41	4.62	4.56	70.62	108.28	0.24	39273.95
	S4	2893	1.01	0.00	2.34	59.10	77.72	0.00	3032.95

Notes: S1: Acid exchangeable form; S2: Oxidizable form; S3: Reducible form; S4: Residual form

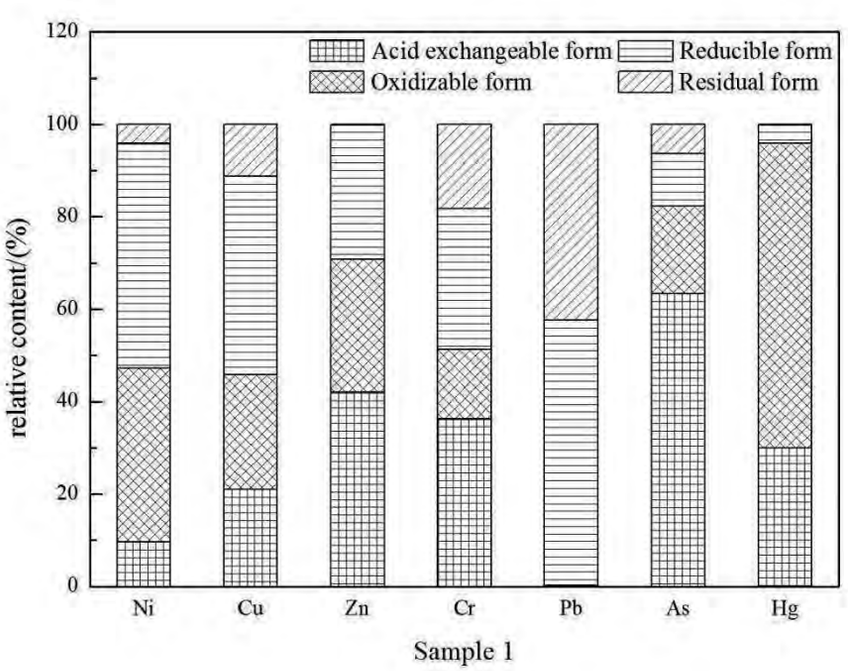

FIGURE 2
Speciation content of heavy metals in Sample 1 based on the BCR procedure

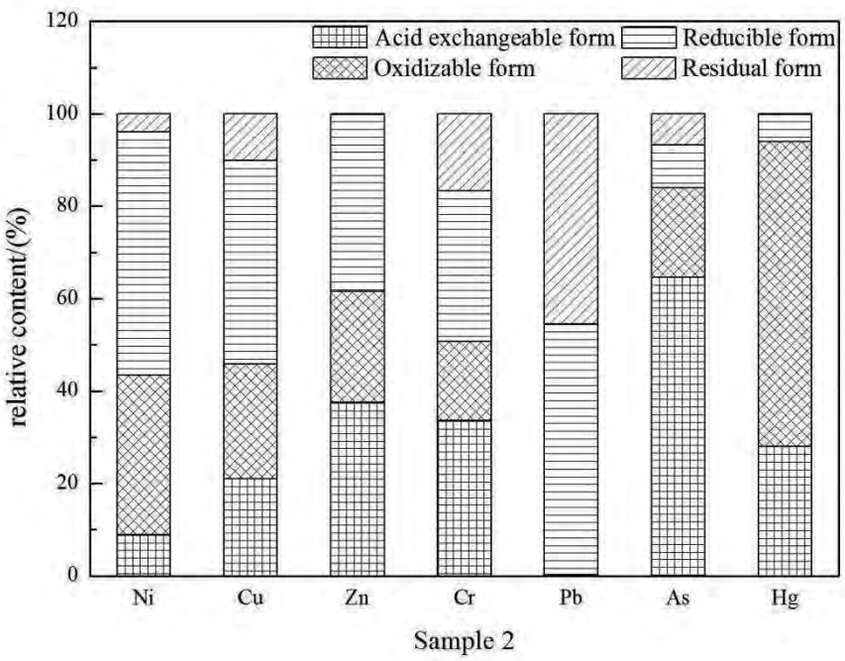

FIGURE 3.
Speciation content of heavy metals in Sample 2 based on the BCR procedure

POTENTIAL ECOLOGICAL RISK ASSESSMENT RESULTS

To assess the potential ecological risk of heavy metals in the spent acrylonitrile catalyst samples, the results of the acid exchangeable form (S1) of the heavy metals were selected to calculate C_i because other researchers have confirmed that the exchangeable form is the direct phase polluting the environment. The potential ecological risk assessment of the heavy metals in the two samples is shown in Table 9.

TABLE 9.
Potential ecological risk assessment results of heavy metals in spent acrylonitrile catalyst

sample	potential ecological risk index values for heavy metals (E_i)						general potential ecological risk (R)	
	Ni	Cu	Zn	Cr	As	Hg	Value	Grade
1	165.00	0.03	0.01	0.03	187.50	29.87	382.43	Severe
2	175.00	0.03	0.01	0.04	175.00	32.00	382.07	Severe

As shown in Table 9, the heavy metal with the highest single potential ecological risk (E_i) was As, with values of 187.50 and 175.00 in the two samples. The values for Ni were 165.00 and 175.00. The potential ecological risk index values for As and Ni were high, whereas the values for Cu, Zn, Cr, and Hg were low, indicating low potential ecological risk for the latter heavy metals. The exchangeable form fraction (S1) of Pb in the samples was very low and below the detection limit; therefore, Pb is not presented in Table 9 and may be classified as no risk. The order of potential ecological risk index values for the heavy metals was As＞Ni＞Hg＞Cr＞Cu＞Zn. The general potential ecological risk, as measured by the potential toxicity index (R), was 382.43 and 382.07 in the two samples, indicating that the spent acrylonitrile catalyst poses severe potential ecological risk. In summary, the heavy metals posing the greatest ecological risk in spent acrylonitrile catalyst are As, Ni and Hg, and because the general ecological risk is severe,

treatment must be carried out before disposal of this material.

CONCLUSIONS

(1) The two spent acrylonitrile catalyst samples contained heavy metals (Ni, Cu, Zn, Cr, Pb, As and Hg). The content of Ni was greater than 7.2%, and the concentrations of Ni, As and Hg exceeded the leaching toxicity identification standard using the sulfuric acid and nitric acid leaching toxicity method according to the identification standard for hazardous wastes. Therefore, the spent acrylonitrile catalyst can be identified as hazardous waste and should be added to the National Hazardous Waste List of China.

(2) Most of the heavy metals in the two spent acrylonitrile catalyst samples existed in either oxidizable form or reducible form (more than 85%), and the contents of the acid exchangeable form were commonly higher than the residual form. The acid exchangeable form fractions were higher than the other fractions for As, Cr and Zn, which indicates that the exchangeable fractions of these metals can be easily distributed in the environment. The environmental availability of heavy metals in spent acrylonitrile catalyst was high, indicating a high potential for leaching.

(3) According to Hakanson's potential ecological risk index method, the potential ecological risk index values for single heavy metals decreased in the order As＞Ni＞Hg＞Cr＞Cu＞Zn. As and Ni pose severe potential ecological risk to the environment, and the general level of potential ecological risk of the two samples was "Severe". Considering these results, treatment of this material must be carried out before disposal.

ACKNOWLEDGMENTS

This study was financially supported by the Grant from the National Environmental Protection Public Welfare Science and Technology Research Program of China (No. 201309021), and the National Natural Science Foundation of China (NSFC) (No. 21307032). Any opinions, findings, conclusions, or recommendations expressed in this publication are those of the authors and do not necessarily reflect the view of the supporting organizations.

REFERENCES

[1] Ware A L, Glass L, Crocker N, Deweese B N, Coles C D, Kable J A, May P A, Kalberg W O, Sowell E R, Jones K L, Riley E P, Mattson S N, Cifasd. (2014) Effects of Prenatal Alcohol Exposure and Attention- Deficit/Hyperactivity Disorder on Adaptive Functioning. Alcoholism-Clinical and Experimental Research 38, 1439-1447.

[2] Schuh K, Kleist W, Hoj M, Trouillet V, Beato P, Jensen A D, Patzke G R, Grunwaldt J D. (2014) Selective oxidation of propylene to acrolein by hydrothermally synthesized bismuth molybdates. Applied Catalysis a-General 482, 145-156.

[3] Simmons D D, Lohr R, Wotring H, Burton M D, Hooper R A, Baird R A. (2014)Recovery of otoacoustic emissions after high-level noise exposure in the American bullfrog. Journal of Experimental Biology 217, 1626-1636.

[4] Lai Y C, Lee W J, Huang K L, Wu C M. (2008) Metal recovery from spent hydrodesulfurization catalysts using a combined acid-leaching and electrolysis process. Journal of Hazardous Materials 154, 588-594.

[5] Vasanthi P, Kaliappan S, Srinivasaraghavan R. (2008) Impact of poor solid waste management on ground water. Environmental Monitoring and Assessment 143, 227-238.

[6] Sayadi M H, Sayyed M R G. (2011) Comparative assessment of baseline concentration of the heavy metals in the soils of Tehran (Iran) with the comprisable reference data. Environmental Earth Sciences 63, 1179-1188.

[7] Du Y J, Wei M L, Reddy K R, Liu Z P, Jin F. (2014) Effect of acid rain pH on leaching behavior of cement stabilized lead-contaminated soil. Journal of Hazardous Materials 271, 131-140.

[8] Du Y J, Jiang N J, Shen S L, Jin F. (2012) Experimental investigation of influence of acid rain on leaching and hydraulic characteristics of cement-based solidified/stabilized lead contaminated clay. Journal of Hazardous Materials 225, 195-201.

[9] Galeano L A, Vicente M A, Gil A. (2011) Treatment of municipal leachate of landfill by Fenton-like heterogeneous catalytic wet peroxide oxidation using an Al/Fe-pillared montmorillonite as active catalyst. Chemical Engineering Journal 178, 146-153.

[10] Yang C, Lv X X, Tian X K, Wang Y X, Komarneni S. (2014) An investigation on the use of electrolytic manganese residue as filler in sulfur concrete. Construction and Building Materials 73, 305-310.

[11] Min X B, Xie X D, Chai L Y, Liang Y J, Li M, Ke Y. (2013) Environmental availability and ecological risk assessment of heavy metals in zinc leaching residue. Transactions of Nonferrous Metals Society of China 23, 208-218.

[12] Kerolli-Mustafa M, Fajkovic H, Roncevic S, Curkovic L. (2015) Assessment of metal risks from different depths of jarosite tailing waste of Trepca Zinc Industry, Kosovo based on BCR procedure. Journal of Geochemical Exploration 148, 161-168.
[13] Mari M, Nadal M, Schuhmacher M, Domingo J L. (2009) Exposure to heavy metals and PCDD/Fs by the population living in the vicinity of a hazardous waste landfill in Catalonia, Spain: Health risk assessment. Environment International 35, 1034-1039.
[14] Dou X S. (2015) Food Waste Generation and Its Recycling Recovery: China's governance mode and Its assessment. Fresenius Environmental Bulletin 24, 1474-1482.
[15] Gu H N, Wang N. (2013) Leaching of uranium and thorium from red mud using sequential extraction methods. Fresenius Environmental Bulletin 22, 2763-2769.
[16] Zhang Z, Zou Q, Xiang L, Lin N, Gao P, Zhan P, Feng Y, Ren N. (2014) Aerobic biodegradation kinetics of 17-beta-estradiol in activated sludge: influence factors and metabolic products prediction. Fresenius Environmental Bulletin 23, 2440-2449.
[17] Bu L, Wang K, Zhao Q L, Wei L L, Zhang J, Yang J C. (2010) Characterization of dissolved organic matter during landfill leachate treatment by sequencing batch reactor, aeration corrosive cell-Fenton, and granular activated carbon in series. Journal of Hazardous Materials 179, 1096-1105.
[18] Moravia W G, Amaral M C S, Lange L C. (2013) Evaluation of landfill leachate treatment by advanced oxidative process by Fenton's reagent combined with membrane separation system. Waste Management 33, 89-101.
[19] Huang Z Y, Xie H, Cao Y L, Cai C, Zhang Z. (2014) Assessing of distribution, mobility and bioavailability of exogenous Pb in agricultural soils using isotopic labeling method coupled with BCR approach. Journal of Hazardous Materials 266, 182-188.
[20] Kulikowska D, Gusiatin Z M. (2015) Sewage sludge composting in a two-stage system: Carbon and nitrogen transformations and potential ecological risk assessment. Waste Management 38, 312-320.
[21] Islam M S, Ahmed M K, Habibullah-Al-Mamun M, Masunaga S. (2015) Potential ecological risk of hazardous elements in different land-use urban soils of Bangladesh. Science of the Total Environment 512, 94-102.
[22] Saeedi M, Salmanzadeh M, Jamshidi-Zanjani A, Li L Y. (2014) Response to the comments of Zhang et al. (2014) on "Heavy metals and polycyclic aromatic hydrocarbons: Pollution and ecological risk assessment in street dust of Tehran". Journal of Hazardous Materials 279, 389-391.
[23] Li R D, Li Y L, Yang T H, Wang L, Wang W Y. (2015) A new integrated evaluation method of heavy metals pollution control during melting and sintering of MSWI fly ash. Journal of Hazardous Materials 289, 197-203.
[24] Jiang X, Lu W X, Zhao H Q, Yang Q C, Yang Z P. (2014) Potential ecological risk assessment and prediction of soil heavy-metal pollution around coal gangue dump. Natural Hazards and Earth System Sciences 14, 1599-1610.
[25] Fu C, Guo J S, Pan J, Qi J S, Zhou W S. (2009) Potential Ecological Risk Assessment of Heavy Metal Pollution in Sediments of the Yangtze River Within the Wanzhou Section, China. Biological Trace Element Research 129, 270-277.
[26] Huang X F, Hu J W, Li C X, Deng J J, Long J, Qin F X. (2009) Heavy-metal pollution and potential ecological risk assessment of sediments from Baihua Lake, Guizhou, PR China. International Journal of Environmental Health Research 19, 405-419.

Received: **13.07.2015**
Accepted: **17.12.2015**

CORRESPONDING AUTHOR

Zhaofu Qiu
East China University of Science and Technology
State Environmental Protection Key Laboratory of Environmental Risk Assessment and Control on Chemical Process
Shanghai 200237 – CHINA

e-mail: zfqiu@ecust.edu.cn

by PSP Volume 25 – No. 1/ 2016, pages 183-190 Fresenius Environmental Bulletin

BUFFER ZONE ASSESSMENT FOR AQUATIC ORGANISMS OF PESTICIDE APPLICATION AGAINST RED SPIDER MITES (*Tetranychus cinnabarinus* B.) IN COTTON

Nigar Yarpuz-Bozdogan

University of Cukurova, Vocational School of Technical Sciences, Misis Adana, Turkey

ABSTRACT

In cotton cultivation, insecticide a.i. against red spider mite (*Tetranychus cinnabarinus* (Biosduval)) has approximately applied as 3,211.6 kg. For this kind of an insect control, in 2013, five active ingredients were used in cotton cultivation in Adana, Turkey. These active ingredients included abamectin, etoxazole, hexythiazox, propargite and spiromesifen. The objective of this research was to determine a buffer zone for the recommended dose by manufacturer (RD) and applied dose by farmers (FD) according to aquatic organisms in cotton cultivation. In this research, all a.i., risk index (RI) values were assessed according to distance (Z) between nozzle and downwind field for Dutch Drift Model (DDM), and field border and downwind field for German Drift Model (GDM). Buffer zones ($Z_{RI=1}$) for all a.i. were calculated by developed equations via RI values at different distances. Buffer zone was found as ≥ 18 m for abamectin and ≥ 16 m for propargite in RD. It was determined as ≥ 27 m for abamectin and ≥ 25 m for propargite in FD. Buffer zone was assessed as ≥ 3 m for etoxazole and ≥ 4 m for spiromesifen in RD. It was calculated as ≥ 4 m for etoxazole and ≥ 5 m for spiromesifen in FD. In this study, buffer zones for FD were determined to be wider than RD's in two models.

KEYWORDS:
Buffer zone; Environment; Aquatic organisms; Cotton; Red spider.

INTRODUCTION

Cotton is cultivated on an area of over 30 million hectares and cotton production is over 25 million tonnes around the world [1]. In Turkey, cotton is mainly produced in the Mediterranean Region, Aegean Region and Southeast Anatolian Region. Located in the south of Turkey, Adana province is in Mediterranean Region and has approximately 540 000 ha agricultural land. In 2012, the harvested area of cotton was 45 584 ha in Adana out of overall 488 496 ha in Turkey [2]. In Adana, cotton production in 2012 was 327 556 tonnes out of overall 2 320 006 tonnes in Turkey. This value equals to 14.1% of cotton production in Turkey [3]. In cotton cultivation, there are insects such as thrips, aphids, cotton bollworm, spider mites, plant bugs, whiteflies and stinkbugs. In Turkey, two species of red spider mites are harmful in cotton cultivation: *Tetranychus cinnabarinus*, damages in Mediterranean Region, and *Tetranychus urticae*, insect in Aegean Region and Southeast Anatolia Region. In winter, red spider mites live on weeds in the field and orchard border, and bushes near cotton fields. When climate starts to warm and cotton seeds germinate in spring, red spider mites settle into cotton fields. In Turkey, population of red spider mites reaches to maximum level in August. In Adana, pesticides are applied against red spider mites from beginning of May to mid-September according to weather conditions and pest population [4].

In Turkey, in 2010, pesticides a.i. were used approximately as 23000 tonnes in agriculture [5]. In 2010, pesticides a.i. were used approximately by 35.14% for insecticides in pesticide applications [5]. In 2013, to control the red spider mites, five a.i. were used in a 22 700 ha cotton cultivation area in Adana. These a.i. included abamectin, etoxazole, hexythiazox, propargite and spiromesifen. Information about these a.i. were given as below and in Figure 1 [6-8].

Abamectin ($C_{49}H_{74}O_{14}$) is a natural fermentation product of this bacterium and acts as a selective acaricide and insecticide for use in ornamentals (Figure 1a). Etoxazole ($C_{21}H_{23}F_2NO_2$) (Figure 1b) and spiromesifen ($C_{23}H_{30}O_4$) (Figure 1c) are insecticides. Hexythiazox ($C_{17}H_{21}ClN_2O_2S$) (Figure 1d) and propargite ($C_{19}H_{26}O_4S$) (Figure 1e) are acaricides.

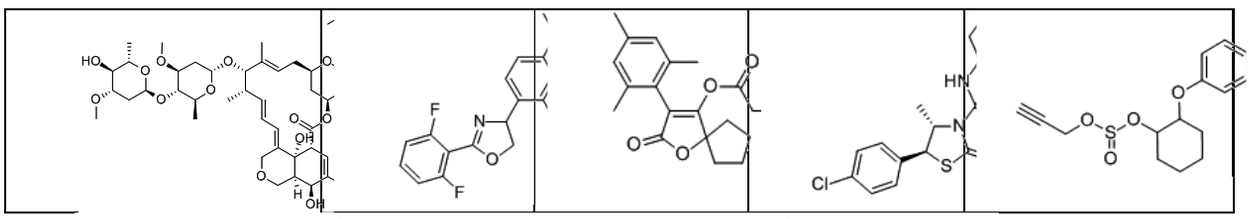

FIGURE 1.
Chemical formulation of active ingredients [6]

In cotton cultivation, in 2013, farmers applied the above shown pesticide a.i. for improving yield and quality of cotton against red spider mites in Adana. Yet, farmers generally apply overdose pesticides instead of the recommended dose (RD) on the product label. Yassin et al. (2002) determined that 43% of the farmers in Gaza Strip applied more than the recommended dose, and 91.3% had toxicity symptoms among these farmers [9]. In addition, Damalas et al. (2006) found that 46.2% of the farmers often apply more doses than the recommended doses [10]. Demircan and Yılmaz (2005) determined that farmers applied 5.71%-186.00% for fungicides, 14.71%-116.67% for insecticides, and 12.00%-105.26% for acaricides more than the recommended dose (RD) in apple production in Isparta province, Turkey [11]. Moreover, Zeren et al. (1996) observed that only 15% of the farmers apply pesticides according to the recommended dose (RD) on the product label in Içel province, Turkey [12].

In pesticide applications, pesticides are harmful for non-target organisms such as human, aquatic organisms, bees, earthworms, soil, groundwater, etc. [13-16]. Pesticide drift depends on meteorological conditions, application equipment and methods, physical properties of pesticide etc. [17-21]. Therefore, pesticide applications have negative effects on human and environment. Yılmaz et al. (2003) detected pesticide in Seyhan and Ceyhan River, Adana. Pesticides that are named as bromacil, chlorpyrifos, dicofol and tetradifon a.i. were determined in these river samples with varying concentrations (0.23-7.14 $\mu g\ l^{-1}$) [22]. Pesticide pollution cannot be eliminated, yet can be minimized. There is a way to minimize the pesticide pollution on aquatic organisms: a buffer zone. Buffer zone is defined as the distance between spray equipment or target field border and sensitive organisms off field. Buffer zone should be used to protect the environment against the negative effects of pesticides [23, 24]. Snoo and Witt (1998) suggested that buffer zones could be well adopted in agricultural practices [25]. Carluer et al. (2011) described that buffer zones can reflect beneficial tools limiting pesticides transferred towards surface water [26]. Syversen and Bechmann (2004) found that drift of pesticides from field to surface waters can induce environmental damage to aquatic organisms and fish. Vegetated buffer zones between surface waters and agricultural field have been proven as effective filters for sediments and sediment bound nutrients. Buffer zone can also be effective filters for pesticides and particles [27]. Buffer zone should be used to protect the environment against the negative effects of pesticides. Payne et al. (1988) informed that buffer zone was guessed by choosing an acceptably low mortality and determining the downwind distance at which this value was obtained [28]. Davis and Williams (1990) reported that buffer zones should be placed according to the downwind of the sprayed areas by estimating the distance at which bees would encounter an LD_{50} dose from spray drift. They assessed that for ground spraying at low wind speeds ($\leq$ 3 m/s) this zone of risk is up to 5 m for the great majority of compounds [29].

The Dutch (DDM) and German Drift Model (GDM) help researchers predict the pesticide drift at certain distances in the downwind field [30-32].

The objective of this study was to assess the buffer zone for the recommended dose by manufacturer (RD) and applied dose by farmers (FD) according to DDM and GDM for aquatic organisms in pesticide application against red spider mites in cotton cultivation, in Adana, Turkey.

MATERIAL AND METHODS

In this research, abamectin, etoxazole, hexythiazox, propargite, and spiromesifen were used for red spider mites control in cotton cultivation in Adana, Turkey, in 2013. Firstly, risk index (RI) values were determined for aquatic organisms according to DDM and GDM, and then buffer zones were calculated for RD and FD in DDM and GDM.

Determination of the Risk Index (RI). RI values for aquatic organisms were calculated by Equation 1 [31, 33].

$$RI_{aquatic\ organisms} = \frac{\left(\frac{D.\%drift.n}{d_{ditch}.1000}\right)}{\min(NORM_w)} \quad \text{(Eq.1)}$$

D: the applied dose of a.i. (mg m^{-2});

%drift: drift deposition of a.i. at a point downwind the field (in %);

n: the number of applied doses;

d_{ditch}: the depth of the ditch (m) and

$\min(NORM_w)$: toxicological reference on aquatic organisms (mg l^{-1}).

%drift was calculated by Equation 2 for DDM, and Equation 3 for GDM [31].

$$\%drift = A_0 e^{-z.A_1} + B_0 e^{-z.B_1} \quad \text{(Eq.2)}$$

z is the distance between the last spray nozzle and a point downwind the field (m) and A_0, B_0, A_1 and B_1 are coefficients that depend on crop [31]. In DDM, there are six categories: bare soil, sugar beets, potatoes, cereals, leaf and leafless fruit trees. In this research, cotton was taken into account as a potato category. For this reason, coefficients were taken as 114 for A_0, 1.74 for A_1, 1.29 for B_0, and 0.139 for B_1 [31].

$$\%drift = A.z^B \quad \text{(Eq.3)}$$

z is the distance between the field border and a point downwind the field (m) and, A and B are coefficients [31]. There are three categories in GDM. These are early fruit application, late fruit application and field crops. In this study, cotton was taken as field crops. Therefore, coefficients were taken as 2.7593 for A, and -0.9778 for B in GDM[31].

In this research, $\min(NORM_w)$ was calculated as toxicological reference by Equation 4 and 5 [31]. Daphnia had the lowest $\min(NORM_w)$, and was used as the toxicological reference for abamectin, etoxazole, hexythiazox, and propargite a.i. (Eq. 4). Fish was used for spiromesifen a.i. because of having the lowest $\min(NORM_w)$ (Eq. 5).

$$\min(NORM_w)\ for\ Daphnia = \frac{EC_{50}}{100} \quad \text{(Eq.4)}$$

$$\min(NORM_w)\ for\ Fish = \frac{LC_{50}}{100} \quad \text{(Eq.5)}$$

In Equations 4 and 5, EC_{50} is the median effect concentration (mg l^{-1}) and LC_{50} is the median lethal concentration (mg kg^{-1}).

Farmers apply overdose pesticide (FD) more than the recommended dose (RD). Table 1 represents the concentration, dose and $\min(NORM_w)$ values of used a.i. in this research.

TABLE 1
Concentration, dose and $\min(NORM_w)$ values of used a.i.

Active ingredient (a.i.)	Concentration of a.i. (g l^{-1})	RD* (kg ha^{-1})	FD** (kg ha^{-1})	$\min(NORM_w)$ (µg l^{-1})
Abamectin	18	0.009	0.0135	0.001
Etoxazole	50	0.055	0.0825	0.071
Hexythiazox	50	0.050	0.0750	4.700
Propargite	570	1.140	1.7100	0.140
Spiromesifen	240	0.096	0.1440	0.160

*RD: Recommended dose of a.i. by manufacturer.**FD: Applied dose of a.i. by farmers.

Assessment of buffer zone. Buffer zone ($Z_{RI=1}$) for DDM and GDM was determined by RI according to z in Eq. 1 and 2. For aquatic organisms, if RI value is higher than 1, it indicates high risk. If RI is equal to or lower than 1, it means minimum risk, and indicates a safe situation.

RESULTS AND DISCUSSION

In this study, RI values at different distances were calculated by Eq. 1. RI values at 1 m ($RI_{w,1}$) for each a.i. were presented in Table 2.

TABLE 2
$RI_{w,1}$ values for each a.i.

Active ingredient (a.i.)	$RI_{w,1}$			
	DDM		GDM	
	RD	FD	RD	FD
Abamectin	84.214	126.320	16.556	24.834
Etoxazole	7.248	10.872	1.425	2.137
Hexythiazox	0.099	0.149	0.019	0.029
Propargite	76.193	114.289	14.979	22.468
Spiromesifen	10.417	15.625	1.103	1.655

As seen in Table 2, $RI_{w,1}$ values for hexythiazox were assessed to be lower than 1.000 in DDM and GDM, and RD and FD. As mentioned above, equal to or lower than 1.000 means minimum risk and safe distance. For this reason, hexythiazox was ignored in the buffer zone calculations because of its $RI_{w,1}$ value. In this study, $RI_{w,1}$ values for other a.i. were determined to be higher than 1. Therefore, we calculated $Z_{RI=1}$ for buffer zone assessment except hexythiazox.

Figure 2 represents the RI values at different distances in downwind for RD and FD for each a.i. in Dutch and German models. RI values were shown in Figure 2a, 2b, 2c and 2d, presented each a.i. with abamectin, etoxazole, propargite and spiromesifen.

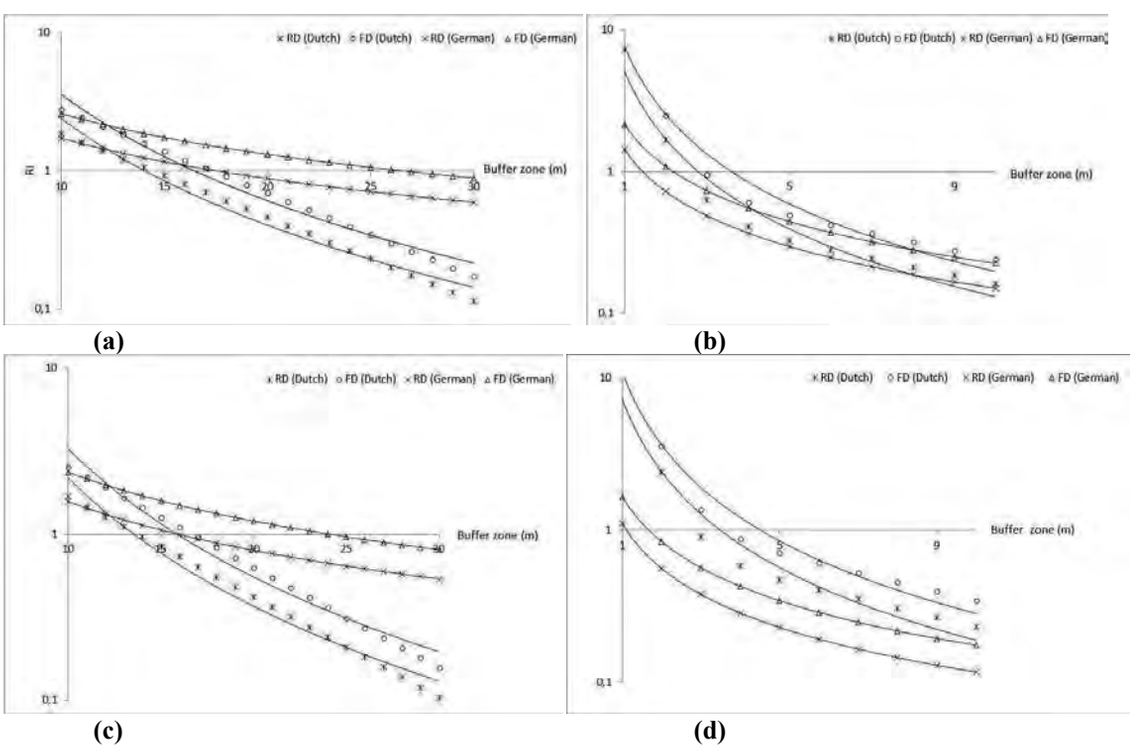

FIGURE 2
Relationship between RI and buffer zone for a.i. in two models and two doses

As seen in Figure 2a, it was observed that buffer zone ($Z_{RI=1}$) was <15 m in DDM and <20 m in GDM for RD, and<20 m in DDM and <30 m in GDM for FD. Figure 2b shows <5 m buffer zones for RD and FD in two models. It was observed that buffer zone was <15 m in DDM and <20 m in GDM for RD, and <20 m in DDM and <25 m in GDM for FD (Figure

2c). Figure 2d represents <5 m buffer zones for RD and FD in two models.

As buffer zone increases, pesticide contamination decreases in aquatic organisms. Yet, wider buffer zone near agricultural land means less arable land in this region. Sieber et al. (2010) assessed that in some rural districts, 30 m buffer zone would result in the conversion of around 12% of the district's area, in Germany [34]. Moreover, they determined that the "gross value added in relation to factor costs" in agriculture declined by 0.08% for 3 m, 1.20% for 30 m, and 2.04% for 50 m buffer zone width.

We have to know the exact buffer zone width to protect the conversion from agricultural land to buffer zone. Therefore, Equations 6 - 9 were developed by using Fig.2a. These equations were used for the exact buffer zone ($Z_{RI=1}$) according to RD and FD in two models for abamectin.

$$y_{RD(DDM)} = 876.09x^{-2.561} \quad (R^2 = 0.98) \quad \text{(Eq. 6)}$$

$$y_{FD(DDM)} = 1314.100x^{-2.561} (R^2 = 0.98) \quad \text{(Eq.7)}$$

$$y_{RD(GDM)} = 16.556x^{-0.978} \quad (R^2 = 1.00) \quad \text{(Eq.8)}$$

$$y_{FD(GDM)} = 24.834x^{-0.978} \quad (R^2 = 1.00) \quad \text{(Eq.9)}$$

Equations 10 - 13 were developed by using Fig.2b. These equations were used for the exact $Z_{RI=1}$ according to RD and FD in two models for etoxazole.

$$y_{RD(DDM)} = 5.076x^{-1.589} \quad (R^2 = 0.96) \quad \text{(Eq.10)}$$

$$y_{FD(DDM)} = 7.614x^{-1.589} \quad (R^2 = 0.96) \quad \text{(Eq.11)}$$

$$y_{RD(GDM)} = 1.425x^{-0.978} \quad (R^2 = 1.00) \quad \text{(Eq.12)}$$

$$y_{FD(GDM)} = 2.138x^{-0.978} \quad (R^2 = 1.00) \quad \text{(Eq.13)}$$

Equations 14 - 17 were developed by using Fig.2c. These equations were used for the exact $Z_{RI=1}$ according to RD and FD in two models for propargite.

$$y_{RD(DDM)} = 792.650x^{-2.561} (R^2 = 0.98) \quad \text{(Eq.14)}$$

$$y_{FD(DDM)} = 1189.000x^{-2.561} (R^2 = 0.98) \quad \text{(Eq.15)}$$

$$y_{RD(GDM)} = 14.979x^{-0.978} (R^2 = 1.00) \quad \text{(Eq.16)}$$

$$y_{FD(GDM)} = 22.469x^{-0.978} (R^2 = 1.00) \quad \text{(Eq.17)}$$

Equations 18 - 21 were developed by using Fig.2d. These equations were used for the exact $Z_{RI=1}$ according to RD and FD in two models for spiromesifen.

$$y_{RD(DDM)} = 7.296x^{-1.589} (R^2 = 0.96) \quad \text{(Eq.18)}$$

$$y_{FD(DDM)} = 10.943x^{-1.589} (R^2 = 0.96) \quad \text{(Eq.19)}$$

$$y_{RD(GDM)} = 1.104x^{-0.978} (R^2 = 1.00) \quad \text{(Eq.20)}$$

$$y_{FD(GDM)} = 1.656x^{-0.978} (R^2 = 1.00) \quad \text{(Eq.21)}$$

According to Equations 6 –9 for abamectin, 10 – 13 for etoxazole, 14 – 17 for propargite and 18 – 21 for spiromesifen, $Z_{RI=1}$were exactly calculated for RD and FD in two models, and presented in Table 3 for each a.i. In addition, Table 3 represents the percentage increase of the $Z_{RI=1}$value for RD and FD in two models.

TABLE 3.
Calculated $Z_{RI=1}$values for each a.i.

Active ingredient (a.i.)	$Z_{RI=1}$ (m)					
	DDM			GDM		
	RD	FD	% increase	RD	FD	% increase
Abamectin	14.09	17.05	21.00	17.64	26.70	51.36
Etoxazole	2.78	3.59	29.00	1.44	2.17	50.69
Propargite	13.55	15.88	17.19	15.92	24.10	51.38
Spiromesifen	3.49	4.51	29.23	1.10	1.67	51.82

As seen in Table 3, $Z_{RI=1}$ for abamectin was calculated as 14.09 for RD-DDM, 17.05 for FD-DDM, and 17.64 for RD-GDM, 26.70 for FD-GDM. $Z_{RI=1}$ for etoxazole were calculated as 2.78 for RD-DDM, 3.59 for FD-DDM, and 1.44 for RD-GDM, 2.17 for FD-GDM. $Z_{RI=1}$ for propargite was calculated as 13.55 for RD-DDM, 15.88 for FD-DDM, and 15.92 for RD-GDM, 24.10 for FD-GDM. $Z_{RI=1}$ for spiromesifen was calculated as 3.49 for RD-DDM, 4.51 for FD-DDM, and 1.10 for RD-GDM, 1.67 for

FD-GDM (Table 3). As seen in Table 3, FD values are higher than RD values in all a.i. Bozdogan and Yarpuz-Bozdogan (2008) assessed that dose in a pesticide application is the major determining factor for buffer zone width [24]. Ucar and Hall (2001) informed that application rate is one of the important factors on buffer zone distance [35]. Marrs et al. (1993) found that increasing need to protect semi-vegetation from potential effects of herbicide drift, and that buffer zones may need to be 20 m wide [36]. Snoo and Witt (1998) indicated that when 3m buffer zone was used the deposition of drift in the ditch decreases minimum of 95% [25]. Sieber et al (2010) determined that the buffer zone width of 0-3 m reduces the pesticide risk by around 60%, whereas going from 30 to 50 m reduces the risk by only 2% [34]. Yarpuz-Bozdogan and Bozdogan (2009) compared the percentage drift of model and field using different types of hydraulic nozzles. They determined that percentage drift at 5 m compared to 1 m distance decreased approximately by 12 folds in flat fan nozzle (F 11006), 10 folds in hollow cone nozzle (D4-45) and 15 folds in low drift nozzle (LD 11003) in the actual pesticide application, 9 folds in Dutch and 5 folds in German models [32].

As seen in Table 3, the percentage of the increase in FD was higher than in RD as 21.00% for abamectin, 29.00% for etoxazole, 17.19% for propargite and 29.23% for spiromesifen in DDM. The percentage of the increase in FD was more than 50% in GDM. The percentage of the increase was lower in DDM than in GDM. deJong et al. (2008) showed that in 2005 with unsprayed buffer zones and other measures in place, percentages are down to 21% for insecticides, 41% for herbicides and 14% for fungicides [37].

CONCLUSION

Results of this research show that buffer zone is important to minimize the pesticide contamination on aquatic organisms. Buffer zone was found as ≥ 18 m for abamectin and ≥ 16 m for propargite in RD. It was determined as ≥ 27 m for abamectin and ≥ 25 m for propargite in FD. Buffer zone for was assessed as ≥ 3 m for etoxazole and ≥ 4 m for spiromesifen in RD. It was calculated as ≥ 4 m for etoxazole and ≥ 5 m for spiromesifen in FD. In all a.i. and two models, buffer zones of FD are higher than RD. Therefore, farmers should conform to the recommended doses on product's label. If not, pesticide contamination in environment occurs as a major problem for aquatic organisms. It can be derived from this study that farmers have to be informed about the importance of the buffer zone, and lectures on agriculture and environment should be given to farmers' children in rural schools for agricultural sustainability.

REFERENCES

[1] Anonymous (2013) 2012 yılı Pamuk Raporu. T.C. Gümrük ve Ticaret Bakanlığı Kooperatifçilik Genel Müdürlüğü. S 46. (In Turkish)

[2] TUIK (2014) URL http://www.tuik.gov.tr (accessed on 09 May 2014).

[3] Anonymous (2014a) Adana İli Ekonomisi 2013. Adana Ticaret Odası, S 99. (In Turkish)

[4] Anonymous (2014b) Adana Tarım İl Müdürlüğü, (accessed on 3 November 2014).

[5] ECPA (2014) URL http://www.ecpa.eu. (accessed 01 August 2014).

[6] Anonymous (2014c) URL http://www.chemicalbook.com. (accessed on 15 August 2014).

[7] BPDB (2014) URL http://sitem.herts.ac.uk/aeru/bpdb/ (accessed on 15 August 2014).

[8] PPDB (2014) URL http://sitem.herts.ac.uk /aeru/ppdb/en/ (accessed on 03 May 2014).

[9] Yassin, M.M.; Abu Mourad, T. A. and Safi, J.M. (2002) Knowledge, Attitude, Practice, and Toxicity Symptomps Associated with Pesticide Use Among Farm Workers in the Gaza Strip. Occup Environ Med, 59, 387-394.

[10] Damalas, C.A.; Theodorou, M. G. and Georgiou, E. B. (2006) Attitudes towards pesticide labelling among Greek tobacco farmers. International Journal of Pest Management 52, 269-274.

[11] Demircan, V. and Yılmaz, H. (2005) The Analysis of Pesticide Use in Apple Production in Isparta Province in terms of Economy and Environmental Sensitivity Perspective. Ekoloji 14, 57, 15-25.

[12] Zeren, O.; Kumbur, H. and Tasdemir, H. (1996) İçel İlinde Tarımsal Ilac Pazarlama Kullanım Tekniği ve Etkinliği Üzerinde Araştırmalar. Tarım-Çevre İlişkileri Sempozyumu, 13-15 May, Mersin, 259-269. (In Turkish).

[13] Bozdogan, A.M. and Yarpuz-Bozdogan, N. (2009) Determination of total risk of defoliant application in cotton on human health and environment. International Journal of Food, Agriculture & Environment 7, 229-234.

[14] Yarpuz Bozdoğan N. (2009) Assessing The Environment And Human Health Risk Of Herbicide Application In Wheat Cultivation. International Journal of Food, Agriculture & Environment 7, 775-781.

[15] Bozdogan A.M. (2014) Assessment Of Total Risk On Non-Target Organisms In Fungicide

Application For Agricultural Sustainability. Sustainability 6, 1046-1058.
[16] Aka Sagliker H.; Kizildag N.; Cenkseven S.; Darici C.; Kocak B.; Yarpuz Bozdogan N. and Daglioglu N. (2014) Effects of Imazamox on Soil Carbon and Nitrogen Mineralization Under Two Different Humidity Conditions. Ekoloji 23, 22-28.
[17] Bozdogan, A.M. and Yarpuz-Bozdogan, N. (2004) A review of the effects of adjuvants on spray drift in pesticide applications. Proc. 7th Int. Symposium on Adjuvants for Agrochemicals, Cape Town, South Africa, 92-98.
[18] Bozdogan, A.M. and Yarpuz-Bozdogan, N. (2008) Determination of dermal bystander exposure of malathion for different application techniques. Fresenius Environmental Bulletin 17, 2103-2108.
[19] Yarpuz-Bozdogan, N. and Bozdogan, A.M. (2009) Assessment of different types of nozzles on dermal bystander exposure in pesticide applications. International Journal of Food, Agriculture & Environment 7, 678-682.
[20] Tobi, İ.; Saglam, R.; Kup, F.; Sahin, H.; Bozdogan, A.M.; Piskin, B. and Saglam, C. (2011) Determination of accuracy level of agricultural spraying application in Sanliurfa/Turkey. African Journal of Agricultural Research 6, 6064-6072.
[21] Yarpuz-Bozdogan, N. (2011) "Drift of Pesticide", *Encyclopedia of Pest Management*, Taylor and Francis, ISBN: 0-8247-0632-3; eISBN: 0-8247-0517-3, Editor David Pimentel, DOI: 10.1081/E-EPM-120009991, pp: 1-4. Published: 21 Oct 2011.
[22] Yılmaz, H.; Erbatur, O. and Erbatur, G. (2003) Monitoring of pesticide and heavy metal discharge of major rivers and drainage canals into the Mediterranean Sea in the north-east coastal zone, Turkey. Fresenius Environmental Bulletin 12, 1407-1411.
[23] SANCO (2005) Landscape and mitigation factors in aquatic ecological risk assessment. European Comission-SANCO/10422, 434 p.
[24] Bozdogan, A.M. and Yarpuz-Bozdogan, N. (2008) Assessment of buffer zones to ditches of dicofol for different applied doses and replication numbers in pesticide applications in Adana province, Turkey. Fresenius Environmental Bulletin 3, 275-281.
[25] Snoo, G.R. and Witt, P.J. (1998) Buffer zones for reducing pesticide drift to ditches and risks to aquatic organisms. Ecotoxicology and Environmental Safety 1, 112-118.
[26] Carluer , N.; Tournebize, J.; Gouy, V.; Margoum, C.; Vincent, B. and Gril, J.J. (2011) Role of buffer zone in controlling pesticides fluxes to surface waters. Procedia Environmental Sciences 9, 21-26.
[27] Syversen, N. and Bechmann, M. (2004) Vegetative buffer zones as pesticide filters for simulated surface runoff. Ecological Engineering 22, 175-184.
[28] Payne, N.J.; Helson, B.V.; Sundaram, K.M.S. and Fleming, R.A. (1988) Estimating buffer zone widths for pesticide applications. Pestic. Sci. 24, 147-161.
[29] Davis, B.N.K. and Williams, C.T. (1990) Buffer zone widths for honeybees from ground and aerial spraying of insecticides. Environmental Pollution 63, 247-259.
[30] Reichenberger, S.; Bach, M.; Skitschak, A. and Frede, H.G. (2007) Mitigation strategies to reduce pesticide inputs into ground-and surface water and their effectiveness; A review. Sci Total Environ. 384, 1-35.
[31] De Schampheleire, M.; Spanoghe, P.; Brusselman, E. and Sonck, S. (2007) Risk assessment of pesticide spray drift damage in Belgium. Crop Protection 26, 602-611.
[32] Yarpuz-Bozdogan, N. and Bozdogan, A.M. (2009) Comparison of Field and Model Percentage Drift Using Different Types of Hydraulic Nozzles in Pesticide Applications. Int. J. Environ. Sci. Tech. 6, 191-196.
[33] Vercruysse, F. and Steurbaut, W. (2002) POCER The pesticide occupational and environmental risk indicator. Crop Protection 21, 307-315.
[34] Sieber, S.; Pannell, D.; Müller, K.; Holm-Müller, K.; Kreins, P. and Gutsche, V. (2010) Modelling pesticide risk: A marginal cost-benefit analysis of an environmental buffer-zone programme. Land Use Policy 27, 653-661.
[35] Ucar, T. and Hall, F.R. (2001) Windbreaks as a pesticide drift mitigation strategy: a review. Pest Management Science 57, 663-675.
[36] Marrs, R.H.; Frost, A.J.; Plant, R.A. and Lunnis, P. (1993) Determination of buffer zones to protect seedlings of non-target plants from the effects of glyphosate spray drift. Agriculture Ecosystems & Environment 45, 283-293.
[37] de Jong, F. M. W.; de Snoo, G. R. and van de Zande, J. C. (2008) Estimated nationwide effects of pesticide spray drift on terrestrial habitats in the Netherlands. Journal of Environmental Management 86, 721-730.

Received: **14.07.2015**
Accepted: **07.01.2016**

CORRESPONDING AUTHOR

Nigar. Yarpuz-Bozdogan
University of Cukurova
Vocational School of Technical Sciences
Misis Adana – Turkey

e-mail: nyarpuzbozdogan@cu.edu.tr

INFLUENCE OF DIFFERENT IRRIGATION LEVEL AND DIFFERENT NICKEL (Ni) DOSES ON PHYTOREMEDIATIVE CAPACITY OF *Tagetes erecta L.*

Derya Onder[1,*], Sermet Onder[2], Hatice Daghan[3], Veli Uygur[4]

[1] Çukurova University, Faculty of Agriculture, Department of Agricultural Structer and Irrigation, Adana-Turkey
[2] Sermet Önder Irrigation Systems Company, Adana-Turkey
[3] Eskişehir Osmangazi University, Faculty of Agriculture, Department of Soil Science and Plant Nutrition, Eskisehir-Turkey
[4] Süleyman Demirel University, Faculty of Agriculture, Department of Soil Science and Plant Nutrition, Isparta-Turkey

ABSTRACT

It is nowadays possible to remedy polluted soils by using various physical, chemical, and biological methods. One of these possible biological remediation methods is phytoremediation, a technique that involves the use of plants to clean up polluted soils. As the quantity of available water decreases in the present-day world, water is becoming an increasingly more valuable resource. In this context, deficit irrigation is a novel approach developed in recent years, aiming for the effective use of water resources.

In this study, *Tagetes erecta*, a plant commonly employed for the cleaning and reclamation of soils polluted with heavy metals, was used at different water levels (IR40, IR60, IR80, and IR100) and at different doses of Nickel (Ni) (0, 50, 100, and 200 mg/kg). Under the study conditions, the Ni and water uptake of the *Tagetes erecta* plant, as well as its uptake of other elements were evaluated and observed that as the Ni doses increased, the plant entered into heavy metal stress and reduced its water consumption. The level of irrigation and deficit irrigation practices significantly affect the leaf area, the chlorophyll content of the young leaves, the fresh (FW) and dry weights (DW) of shoot, the root dry weight, and the level of Ni removed through the action of plant organs above the soil. *Tagetes erecta L.* reacted to both heavy metal and water stresses by reducing the amount of biomass produced and the area of its leaves. In addition, the plant removed the largest amount of Ni from the soil in 50 mg/kg Ni application (682 µg/shoot), with higher doses of Ni, resulting in a slight decrease in the amount of Ni removed from the soil.

KEYWORDS:
Phytoremediation, Ni, irrigation, deficit, soil, pollution

INTRODUCTION

The water and soil resources of our world are decreasing with each passing day. The expected growth in world population, the potential changes in climate, and the continually growing demand for water are very likely to further worsen the depletion of these highly valuable resources around the world [1-7].

The rapid and accelerating growth in world population has led to a parallel increase in food demand, and, by extension, to a parallel increase in the utilization of natural resources. In Europe, for instance, the amount of land irrigated per person has, over the years, increased from 0.022 to 0.035 [8]. Under these circumstances, it has nowadays become necessary to decrease agricultural water consumption by employing different methods, such as reducing the amount of water required by crops [9, 10]. One of the methods employed for ensuring water use efficiency (WUE) is deficit irrigation [11, 12], a practice where crops are systematically irrigated with less water than they normally require with the aiming of achieving greater yields for a given level of irrigation [13, 14]. In this approach, crops are subject to water stress during part or all of their growing period, without causing a considerable decrease in crop yield [15].

In addition to the decrease and pollution of water resources, another factor that threatens human societies is soil pollution [16]. Wastes generated by residential areas, exhaust gases, industrial wastes, pesticides, and chemical fertilizers are the main contributors of soil pollution. Heavy metals represent one of the most important groups of environmental pollution, with 129 heavy metals being classified as priority pollutants in the list prepared by the United States Environmental Protection Agency (EPA) [17, 18]. Heavy metal pollution represents a significant environmental issue, since heavy metals cannot be easily removed or eliminated from nature, and can have toxic effects on animals, plants, and microorganisms even at low doses; moreover, heavy metals tend to

accumulate in water, soil, and living organisms, such that even relatively small quantities of heavy metals released into the environment can eventually reach toxic levels [19]. As a heavy metal and pollutant, Nickel (Ni) is commonly found in soils. Although Ni is used as a nutrient required by many organisms, it is only necessary in small quantities; consequently, large concentrations of Ni have toxic effects on plants and animals [20, 21]. The mean concentration of Ni in soil is generally about 50 mg/kg soil, and ranges between 5 and 500 mg/kg soil. However, in agricultural soil and soils formed from igneous rocks, Ni concentrations tend to be higher, ranging between 3 to 1000 mg/kg soil and 2000 to 6000 mg/kg soil, respectively [22].

Nowadays, it is possible to remedy polluted soils by using various physical, chemical, and biological methods. Phytoremediation, which is a biological remediation method, represents a low-cost and effective alternative compared to other remediation approaches. Phytoremediation is recently developed environmentally friendly approach involving the utilization of plants for remedying soils, surface and ground waters, and sediments by eliminating organic pollutants, radionuclide's and heavy metals [23].

In this study, Ni removal, accumulation, and tolerance of the *Tagetes erecta* – a plant commonly used for the phytoremediation of soils polluted with certain heavy metals doses and different levels of irrigation.

MATERIALS AND METHODS

Soil obtained from the first 0 to 30 cm layer of the Paşaköy series was used. The Paşaköy series is one of the commonly found soils of the Amik plain in Hatay, Turkey. The soils used in this study had a pH of 7.56, a lime content of 5.06%, and an organic content of 1.48%; the soils also had a clayey texture (Table 1).

Prior to planting, a Ni solution was applied at four different concentrations (0, 50, 100, and 200 mg/kg) to the soil in the pots. The pots were then incubated under controlled conditions for three weeks at 80% field capacity. Immediately before planting, 200 mg/kg of N (from $(NH_4)_2SO_4$), 100 mg/kg of P, and 125 mg/kg of K (from KH_2PO_4), and 2.5 mg/kg of Fe (from Fe-EDTA) were added to the soil. The *Tagetes erecta* L. plant species was used in the experiments. *Tagetes erecta* L. (Compositae) is a commonly found plant, also called the *Marigold* [24].

TABLE 1
The chemical and physical properties of the study soil

Properties	Unit	Content	Properties	Unit	Content
Organic Matter	%	2.55	pH		7.56
Organic carbon	%	1.48	Salt	%	0.216
K	%	77.28	EC	dS/m	4.35
P	%	19.14	Texture		Clay
$CaCO_3$ (Lime)	%	5.06	Field Capacity	Pw/Pw (%)	43

The plant seeds were germinated in a peat and perlite mix (1:1 ratio) [25], under a 16/8 hour light/dark cycle, and at 60-70% relative humidity and a temperature of 22-25°C. After the plants developed two to three leaves and an adequate root system, they were transferred to experiment pots. Fertilizers were provided only one to the plants at the beginning of the experiment. The experiment was based on three repeats according to a factorial experiment design in randomized parcels. The experiment was performed in a climate chamber with light, temperature, and humidity control. Four different levels of irrigation were used during the experiment. These irrigation levels were 40% of full irrigation (IR40; 60% deficit), 60% of full irrigation (IR60; 40% deficit), 80% of full irrigation (IR80; 20% deficit) and full irrigation (IR100).

After the plants adapted to the soil and became lively, the irrigation program was applied under vegetation cover of 20%. All pots were weighed before irrigation (IR40, IR60, IR80, and IR100). For each pot, the amount of water necessary for IR100 irrigation was calculated based on the difference between their weight at field capacity and their current weight. Irrigation at IR80, IR60, and IR40 was performed by applying 80%, 60%, and 40% of the amount of water calculated for IR100. Irrigation was performed every three days and continued until harvest.

After being transferred to pots, plants were grown for approximately six weeks until reaching the highest biomass before their flowering. Certain morphological and phonological observations were made of the plant during the experiments. The areas of the leaves and fresh weights (FW) of plants were measured at the time of harvest. The chlorophyll content of the leaves was measured using the Chlorophyll meter (Konica-Minolta SPAD-502) device according to [26] method.

After harvesting, the plant samples were rinsed in de-ionized water and then dried at 70ºC. The dry weights (DW) of the plants shoots (the plants above ground biomass) were measured and plant samples grind with an agate mill (Retcsh RM200). Then the plant samples were wet composted with HNO_3 and H_2O_2 in microwave oven (MarsXpress CEM). The cadmium (Cd), lead (Pb), nickel (Ni), zinc (Zn), copper (Cu), iron (Fe), manganese (Mn), phosphor (P), calcium (Ca), and magnesium (Mg) concentrations of the plant samples were determined by Inductively Coupled Plasma-Atomic Emission Spectrometry (ICP-AES; Varian Series-II). Using the wet decomposition method, K and Na concentrations were measured with a flame photometer [27].

In addition to performing morphological and chemical analyses, we also evaluated the physiological changes of the plants, as well as the level of sulfhydryl group/reduced glutathione (–SH), superoxide dismutase (SOD), and proline, which are enzymes/chemicals that eliminate reactive oxygen species, were also evaluated. To assay the enzymes/chemicals in question, fresh leaf samples were taken from shoot, weighed, and then subjected to chemical content analysis.

The analysis of -SH (reduced glutathione) and (SOD) superoxide dismutase activity was performed according to [28]. Proline concentration was determined according to [29]. Nitrogen (N) analysis of the plant samples was performed according to the Kjheldal method [30].

Analysis of variance for data was performed using the SPSS-17 statistical analysis program, and according to the factorial experiment design in random parcels. Comparisons between means were performed using the LSD test [31].

RESULTS AND DISCUSSION

In accordance with the irrigation program, the amount of irrigation gradually decreased from IR100 plants to the IR40 plants (Table 2). On the other hand, a gradual increase in the dose of Ni from 0 to 200 mg/kg was associated with a decrease in the amount of irrigation. The only exception to this was the slight increase in the level of irrigation for IR80 plants at the Ni doses of 50 mg/kg.

An increase in the level of irrigation was associated with an increase in ET values. However, as the level of irrigation increased from IR80 to IR100, a slight decrease was observed in the ET value. On the other hand, at all levels of irrigation, a decrease in Ni levels from 200 to 0 g/kg was associated with an increase in ET values. It is therefore possible to state that an increase in Ni doses resulted in heavy metal stress that reduced evapotranspiration.

Table 3 shows the effect of Ni doses and irrigation levels on the plant's growth parameters. The biomass of the plants above ground (shoot), which was 79.3 g/shoot in the control application decreased to 51.2 g/shoot during 200 mg/kg Ni applications. According to the LSD test, there were three homogenous groups: a control group, a 200 mg/kg Ni group, and a group comprising both the 50 and 100 g/kg Ni applied plants. Increasing water stress led to a noticeable decrease in FW; while biomass was 88.1 g/plant in the control applications, it decreased to 46.5 g/shoot following 60% reduction in irrigation. According to the LSD test, every irrigation level represented a different group. The DW of plant parts above the surface demonstrated a behavior and grouping statistically similar to that the FW. This indicated that these irrigation practices/levels can be an important problem for the phytoremediation of Ni.

TABLE 2
Level of irrigation and ET values of the *Tagetes* plants according to the IR level and Ni doses.

Irrigation Levels	Irrigation Amount, gram/pot				Evapotranspiration, gram/pot			
	Nickel Doses				Nickel Doses			
	200	100	50	0	200	100	50	0
IR 40	1826.5	2120.0	2439.0	2520.3	2054.8	2298.0	2695.2	2781.9
IR 60	2335.6	2634.6	3096.1	3155.9	2454.9	2627.7	3069.1	3120.1
IR 80	2604.7	3220.8	3760.9	3686.5	2682.0	2923.7	3441.3	3642.1
IR 100	3058.7	3764.0	4271.3	4380.0	2623.3	3589.0	3956.7	4113.7

TABLE 3
The effect of Ni doses and irrigation levels on parameters relating to growth.

Treatments	Shoot FW (g/shoot)	Shoot DW (g/shoott)	Chlorophyll Old Leaves	Chlorophyll Young Leaves	Leaf Area (cm^2)	Root Dry Weight (g/root)
Ni 0 mg/kg	79.3 a	8.87 a	59.8 n.s	48.5 b	1342.4 a	1.455 n.s
Ni 50 mg/kg	70.2 b	7.76 b	60.8 n.s	55.4 a	1497.4 a	1.603 n.s
Ni 100 mg/kg	71.1 b	7.77 b	57.3 n.s	50.6 b	1366.6 a	1.384 n.s
Ni 200 mg/kg	51.2 c	5.91c	54.5 n.s	51.6 ab	1031.4 b	0.856 n.s
Irrigation Level (IR) %40	46.5 D	5.72 D	56.7 n.s	47.0 B	872.5 D	1.028 C
Irrigation Level (IR) %60	63.5 C	7.30 C	57.2 n.s	49.6 B	1205.6 C	1.145 BC
Irrigation Level (IR) %80	73.5 B	7.96 B	61.7 n.s	54.5 A	1432.4 B	1.305 B
Irrigation Level(IR) %100	88.1 A	9.34 A	56.9 n.s	55.0 A	1727.3 A	1.820 A

Different letters indicate significant (0.05) difference between the means. n.s: no significant

Table 4 shows the multivariate analysis of the macro-element content of plant organs above the surface. This table indicates that Ni had a very significant effect on the concentrations of the macro-elements phosphorus and potassium. The level of irrigation did not have a significant effect on the concentration of any of the macro-elements. The interaction of Ni doses and irrigation levels had a significant effect on the macro-elements N and Ca. The effect of Ni doses and irrigation levels of the macro-element and Na concentration of the plants' green parts is shown in Table 4. Increasing Ni concentrations was associated with a decrease in N concentration in the green parts. On the other hand, the N concentration varied only with a narrow range of 2.39% and 2.44% depending on the level of irrigation. Increasing doses of Ni were associated with a decrease in phosphorus concentration. Based on the LSD test, three different groups were identified; the first group comprised the 0 and 50 mg/kg Ni applications; the second group comprised the 100 mg/kg Ni application; and the third group comprised the 200 mg/kg Ni application. No changes were observed in phosphorus levels due to the level of irrigation.

The K content decreased significantly in high dose (200 mg/kg) Ni applications. Up to 100 mg/kg Ni application, the K concentrations remained more or less the same. The concentration of K did not vary according to the irrigation level.

The Ca concentration of the plants was not significantly affected by irrigation or Ni doses. However, an increase in Ni doses and irrigation levels was nevertheless associated with a slight increase in Ca concentrations.

TABLE 4
The mean N, P, K, Ca, Mg and Na concentrations in the *Tagetes* plants' shoots according to different Ni doses and irrigation levels

	N	P	K	Ca	Mg	Na
Stress Factors			%			mg/kg
Ni 0 mg/kg	2.52 n.s	0.244 a	2.928 a	1.088 n.s	0.379 n.s	90.9 n.s
Ni 50 mg/kg	2.45 n.s	0.223 a	2.751 b	1.092 n.s	0.400 n.s	88.0 n.s
Ni 100 mg/kg	2.45 n.s	0.195 b	2.833 b	1.144 n.s	0.374 n.s	114.6 n.s
Ni 200 mg/kg	2.27 n.s	0.165 c	2.458 c	1.152 n.s	0.374 n.s	77.5 n.s
IR %40	2.39 n.s	0.200 n.s	2.666 n.s	1.098 n.s	0.371 n.s	84.5 n.s
IR %60	2.43 n.s	0.199 n.s	2.717 n.s	1.088 n.s	0.384 n.s	112.5 n.s
IR %80	2.44 n.s	0.215 n.s	2.757 n.s	1.175 n.s	0.392 n.s	87.6 n.s
IR %100	2.44 n.s	0.213 n.s	2.830 n.s	1.115 n.s	0.380 n.s	86.4 n.s

Different letters indicate significant (0.05) difference between the means. n.s: no significant

The Mg concentration of the plants increased only at a Ni dose of 50 mg/kg; other Ni doses were not associated with any noticeable changes in Mg concentrations. On the other hand, the level of irrigation had no effect on Mg concentrations.The Na concentration of the plants increased only at a Ni dose of 100 mg/kg; other Ni doses were not associated with any noticeable changes in Na concentrations. Similarly, Na concentrations increased only at an irrigation level of 60%. This behavior might have stemmed from a combination of water consumption, biomass production, and dilution effects, rather than differences in Na uptake.Table 5 shows that the Ni doses had a significant effect on the plants' Ni, Fe, Cu and Zn concentration. On the other hand, the level of irrigation did not have a significant effect on the concentrations of elements other than Mn. The interaction of Ni doses and irrigation levels had a significant effect on Fe, Zn and root Ni concentration, but no significant effects on other parameters of this group.The effect of Ni doses and irrigation levels on the concentrations of Fe, Cu, Mn, Zn, Ni, the content of Ni by shoots, and the Ni concentration at the roots is shown in Table 5. Ni applications generally had the effect of reducing the Fe concentration of the shoots. While the Fe concentration was 316.8 mg/kg in the control groups, the Fe concentration of the groups applied with 100 and 200 mg/kg Ni decreased to 69.3 and 90.1 mg/kg, respectively. As a result of this variability, two groups were identified based on the LSD test. The first group comprised the controls Ni applications, while the other groups comprised the other high dose Ni applications (50, 100 and 200 mg/kg). Water stress resulted in behavior similar to heavy metal stress. The irrigation level of 100%, which involved the lowest level of water stress for the plants, was associated with the high Fe concentration, while increasing water stress led to a decrease in the Fe concentration. This behavior is in agreement with the expected decrease in redox potential due to the decrease in the amount of irrigation [32, 33].

The Cu concentration of shoots was significantly affected by the Ni applications, with Cu concentrations showing a considerable decrease with increasing Ni doses (Table 5). This behavior can be explained by the similarity of the two elements uptake mechanisms in plants [34, 35]. The decrease in the level of irrigation was associated with a decrease in the Cu concentration within the plant. However, the level of irrigation had no effect on Cu concentration.The level of Ni and irrigation did not have a significant effect on the Mn concentration of the shoots (Table 5). On the other hand, an increase in Ni concentration was associated with an increase in Zn concentration. The highest Zn concentrations were obtained during the 100 and 200 mg/kg Ni applications. According to the LSD test, 100 and 200 mg/kg Ni-applied plants for one group while the control and 50 mg/kg Ni-applied treatments formed another group. Water stress similarly led to an increase in Zn concentrations, with the Zn concentrations varying between 5.3 and 11.3 mg/kg depending on the level of water stress. According to the LSD test, the level of irrigation led to the formation of two groups: a group with high Zn concentrations, comprising IR40 and IR60 treatment and a group with lower Zn concentrations, comprising IR100 and IR80. Ni concentrations within the *Tagetes* plant increased in parallel to the Ni applications. However, according to the LSD test, all plants applied with Ni were within the same group. This indicates that the *Tagetes* plants were not able to effectively remove Ni from the soil at concentrations above 50 mg/kg. The Ni concentration decreased with a decrease in irrigation level. However, according to the LSD test, all Ni doses were within the same group.

TABLE 5
The mean Fe, Cu, Mn, Zn, and Ni concentrations and Ni content of shoots and the Ni concentration at the roots for *Tagetes* plants at different Ni doses and irrigation levels

Stress Factors	Fe	Cu	Mn	Zn	Ni	Ni Removed	Ni Root
	mg/kg					µg/ shoot	mg/kg
Ni 0 mg/kg	316.8 a	9.37 a	143 n.s	2.4 c	16.8 b	167 b	28.5 d
Ni 50 mg/kg	156.9 b	7.07 ab	141 n.s	6.2 b	91.6 a	682 a	95.0 c
Ni 100 mg/kg	69.3 b	5.70 bc	147 n.s	13.7 a	81.5 a	626 a	253.2 b
Ni 200 mg/kg	90.1 b	3.99 c	147 n.s	11.1 a	91.7 a	539 a	453.1 a
IR %40	77.8 B	6.02 N.S	136 N.S	11.3 A	59.6 N.S	335 C	220.3 B
IR %60	71.8 B	5.65 N.S	148 N.S	10.6 A	61.7 N.S	435 BC	157.9 BC
IR %80	165.9 AB	5.78 N.S	148 N.S	5.3 B	81.1 N.S	558 AB	315.6 A
IR %100	318.1 A	8.67 N.S	146 N.S	6.2 B	79.2 N.S	687 A	135.9 C

Different letters indicate significant (0.05) difference between the means. n.s: no significant

The *Tagetes* plant was able to remove the highest level of Ni from the soil (682 µg/ shoot) during a 50 mg/kg Ni application; higher doses of Ni resulted in a slight, non-significant decrease in the level of Ni removed from the soil. With regards to the level of water, the highest level of Ni was removed from the soil at an irrigation level of 100%. Although the 80% irrigation was within the same group as 100% irrigation in terms of Ni removed, the level of Ni removed at 80% irrigation was comparatively lower at 558 µg/ shoot. With increasing water stress, the level of Ni content decreased to 335 µg/ shoot. According to the LSD test, all plants exposed to water stress constituted a single group.

Root Ni concentration increased with the dose of applied Ni and each Ni dose constituted a different group according to the LSD test (Table 5). Although the increase in irrigation level was not associated with a specific and discernable trend, each irrigation level formed a different group according to the LSD test.

The analysis of variance concerning the biochemical responses of the *Tagetes* plant to Ni concentration and various levels of water deficit is shown in Table 6. It was determined that the application of a heavy metal (i.e. Ni) did not result in a significant difference in the plants' SOD and proline levels.

According to the LSD test, the -SH concentrations were similar in 100%, 80%, 60% and 40% irrigation levels (Table 6). Proline concentration was the highest at 60% irrigation level.

Table 6 provides the LSD comparisons and the mean values concerning the effect of Ni applications on the biochemical parameters SOD activity and proline activity. As shown on this table, the SOD activity of the control plants (i.e. applied with 0 mg/kg Ni) was higher than that of a volume of enzyme extract necessary for reducing NBT concentration to 50% within a confidence interval of 95% ($P<0.05$). No statistically significant difference between the different Ni applications in terms of SOD activity, with all levels of Ni application being assigned to the same group. This indicated that the plants produced more SOD to counter the damage caused in the plants by heavy metal stress.

TABLE 6
The effect of Ni doses and irrigation levels on the biochemical parameters of the *Tagetes* plant

Stress Factors	-SH µg/g FW	SOD (µL/g FW)	Proline (µmol/gFW)
Ni 0 mg/kg	1111.9 b	202.6 n.s	13.28 n.s
Ni 50 mg/kg	1105.6 b	152.2 n.s	19.07 n.s
Ni 100 mg/kg	1060.1 b	146.7 n.s	23.05 n.s
Ni 200 mg/kg	1360.4 a	144.8 n.s	23.22 n.s
IR %40	1209.4 N.S	195.0 N.S	22.10 B
IR %60	1305.5 N.S	233.7 N.S	22.23 BA
IR %80	1103.5 N.S	186.0 N.S	23.33 A
IR %100	1019.6 N.S	188.4 N.S	10.96 C

Different letters indicate significant (0.05) difference between the means. n.s: no significant

The proline concentration in *Tagetes* plant leaves increased with to the increase in the applied dose of Ni, with the proline concentration varying between a range of 13.28 µmol/g FW and 23.22. However, the Nickel concentration had no significant effect on proline concentration. Although, the proline concentration continued to increase slightly with increasing Ni concentration (Table 6). Thus, increasing Ni doses were generally associated with an increase in proline concentrations. On the other hand, considering the proline activity is a parameter that generally increases under conditions of water and salt stress, the increase in proline activity as a result of Ni application suggests that the Ni ion might play an important role in the water balance of plants.

Water stress had a significant effect on the proline levels of the plants, with higher water deficit being associated with a higher proline concentration in *Tagetes* leaves (Table 6). Proline concentration was the lowest at IR100, which involved full irrigation and no water stress; according to the LSD test, IR100 formed another group by itself. Irrigation levels involving increasingly higher water deficits led to higher proline concentrations.

CONCLUSIONS

It is believed that higher Ni doses induce heavy metal stress in plants that reduce water consumption. Applications of different irrigation (or water deficit) levels significantly affected the leaf area, the chlorophyll level of the young leaves, FW and DW, the root dry weights, and Ni content. In general, increasing Ni doses led to higher proline concentrations. Considering that proline activity is a parameter that increases under water and salt stress conditions, the parallel increase in Ni doses and proline activity suggests that the Ni ion might play an important role in the water balance of plants.

The *Tagetes* plant was able to remove the most Ni from the soil (682 µg/shoot) at an applied Ni dose of 50 mg/kg. Higher Ni doses led to a slight and non-significant decrease in Ni removal. With respect to the level of irrigation, the highest amount of Ni content (µg/shoot) took place at 100% irrigation. According to the LSD test, the irrigation level of 80% belonged to the same group as 100% irrigation in terms of Ni removal; however, the level of Ni removal with 80% was slightly lower at 558 µg/ shoot. With increasing water stress, the level of Ni removal by the plants decreased to 335 µg/ shoot.

Water is one of the most important inputs of plant growth, with increasing amount of water leading to higher plant biomass. Higher plant biomass also has the effect of decreasing concentration (or "diluting") the elements within the plants. When there is insufficient water, or when plants use less water, a significant decrease will also be observed under normal circumstances in the amount of nutrient elements collected by plants from the soil. However, in case a plant cannot produce sufficient biomass, no reduction or dilution will be observed in the concentration of such elements, with even a small amount of nutrient element uptake causing noticeable increases in the concentrations within the plant.

ACKNOWLEDGEMENTS

This project was supported by the scientific and technological research council of turkey (TUBİTAK) (110-O-837).

REFERENCES

[1] Kiguchi, M., Shen, Y., Kanae, S. and Oki, T. (2015). Reevaluation of future water stress due to socio-economic and climate factors under a warming climate. Hydrol. Sci. J., 60 (1):14–29.

[2] Lehner, B., Döll, P, Alcamo, J., Henrichs, T. and Kaspar, F. (2006). Estimating the impact of global change on flood and drought risks in Europe: a continental, integrated analysis Clim. Change. 75:273–299.

[3] Önder, S., Gümüş Z., Önder D. (2002). Türkiye Su Kaynaklarının Havzalar Düzeyinde Değerlendirilmesi. Su Havzalarında Toprak ve Su Kaynaklarının Korunması, Geliştirilmesi ve Yönetimi Sempozyumu. 18-20 Eylül 2002. Antakya (in Turkish). 203-209.

[4] Prudhomme, C., Giuntoli, I., Robinson, E.L., Clark, DB., Arnell, N.W., Dankers, R., Fekete, B.M., Franssen, W., Gerten, D., Gosling, S.N., Hagemann, S., Hannah, D.M. Kim, H., Masaki, Y., Satoh, Y., Stacke, T., Wada, Y. and Wisser, D. (2014). Hydrological droughts in the 21st century, hotspots and uncertainties from a global multimodel ensemble experiment. Proc. Natl. Acad. Sci. U. S. A. 111(9): 3262–3267.

[5] Wada, Y., van Beek, L.P.H. and Bierkens, M.F.P. (2011). Modeling global water stress of the recent past: on the relative importance of trends in water demand and climate variability. Hydrol. Earth Syst. Sci., 15: 3785–3808.

[6] Gikas, D.G., Dimou, D. and Tsihrintzis, A.V. (2013). River water quantity and quality monitoring in an agricultural basin in North Greece. Fresenius Environmental Bulletin. 22(7a): 2006-2016.

[7] Oikonomou, E.K. and Ioannidou, V. (2014). Implementation and evaluation of water hammer software in flow problems in irrigation networks. Fresenius Environmental Bulletin.23(11): 2785-2790.

[8] Marm, M. (2009). Estudio de la cadena de valor y formación de precios del sector cítricos. Observatorio de precios de los alimentos. Ministerio de Medio Ambiente, Rural y Marino. Gobierno de España, Madrid, Spain.

[9] Katerji, N. (1997). Les indicateurs de l'état hydrique de la plante Ch. Riou, R. Bonhomme, P. Chassin, A. Neven, F. Papy (Eds.), L'eau dans l'espace Rural: Production végétale et qualité de l'eau. Aupelf-UREF/INRA editions. France (1997). 169-177.

[10] Rana, G., Katerji, N. and Lorenzi, F. (2005). Measurement and modelling of evapotranspiration of irrigated citrus orchard under Mediterranean conditions Agric. For. Meteorol., 128:199–209.

[11] English, M.J. and Musick, J.T. (1990). Murty deficit irrigation G.J. Hoffman, K.H. Soloman (Eds.), Management of Farm Irrigation Systems, American Society of Agricultural Engineers, St. Joseph, MI. 631–663.

[12] Jurriens, M. and Wester, P. (1994). Protective irrigation in India. 1994 Annual Report International Institute for Land Reclamation and Improvement, Wageningen, the Netherlands.

[13] Saeed, H., Grove, I.G., Kettlewell, P.S. and Hall, N.W. (2008). Potential of partial rootzone drying as an alternative irrigation technique for potatoes (*Solanum tuberosum*) Ann. Appl. Biol., 152:71–80.

[14] Domínguez,A., De Juan, J.A., Tarjuelo, J.M., Martínez, R.S. and Martínez-Romero, A. (2012). Determination of optimal regulated deficit irrigation strategies for maize in a semi-arid environment. Agriculturual Water Management. 110: 67–77.

[15] Topac, F.O., Başkaya, H.S., Alkan, U. and Katkat, A.V. (2008). Variations in chemical properties and enzyme activities of soil irrigated with low quality stream water. Fresenius Environmental Bulletin.17(12a): 2020-2026.

[16] Kirda, C.R. (2002). Deficit ırrigation scheduling based on plant growth stages showing water stress tolerance. FAO (Ed.), Deficit Irrigation Practices. Food and Agriculture Organization of the United Nations, Water Reports 22 View Record in Scopus Citing articles. 32: 3–10

[17] Anonymous. (2008). Metallerle Kirlenmiş Toprakların Temizlenmesinde Fitoremediasyon Tekniği. http//www.inepo.com/english/uplFiles_resim/A%C4%9EIR (in Turkish).

[18] Önder, D. and Dağhan, H. (2007). Tarımsal Uygulamalar ve Su Kirliliği İlişkileri. 5. GAP Tarım Kongresi. 17-19 Ekim. Şanlıurfa (in Turkish)

[19] MacFarlane, G.R. and Burchett, M.D. (2000). Cellular distribution of Cu, Pb, and Zn in the grey mangrove *Avicennia marina* (Forsk.)Vierh. Aquat. Bot., 68:45–59.

[20] Grimsrud, T. and Andersen, A. (2010). Evidence of carcinogenicity in humans of

water-soluble nickel salts. J. Occup. Med. and Toxic. 5:1-7.
[21] Lukowski, A. and Wiater, J. (2009). The influence of mineral fertilization on heavy metal fraction contents in soil. Part II: Copper and Nickel. Polish J. of Environ. Stud. 18(4):645-650.
[22] Brown, P.H. (2008). Micronutrient use in agriculture in the United States of America: current practices, trends and constraints. In micronutrient deficiencies in global crop production. Alloway, Brian J. (Ed.) Springer International, Dordrecht. 267-286.
[23] Pradhan, S.P., Conrad, J.R., Conrad Paterek, J.R. and Srivastava, V.J. (1998) Potential of phytoremediation for treatment of PAHs in soil at MGP sites. J. Soil Contam., 7: 467–480.
[24] Maity N, Nema N.K., Abedy M.K., Sarkar B.K. and Mukherjee P.K. (2011). Exploring Tagetes erecta linn flower for the elastase, hyaluronidase and MMP-1 inhibitory activity. Journal of Ethnopharmacology. 137(3):1300–1305.
[25] Dağhan, H. (2004). Phytoextraction of heavy metal from contaminated soils using genetically modified plants. PhD thesis. Mathematik. Informatik und Naterwissenschaften Fakultaet der RWTH-Aachen.
[26] Wellburn, A.R. (1994). The spectral determination of chlorophylls A and B. As well as total carotenoids, using various solvents with spectrophotometers of different resolution. Journal of Plant Physiology, 144:307-313.
[27] Kacar. B., (1995). Bitki ve Toprağın Kimyasal Analizleri. III. Toprak Analizleri. A.Ü. Ziraat Fak. Eğitim. Araştırma ve Geliştirme Vakfı Yayınları No. 3. Ankara (in Turkish).
[28] Cakmak I. and Marschner H., (1992). Magnesium deficiency and high light intensity enhance activities of superoxide dismutase, ascorbate peroxidase and glutathione reductase in bean leaves. Plant Physiology. 98. 1222-1227.
[29] Bates, L. S., Waldren R.P., Teare I.D. (1973). Rapid determination of free proline for water-Stress studies. Plant and Soil, 39:205–207
[30] Kacar, B. (1972). Bitki ve toprağın kimyasal analizleri. 2. Bitki analizleri. Ankara Üniversitesi, Ziraat Fakültesi Yayınları, (in Turkish). p: 453
[31] Yurtsever, N. (1984). Deneysel İstatistik Metotları, Tarım Orman ve Köyişleri Bakanlığı, Köy Hizmetleri Genel Müdürlüğü Yayınları (in Turkish).
[32] Usta, S. (1995). Toprak Kimyası. Ankara Üniversitesi Ziraat Fak. Yayınları , No: 1387, Ders Kitabı No: 401, Ankara (in Turkish).
[33] Kabata-Pendias, A. (2011). Trace elements in soils and plants. 4th edition. CRC Press. Boca Raton.
[34] Marschner, H. (2011). Mineral nutrition of higher plants, 3rd ed.(London:Academic Press)
[35] Kacar, B. (2012). Temel Bitki Besleme. Nobel yayınevi, Ankara (in Turkish).

Received: **20.07.2015**
Accepted: **17.12.2015**

CORRESPONDING AUTHOR

Derya Önder
Cukurova University
Agricultural Faculty
Department of Agricultural Structures and Irrigation
Balcalı-Yuregir, Adana – TURKEY

e-mail: donder@cu.edu.tr
deryaonder2007@gmail.com

by PSP Volume 25 – No 1/ 2016, pages 200-209 Fresenius Environmental Bulletin

THE ABILITY OF *Brassica napus L.* TO REMOVE LEAD (Pb) FROM THE SOIL AT DIFFERENT IRRIGATION LEVELS AND Pb CONCENTRATIONS

Derya Onder[1,*], Sermet Onder[2], Hatice Daghan[3], Veli Uygur[4]

[1]Çukurova University, Faculty of Agriculture, Department of Agricultural Structer and Irrigation, Adana-Turkey
[2]Sermet Önder Irrigation Systems Company, Adana-Turkey
[3]Eskişehir Osmangazi University, Faculty of Agriculture, Department of Soil Science and Plant Nutrition, Eskisehir-Turkey
[4] Süleyman Demirel University, Faculty of Agriculture, Department of Soil Science and Plant Nutrition, Isparta-Turkey

ABSTRACT

Limited numbers of studies have been performed to date on the removal of heavy metals from the soil through phytoextraction. The number of plants species used in such studies is also restricted. One of the plants used for phytoremediation is the *Brassica*.

Four different doses of lead (0, 500, 1000, and 2000 mg Pb /kg) were applied under four different levels of irrigation (IR40, IR60, IR80, and IR100) to the plant *Brassica napus L*, which is used in the remediation of soil polluted with certain heavy metals. Therefore, the ability of *Brassica napus L* to remove lead (Pb) from the soil at different irrigation levels and Pb concentrations was investigated.

The result of current study indicated that the highest water requirement was generally observed at higher Pb doses, namely at 1000 and 2000 mg Pb/kg. Similarly, the minimum water requirement was generally observed when the Pb dose was lower. Under experimental conditions, it was determined that irrigation water requirement and water consumption for the Brassica was not significantly affected by doses of Pb. No significant differences were observed between the level of irrigation and the amount of Pb removed from the soil by the plant.

KEY WORDS:
Lead, Brassica, phytoremediation, deficit irrigation.

INTRODUCTION

Soils, which represent one of the most important and indispensable natural resources for the continuity of life, is polluted by various quantities of heavy metals as a result of human activities. Due to their high toxicity and the difficulty of their elimination/removal from natural environments, heavy metals pose a growing risk for both the environment and human health [1]. For this reason, to ensure the well-being of ecosystems and humans, it is both necessary and important to use various methods to remedy heavy metal pollution, especially for heavy metals that have reached hazardous levels. The heavy metal, lead (Pb), is an element found in the earth's crust at an average concentration of 15 mg/kg. Lead is a highly toxic metal that can accumulate over time in natural environments and living organisms. Over the past centuries, human activity has had a significant effect on the biogeochemical cycle of Pb [2]. Lead pollution is caused largely by the direct release of Pb into the atmosphere as a result of industrial and transportation-related activities. The removal of heavy metals from polluted soils is a very difficult and high cost activity. Among the different methods currently used around the world, the most environmentally friendly and low-cost approach is the use of plants for removing heavy metals from soils. There is, in fact, a clear need for an effective and applicable technological solution for eliminating heavy metal pollution in soils. Nowadays, various physical, chemical, and biological methods can be used for the reclamation of polluted soils. Phytoremediation, which is a biological reclamation method, is the most suitable and low-cost among the different methods and novel approaches that are available. Phytoremediation is defined as the use of plants to clean up contaminants from polluted soils.

Like water, soil is also a resource whose availability has decreased in recent years. Climate change has led to growing problems concerning the management of water resources. Many studies emphasize that water-related problems will become especially prominent in the near future [3, 4]. For these reasons, it is necessary to implement new strategies that will help decrease the level of water used in agricultural activities. One example of such strategies is deficit irrigation associated with many advantages such as significantly reducing the amount of water consumed while having little effect on the quantity and quality of harvests; improving productivity per unit water, as well as

profitability in agricultural activities; and improved environmental protection [5, 6]. As the availability of water resources gradually diminishes, it is very likely that deficit irrigation will be implemented on a larger scale, especially in regions where water resources are scarce [7].

The *Brassica napus* plant, which has been cultivated for over 4000 years, is an important oil crop in many regions around the world [8]. *Brassica* is also one of plant that has been used for biologically removing heavy metals such as cadmium (Cd), chromium (Cr), copper (Cu), and lead (Pb) from soils [9-14].

In this study, four different doses of Pb (0, 500, 1000, and 2000 mg Pb/kg) were applied under four different levels of irrigation (IR40, IR60, IR80, and IR100) to the *Brassica napus L*, which is used in the remediation of soil polluted with certain heavy metals.

MATERIAL AND METHODS

In the current study, Paşaköy variety of soil, which is a common type of soil found in the Amik Plain of Turkey's Eastern Mediterranean Region was used. The organic matter of the soil was 2.55 % [15], while its potassium (K), phosphorus (P), and lime contents were 77.28% [16], 19.14% [17], and 5.06% [18], respectively. The pH value of this soil was 7.56 [16], while its salt content and EC value were 0.216% and 4.35 dS/m [19], respectively. The soil had a clayey texture) [20], and a field capacity value of 43% [21]. DTPA-extractable Pb.mg/kg [22].

The plant seeds were germinated in a peat and perlite mix (1:1 ratio) [23] under a 16/8 hour light/dark cycle, at a relative humidity of 60-70%, and temperature of 22-25^{o}C. The plants were transferred to pots after they developed two to three leaves and an adequate root system. Fertilizers were provided only once to the plants at the beginning of the study was based triplicate according to a factorial experiment design in randomized parcels. The experiment was performed in a climate chamber with light, temperature, and humidity control. Different levels of irrigation were applied during the experiment. These irrigation levels were 40% of full irrigation (IR40; 60% deficit) 60% of full irrigation (IR60; 40% deficit) 80% of full irrigation (IR80; 20% deficit) and full irrigation (IR100).

A Pb solution prepared by using $Pb(NO_3)_2$ was applied to the potting soils before planting, to provide that the soils would have final Pb concentrations of 0, 500, 1000, and 2000 mg Pb /kg. The pots soils were then incubated under controlled conditions for three weeks at 80% field capacity. Immediately before planting, 200 mg/kg of N (from $(NH_4)_2SO_4$), 100 mg/kg of P, 125 mg/kg of K (from KH_2PO_4), and 2.5 mg/kg of Fe (from Fe-EDTA) was added to the soil. The experiment was performed using the *Brassica napus L* plant. *Brassica napus* L. (*B. napus*) is widely used and protein rich staple food that is also used as a source of vegetable oil. The cultivation of *B. napus* has considerably increased over the past ten years [24].

The experiment's irrigation program was initiated after the plants had a vegetation cover of 20%. All pots (IR40, IR60, IR80, and IR100) were weighed prior to irrigation. For each pot, the amount of water necessary for IR100 irrigation was calculated based on the difference between their weight at field capacity and their current weight. Irrigation at IR_{80}, IR_{60}, and IR_{40} was performed by applying 80%, 60%, and 40% of water calculated for IR_{100} respectively. Irrigation was performed every three days. This irrigation program was continued until the time of harvest.

After being transferred to pots, plants were grown until they reached their highest biomass (for approximately six weeks). Certain morphological and phonological observations were also made during the experiment. The leaves area was measured at the time of harvest, and the fresh (FW) and dry weights (DW) of the shoots (plants above ground biomass) were determined. The chlorophyll content of the leaves was measured using the Konica-Minolta SPAD-502 device according to [25] method.

The physiological changes of the plants, as well as the levels of sulfhydryl group/reduced glutathione (–SH), superoxide dismutase (SOD), and proline, which are enzymes/chemicals that eliminate reactive oxygen species were also evaluated. To assay the enzymes/chemicals in question, fresh leaf samples were collected from shoot, weighed, and then subjected to chemical content analysis.

The cadmium (Cd), lead (Pb), nickel (Ni), zinc (Zn), copper (Cu), iron (Fe), manganese (Mn), calcium (Ca), and magnesium (Mg) concentrations of the shoots were determined by Inductively Coupled Plasma-Atomic Emission Spectrometry (ICP-AES; Varian Series-II). Potassium (K) and sodium (Na) concentrations were measured with a flame photometer using the wet decomposition method [26]. The analysis of -SH (reduced glutathione) and (SOD) superoxide dismutase activity in the plant samples was performed according to [27]. Proline concentration was determined according to [28]. Nitrogen (N) analysis of the plant samples was performed according to the Kjheldal method, while the ICP-AES device

was used for the phosphor (P) analysis of the plant samples [29].

Analysis of variance for data was performed using the SPSS-17 statistical analysis program, and according to the factorial experiment design in random parcels. Comparisons between means were performed using the LSD test [30].

RESULTS AND DISCUSSION

The effect of different lead doses and irrigation levels on the water requirement and water consumption of the *Brassica napus* L is shown in Figure 1.

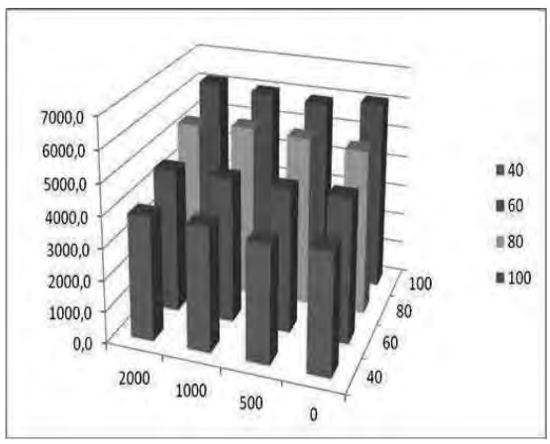

FIGURE 1
Water requirement of the *Brassica napus* L. at different irrigation levels and Pb doses.

The plants' water requirements (i.e. the amount of irrigation water used) decreased gradually from IR100 to IR40. On the other hand, with the exception of plants that received Pb at a dose of 500 mg/kg, the application of Pb had the effect of slightly increasing the amount of water used in comparison to plants that were not administered with Pb. However, these differences were negligible. At all irrigation levels, the effect of the different Pb doses on the plants' water requirement was very similar. The results indicate that the highest water requirement was generally observed at the highest Pb doses of 1000 and 2000 mg/kg. On the other hand, the minimum water requirement was generally observed at the lowest Pb doses. The relationship between Pb doses and plant water consumption was similar to the relationship between Pb doses and water requirement (Figure 2). However, plants under no water stress (IR100) and the highest level of water stress (IR40) showed higher levels of water consumption than the other plants. Based on these results, it is possible to state that the water requirement and water consumption of the *Brassica* was not significantly affected by the dose Pb.

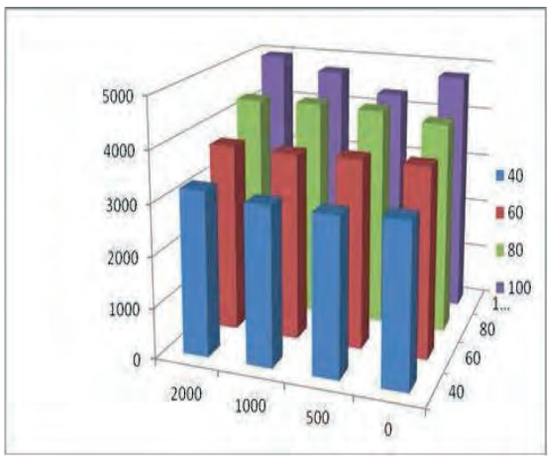

FIGURE 2
Water consumption of the *Brassica napus* L. at different irrigation levels and Pb doses.

Table 1 shows the variance analysis concerning the effect of different Pb doses and irrigation levels on the *Brassica* plant's different growth parameters their shoot and root biomass, chlorophyll, and leaf area. Lead had a significant effect on all of the plant growth parameters. The level of irrigation affected all growth parameters, except for the chlorophyll content of the plants' older leaves. In addition, the interaction of Pb doses and irrigation levels had no significant effect on any of these parameters.

An evaluation of the effect of irrigation levels and Pb doses on the growth performance parameters indicated the existence of different groups with respect to FW and DW. The FW of the plant varied between 46.8 and 78.3 g/shoot depending on the level of irrigation, while the FW of Pb-applied plants varied between a narrower range of 57.7 and 65.0 g/shoot. This indicated that between these two stress factors, the level of irrigation had a more limiting effect on plant growth.

TABLE 1
Multivariate analysis of the growth performance of *Brassica* plants under different Pb and irrigation levels.

Variation Source	Variable	D.F.	Mean Squares	F
Heavy Metal Doses (HMD)	Shoot FWs	3	202.710	8.710**
	Shoot DWs	3	4.359	8.143**
	Root DWs	3	0.187	10.260**
	Chlorophyll old leaves	3	48.206	10.477**
	Chlorophyll young leaves	3	32.132	4.693**
	Leaves Area (LA)	3	149727.515	8.824**
Irrigation Level (IR)	Shoot FWs	3	2143.059	92.084**
	Shoot DWs	3	32.952	61.552**
	Root DWs	3	0.134	7.315**
	Chlorophyll old leaves	3	7.937	1.725
	Chlorophyll young leaves	3	61.129	8.929**
	Leaves Area (LA)	3	379063.552	22.340**
Interreaction (HMDxIR)	Shoot FWs	9	22.769	0.978
	Shoot DWs	9	0.548	1.023
	Root DWs	9	0.034	1.871
	Chlorophyll old leaves	9	8.599	1.869
	Chlorophyll young leaves	9	7.383	1.078
	Leaves Area (LA)	9	16770.381	0.988

*Significance level of P=0.05, **Significance level of P<0.01.

The highest level of chlorophyll in the old leaves was observed at the 1000 mg/kg Pb application, which was also associated with the highest level of biomass. In terms of the highest levels of chlorophyll in the old leaves, the 1000 mg/kg Pb dose was followed by 2000 mg/kg Pb dose, the control group, and the 500 mg/kg Pb dose. In other words, the chlorophyll content of the older leaves did not vary or change in a single direction depending on the Pb dose. The plants' younger leaves, on the other hand, displayed a different behavior, with higher Pb concentrations being associated with higher chlorophyll levels. It was observed that only the 60% irrigation level was associated with lower chlorophyll content in the older leaves compared to the other irrigation levels; according to the LSD test, irrigation levels had not significant effect. In the younger leaves, on the other hand, an increase in irrigation level was associated with an increase in chlorophyll content (Table 2). This indicates that the level of water stress affected the accumulation of nutrient elements and/or metabolites in younger leaves. The leaf area, the FW,the DW and root DW exhibited parallel behaviors. The largest leaf area was observed in the control plants (1278.3 cm^2/ plant); which was followed by the 100 mg/kg Pb dose, the 500 mg/kg Pb dose, and the 2000 mg/kg Pb dose. While the leaf area of the *Brassica* plants varied between 1019.9 and 1278.3 cm^2 depending on the Pb dose, the leaf area varied over a greater range between 945.7 and 1374.9 cm^2 depending on the level of irrigation. In addition, according to the LSD test, the 80% and 60% irrigation levels formed a single group with respect to leaf area; while other irrigation levels (100% and 40%) each formed a separate group.

The application of Pb had the effect of enhancing root weight, and increasing Pb doses gradually increased the root biomass (DWs) from 0.611 g/root to 0.894 g/root (Table 2). Increasing irrigation levels similarly increased the amount of root biomass produced.

According to the LSD test, the lower irrigation levels of 40% and 60% formed a single group with respect to root biomass, while the higher irrigation levels (80% and 100%) formed a single separate group. This indicates that an irrigation level of 80% can be used to achieve maximum root development in phytoremediation studies.

TABLE 2
The effect of Pb doses and irrigation levels on the growth performance parameters of the *Brassica* plant

Stress Factors	Shoot FWs (g/shoot)	Shoot DWs (g/shoot)	Chlorophyll old leaves	Chlorophyll young leaves	Leaf Area (cm^2)	Root DWs (g/root)
Pb 0 mg/kg	65.0 ab	8.2 a	33.1 bc	46.3 b	1278.3 a	0.611 c
Pb 500 mg/kg	62.8 b	8.5 a	31.8 c	46.4 b	1139.5 b	0.656 bc
Pb 1000 mg/kg	67.2 a	8.7 a	36.5 a	49.5 a	1218.9 ab	0.746 b
Pb 2000 mg/kg	57.7 c	7.3 b	33.9 b	48.7a	1019.9 c	0.894 a
IR %40	46.8 D	6.1 D	34.3 N.S	50.0 A	945.7 C	0.608 B
IR %60	59.4 C	7.8 C	32.6 N.S	48.4 AB	1132.1 B	0.669 B
IR %80	68.2 B	8.7 B	34.1 N.S	47.9 B	1203.9 B	0.797 A
IR %100	78.3 A	10.1 A	34.3 N.S	44.6 C	1374.9 A	0.833 A

Different letters (upper case letters used for irrigation levels and lower case letters used for heavy metal applications) indicate that the difference between the relevant items is greater than the 5% significance level. n.s: no significant

The P, K, and Mg concentrations within the shoots were not significantly affected by these two stress factors, with their behavior showing very minor changes according to the degree/level of the stress factors.

Table 3 provides the results of the multivariate analysis regarding the effect of different Pb doses and irrigation levels on the microelement concentration in shoots; the total amount of Pb content by the shoot; and the concentration of Pb in the roots. Different Pb doses only affected the Pb concentrations in the plant tissues and the Pb content, while having no significant effect on the concentrations of other microelements. The level of irrigation also had no significant effect on any of the microelements. The interaction of the Pb doses and irrigation levels had a significant effect on the Pb concentration and the Pb content.

An evaluation of the effect of heavy metal and water stress on the concentration of microelements in the shoots revealed that these sources of stress did not have a significant effect on the levels of Fe, Cu, Mn, and Zn (Table 4). Only the Pb in the shoots increased with increasing Pb doses. According to the LSD test, the average values determined for each Pb dose application formed a separate group.

However, despite the high concentrations of Pb applied to the plants, the concentration of Pb in the plant tissues still remained at trace levels compared to the other elements.

TABLE 3
Multivariate analysis of the effect of different Pb doses and irrigation levels on the microelement concentrations in plant parts above the surface; the total amount of Pb removed from the soil by the plant parts above the surface; and the concentration of Pb in the roots of the *Brassica* plant.

Variation Source	Variable	D.F.	Mean Squares	F
Heavy Metal Doses (HMD)	Fe	3	87010.23	1.060
	Cu	3	2.693851	0.292
	Mn	3	2386.777	0.500
	Zn	3	43.98961	0.298
	Pb	3	39.75293	41.875**
	Pb removed	3	2265.74	26.226**
Irrigation Level (IR)	Fe	3	93070.17	1.134
	Cu	3	7.878506	0.855
	Mn	3	6258.819	1.312
	Zn	3	187.2435	1.269
	Pb	3	2.57329	2.711
	Pb removed	3	204.5663	2.368
Interreaction (HMDxIR)	Fe	9	82662.32	1.007
	Cu	9	2.750805	0.299
	Mn	9	4359.429	0.914
	Zn	9	170.616	1.157
	Pb	9	3.04415	3.207**
	Pb removed	9	206.4705	2.390*

*Significance level of P=0.05, **Significance level of P<0.01

TABLE 4
The mean Fe, Cu, Mn, Zn, and Pb concentrations and the Pb content by the *Brassica* plant.

Stress Factors	Fe	Cu	Mn	Zn	Pb Consentration	Pb Content
	mg/kg					µg/shoot
Pb 0 mg/kg	104.5 n.s	11.9 n.s	114.3 n.s	10.12 n.s	0.27 d	2.11 c
Pb 10 mg/kg	262.4 n.s	12.3 n.s	140.6 n.s	7.66 n.s	2.60 c	20.8 b
Pb 20 mg/kg	84.2 n.s	13.0 n.s	109.5 n.s	10.18 n.s	3.31 b	29.0 a
Pb 40 mg/kg	90.1 n.s	12.1 n.s	114.4 n.s	6.30 n.s	4.62 a	33.1 a
IR %40	100.1 N.S	11.9 N.S	108.8 N.S	4.09 N.S	3.13 N.S	19.0 N.S
IR %60	266.0 N.S	13.5 N.S	153.4 N.S	11.09 N.S	2.91 N.S	22.1 N.S
IR %80	73.4 N.S	12.2 N.S	103.4 N.S	12.59 N.S	2.05 N.S	17.3 N.S
IR %100	101.8 N.S	11.8 N.S	113.2 N.S	6.50 N.S	2.72 N.S	26.7 N.S

Different letters indicate that the difference between the relevant items is greater than the 5% significance level. n.s: not significant

Although the Pb concentration varied in the range of 0.27 to 4.62 mg/kg, a significant difference was identified between the different Pb dose applications. An evaluation of the effect of the irrigation level indicated that the highest values were obtained at 40% and 60% irrigation.

The amount of Pb content increased in parallel with the applied dose of Pb. According to the LSD test, each applied dose of Pb formed a different

group with respect to the amount of Pb content (Table 4). The irrigation levels, on the other hand, had not significant effect according to the LSD test.

The multivariate analysis regarding the *Brassica* plants' biochemical response to different Pb doses and irrigation levels is shown in Table 5. The plants showed a significant reaction to higher levels of Pb and water stress by activating their SOD and -SH defense mechanisms. The interactions of these two stress factors had a significant effect on the SOD biochemical parameter.

TABLE 5
Multivariate analysis of the *Brassica* plants' biochemical response to Pb and water stress

Variation Source	Variable	D.F.	Mean Squares	F
Heavy Metal Doses (HMD)	-SH concentration	3	12641.983	5.575**
	SOD concentration	3	207.730	14.655**
	Prolin concentration	3	3227.266	1.984
Irrigation Levels (IR)	-SH concentration	3	23941.255	10.558**
	SOD concentration	3	1757.791	124.005**
	Prolin concentration	3	1237.367	0.761
Interreaction (HMDxIR)	-SH concentration	9	2367.159	1.044
	SOD concentration	9	128.031	9.032**
	Prolin concentration	9	2822.306	1.735

*Significance level of P=0.05, **Significance level of P<0.01.

The effect of the Pb doses and irrigation levels on the biochemical parameters is shown in Table 5. The -SH concentration gradually increased as the Pb level increased to 1000 mg/kg; however, further increased in Pb levels led to a decrease in -SH concentrations. At all applied doses of Pb, the level of -SH activity was higher compared to the controls. An evaluation of the effect of irrigation levels showed that increasing water stress increased the -SH concentration from 205.0 at 100% irrigation to 302.4 at 40% irrigation. According to the LSD test, irrigation levels of 60-80% and higher formed a single group, while irrigation at 40% formed a separate group.

The highest SOD value observed at a Pb dose of 0 was 3.7 µL/g FW. The SOD activity at 500 mg/kg Pb application was 13.2 µL/g FW, which is the lowest level of activity among Pb-applied plants (Table 6). According to the LSD test, three groups were identified with respect to the effect of Pb on SOD activity: the control, 500, 1000, 2000 mg/kg Pb doses. Many researchers have reported that different doses of Pb can either increase or decrease SOD activity depending on the plant. [31] Previously reported that SOD activity in *Oriza sativa* decreased with increasing Pb doses, while [32, 33], respectively, reported that increasing Pb doses increased SOD activity in *Triticum aestivum* and *Potamogeton crispus*. According to the LSD test, three groups were identified with respect to the effect of irrigation level on SOD activity: the 40% irrigation level had the lowest SOD activity (i.e. required the highest amount of plant extract to reduce NBT concentration by half), while increasing irrigation levels led to higher SOD activity.

The multivariate analysis indicated that the effect of the two stress factors on proline levels was not significant.

TABLE 6
The effect of different Pb doses and irrigation levels on the *Brassica* plants' biochemical parameters.

Stress Factors	-SH (µg/g shoot FW)	SOD (µL/g shoot FW)	Prolin (µmol/gshoot FW)
Pb 0 mg/kg	191.8 b	3.7 c	217.5 n.s
Pb 500 mg/kg	256.0 a	13.2 a	186.0 n.s
Pb 1000 mg/kg	264.5 a	11.0 a	187.1 n.s
pb 2000 mg/kg	238.4 a	7.4 b	181.9 n.s
Irrigation Level (IR) %40	302.4 A	26.2 A	188.8 N.S
Irrigation Level (IR) %60	211.4 B	8.2 B	206.4 N.S
Irrigation Level (IR) %80	232.0 B	0.4 C	194.6 N.S
Irrigation Level (IR) %100	205.0 B	0.6 C	182.6 N.S

Different letters (upper case letters used for irrigation levels and lower case letters used for heavy metal applications) indicate that the difference between the relevant items is greater than the 5% significance level.
n.s: not significant

CONCLUSION

Brassica napus L. reacted to both heavy metal stress and water stress by decreasing its biomass levels and leaf surface area.

The application of heavy metal and water stress significantly affected not only the concentrations of heavy metals within the plants, but also the levels of the plant nutrients analysed. This was possibly due to mechanisms such as the reaction of heavy metals with the elements in the soil; the alteration of element uptake by the plants due to the heavy metal's effects on plant root development and water consumption; the interaction of elements within the plant; and the dilution effect.

It was observed that the *Brassica* plants exhibited biochemical responses to heavy metal and water stress, and that one or several of the enzymes/substances -SH, SOD.

Independently of the level of irrigation, the level of Pb content by *Brassica* varied between 2.11 and 33.1 µg/ shoot. The highest level of Pb was removed at an irrigation level of 100%. A study performed by [34] determined that *Brassica* has the highest level of Cu and Zn uptake (or removal) at higher soil moisture levels. Higher levels of heavy metal stress in *Brassica* plants (due to the application of high lead doses) was associated with an 11.5% biomass loss compared to the controls.

The results of this study indicated that higher irrigation levels had a positive effect of the development of *Brassica napus* L. plants, which in turn increased the amounts of Pb they removed from the soil, and hence their effectiveness in soil phytoremediation. The results also suggested that growing plants at an irrigation level of 100% (IR100) offered the best advantages in terms of higher biomass and efficient Pb removal.

ACKNOWLEDGEMENTS

This project was supported by the scientific and technological research council of turkey (TUBİTAK) (110-O-837).

REFERENCES

[1] Yanez, L., Ortiz, D., Calderon, J., Batres, L., Carrizales, L., Mejia, J., Martinez, L., Garcia-Nieto, E. and Diaz-Barriga. F. (2002). Overview of human health and chemical mixtures: problems facing developing countries.Environ. Health Perspect, 110 (6): 901–909.

[2] Komárek, M., Ettler, V., Chrastn, V. and Mihaljevic, M. (2008). Lead isotopes in environmental sciences: a review. Environment International. 34: 562-577.

[3] Rijsberman, F.R. (2006). Water scarcity: factor or fiction. Agricultural Water Management. 80:5-212.

[4] EU (2007). Addressing the challenge of water scarcity and droughts in the European Union, communication from the commission to the European parliament and the council, Eur. Comm., DG Environ., Brussels.

[5] Onder, S., Kanber R., Onder D., Kapur B. (2005). Global iklim değişimlerine bağlı olarak sulama yöntem ve işletim tekniklerinde gelecekte ortaya çıkabilecek değişiklikler. GAP IV. Tarım Kongresi, 23.09.2005, Şanlıurfa (in Turkish). 1128-1135.

[6] Fereres, E. and Soriano, M.A. (2007). Deficit irrigation for reducing agricultural water use. J. Exp. Bot., 58:147–159.

[7] Aragüés, R., Medina, E.T., Martínez-Cob, A. and Faci, J. (2014). Effects of deficit irrigation strategies on soil salinization and sodification in a semiarid drip-irrigated peach orchard. Agricultural Water Management. 142:1-9.

[8] Ericson, M., Rödin, J., Lenman, M., Glimelius, K., L., Josefsson, G. and Rask, L. (1986). Structure of the rapeseed 1.7 S storage protein, napin, and its precursor. J. Biol. Chem., 261:14576–14581.

[9] Kanwal, U., Ali, S., Shakoor, M.B., Farid, M., Hussain, S., Yasmeen, T., Adrees, M., Bharwana, S.A. and Abbas, F. (2014). EDTA ameliorates phytoextraction of lead and plant growth by reducing morphological and biochemical injuries in *Brassica napus* L. under lead stress. Environ. Sci. Pollut. Res. 21:9899–9910.

[10] Rizwan, M., Meunier, J.D., Miche, H. and Keller, C. (2012). Effect of silicon on reducing cadmium toxicity in durum wheat (*Triticum turgidum* L. cv. Claudio W.) grown in a soil with aged contamination. J. Hazard Mater. 209:326–334.

[11] Wuana, R.A. and Okieimen, F.E. (2011). Heavy metals in contaminated soils: a review of sources, chemistry, risks and best available strategies for remediation. ISRN Ecol. Article ID 402647.

[12] Barajas-Aceves, M., Camarillo-Ravelo, D., Juarez-Sanches, F. and Rodriguez-Vazquez, R. (2012). Lead and zinc distrubition in Brassica juncea and arid soil amended with mine tailing and bokash. Fresenius Environmental Bulletin. 21(9): 2626-2637.

[13] Novo, L. and González, L. (2013). The effects of variable soil moisture on the phytoextraction of Cd and Zn by Brassica juncea. Fresenius Environmental Bulletin. 22(1a): 299-304.

[14] Novo, L., Manousaki, E., Kalogerakis. N. and González, L. (2014). The effect of cadmium and salinity on germination and early growth of Brassica juncea (L.) var. juncea. Fresenius Environmental Bulletin. 22(12a): 3709-3717.

[15] Nelson, D. and Sommers, L.E.(1996). Total carbon, organic carbon, and organic matter. In: methods of soil analysis, Ed: D.L. Spark, Madison, Wisconsin, USA. 961-1010.

[16] Richards, L.A. 1954. Diagnosis and Improvement of Saline and Alkali Soils. United States Department.

[17] Olsen, S.R., Cole C.V., Watanabe F.S. and Dean L.A. (1954). Estimation of Available Phosphorus in Soils by Extraction with Sodium Bicarbonate. US Dept. Of Agric. Cric. 939.

[18] Loeppert, R. H. and Suarez, D. L. (1996). Carbonate and Gypsum. In Methods of soil analysis. Part 3. Chemical Methods. pp. 437-474. Edited by D.L. Spark. Madison. Wisconsin. USA.

[19] Soil Survey Staff 1951. Soil Survey Manual. U.S. Department of Agriculture, Handbook No,18. U.S Goverment Print Office. Washington.

[20] Bouyoucus, G. J. (1952). "A Recalibration of Hydrometer for Making Mechanical Analysis of Soils". Agronomy Journal. 43:434-438.

[21] Alpaslan, M., Güneş, A. and İnal, A. (1998). Deneme Tekniği. Ankara Üniversitesi Ziraat Fakültesi Yayınları No,1502. Ders Kitabı, 455.

[22] Lindsay, W.L. and Norvell W.A. (1978). Development of a DTPA test for zinc, iron, manganese, and copper. Soil Sci. Soc. Amer. J. 42:421-428

[23] Daghan, H. (2004). Phytoextraction of heavy metal from contaminated soils using genetically modified plants. PhD thesis, Mathematic informatik und naterwissenschaften fakultaet der RWTH-Aachen.

[24] Yang, H., Liu, J., Huang, S., Guo, T., Deng, L. and Hua, W. (2014). Selection and evaluation of novel reference genes for quantitative reverse transcription PCR (qRT-PCR) based on genome and transcriptome data in *Brassica napus* L. Gene. 538(1):113-122.

[25] Wellburn, A.R. (1994). The spectral determination of chlorophylls a and b as well as total carotenoids, using various solvents with spectrophotometers of different resolution. Journal of Plant Physiology, 144:307-313.

[26] Kacar. B. (1995). Bitki ve toprağın kimyasal analizleri. III. Toprak analizleri. A.Ü. Ziraat Fak. Eğitim Araştırma ve Geliştirme Vakfı Yayınları No:3. Ankara (in Turkish).

[27] Cakmak, I. and Marschner, H. (1992). Magnesium deficiency and high light intensity enhance activities of superoxide dismutase, ascorbate peroxidase and glutathione reductase in bean leaves. Plant physiology. 98:1222-1227.

[28] Bates, L.S., Waldren R.P. and Teare, I.D. (1973). Rapid determination of free proline for water-stress studies. Plant and Soil, 39:205–207.

[29] Kacar, B. (1972). Bitki ve toprağın kimyasal analizleri. 2. Bitki Analizleri. Ankara Üniversitesi Ziraat Fakültesi Yayınları, 453 Ank. Üniv. Basımevi Ankara (in Turkish).

[30] Yurtsever, N. (1984). Deneysel İstatistik Metotları, Tarım Orman ve Köyişleri Bakanlığı, Köy Hizmetleri Genel Müdürlüğü Yayınları (in Turkish).
[31] Panda, P., Nath, S., Chanu, T.T., Sharma, G.D. and Panda, S.K. (2011). Cadmium stress-induced oxidative stress and role of nitric oxide in rice oryza sativa l. Acta Physiol Plant. 33:1737–1747.
[32] Lamhamdi, M, Bakrim A., Aarab A., Lafont R. and Sayah, F. (2011). Lead phytotoxicity on wheat triticum aestivum l. seed germination and seedlings growth. C R Biology. 334:118–126.
[33] Hua, B. and Guo, W.Y. (2002). Effect of exogenous proline on SOD and POD activity of Soyabean callus under salt stress. Acta Agriculturae Boreali-Sinica, 17:37–40.
[34] Novo, L.A.B. and Gonzalez, L. (2014). The influence of soil moisture on brassica juncea grown in copper mine soil amended with technosol and its impact on phytoremediation. Fresenius environmental bulletin. 23(7): 1560-1563.

Received: **20.07.2015**
Accepted: **17.12.2015**

CORRESPONDING AUTHOR

Derya Önder
Cukurova University
Agricultural Faculty
Department of Agricultural Structures and Irrigation
Balcalı-Yuregir, Adana – TURKEY

e-mail: donder@cu.edu.tr,
deryaonder2007@gmail.com

by PSP Volume 25 – No 1/ 2016, pages 210-218 Fresenius Environmental Bulletin

ADSORPTION OF POLYVINYL ALCOHOL BY LOW-COST ACTIVATED COKE

Zilin Meng[1], Yihe Zhang[1*], Qian Zhang[1], Guocheng Lv[1], Fengzhu Lv[1], Bin Fei[2], Pan Hu[1]

[1]Beijing Key Laboratory of Materials Utilization of Nonmetallic Minerals and Solid Wastes, National Laboratory of Mineral Materials, School of Materials Science and Technology, China University of Geosciences, Beijing, 100083
[2]Institute of Textile and Clothing, The Hong Kong Polytechnic University, Kowloon, Hong Kong, China

ABSTRACT

In this study, low-cost activated coke (AC) was used as absorbents to remove polyvinyl alcohol (PVA) from wastewater and zeolite with similar surface area and pore volume was employed as check experiment to analyze the relevant mechanism. The adsorption kinetics were studied and the data well fitted the pseudo-second-order kinetics model to various initial PVA concentrations both AC and zeolite. The adsorption process was controlled by external mass transfer and Freundlich isotherm model fitted the equilibrium adsorption data better than Langmuir. Adsorption effect of AC (8.63 mg/g) was far better than that of zeolite (1.42 mg/g) at 100 mg/L initial concentration. Thermodynamic parameters were also calculated indicating that the process was physical adsorption. The formation of hydrogen bonding was the main factor of adsorption mechanisms and FT-IR also proved the same conclusion.

KEYWORDS:
Adsorption; Activated coke; polyvinyl alcohol; Mechanism

INTRODUCTION

Polyvinyl alcohol (PVA) is a water-soluble polymer, which is prepared by the hydrolysis of polyvinyl acetate. PVA is widely used in the textile, pharmaceutical and paper coating industry for its good flexibility, high tensile strength, chemical stability, water-solubility and good film-forming capability [1]. PVA as a refractory organic whose ratio of BOD_5 to COD is low to 0.1 is difficult to be biodegraded. Lots of discharged PVA are harmful to the environment and accumulate in the human body via the food chain.

Many studies have been reported to remove PVA. Physical methods such as adsorption [2], electrocoagulation [3] and membranes [4] are used to treat PVA wastewater. Chemical methods were focused on oxidation such as wet air oxidation [5], Fenton Oxidation [6], supercritical water gasification [1], electrochemical oxidation [7], photo catalysis [8] and ionizing radiation [9]. Chemical methods convert PVA to CO_2 and H_2O as a pretreatment followed by bio-treatment. The biological methods [10] using activated sludge process aimed at degrading the organic pollutants by microorganism.

Carbon-based materials possess large surface area [11, 12], extensive sources [13-15] and favorable affinity to organic contaminants [16]. Activated coke (AC) which is much cheaper also own those similar advantages. AC is produced from naturally carbonaceous materials like lignite, petroleum coke, wood and other biomasses [17], which often are treated as waste in industry. Appropriate use of AC is a reuse to industrial waste and environmental sustainable [18]. However, there are still no studies reported on the adsorption treatment of PVA wastewater by AC or zeolite. Therefore, in the present study the mechanisms of AC as an adsorbent for removal of PVA by batch experiments was analyzed. Zeolite was selected as a comparison to explain the adsorption mechanism. The relevant dynamics, isotherm and thermodynamics were also analyzed. The adsorption mechanism was also put forward and mutual authentication for the relevant data. The adsorption of removal PVA on AC has reference meaning for PVA treatment in the future research.

MATERIALS AND METHODS

Materials. The AC made by lignite was supplied by Datang Yima coke plant and Zeolites were taken from Hencheng Water purification materials plant. The selected AC and zeolite have similar surface area and pore volume (shown in Table 1).

TABLE 1
Physical properties for the AC and Zeolite

	Surface area (m^2/g)	Pore volume (cm^3/g)
Activated Coke	439.7	0.271
Zeolite	3984.	0.238

AC and zeolite were washed with distilled water and dried in the oven at 80 °C for 24h. The PVA was purchased from Tianjin Fuchen Chemical Plant.

Batch equilibrium studies. Batch adsorption experiments were carried out using 0.5g AC or zeolite as the adsorbent in a 100ml flask, containing 50ml PVA solution. The samples were shaken at 150rpm in a SHA-BA water bath. The adsorption isotherms were carried out at 303K, 313K and 323K with different initial concentrations (100-500mg/L). Samples were separated by filtration. The concentrations of PVA were determined at the wavelength of 640nm using an uv-vis spectrophotometer by reacting with appropriate amounts of I_2-KI and boric acid solution. The amount of PVA adsorbed by adsorbent was calculated by:

$$q_e = \frac{(C_0 - C_e)V}{M}$$

where q_e (mg/g) is the amount of adsorption at equilibrium; C_0 (mg/L) and C_e (mg/L) are the initial and final or equilibrium concentrations in the solution; M (g) is mass of adsorbent and V (L) is volume of solution.

Characterization. The Fourier transform infrared (FT-IR) spectra of AC and zeolites were acquired on a Perkin Elmer spectrum 100 (Waltha, MA, USA). The samples were prepared using the KBr pressed-disk method and the samples were scanned in the range of 450-4000cm^{-1}. BET surface area was measured using an ASAP 2010 Micrometrics instrument.

RESULTS AND DISCUSSION

Adsorption kinetics. The kinetics that describe the solute uptake rate governing the residence time of the adsorption reaction is one of the important characteristics defining the efficiency of sorption [19]. The relationship between contact time and absorbed PVA onto AC and zeolite at different initial was shown in Fig. 1.

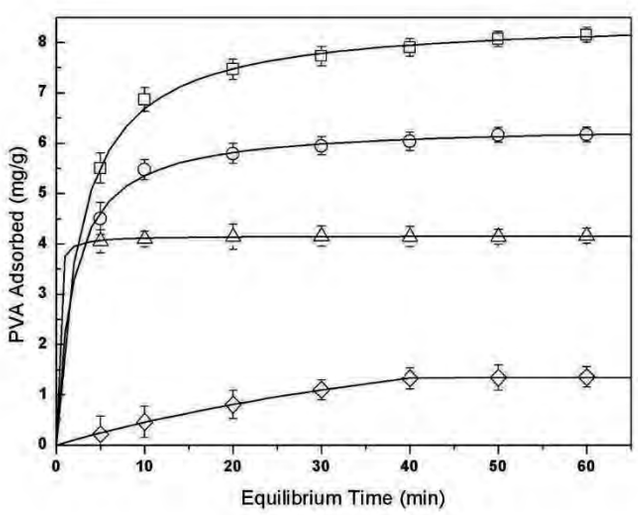

FIGURE 1
Adsorption kinetics for PVA onto activated coke (C_0=100mg/L,□; 75mg/L,○;50mg/L, Δ), and onto zeolite (C_0=100mg/L,◇). The solid lines are the Pseudo-second-order model fits to the observed data.

From the Fig. 1, it is observed that PVA uptake was fast in the first 10 min, thereafter the adsorption kinetics decreased progressively and finally the adsorption approached to the equilibrium in all the case. The fast adsorption at the initial stage was probably because of the increased concentration gradient between the adsorbate in the solution and adsorbate in adsorbent where many vacant sites were available at the beginning. The progressive increase in the adsorption process and consequently the attainment of equilibrium adsorption may be due to lim-

ited mass transfer of the adsorbate molecules from the bulk liquid to the external surface of AC. In the later stage, diffusion must break through the barrier of adsorbed PVA and it was also slow for internal mass transfer within AC particles. The adsorption capacities corresponding to equilibrium adsorption increased from 4.16 to 8.15mg/g with the increased initial PVA concentration 50 to 100 mg/L. It was also shown that the zeolite had little adsorption effect and the amount of PVA adsorbed was 0.6mg/g. According to adsorption equilibrium removal efficiency, it was 92.33% and 26.44% by AC and zeolite, respectively.

The adsorption of PVA onto AC was evaluated by utilizing commonly used kinetic models including the Pseudo-first-order model and the Pseudo-second-order model [20]. The Pseudo-first-order model presents as the following form:

$$\frac{dq}{dt} = k_1(q_e - q)$$

where q_e (mg/g) and q (mg/g) refer to the amount of PVA adsorbed at equilibrium and at any time. k_1 (min^{-1}) is the equilibrium rate constant of pseudo-first-order sorption and t (min) is time. The pseudo-second-order model assumes that the rate-limiting step is chemical adsorption and predicts the behavior over the whole range of adsorption. Currently the pseudo-second-order model has been widely used for sorption systems due to its good representation of the experimental data for most of the adsorbent adsorbate systems. The model presents as the following form:

$$\frac{dq}{dt} = k_2(q_e - q)^2$$

where k_2(g/mg·min) is the equilibrium rate constant of pseudo-first-order sorption. The nature of the adsorption process will depend on physical or chemical characteristics of the adsorbent system. The kinetic constants and the correlation coefficients (R^2) were given in Table 2.

TABLE 2
Comparison of the first- and second-order adsorption rate constants and calculated and experimental q_e values for different initial concentrations

Initial concentration (mg/L)	$q_{e,exp}$ (mg/g)	Pseudo-first-order kinetics			Pseudo-second-order kinetics		
		$k_1(min^{-1})$	q_e(mg/g)	R^2	$k_2(min^{-1})$	q_e(mg/g)	R^2
50	4.27	0.003	0.15	0.376	2.240	4.16	1.000
75	6.28	0.018	1.17	0.977	0.084	6.36	1.000
100	8.63	0.011	2.06	0.980	0.044	8.48	1.000
500	26.25	0.006	12.51	0.977	0.0007	22.22	0.996

The correlation coefficient (R^2) for the pseudo-first-order model (R^2=0.980) was relatively lower than that of pseudo-second-order model (R^2=1.000). The calculated equilibrium adsorption capacity (q_e=8.63mg/g) had great difference from the experimental value ($q_{e,exp}$=2.06mg/g). It indicated that the pseudo-first-order model cannot describe PVA absorbed onto AC exactly. The equilibrium PVA amount from the experimental date (qe=8.63 mg/g) was in accordance with the calculated values ($q_{e,exp}$=8.48 mg/g).

Prediction of rate-determining step is important for the design purpose. Generally, for a solid liquid adsorption process, the solute transfer is usually characterized by either external mass transfer or intraparticle diffusion or both [21]. The overall rate of sorption will be controlled by the slowest step, which would be either film diffusion or pore diffusion. However, the controlling step might be distributed between intraparticle and external transport mechanisms. In order to predict the actual slow step involved, the kinetic data were further analyzed using the Boyd kinetic expression. The Boyd kinetic expression is given by

$$F = 1 - \frac{6}{\pi^2}\exp(-Bt) \text{ and } F = \frac{q}{q_e}$$

where F represents the fraction of solute adsorbed at any time, and Bt is a mathematical function of F.

The calculated Bt values were plotted against t as shown in Fig. 2 and identified whether external transport or intraparticle transport control the rate of sorption.

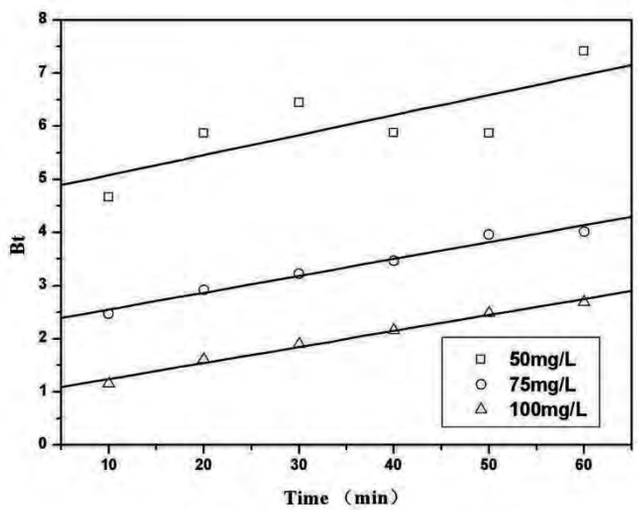

FIGURE 2
Plot of Bt versus t (Boyd plot)

Fig.2 showed that the Boyd plot was linear and did not pass through the origin suggesting that the external mass transfer mainly governs the rate of the reaction.

Adsorption isotherms. The adsorption isotherm indicates the functional relationship between the amount of solute adsorbed per unit weight of the adsorbent and the concentration of adsorbate in bulk solution at a given temperature under equilibrium conditions. It plays an important role in predictive modeling procedures for analysis and design of adsorption systems. Langmuir and Freundlich models have been developed and employed for such analysis [22]. Langmuir isotherm assumes monolayer adsorption onto a surface containing a set of well-defined localized adsorption sites of the same adsorption energy with no transmigration between adsorbed molecules. The theoretical Langmuir isotherm equation can be given by:

$$q_e = \frac{Q_0 b C_e}{1 + b C_e}$$

where Q_0 is a Langmuir adsorption constant reflecting the maximum adsorption capacity (mg/g), b is also a constant. R_L, the separation factor, is defined to estimate the adsorption condition. And the equation is given by:

$$R_L = \frac{1}{1 + b C_0}$$

Freundlich isotherm assumes the surface heterogeneity and encompassed exponential distribution of the active sites and their energies. The empirical Freundlich isotherm equation can be given by:

$$q_e = K_F C_e^{1/n}$$

where K_F ((mg/g)(L/mg)$^{1/n}$) and n (dimensionless) are the Freundlich constants which indicate the adsorption capacity and adsorption intensity respectively.

The relevant results were showed in Fig. 3 and Table 3.

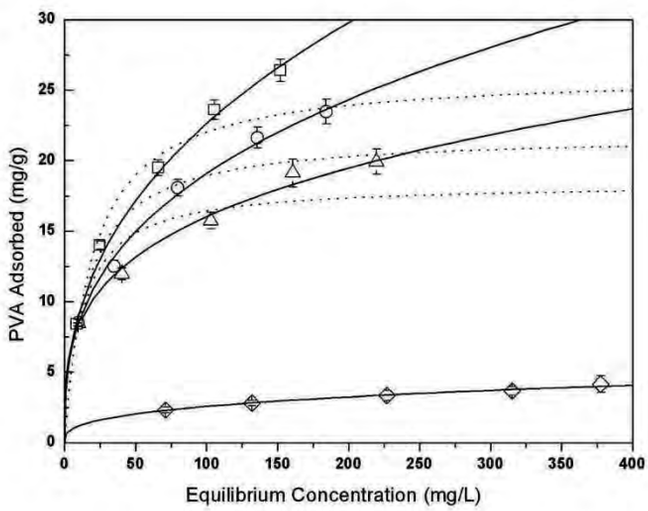

FIGURE 3

Equilibrium curves for adsorption of PVA onto AC at 30ºC (□), 40ºC (○), 50ºC (Δ) and onto zeolite at 30ºC (◇). The solid and dash lines are the Freundlich and Langmuir fits to the observed data (C_0=100mg/L; AC, 0.5g; V, 100 ml).

TABLE 3
Isotherm constants for Langmuir and Freundlich isotherm

	Langmuir			Freundlich		
	Q_0(mg/g)	b(L/mg)	R^2	K_F((mg/g)(L/mg)$^{1/n}$)	n	R^2
303K	26.18	0.053	0.972	3.64	2.52	0.995
313K	21.83	0.066	0.929	3.82	2.86	0.994
323K	18.38	0.085	0.912	4.38	3.55	0.992

The calculated correlation coefficient (R^2) for AC can be found that the Freundlich model in different temperature (R^2= 0.972, 0.929, 0.912) was more suitable than Langmuir model (R^2= 0.995, 0.994, 0.992) and the state of fitting was also showed in Fig. 3 (solid or dashed lines). The fitted to Freundlich model indicated that AC has heterogeneous surface and exponential distribution of the active sites. The Freundlich constant n given an idea for favorability of the adsorption process. The calculated n were 2.52, 2.86, 3.55 at 303K, 313K and 323K, respectively, which indicating that a favorable adsorption process.

Experimental data of PVA adsorption on zeolite at 30 ºC was further fitted to the Freundlich model by a linear regression technique as shown in Fig. 3. But the calculated Freundlich constant n was only 0.98, indicating poor adsorption characteristics.

Adsorption Thermodynamics. The thermodynamic parameters at equilibrium at 293,298,303 K were calculated. The Gibbs' free energy change (ΔG) can be calculated from:

$$\Delta G = -RTlnK_c$$

where R is the universal gas constant and equal to 8.314l/mol k; T is temperature (K) and K_c is the equilibrium constant (m^3/mol). The thermodynamics parameters of enthalpy change (ΔH) and entropy change (ΔS) were evaluated using the following equation:

$$lnK_c = \frac{\Delta S}{R} - \frac{\Delta H}{RT}$$

The value of ΔH and ΔS were calculated from the slope and intercept of the plot of 1/T versus lnK_c (Fig. 4) and the values of ΔG, ΔH and ΔS were summarized in Table 4.

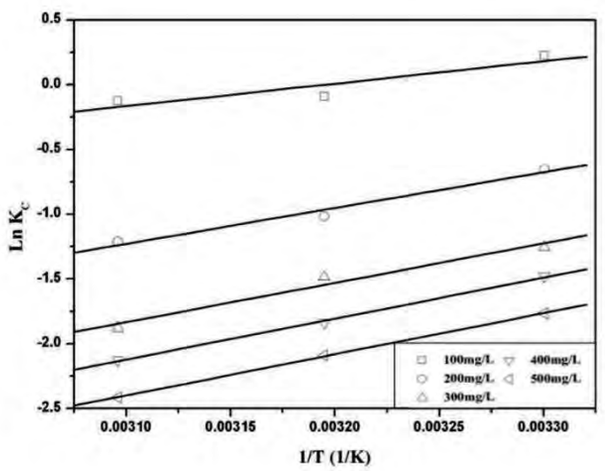

FIGURE 4
Plot of Ln K_c vs. (1/T) for the estimation of the modynamic parameters for adsorption of PVA onto AC.

TABLE 4
Thermodynamic parameters for the adsorption of PVA on AC

C_0 (mg/L)	ΔH(KJ/mol)	ΔS(KJ/molK)	ΔG(KJ/mol)		
			303K	313K	323K
100	-14.4	-0.05	-0.46	0.004	0.46
200	-22.9	-0.08	1.71	2.52	3.34
300	-25.3	-0.09	3.09	4.03	4.96
400	-26.3	-0.10	3.75	4.75	5.74
500	-26.4	-0.10	4.45	5.46	6.48

The negative values of ΔH indicated that the adsorption of PVA on AC was an exothermic process. The lower temperature was conducive to the adsorption. In addition, the absolute value of ΔH was between 14.4 and 26.4 KJ/mol indicating a physical adsorption characteristics. The negative entropy change ΔS reflected the affinity of the adsorbent material toward PVA and indicated the decrease of the randomness of the system [23].

FTIR analysis. The surface functional groups of sample were determined by FTIR and the spectrum was displayed in Fig. 5.

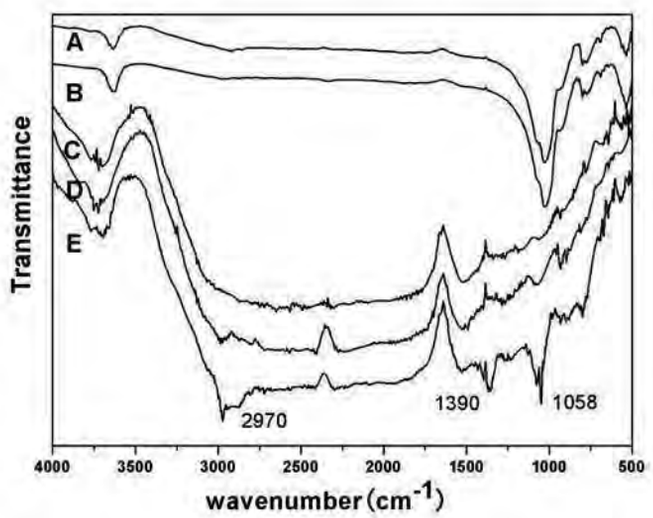

FIGURE 5
FTIR spectra of zeolite(A), zeolite after adsorption PVA 100mg/L(B), AC(C), AC after adsorption PVA 100mg/L(D), AC after adsorption PVA 500mg/L(E).

For zeolite, 795 and 775 cm^{-1} was respective Si-O-Si absorption peak in the silicon oxygen tetrahedron and Al-O-Si adsorption peak in aluminum oxygen octahedron. The absorption peak of 1620 and 470 cm^{-1} was caused by bending vibration of Si-O and Al-O. 1048 cm^{-1} was stretching vibration peak of Si-O-Si skeleton and 540 cm^{-1} was stretching vibration absorption peak of tetrahedral structure. 3429 cm^{-1} was absorption peaks of combined water in the zeolite. For AC, 3407 cm^{-1} was O-H stretching vibration peak. 1720 cm^{-1} was C-O stretching vibration peak showing that the surface of AC have aldehyde group and ketone group. 1080 cm^{-1} indicated C-O vibrating peaks of a variety of functional groups, such as ether, phenolic hydroxyl group, etc. in AC [24].

Compared with pure zeolite, zeolite after adsorption in the effluent remained unchanged. It meant that the contaminants could not be absorbed by zeolite. The adsorption data also showed same results. For AC after adsorption, three peaks (1058, 1390 and 2970 cm^{-1}) appeared on the FTIR spectrum. 1390 and 2970 cm^{-1} was the bending vibration and stretching vibration absorption peak of C-H, respectively. 1058 cm^{-1} was the C-O stretching vibration peak of hydroxyl. PVA adsorbed on the surface of AC and larger adsorption capacity is corresponding to stronger characteristic peaks.

Adsorption mechanism. The two adsorbent with very similar surface area and pore volume had very different adsorption capacity to PVA, so the affinity of adsorbent for PVA played an extremely essential role in the adsorption process. As demonstrated by the results of FT-IR analysis, the surfaces of AC and zeolite had distinct functional group for the adsorption process. The oxygen atom in some functional group on the surface of AC, such as carbonyl, hydroxyl or ester can form stable hydrogen-bonding structure with hydrogen atom in hydroxyl of PVA. On the other hand, oxygen atom in PVA also can form hydrogen-bonding structure with hydrogen atom in surface functional group of AC (shown in Fig. 6).

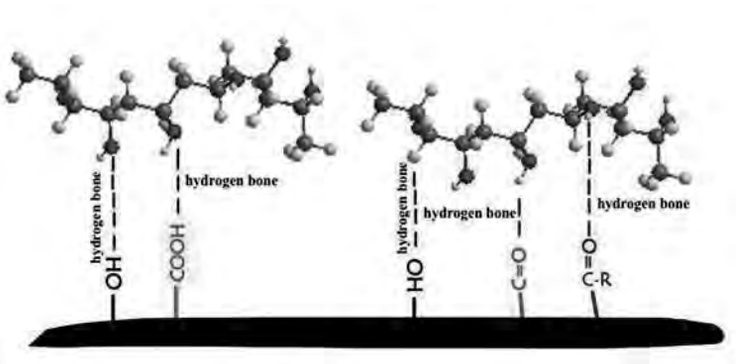

FIGURE 6
The adsorption mechanism of hydrogen bonding between Activated Coke and PVA from aqueous solution.

However, according to FT-IR results, the surface functional group of zeolite cannot form hydrogen-bonding structure. So the adsorption capacity of AC was much larger than that of zeolite. The calculated thermodynamic results can also prove the role of hydrogen-bonding for the adsorption process. The formation of hydrogen bond as the main factors well explained that the two adsorbents with similar surface area and pore volume had very different adsorption effect for PVA removal.

CONCLUSION

AC is an effective adsorbent for removal of PVA from aqueous solution. The adsorption reached equilibrium within 60 min in all different concentration. The amount of PVA uptake was found to enlarge with increase of concentration. The adsorption data were found to follow pseudo-second-order kinetics. A Boyd plot confirms the external mass transfer as the slowest step involved in the sorption process. The equilibrium data were best fitted to the Freundlich isotherm model. The thermodynamic analyses indicate that adsorption of PVA by AC is an exothermic process and physical adsorption. Compared with the low adsorption capacity of zeolite and the results of FT-IR, the mechanism is related with hydrogen-bonding formation. AC shows excellent adsorption characteristics and can be used in the removal of PVA from aqueous solution.

ACKNOWLEDGMENTS

The work was jointly supported by National High Technology Research and Development Program (863 Program 2013AA06A109) of China.

REFERENCES

[1] Yan, B.O., Wei, C.H., Hu, C.S., Xie, C. and Wu, J.Z. (2007) Hydrogen generation from polyvinyl alcohol-contaminated wastewater by a process of supercritical water gasification. *J. Environ. Sci.* 19, 1424-1429.

[2] Behera, S. K., Kim, J. H., Guo, X. and Park, H. S. (2008) Adsorption equilibrium and kinetics of polyvinyl alcohol from aqueous solution on powdered activated carbon. *J. Hazard. Mater.* 153, 1207-1214.

[3] Chou, W.L. (2010) Removal and adsorption characteristics of polyvinyl alcohol from aqueous solutions using electrocoagulation. *J. Hazard. Mater.* 177, 842-850.

[4] Porter, J.J. (1988) Recovery of polyvinyl alcohol and hot water from the textile wastewater using thermally stable membranes. *J. Membr. Sci.* 151, 45-53.

[5] Chen, G., Lei, L., Yue, P.L. and Cen, P. (2000) Treatment of desizing wastewater containing poly (vinyl alcohol) by wet air oxidation. *Ind. Eng. Chem. Res.* 39, 1193-1197.

[6] Chou, W. L., Chen, L. S., Wang, C.T. and Lee, S. R. (2012) Electro-fenton removal of polyvinyl alcohol from aqueous solutions using an activated carbon fiber cathode. *Fresen. Environ. Bull.* 21, 3735-3742.

[7] Kim, S., Kim, T.H., Park, C. and Shin, E.B. (2003) Electrochemical oxidation of polyvinyl alcohol using a RuO_2Ti anode. *Desalination* 155, 49-57.

[8] Hsu, L.J., Lee, L.T. and Lin, C.C. (2011) Adsorption and photocatalytic degradation of polyvinyl alcohol in aqueous solutions using P-25 TiO_2. *Chem. Eng. J.* 173, 698-705.

[9] Zhang, S.J. and Yu, H.Q. (2004) Radiation-induced degradation of polyvinyl alcohol in aqueous solutions. *Water Res.* 38, 309-316.

[10] Rongrong, L., Xujie, L., Qing, T., Bo, Y. and Jihua, C. (2011) The performance evaluation of hybrid anaerobic baffled reactor for treatment of PVA-containing desizing wastewater. *Desalination* 271, 287-294.

[11] Xie, R. Z., Jiang, W. J., Wang, H., Jiang, Y. X., Huang, X. and Chen, Y. (2014) Adsorption of Cr (VI) from aqueous solution by sludge-base activated carbons obtained from chemical and physical activation. *Fresen. Environ. Bull.* 23, 2388-2394.
[12] Qi, Z. F., Li, X. D., Liu, J., Bai, S. H., Chen, T., Lu, S. Y., Buekens, A. and Yan, J. H. (2014) Adsorption of PCBS in flue gas by activated carbon. *Fresen. Environ. Bull.* 23, 290-296
[13] Turkyilmaz, A., Dogan, M. and Alkan, M. (2014) Characterization and adsorptive properties of activated carbon prepared from olive stones. *Fresen. Environ. Bull.* 23, 1585-1593
[14] Asyhar, R., Wichmann, H., Bahadir, M. and Cammenga, H. K. (2002) Preparation of active sorbent from petroleum coke and its application for phenol and 4-nitrophenol reduction from aqueous solution. *Fresen. Environ. Bull.* 3, 143-149.
[15] Turkyilmaz, A., Dogan, M. and Alkan, M. (2013) Surface and adsorptive properties of activated carbon prepared from pomegranate shell. *Fresen. Environ. Bull.* 22, 3317-3325
[16] Li, Q. M., Qi, Y. S. and Gao, C. Z. (2015) Thermal regeneration of spent powered activated carbon used in decolorization for pharmaceutical industry. *Fresen. Environ. Bull.* 24, 1440-1445
[17] Kojima, N., Mitomo, A., Itaya, Y., Mori, S. and Yoshida, S. (2002) Adsorption removal of pollutants by active cokes produced from sludge in the energy recycle process of wastes. *Waste Manage.* 22, 399-404.
[18] Asyhar, R., Wichmann, H., Bahadir, M. and Cammenga, H. K. (2002) Equilibrium adsorption studies of activated coke towards phenol and 4-nitrophenol. *Fresen. Environ. Bull.* 11, 270-277.
[19] Xue, Y., Hou, H. and Zhu, S. (2009) Adsorption removal of reactive dyes from aqueous solution by modified basic oxygen furnace slag: Isotherm and kinetic study. *Chem. Eng. J.* 147, 272-279.
[20] Wei, F.F., Zhang, Y.H., Lv, F.Z., Chu, P.K. and Ye, Z.F. (2011) Extraction of organic materials from red water by metal-impregnated lignite activated carbon. *J. Hazard. Mater.* 197, 352-360.
[21] Vadivelan, V. and Kumar, K.V. (2005) Equilibrium, kinetics, mechanism, and process design for the sorption of methylene blue onto rice husk. *J. Colloid Interface Sci.* 286, 90-100.
[22] Fu, D., Zhang, Y.H., Lv, F.Z., Chu, P.K. and Shang J.W. (2012) Removal of organic materials from TNT red water by Bamboo Charcoal adsorption. *Chem. Eng. J.* 193, 39-49.
[23] Gasser M.S., Morad, G.H. and Aly, H.F. (2007) Batch kinetics and thermodynamics of chromium ions removal from waste solutions using synthetic adsorbents. *J. Hazard. Mater.* 142, 118-129.
[24] Vargas, A.M., Cazetta, A.L., Kunita, M.H., Silva, T.L. and Almeida, V.C. (2011) Adsorption of methylene blue on activated carbon produced from flamboyant pods (Delonix regia): Study of adsorption isotherms and kinetic models. *Chem. Eng. J.* 168, 722-730.

Received: **28.07.2015**
Accepted: **27.12.2015**

CORRESPONDING AUTHOR

Yihe Zhang
China University of Geosciences
School of Materials Science and Technology
National Laboratory of Mineral Materials
Beijing Key Laboratory of Materials Utilization of Nonmetallic Minerals and Solid Wastes
Beijing 100083 – CHINA

e-mail: zyh@cugb.edu.cn

by PSP Volume 25 – No 1/ 2016, pages 219-239 Fresenius Environmental Bulletin

USE OF RCPTU METHOD FOR PESTICIDES CONTAMINATED SOILS PROPERTIES IDENTIFICATION

Guojun Cai, Hanliang Bian, Songyu Liu

Institute of Geotechnical Engineering, Southeast University, Nanjing, China 210096

ABSTRACT

Electrical resistivity is one of the fundamental parameters of the soil, it is an index can be used to evaluate whether the soil was contaminated or not. Resistivity piezocone penetration test (RCPTU) is a reliable in situ technique which can measure the soil resistivity. By conducted four RCPTU soundings at one pesticides contaminated site, soil parameters such as cone tip resistance (q_t), sleeve friction (f_s), pore pressure (u_2), soil resistivity (ρ) and so on were obtained. Based on the data from different types of soil, correlations of q_t, f_s, u_2, relative density (D_r), constrained modulus (E_s) and ρ were established. The correlations are linearly independent, resistivity decrease with the increase of other parameters. It is shown that different pollutants had different effects on the same type of soil. Uncontaminated soils had the highest resistivity, nitidine chloride contaminated soils had higher resistivity than organophosphorus contaminated soils. Soils contaminated by same kind of pollutant have similar resistivity. Contaminated soils and uncontaminated soils were identified at different zones in Robertson et al. (1986) soil classification charts based on CPTU data.

KEYWORDS:
Pesticides contaminated site; in situ testing; RCPTU; soil classification

INTRODUCTION

The cone penetration test (CPT), as a fast, repeatable, simple, cost effective in-situ technique to detect the geological data, is widely used in subsurface soil characterization studies. It is used to estimate geotechnical parameters and provide results for direct geotechnical design (Lunne et al. 1997). Cones with different type of sensors were developed for various purposes, such as pressure transducers, electrical resistivity, temperature, geophones, radioisotope, and so on (Lunne et al. 1997; Cai et al. 2010, 2011a, 2012; Robertson et al. 2012). Cone with pressure transducer capable of measuring pore water pressure simultaneously with cone tip resistance (q_t) and sleeve friction (f_s), is commonly referred as piezocone penetration test (CPTU) (Baligh et al. 1980; Tumay et al. 1981; Zuidberg et al. 1982; Lunne et al. 1997; Cai et al. 2011b). CPTU with an electrical resistivity sensor can obtain soil resistivity named RCPTU, which can be used as a direct detection tool in geoenvironmental site assessment.

RCPTU cone consist of four conducting rings in the rod, two outer of them providing a constant current and other two measuring the resulting potential field. The probe can measure stationary electrical resistance. During the process of testing, geometrical effects are not accounted for. Therefore, an apparent resistance is found instead of an absolute value for the electrical resistance. The measurement of electrical properties was first developed to evaluate in situ density of sands, more recently it can be used to evaluate other properties of soil.

The resistivity of soil is depend on soil type, fluid resistivity, soil porosity, compositions, structure, water content, degree of saturation and so on. Davies (1999) studied the correlation of bulk resistivity and sulphate ion concentration, as shown in Fig. 1, it is noted that bulk resistivity decrease with the increase of sulphate concentration.

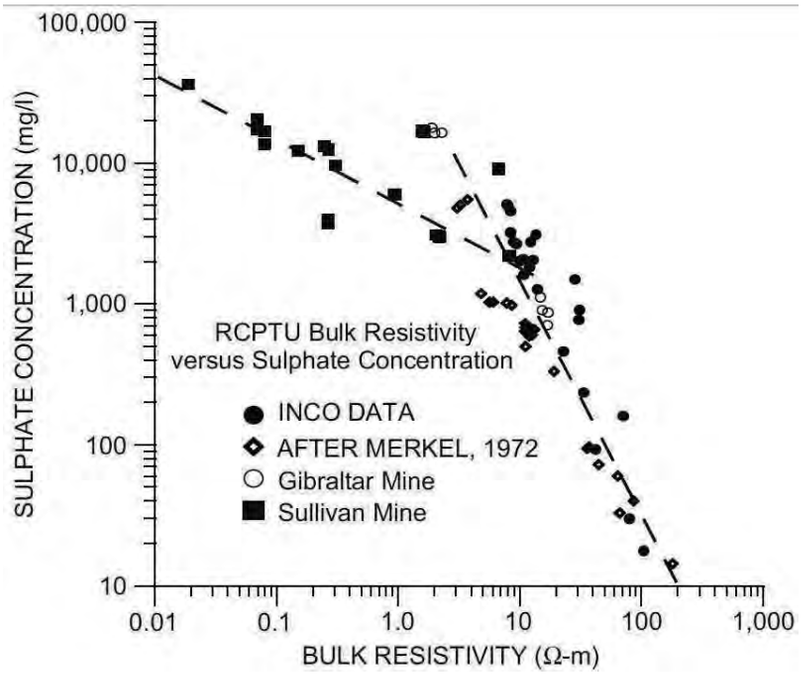

FIGURE 1
Sulphate ion concentration versus bulk resistivity (Davies 1999)

Hassona et al. (2008) built mathematical relationships of resistivity and bulk density, water content, specific gravity, Atterberg limits, grain size distribution of clayey soil, proved that resistivity is an easily and rapidly method to determine soil mechanical properties. It has been recognized that resistivity of soil is changed by the presence of pollutants. In geoenvironmental tests, resistivity of contaminated soils is much difference compared with uncontaminated soils. So it is feasible to distinguish contaminated soil from uncontaminated by resistivity. Fukue et al. (2001) performed field experiments with resistivity cone to detect contaminated soil layers. It was concluded that the resistivity cone can be used for detecting contaminated layer in soils whose background values are known. Campanella (2008) successfully using RCPTU to characterize the contaminated sites, which including mine tailing, oxidized sulphide leachate, creosote-contaminated saturated sediments, and salt water intrusion. Liu et al. (2012) used RCPTU to detect organic contaminated soils, concluded that RCPTU is a helping tool in geoenvironmental site detecting.

There are several literatures based on field tests and laboratory experiments about resistivity cone penetrometer for contaminant assessment (Campanella and Weemees 1990; Kim et al. 2007, 2009; Mondelli et al. 2007; Chan 2008; Liu et al. 2008; Oh et al. 2008; Peixoto et al. 2010; Marluci et al. 2011; Siddiqui et al. 2013). It was concluded that resistivity is a useful index in determine whether the soil was contaminated, and resistivity cone penetrometer is a helping tool in geoenvironmental site detecting. Relationships of resistivity and other parameters also established.

In contaminated sites, soil resistivity varied with different pollution compositions. RCPTU can be used to detect the change of soil resistivity (ρ). Meanwhile, other parameters such as cone resistance (q_t), sleeve friction (f_s), pore water pressure (u) could be obtained. Furthermore, the geotechnical parameters such as soil overconsolidation ratio (*OCR)*, undrained shear strength (S_u), sensitivity (S_t), constrained modulus (E_s), relative density (D_r), shear wave velocity (V_s), and so on, can be obtained. However, the correlations between soil electrical property and other physical and mechanical properties are very complex, because many soil properties may influence in-situ measured electrical parameters (Rhoades et al. 1976; Abu-Hassanein et al. 1996; Banton et al. 1997).

This paper presents a case study of RCPTU method used in one pesticides contaminated site located in Jiangsu Province, Eastern China, providing geology information about the test site. The main purposes of this paper are to establish correlations between measured resistivity and parameters based on RCPTU data, determine soil types using the classification chart proposed by Robertson et al. (1986), to find how pollutants influence soil classification.

SITE DESCRIPTION

The site is located at northwest of Nantong City, Middle of Jiangsu Province, as shown in Fig. 2.

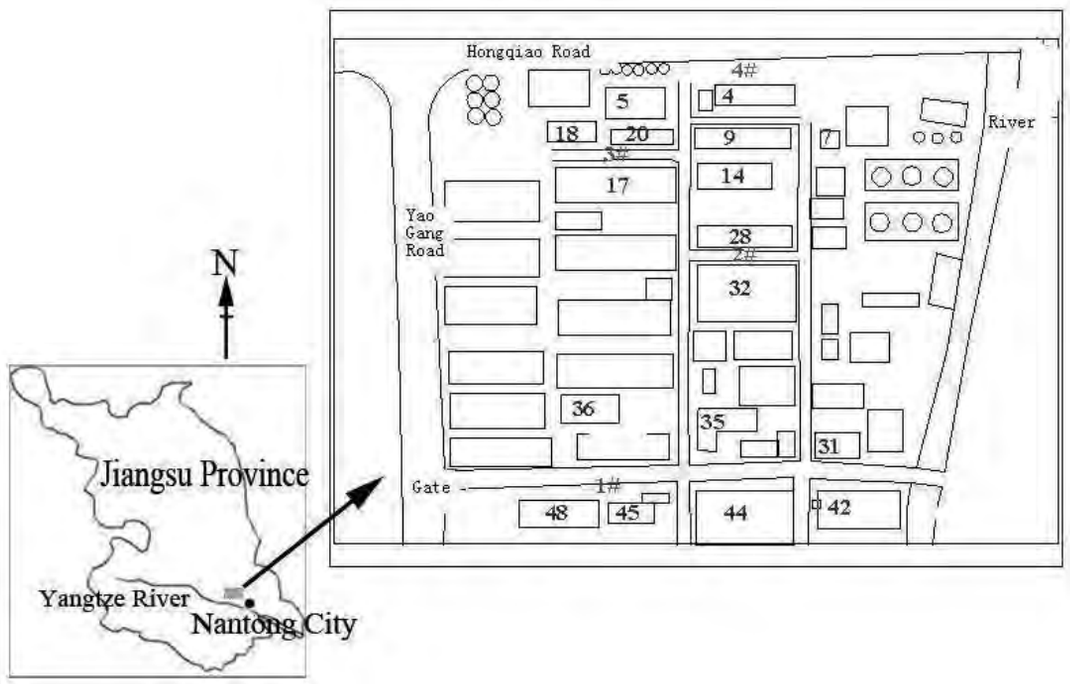

FIGURE 2
Locations of four RCPTU tests carried out at the pesticides contaminated site

It was an agrochemical & fine chemical factory. Nantong City is located in north of the Yangtze River, belong to Yangtze River alluvial plain, characterized by alluvial deposit. Based on the data from drilling bores logs in the test site, subsurface deposits of the site consist of alternating layers of clayey silt, silty clay, sandy silt, medium sand, silt, silty sand, medium sand. Detailed soil layers are listed in Table 1, and soil properties are listed in Table 2.

TABLE 1
Soil layers description of the study area

Layer number	Soil type	Layer thickness (m)	Description
1	Fill	0.50~1.50	Gray to greyish, most of the soils are silt soil with silty clay, density of the soil is uneven, including construction waste
2	Silty with silty clay	1.50~2.00	Greyish to gray, silt soil is slightly dense, with high moisture, has low dry strength and low toughness; silty clay is soft-plastic, has high strength and high toughness, with smooth section
3	Mucky silty clay	1.20~2.60	Dust color, with thin layer gray silt soil, flow-plastic, middle dry strength, high toughness, with smooth section
4	Silty with silty clay	2.00~3.10	Greyish to gray, silt soil is slightly dense, with high moisture, has low dry strength and low toughness; silty clay is soft-plastic, has high strength and high toughness, with smooth section
5	Silty sand	4.00~4.10	Gray, with thin layer dust colour silty clay, middle density, saturation
6	Silty with silty clay	2.50~2.80	Greyish to gray, silt soil is slightly dense, with high moisture, has low dry strength and low toughness; silty clay is soft-plastic, has high strength and high toughness, with smooth section
7	Medium sand		Gray, with thin layer dust colour silty clay, middle density, partial density, saturation,

Resistivity piezocone penetration tests were conducted at the test site. Four different locations

TABLE 2
Soil layers and properties of the study area

Soil layer	Water content w (%)	Unit weight γ (kN/m^3)	Porosity e	Liquidity Index I_L	Consolidated-quickly shear	
					Cohesion (c)	Friction angle φ (°)
Silt with silty clay	32.5	18.6	0.921	0.97	8.0	22.6
Mucky silty clay	36.8	18.1	1.053	1.12	19.5	8.9
Silt with silty clay	32.5	18.5	0.924	1.09	9.3	22.8
Slit sand	27.5	19.3	0.772		1.0	31.2

RCPTU-1 to RCPTU-4 (labeled as 1#, 2#, 3#, 4#) have been chosen to conduct RCPTU test, approximate location of the soundings were shown in Fig. 2. Each sounding has a different depths and the deepest one is RCPTU-1 with a depth of 23 m. Others are between the depth of 10~11 m. Four soundings are contaminated by different pesticides. RCPTU-1 was contaminated by nitidine chloride; RCPTU-2 and RCPTU-3 were contaminated by organophosphorus; RCPTU-4 was uncontaminated, just as a comparison sounding.

RCPTU soundings were conducted using Hogentogler 200 kN digital resistivity pizeocone penetrometer and field data were acquired using E4FCS software. The RCPTU system consist of a hydraulic pushing and leveling system, 1 m length segmental rods, cone penetrometers and a data acquisition system. The piezocone is equipped with various sensors to measure depth of penetration, inclination, resistivity, cone resistance, sleeve friction and pore water pressure. The area of the cylindrical cone is 10 cm^2 with a tip angle of 60 °. The surface area of the friction cylinder is 150 cm^2. The pore pressure is measured at the cone shoulder (u_2). This equipment can be operated with the maximum depth of 40 m with a rate of penetration of 20 mm/s. Fig. 3 shows the schematic of the used resistivity piezocone probe with a four-electrode array (Liu et al. 2012).

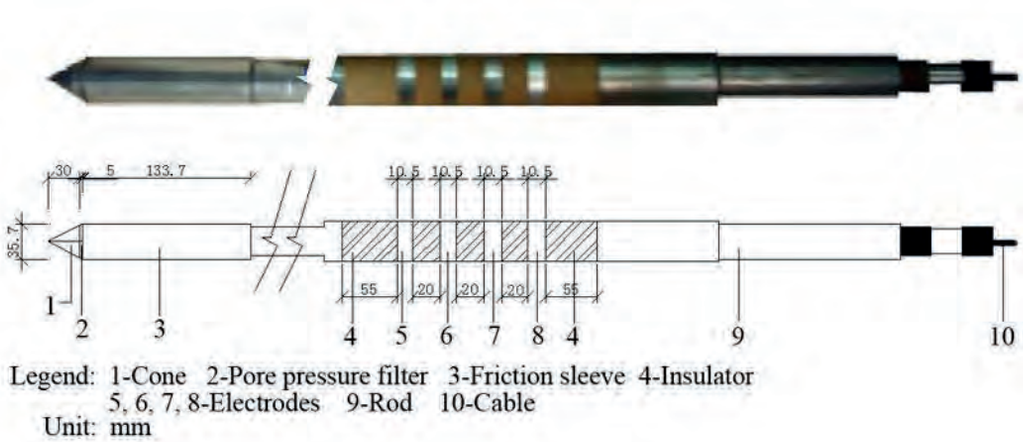

FIGURE3
Schematic representation of a resistivity piezocone probe with a four-electrode array (Liu et al. 2012)

Most of the RCPTU cones were arranged as shown in Fig. 3, which has four electrodes, known as Wenner array. A large part of RCPTU cones were built with four electrodes because they are less subject to the effect of polarization in the electrodes. Devices with two electrodes working at low frequencies are subject to the effect of polarization in the electrodes, which strongly interferes in resistivity readings. However, as higher frequencies are used, this effect tends to decrease as the ions cannot polarize in the electrodes (Weemees 1990).

Typical RCPTU data and soil profiling are showing in Fig. 4 for the test site.

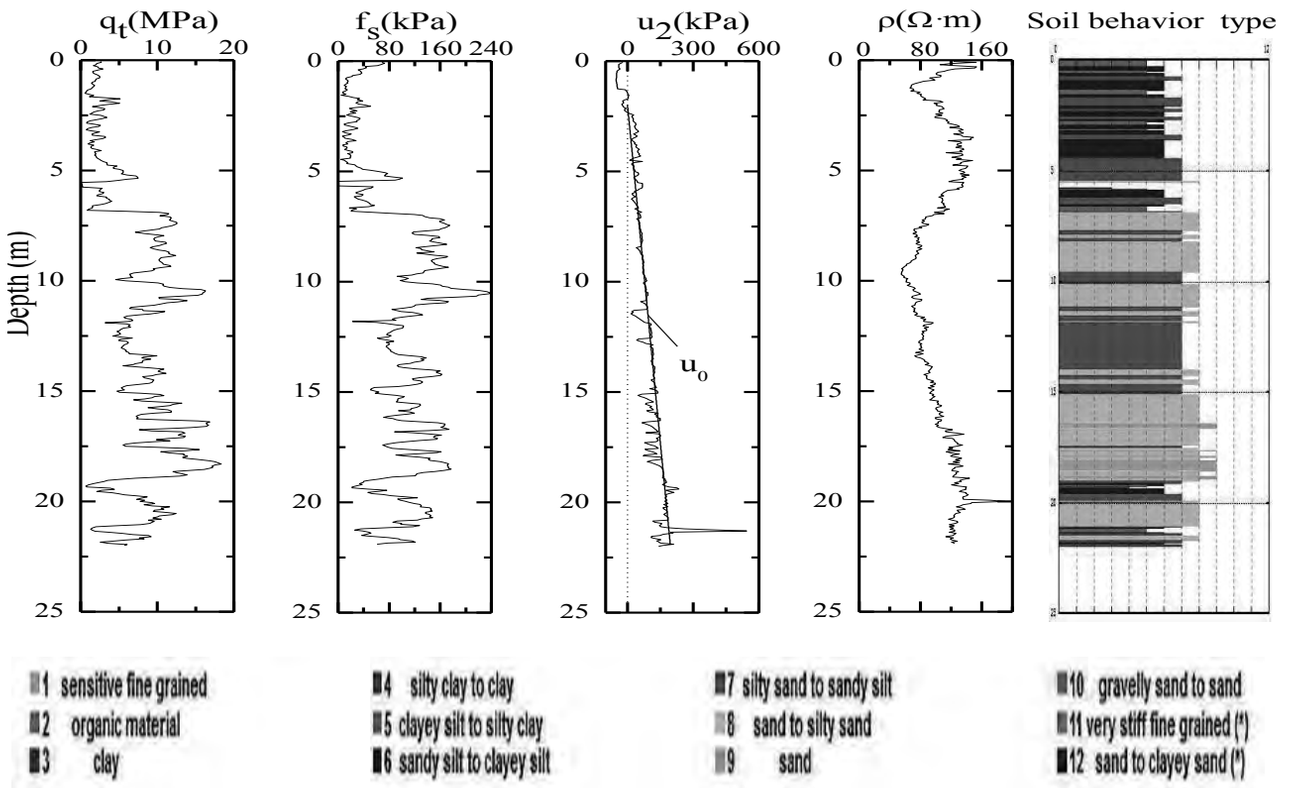

FIGURE 4
Typical RCPTU data of test site in Nantong

The groundwater table is also indicated in the Fig. 4 (u_2). Based on RCPTU data, soil stratums can be distinguished as follows. The soil layer shows fills to depth of about 1.6 m, the tip resistance is about 1.8 MPa, and decrease slightly with depth. A silty clay layer about 0.7 m with tip resistance about 3.1 MPa is layed below. At the depth of 4 m, there is a sandy silt layer, its thickness is about 1.5 m. Under the depth of 6.8 m, there is a mediun sand layer, its resistance is about 10.5 MPa, its thickness is about 2.6 m. At the depth of 10.1 m, there is another medium sand layer, which cone tip resistance is about 12.5 MPa. The sublayer is silty sand, with thickness of about 4.1 m, whose cone resistance is about 7.0 MPa. The soil layer below is medium sand, which cone tip resistance is about 12.2 MPa, with the thickness of about 3.9 m.

According to RCPTU data, soil profile is shown in Fig 5.

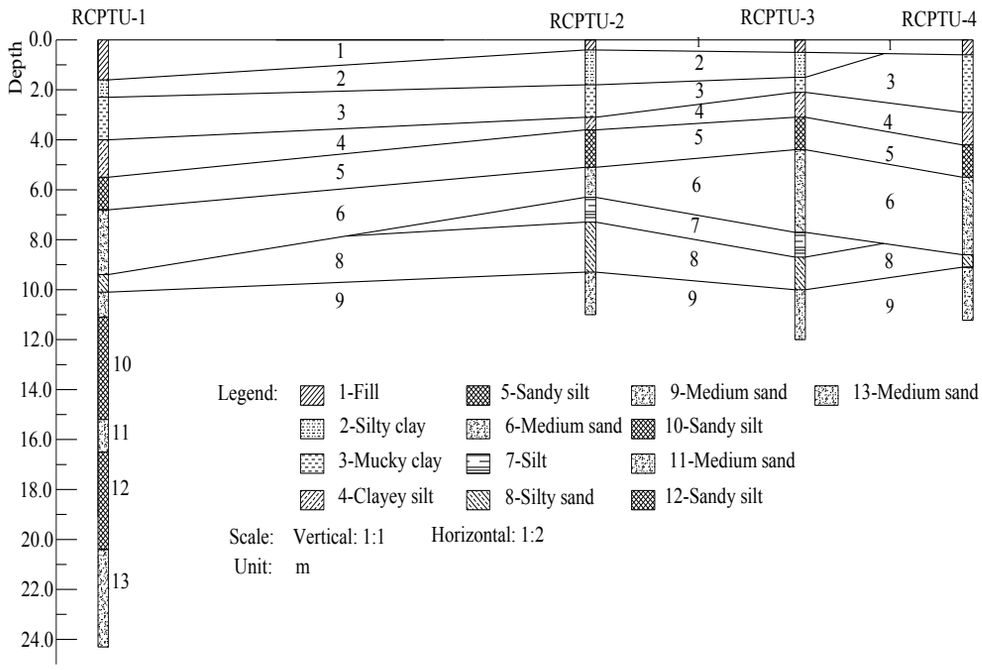

FIGURE 5
Soil profile according to RCPTU data

It can be seen in Fig. 5 that soil layers of the four RCPTU soundings are similar. Differences of soil layers are RCPTU-2 has a silt soil layer which is not exist in other soundings, and RCPTU-4 lacks of the silty clay layer just layed below the fill.

THEORY OF SOIL RESISTIVITY

According to Campanella and Weemees (1990), soil resistivity is determined first by measuring the electrical resistance. According to Ohm's law, when the voltage of a pair of electrodes fed with an alternating current at a known frequency is known, resistivity of soil measured by this cone can be calculated from the following equation:

$$\rho = 2a \times \frac{\Delta v}{I} \quad (1)$$

where ρ is the resistivity of soil (Ω·m); a is the distance between the electrodes (m); I is the electric current (mA); Δv is electric potential difference (mV).

Measured soil resistivity is affected by several factors, such as pore fluid chemistry, degree of fluid saturation, porosity of soil matrix, clay content, mineralogy, and so on (Campanella 2008). According to Archie's law (1942), soil bulk resistivity is relates to pore fluid resistivity, degree of saturation, soil porosity, and so on, the law was defined as following equation:

$$F = \rho_b / \rho_f = a \cdot (n)^{(-m)} \cdot (S_r)^{(-S)} \quad (2)$$

where F is formation factor; ρ_b is soil bulk resistivity, (Ω·m); n is soil porosity; S_r is degree of saturation, (%); ρ_f is fluid resistivity, (Ω·m); a is the scale factor of the equation, depends on the soil mineralogy; m is a constant value, depends on the soil type; s is exponent of the equation, depends on the soil mineralogy.

RELATIONSHIPS BETWEEN RESISTIVITY AND ENGINEERING PROPERTIES OF CONTAMINATED SOIL

As the cone tip resistance and sleeve friction were influenced by soil type, porosity, soil structure. According to equation (2), soil resistivity also influenced by soil structure, porosity, soil type. There must be relationships between the cone tip resistance, sleeve friction and soil resistivity. This paper tries to establish the relationships of these parameters. In this section, correlated cone tip resistances (q_t), sleeve frictions (f_s) plotted against the values of soil resistivity (ρ) measured in the field by RCPTU. Every relation had a best fit line. The line is determined statistically based on the method of least squares. A coefficient of determination (R^2) was also computed for the suggested equation.

Correlations between resistivity and RCPTU measurements

Soil resistivity versus cone tip resistance

Figure 6 illustrates the best fit correlation lines of corrected cone resistance (q_t) values and soil resistivity (ρ) of four soundings.

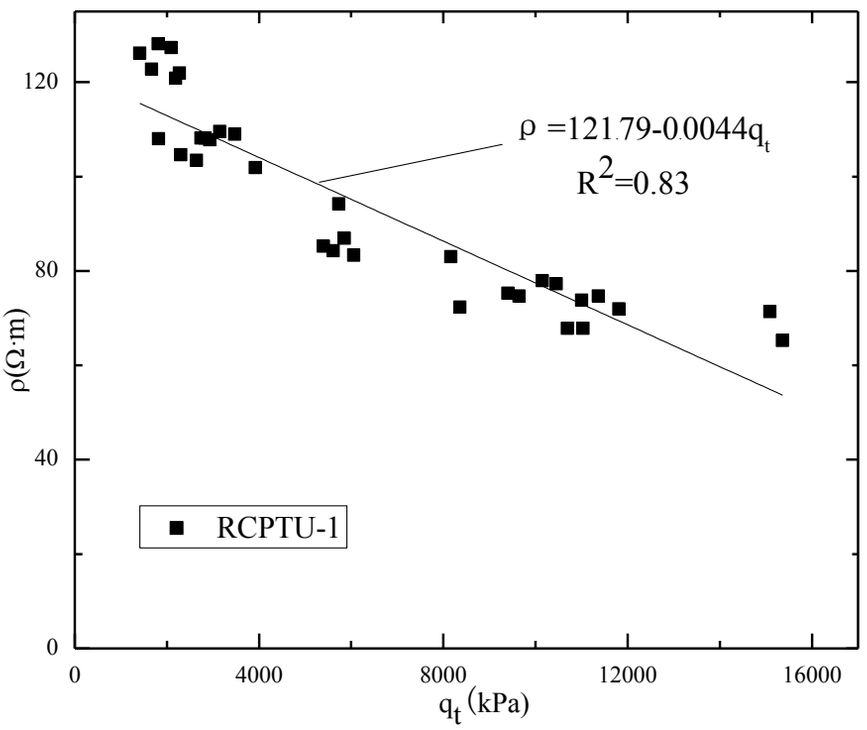

6(a)

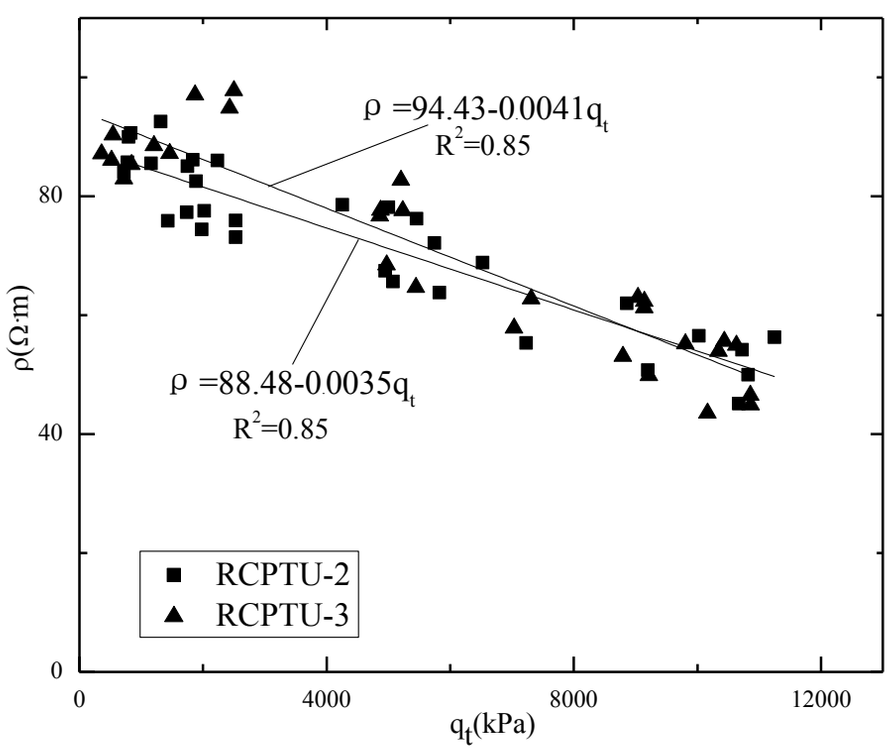

6(b)

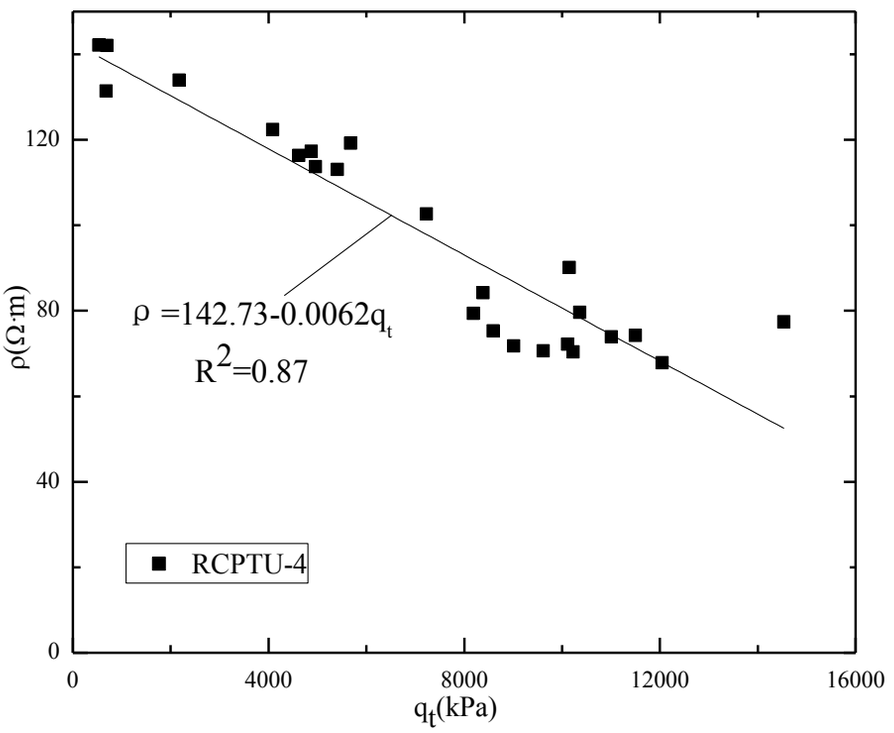

6(c)

FIGURE 6
Variation of cone tip resistance with resistivity: (a) nitidine chloride contaminated soil (b) organophorus contaminated soil (c) uncontaminated soil

Fig. 6(a) shows the relationship of the nitidine chloride contaminated soils. Fig.6(b) shows the relationships of two soundings contaminated by organophosphorus. Fig. 6(c) shows the relationship of uncontaminated soils. It is noted that in all figures, relationships between cone tip resistance (q_t) and resistivity (ρ) are linearly, every relation has an acceptable coefficient of determination. Resistivity decreases linearly with the increase of cone tip resistance. It also can be seen that different pollutants had different effects on the soil resistivity.

Resistivity of nitidine chloride contaminated soils range between 65.21~128.17 Ω·m. Resistivity of organophosphorus contaminated soils range between 45.13~92.5 Ω·m and 43.55~97.80 Ω·m. Resistivity of uncontaminated soils range between 70.35~142.11 Ω·m. Cone tip resistance of nitidine chloride contaminated soils range between 1415~15360 kPa. Cone tip resistance of organophosphorus contaminated soils range between 360~10862 kPa and 420~11250 kPa. Uncontaminated soils' cone tip resistance range between 532~14533 kPa. Uncontaminated soils have the highest resistivity, middle range of cone resistance; nitidine chloride contaminated soils have middle resistivity, and the highest cone resistance; organophosphorus contaminated soils have the lowest resistivity, and the lowest cone resistance. Same pollutant has similar effects on soil resistivity and cone resistance.

Soil resistivity versus sleeve friction

Figure 7 illustrates the best fit correlation lines of sleeve friction (f_s) and soil resistivity (ρ) of four soundings.

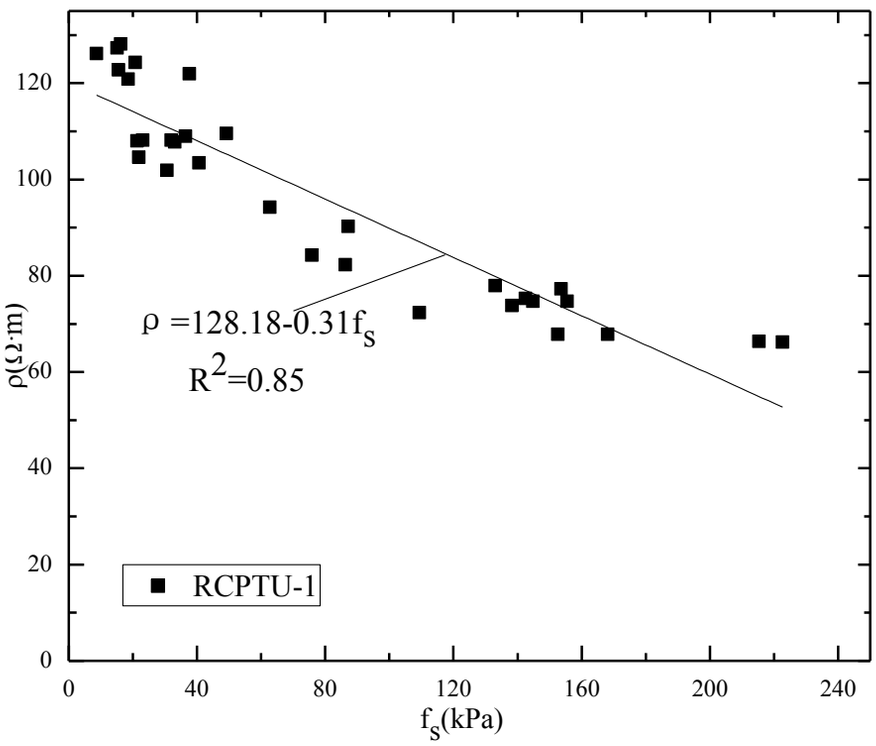
ρ =128.18-0.31f_s
R^2=0.85
RCPTU-1
ρ(Ω·m)
f_s(kPa)
0
20
40
60
80
100
120
0
40
80
120
160
200
240

7(a)

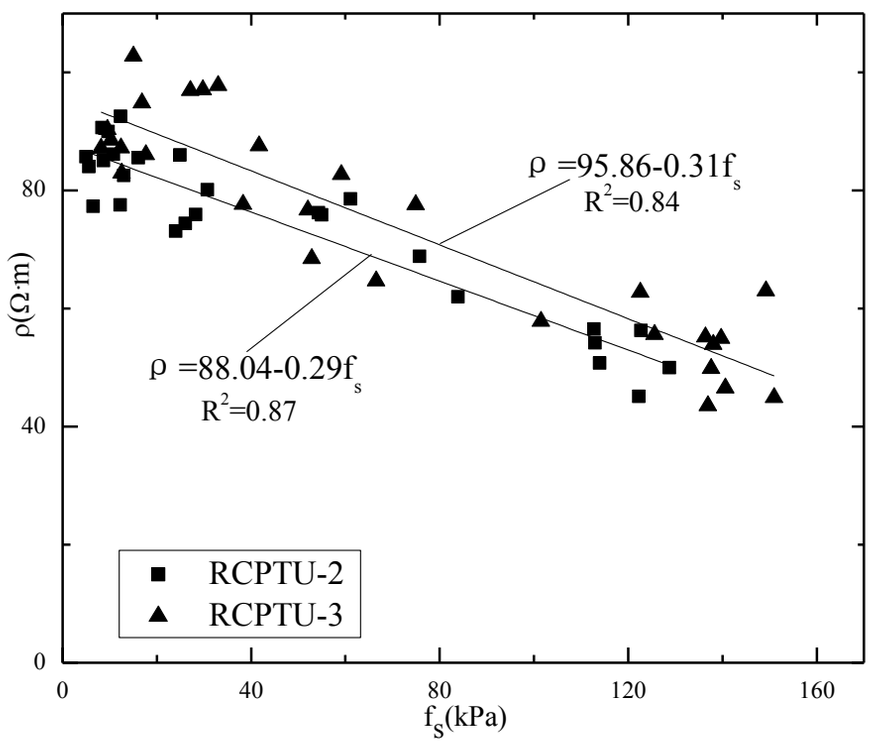
ρ =95.86-0.31f_s
R^2=0.84
ρ =88.04-0.29f_s
R^2=0.87
RCPTU-2
RCPTU-3
ρ(Ω·m)
f_s(kPa)
0
40
80
0
40
80
120
160

7(b)

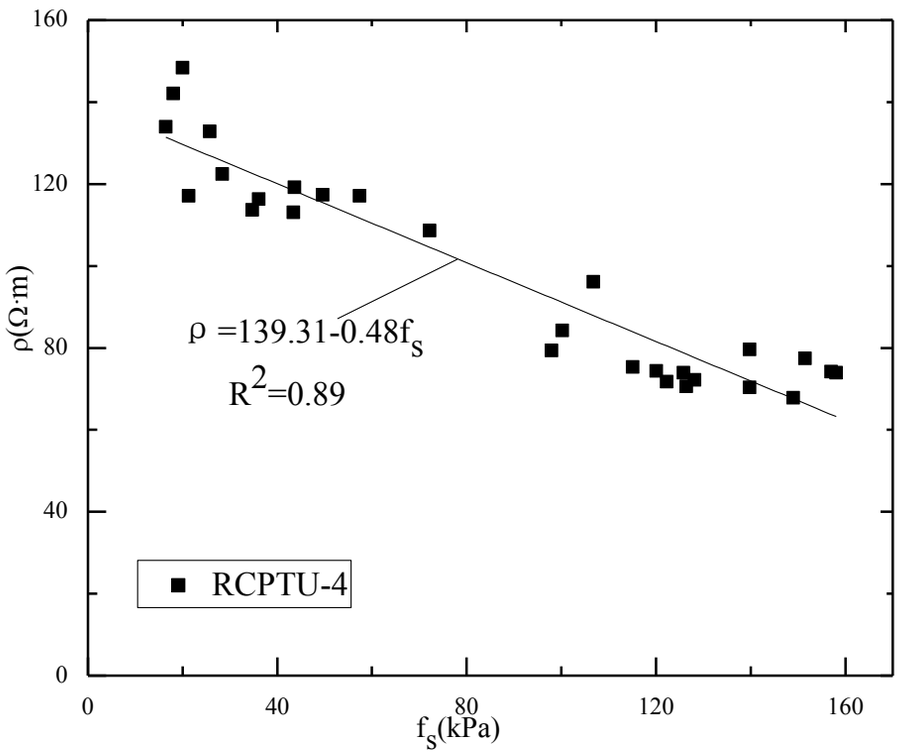

7(c)

FIGURE 7
Variation of sleeve friction with resistivity: (a) nitidine chloride contaminated soil (b) organophorus contaminated soil (c) uncontaminated soil

Fig. 7(a) shows the relationship of the nitidine chloride contaminated soil. Fig. 7(b) shows the relationships of two soundings contaminated by organophosphorus. Fig. 7(c) shows the relationship of uncontaminated soils. It is noted that in all figures, the relationship of sleeve friction (f_s) versus resistivity (ρ) are linearly, every relation has an acceptable coefficient of determination. Resistivity decreases linearly with the increase of sleeve friction.

Sleeve friction of nitidine chloride contaminated soils range between 8.69~222.64 kPa. Sleeve friction of organophosphorus contaminated soils range between 5.01~128.8 kPa and 8.18~150.9 kPa. Uncontaminated soils' sleeve friction range between 16.43~158.1 kPa. Uncontaminated soils have the highest resistivity, middle range of sleeve friction; nitidine chloride contaminated soils have middle resistivity, the highest sleeve friction; organophosphorus contaminated soils have the lowest resistivity, and the lowest sleeve friction. Same pollutant has similar effects on soil resistivity and sleeve friction.

Soil resistivity versus pore water pressure

It is generally accepted that the pore pressure around a penetrating cone influence the measured cone tip resistance and sleeve friction (Lunne et al. 1997). On the RCPTU cone we used, pore pressure was measured at the cone shoulder (u_2). Fig. 8 demonstrates the best fit correlation lines of pore pressure (u_2) values and soil resistivity (ρ) of four soundings.

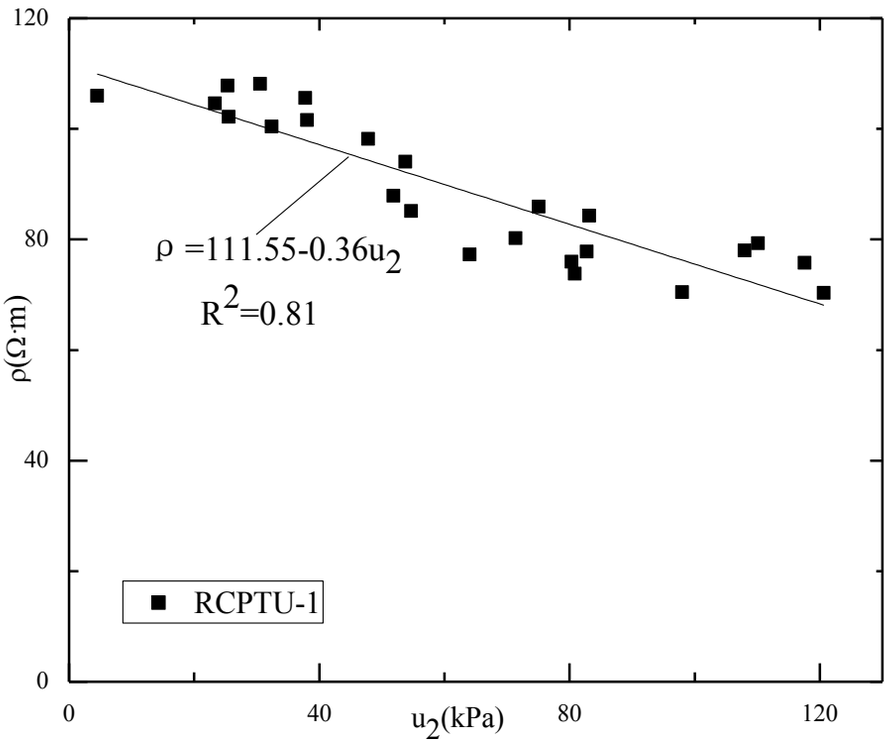
120
80
40
0
0
40
80
120
ρ(Ω·m)
u2(kPa)
ρ =111.55-0.36u2
R2=0.81
RCPTU-1

8(a)

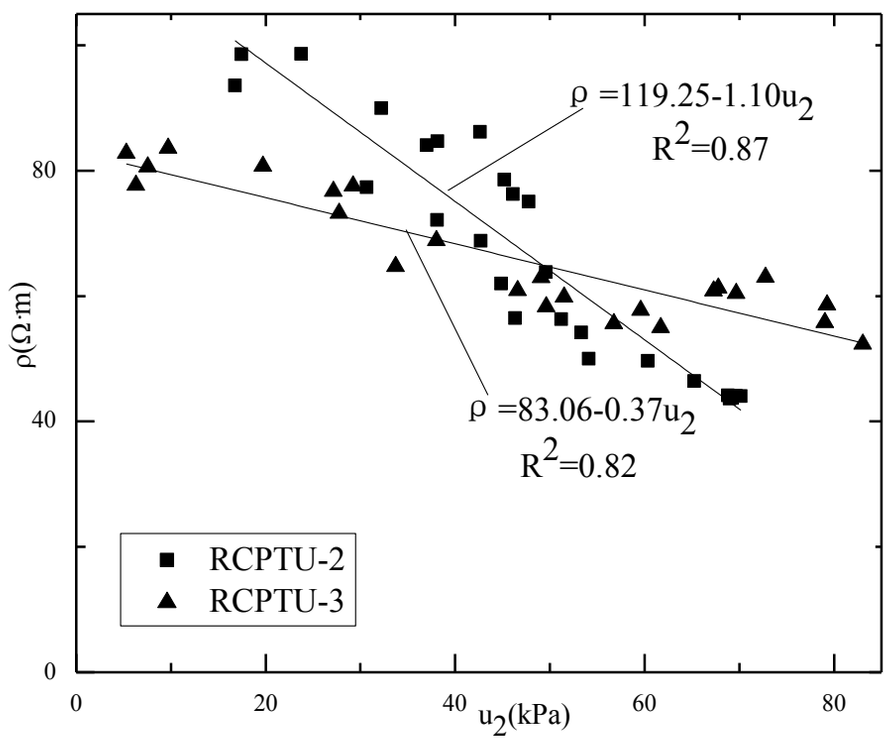
80
40
0
0
20
40
60
80
ρ(Ω·m)
u2(kPa)
ρ =119.25-1.10u2
R2=0.87
ρ =83.06-0.37u2
R2=0.82
RCPTU-2
RCPTU-3

8(b)

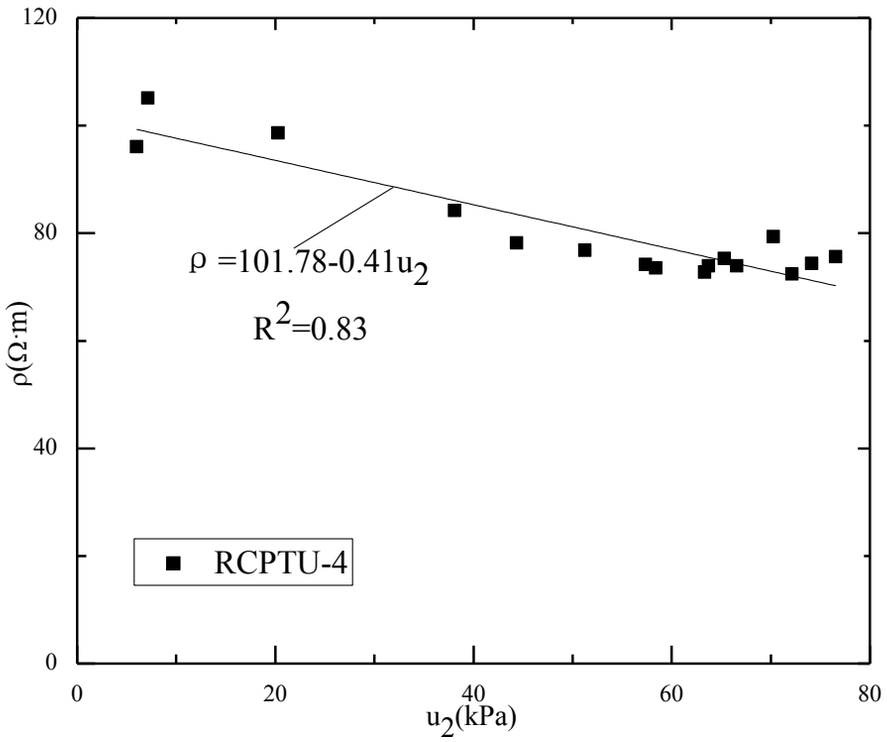

8(c)

FIGURE 8
Variation of pore pressure with resistivity: (a) nitidine chloride contaminated soil (b) organophorus contaminated soil (c) uncontaminated soil

Fig. 8(a) shows the relationship of the nitidine chloride contaminated soils. Fig. 8(b) shows the relationships of two soundings contaminated by organophosphorus. Fig. 8(c) shows the relationship of uncontaminated soils. It can be seen that in all figures, the relationship versus pore pressure (u_2) and resistivity (ρ) are linearly, every relation has an acceptable coefficient of determination. Resistivity decreases with the increase of pore pressure.

Pore pressure of nitidine chloride contaminated soils range between 4.50~120.64 kPa. Pore pressure of soils contaminated by organophosphorus range between 16.8~70.17 kPa and 5.30 ~83.02 kPa. Pore pressure of uncontaminated soils range between 6.01~74.20 kPa.

Correlations between resistivity and mechanical parameters

Soil resistivity versus relative density

In the test site, several stratums are silty sand and middle sand, their properties are all relate with relative density. Fig. 9 illustrates the best fit lines of relative density (D_r) and soil resistivity (ρ) of four soundings.

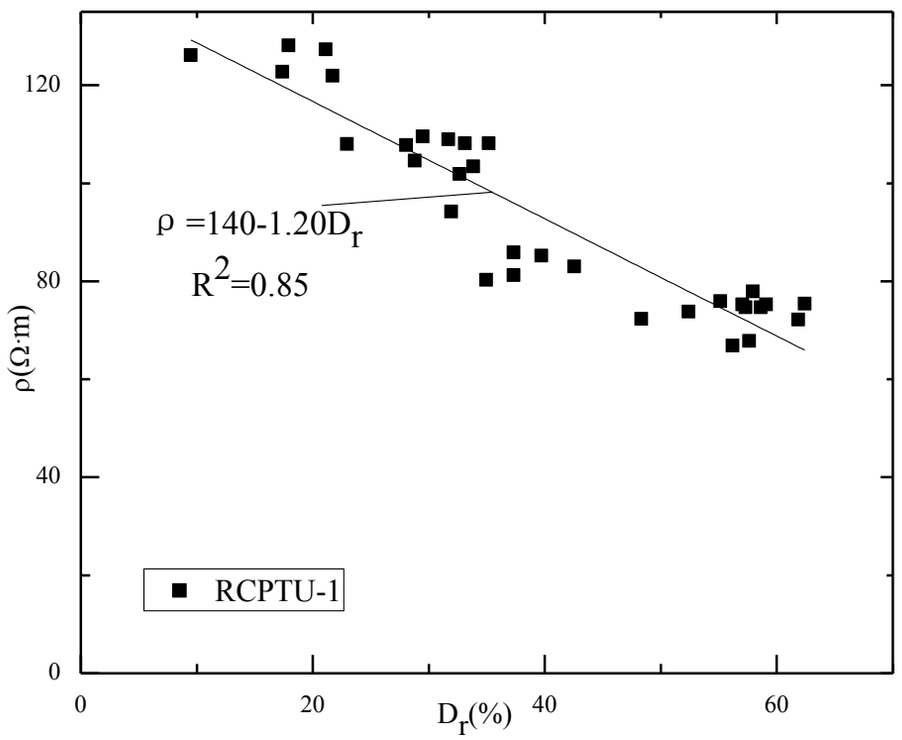
120
80
40
0
0
20
40
60
ρ(Ω·m)
D_r(%)
ρ =140-1.20D_r
R^2=0.85
RCPTU-1

9(a)

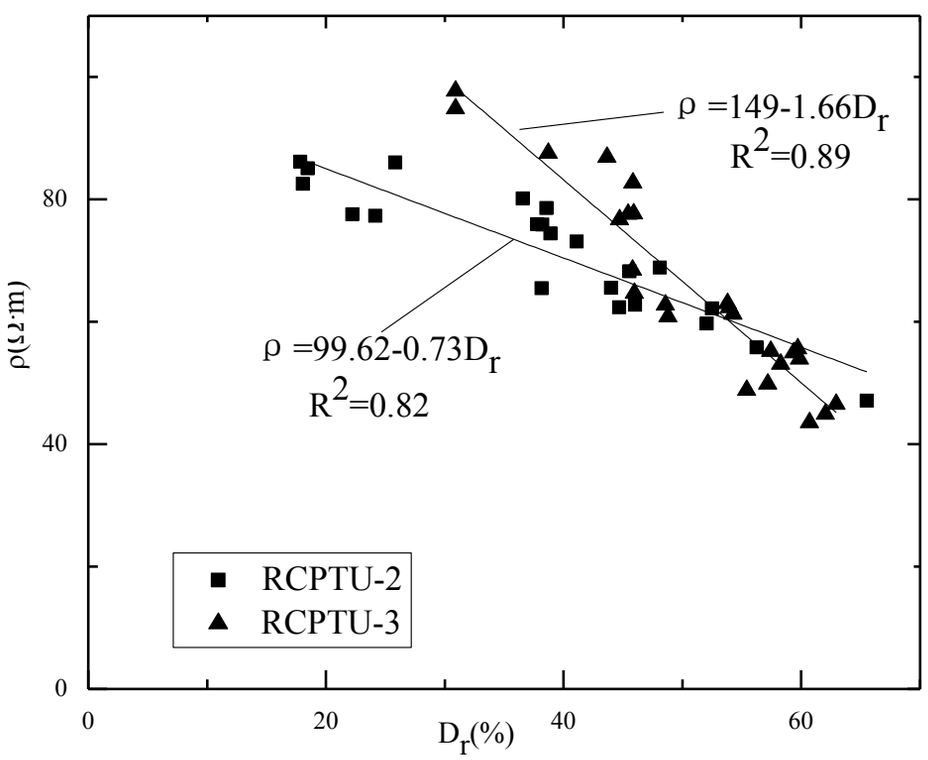
80
40
0
0
20
40
60
ρ(Ω·m)
D_r(%)
ρ =149-1.66D_r
R^2=0.89
ρ =99.62-0.73D_r
R^2=0.82
RCPTU-2
RCPTU-3

9(b)

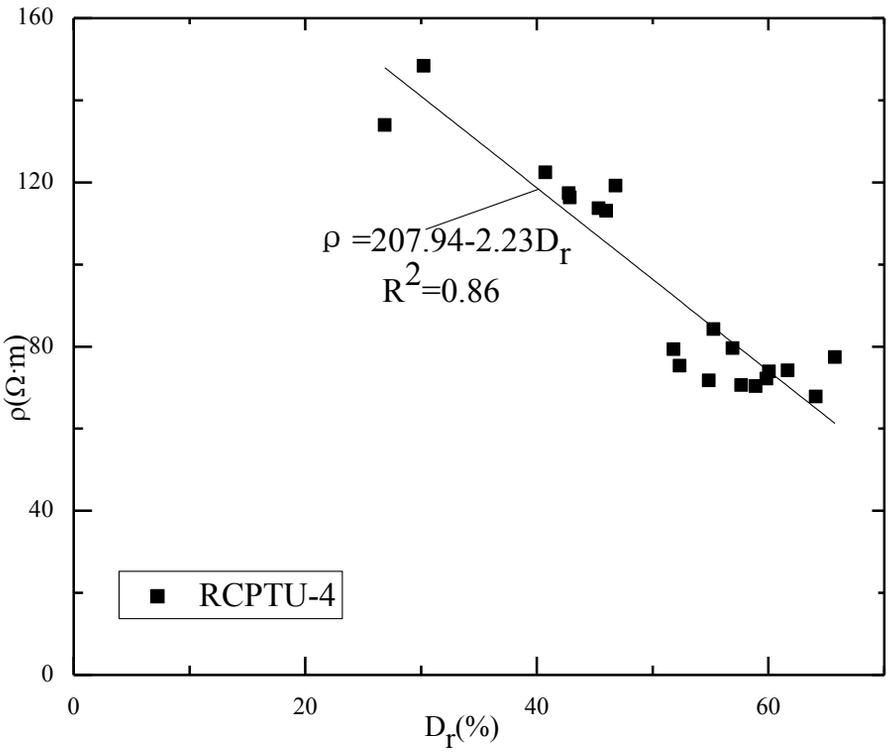

9(c)

FIGURE 9
Variation of relative density with resistivity: (a) nitidine chloride contaminated soil (b) organophorus contaminated soil (c) uncontaminated soil

Fig. 9(a) shows the relationship of the nitidine chloride contaminated soils. Fig. 9(b) shows the relationships of two soundings contaminated by organophosphorus. Fig. 9(c) shows the relationship of uncontaminated soils. It is noted that in all figures, the relationship between relative density (D_r) and resistivity (ρ) are linear correlation, and every relation with an acceptable coefficient of determination. Resistivity decreases linearly with the increase of relative density. Uncontaminated soils have the highest resistivity, while organophosphorus contaminated soils have the lowest values. The relative density of uncontaminated soils range is 26.87~65.75 %, and for the nitidine chloride contaminated soils range is 9.5~63.8 %. While the relative density of organophosphorus contaminated soils are 17.86~60.50 %, 30.9~62.9 %, respectively.

Soil resistivity versus constrained modulus

Figure 10 illustrates the best fit lines of constrained modulus (E_s) and soil resistivity (ρ) of four soundings.

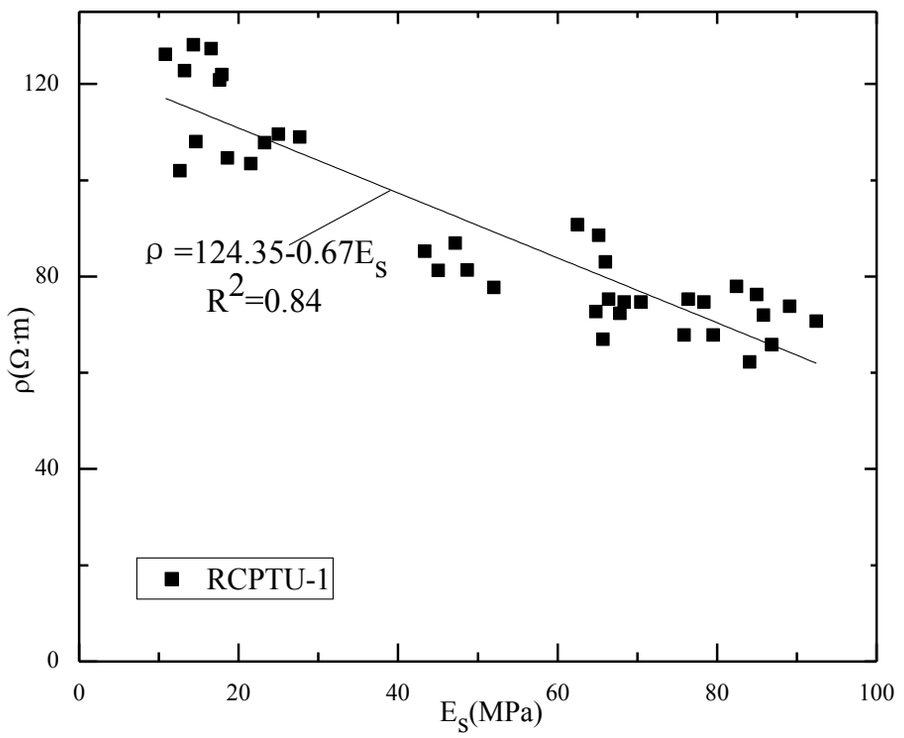
ρ =124.35-0.67E_S
R^2=0.84
RCPTU-1
ρ(Ω·m)
E_S(MPa)
0
40
80
120
0
20
40
60
80
100

10(a)

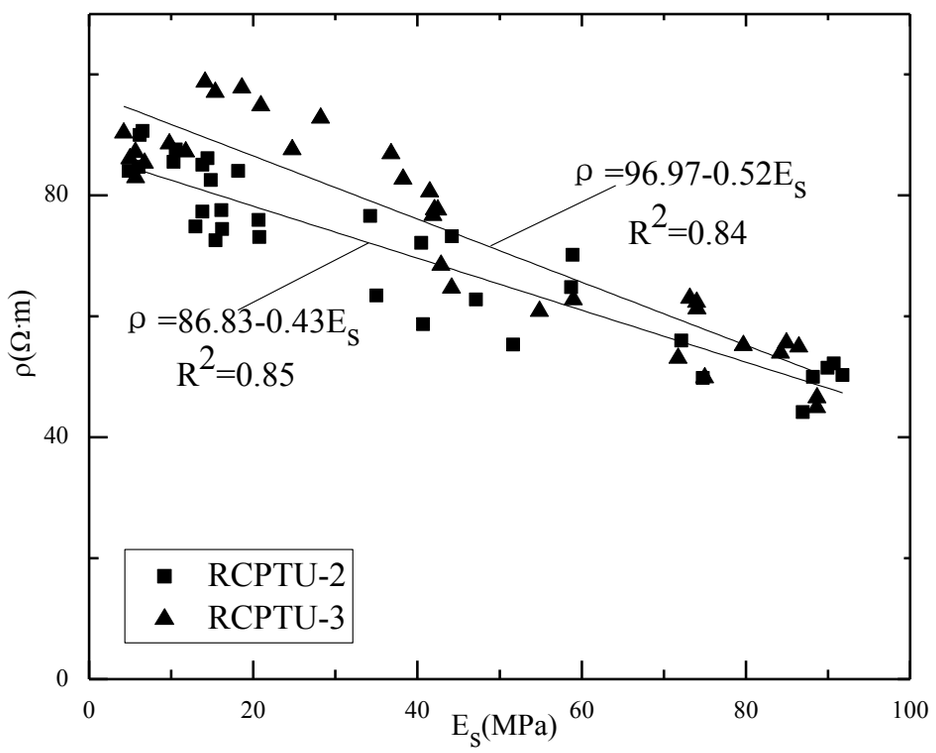
ρ =96.97-0.52E_S
R^2=0.84
ρ =86.83-0.43E_S
R^2=0.85
RCPTU-2
RCPTU-3
ρ(Ω·m)
E_S(MPa)
0
40
80
0
20
40
60
80
100

10(b)

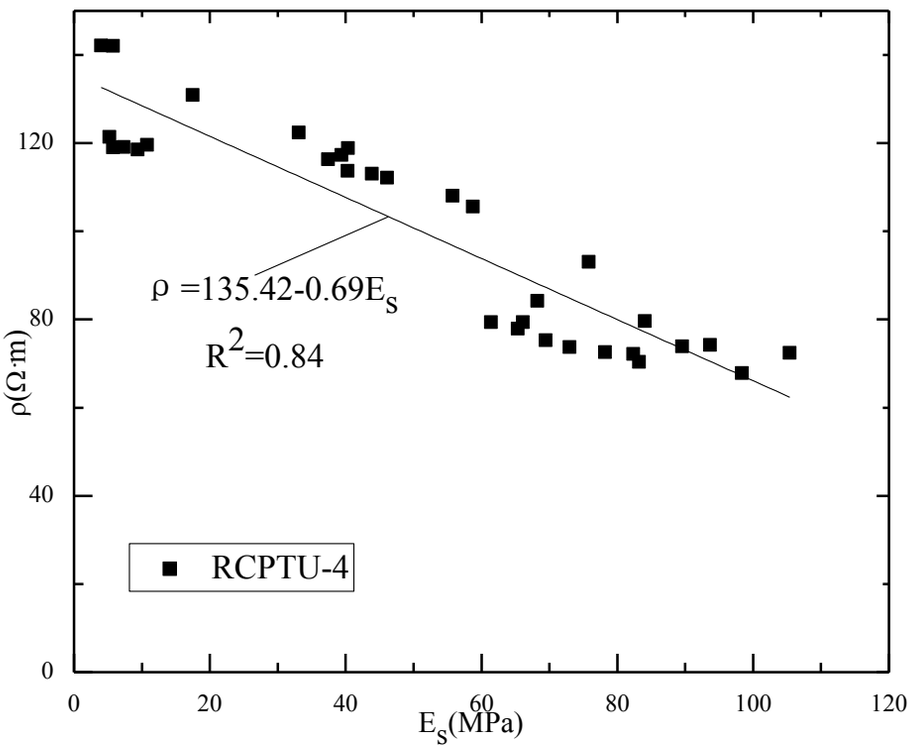

10(c)

FIGURE 10
Variation of constrained modulus with resistivity: (a) nitidine chloride contaminated soil (b) organophorus contaminated soil (c) uncontaminated soil

Fig. 10(a) shows the relationship of the nitidine chloride contaminated soils. Fig. 10(b) shows the relationships of two soundings contaminated by organophosphorus. Fig. 10(c) shows the relationship of uncontaminated soils. It is noted that in all figures, the relationships between constrained modulus (E_s) and resistivity (ρ) are linear correlation, every relation has an acceptable coefficient of determination. Resistivity linearly decreases with the increase of constrained modulus. Range of nitidine chloride contaminated soils' constrained modulus is 10.78~92.52 MPa. Range of organophosphorus contaminated soils' constrained modulus are 4.50~91.76 MPa and 4.22~88.68 MPa. Range of uncontaminated soils' constrained modulus is 4.15~105.53 MPa. Uncontaminated soils have the highest resistivity and constrained modulus, and nitidine chloride contaminated soils have middle resistivity and constrained modulus. While organophosphorus contaminated soils have the lowest resistivity and constrained modulus. Same pollutant has similar effects on soil resistivity and constrained modulus.

The results in Fig. 6 to Fig. 10 demonstrate that with the increase of soil cone tip resistance (q_t), sleeve friction (f_s), pore pressure (u_2), relative density (D_r), and constrained modulus (E_s), resistivity of soil (ρ) decrease in different degree. As aforementioned, there are several factors affect soil resistivity, pore fluid chemistry changed in pesticides contaminated soils, so resistivity changed. When soil relative density increase, the void ratio decrease, cone tip resistance and sleeve friction increase, soil microstructure variation, the porosity of soil decrease, and so soil resistivity change. In pesticides contaminated soils resistivity decrease. It is also shown that organophorus has much more influence on the properties of soil than nitidine chloride does.

IDENTIFICATION OF PESTICIDE CONTAMINATED SOILS

Identify soil type is one of the most common applications of CPTU test. This has been accomplished by using charts that link cone parameters with soil type, or accomplished by empirical correlations of cone parameters. A number of classification methods have been reported for predict soil type from either CPT or/both CPTU data. Several common used soil classify methods found in literature were list in Table 3.

TABLE 3
Soil classification methods based on CPT/CPTU data in literatures

References	Index of classification	Characteristic
Begemann (1965)	q_t , f_s	Site-specific, for Dutch soils
Jones and Rust (1982)	q_t , u	
Robertson et al. (1986) Campanella and Robertson (1988)	q_t , R_f/ Bq	Separate soil type into 12 zones,
Olsen and Malone (1988) Olsen and Mitchell (1995)	R_f , corrected q_{ct} Corrected R_f , corrected q_t	
Senneset and Janbu (1989)	B_q , q_t	Suitable for q_t<16MPa
Robertson (1990)	F_R, Q_t, q_t, Bq, R_f	
Jefferies and Davies (1991) Robertson and Wride (1998)	I_c	
Eslami and Fellenius (1997)	B_E, q_t	
Zhang and Tumay (1999, 2003) Kotzias et al. (2000)	U	
Liao (2005) Liao and Mayne (2012)	q_t, f_s, B_q	Truly three-dimensional soil classification scheme

Note: q_t - Cone tip resistance; f_s - Sleeve friction; u - Excess pore pressure; R_f - Friction ratio; B_q -Pore pressure ratio; B_E - Effect pore pressure ratio; Q_t - Normalized cone tip resistance; F_R - Normalized sleeve friction; I_c - Soil behavior type index; U - Soil classification index.

Douglas and Olsen (1981) first used electrical cone penetrometer to profile soils, they proposed a soil classification chart use parameters of q_t and R_f. The chart also indicates soil liquidity trends and earth pressure coefficient. Senneset and Janbu (1985) proposed pore pressure ratio, B_q, which is defined by Equation (3):

$$B_q = \frac{u_2 - u_0}{q_t - \sigma_{v0}} = \frac{\Delta u}{q_t - \sigma_{v0}} \quad (3)$$

where B_q is pore pressure ratio, u_0 is in-situ pore pressure, σ_{v0} is in situ total vertical stress, Δu is the excess pore pressure.

Robertson et al. (1986) defined soil classification charts used q_t, B_q, and R_f. Soil behavior type was divided into 12 zones in the charts. They point out occasionally soil will fall within different zones in each chart. Account for the influence of overburden stress, Robertson (1990) refined soil behavior type classification charts using normalized cone tip resistance Q_t and normalized friction ratio F_r, defined as follows:

$$Q_t = \frac{q_t - \sigma_{v0}}{\sigma'_{v0}} \quad (4)$$

$$F_r = \frac{f_s}{q_t - \sigma_{v0}} \quad (5)$$

where σ'_{v0} is effective vertical stress, equal to (σ_{v0}-u_0); other symbols are same as Equation (3) defined.

Among these classification methods, the charts proposed by Robertson et al. (1986) and Robertson (1990) are used commonly. According to Cai et al. (2011), the Robertson et al. (1986) classification charts are best appropriate for classifying recent clayey deposits in Jiangsu Province of China. Hence, this paper use the Robertson et al. (1986) charts to classify the soil type in the research site, to check whether the contaminated soils and uncontaminated soils locate at same zone in each chart.

In the test site, soil properties of q_t and B_q were obtained by RCPTU. According to the Robertson et al. (1986) soil classification charts, test site soil types are illustrated in Fig. 11.

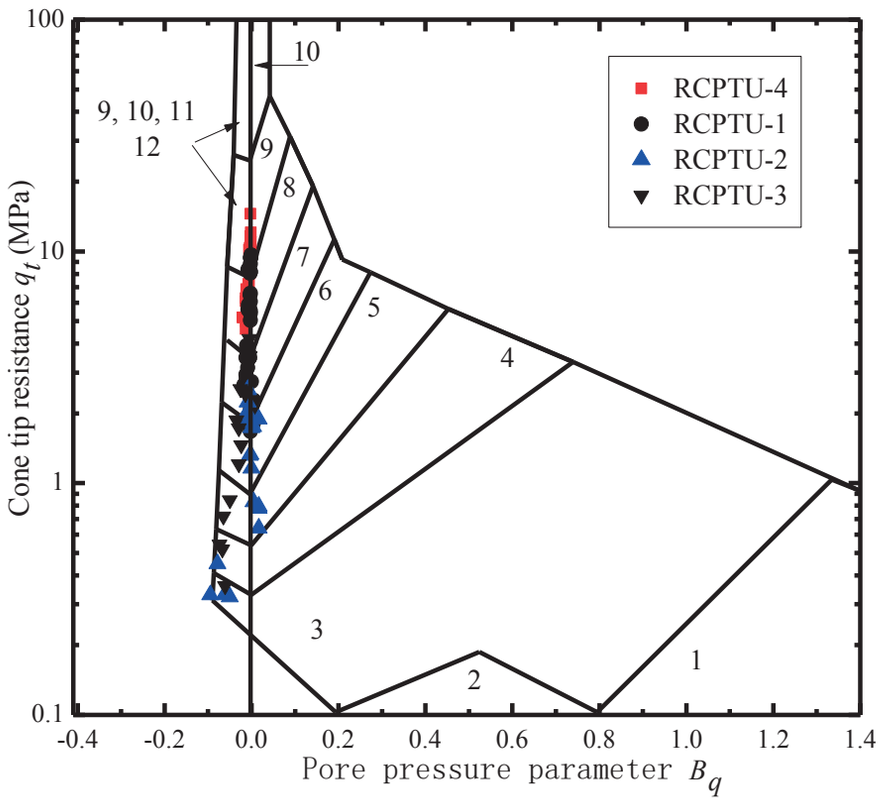

11(a) Soil classification chart based on q_t-B_q

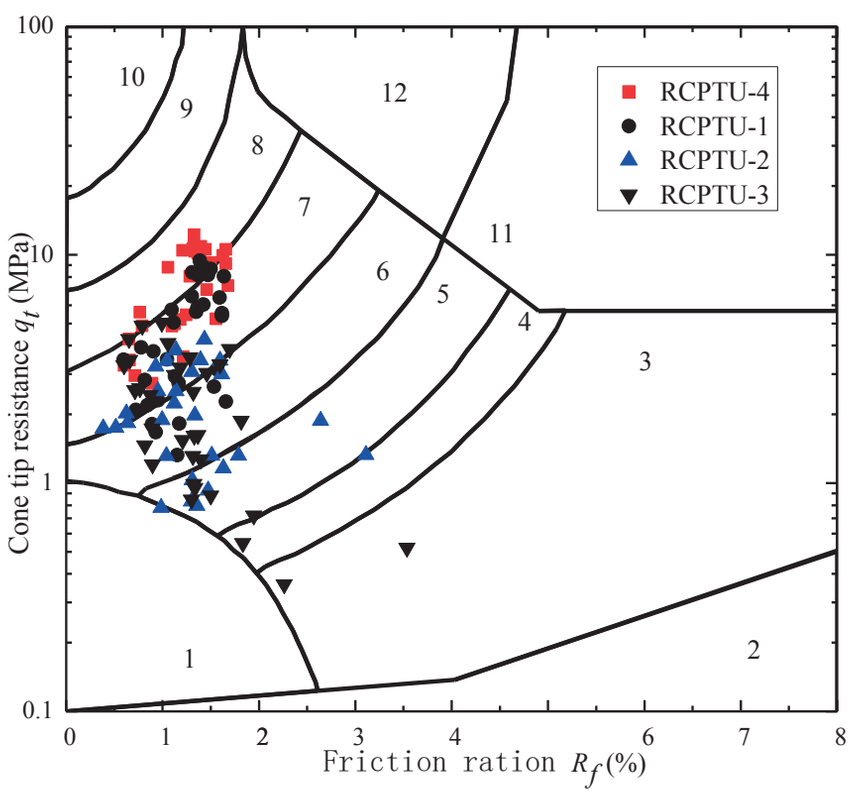

11(b) Soil classification chart based on q_t-R_f

FIGURE 11
RCPTU data plotted in Robertson et al. (1986) charts

Zones/Soil behavior type (from Robertson et al. 1986)

1. Sensitive fine grained	4. Silty clay to clay	7. Silty sand to sandy silt	10. Gravelly sand to sand
2. Organic material	5. Clayey silt to silty clay	8. Sand to silty sand	11.Very stiff fine grained*
3. Clay	6. Sandy silt to clayey silt	9. Sand	12. Sand and clayey sand*

Note: *(over consolidation or cemented)

Fig. 11(a) shows the results of classification by index of cone resistance (q_t) and pore pressure ratio (B_q). It is noted that uncontaminated soils belong to zones of 8 and 9; nitidine chloride contaminated soils belong to zones of 6 to 8, few of the data located at the dividing line of zone 8 and zone 9; organophorus contaminated soils belong to zones of 3 to7. As soil types in the research site mostly are sand, the B_q of the soil are very close, that is why the soil locations were so close to each other.

Fig. 11(b) is classified by cone tip resistance (q_t) and friction ration (R_f), it could be clearly seen that uncontaminated soils belong to zones of 7 and 8; nitidine chloride contaminated soils belong to zones of 6 and 7, few of the data located at the dividing line of zone 7 and zone 8; organophorus contaminated soils belong to zones of 3 to 7. It can be concluded that contaminated soils belong to different zones compare with uncontaminated soils, as the soil mechanical properties are affected by the pollutants.

SUMMARY AND CONCLUSIONS

This paper analyzed data of one pesticides contaminated site obtained by RCPTU, established the relationship of different type of soils resistivity with cone resistance, sleeve friction, pore pressure, relative density and constrained modulus. Some conclusions can be reached as follows:

(1) The relationship of each one is a linear correlation and has a similar trend with each other. Resistivity decrease linearly with the increase of soils properties. Each of the linear correlation has an acceptable coefficient of determination ($R^2 > 0.80$).

(2) It is noted that properties of contaminated soils such as cone tip resistance, sleeve friction, relative density, constrained modulus are lower than uncontaminated soils. Different pollutants influenced different degree of soil properties. Properties of nitidine chloride contaminated soils are higher than that of organophosphorus contaminated soils. They all have similar trend as uncontaminated soils, that is with increase of properties value, soil resistivity decrease.

(3) When using Robertson chart to classify soil type, contaminated soils located at different zones from uncontaminated soil. In this test site, uncontaminated soils belong to zones of 8 and 9 (q_t-B_q) or 7 and 8 (q_t-R_f), nitidine chloride contaminated soils belong to zones of 6 to 8 (q_t-B_q) or 6 and 7 (q_t-R_f), organophosphorus contaminated soil belong to zones of 3 to 7 (q_t-B_q) or 3 to 7 (q_t-R_f). Uncontaminated soils locate at higher zones than contaminated soil in the chart.

(4) It is feasible to use RCPTu as a help tool to judge whether the soil was contaminated. As the resistivity of organic pesticides contaminated soil is lower than uncontaminated soil. By the degree of the contaminated soils' resistivity decrease, whether the soil was contaminated can be judged, and proper measures can be taken to deal with the site.

ACKNOWLEDGMENTS

Majority of the work presented in this paper was funded by the National Natural Science Foundation of China (Grant No. 41202203), the Foundation for the New Century Excellent Talents of China (NCET-13-0118), the Foundation of Jiangsu Province Outstanding Youth (Grant No. BK20140027) and the Foundation for the Author of National Excellent Doctoral Dissertation of PR China (Grant No. 201353). These financial supports are gratefully acknowledged. The authors would like to express appreciations to the editor and anonymous reviewers for their valuable comments and suggestions.

REFERENCES

[1] Abu-Hassanein ZS, Benson CH, Blotz LR (1996) Electrical resistivity of compacted clays. J Geotech Engrg 122:397-406.

[2] Archie GE (1942) The electrical resistivity log as an aid in determining some reservoir characteristics. Trans Am Inst Min Eng 146:54-62.

[3] Baligh MM, Vivatrat V, Ladd CC (1980) Cone penetration in soil profiling. J Geotech Engrg 112(7):727-745.
[4] Banton O, Seguin MK, Cimon MA (1997) Mapping field-scale physical properties of soil with electrical resistivity. Soil Sci Soc Am J 61:1010-1017.
[5] Begemann HKS (1965) The friction jacket cone as an aid in determining the soil profile. Proc. Int. Conf. Soil Mech. Found. Eng. 6th, Montreal, Quebec, Canada, I:17-20.
[6] Cai GJ, Liu SY, Tong LY (2010) Field evaluation of deformation characteristics of a lacustrine clay deposit using seismic piezocone tests. Eng Geol 116:251-260.
[7] Cai GJ, Liu SY, Puppala AJ, Tong LY (2011a) Assessment of the coefficient of lateral earth pressure at rest (K_0) from in situ seismic tests. Geotech Test J 34(4):310-320.
[8] Cai GJ, Liu SY, Puppala AJ (2011b) Comparison of CPT charts for soil classification using PCPT data: Example from clay deposits in Jiangsu Province, China. Eng Geol 121:89-96.
[9] Cai GJ, Liu SY, Puppala AJ (2012) Liquefaction assessments using seismic piezocone penetration (SCPTU) test investigations in Tangshan region in China. Soil Dyn Earthq Eng 41:141-150.
[10] Campanella RG, Robertson PK (1988) Current status of the piezocone test. ISOPT-1, Orlando, March 22-24, 1:93-116.
[11] Campanella RG, Weemees I (1990) Development and use of an electrical resistivity cone for groundwater contaminated studies. Can Geotech J 27(5):557-567.
[12] Campanella RG (2008) The third James K Mitchell lecture: Geo-environmental site characterization. Geomechanics and Geoengineering: An International Journal 3:155-165.
[13] Cetin KO, Ozan C (2009) CPT-based probabilistic soil characterization and classification. J Geotech Geoenviron 135(1):84-107.
[14] Chan CM (2008) Evaluation of strength and electrical resistivity of a cement-stabilised malaysian clay. ISC'3. Taipei, Taiwan. Geothecnical and Geophysical Site Characterization. Londres. Taylor & Francis Group Ed: 285-288.
[15] Davies MP (1999) Piezocone technology for the geoenvironmental characterization of mine tailings. Dissertation, University of British Columbia.
[16] Douglas BJ, Olsen RS (1981) Soil classification using electric cone penetrometer. ASCE, Proceedings of Conference on Cone Penetration Testing and Experience, St. Louis, Oct 26-30:209-227.
[17] Eslami A, Fellenius BH (1997) Pile capacity by direct CPT and CPTU methods applied to 102 case histories. Can Geotech J 34(6):886-904.
[18] Fukue M, Minato T, Matsumoto M, et al. (2001) Use of a resistivity cone for detecting contaminated soil layers. Eng Geol 60:361-369.
[19] Hassona FA, Hassan MA, Abu-Heleika MM, et al. (2008) Correlations between electrical resistivity and some properties of clayey soil. ISC'3. Taipei, Taiwan. Geothecnical and Geophysical Site Characteriza-tion. Londres. Taylor & Francis Group Ed:837-841.
[20] Jefferies MG, Davies MP (1991) Soil classification using the cone penetration test. Discussion. Can Geotech J 28(1):173-176.
[21] Jones GA, Rust E (1982) Piezometer penetration testing, CUPT. ESOPT-2, Amsterdam, May 24-27, 2:607-614.
[22] Jung BC, Gardoni P, Biscontin G (2008) Probabilistic soil identification based on cone penetration tests. Geotechnique 58(7):591-603.
[23] Kim YS, OH MH, Park J (2007) Laboratory study on the dielectric properties of contaminated soil using CPT deployed probe. Geosci J 11(2):121-130.
[24] Kim YS, OH MH, Park J (2009) Analysis of resistivity data obtained from cone penetrometer in contaminated soil layers. Environ Geol 58:1309-1317.
[25] Kotzias P, Stamatopoulos A, Zhang Z, Tumay M (2000) Statistical to Fuzzy Approach toward CPT Soil Classification. J Geotech Geoenviron Eng. 126(6):577-580.
[26] Liao TF (2005) Post Processing of Cone Penetration Data for Assessing Seismic Ground Hazards, with Application to the New Madrid Seismic Zone. Dissertation, Georgia Institute of Technology.
[27] Liao T, Mayne PW (2012) True Three-Dimensional Soil Classification Based On CPTu Data. GeoCongress 2012, ASCE:2599-2608.
[28] Liu SY， Cai GJ， Du YJ，et al. (2012) Site Investigation of a Pesticide Contaminated Factory Based on In-situ Resistivity Piezocone Tests in Southeastern China. ISC-4. London: Taylor & Francis Group:1757-1764.
[29] Liu SY, Du YJ, Han LH, et al. (2008) Experimental study on the electrical resistivity of soil–cement admixtures. Environ Geol 54:1227–1233.
[30] Lunne T, Robertson PK, Powell JJM (1997) Cone Penetration Testing in Geotechnical Practice. Blackie Academic and Professional, London.
[31] Marluci CP, Peixoto ASP, Yamasaki MT (2011) Electrical potential field around the laboratory resistivity equipment. Pan-Am CGS Geotechnical Conference.

[32] Mondelli G, Giacheti HL, Boscov MEG et al. (2007) Geoenvironmental site investigation using different techniques in a municipal solid waste disposal site in Brazil. Environ Geol 52:871-887.
[33] Oh MH, Kim YS, Park JB, et al. (2008) Laboratory study on applicability of resistivity cone for investigation of subsurface contamination. ISC'3. Taipei, Taiwan. Geothecnical and Geophysical Site Characteriza-tion. Londres. Taylor & Francis Group Ed:737-743.
[34] Olsen RS, Malone PG (1988) Soil classification and site characterization using the cone penetrometer test. ISOPT-1, Orlando, March 22-24, 2:887-893.
[35] Olsen RS, Mitchell JK (1995) CPT stress normalization and prediction of soil classification. Proc Int Symp on Cone Penetration Testing, CPT 95, Linkoping, Sweden. 257-262.
[36] Peixoto ASP, Pregnolato MC, Silva ACCL, et al. (2010) Development of an electrical resistivity measure for geotechnical and geoenvironmental characterization. CPT'10. Huntington Beach, CA, USA: 1-7.
[37] Rhoades JD, Schilfgaarde JV (1976) An electrical conductivity probe for determining soil salinity. *S*oil Sci Soc Am J 40:647-650.
[38] Robertson PK, Campanella RG, Gillespie D, et al. (1986) Use of piezometer cone data. Proc of ASCE, In-Situ 86 Specialty Conference, Edited by S. Clemence, Blacksburg, June 23-25, Geotechnical Special Publication No.6:1263-1280.
[39] Robertson PK (1990) Soil classification using the cone penetration test. Can Geotech J 27 (1):151-158.
[40] Robertson PK, Wride CE (1998) Evaluating cyclic liquefaction potential using the cone penetration test. Can Geotech J 35(3):442-459.
[41] Robertson PK, Robertson CKL (2012) Guide to Cone penetration testing for geotechnical engineering (5th edition). Gregg Drilling & Testing Inc.
[42] Senneset K, Sandven R, Janbu N (1989) Evaluation of soil parameters from piezocone test. In-situ testing of soil properties for transportation, Transportation Research Record, No. 1235, Washington, D. C.: 24-37.
[43] Siddiqui FI, Baharom SABSO (2013) Simple and multiple regression models for relationship between electrical resistivity and various soil properties for soil characterization. Environ Earth Sci (2013) 70:259–267.
[44] Tumay MT, Boggess RL, Acar Y (1981) Subsurface investigation with piezocone penetrometer. ASCE GSP on Cone Penetration Testing and Experience, St Louis, MO: 325-342.
[45] Weemees IA (1990) Development of an electrical resistivity cone for groundwater contamination studies. Dissertation. University of British Columbia.
[46] Zhang Z, Tumay MT (1999) Statistical to fuzzy approach toward CPT soil classification. J Geotech Geoenviron Eng 125(3):179-186.
[47] Zhang Z, Tumay MT (2003) Non-traditional approaches in soil classification derived from the cone penetration test, ASCE Special Publication No. 121 on Probabilistic Site Characterization at the National Geotechnical Experimentation Sites:101-149.
[48] Zuidberg HM, Schaap LHJ, Beringen FL (1982) A penetrometer for simultaneously measuring of cone resistance, sleeve friction and dynamic pore pressure. Proceedings of the Second European Symposium on Penetration Testing, ESOPT-2, 2:963-970.

Received: **31.07.2015**
Accepted: **06.12.2015**

CORRESPONDING AUTHOR

Guojun Cai
Southeast University
Institute of Geotechnical Engineering
210096 Nanjing – CHINA

e-mail: focuscai@163.com

by PSP Volume 25 – No 1/ 2016, pages 240-248 Fresenius Environmental Bulletin

MEASURING ENVIRONMENTAL EFFICIENCY IN THE EU AGRICULTURAL SECTOR "CONSIDERING DESIRABLE AND UNDESIRABLE OUTPUTS"

Altug Özden

Adnan Menderes University,Faculty of Agroculture,Department of Agrocultural Economics, Aydin-Turkey

ABSTRACTS

One of the major objectives of the European Union economic policy is to become a low-carbon and resource efficient economy. Therefore, aiming to increase the efficiency of inputs used in the agricultural production is gaining importance. Efficiency scores are calculated for the goal of the new CAP framework 2014-2020 and 20-20-20 strategy by single and multi-output models. Value of agricultural Production and CO_2 emission levels are considered as desirable and undesirable outputs. Environmental, production and emission efficiencies of EU countries and the candidate country Turkey are determined with a new index which can be used by Data Envelopment Analysis methodology and existing software. In this paper its determined that, CO_2 emission and energy consumption can be reduced by 19.62% and 11.51% while the agricultural production value increased by 15.80%. Also its determined that countries should be reduce capital stock by 8.83%, cattle population by 3.67%, fungicide and bactericide use by 4.57%, herbicide use by 4.41%, insecticide use by 5.04%, and nitrogen, phosphate and potassium fertilizer consumption by 11.87%, 10.59%, and 10.34%.

KEYWORDS:
DEA, Desirable and Undesirable Outputs, Environmental Efficiency.

INTRODUCTION

After the 1950's the first aim of production was to produce more. In this respect many studies were carried out to increase the production. This was especially true in agricultural production, due to the increase of population and hunger. Earlier attempts to increase agricultural production, such as plant breeding, use of pesticides, and chemical fertilizers led to more modern techniques such as GMO (Genetically Modified Organism) crops. Over the time, these techniques included economic aspects such as resource utilization, and efficiency has been gaining importance. However, environmental problems constitute a serious threat, both domestically and globally [1]. Nowadays, sustainability and reducing environmental impact, such as pollution, is considered an integral part of production. The products which produced in this way have higher market prices and more preferable [2]. This condition has brought forward the undesirable outputs which was previously unheeded and production processes reached to a new level. To ensure that economic and environmental productivity continues to increase in the agricultural sector, agricultural inputs must be used at their optimum levels [3].

There are undesirable outputs in the agricultural production, even agricultural practices contribute about 20% of the global annual emission of carbon dioxide (CO_2) [4]. Due to this, environmental efficiency analysis in agriculture and undesirable outputs have received attention and many researchers have made researches in this field [5-6-7-8-9-10-11-12-13-14].

One of the major objectives of the European Union (EU) economic policy is to become a low-carbon and resource efficient economy. According to this goal by the year 2020 EU needs to decrease the CO_2 emissions by 20%, increase the efficiency of energy use by 20% and produce the 20% of the overall energy being consumed by renewable energy resources (20-20-20 strategy) [15]. Using statistical relationships between agricultural production and undesirable outputs, it is concluded that there is considerable potential for CO_2 mitigation by total European agriculture [16]. The Common Agricultural Policy (CAP), has set a series of environmental preconditions which should be satisfied by the farmers. The new CAP framework for the 2014-2020 programming period reinforces the environmental conservation agenda, aiming to increase the efficiency of inputs used in the agricultural production [14].

The main purpose of this paper is to calculate the agricultural efficiency scores of the EU countries and the candidate country, Turkey, considering desirable and undesirable outputs with the aim of CAP framework (2014-2020). The

secondary purpose is to determine the input levels which will decrease CO_2 emissions levels for the goal of 20-20-20 strategy.

MATERIALS AND METHODS

The main methodology used is the estimation of a production frontier function with eleven inputs and two outputs in order to measure the technical efficiency in agricultural sector. EU countries and candidate country Turkey, which produce 16% of the total agricultural production value of the EU have considered as the decision making units (DMU). The data for these countries were obtained from Food and Agriculture Organization of the United Nations (FAO). Total Value of Agricultural Production (million US$) and Emissions from agriculture (CO_2 equivalent) (Giga kilograms) (FAO, 2012) have been determined as output. Inputs are determined as;

I_1: Energy used in agriculture (Calculated by multiplication of the ratio of the energy used in agriculture to total energy production [17] and the total energy production [18] **(Energy)**

I_2: Agricultural land **(Land)**

I_3: Agricultural net capital stock **(Cap.)**

I_4: Total economically active population in agriculture **(Pop.)**

I_5: Cattle stock **(Cattle)**

I_6: Usage of total Fungicides & Bactericides **(F&B)**

I_7: Usage of total Herbicides **(Herb.)**

I_8: Usage of total Insecticides **(Ins.)**

I_9: Consumption of Nitrogen Fertilizers (N total nutrients) **(N)**

I_{10}: Consumption of Phosphate Fertilizers (P205 total nutrients) **(P)**

I_{11}: Consumption of Potash Fertilizers (K20 total nutrients) **(K)**

As agricultural land and population inputs can only be interfered with long term policies they are calculated as uncontrolled inputs.

Data Envelopment Analysis (DEA) has been used for estimation of efficiency scores. This non-parametric efficiency estimate method applying frontier functions was introduced by Charnes, Cooper and Rhodes [19] and has been modified and extended after further research [20-21]. DEA allows for the evaluation of each DMU by producing one or several outputs from a common set of inputs. Technical efficiency scores have been calculated as single-output and multi-output. In the single output model, value of agricultural production (desirable output) has been determined as output and named as Production Efficiency **(PE)**. In the second model only the emission values (undesirable output) have been determined as output and named as Emission Efficiency **(ESE)**. Lastly in the third model, value of agricultural production and emission values determined as outputs at the same time and named as Environmental Efficiency **(EE)**.

Framework. The efficiency of each unit is defined as the ratio of the weighted sum of outputs in relation to the weighted sum of inputs. In other words, technical efficiency criterion (for j^{th} decision point) for any decision point can be determined by;

$$TE = \frac{u_1 y_1 + u_2 y_2 + \ldots + u_n y_n}{v_1 x_1 + v_2 x_2 + \ldots + v_m x_m} \qquad (1)$$

There are *"n"* pieces output and *"m"* pieces input for j^{th} decision point. Here u_n represents the weight of n^{th} output, y_n represents the amount of n^{th} output, v_m represents weight of m^{th} input and x_m represents the amount of m^{th} input. As can be seen from equation 1, DEA includes a fractional programming process. However, it is difficult to solve the fractional programming. Therefore fractional programming set can be solved by converting to linear programming set with the assumption that the denominator of the equation equals to one. Generally in DEA two models are used. These are CCR (Charnes-Cooper-Rhodes) [19] model and BCC (Banker-Charnes-Cooper) [22] model. In both models, fractional programming-linear programming transformation can be used for calculation. CCR model is based on assumptions of Constant Returns to Scale (CRS). If the efficiency of the j^{th} *DMU is* g_j, the aim should be the maximization of this value. In this case, under the assumption of output orientation, the objective function and the constraints should be defined as :

$$OFh_j = \frac{\sum_{r=1}^{n} u_r y_r}{\sum_{i=1}^{m} v_i x_i} \qquad (2)$$

Constraints;

$$\frac{\sum_{r=1}^{n} u_r y_r}{\sum_{i=1}^{m} v_i x_i} \leq 1$$

$$u_r \geq 0 \qquad (3)$$

$$v_i \geq 0$$

When equations 2 and 3 expressed with linear programming logic, equations 4 and 5 will be obtained.

$$OFh_j = \sum_{i=1}^{m} v_i x_i \quad (4)$$

$$\sum_{r=1}^{n} u_r y_r = 1$$

$$-\sum_{r=1}^{n} u_r y_r + \sum_{i=1}^{m} v_i x_i \geq 0$$

$$u_r, v_i \geq 0 \quad (5)$$

BCC model is based on the assumption of the VRS. The only difference from CCR model of BCC model is the sum of λ (Values that provide the information which is necessary to create a possible efficient input-output combination for an inefficient DMU) values equals to one. In this case the model will be as follows:

s.t.

$$OFh_k$$

$$\sum_{j=1}^{N} y_{rj}\lambda_{jk} \geq y_{rk}$$

$$h_k x_{ik} - \sum_{j=1}^{N} x_{ij}\lambda_{jk} \geq 0 \quad (6)$$

$$\sum_{j=1}^{N} \lambda_j = 1$$

Scale efficiency (SE) can be calculated by the ratio of CRS and VRS technical efficiency scores.

$$SE = \frac{TE_{crs}}{TE_{vrs}} \quad (7)$$

In many studies, there are environmental based efficiency scores that named eco-efficiency or environmental efficiency which were calculated by different models. However, these models cannot be included in the commonly used basic DEA software. Unlike other studies in this paper, the undesirable output (emission value) is included to the model as CO_2^{-1}. In the output-oriented efficiency models, the aim is to maximize the output. So in this condition, the fact that when the model try to maximize the output, emissions will be minimized. It is thought that although there are models which can minimize the output, this new simple indexing method can be used with all DEA software's for the models that have desirable and undesirable outputs. The data were analysed by Banxia Frontier Analyst, Stata and SPSS software.

RESULTS AND DISCUSSION

In this study all data were analysed for 29 countries. In terms of their contribution to total value of agricultural production, the leading countries are France (17%), Turkey (16%), Germany (12%), Italy (9%), Spain (9%), UK (5%), Poland (5%), Romania (4%) and Greece (4%). These nine countries constitutes more than 80% of the total value of agricultural production. The remaining 20 countries are relatively smaller countries and specialized in other producing areas. The same nine countries are responsible for more than 80% of the total CO_2 emissions from agriculture and their shares are respectively, France (16%), Germany (14%), UK (10%), Turkey (9%), Spain (9%), Poland (9%), Italy (8%), Romania (4%) and Greece (3%). In the Analysis, 2 outputs and 11 inputs have been used. Descriptive statistics for inputs and outputs are given in Table 1.

TABLE 1
Descriptive Statistics of Inputs and Outputs

N=29	Mean	STD	Min.	Max.
Value of agricultural production (million US$)	15832	21743	147	77901
CO_2^{-1} (Giga kilograms^{-1})	0.616	2.024	0.012	10.917
Energy used in agriculture (Quadrillion Btu)	2.600	1.540	0.310	6.460
Agricultural land (1000 ha)	7758	9777	10	38407
Agricultural net capital stock (million US$)	26721	33304	96	123247
Total economically active population in agriculture (1000)	616	1485	2	7809
Cattle stock (1000 head)	3466	4680	16	19006
Usage of total Fungicides & Bactericides (tonnes)	5371	9666	47	42537
Usage of total Herbicides (tonnes)	4180	5349	36	22632
Usage of total Insecticides (tonnes)	1610	3439	13	14335
Consumption of Nitrogen Fertilizers (tonnes)	422417	549899	1969	1914915
Consumption of Phosphate Fertilizers (tonnes)	111986	146411	10	612825
Consumption of Potash Fertilizers (tonnes)	99305	130627	30	446185

The efficiency calculations have been done as single-output and multi-output. Primarily only value of agricultural production, then only CO_2 emission has been included to the calculations as an output. In the multi output model value of agricultural production (as desirable output) and CO_2 emission (as undesirable output) were included to the calculations. Technical efficiency scores about desirable and undesirable outputs are given in Table 2. Density distributions about efficiency scores can be seen in Figure 1.

TABLE 2
Descriptions of the Technical Efficiency Scores

Models	Production Efficiency			Emission Efficiency			Environmental Efficiency		
	CCR	BCC	SCA	CCR	BCC	SCA	CCR	BCC	SCA
Mean	0.81	0.84	0.96	0.32	0.39	0.69	0.69	0.71	0.92
SD	0.59	0.65	0.87	0.12	0.15	0.61	0.47	0.52	0.87
Min.	1.00	1.00	1.00	1.00	1.00	1.00	1.00	1.00	1.00
Max.	0.09	0.13	0.11	0.12	0.19	0.17	0.16	0.11	0.07
%Efficient Countries	35	45	35	14	17	18	21	24	35
Correlation between CCR-BCC	0.816***			0.811***			0.571**		
Correlation between BCC-SCA	0.479**			0.779***			0.129		
Correlation between CCR-SCA	0.901***			0.732***			0.857***		

*** Significant at level 0.01, **Significant at level 0.05

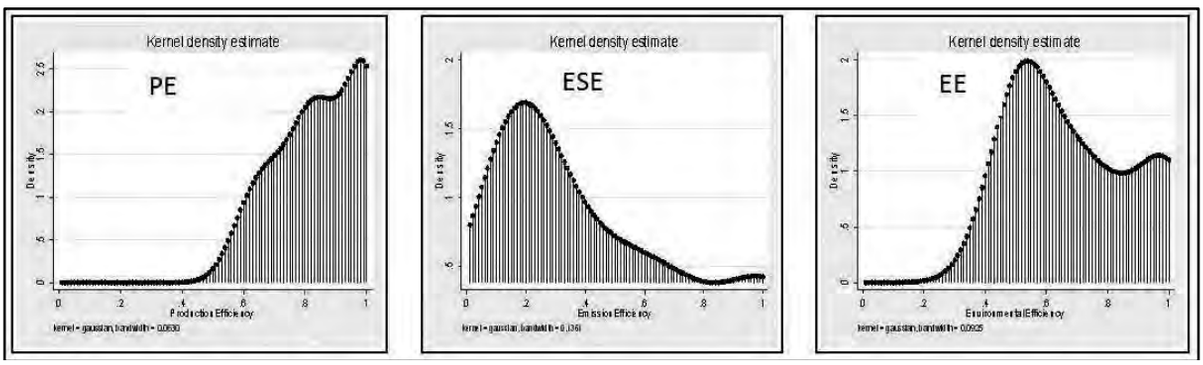

FIGURE 1
Kernel Density Estimates of the Technical Efficiency Scores

BCC model scores that computed for both PE and ESE are higher than the CCR model scores as expected. The reason for this is, in BCC models more DMUs can find their way to the frontier [23-24-25]. PE scores are in medium-high level and in concordance with many other studies [5-6-8-11]. The referenced countries for CCR and BCC models are Germany, France, Holland, Spain, Sweden, Italy, Romania, Slovenia, Turkey and Greece. These countries are also determined as full efficient. The lowest score is belongs to Latvia with 59.32%. When a comparison for agricultural production is made from the production efficiency, although England (87.35%) and Poland (69.04%) have high production values it is observed that they have not managed to reach the required achievement. However the impact of natural conditions on agricultural production should not be forgotten. The countries have high scale efficiencies and it is determined that the disadvantage due to scale is about 4%. There are statistically significant positive relationships between the CCR, BCC and SCA efficiency scores. In terms of value of agricultural production, it is determined that Hungary, UK, Portugal, Czech Republic and Slovakia are producing subject to non-increasing returns to scale, Croatia and Poland are producing subject to decreasing returns to scale and the remaining countries are producing subject to constant returns to scale.

ESE scores are quite low compared to the PE scores. The means of technical efficiency scores are 32% (CCR), 39% (BCC) and 69% (SCA) and these scores shows that the emission efficiencies of the countries are rather low. This condition represents that the countries can have a lower CO_2 emission levels with the same amount of input or with the lower levels of input have the same emission levels. The main issue here is the reduction of CO_2 emission levels. In order to reduce agricultural CO_2 emission levels, inputs should be reduced. Malta, Estonia, Sweden and Bulgaria are appeared as a reference point for both CCR and BCC models and it is also seen that they are 100% efficient. In accordance with the input levels of these four countries, it is observed that these countries produced the lowest levels of CO_2 emission. From perspective of the agricultural input, among the 29 countries Malta has the lowest emission level, Estonia has the lowest 7th, Bulgaria 11th and Sweden has the lowest 15th. Malta and Estonia in comparison to other countries have low and similar agricultural production and input usage. But Sweden and Bulgaria have a perceivable share for total agricultural production. Due to this reason both the countries ESE scores and the used agricultural input and CO_2 emission scale between them is rather important. When examining the inputs of the both countries it is seen that their input amounts are very similar to each other. In Sweden it is observed that the cattle number and the amount of phosphate fertilizers and in Bulgaria amounts of pesticides and other chemical fertilizers are commonly used. As per the CCR model the lowest ESE scored countries are Poland (12%), Turkey (18%), Greece (19%), Hungary (19%) and France (20%) and as per the BCC model are Poland (15%), Turkey (19%), France (%22), Hungary (22%) and Greece (23%). There are also statistically significant positive relationships between the CCR, BCC and SCA efficiency scores. As a result of the calculations for CO_2 emission, only five countries (Sweden, Bulgaria, Malta, Estonia, Lithuania) produce subject to constant returns to scale and the remaining countries produce subject to increasing returns to scale or decreasing returns to scale and as per the ESE scores the %100 efficient countries are the countries that produce subject to constant returns to scale.

As expected, the mean of EE scores are between the means of PE and ESE scores. In the previously mentioned papers for agricultural sector,

differently named efficiency studies like eco-efficiency, environmental efficiency or sustainable efficiency which were considered the desirable and undesirable outputs have been studied. The results of this paper are in concordance with these studies [5-6-9-11-14]. In terms of EE scores Netherlands, Sweden, Germany, France and Bulgaria are determined as reference countries (100% efficient both in CCR and BCC models.

Only Sweden within these counties have been determined as not alone single output but also multi-output as most efficient country. In the study done for the 15 European countries, Sweden has been determined as the most efficient country for environmental efficiency and in the other studies done for the EU countries, Netherlands and Bulgaria have been pointed out as reference countries [11-14]. The lowest EE scored countries are Portugal (47%) and Czech Republic (48%) for CCR model and Czech Republic (52%) and Portugal (53%) for BCC model. Also in the previously studies, Czech Republic and Portugal determined as with lowest efficiency scores. EE scores of the main countries with the highest agricultural production values are listed as Spain (84%), UK (79%), Italy (74%), Greece (71%), Turkey (66%), Poland (55%), and Romania (54%). In other studies the calculated scores for UK were 82% and 89%. In addition, in this study the calculated score rankings for these countries show similarities with the other studies [9-11-14].

As a result of the calculations, it is observed that six countries (Hungary, UK, Portugal, Latvia, Czech Republic, Slovakia) produce subject to decreasing returns to scale, two countries (Croatia, Poland) produce subject to increasing returns to scale and the remaining countries produce subject to constant returns to scale. It is also seen that the %100 efficient countries are the ones that produce subject to constant returns to scale. The mean of SCA scores are at a high level. After an efficiency estimate is obtained, it is interesting to analyse the magnitude of the slacks for each output in order to find out the increase percentage they could achieve if we eliminated inefficiency. Table 3 shows the total slacks, as well as those corresponding to the decrease in inputs given the output orientation.

TABLE 3
Total Improvements in Variables (%)

	VAP	CO_2	Energy	Cap.	Cattle	F&B	Herb.	Ins.	N	P	K
PE	8.92 (5.16)	-	7.06 (7.11)	4.88 (3.47)	1.55 (1.98)	3.09 (2.17)	4.05 (5.73)	5.18 (4.78)	12.23 (9.14)	13.10 (8.11)	11.54 (7.12)
ESE	-	37.94 (14.47)	17.77 (1.41)	1.37 (1.59)	5.48 (6.12)	7.35 (4.51)	8.41 (5.42)	6.21 (4.19)	13.85 (8.83)	14.13 (9.21)	12.56 (9.61)
EE	15.80 (11.54)	19.62 (13.91)	11.51 (10.28)	8.83 (6.36)	3.67 (6.11)	4.57 (5.78)	4.41 (6.05)	5.04 (9.09)	11.87 (9.97)	10.59 (8.16)	10.34 (8.84)

*Values in parentheses are standard deviations

In view of the slacks in technically inefficient countries, an increase of up to 8.92% on average in value of agricultural production should be possible; the potential decline in CO_2 emissions (37.94%) and the potential improvement for value of agricultural production and decline for CO_2 in multi-output performance rises to 15.80% for VAP and 19.62 for CO_2 emission on average. As to inputs, it is relevant to highlight the mean slack of N, P, and K for value of agricultural production, CO_2 emission and multi-output performance. A noticeable variability in the slacks of variables is shown all over the sampling (Table 3). While there are some completely efficient countries that make an optimum use of resources, there are some other countries with a very low level of efficiency. EE scores and improvements in variables of 29 countries can be seen in Table 4.

In view of slacks, the main countries with the highest agricultural production values, Romania and Turkey especially should reduce their energy consumption, Poland and U.K. especially should reduce their N, P, K fertilizers consumption and cattle stock, Spain, Italy and Greece should reduce all inputs in a balanced way.

TABLE 4
EE Scores and Improvements in Variables (%)

Countries	EE (%)	VAP	CO2	Energy	Capital	Cattle	F&B	Herb.	Ins.	N	P	K
Austria	71.25	12.23	20.24	8.21	2.11	0	3.31	0	0	15.51	12.10	9.48
Belgium	66.36	8.81	19.48	12.54	5.21	0	2.16	5.16	7.45	21.25	14.54	7.65
Bulgaria	100.00	0	0	0	0	0	0	0	0	0	0	0
Croatia	49.12	31.25	41.48	13.30	11.23	17.50	5.50	3.31	4.86	36.60	26.20	25.50
Cyprus	51.26	12.10	26.25	39.91	18.23	0	1.10	6.16	10.54	2.25	8.10	24.40
Czech Rep.	48.23	27.23	27.23	8.31	15.53	0	12.85	13.00	43.16	24.10	11.00	11.90
Denmark	90.32	9.25	10.21	4.56	0	2.36	0	0	0	2.51	1.18	3.47
Estonia	68.45	14.33	14.25	2.23	7.25	4.16	2.21	4.12	1.25	17.41	11.24	5.36
Finland	75.18	25.23	5.23	5.28	3.21	0	0	0	0	8.16	15.35	14.84
France	100.00	0	0	0	0	0	0	0	0	0	0	0
Germany	100.00	0	0	0	0	0	0	0	0	0	0	0
Greece	70.85	8.21	20.01	12.20	9.29	3.11	4.56	2.20	3.32	14.41	10.25	9.96
Hungary	52.21	16.80	6.80	13.29	12.53	0	0	22.20	26.90	17.70	10.54	7.89
Ireland	54.29	22.21	22.21	9.25	8.22	3.20	2.11	3.41	8.12	11.24	12.14	9.46
Italy	74.42	6.31	25.12	9.15	5.21	1.18	4.12	0	5.21	10.35	8.85	12.54
Latvia	63.25	36.69	19.69	19.11	17.2	0	0	0	3.50	12.60	13.20	9.20
Lithuania	59.56	29.20	29.20	15.50	14.20	16.92	0	17.70	3.90	0	14.80	13.40
Luxembourg	67.21	18.80	15.80	8.90	5.80	19.30	3.28	4.57	11.60	19.10	0	10.60
Malta	61.58	31.05	11.05	33.26	18.80	0	1.29	2.36	3.33	2.23	1.02	1.14
Netherlands	100.00	0	0	0	0	0	0	0	0	0	0	0
Poland	55.05	44.80	44.80	12.25	11.90	5.16	13.50	10	0	29.80	21.60	24.70
Portugal	47.10	14.25	24.50	5.41	12.50	4.18	17.20	13.80	7.51	5.27	12.30	14.40
Romania	53.68	17.21	27.45	32.25	14.15	2.10	18.80	0	0	12.10	7.11	4.48
Slovakia	50.96	21.25	54.00	19.25	16.40	0	16.21	14.40	0	17.10	19.20	5.24
Slovenia	50.54	9.25	34.65	20.30	13.30	1.80	9.90	0	0	25.0	28.90	25.50
Spain	84.12	15.96	15.96	1.21	5.16	0	5.51	3.16	4.18	4.48	12.10	8.08
Sweden	100.00	0	0	0	0	0	0	0	0	0	0	0
Turkey	66.22	7.85	35.66	21.25	10.21	6.18	8.89	2.21	1.32	11.41	10.15	6.56
U.K.	79.31	17.80	17.80	6.91	18.50	19.40	0	0	0	23.70	25.10	34.00

CONCLUSION

This paper studies the level of technical efficiency of production and environmental management in the agricultural sector. The technique used is on a non-parametric frontier method. When output oriented efficiency is to be measured, desirable and undesirable outputs cannot be used together due to the maximization of both outputs. Therefore it is necessary to design and evaluate a new index in order to measure the technical efficiency of production and environmental management, which can then be used with the existing software. In order to accomplish this, a new index was produced by changing the place of the numerator and denominator for undesirable outputs (CO_2 emissions).

The countries analysed have a medium-high technical efficiency level for value of agricultural production, medium-low level for CO_2 emissions, and medium-level for multi-output. It was also found that the countries that are technically most

efficient were those which produce subject to Constant returns to scale.

As a conclusion, in order for the countries to reach optimal levels of production while controlling both value of agricultural production and CO_2 emissions, they must reduce their energy consumption by 11.51%, capital by 8.83%, cattle population by 3.67%, fungicide and bactericide use by 4.57%, herbicide use by 4.41%, insecticide use by 5.04%, and nitrogen, phosphate and potassium fertilizer consumptions by 11.87%, 10.59%, and 10.34%, respectively. With the purpose of 20-20-20 strategy, we determined that CO_2 emission and energy consumption can be reduced by 19.62% and 11.51%. It goes without saying that, in this case, countries can adjust their inputs without impacting value of agricultural production, while reducing their emissions. In a study carried out in Spain, it has been shown that reducing the environmental pressure would not affect the economic performance [13]. Agricultural land and population are parameters influenced by long term policies, and hence have been used as uncontrolled inputs in this study. Because of this, no improvement due to these parameters have been investigated.

The efficiency scores calculated in this study display similarities with the scores calculated by different models in different studies. Therefore, a simple index (1/undesirable output) can be utilized in DEA calculations and software and this index can be added to the minimized and maximized efficiency calculations.

REFERENCES

[1] Armagan, A., Turgut, C. (2008). Analysis of Environmental Pollution with Multivariate Statistical Tecniques. Fresenius Environmental Bulletin, 17(8), 978-984.

[2] Buller, H., Morris, C. (2004). Growing goods: the market, the state, and sustainable food production. Environment and Planning, A 36(6), 1065 – 1084.

[3] Ozer, O. O. (2014). Analysİs of the Factors That Affect the Informatıon Sources for Wheat Farmers Using Pesticides in Turkey. Fresenius Environmental Bulletin, 13(4), 1068-1023.

[4] Lal, R. (2004). Carbon emission from farm operations. Environment International, 30(7), 981-990.

[5] Reinhard, S., Knox Lovell, C. A., Thijssen, G. J. (1999). Econometric Estimation of Technical and Environmental Efficiency: An Application to Dutch Dairy Farms. American Journal of Agricultural Economics, 81(1), 44-60.

[6] Reinhard, S., Knox Lovell, C. A., Thijssen, G. J. (2000). Environmental efficiency with multiple environmentally detrimental variables; estimated with SFA and DEA. European Journal of Operational Research, 121(2), 287-303.

[7] Zaim, O., Taskin, F. (2000). Environmental efficiency in carbon dioxide emissions in the OECD: A non-parametric approach. Journal of Environmental Management, 58(2), 95-107.

[8] Coelli, T., Lauwers, L., Huylenbroeck, G. V. (2007). Environmental efficiency measurement and the materials balance condition. Journal of Productivity Analysis, 28, 3-12.

[9] Serrao, A. (2008). Measuring Eco-efficiency of Agricultural Activity in European Countries: A Malmquist Index Analysis. American Agricultural Economics Association (New Name 2008: Agricultural and Applied Economics Association), Annual Meeting, July 27-29, Orlando, Florida.

[10] Gomez-Limon, J. A., Picazo-Tadeo, A. J., Reig-Martinez, E. (2012). Eco-efficiency assessment of olive farms in Andalusia. Land Use Policy, 29, 395-406.

[11] Hoang, V., Alauddin, M. (2012). Input-Orientated Data Envelopment Analysis Framework for Measuring and Decomposing Economic, Environmental and Ecological Efficiency: An Application to OECD Agriculture. Environmental and Resource Economics, 51(3), 431-452.

[12] Falavigna, G., Manello, A., Pavone, S. (2013). Environmental efficiency, productivity and public funds: The case of the Italian agricultural industry. Agricultural Systems, 121, 73-80.

[13] Beltran-Esteve, M., Gomez-Limon, J. A., Picazo-Tadeo, A. J., Reig-Martinez, E. (2014). A metafrontier directional distance function approach to assessing eco-efficiency. Journal of Productivity Analysis, 41(1), 69-83.

[14] Vlontzos, G., Niavis, S., Manos, B. (2014). A DEA approach for estimating the agricultural energy and environmental efficiency of EU countries. Renewable and Sustainable Energy Reviews, 40, 91-96.

[15] European Commission. (2010). Communication from the Commission: Europe 2020. A Strategy for smart, sustainable and inclusive growth. 3.3.2010, COM(2010) 2020.

[16] Smith, P., Powlson, D. S., Smith, J. U., Falloon, P., Coleman, K. (2000). Meeting Europe's climate change commitments: quantitative estimates of the potential for

carbon mitigation by agriculture. Global Change Biology, 6(5), 525-539.
[17] Anonymous. (2012a). http://www.fao.org, [May, 2015]
[18] Anonymous. (2012b). http://www.eia.gov, [June, 2015]
[19] Charnes, A., Cooper, W. W., Rhodes, E. (1978). Measuring the efficiency of decisionmaking units. European Journal of Operational Research, 2, 429-444.
[20] Färe, R., Grosskopf, S., Lovell, C. (1994). Production Frontiers. Cambridge University Press, London.
[21] Cooper, W., Seiford, L., Kaoru, T. (2006). Data Envelopment Analysis: A Comprehensive Text with Models, Applications, References and DEA-Solver Software. Springer, New York, NY.
[22] Banker, R. D., Charnes, R. F., Cooper, W. W. (1984). Some Models for Estimating Technical and Scale Inefficiencies in Data Envelopment Analysis. Management Science. 30, 1078-1092.
[23] Ozcan, Y. A. (2014). Health Care Benchmarking and Performance Evaluation: : An Assessment Using Data Envelopment Analysis (DEA). Springer, New York, NY.
[24]Cankurt,M.,Miran,B.,Gunden,C(2013.A comparative analysis on productivity and efficiency of agricultural production of the EU andTurkey.JournalofFood,Agriculture&Environment 11(2),433-439.
[25]Cankurt,M.,Gunden,C.,Terrence,T.,Miran,B.,Sahin,A.(2013)Measuring Economic Efficiency of Selected Crops Produced in Costal Aegean Basin of Turkey.Journal of Food,Agriculture&Environment 11(2);481-484.

Received: **04.08.2015**
Accepted: **08.12.2015**

CORRESPONDING AUTHOR

Altug Özden

Adnan Menderes University
Faculty of Agroculture
Department of Agrocultural Economics
Aydin – TURKEY

by PSP Volume 25 – No 1/ 2016, pages 249-274 Fresenius Environmental Bulletin

NUMERICAL ANALYSIS OF ESSENTIAL FACTORS AFFECTING PIEZOCONE PENETRATION TEST IN CLAYS BY APPLYING FINITE ELEMENT METHOD

Guojun Cai, Jun Lin

Institute of Geotechnical Engineering, Southeast University, Nanjing, China 210096

ABSTRACT

Due to its repeatability and reliability, the piezocone penetration test (PCPT or CPTu) is widely used in geotechnical site characterization. This paper presents a numerical technique for the analysis of the PCPT in cohesive soil. The Mohr-Coulomb yield criterion with the associated flow rule is assumed to model the elasto-plastic behavior of clays under undrained condition. A volumetric weighting algorithm adjusts the relative positions of nodes after each loading increment. The variation of the cone resistance is examined in relation to various parameters such as the in situ stress state, cone apex angle and penetration rate. For different penetration rates and cone sizes, the cone tip resistance profile and excess pore pressure profile are provided. A full parametric study was undertaken, quantifying the influences of the rigidity index, in situ stress anisotropy and the cone roughness. The trends of these variations are highlighted and compared with those found by other researchers. This technique can be extended to analyze the plastic behavior of elastoplastic sands often modelled using either the Drucker–Prager yield criterion or a critical state model. The results show this study would provide some useful insights into the factors affecting the data interpretation of PCPT in clays.

KEYWORDS: Piezocone; clays

INTRODUCTION

Cone penetration test (CPT) is one of the most popular in-situ testing methods used to investigate the soil properties [1, 2]. Essentially, the device comprises a pushing penetrometer with a standard geometry (cylindrical with a diameter of 35.7 mm and a conical point with an apex angle of 60^o) that is pushed into the soil at a rate of 20 mm/s, while measures a number of parameters. It has been increasingly used because of its important advantages, such as simplicity, speed and continuous profiling [3, 4, 5]. The piezocone penetration test (PCPT or CPTu) is an extension of the CPT and is able to measure cone tip resistance, sleeve friction and generated pore-water pressures simultaneously. The PCPT data are affected by many variables [6, 7, 8, 9, 10], including piezocone design, geometric size, rate of penetration, testing procedures and soil characteristics. More importantly, some factors that affect measurements are significant. It calls for the research to be continued and different methods, including the numerical analysis, may be applied. A group of researchers [11, 12, 13, 14] have investigated the penetration problem using the finite-element technique. Teh and Houlsby [15] proposed a combination of the strain path method with the finite-element technique to analyze the piezocone penetration test. The finite-element technique has many advantages over the other methods: (1) the piezocone geometry can be properly modeled; (2) the equilibrium equations are fully satisfied; and (3) The soil-piezocone interface friction can be addressed. The current finite-element models assume an existing prebored cone hole with the surrounding in situ stresses remaining unchanged. The incremental vertical displacements are then applied to simulate the continuous penetration. Finite-element analysis shows that small penetrations can develop high soil stresses around the piezocone shaft and tip [13]. The developed high soil stresses around the tip will influence the penetration resistance of the piezocone, resulting in higher cone penetration pressures than are predicted assuming a prebored piezocone hole [15].

The finite element method, besides the methods based on semi-empirical approaches, bearing capacity models, cavity expansion theory and strain path methods, has been used and become an important method to analyze the complex cone penetration mechanism considering the influence factors [16, 17]. The purpose of this paper, therefore,

is to present a numerical technique for the analysis of the piezocone penetration test in cohesive soil. The Mohr-Coulomb yield criterion with the associated flow rule is assumed to model the elasto-plastic behavior of clays under undrained condition. The variation of the cone resistance is examined in relation to various parameters such as the in situ stress state (K_o), cone apex angle and the penetration rate. For different factors of penetration rate and cone size, the cone tip resistance profile and excess pore pressure profile are provided. The trends of these variations are highlighted and compared with those found by other researchers. The results show this study would provide some useful insights into the factors affecting the data interpretation of PCPT in clays.

FINITE-ELEMENT MODELING

To determine soil properties from measured piezocone data, it is necessary to establish some relationships among them. For this purpose, much previous work has focused on cone-penetration analysis over the past two decades. The difficulties lie in the complicated deformation of the soil, which results from the punching of the penetrometer, as well as the complex interfacial behavior. Rigorous closed form solutions are not available for penetration problems, and analyses are often based on simplified theories. One approach treats the steady-state penetration of the cone as a limit equilibrium problem of a circular footing, and proposes correlations based on its bearing capacity. The applicability of correlations of this type is limited due to the assumption that soil compressibility and elastic deformation are neglible. Another type of correlation often used in practice is based on the solutions of cavity expansion theory. This approach includes parameters related to soil deformation, and is therefore more flexible for applications. Several approaches have been proposed to analyze and interpret the deep piezocone penetration problem. The first approach is based on the bearing capacity theory, in which penetration is considered as a simple failure of a rigid plastic material. In the second approach, the penetration problem is analyzed using the cavity expansion theories in elasto-plastic materials. The third approach is based on the strain path method, in which the penetration process is treated as a strain controlled problem.

Small strain finite-element analyses of PCPT were carried out using the finite-element program PLAXIS (PLAXIS 1998). PLAXIS Version 7.0 was used for the initial cases with isotropic soil strengths, while Version 8.0, which can incorporate user-defined constitutive models, was used to explore strength anisotropy and strain softening. The finite element mesh as well as the boundary condition is presented in Figure 1.

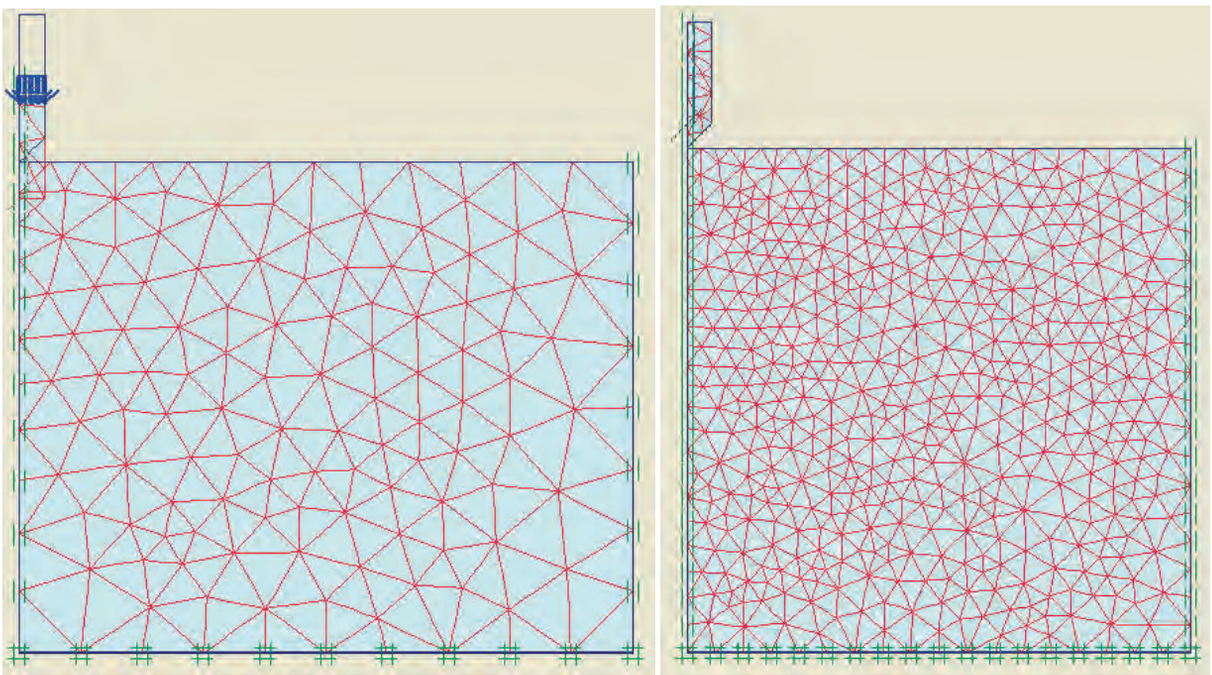

(a) (b)

FIGURE 1
Finite element meshes used for Plaxis analyses: (a) fine mesh; (b) ultrafine mesh

In PLAXIS, all boundaries must have one boundary condition in each direction. When no explicit boundary condition is given to a certain boundary (a free boundary), the natural condition applies, which is a prescribed force equal to a zero and a free displacement.

To avoid the situation where the displacements of the geometry are undetermined, some points of the geometry must have prescribed displacements. The form of a prescribed displacement is a fixity (zero displacement), but non-zero prescribed displacements may also be given. As a result PLAXIS generates a full fixity at the base of the geometry and roller conditions at the vertical sides (u_x=0; u_y=free). A fixity in a certain direction appears on the screen as two parallel lines perpendicular to the fixed direction. Hence, roller supports appear as two vertical parallel lines and full fixity appears as crosshatched lines.

Meshes of differing refinement were investigated, with example "fine" and "ultrafine" meshes illustrated in Figure 1. The latter was used for strain-softening cases. The piezocone penetration analysis is treated as an axi-symmetric boundary value problem with the need of changing the boundary conditions as the piezocone penetrometer advances. The penetrometer is assumed to be infinitely stiff and no tensile stresses are allowed to develop along the centerline boundaries. The continuous penetration of the piezocone was simulated by applying an incremental vertical displacement at the nodes representing the piezocone boundary. The Mohr-Coulomb frictional model is used to define the sliding potential between the cone surface and the soil. The soil-penetrometer interface friction coefficient $\mu=\tan(\delta)$. $\delta=14^o$ and it is the friction angle between the soil and the piezocone surface. So, μ is taken to be 0.25. Table 1 gives the mechanical parameters of the clay soil as well as the cone body and consolidation parameters.

TABLE 1
The mechanical parameters of the clay soil as well as the cone body

Parameters	Cone body	Clay soil
E	200 GPa	30 MPa
ν	0.30	0.49
Cc		0.13
Cs		0.022
k		1.0×10^{-9} m/s

Note: Young's modulus, E; Poisson's Ratio, ν; Compression Index, Cc; Recompression Index, Cs; Permeability, k.

The cone body is assumed to be elastic with Young's modulus of 200 GPa and Poisson's ratio of 0.3. The cone surface is smoothed, with the smoothing parameter 1/6. The cone-soil interface is assumed to be smooth along the cone rod.

CONTACT INTERFACE

This section will describe how this simulation establishes contact and calculates the resulting deformation in the model. It is extremely important to set up the governing equations of the interaction between the lateral surface of the penetrometer and the soil [18]. This purpose can be achieved by using interface elements. The most commonly used interface elements can be grouped into three main classes; namely the zero-thickness interface elements, thin-layer interface elements and the constraint approach. In this paper, the penetrometer is assumed to be a rigid body and the surrounding soil is deformable. The interaction occurs between these two bodies in terms of two surfaces that may interact.

The lateral surface of the penetrometer is called "master surface" which is rigid. The soil surface is called "slave surface" which is deformable. The nodes on the slave surface are constrained not to penetrate into the master surface; however, the nodes of the master surface can, in principle, penetrate into the slave surface. After this contact pair is defined, a family of contact elements is automatically generated. At each integration point, these elements construct series measures of clearance and relative shear sliding. These kinematic measures are then used, together with appropriate Lagrange multiplier techniques, to introduce surface interaction theories. The interaction simulation consists of two components: one normal to the surfaces and one tangential to the surfaces [19].

A pure master-slave relationship is used to model contact between two surfaces [20]. In this work, the steel cone was chosen as the master and the soil as the slave. Nodes of the master surface can penetrate the slave surface, but not vice versa. It is believed that this algorithm gives a relatively accurate solution for cone penetration. A balanced master-slave model, which completely prohibits penetration, was not chosen to avoid very expensive calculation. Penetration of the master into the slave surface is minimized by refining the mesh of the slave. The present model uses a kinematic, predictor/corrector contact algorithm as opposed to a penalty method, which has a weaker enforcement of contact constraints. In the kinematic predictor/corrector algorithm, the resisting force is based on the depth of a slave node's penetration, the mass associated with the penetration, and the time increment [19]. The resisting forces of all slave nodes are distributed to the nodes on the master surface. The mass of the slave nodes is also distributed to the master surface nodes. The total inertial mass of the contacting surfaces can be calculated from the additional node mass of the slave and master surfaces [19].

The contact interface is modelled in such a way that it will not transmit contact pressure in either the normal or tangential direction unless the nodes of the slave surface contact the master surface. The magnitude of the transmitted contact pressure is not limited. Transfer of tensile stress is not allowed across the interface. For the tangential direction, the classical isotropic Coulomb friction model without a cap was chosen. The coefficient of interface friction is assumed to be a function of the angle of internal friction and the value is maintained constant throughout an analysis.

For tracking contact nodes, this analysis uses a "finite sliding algorithm" to ensure correct pairing of nodes and elements of master and slave surfaces.

This algorithm can guarantee better quality results compared to a "small sliding algorithm". The finite sliding algorithm tracks and pairs node and element pairs between master and slave surfaces until the calculation stops. By contrast, a small sliding algorithm would have tracked and paired node and element pairs only at the beginning of the first step [19].

CONSTITUTIVE SOIL MODEL AND SOIL PROPERTIES

The word soil actually implies a mixture because the voids of soil skeleton are generally filled with water and air or gas [18]. Hence, soil in general can be considered as a multiphase material whose state can be described by the stresses and displacements (or velocities) within each phase. The stresses carried by the soil skeleton are conventionally called "effective stress", and the parts carried by water are called "pore water pressures". If the free drainage condition holds, the steady state pore water pressure depends only on the hydraulic conditions and is independent of the soil skeleton response to external loads. In this case, the soil behavior can be described in a single phase way. The same description can be applied to the soil if no drainage condition prevails. However, in an intermediate case, in which some flow can take place, there is an interaction between the skeleton strains and the pore water flow. The solution of these problems requires that the soil behavior be analyzed by incorporating the effect of the transient flow of the pore water through the voids and the stress-strain behavior of soils. Therefore, a multiphase continuum formulation is required for porous media. In this research, it is assumed the soil is fully saturated and is treated as a two-phase problem.

The equilibrium equation for porous media can be derived from the principle of effective stress. The porous media here will be approximately modeled by attaching the finite element mesh to the solid phase. The liquid can flow through this mesh. A continuity equation is, therefore, required for the liquid, equating the rate of increase in liquid mass stored at a point to the rate of mass of liquid flowing into the point within the time increment. The liquid flow is assumed to obey Darcy's law. The continuity equation is satisfied approximately in the finite element model by using excess pore pressure as nodal variables, interpolated over the elements. The equation is integrated in time by using the backward Euler approximation. The total derivative of this integrated variational statement of continuity with respect to the nodal variables is required for the Newton iterations used to solve the nonlinear, coupled, equilibrium and continuity equations.

In the piezocone penetration test (PCPT), the area close to the cone tip is under very large strain [20]. It is always in a yield (plastic) condition. Therefore, it is essential to model the soil with a nonlinear soil constitutive model. For this work, an elastic-plastic model was chosen. In the elastic-plastic model, soil modulus is characterized by 4 components: (1) The elastic parameters that determine deformation in the elastic region. (2) A yield criterion that describes the stress state necessary for plastic deformation. (3) A hardening rule that defines how the material's resistance to further yield changes with increasing strain. (4) A flow rule that characterizes the incremental plastic strains as a function of stresses.

A large number of constitutive models exist for different soils [21]. Some authors gave the FEM simulation of cone penetration using different soil models shown in Table 2.

TABLE 2
Summary of different soil constitutive models in the FEM simulation

Authors	Constitutive model	Flow rule	Soils	References
Markauskas	Elastic-perfectly plastic uncompressible Mises material		Undrained clay	[22]
Endra	Drucker-Prager constitutive model	Non-associated	Sand	[20]
Abu-Farsakh	Modified Cam clay model		Clay	[10, 13]
Lu Q	Tresca yield criterion		Clay	[23]
Lei Wei	Anisotropic Modified Cam Clay Model	Non-associated	Clay	[18]
Huang	Mohr-Coulomb criterion		Sand	[21]
Ahmadi	Mohr-Coulomb elastic-plastic material		Sand	[24]
Walker	Von Mises yield criterion	Associated	Clay	[25]
Walker	Drucker-Prager failure criterion	Associated	Clay	[26]

To capture as many aspects of soil behavior as possible, some of these are very sophisticated and involve lots of parameters. However, in engineering practice, simple models are often sufficient as only the key features of soil behavior are of importance. In this study, a simple elasto-perfectly plastic model with the Mohr-Coulomb yield criterion is used to describe the behavior of a cohesive soil. The elastic deformation is described by the elastic modulus E (or the shear modulus G) and the Poisson's ratio, while the plastic deformation is characterized by the friction angle, the dilation angle and the cohesion. A non-associated flow rule is used to simulate the dilatant behavior of the soil. Loading and unloading within the current yield surface are assumed elastic (defined by a separate modulus, E_{ur}), and the Mohr–Coulomb failure criterion is employed. Specification of the peak dilation angle (ψ) and friction angle (φ) defines the critical-state friction angle (φ_{cv}). The clay under undrained condition modelled as elasto-perfectly plastic uncompressible material with elastic parameters Young's modulus E = 30 MPa, Poisson's ratio$v$ = 0.49 and the undrained shear strength S_u = 20 kPa is considered in PCPT. Table 3 presents a summary of the input parameters for FEM analysis.

TABLE 3
Input Parameters of the FEM Simulation

Parameters	Quantity
Friction angle	23°
Dilation angle	0°
Slope of critical line, M	1.1
Initial void ratio	1.2
Unit weight of water	9.8 KN/m^3
Effective unit weight	5.7 KN/m^3
Harding parameter c	0.04
Harding parameter x	2.2

The initial stress state can be obtained by changing in situ horizontal effective stress.

RESULTS OF THE NUMERICAL SIMULATION

Cone penetration was imposed by applying positive volumetric strain to the spherical soil cluster, and the cavity pressure–radial displacement variation during expansion was deduced by selecting and averaging the output from appropriate nodes and Gauss points. The procedure, as required by PLAXIS, involved three steps:

(a) 'input', including mesh set-up and initial stress generation;

(b) 'calculation', including definition of calculation phases and selection of nodes and stress points for output;

(c) 'output', involving extraction of the output using the PLAXIS curve program and subsequent post-processing to generate pressure–expansion curves and determine cone tip resistance and sleeve friction. The cone penetrometer steady-state resistance could then be derived from the relationship proposed by Randolph [27]. Coupled-consolidation, updated Lagrangian finite-element analyses were performed to study the effects of partial consolidation during cone penetration on the cone tip resistances and excess pore pressures. The effects of pore pressure generation and dissipation on the cone response caused by different penetration rates spanning the fully drained to fully undrained conditions were examined by the effective-stress-based finite-element method. The effect of penetrometer size can be accounted for by using non-dimensional and normalised quantities to present and interpret the results.

For each different initial stress state, vertical penetration analysis was performed. Kiousis et al. [8] reported a steady state about tip resistance that is almost reached when the penetration depth is about 2/3 the radius of the cone. In this study, the penetration depth of the penetrometer into the soil was chosen to be 20 mm, which is a little bit larger than the radius of the penetrometer (17.8 mm). If the penetration distance is too long, the soil elements may be distorted too much and fail to yield accurate results. For the consideration of stress concentration besides of the cone, the updated Lagrangian (UL) formulation with logarithmic strains was used in this study. This approach could still result in severe element distortions in the soil–cone vicinity, but these were controlled by modifying the mesh density and element aspect ratio in the vicinity of the cone by way of a trial-and-error process.

Tip resistance profiles. The tip resistance for vertical penetration is defined as the vertical force acting on the tip of the penetrometer divided by the projected area of the tip (10 cm^2). This projected area of the tip is related only to the geometry of the penetrometer. Figure 2 shows the tip resistance profiles for each K_o value.

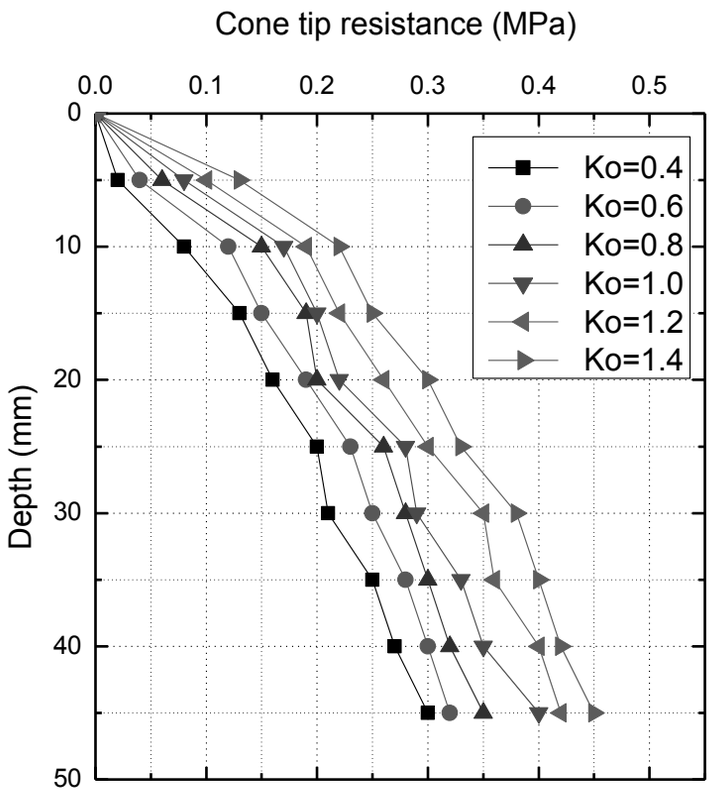

FIGURE 2
Tip resistance profiles at different K_o values

Here, the K_o is defined as the coefficient of lateral earth pressure (ratio of effective stresses, i.e., $K_o = \sigma_{ho}/\sigma_{vo}$). For $K_o = 1$, the initial stress state is isotropic. The tip resistance value at about 45 mm penetration depth for each different K_o are compared in Figure 3.

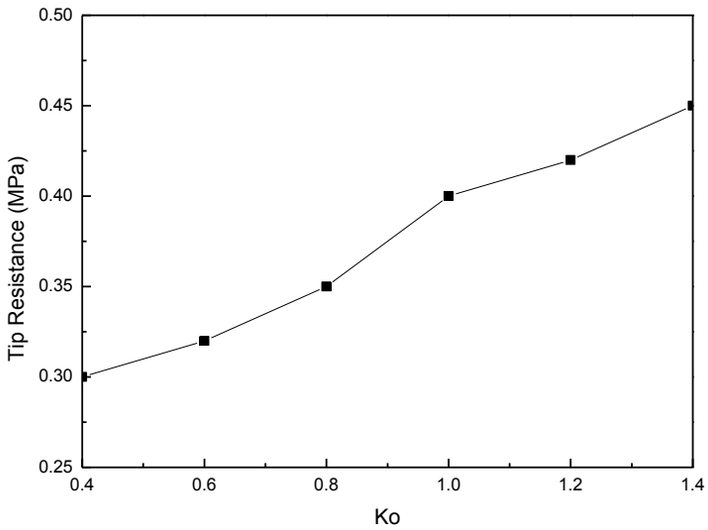

FIGURE 3
Comparison of steady-state tip resistance for different K_o values (σ_{vo} = 100 kPa)

As can be seen from both Figure 2 and Figure 3, the tip resistance is strongly affected by the initial stress state. The higher the initial stresses are, the higher the tip resistance will be. It should be noted that this trend is observed based on a constant initial vertical stress (σ_{vo} = 100 kPa), in which condition a higher K_o value means a higher initial stress state. For vertical penetration, the tip resistance increases from 0.30 MPa to 0.45 MPa when K_o increases from 0.4 to 1.4.

Sleeve Friction Profiles. The sleeve friction is defined as the total shear force in the penetration direction divided by the sleeve surface area (150 cm^2). Figure 4 shows the sleeve friction profiles for different K_o values.

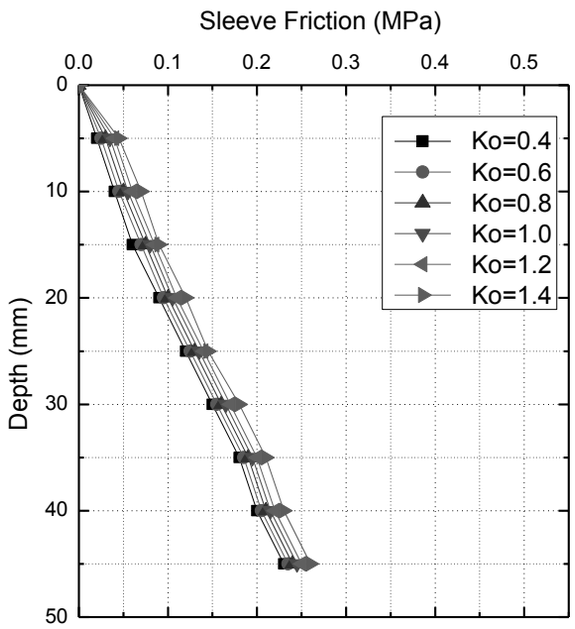

FIGURE 4
Sleeve friction profiles at different K_o values

Obviously, at the penetration depth of 45 mm, a steady state for the sleeve friction still has not been reached. However, when the penetration distances are large, severe mesh distortions happen in zones of high strain concentrations around the cone tip, which lead to a severe loss of accuracy and numerical divergence. Therefore, the simulated penetration depth in this study was limited to 45 mm. The standard penetrometer has a sleeve friction area of 150 cm^2, which corresponds to a friction sleeve length of 134 mm. Since the penetration distance is only 30% of the friction sleeve length, one expects most of the normal and shear stresses on the sleeve have not been fully mobilized with such a short penetration distance as compared to the friction sleeve length. The sleeve friction values at penetration depth of 45 mm for different K_o values are presented in Figure 5.

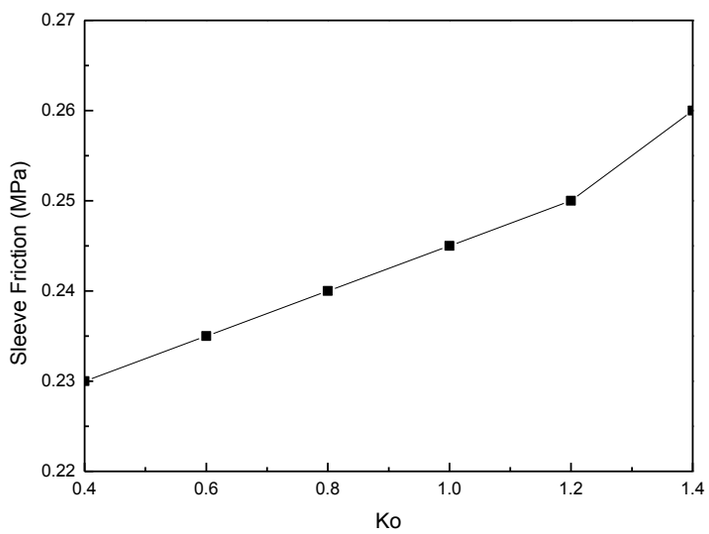

FIGURE 5
Comparison of sleeve friction for different K_o values (σ_{vo} = 100 kPa)

As can be seen from both Figure 4 and Figure 5, the sleeve friction is affected by the initial stress state. The higher the initial stresses are, the higher the sleeve friction will be. It should be noted that this trend is observed based on a constant initial vertical stress (σ_{vo} = 100 kPa), in which condition a higher K_o value means a higher initial stress state. For vertical penetration, the sleeve friction increases from 0.23 MPa to 0.26 MPa when K_o increases from 0.4 to 1.4.

Pore water pressure profiles. One important aspect of the piezocone that has not yet been standardized is the location of the porous element [28, 29, 30]. The piezocones used in the current practice have three common locations for the porous elements: (1) at the cone tip (u_1 configuration), generally mid-way for 10 or 15 cm^2 cones and the very tip for mini-cones, (2) 0.5 mm above the base of the cone (u_2 configuration), and (3) behind the friction sleeve (u_3 configuration), as illustrated in Figure 6.

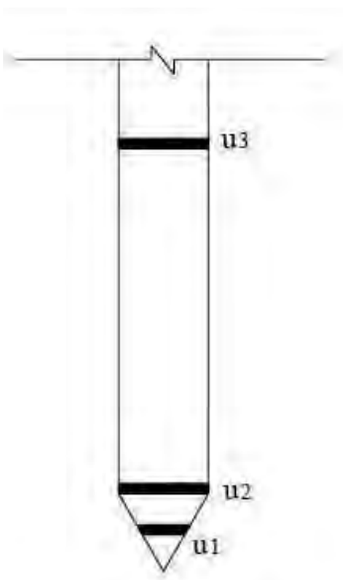

FIGURE 6
Schematic showing common locations of porous filter element

The u_2 configuration at the cone shoulder is utilized in this study. Figure 7 shows the pore pressure u_2 profiles for each K_o value.

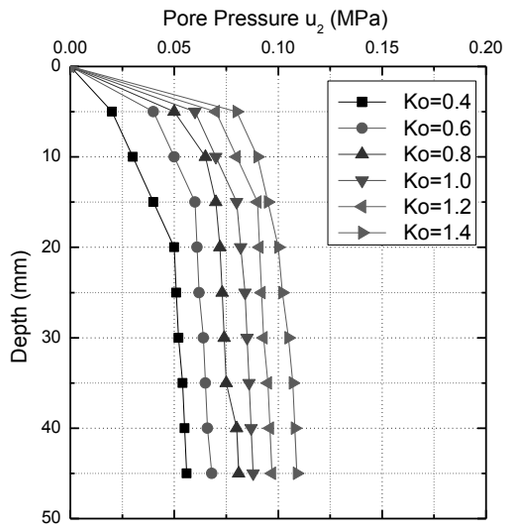

FIGURE 7
Pore pressure u_2 profiles at different K_o values

The pore pressure u_2 almost reaches the steady state value at about 20 mm penetration depth, which is less than the steady state distance of tip resistance. These steady state values for each different K_o values are compared in Figure 8.

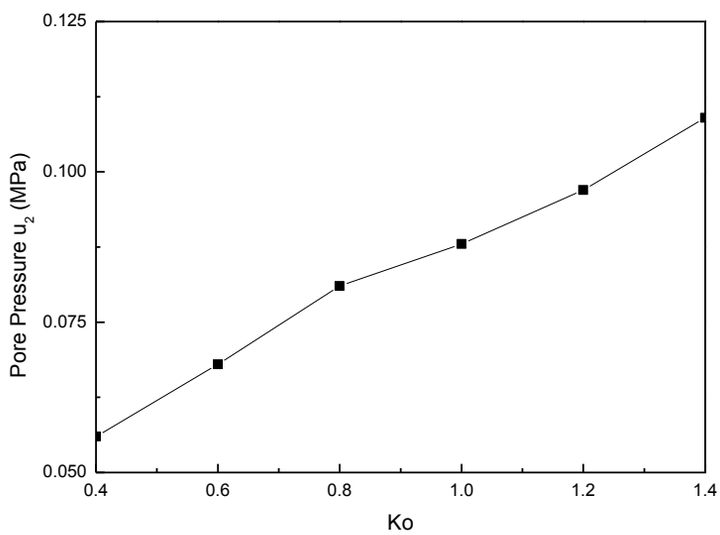

FIGURE 8
Comparison of steady-state pore pressure u_2 for different K_o values (σ_{vo} = 100 kPa)

As can be seen from both Figure 7 and Figure 8, the pore pressure u_2 is strongly affected by the initial stress state. The higher the initial stresses are, the higher the tip pore pressure will be. It should be noted that this trend is observed based on a constant initial vertical stress (σ_{vo}=100 kPa) in which

condition a higher K_o value means a higher initial stress state. For vertical penetration, the pore pressure increases from 56 kPa to 109 kPa when K_o increases from 0.4 to 1.4.

ANALYSIS OF FACTORS AFFECTING PCPT MEASUREMENT

Effect of cone size. The effect of scale size on penetration testing was examined by comparing results from different cone size penetrometers. The piezocone with different cross-sectional area (A_c) of 1, 5, 10, 15, 20, and 30 cm^2 were facilitated by the numerical simulation. The cone tip resistance profiles at about 45 mm penetration depth for each different cone area are compared in Figure 9.

Cone resistance increases as the cone area decreases. Results of some field cone penetration tests indicated that the cone size may have had some minor effect on the recorded parameters [31].

As can be seen from Figure 10, the cone tip resistance is strongly affected by the cross-sectional area.

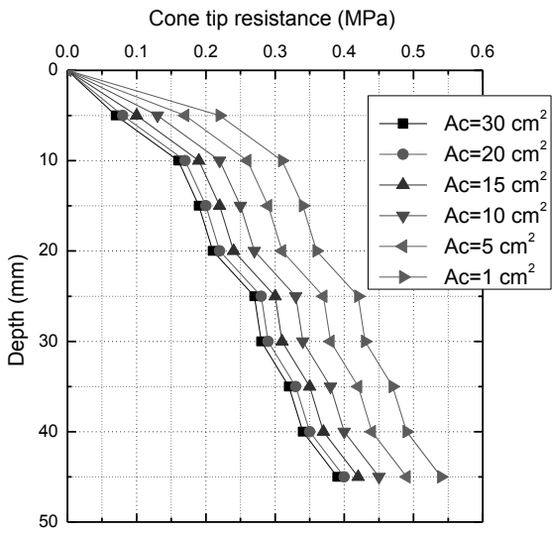

FIGURE 9
Comparison of cone tip resistance profiles at different cross-sectional area

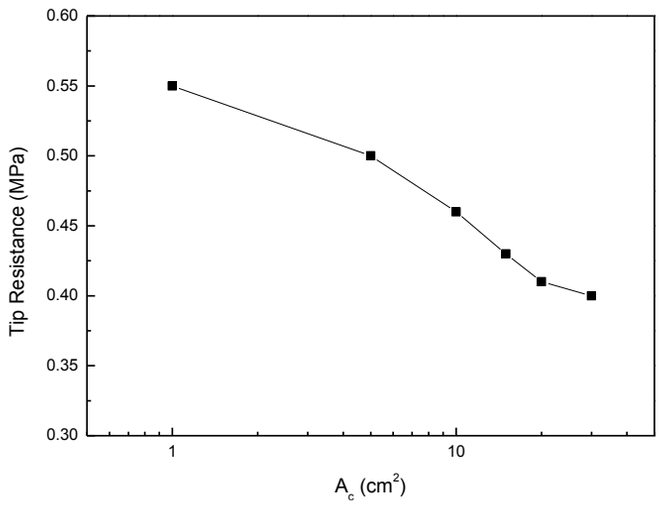

FIGURE 10
Effect of cone cross-sectional area on tip resistance (σ_{vo} = 100 kPa)

The higher the cross-sectional area is, the lower the cone tip resistance will be. It should be noted that this trend is observed based on a constant initial vertical stress (σ_{vo} = 100 kPa), in which condition a higher K_o value means a higher initial stress state. For vertical penetration at the standard 20 mm/s rate, the cone tip resistance increases from 0.40 MPa to 0.55 MPa when the cross-sectional area decreases from 30 to 1 cm^2.

The piezocone with different sleeve friction area (A_s) of 10, 50, 100, 150, 200, and 300 cm^2 were facilitated by the numerical simulation. The sleeve friction profiles at about 45 mm penetration depth for each different cone sleeve friction are compared in Figure 11.

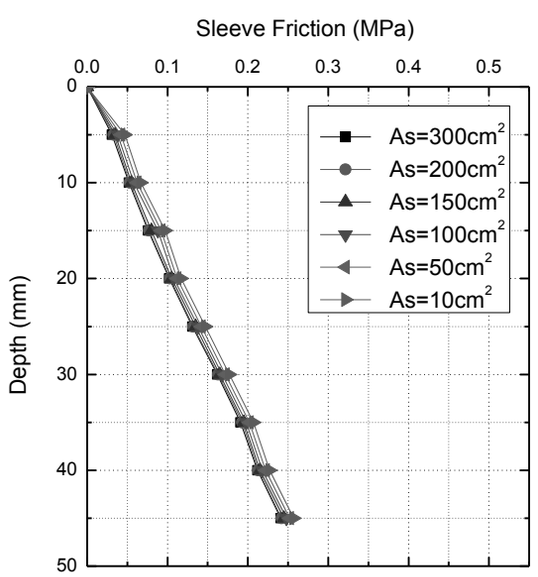

FIGURE 11
Comparison of sleeve friction profiles at different sleeve friction area

Sleeve friction increases as the sleeve friction area decreases. Results of some field cone penetration tests indicated that the cone size may have had some minor effect on the recorded parameters [31].

As can be seen from Figure 12, the sleeve friction is affected by the sleeve friction area.

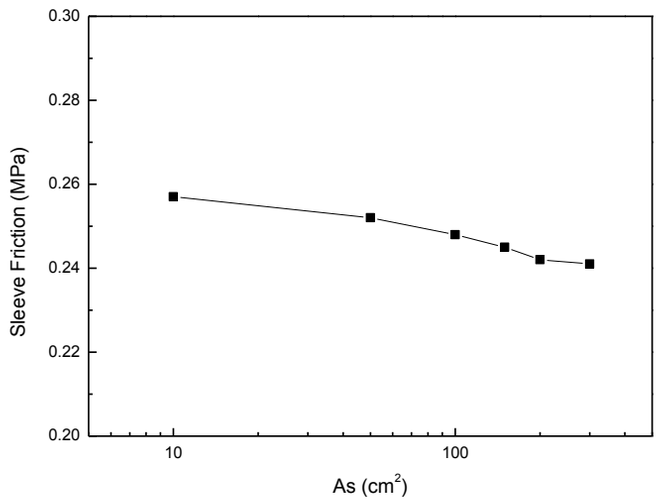

FIGURE 12
Effect of the sleeve friction area on sleeve friction (σ_{vo} = 100 kPa)

The higher the cross-sectional area is, the lower the cone tip resistance will be. It should be noted that this trend is observed based on a constant initial vertical stress (σ_{vo}=100 kPa), in which condition a higher K_o value means a higher initial stress state. For vertical penetration, the sleeve friction increases from 0.241 MPa to 0.257 MPa when Ac decreases from 300 to 10 cm^2.

The cone with a cone apex angle of 18, 30, 60, 90, 120, and 180º were facilitated by the numerical simulation. To simulate the experimental setup of the tests, the cone is initially in contact with the weightless soil. A pressure load is then applied to the soil top surface, while the cone is allowed to settle vertically with the soil. This step is used to establish an initial stress field in the soil that is in equilibrium with the boundary conditions. Once the initial stresses are set up, all displacements in the soil and the cone are set to zero. The cone is then pushed down in the soil by prescribing a vertical displacement of 50 mm at the cone tip. The cone tip resistance values with depth are shown in Figure 13.

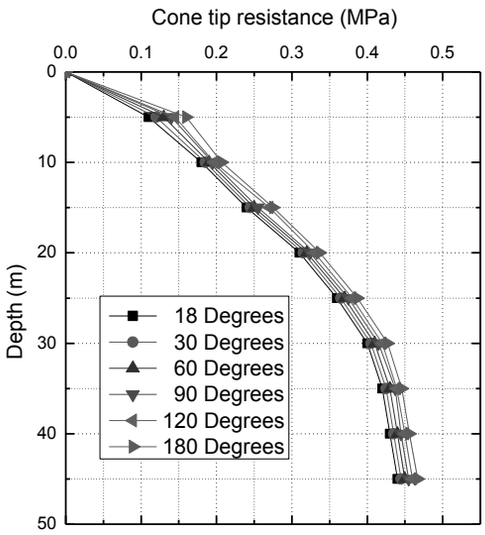

FIGURE 13
Comparison of predicted cone tip resistance values with depth (σ_{vo} = 200 kPa)

Figure 14 illustrates the effects of the increased cone apex angle with the cone resistance showing some overall increase.

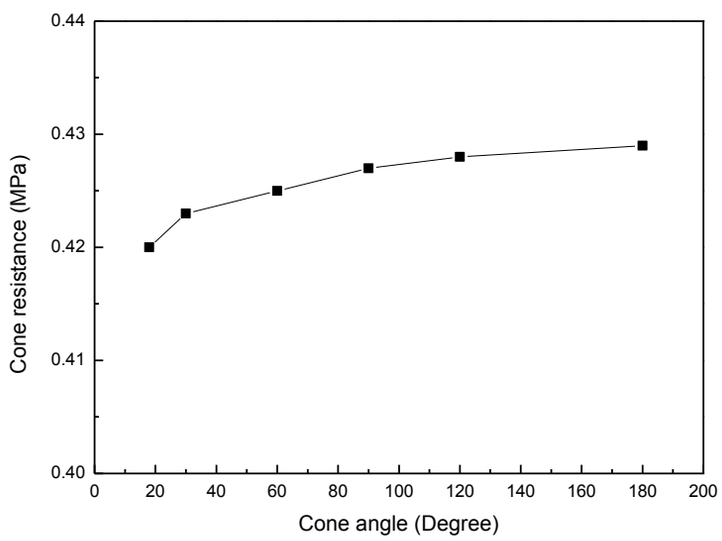

FIGURE 14
Effect of the cone angle on cone tip resistance (σ_{vo} = 200 kPa)

As can be seen from Figure 14, the cone tip resistance is affected by the cone apex angle. The higher the cone apex angle is, the higher the cone tip resistance will be. It should be noted that this trend is

observed based on a constant initial vertical stress (σ_{vo} = 200 kPa), in which condition a higher K_o value means a higher initial stress state. For vertical penetration, the sleeve friction increases from 0.241 MPa to 0.257 MPa when cone apex angle increases from 18 to 180°.

Effect of cone penetration rate. Rate effects can be significant for CPT results in soil. The effect of penetration rate on the cone resistance is obvious. A number of studies have considered rate effects in CPT testing for both clays and sands [32, 33, 34, 35, 36, 37, 38, 39, 40]. Results of some field cone penetration tests indicated that cone resistance increases and excess pore pressure drops as the penetration rate decreases [34], and recent centrifuge test results showed that the increase in cone resistance was due to enhanced drainage [36, 37, 41]. Silva et al. [38] presented a set of numerical analyses investigating the effect of penetration rate on piezocone test results in clay. A coupled cavity expansion finite element method was used to simulate the penetration of a piezocone. The rate of cavity expansion was linked to the penetration rate of the cone and the cone angle, using the assumption that the deformation was wholly radial, and took place only between the cone tip and the cone shoulder.

The PCPTs were performed at seven different penetration rates, which range from 200 to 0.02 mm/s (0.02 mm/s，0.2 mm/s，2 mm/s，5 mm/s，10 mm/s，20 mm/s，200 mm/s) in the clays. Additionally, only soil layers located below the groundwater level were considered, so that the data are for fully saturated conditions. Average values of cone tip resistance, pore pressure (u_2), and sleeve friction versus cone penetration rate are shown in Figure 15.

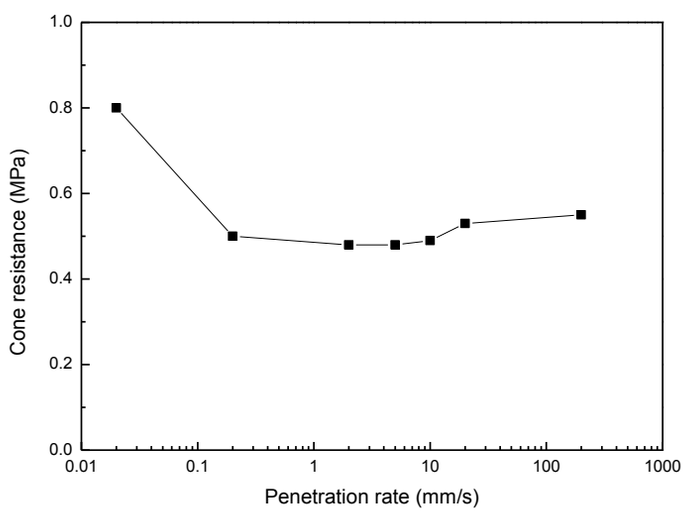

(a) Cone tip resistance

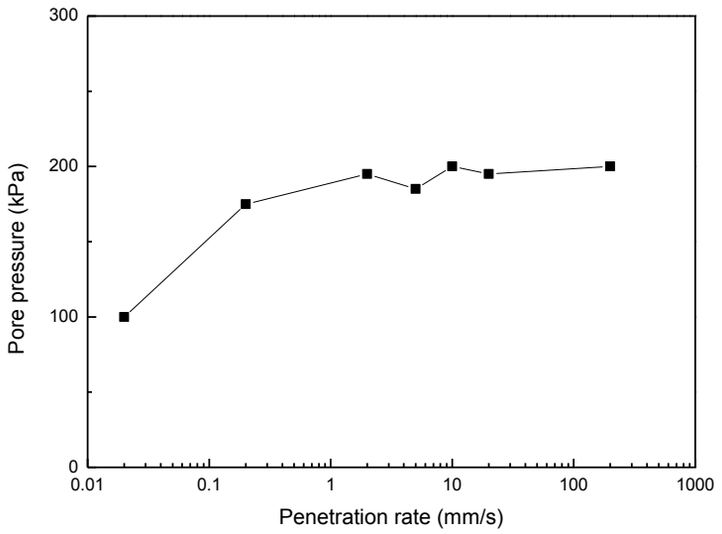

(b) Pore pressure (u_2)

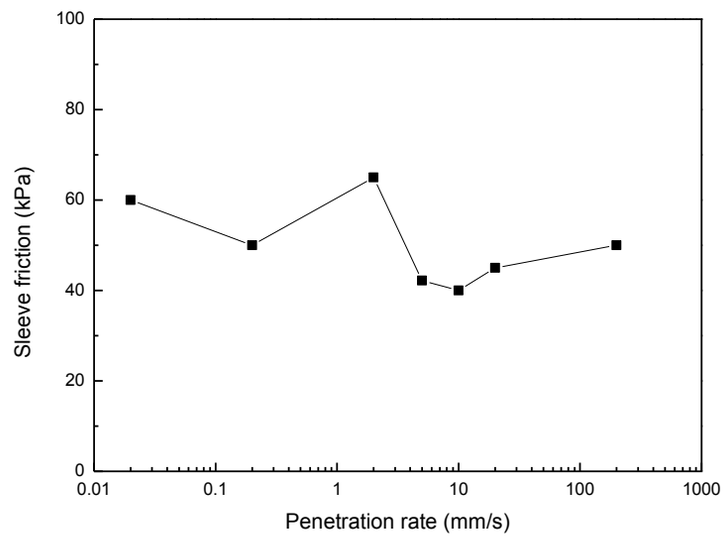

(c) Sleeve friction

FIGURE 15
Effect of penetration rate on cone tip resistance, pore pressure and sleeve friction (σ_{vo} =100 kPa)

For penetration rates in the range between 200 and 0.2 mm/s, penetration seems to occur under undrained conditions. The average cone tip resistance for a penetration rate between 10 and 0.2 mm/s was about 0.49 MPa. As penetration rate was reduced to 0.02 mm/s, the average cone tip resistance increased abruptly to 0.8 MPa. If we compare the cone tip resistance profiles with the corresponding excess pore pressure profiles, it is clear that the main reason for the increase in cone resistance with decreasing penetration rate is the change in drainage conditions. The excess pore pressure decreased from an average of 195 kPa for penetration rates in the range between 0.2 and 200 mm/s to about 100 kPa for v = 0.02 mm/s. It has been stated that the sleeve friction measurement of a cone does not give consistent

results during cone penetration [42]. The values of sleeve friction increased as the cone velocity decreased. However, it can be seen from Figure 15(*c*) this tendency was not evident.

Loading rate effects (which may be attributed to soil "viscosity") were studied by several researchers [43, 44, 45]. It is known that the shear strength of clay increases with loading rate; however, only a small increase in the shear strength of sand is observed with changes in the loading rate. O'Reilly et al. [45] performed a series of undrained triaxial compression tests at various strain rates and showed that, for the soil they studied (silty clay), the strength increased 15% for every tenfold increase in strain rate.

Increases in cone resistance due to increases in penetration rate have been reported by [35, 46] for field and calibration chamber CPTs performed under undrained conditions (at fast penetration rates). Since cone resistance is directly related to the undrained shear strength s_u of the clay, the same loading rate effects observed in the laboratory for S_u can be expected to influence q_t measurements. Accordingly, cone resistance measured under undrained conditions is expected to increase as a result of the increase in S_u caused by penetration rate increases. Miniature cone test results reported by Tani and Craig [46] showed that cone resistance increased by 10% for every tenfold increase in the penetration rate range between 0.1 and 5 mm/s on clay till soils. Powell and Quarterman [35] also reported a 10% increase of cone resistance measured in field CPTs in clay for an increase in penetration rate from 1.7 to 16.7 mm/s. CPTs performed under undrained conditions (0.2–200 mm/s) for the clay showed viscous effects at high penetration rates (Figure 15). The average q_t at 200 mm/s was 0.55 MPa, 15% higher than q_t (q_t = 0.48 MPa) at 2 mm/s.

PARAMETRIC STUDY

A full parametric study has been undertaken, quantifying the influences of the rigidity index, in situ stress anisotropy and the cone roughness. A theoretical correlation for the cone factor, N_{kt}, is developed from this study, and compared with previous correlations developed using the strain path method [23].

In saturated clays and other fine-grained soils, the test is carried out at a penetration rate that does not permit drainage, and the cone resistance may then be interpreted directly as a measure of the undrained shear strength of the clay. Conventionally, the shear strength is derived by dividing the (net) cone resistance by a cone factor and, ideally, it would be helpful to have a sound theoretical basis for this cone factor.

$$q_c = N_{kt} S_u + \sigma_{v0} \tag{1}$$

In practical applications, it may still be appropriate to establish an empirical cone factor, for example by correlating the cone resistance with shear strengths determined in the laboratory or with an alternative in situ device. Typical ranges of cone factor, N_{kt} (see later, equation (3)) may be found in the literature [2], and can range from as low as 6 to over 20, but more commonly are in the range 9–17, with the shear strength measured in triaxial compression generally used to normalize the cone resistance. In principle, comparison of the empirically derived cone factor with the theoretical values for idealized soil provides additional information on the soil characteristics. Indeed, it may also be appropriate to adjust theoretical geotechnical design equations in a manner that is consistent with any difference between empirical and theoretical cone factors.

Smooth conditions at the cone interface. In this section, the proposed numerical technique is applied to the cone penetration test in a weightless material. Sliding is allowed at the soil-penetrometer interface and no initial stress is imposed on the soil domain. In this case, the cone factor (N_{kt}) is defined as the net cone tip resistance (q_{net}) normalized by the undrained shear strength of the soil (S_u).

$$N_{kt} = \frac{q_c - \sigma_{v0}}{S_u} \tag{2}$$

Figure 16 shows the evolution of the cone resistance as the cone penetrometer is pushed into three materials obeying the Drucker-Prager failure criterion.

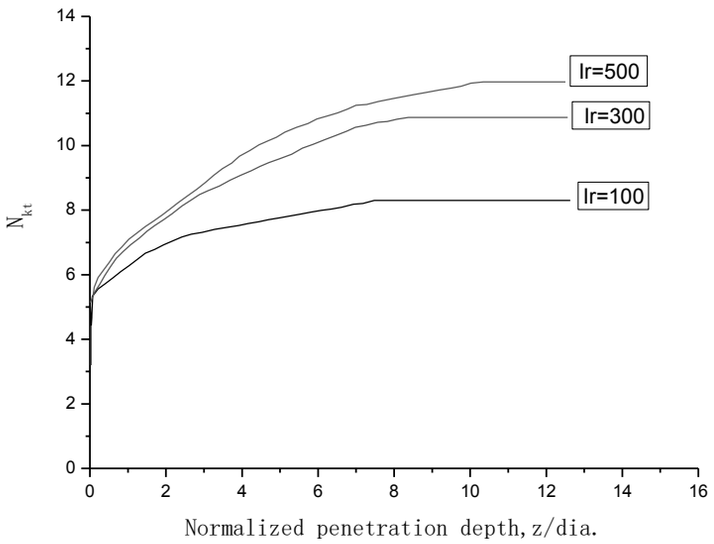

FIGURE 16
Evolution of cone resistance in clays with different rigidity indices

It can be concluded from Figure 16, that it is not necessary to continue the analyses after a penetration depth of 12 diameters because a steady state condition has been reached. The depth required to achieve a steady state condition increases with I_r. These results show that a steady state condition is achieved after a penetration depth of approximately 8 cone diameters in a Drucker-Prager material with an I_r of 100 and a steady state condition is achieved after a depth of approximately 12 cone diameters in a Drucker-Prager material with an I_r of 500. The final cone factors for the three different material stiffnesses are plotted on a logarithmic scale and are shown in Figure 17.

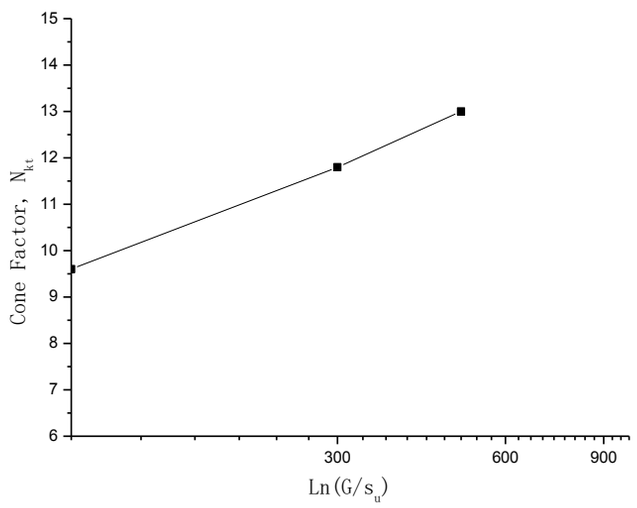

FIGURE 17
Effect of the rigidity index on the cone factor

The labels in Figure 17 represent the cone factors at rigidity indices of 100, 300 and 500. The equation represents a fit to the numerical results. In order to validate these results, it is necessary to compare this equation with others, as shown in Figure 18.

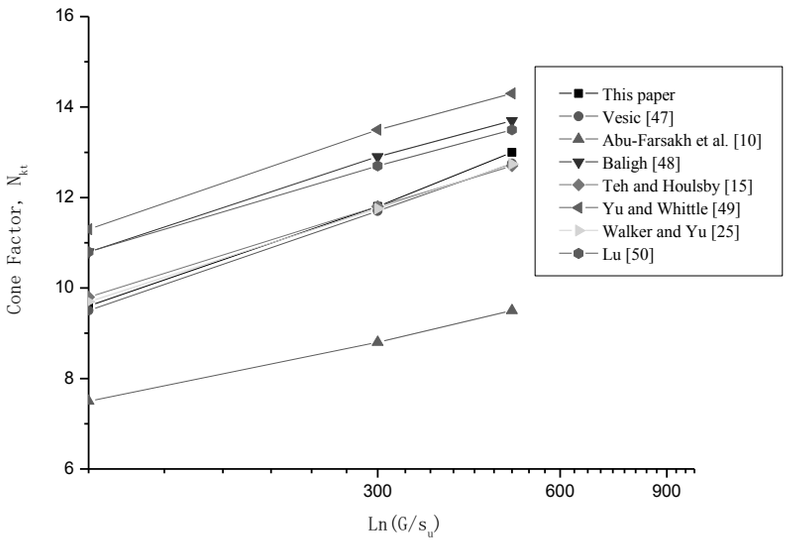

FIGURE 18
Comparison of the cone factors from different studies

It can be seen that the result obtained using the proposed method agrees well with others. Of particular note is the extremely close agreement between the current work and Walker and Yu [25] novel method which cannot be seen on the graph because the results virtually coincide with each other. This is comparable to others in the literature and these are summarized in Table 4.

TABLE 4
Comparison of the cone factors

Authors	I_r		
	100	300	500
Walker and Yu [25]	9.50	11.71	12.75
Vesic [47]	7.45	8.92	9.60
Abu-Farsakh et al. [10]	10.74	12.72	13.64
Baligh [48]	10.72	12.92	13.94
Teh and Houlsby [15]	9.77	11.80	12.75
Yu and Whittle [49]	11.14	13.34	14.36
Lu [50]	10.77	12.53	13.34
Yu and Mitchell [51]	9.54	11.74	12.76
This paper	9.60	11.80	13.00

Rough cone face and shaft. The investigation is extended to examine the effect of the roughness of the penetrometer on the cone factor. No special contact elements are needed because the explicit

algorithm can handle complicated contact conditions. The friction conditions at both the cone face-soil interface and the shaft-soil interface are identical. It is assumed that the soil sticks to the penetrometer until the shear stress at the interface equals a predetermined fraction of the shear strength of the soil. At this point the material is allowed to slide freely. The maximum shear stress that can be reached in a von Mises material is given by:

$$\tau_{\max} = \frac{2s_u}{\sqrt{3}} \tag{3}$$

where s_u is the undrained shear strength of the material under triaxial conditions. Interface friction is proportional to the roughness of the cone penetrometer itself. Hence, to simulate different levels of roughness the maximum permissible shear stress at the interface is varied. The fraction of permissible shear stress at the interface can be described by the following equation:

$$\alpha = \frac{\tau_{\text{int}}}{\tau_{\max}} \tag{4}$$

where τ_{int} is the permissible shear stress at the penetrometer-soil interface.

The final cone factors for four different values of α (=0, 1/3, 0.5, 2/3) are presented in Figure 19 for three different rigidity indices (100, 300, 500).

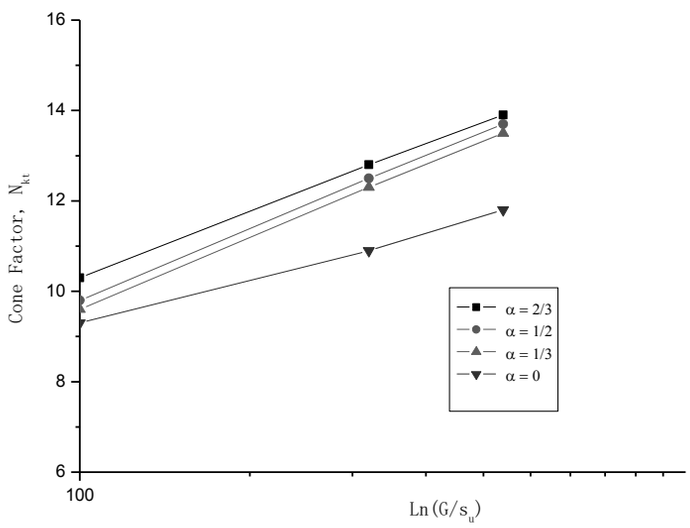

FIGURE 19
Effect of a rough cone and shaft on the cone factor

It can be seen that the cone factor increases with friction at the interface. The four equations in Figure 19 represent the trend lines of the data and it can be seen that for the range of values considered, the inclusion of friction at the interface increases the gradient of the trends. Whilst the gradient is constant if friction is included, the intercept of each trend line varies with a and a curve fitting analysis has shown that the intercepts adhere to the following trend

$$\text{Intercept} = \alpha\left(0.0026\left(I_r\right)-1.1919\right) \tag{5}$$

Hence the following relation is obtained for $1/3 \le \alpha_{cs} \le 2/3$.

$$N_c = 2.1907\ln\left(I_r\right)+\alpha_{cs}\left(0.0026\left(I_r\right)-1.1919\right) \tag{6}$$

where α_{cs} is the value of α at the penetrometer-soil interface. Many results in the literature use a linear term to describe the effect of the roughness of the penetrometer. However, the results in this paper show that this term is non-linear and dependent on I_r.

The values are comparable to the other solutions listed in Table 5, although there are some outlying results, such as the values for a rough cone from van den Berg [11].

TABLE 5
Comparison of cone factors derived using different methods

I_r	Cavity expansion						Strain path		Strain path and finite element		Finite element method			
	Ladanyi and Johnson [52]		Baligh [48]		Yu [53]		Teh and Houlsby [15]				Van den Berg [11]		This paper	
	S	R	S	R	S	R	S	R	S	R	S	R	S	R
50	6.5	8.5		15.9	8.5	13.8	8.5	10.5	8.4	10.8	9.5	13.8	8.6	10.2
100	8.0	10.0		17.0	9.8	15.0	10.5	12.5	10.6	13.0			9.6	11.3
150	8.3	10.3		17.2	10.1	15.2	10.9	12.9	10.9	13.9			10.5	11.8
300	8.9	10.9		17.7	10.6	15.8	11.7	13.7	12.5	14.9			11.8	12.7
500	9.6	11.6		18.2	11.2	16.4	12.7	14.7	14.4	16.8	12.0	17.5	13.0	13.9

Note: S = Smooth, R = Rough.

With both cone roughness and soil rigidity taken into consideration, the range from the present work is slightly narrower than the solutions by Yu [53], Teh & Houlsby [15] and van den Berg [11]. Closest agreement is with the solutions for a rough cone expressed in equation (5) obtained by Teh & Houlsby [15], using a pure strain path method but including a quasi-analytical term for the cone roughness [54, 55].

SUMMARY AND CONCLUSIONS

In this paper, finite-element analyses were performed to analyze the effect of in situ stress state, cone size and penetration rate on piezocone penetration test in clays, using the commercial finite-element code PLAXIS. The saturated clay was modeled as a multiphase material and the effective stress principle was used to describe its behavior. A frictional contact interface utilizing Mohr-Coulomb's theory was chosen to represent interactions between the surface of the cone and the soil. The variation of the cone resistance was examined in relation to various parameters such as the in situ stress state (K_o), cone size, cone apex angle, penetration rate and the material strength. For different penetration rate and cone size, the cone tip resistance profile and excess pore pressure profile are provided. A full parametric study has been undertaken, quantifying the influences of the rigidity index, in situ stress anisotropy and the cone roughness. The results show this study would provide some useful insights into the factors affecting the data interpretation of PCPT in clays. Based on this study, the following conclusions can be drawn:

The initial stress state (K_o) affects the cone tip resistance, sleeve friction and the generated excess pore pressures; the higher the initial stresses, the higher the tip resistance and the excess pore pressures. The cone tip resistance is strongly affected by the cross-sectional area. The higher the cross-sectional area is, the lower the cone tip resistance will be. The sleeve friction is affected by the sleeve friction area. The higher the cross-sectional area is, the lower the cone tip resistance will be. The higher the cone apex angle is, the higher the cone tip resistance will be. It should be noted that these trends are observed based on a constant initial vertical stress (σ_{vo} = 100 kPa). Rate effects can be significant for CPT results in soil. The effect of penetration rate on the cone resistance is obvious. The values of f_s increased as the cone velocity decreased. However, this tendency was not evident.

ACKNOWLEDGEMENTS

Majority of the work presented in this paper was funded by the Foundation for the New Century Excellent Talents of China (NCET-13-0118), the Foundation of Jiangsu Province Outstanding Youth (Grant No. BK20140027) and the Foundation for the Author of National Excellent Doctoral Dissertation of PR China (Grant No. 201353). These financial supports are gratefully acknowledged.

REFERENCES

[1] Acar, Y.B.: Piezocone penetration in soft chesive soils. Fugro Post-Doctoral Fellowship Activity Report No. 4, Louisiana State University, pp. 81 (1981)

[2] Lunne, T.; Robertson, P.K.; Powell, J.J.M.: Cone penetration testing in geotechnical practice. Blackie Academic and Professional, London, pp. 312 (1997)

[3] Salgado, R.; Mitchell, J.K.; Jamiolkowski, M.: Cavity expansion and penetration resistance in sand. J Geotech Geoenviron Eng. **123**(4), 344–354 (1997)

[4] Cai, G.J.; Liu, S.Y.; Tong, L.Y.; Du, G.Y.: Assessment of direct CPT and CPTU methods for predicting the ultimate bearing capacity of single piles. Eng Geol. **104**(1), 211–222 (2009)

[5] Cai, G.J.; Liu, S.Y.; Tong, L.Y.; Puppala, A.J.: Finite element analysis of some factors affecting piezocone penetration test (CPTU) in clays. In Proceedings of the International Symposium on Geomechanics and Geotechnics: From Micro to Macro (IS-Shanghai 2010), Oct. 10-12, 2010, Tongji University, Shanghai, China. Vol. 2, pp. 781-788. (2010)

[6] Tumay, M.T.; Acar, Y.B.: Pore pressures in piezocone penetration test (PCPT) in soft cohesive soils. Special Technical Publ. No. 833, Strength testing of marine sediments: Laboratory and in situ measurements, American Society of Testing and Materials, West Conshohocken, Pa., pp. 72–82 (1985)

[7] Kiousis, P.D.: Large strain theory as applied to penetration mechanism in soils. Ph.D. Dissertation, Louisiana State University, pp. 98 (1985)

[8] Kiousis, P.D.; Voyiadjis, G.Z.; Tumay, M.T.: A large strain theory and its application in the analysis of the cone penetration mechanism. Int J Numer Analyt Meth Geomech. **2**(1), 45–60 (1988)

[9] Kurup, P.U.; Voyiadjis, G.Z.; Tumay, M.T.: Calibration chamber studies of piezocone test in cohesive soils. J Geotech Engrg. 120(1), 81–107 (1994)

[10] Abu-Farsakh, M.Y.; Tumay, M.; Voyiadjis, G.Z.: Numerical parametric study of piezocone penetration test in clays. International Journal of Geomechanics. **3**(2), 170–181 (2003)

[11] Van den Berg, P.: Analysis of soil penetration, PhD Thesis, Delft University. (1994)

[12] Voyiadjis, G.Z.; Abu-Farsakh, M.Y.: Coupled theory of mixtures for clayey soils. Journal of Computers and Geotechnics. **20**(3), 195–222 (1997)

[13] Abu-Farsakh, M.Y.; Voyiadjis, G.Z.; Tumay, M.: Numerical analysis on the miniature piezocone penetration tests (PCPT) in clays. Int J Numer Analyt Meth Geomech. **22**(8), 791–818 (1998)

[14] Hu, Y.; Randolph, M.F.: A practical numerical approach for large deformation problems in soil. Int. J. Numer. Anal. Meth. Geomech. **22**(5), 327-350 (1998)

[15] Teh, C.I.; Houlsby, G.T.: An analytical study of the cone penetration test in clay. Geotechnique. **41**(1), 17–34 (1991)

[16] Zhou, L.; Deng, H.P.; Zhang, W.; Gao, Y.H.: Photodegradation of sulfamethoxazole and photolysis active species in water under UV-VIS light irradiation. Fresenius Environmental Bulletin. **24**(5), 1685–1691 (2015)

[17] Kiurski, J.; Ranogajec, J.; Oros, I.; Zoric D.: Fired clay, an effective natural adsorbent for printing developer purifying. Fresenius Environmental Bulletin. **22**(12), 3860–3864 (2013)

[18] Wei, L.; Abu-Farsakh, M.Y.; Tumay, M.T.: Finite-element analysis of inclined piezocone penetration test in clays. International Journal of Geomechanics. **5**(3), 167–178 (2005)

[19] Walker, J.; Yu, H.S.: Cone penetration analysis in cohesive-frictional materials. Proceedings of ISC-3 on Geotechnical and Geophysical Site Characterization, Huang A B & Mayne P W, 2008 Taipei, 1217–1222 (2008)

[20] Endra, S.; Roman, D.H.: Large displacement FEM modelling of the cone penetration test (CPT) in normally consolidated sand. Int. J. Numer. Anal. Meth. Geomech. 27, 585–602 (2003)

[21] Huang, W.; Sheng, D.; Sloan, S.W.; Yu, H.: Finite element analysis of cone penetration in cohesionless soil. Computers and Geotechnics. **31**(10), 517–528 (2004)

[22] Markauskas, D.; Kacianauskas, R.; Suksta, M.: Modeling the cone penetration test by the finite element method. Foundation of Civil and Environmental Engineering. **2**, 125–140 (2002)

[23] Lu, Q.; Randolph, M.F.; Hu, Y.; Bugarski, I.C.: A numerical study of cone penetration in clay. Geotechnique. **54**(4), 257–267 (2004)

[24] Ahmadi, M.M.; Byrne, P.M.; Campanella, R.G.: Cone tip resistance in sand: modeling,

verification, and applications. Can. Geotech. J. 42(4), 977–993 (2005)
[25] Walker, J.; Yu, H.S.: Adaptive finite element analysis of cone penetration in clay. Acta Geotech. 1(1), 43–57 (2006)
[26] Walker, J.; Yu, H.S.: Analysis of the cone penetration test in layered clay. Geotechnique. 60(12), 939–948 (2010)
[27] Randolph, M.F.; Dolwin, J.; Beck, R.: Design of driven piles in sand. Geotechnique. **44**(3), 427–448 (1994)
[28] Tumay, M.T.; Acar, Y.B.; Boggess, R.: Subsurface investigations with piezocone penetrometer, ASCE Special Publication on Cone Penetration Testing and Experience, pp. 325–342 (1981)
[29] Rad, N.S.; Tumay, M.T.: A study of pore pressure response of piezocone penetration test (PCPT). Geotechnical Testing Journal. **8**(1), 125–131(1985)
[30] Chen, B.S.Y.; Mayne, P.W.: Profiling the OCR of clays by piezocone tests. Report CEEGEO–94–1, Georgia Institute of Technology, Atlanta, pp. 98 (1994)
[31] Finke, K.A.; Mayne, P.W.; Klopp, R.A.: Piezocone penetration testing in Atlantic Piedmont residuum. J Geotech Geoenviron Eng. **127**(1), 48–54 (2001)
[32] Bemben, S.M.; Myers, H.J.: The influence of rate of penetration on static cone resistance in Connecticut river valley varved clay. In: Proceedings of the European Symp. on Penetration Testing, National Swedish Council for Building Research, Stockholm, Vol. 2.2, pp. 33–34 (1974)
[33] Roy, M.; Tremblay, M.; Tavenas, F.; Rochelle, P.L.: Development of pore pressures in quasi-static penetration tests in sensitive clay. Can Geotech J. **19**(2), 124–138 (1982)
[34] Campanella, R.G.; Robertson, P.K.; Gillespie, D.: Cone penetration testing in deltaic soils. Can Geotech J. **20**(1), 23–35 (1983)
[35] Powell, J.J.M.; Quarterman, R.S.T.: The interpretation of cone penetration tests in clays, with particular reference to rate effects. In: Proceedings of the Int. Symp. on Penetration Testing, A. A. Balkema, Rotterdam, pp. 903–909 (1988)
[36] Randolph, M.F.; Hope, S.: Effect of cone velocity on cone resistance and excess pore pressures. In: Proceedings of the Int. Symp. on Eng. Practice and Performance of Soft Deposits, Yodogawa Kogisha, Osaka, pp. 147–152 (2004)
[37] Chung, S.F.; Randolph, M.F.; Schneider, J.A.: Effect of penetration rate on penetrometer resistance in clay. J Geotech Geoenviron Eng. **132**(9), 1188–1196 (2006)
[38] Silva, M.F.; White, D.J.; Bolton, M.D.: An analytical study of the effect of penetration rate on piezocone tests in clay. Int J Numer Analyt Meth Geomech. **30**(1), 501–527 (2006)
[39] Yafrate, N.J.; DeJong, J.T.: Influence of penetration rate on measured resistance with full flow penetrometers in soft clay In: Proceedings of Sessions of Geo-Denver 2007, GSP 173 Advances in measurement and modeling of soil behavior, pp. 10 (2007)
[40] Kim, K.; Prezzi, M.; Salgado, R.; Lee, W.: Effect of penetration rate on cone penetration resistance in saturated clayey soils. J Geotech Geoenviron Eng. **134**(8), 1142–1153 (2008)
[41] House, A.R.; Oliveira, M.S.; Randolph, M.F.: Evaluating the coefficient of consolidation using penetration tests. Int. J. Phys. Model. in Geotechnics. **1**(3), 17–26 (2001)
[42] Lunne, T.; Eidsmoen, T.; Gillespie, D.; Howland, J.D.: Laboratory and field evaluation of cone penetrometers. In: Proceedings of the In Situ '86, Use of In Situ Tests in Geotech Engrg ASCE GSP 6, ASCE, Blacksburg, Va., pp. 714–729 (1986)
[43] Richarsdson, A.M.; Whitman, R.V.: Effect of strain-rate upon undrained shear resistance of a saturated remolded fat clay. Geotechnique. **13**(4), 310–324 (1963)
[44] Vaid, Y.P.; Campanella, R.G.: Time dependent behavior of undisturbed clay. J Geotech Engrg. **103**(7), 693–709 (1977)
[45] O'Reilly, M.P.; Brown, S.F.; Overy, R.F.: Viscous effects observed in tests on an anisotropically normally consolidated silty clay. Geotechnique. **39**(11), 153–158 (1989)
[46] Tani, K.; Craig, W.H.: Bearing capacity of circular foundations on soft clay of strength increasing with depth. Soils Found. **35**(4), 21–35 (1995)
[47] Vesic, A.S.: Expansion of cavities in an infinite soil mass. J Soil Mech Found Div ASCE **98**:265–290 (1972)
[48] Baligh, M.M.: Strain path method. J Geotech Eng, ASCE 111(3):1108–1136 (1985)
[49] Yu, H.S.; Whttle, A.J.: Combining strain path analysis and cavity expansion theory to estimate cone resistance in clay. Unpublished Notes (1999)

[50] Lu, Q.: A numerical study of penetration resistance in clay. PhD Thesis, The University of Western Australia (2003)
[51] Yu, H.S.; Mitchell, J.K.: Analysis of cone resistance: review of methods. J Geotech and Geoenvironment Eng. **124**(2):140–149 (1998)
[52] Ladanyi, B.; Johnson, G.H.: Behavior of circular footings and plate anchors embedded in permafrost. Can. Geotech. J. 11, 531–553 (1974)
[53] Yu, H.S.: Discussion on: Singular plastic fields in steady penetration of a rigid cone. J. Appl. Mech. 60, 1061–1062. (1993)
[54] Yu, H.S.: Cavity expansion methods in Geomechanics. Kluwer, Dordrecht (2000)
[55] Voyiadjis, G.Z.; Kurup, P.U.; Tumay, M.T.: Preparation of large size cohesive specimens for calibration chamber testing. Geotechnical Testing Journal. 16(3), 339–349 (1993)

Received: **07.08.2015**
Accepted: **21.12.2015**

CORRESPONDING AUTHOR

Guojun Cai
Southeast University
Institute of Geotechnical Engineering
210096 Nanjing – CHINA

e-mail: focuscai@163.com

by PSP Volume 25 – No. 1/ 2016, pages 275-283 Fresenius Environmental Bulletin

PREPARATION OF PALLADIUM/POLYMERIC PYRROLE-MULTIWALL CARBON NANOTUBES/TITANIUM ELECTRODE FOR HYDRODECHLORINATION OF PENTACHLOROPHENOL

Zhirong Sun[1,*], Sisi Zhao[1], Xuefeng Wei[1,3], Xiang Hu[2,]**

[1]College of Environmental & Energy Engineering, Beijing University of Technology, Beijing 100124, P.R. China
[2]College of Chemical Engineering, Beijing University of Chemical Technology, Beijing, 100029, P.R. China
[3]College of Chemical Engineering & Pharmaceutics, Henan University of Science and Technology, Luoyang 471003, P.R. China

ABSTRACT

A composite Pd coated electrode was prepared, which was modified with polypyrrole (PPy) and multiwall carbon nanotubes (MWCNTs), named Pd/PPy-MWCNTs/Ti electrode. The preparation parameters of Pd/PPy-MWCNTs/Ti were discussed. The content of MWCNTs adsorbed on Ti substrate was 1.0 mg, the polymerization current of pyrrole was 5 mA for 4 min and the depositing current of Pd was 40 mA for 45 min. The prepared electrode was characterized by scanning electron microscopy (SEM) and X-ray diffraction (XRD). It was used for pentachlorophenol (PCP) dechlorination in aqueous solution. PCP with initial concentration of 10 mg/L was completely removed by Pd/PPy-MWCNTs/Ti electrode in 90 min under the conditions of the electrolysis current of 5 mA and the initial pH of 2.2 at ambient temperature. The removal of PCP was maintained at 100% when Pd/PPy-MWCNTs/Ti electrode was reused eight times. It revealed that the self-made electrode had good stability for electrochemical dechlorination.

KEYWORDS:
Multiwall carbon nanotubes; polymeric pyrrole; pentachlorophenol; dechlorination

INTRODUCTION

Chlorophenols have been widely used as preservative, disinfectant, pesticide and industrial intermediates. However, they are highly toxic substances with carcinogenic, teratogenic and mutagenic effects [1, 2]. Some of them including pentachlorophenol (PCP) have been listed as the priority pollutants by United States Environmental Protection Agency [3, 4].

There are many ways to remove chlorophenols including physical, biological and chemical methods. Physical methods [5-8] just achieve a transfer of pollutants but not real transformation, such as adsorption, extraction and membrane separation. Biological treatments [9, 10] take a long time to domesticate specific microorganisms for the degradation of persistent organic compounds. Chemical methods can be divided into oxidative and reductive process, but the oxidation of chlorophenols tends to produce virulent byproducts such as PCBs, dioxins and dibenzofurans [11, 12].

Electrocatalytic hydrodechlorination (ECH) which belongs to reduction methods has received much attention due to its mild reaction conditions, rapid reaction rate and the absence of secondary contaminants [13]. The mechanism of ECH [14, 15] is that atomic hydrogen (H*) generated from electrochemical reduction of water molecules or hydrogen ions attacks chlorophenols adsorbed on the electrode surface to form products without chlorine atoms.

The process of electrochemical reaction could be influenced greatly by the electrode material and nature. Palladium (Pd) is one of the most commonly used catalysts in the preparation of electrode for ECH due to its unique hydrogen sorption/desorption properties [16-18]. Titanium (Ti) is used as the cathode substrate for its strong corrosion resistant ability. Chen et al. [19, 20] found that cathode modified by Pd showed high electrochemical activity and long-term stability, especially for the Pd/Ti electrode. Polymeric pyrrole (PPy) is a kind of conductive polymer which has the advantages of environmental stability and good conductivity [21, 22]. It could be used as proper host matrices to obtain highly dispersed metallic particles. In particular, metal microparticles dispersed on polymer modified electrodes have been recognized to have potential applications in electrocatalysis [23]. Carbon nanotubes (CNTs) have been the subject of research

effort due to their unique chemical and mechanical properties [24-25].

They also have the capability of hydrogen storage because of the unique behavior between hydrogen and CNTs [26]. They have become novel promising materials which were employed to modify composite electrode.

In this study, the Pd composite electrode modified with multiwall carbon nanotubes (MWCNTs) and PPy was prepared. The properties of the electrode were characterized and the dechlorination process of PCP was also investigated.

EXPERIMENTAL

Chemicals and materials. PCP (99%) was analytical purity and purchased from Chem Service Inc. Experimental chemicals including palladium chloride ($PdCl_2$) powder, pyrrole (Py), sodium sulfate (Na_2SO_4) and acetone were analytical purity and supplied by Beijing Reagent Co. Perchloric acid ($HClO_4$, 72%) and nitric acid (HNO_3, 68%) were purchased from Beijing Chemical Works. MWCNTs (95%, 15-20 nm) were chemical purity and provided by Beijing Nachen S&T Ltd. Meshed Ti (aperture density 150 PPI, line diameter 0.10 mm) was from Anping Wire Screen Mesh Plant, China. Platinum (Pt) foil was from General Research Institute for Nonferrous Metals, China. Cation-exchange membrane Nafion-324 (DuPont) was supplied by Sigma Aldrich Chemical Co. All aqueous solutions were prepared using ultrapure water (Millipore-Q system, 18.2 MΩ•cm).

Pretreatment of MWCNTs. MWCNTs were suspended in mixed acid (V_{HNO3}/V_{HClO4}=1/3) and sonicated for 8 hours. Subsequently, the mixture was filtered through mixed cellulose ester membrane with aperture of 0.22 μm and washed thoroughly with ultrapure water. Finally, they were dried under the temperature of 373K.

Electrode preparation. Meshed Ti was pretreated before use. It was put into hot sodium carbonate solution for 30 min to remove grease and put into boiling oxalic acid for 30 min to remove surface oxides. Then it was rinsed thoroughly with ultrapure water and stored in ethanol for later use. Py was distilled before use and stored in a light protected bottle.

The pretreated MWCNTs were dispersed in 10 mL acetone solvent and were adsorbed on meshed Ti surface by dip-coating method. Secondly, PPy-MWCNTs/Ti was prepared by electro-polymerization. PPy was synthesized on MWCNTs/Ti substrate in a mixed solution containing 0.5 mol/L H_2SO_4 and 0.06 mol/L Py. Lastly, Pd particles were electrodeposited on PPy-MWCNTs/Ti supporting electrode in $PdCl_2$ solution with the concentration of 33.75 mmol/L under constant current. The self-made electrode was named Pd/PPy-MWCNTs/Ti electrode.

Dechlorination experiments. The dechlorination experiments of PCP were conducted in a two-compartment cell. It was separated by a cation-exchange membrane Nafion-324 which was used to prevent the oxidation of chlorophenols and dechlorination products on the anode. The catholyte was 10 mg/L PCP aqueous solution containing 0.05 mol/L Na_2SO_4 as a supporting electrolyte. The anolyte was only 0.05 mol/L Na_2SO_4 solution. The initial pH of catholyte was adjusted by addition of H_2SO_4. Pd/PPy-MWCNTs/Ti electrode was used as cathode and Pt was used as anode. The dechlorination process was carried out at ambient temperature and conducted under constant current. The catholyte was stirring with magnetic stir at the speed of 400 rpm to eliminate the effect of concentration polarization.

Analysis methods. The electrode was characterized by cyclic voltammetry (CV) with three-electrode system using electrochemical workstation (CHI660C, Shanghai Chenhua Instrument Co., Ltd., China). Pd/PPy-MWCNTs/Ti electrode was used as working electrode, Pt was used as counter electrode and Hg/Hg_2SO_4-saturated K_2SO_4 was used as reference electrode. The CV tests were performed in a 0.5 mol/L H_2SO_4 solution with scan rate of 50 mV/s. The morphology of the electrode was recorded by scanning electron microscope (SEM, S4700, Hitachi Ltd., Japan) with an accelerating voltage of 20.0 kV. The lattice structure of Pd particles on the surface of the electrode was analyzed by X-ray diffraction (XRD, D8 Advance, Bruker/AXS, Germany) using Cu-Kα radiation with k=1.5405˚A and operating at 40 kV and 50 mA. The concentration of PCP was determined by high performance liquid chromatography (HPLC, Waters 1525, USA).

The removal efficiency (η) was expressed as follows:

$$\eta(\%) = \frac{C_0 - C_t}{C_0} \times 100\% \quad (1)$$

where C_0 was the initial concentration of PCP (mg/L), and C_t was PCP concentration at electrolysis time t (mg/L).

RESULTS AND DISCUSSION

Preparation parameters of Pd/PPy-MWCNTs/Ti electrode. According to the mechanism of ECH [14, 15], sufficient hydrogen atoms adsorbed on the electrode were beneficial to remove chlorine atoms from chlorophenols. The value of hydrogen adsorption peak of CV curves indicated the amount of hydrogen atoms adsorbed on the electrode [27, 28]. Therefore, the electrode with high hydrogen adsorption peak current showed its great potential for dechlorination.

MWCNTs content. Pd/PPy-MWCNTs/Ti electrodes were prepared with different content of MWCNTs (0.6, 1.0, 1.4 and 1.8 mg, respectively). PPy with the concentration of 0.06 mol/L was eletro-polymerizated at constant current of 5 mA for 4 min. Pd was eletrodeposited with constant current of 40 mA for 45 min.

Fig.1 shows the CV curves of Pd/PPy-MWCNTs/Ti electrode which affected by the content of MWCNTs. With the increase of MWCNTs content, the value of hydrogen adsorption peak current increased first and then decreased after reaching a maximum. When the content of MWCNTs was 1.0 mg, the hydrogen adsorption peak current obtained the maximal value. It may be referred to that when the content of MWCNTs was low, the ability of catalysis and conductivity couldn't be performed to the best. When the content was high, MWCNTs combined with
meshed Ti weren't stable and it was unfavorable to the deposition of PPy and Pd.

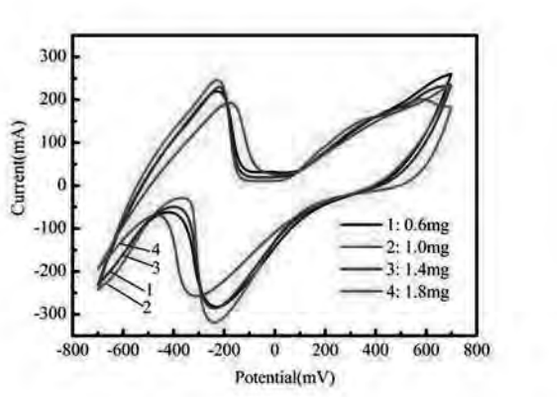

FIGURE 1
CV curves of Pd/PPy-MWCNTs/Ti electrodes prepared at different MWCNTs content

Electro-polymerization current and time of PPy. Pd/PPy-MWCNTs/Ti electrodes were prepared with 0.06 mol/L Py under different electro-polymerization current and time. The content of MWCNTs was 1.0 mg which adsorbed on the electrode. Pd was eletrodeposited on the electrode with the electrodepositing current of 40 mA for 45 min.

Fig.2a shows the CV curves of Pd/PPy-MWCNTs/Ti electrodes prepared under different electro-polymerization current for PPy (3, 4, 5 and 6 mA, respectively), the polymerization time was 5 min. The hydrogen adsorption peak current reached the maximum with electro-polymerization current of 5 mA. At the current of 5 mA, the effect of electro-polymerization time on Pd/PPy-MWCNTs/Ti electrode was investigated further. Fig.2b shows the CV curves of Pd/PPy-MWCNTs/Ti electrodes affected by different electro-polymerization time (2, 3, 4 and 5 min, respectively). The maximal hydrogen adsorption peak current was obtained at the polymerization time of 4 min.

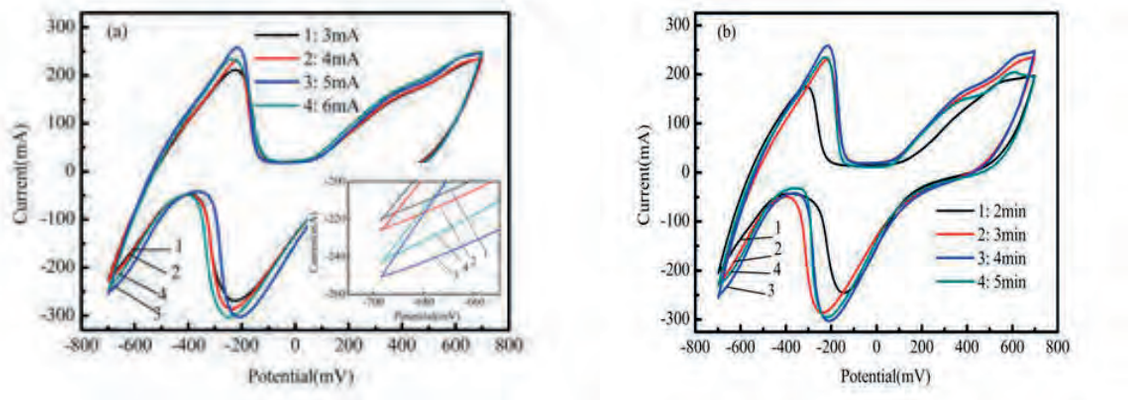

FIGURE 2

CV curves of Pd/PPy-MWCNTs/Ti electrodes prepared at (a) different electro-polymerization current and (b) different time (The inset is the partial enlarged details)

The electro-polymerization condition of Py affected electrochemical properties of Pd/PPy-MWCNTs/Ti electrode greatly. When polymerization current was low and the time was short, the PPy film was too thin to have effect on the dispersion of Pd particles. However, if the current was high and time was long, the PPy film would become too thick to promote the electron transfer and the hydrogen adsorption current would decrease. Therefore, the appropriate conditions for preparing Pd/PPy-MWCNTs/Ti electrode was 0.06 mol/L Py with polymerization current of 5 mA and time of 4 min.

Electrodepositing current and electrodepositing time of Pd. Different current and time of Pd electrodepositing for Pd/PPy-MWCNTs/Ti electrodes preparation were investigated. The MWCNTs with the content of 1.0 mg were adsorbed on the electrode and Py with the concentration of 0.06 mol/L was eletro-polymerizated under the current of 5 mA for 4 min.

Fig. 3a shows the CV curves of Pd/PPy-MWCNTs/Ti electrodes prepared at different electro-depositing current (30, 35, 40 and 45 mA, respectively) with the fixed electrodepositing time of 45 min. The hydrogen adsorption peak performed the best with the current of 40 mA. Electrodepositing time of Pd was studied further when the depositing current was 40 mA. Fig. 3b shows the CV curves of Pd/PPy-MWCNTs/Ti electrodes at different depositing time (35, 40, 45 and 50 min, respectively). When the depositing time was 45 min, the hydrogen adsorption peak current was the maximum.

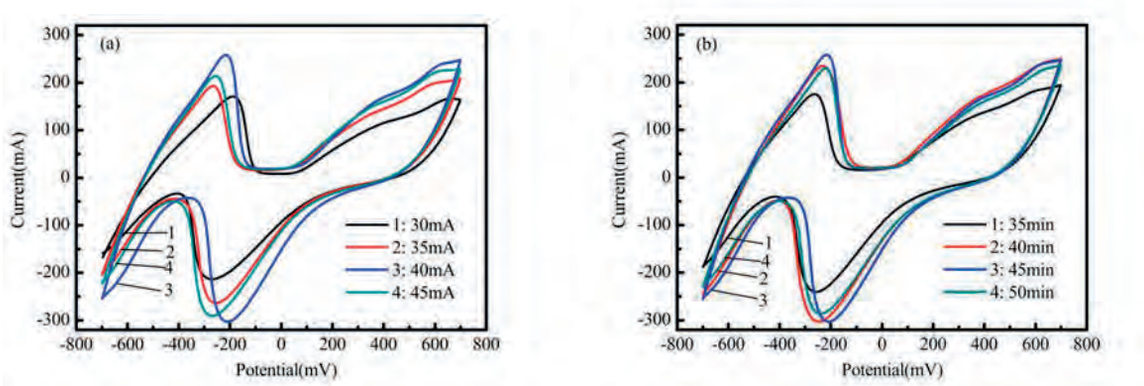

CV curves of Pd/PPy-MWCNTs/Ti electrodes prepared at (a) different electrodepositing current and (b) different time

The results indicated that the depositing condition of Pd microparticles had great impact on the performance of Pd/PPy-MWCNTs/Ti electrode. The amount of Pd deposited on the electrode became larger with the increase of electrodepositing current and time. However, when the content of Pd was too large, it could aggregate on the surface. The value of hydrogen adsorption peak current decreased and the electrocatalytic capability of Pd/PPy-MWCNTs/Ti electrode also decreased, accordingly. In addition, when the electrodepositing current was low or the time was insufficiency, the content of Pd catalyst was insufficient and the hydrogen adsorption peak current of the electrode would reduce. Therefore, the electrodepositing current of 40 mA and time of 45 min for depositing Pd on the electrode were selected as the proper preparation conditions.

In brief, the MWCNTs content of 1.0 mg, Py electro-polymerization current of 5 mA , polymerization time of 4 min, Pd electrodepositing current of 40 mA and depositing time of 45 min were selected as the optimized parameters for preparing Pd/PPy-MWCNTs/Ti electrode.

Characterization of Pd/PPy-MWCNTs/Ti electrode. Fig. 4 shows the morphology of Pd/PPy-MWCNTs/Ti electrode under different zoom scales. As shown in Fig. 4a (2,000×), Pd particles were dispersed on PPy-MWCNTs/Ti substrate with lacebark pine shape. From the high magnification Fig.4b (50,000×), Pd microparticles presented flocculent and intertwined-flaky shape. The structure of the electrode surface performed good spatial extensibility which could have higher surface areas and supply more catalytic sites for dechlorination.

Fig. 5 shows the crystallographic information of the Pd/PPy-MWCNTs/Ti electrode. The peaks at 2θ values of 40.1, 46.7, 68.1, 82.1 and 86.6 could be ascribed to (111), (200), (220), (311) and (222) reflection of the crystal lattice of Pd. The results represented that Pd particles with crystal lattice were successfully deposited on the electrode. The metal Lorentz grain size of Pd was 17.1 nm and the lattice parameter was calculated by the XRD bundle software (EVA).

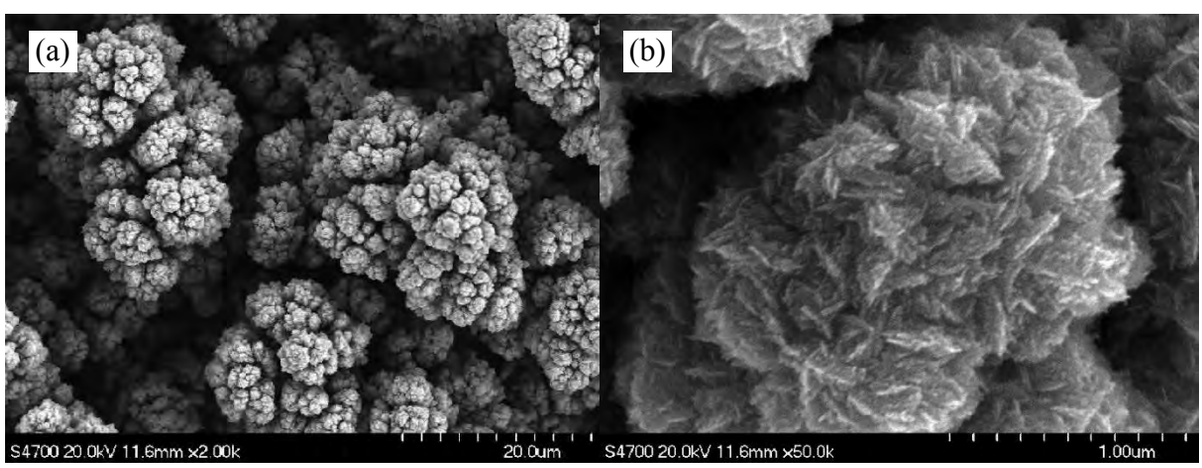

FIGURE 4
SEM images of Pd/PPy-MWCNTs/Ti electrode under different zoom scales

ELECTROCHEMICALLY REDUCTIVE DECHLORINATION OF PCP

Effect of dechlorination current. The effect of dechlorination current (1, 3, 5, 8 and 10 mA, respectively) on the removal of PCP was investigated under the condition of initial pH of 2.0. Fig.6 shows the removal of PCP changed with different electrolysis currents. At the current of 1 mA, the removal of PCP reached 79.4%. When the current increased to 5mA, PCP was completely removed within 90 min. However, when the dechlorination current increased further, the removal efficiency of PCP on Pd/PPy-MWCNTs/Ti electrode decreased. It may be inferred that the side reaction of hydrogen evolution reaction (HER) on the electrode was

intensified under the higher current. Hydrogen formed from HER restrained the diffusion of PCP molecules and then prevented PCP molecules adsorbing on the electrode surface for dechlorination.

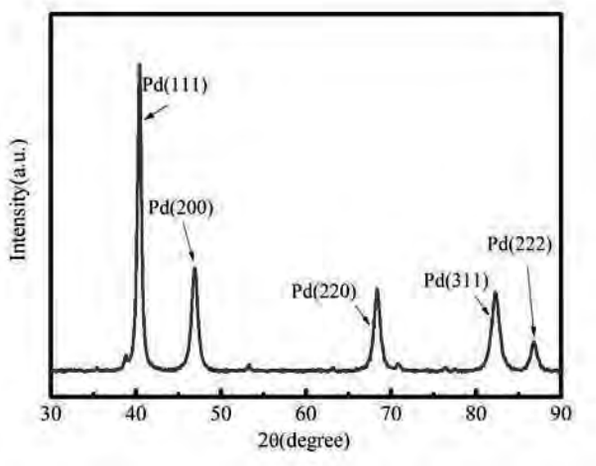

FIGURE 5
XRD pattern for Pd/PPy-MWCNTs/Ti electrode

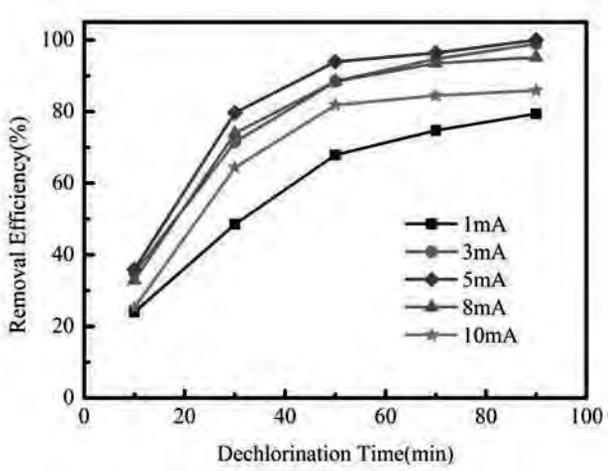

FIGURE 6
Effect of dechlorination current on removal efficiency of PCP (PCP concentration: 10 mg/L, initial pH: 2.0)

Effect of initial pH. The effect of initial pH (1.8, 2.0, 2.2, 2.8 and 3.4, respectively) on the removal of PCP was investigated under the condition of dechlorination current of 5 mA. Fig.7 shows the removal of PCP improved with the solution acidity increasing. When initial pH was 2.8 and 3.4, only a small amount of PCP was removed from the solution. The result could be explained that active hydrogen atoms formed from the reduction ofhydrogen ions were insufficient for dechlorination of PCP. When pH decreased to 2.2, the removal of PCP reached 100% and the finial pH of solution was 6.5, which was close to neutral. When pH was 2.0 and 1.8, PCP still could be successfully removed, but the solution was acidic at the end of the reaction, which was bad for the subsequent treatment.

The stability of Pd/PPy-MWCNTs/Ti electrode. The stability of Pd/PPy-MWCNTs/Ti electrode was studied by batch dechlorination experiments and SEM images. The electrocatalytic hydrodechlorination of PCP were conducted continuously under the selected conditions, i.e., initial concentration of 10 mg/L, electrolysis current of 5 mA, initial pH of 2.2 and dechlorination time of 90 min. Fig.8 indicated that the conversion efficiency of PCP still reached 100% during eight times

dechlorination. Compared the SEM images (Fig.9) used for 8 times with the SEM observation of the initial one (Fig.5), there was little change on the surface of Pd/PPy-MWCNTs/Ti electrode. This suggested that the self-made electrode have good stability within the investigation range.

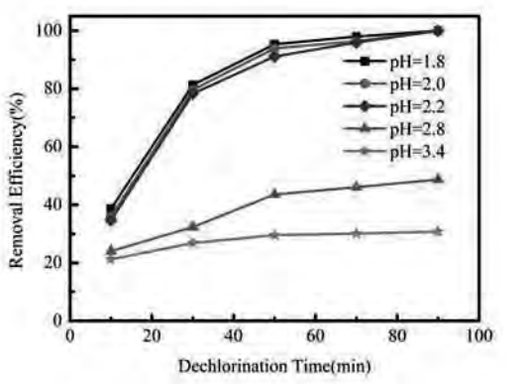

FIGURE 7
Effect of initial pH on removal efficiency of PCP
(PCP concentration: 10 mg/L, dechlorination current: 5mA)

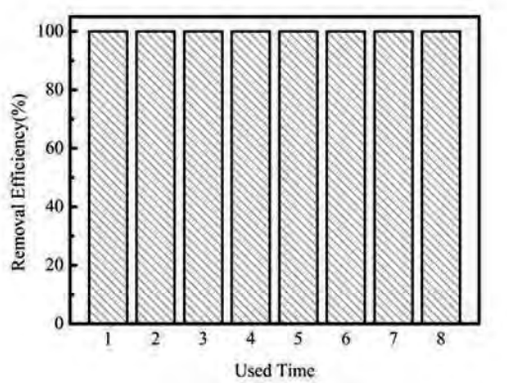

FIGURE 8
Effect of electrode reused times on removal efficiency of PCP

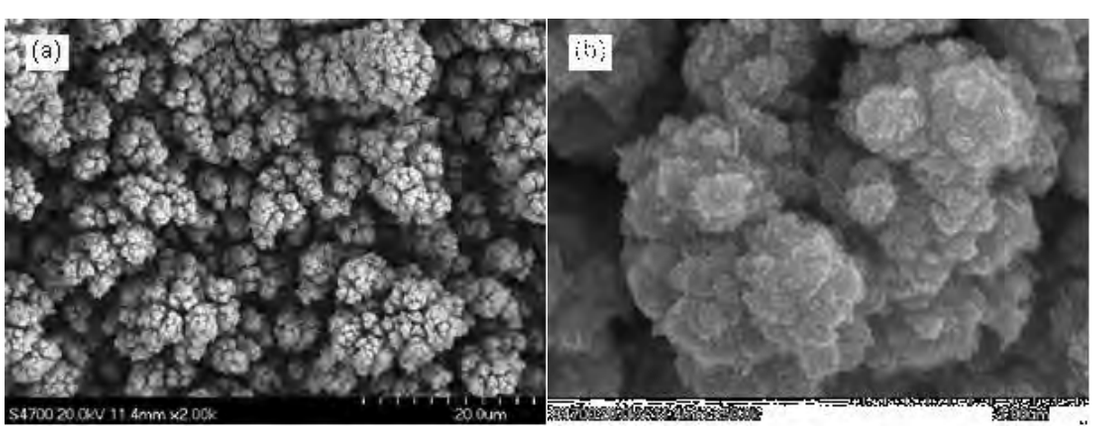

FIGURE 9
SEM images of Pd/PPy-MWCNTs/Ti electrode which was used 8 times

CONCLUSIONS

A composite Pd/PPy-MWCNTs/Ti electrode was prepared and was employed to dechlorination of PCP in aqueous solution. The parameters for preparing the electrode were optimized .i.e. the content of MWCNTs was 1.0 mg, 0.06 mol/L Py was electro-polymerizated under the current of 5 mA for 4 min and 33.75 mmol/L $PdCl_2$ was electrodeposited under the current of 40 mA for 45 min. 10 mg/L PCP was completely removed by Pd/PPy-MWCNTs/Ti electrode within 90 min under the conditions of the dechlorination current of 5 mA and the intial pH of 2.2 at ambient temperature. The composite Pd/PPy-MWCNTs/Ti electrode performed good stability in successively repeated experiments.

ACKNOWLEDGEMENTS

The work was supported by National Natural Science Foundation of China (51278006, 51478014), Research Fund for the Doctoral Program of Higher Education of China (20111103110007), The Importation and Development of High-Caliber Talents Project of Beijing Municipal Institutions (CIT&TCD20130311).

REFERENCES

[1] Wu T.N. (2010) Electrochemical removal of pentachlorophenol in a lab-scale platinum electrolyzer. *Water Sci. Technol.*, 62(10): 2313-2320.

[2] Miao M.S., Zhang Y.J., Shu L., Zhang J., Kong Q., Li N. (2014) Development and characterization of the 2,4,6-trichlorophenol (2,4,6-TCP) aerobic degrading granules in sequencing batch airlift reactor. *Int. Biodeter. Biodegr.*, 95: 61-66.

[3] Liu X.C., Wang X.Y. (2014) Highly dispersive PdCoB catalysts for dechlorination of chlorophenols. *J. Hazard. Mater.*, 274: 63-71.

[4] Garg S.K., Tripathi M., Singh S.K., Singh A. (2013) Pentachlorophenol dechlorination and simultaneous Cr^{6+} reduction by Pseudomonas putida SKG-1 MTCC (10510): characterization of PCP dechlorination products, bacterial structure, and functional groups. *Environ. Sci. Pollut. R.*, 20(4): 2288-2304.

[5] Zhou L.C., Meng X.G., Fu J.W., Yang Y.C., Yang P., Mi C. (2014) Highly efficient adsorption of chlorophenols onto chemically modified chitosan. *Appl. Surf. Sci.*, 292: 735-741.

[6] Wang K.D., Chen P.S., Huang S.D. (2014) Simultaneous derivatization and extraction of chlorophenols in water samples with up-and-down shaker-assisted dispersive liquid-liquid microextraction coupled with gas chromatography/mass spectrometric detection. *Anal. Bioanal. Chem.*, 406(8): 2123-2131.

[7] Yogesh, Popat K.M., Ganguly B., Brahmbhatt H., Bhattacharya A. (2008) Studies on the separation performances of chlorophenol compounds from water by thin film composite membranes. *Macromol. Res.*, 16(7): 590-595.

[8] Ghosh U.K., Pradhan N.C., Adhikari B. (2006) Separation of water and o-chlorophenol by pervaporation using HTPB-based polyurethaneurea membranes and application of modified Maxwell-Stefan equation. *J. Membrane Sci.*, 272(1-2): 93-102.

[9] Carucci A., Milia S., Cappai G., Muntoni A. (2010) A direct comparison amongst different technologies (aerobic granular sludge, SBR and MBR) for the treatment of wastewater contaminated by 4-chlorophenol. *J. Hazard. Mater.*, 177(1-3): 1119-1125.

[10] Pal N., Korfiatis G.P., Patel V. (1997) Sonochemicalextractionand biological treatment of pentachlorophenol contaminated wood. *J. Hazard. Mater.*, 53(1-3): 165-182.

[11] Munoz M., de Pedro Z.M., Casas J.A., Rodriguez J.J. (2011) Assessment of the generation of chlorinated byproducts upon Fenton-like oxidation of chlorophenols at different conditions. *J. Hazard. Mater.*, 190(1-3): 993-1000.

[12] Vallejo M., San Román M.F., Ortiz I., Irabien A. (2014) The critical role of the operating conditions on the Fenton oxidation of 2-chlorophenol: Assessment of PCDD/Fs formation. *J. Hazard. Mater.*, 279: 579-585.

[13] He Z.Q., Zhan L.Y., Wang Q., Song S., Chen J.M., Zhu K.R., Xu X.H., Liu W.P. (2011) Increasing the activity and stability of chemi-deposited palladium catalysts on nickel foam substrate by electrochemical deposition of a middle coating of silver. *Sep. Purif. Technol.*, 80(3): 526-532.

[14] Cui C.Y., Quan X., Yu H.T., Han Y.H. (2008) Electrocatalytic hydrodehalogenation of pentachlorophenol at palladized multiwalled carbon nanotubes electrode. *Appl. Catal. B*, 80(1-2):122-128.

[15] Xu Y.H., Cai Q.Q., Ma H.X. (2013) Optimisation of electrocatalytic dechlorination o f 2,4- dichlorophenoxyacetic acid on a roughened silver-palladium cathode. *Electrochim. Acta,* 96: 90-96.

[16] Dabo P., Cyr A., Laplante F., Jean F., Menard H., Lessard J. (2000) Electrocatalytic dehydrochlorination of pentachlorophenol to phenol or cyclohexanol. *Environ. Sci. Technol.,* 34(7): 1265-1268.

[17] Cheng I.F., Fernando, Q., Korte, N. (1997) Electrochemical dechlorination of 4-chlorophenol to phenol. *Environ. Sci. Technol.*, 31(4): 1074-1078.

[18] Wu Y.Y., Hsu C.T., Mark Chang T.F., Sone M., Hu C.C. (2015) Preparation and characterization of palladium-hydride-coated titanium as a reference electrode for the supercritical carbon dioxide emulsion electrochemical system. *Electrochimi. Acta*, 155: 209-216.

[19] Cheng H., Scott K., Christensen P. A. (2003) Electrochemical hydrodehalogenation of chlorinated phenols in aqueous solution-I. Material aspects. *J. Electrochem. Soc.*, 150(2): D17-D24.

[20] Cheng H., Scott K., Christensen P. A. (2003) Electrochemical hydrodehalogenation of chlorinated phenols in aqueous solution-II. Effect of operating parameters. *J. Electrochem. Soc.*, 150(2): D25-D29.

[21] Hosseini S.H., Abadi A.J.N. (2015) Preparation of magnetic and conductive graphite nanoflakes/Fe_3O_4 nanoparticles/polypyrrole nanocomposites. *Synth. React. Inorg. M.*, 45(4): 591-596.

[22] Yang Q.H., Hou Z.Z., Huang T.Z. (2015) Self-assembled polypyrrole film by interfacial polymerization for supercapacitor applications. *J. Appl. Polym. Sci.*, 132(11): 41615.

[23] Mourato A., Correia J.P., Siegenthaler H., Abrantes L.M. (2007) Palladium eletrodeposition on polyaniline films. *Electrochim. Acta*, 53(2): 664-672.

[24] Ling X.L., Wei Y.Z., Zou L.M., Xu S. (2013) Preparation and characterization of hydroxylated multi-walled carbon nanotubes. *Colloid. Surface. A*, 421: 9-15.

[25] Karousis N., Tsotsou G.E., Evangelista F., Rudolf P., Ragoussis N., Tagmatarchis N. (2008) Carbon nanotubes decorated with palladium nanoparticles: synthesis, characterization, and catalytic activity. *J. Phys. Chem. C*, 112(35): 13463-13469.

[26] Liu C., Fan Y.Y., Liu M., Cong H.T., Cheng H.M., Dresselhaus M.S. (1999) Hydrogen storage in single-walled carbon nanotubes at room temperature. *Science*, 286(5442): 1127-1129.

[27] Hu X., Ge H., Li B.H., Sun Z.R. (2008) Preparation and characterization of codeposited palladium-nickel/titanium electrodes and palladium-nickel/polymeric pyrrole film/titanium electrodes. *Chem. Eng. Technol.*, 31(10): 1396-1401.

[28] Zhang J.T., Huang M.H., Ma H.Y. (2007) High catalytic activity of nanostructured Pd thin films electrochemically deposited on polycrystalline Pt and Au substrates towards electro-oxidation of methanol. *Electrochem. Commun.*, 9(6):1298-1304.

Received: **11.08.2015**
Accepted: **16.01.2016**

CORRESPONDING AUTHORS

Prof. Dr. Zhirong SUN
Beijing University of Technology
College of Environmental & Energy Engineering
100 Pingleyuan, Chaoyang District
Beijing 100124 – CHINA

e-mail: zrsun@bjut.edu.cn

Prof. Dr. Xiang HU
Beijing University of Chemical Technology
College of Chemical Engineering
Chaoyang District
Beijing 100029 – CHINA

e-mail: huxiang99@163.com

by PSP Volume 25 – No. 1/ 2016, pages 284-291 Fresenius Environmental Bulletin

APPLYING OF LOW DOSE GAMMA-RADIATION TO ENHANCE *T. HARZIANUM* AND *T. VIRIDE* FUNGI FOR CARBOFURAN PESTICIDE BIODEGRADIATION

Abd El-Moneim M.R. Afify[1], Ghada I. Mahmoud[1], Mohamed A. Abo-El-Seoud[2], Bassam W. Kassem[2]

[1] Biochemistry Dept., Faculty of Agriculture, Cairo University, Giza, Egypt.
[2] Plant Research Dept., Nuclear Research Center, Egyptian Atomic Energy Authority, Abu-Zabal 13759, Egypt.

ABSTRACT

This investigation has been carried out to study the possibility of enhancing *Trichoderma* spp. with low dose gamma radiation for biodegradation of carbofuran pesticide. Five fungi strains are identified as *Trichoderma* spp. including *T. harzianum* and *T. viride*, *Aspergillus niger*, *Fusarium oxysporum* and *Penicillium cyclopium*. The results showed that *Trichoderma* spp. reached its maximum growth using carbofuran concentration of 200 mg/L (*T. harzianum* and *T. viride*, 167.6 and 222.0 mg/L respectively). On the other hand, *Aspergillus niger* reached its maximum yield 203.2 with 20 mg/L while the growth of *Fusarium oxysporum* and *Penicillium cyclopium* were dose dependence. This indicated that the isolates of *Trichoderma* spp. were potentially useful for carbofuran bioremediation after enchantment by low dose of gamma radiation. The biomass of *Trichoderma* spp. strain were increased and reached its maximum at 250 Gy of gamma radiation with *Trichoderma* spp. This dose showed increase in carbofuran biodegradation by 79% and 83.5% with *T. harzianum* and *T. viride*, respectively.

KEYWORDS:
Carbofuran; Trichoderma harzianum; Trichoderma viride; biodegradation; gamma-irradiation.

INTRODUCTION

Although it might take a larger dose of pesticide to harm humans than pests such as insects, many pesticides are still toxic to humans (Afify *et al.*, 2010 and Afify, 2011). The doses needed to kill a pest might not kill us, but may still harm us. Many pesticides classified as herbicides are designed as species specific to the target plant pest. The exceptions to this are broad spectrum herbicides that are designed to kill a wide variety of plants. A herbicide that is specific to one or more species of plants does not insure that it is safe to enter the water system. Some of the dangers from these chemicals are yet to be fully understood.

Organophosphate and carbamate compounds are considered widely used pesticides. Contamination of surface water with carbofuran, carbamate pesticide is of interest because of potential toxicity to aquatic organisms. Although it might take a larger dose of pesticide to harm humans than pests such as insects.

Fungi degrade pesticides by introducing minor structural changes to the pesticides where it is susceptible to further biodegradation (Kim *et al*., 2004). Several fungi such as *Agrocybe semiorbicularis, Auricularia auricula, Coriolus versicolor, Dichomitus squalens, Flammulina velupites, Hypholoma fasciculare, Pleurotus ostreatus, Stereum hirsutum,* and *Avatha discolor* have shown their ability to degrade various pesticide groups (Rani and Dhania, 2014).

The biodegradation of carbamate has been investigated by different microorganisms that metabolize carbamate pesticides to other products (Afify *et al.*, 2013). In most cases, the studies did not eliminate the possibility that abiotic processes are involved in the degradation. A number of bacteria capable of degrading carbofuran (*Pseudomonas*, *Flavobacterium*, *Sphingomonas* and *Arthrobacter*) have been isolated and characterized in an effort to better understand the bacterial role to remove carbofuran from the environment. Carbofuran is one of the pesticides belonging to the *N*-methylcarbamate class used extensively in agriculture. It exhibits high mammalian toxicity and has been classified as highly hazardous. Biomarkers are analyzed directly in cells and tissues of exposed organisms, and are traditionally defined as molecular, biochemical, cellular and physiological alterations caused by external stressors (Afify *et al.*, 2008; Afify, 2009 and Afify *et al.*, 2009). Biomarkers of exposure indicate exposure reflective of the internal concentration of pesticide(s) or metabolite(s), and can be applied as screening tools for specific chemical groups, for example the proteins metallothionein as indicators of elevated concentrations of bioavailable heavy

metals (Connon *et al.*, 2012). Environmental of oral and dermal exposure of rats to pesticide cyanophos was characterized by studying acetylcholine esterase, aspartate transaminase, alanine transaminase and alkaline phosphatase enzyme activities (Afify and El-Beltagi, 2011) as biomarker for pesticides pollution.

A number of isolates capable of carrying out some form of degradation of pesticide have been isolated from soils and several fungi have been isolated and studied, including *Aspergillus niger* (Qing *et al.*, 2006), *Fusarium graminearum* (Salama, 1998), *Mucor ramannianus* (Seo *et al.*, 2007) and *Gliocladium* sp. (Slaoui *et al.*, 2007). Recently a strain of *Trichoderma harzianum* has been shown to degrade carbofuran (Wootton *et al.*, 1993, Afify *et al.*, 2013).

Low dose of ionizing radiation on microorganisms is responsible of accelerated enzyme activity (Chakravarty and Sen, 2001). The lowest dose of gamma irradiation (1 MCi for 10 min) enhanced three isolates of *Aspergillus niger* investigated to produce more biomass and polygalacturonase, cellulase and protease (Gherbawy, 1998). *Trichoderma harzianum*, *T. viride* and *T. knoingii* irradiated with 500 Gy dosage resulted in the highest percentage of pathogen growth reduction by producing highly active exo-enzymes (Haggag and Mohamed, 2002).

The present investigation aimed to activate *Trichoderma* spp. (*T. viride*. and *T. harzianum*) by low dose gamma radiation to accelerate the biodegradation of carbofuran pesticides.

MATERIALS AND METHODS

Soil sampling and characterization. Soil sample were collected from 10 different sub-samples and taken from the areas of 25 m², (0–20 cm) depth, from heavy clay soil had a previous history of treatment with carbofuran in the last 10 years at field located in El-Fayoum governorate, Egypt.

The soil was gently air-dried to the point of soil moisture suitable for sieving. After sieving to a maximum particle size of < 2 mm, the soil kept in a plastic bag at 4 ºC for 7 days before use.

Chemicals and reagents. Technical grade carbofuran (99.1% purity) was purchased from Sigma Aldrich Co., Nasr city, Egypt. All other chemicals and solvents were ultra pure grade and obtained from El-Gomhouria Co. For Trading Chemicals And Medical Appliances, Egypt.

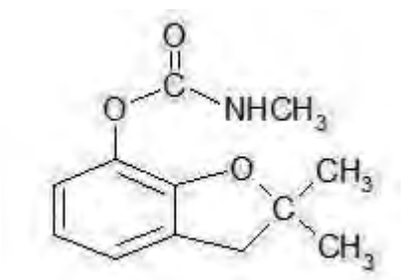

FIGURE 1
Chemical structure of carbofuran

ENRICHMENT PROCEDURE AND ISOLATION OF MICROORGANISMS

Soil contamination. The aim of this step was to adapt the soil microflora to carbofuran. To obtain this effect, prepared soil (200 g) was supplemented with carbofuran at concentration of 50 mg/kg soil, introduced in a form of methanol solution. After mixing and solvent evaporation the soil was incubated in the dark at 30 ± 1 ºC, in a thermostatic chamber for 90 days. The water content of the soil was adjusted to 50% of the maximum water holding capacity. Throughout the incubation period, water losses exceeding 5% of the initial values were compensated by the addition of deionized water. After 30 and 60 days of incubation the soil was contaminated again with the same dosage of carbofuran.

Cultivation in liquid medium. In this step of enrichment procedure the mineral salt medium (MSM) was used. The medium contained: $(NH_4)_2SO_4$, 2 g; KH_2PO_4, 3 g; $MgSO_4.7H_2O$, 0.5 g; glucose, 3 g, micro-elements mineral solution, 2 ml (Cooney and Levine, 1972) and distilled water,1 liter. The solid synthetic medium was obtained by

addition of agar, 15 g L^{-1}. The pH was adjusted to 7 and the media were sterilized at 121°C for 15 min.

After autoclaving and cooling, the medium was supplemented with carbofuran as a sole of carbon source. Insecticide was introduced in a form of methanol solution to give the final concentration of 50 mg L^{-1}. After 24 h of shaking and solvent evaporation 10 g of contaminated soil was added into 250 mL flasks with 100 mL of liquid medium supplemented with carbofuran. Flasks were incubated at 30 ± 1 ºC on a rotary shaker (120 rpm) for 72 h and kept in a dark to avoid photo-degradation of carbofuran. After this time, 1 mL of soil suspension was transferred into flasks containing the same fresh medium supplemented with the higher concentration of insecticide (100 mg L^{-1}) and incubated for a further 72 h under the same conditions.

Cultivation and selection of isolates on agar medium. The fungal strains were isolated by plating 10-fold dilutions of the liquid medium onto MSM agar supplemented with carbofuran at concentration of 100 mg L^{-1} as a sole of carbon source and incubated at 30 ± 1 ºC for 7 days. The fungal isolates were purified by using single spore or hyphal tip technique. Based on morphological properties the individual strain colonies were selected and subcultured to obtain pure culture. For further analyses five fungal isolates (carbofuran-degrading fungi) were reserved.

Identification of isolates. The pure isolated fungi were identified according to the most documented keys in fungi identification (Carmichael *et al.*, 1980; Barnett and Hunter, 1998). The morphological identification of isolated fungal strains is based on the morphology of the fungal culture colony or hyphae and the characteristics of spores.

Exposure of *T. harzianum* and *T. viride* to gamma radiation. The most effective carbofuran degrading fungi (*Trichoderma* spp., including *T. harzianum* and *T. viride*) selected and exposed to different doses of gamma radiation. Slants of 7 days old culture were irradiated with doses of 0.0, 20.0, 50.0, 100.0, 250.0, 500.0, 1000.0, 2000.0 and 5000.0 Gy, and three replicates were used for each dose. Radiation treatments were carried out at Atomic Energy Authority, Abu-Zabal at dose rate of Egypt's Mega-gamma-1 type, J 6600-Cobalt-60 Irradiator.

Biodegradation of carbofuran in liquid medium. Growth experiments with carbofuran as a sole of carbon source were performed in 100 mL Erlenmeyer flasks containing 50 mL of sterile MSM. Carbofuran was introduced in a form of methanol solution to give the final concentration of 200 mg L^{-1}. After 24 h of shaking and solvent evaporation, 1ml of spore suspension (10^7 spore/ml) of each isolate was inoculated into MSM to evaluate the degradation dynamics of carbofuran in liquid medium. Non-inoculated MSM with the fungal suspension were kept as controls. Flasks were incubated at 30 ± 1 ºC for 7 days. After the incubation period, the produced mycelia were oven-dried at 70 ºC till constant weight.

CHEMICAL ANALYSIS

Extraction and Purification of carbofuran. Carbofuran was analyzed by high performance liquid chromatography (HPLC) at Atomic Energy Authority, Abu-Zabal, Egypt. In order to extract carbofuran from the soil and liquid phases, the soil was slurry centrifuged at 6000 rpm at 25 ºC for 15 min to separate the liquid from the soil. The liquid phase was filtered through cellulose acetate paper (Whatman- number 1, England) prior to the liquid–liquid partitioning extraction procedure. Briefly, 2 mL of methanol were added to 2 mL of liquid sample and then the mixture was sonicated twice for 10 min on a 50/60 voltage cycle. After sonication, carbofuran was extracted in a separation funnel with dichloromethane. For the method of high-performance liquid chromatography (HPLC), the supernatant was dissolved in the same volume of pure grade methanol and filtrated by membrane filters (0.45 μm). An aliquot of the residue in a 20 μL sample size was injected into a HPLC. The analytical column was Zorbax SB-C18 column (250×4.6 mm, 5 μm), and the solutes were detected using PDA detector with gradient UV-VIS detection ranging from 200 to 600 nm. The mobile phase consisted of 70% methanol and 30% water at a flow rate of 1.0 mL min^{-1}.

Data analysis. Data was analyzed by SPSS program Version 11.5.0. The significance of treatments was set at p-value less than or equal to 0.05 by the one-way ANOVA test.

RESULTS AND DISCUSSION

Contamination of surface water by carbofuran carbamate pesticides compounds is of concern because of potential toxicity to aquatic organisms (Bondarenko *et al.*, 2004). The ability of enhancements fungi by low dose of gamma radiation to biodegrade carbofuran pesticides will

reduce the concentration of xenobiotics (Afify, 2009). Therefore gamma irradiation was used to activate several fungi and determine the activities of their growth under these conditions. The biodegradation of carbofuran is often complex and involves biochemical reactions. Although many enzymes efficiently catalyze the biodegradation of pesticides.

Isolation and Identification of fungi. Five fungi strains were identified as *Trichoderma* spp. including *T. harzianum* and *T. viride, Aspergillus niger, Fusarium oxysporum* and *Penicillium cyclopium* (Fig 1). The results showed that *Trichoderma* spp. reached its maximum growth using carbofuran concentration of 200 mg/L (*T. harzianum,* and *T. viride,* 167.6 and 222.0 mg/L respectively). On the other hand, *Aspergillus niger* reached its maximum yield 203.2 with 20 mg/L while the growth of *Fusarium oxysporum* and *Penicillium cyclopium* were dose dependence. From the above results *Trichoderma* spp. possesses enzyme(s) which acts on amide and ester bond in carbofuran and initiates the biodegradation. It is very important to note that half-life carbofuran 45 days in water indicating that the isolates of *Trichoderma* spp. were potentially useful for carbofuran bioremediation and prevent accumulation in the environments. These results agree with those of Rajagopal *et al.* (1984) who isolated *Bacillus* sp., *Micrococcu*s sp., *Arthrobacter* sp. and *Azospirillum* sp. capable of using pesticides as source of carbon and nitrogen. This increase in the biomass of the culture with carbofuran could be explained by the fact that this product constitutes, an additional carbon and nitrogen contribution which allows the synthesis of new secondary metabolites favoring the production of microbial biomass and in consequence support a faster use of carbofuran. The increase in biomass was reported when *T. viride* strain incubated with pesticides (Wootton *et al.*, 1993). Therefore *Trichoderma* spp. have been selected for enhancement by different doses of gamma radiation for better biodegradation of carbofuran pesticide.

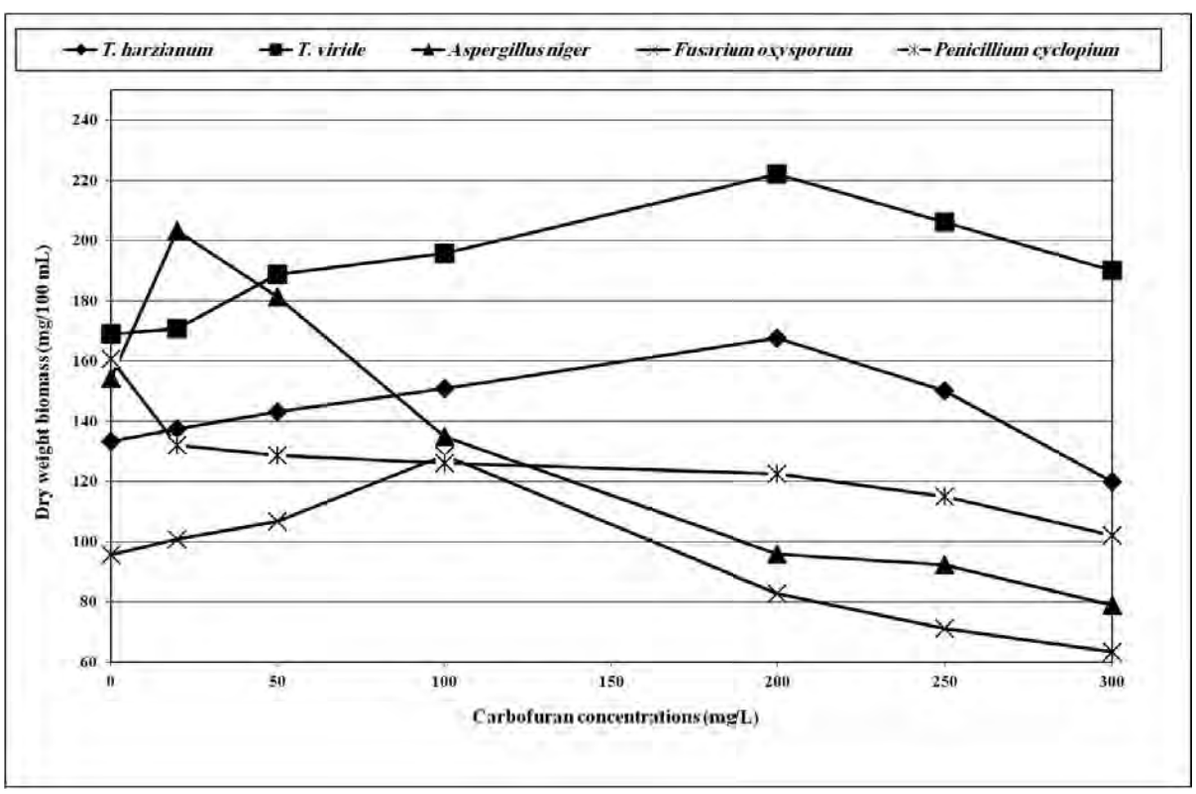

FIGURE 2
Effect of carbofuran on dry weight biomass for all tested fungi within 7 days of incubation at 30°C

TABLE 1
Mycelial dry weight (mg /100 ml) of gamma irradiated *Trichoderma* spp. grown on MSM with 200 mg L^{-1} of carbofuran at 30 ºC for 7 days of incubation

Gamma irradiation dose (Gy)	Mycelial dry weight (mg/100 ml)*			
	T. harzianum		*T. viride*	
	growth(mg /100 ml)	% of change	growth(mg /100 ml)	% of change
0	168 ± 0.11^{f}	0.0	222 ± 0.58^{e}	0.0
20	176 ± 0.58^{e}	4.76	236 ± 0.11^{d}	6.31
50	178 ± 0.52^{d}	5.95	240 ± 0.58^{c}	8.11
100	191 ± 0.29^{b}	13.69	248 ± 1.15^{b}	11.71
250	206 ± 0.17^{a}	22.61	258 ± 1.73^{a}	16.21
500	188 ± 0.98^{c}	11.90	215 ± 1.15^{f}	-3.15
1000	144 ± 0.63^{g}	-14.29	205 ± 2.31^{g}	-7.65
2000	122 ± 0.40^{h}	-27.38	187 ± 0.58^{h}	-15.77
5000	83 ± 0.29^{i}	-50.59	144 ± 1.21^{i}	-35.14

* The values are means ± SE. The mean values with different small letters within a column indicate significant differences ($P < 0.05$).

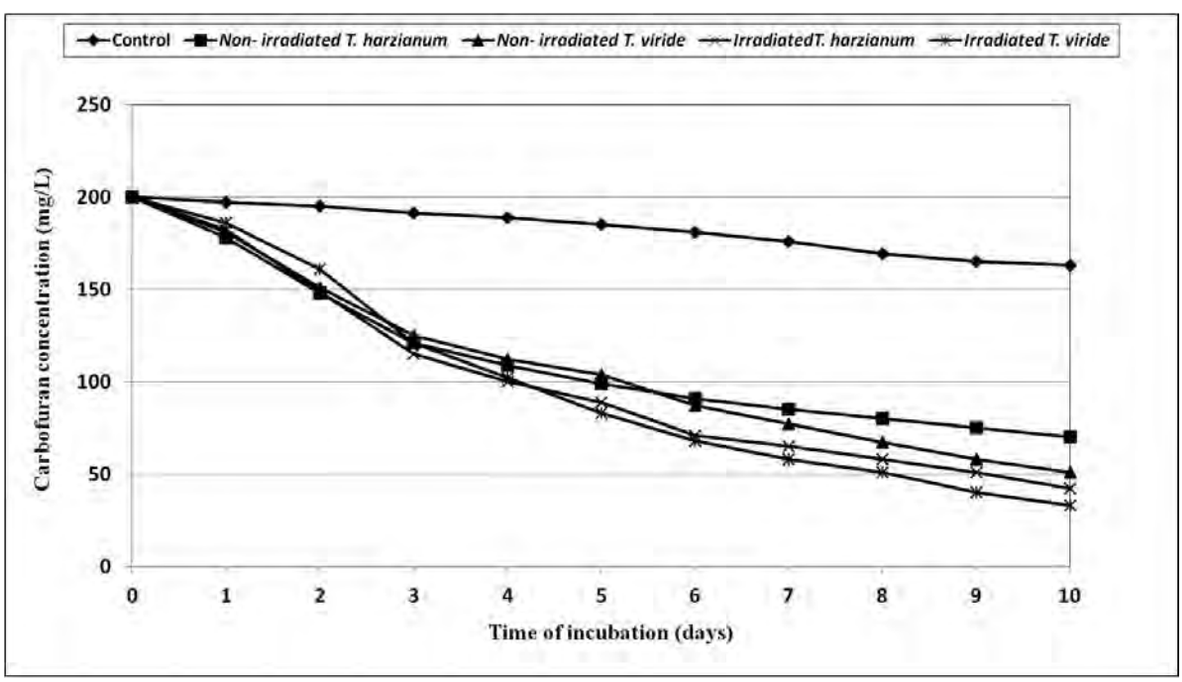

FIGURE 3
Biodegradation of carbofuran in mineral salt medium by non-irradiated and irradiated *Trichoderma* spp.

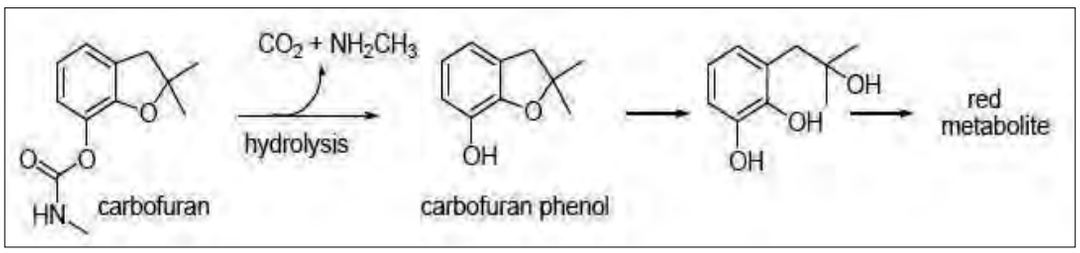

FIGURE 4
Proposed biodegradation of carbofuran pesticides

Effect of low dose gamma radiation on *Trichoderma* spp. The most effective carbofuran degrading fungi (*Trichoderma* spp., including *T. harzianum* and *T. viride*) selected and exposed to different doses of gamma radiation (0.0, 20.0, 50.0, 100.0, 250.0, 500.0, 1000.0, 2000.0 and 5000.0 Gy). Results in Table (1) indicated the biomasses of *Trichoderma* spp. (*T. viride* and *T. harzianum*) grown on MSM with carbofuran at concentration of 200 mg L^{-1} within 7 days of incubation. The biomass of *Trichoderma* spp. strain were increased and reached its maximum at 250 Gy by 22.61 and 16.21% when using *T. harzianum* and *T. viride* respectively. As a general trend the gamma radiations over than 250 Gy reduce the growth of *Trichoderma* spp. (*T. viride* and *T. harzianum*). Therefore the gamma radiation over 250 Gy inhibit the growth of the fungi and reached 50.59% and 35.14% inhibition with gamma radiation dose 5000 Gy using *T. harzianum* and *T. viride* respectively.

Biodegradation of carbofuran in mineral salt medium (MSM). The isolates of *T. harzianum* and *T. viride* were able to degrade carbofuran and use it as the sole carbon source in MSM. The abilities of strains *T. harzianum* and *T. viride* to degrade of carbofuran in MSM were investigated. Figure 2 shows biodegradation of carbofuran at concentration of 200 mg/L by *T. harzianum* and *T. viride* cultivated in MSM. The results indicate that both fungal isolates used carbofuran as source of carbon and nitrogen. The results showed that 65% and 74.5% of carbofuran were degraded within 10 days of incubation by *T. harzianum* and *T. viride*, respectively. The ionizing radiation to *Trichoderma* spp. at dosage of 250 Gy was showed increase in biodegradation of carbofuran by 14% (79 % total biodegradation) and 9% (83.5 % total biodegradation) by *T. harzianum* and *T. viride*, respectively.

Previous studies have shown that, relatively low dose of ionizing radiation on microorganisms is responsible of accelerated enzyme activities (Chakravarty and Sen, 2001). The low doses of gamma ray (10 and 20 Gy) significantly increased the alcohol-dehydrogenase enzyme activity of *Saccharomyces cerevisiae* (Ben-Akacha *et al.*, 2008). *T. harzianum*, *T. viride* and *T. knoingii* irradiated with 500.0 Gy dosage resulted in the highest percentage of pathogen growth reduction by producing highly active exo-enzymes (cellulase and chitinase isoenzymes) as confirmed by Haggag and Mohamed (2002). These results are in agreement with the results stated that growth of *T. viride* was increased at 500.0 Gy of gamma-radiation. Mycelial dry weight increased in isolates of *Aspergillus tamaru, A. flavus* and *A. niveus* when exposed to gamma-irradiation doses of 200.0 and 500.0 Gy (Younis, 1999). The results showed that *Trichoderma* sp. presented a good growth in the presence of pesticide and 21% of the pesticide was degraded (Ortega *et al.*, 2011). Haggag and Mohamed (2002) found that mutagenesis of three *Trichoderma* species by gamma irradiation exhibited high capabilities to produce efficient antibiotics, enzymes and phenols. On the other hand the tested UV-induced mutants were higher in their production of enzymes (cellulases, chitinases and β-1,3-glucanases) than their parental wild type strain (*T. viride*). Cellulase was the greatest enzyme production by the tested *T. viride* strains followed by β-1,3-glucanase then chitinase. Therefore the enhancement of *Trichoderma* spp. by gamma radiation induce the activation of the main enzymes cellulases, chitinases and β-1,3-glucanases which depend mainly on the dose of radiation (Shafique *et al.*, 2009). Carbofuran was degraded first to carbofuran phenol and then degraded to 2-hydroxy-3-(3-methylpropan-2-ol) phenol by *Sphingomonas* sp. as proposed by Kim *et al.* (2004) as shown in Fig (3).

CONCLUSION

Biodegradation is a major way of carbofuran degradation in the environment in the presence of

stimulated fungi with low dose of gamma radiation (Salama, 1998). Data in this work indicate the possibility of applying low dose gamma-radiation to increase carbofuran degradation by enhancement *T. harzianum* and *T. viride.* An enrichment procedure allowed isolating of two effective fungal strains belonging to *T. harzianum* and *T. viride* that may participate in efficient degradation of the carbofuran. Obtained results have implicated for the development of a bioremediation strategy of carbofuran polluted in environments. There is a need for further research on the biochemical and genetic aspects of carbofuran biodegradation by the isolated fungi. Esterases are the enzymes that catalyze the hydrolysis of carboxylic esters (carboxylesterases), amides (amidases), phosphate esters (phosphatases), etc. (Bansal, 2012 and Ortiz-Hernández *et al.*, 2013). In the reaction catalyzed by esterases, a wide range of ester substrates can be hydrolyzed into their alcohol and acid components. Carbofuran carbamate has a carboxylic ester component, and the enzymes capable of hydrolyzing this type of ester bond are known as carboxylesterases. In the future it could even apply *Trichoderma* spp. directly under special condition or producing carboxylesterases enzyme from fungi and apply in the field for biodegradation of carbofuran pesticides to clean environments from pollutants. Therefore biodegradation can offer an efficient and cheap option for the decontamination of polluted ecosystems and the destruction of pesticides. Finally applying enzymes to degrade pesticides is an innovative technique for the removal of these pesticides from polluted environments.

ACKNOWLEDGEMENTS

This work was supported by Scientists Next Generation Program, Academy of Scientific Research and Technology, Egypt and Faculty of Agriculture, Biochemistry Department, Cairo University.

REFERENCES

[1] Afify, A. M. R. (2009). Biological function of xenobiotics through protein binding and transportation in living cells. Int J Agric Res 5: 562-575.

[2] Afify, A. M. R. (2011). Recent techniques applied for pesticides identification and determination in natural products and its impact to human health risk, Pesticides in the Modern World - Trends in Pesticides Analysis ,open access, ISBN, ISBN 978-953-307-437-5 Edited by: Margarita Stoytcheva, Publisher: InTech, October 2011.

[3] Afify, A. M. R., Abo-El-Seoud, M. A., Ibrahim, G.M., Kassem BW (2013). Stimulating of biodegradation of oxamyl pesticide by low dose gamma irradiated Fungi. J Plant Pathol Microb 4 (9): 3-5 ,201. doi:10.4172/2157-7471.1000201.

[4] Afify, A. M. R., Aboul-Soud, M. A., Mohamed, S. F., Mahmoud, W. A., Tarek, K., Asar A. R. and Al-Khedhairy, A. A. (2009). Production of alkaline protease and larvicidal biopesticides by an Egyptian Bacillus sphaericus isolate. Afr J Biotechnol 8 (16): 3864-3873.

[5] Afify, A. M. R. and El-Beltagi, H.S. (2011). Effect of the insecticide cyanophos on liver function in adult male rats. Fresenius Environ Bull, 20, (4a):1084-1088.

[6] Afify, A. M. R., Mohamed, S. F., Aboul-Soud, M. A., Mohamed, A.M., Tarek, K. and Asar A. R. (2008). Purification and biochemical characterization of alkaline protease from biopesticide-producing strain of Bacillus Sphaericus. Egypt J Biotechnol 29: 139-156.

[7] Afify, A. M. R., Mohamed, M. A., El-Gammal, H. A. and Attalla, E. R. (2010). Multiresidue method of analysis for determination of 150 pesticides in grapes using quick and easy method (QuEChERS) and LC-MS/MS determination. J Food Agric Environ 8(2): 602-606.

[8] Bansal, O. P. (2012). Degradation of pesticides. In: Pesticides Evaluation of environmental pollution (S. Hamir, Rathore and L. M. L. Nollet, Ed.). CRC Press, New York, United States of America, pp. 47-77.

[9] Barnett, H. L. and Hunter, B. B. (1998). Illustrated Genera of Imperfect Fungi. APS Press, St. Paul, Minnesota, USA.

[10] Ben-Akacha, N., Zehlila, A., Mejri, S., Jerbi, T. and Gargouri, M. (2008). Effect of gamma-ray on activity and stability of alcohol-dehydrogenase from *Saccharomyces cerevisiae.* Biochem Engineering J 40: 184–188.

[11] Bondarenko, S., Gan, J., Haver, D. L. and Kabashima, J. N. (2004). Persistence of selected organophosphate and carbamate insecticides in waters from a coastal

watershed. Environ Toxicol Chem 23(11): 2649–2654.
[12] Carmichael, J. W., Kendrick, B. W., Conners, I. L. and Lynne, S. (1980). Genera of Hyphomycetes. The University of Alberta, CA.
[13] Chakravarty, B. and Sen, S. (2001). Enhancement of regeneration potential and variability by gamma-irradiation in cultured cells of *Scilla indica*, Biol Plant 44: 189–193.
[14] Gherbawy, Y. A. (1998). Effect of gamma irradiation on the production of cell wall degrading enzymes by *Aspergillus niger*. Inter. J Food Microbiol 40:127–131.
[15] Connon, R. E., Geist, J. and Werner, I. (2012). Effect-based tools for monitoring and predicting the ecotoxicological effects of chemicals in the aquatic environment. Sensors 12: 12741-12771.
[16] Cooney, N. L. and Levine, D. W. (1972). Microbial utilization of methanol. Adv Appl Microbiol 15: 337–365.
[17] Haggag, W. M. and Mohamed, H. A. A. (2002). Enhancement of antifungal metabolites production from gamma-rays induced mutants of some *Trichoderma sp.* for control onion white rot disease. Plant Pathol Bull 11: 45-56.
[18] Kim, I. S., Ryu, J. Y., Hur, H. G., Gu, M. B., Kim, S. D. and Shim, J. H. (2004). *Sphingomonas* sp. strain SB5 degrades carbofuran to a new metabolite by hydrolysis at the furanyl ring. J Agric Food Chem 52(8): 2309- 2314.
[19] Ortega, N. O., Nitschke, M., Mouad, A. M., Landgraf, M. D., Rezende, M. O. O., Seleghim, M. H. R., Sette, L. D. and Porto, A. L. M. (2011). Isolation of Brazilian marine fungi capable of growing on DDD pesticide. Biodegradation 22(1): 43-50.
[20] Ortiz-hernández, M. A. L., Sánchez-salinas, E., Castrejón godíne, M. L. Z., Dantan González, E. and Popoca ursine, Y. E. C. (2013). Mechanisms and strategies for pesticide biodegradation: opportunity for waste, soils and water cleaning. Rev. Int Contam Ambie 29: 85-104
[21] Qing, Z., Yang, L. and Huan, L. Y. (2006). Purification and characterization of a novel carbaryl hydrolase from *Aspergillus niger* PY168. *FEMS Microbiology Letters* 228(1): 39-44.
[22] Rajagopal, B. S., Rao, V. R., Nagendrappa, G. and Sethunathan, N. (1984). Metabolism of carbaryl and carbofuran by soil –enrichment and bacterial cultures. Can J Microbiol 30: 1458 – 1466.
[23] Rani, K. and Dhania, G. (2014). Bioremediation and biodegradation of pesticide from contaminated soil and water- A Noval Approach. Int J Curr Microbiol App Sci 3(10): 23-33.
[24] Salama, A. K. (1998). Metabolism of carbofuran by *Aspergillus niger* and *Fusarium graminearum*. J Environ Sci Health 33(3): 253-266.
[25] Seo, J., Jeon, J., Kim, S. D., Kang, S., Han, J. and Hur, H. G. (2007). Fungal biodegradation of carbofuran and carbofuran phenol by the fungus *Mucor ramannianus*: identification of metabolites. Water Sci Technol 55 (2): 163–167.
[26] Shafique S., Bajwa, R. and Shafique, S. (2009). Cellulase biosynthesis by selected *Trichoderma* species. Pak J Bot 41(2): 907-916,
[27] Slaoui, M., Ouhssine, M., Berny, E. and El-Yachioui, M. (2007). Biodegradation of the carbofuran by a fungus isolated from treated soil. Afr J Biotechnol 6 (4): 419-423.
[28] Wootton, M. A., Kremer, R. J. and Keaster, A. J. (1993). Effects of carbofuran and the corn rhizosphere on growth of soil microorganisms. Bull Environ Contam Toxicol 50: 49-56.
[29] Younis, N. A. (1999). A comparison study on protease, alpha-amylase and growth of certain fungal strains of *Aspergillus* sp. after exposure to gamma-rays. Arab J Nuclear Sci App 32(2): 257-264.

Received: **28.08.2015**
Accepted: **19.12.2015**

CORRESPONDING AUTHOR

Abd El-Moneim M.R. Afify
Cairo University
Faculty of Agriculture
Biochemistry Dept.
Giza, Egypt

e-mail: abdelmoneimafify@yahoo.com

by PSP Volume 25 – No. 1/ 2016, pages 292-299 Fresenius Environmental Bulletin

COMPONENT ANALYSIS OF THE DIFFERENT FISH SAMPLES CONTAINING HEAVY METALS IN ISTANBUL BOSPORUS

Emre Eroglu[1], Namik Ak[2], Ibrahim Guney[3] and Ersin Sener[1]

[1]Department of Mathematics, Kirklareli University, Kirklareli, Turkey
[2]Energy Systems Engineering, Adiyaman University, Adiyaman, Turkey
[3]Department of Management, Istanbul Sabahattin Zaim University, Istanbul, Turkey

ABSTRACT

Fish and fish products are important sources in nutrition, especially for kids and youths. Turkey has the geographical advantage of being surrounded on three sides by the sea. However, the usage of seas unconsciously and fishing illegally cause pollution, which threatens human health, and decrease fish rates.

In this study, distinguishable heavy metals are found (Pb, Cu, Ni, Al, Zn, etc.) that may affect human beings permanently in a negative way. The fish samples are analyzed, and significant heavy metal levels are displayed. The levels of heavy metals are introduced by using a mathematical approach and a statistical modeling. *Original* and *new* data are obtained from fishes related to levels of heavy metals. Data are analyzed by means of correlation-regression that is a linear model and a factor analysis method. Besides, regression equations and factor loadings are exhibited.

KEYWORDS:
Heavy metals, Factor analysis, Statistical model

INTRODUCTION

Determination of the toxic heavy metal levels in seafood is important for community health. Therefore, much more researches have focused on the effects of heavy metals on humans. Yang et al. investigated the concentrations of heavy metals (Cr, Cd, Hg, Cu, Zn, Pb and As) in water, sediment, and fish from the middle and lower levels of the Yangtze River, China [1].

The health risk analysis of each heavy metal in fish tissues indicates the safe levels for the general population and fishermen, but there is a possible risk in total target hazard quotients [1]. Heavy metal concentrations are investigated in Gaza Strip. It is studied to get information about heavy metal concentrations in the muscles of six commercial fish species available in Gaza Strip markets and the possible risk associated with their consumption is evaluated [2]. The amount of Cd, Cu, Cr, Hg, Ni and Zn in the muscles, livers and gills of whitefish, perch, pike, brown trout, burbot and vendace, which are taken from the lake in the vicinity of mining activity and several metallurgic smelters between Norway and Russia, is searched [3]. The levels and bioaccumulation of the organochlorine pesticides (OCPs) and heavy metals in muscles and livers of three fish species, with two trophic levels, from Lake Awassa, Ethiopia, are studied [4]. In Turkey a comprehensive study has been planned in 2010 and carried out to determine the radioactivity levels and heavy metal concentrations in the most common four fish species samples collected from eight stations in the Black Sea Region, which is affected by Chernobyl in 1986 [5]. Heavy metal (Cd, Cr, Cu, Hg, Pb, Zn) concentrations determined in the muscle tissues of the seven fish species (silver carp Hypophthalmichthys molitrix, grass carp Ctenopharyngodon idellus, crucian carp Carassius auratus, carp Cyprinus carpio, Coreius heterodom, catfish Silurus asotus, and yellow-head catfish Pelteobagrus fulvidraco) in Yangtze River are measured [6]. The heavy metal pollution in marine life has been taken into consideration as a serious environmental issue [7,8]. The pollutants are potentially accumulated in sediments and livings in seas and subsequently they are transferred to people through nutrition [9]. Metals, playing an important role in biological system, such as iron, copper, zinc and manganese, are essential metals, whereas mercury, lead and cadmium, which are toxic even in small amounts, are non-essential metals [10,11]. A formula is obtained for the quantification of benefit-risk ratio (hazard quotient) for the intake of a product containing essential polyunsaturated fatty acids e.g, heavy metals [12]. Monitoring fishes and shells is important for water ecosystem because people may get affected by nutrition [13]. Eventually, various researches have been carried out on metal accumulation in different fish species [14-18]. Fortunately the situation is not inextricable for now [19].

In the seas of Turkey, the investigation of heavy metals assessment (for two commercial fish species) is extensive [20]. The studies show that the high concentrations of metals in fish samples may be related to industry [20]. In addition, it is found that heavy metal levels are low in fish species sampled from relatively unpolluted areas [20,21]. The statistical comparison revealed that the metal concentrations are significantly different in each tissue of different fish species. There is a negative relationship between fish sizes and metal levels in most cases. The data show that the positive relationship is only between zinc and lead levels in the gill of Mugil cephalus and size. The relationship between the size of fish and metal concentration in the marine life should also be monitored occasionally in the field to understand better the effects of metals on fish growing and the current situation of population dynamics [21].

Heavy metal concentrations of the fishes in Beymelek Lagoon (Antalya/Turkey) are lower than those from other contaminated Mediterranean regions of Turkey. This research shows that the heavy metal concentrations in muscles of the observed species are also lower than the maximum levels set by law [22].

The results may be considered as a bioindicator of the contamination by estimating the bioavailability of metals in marine biota. Moreover, these results can also be used to test the chemical levels of the sea food and the possible risk associated with their consumption can be evaluated [23]. The method that is used for the new and original data is remarkable [24,25].

The goal of this study is to analyze the heavy metals statistically with the data that is implemented by data analysis, correlation-regression, general linear model, dendogram, factor loadings and regression equations.

MATERIALS AND METHODS

Sampling. Barb fish species used in this study (Red Mullet- Mullus barbatus), horse mackerel (Mackerel- Trachurus spp Horse), bluefish (Blue fish- Pomatomus saltatriks), sea bass (Seabass - Dicentrarchus labrax), Bonito (Bonito-Sarda sarda), Zargan (needlefish -Belo to vulgaris), Swallow (Red Gurnard- Triglidae), Haddock (Whiting fish-Merlangius merlangus), anchovy (Anchovy-Engraulis encrasicolus), mussels (Mussel-Mytilus galloprovincialis), Blue Fish (Young Blue fish-pomatomus saltatrix) Shrimp (Shrimp-Lysmat to rathbuna), the sardine (Sardina-Sardina pilchardus) are chosen. This analysis deals with the fish species in the Sea of Marmara, which are the most commonly consumed and economic in Februaries and Marches. Moreover, those ones affected by the heavy metals are joined in national and international trade and other industrial activities.

Analytical procedures. The fish samples in polyethylene containers together with ice are brought to the laboratory on the same day [20]. Firstly, the samples are washed with tapwater and then distilled water [27]. The liver and muscle samples taken from the big (sea bass, bonito, bluefish and Zargan), and small fish species are cut into small pieces with a plastic knife and dried in a 90 ° C-oven down to fixed weight and the ground has been homogenized [15,26].

0.25 grams of the dried tissue samples are mixed in PTFE containers (PTFE vessel) and by adding HNO3-H2O2 (5: 2, v / v) mixture it is put into the microwave for solubilization process [28,29]. The samples taken from microwave are completed to 50 ml with ultrapure water. The levels of heavy metal accumulation in examined tissues are determined by optical emission spectrometry with the 7000 DV ICP-OES model of brand Perkin Elmer Samples are passed through a 0.45 mm membrane filter before analysis.

Li, Ba, V, Cr, Fe, Ni, Cu, Zn, Al, Pb, Mn, Cd, Co, Sr, Na, K, Mg, Ca, P in the analyzed samples has been examined and the results are given in terms of mg / kg.

Element analysis. 0.2-0.5 gram of homogenously mixed samples is put into teflon containers in their dry forms. 9 ml pure HNO_3, 3 ml HCl and 2 ml HF are added for soil while this is 8 ml pure HNO_3 for plants (and diluted HNO_3 for tissues). The teflon containers are capped and placed in a microwave oven. The heat is gradually increased up to 185 °C and the container was kept at this heat for 20 minutes. Then, teflon containers are taken out and contents are poured to 50 ml HDPE volumetric flasks where they were complemented to 50 ml volume by addition of ultra-pure water. After those processes the conditions are convenient for heavy metal analysis at ICP-OES. The elemental heavy metal analysis of the collected soil samples has been carried out by Perkinelmer for the brand model (Optima 7000 DV) ICP-OES (Inductively Coupled Plasma Optical Emission Spectrometer).

In ICP, the sample collected through auto sampler is transferred to the nebulizer and therein it is mixed with argon gas to form aerosol. After that, it becomes plasm state at a temperature about 600-700°K. The 'Torch' where the plasm is constituted is composed of 2 nested quartz canals. Aragon is injected via two outside canals while the sample and aragon are injected together through small inside canals. The sample, which is sprayed with aragon through the injector, is brought into a form of plasm after being induced with an RF (Radio

Frequency) signal applied to metal coil on the side of the area. Emissions from the hot spot in the middle of the plasm are used for the analysis.

Five standards and a blank are prepared in order to constitute the calibration curve. The concentration of the standards is as follows: STD 1 10 ppb; STD 2 25 ppb; STD 3 50 ppb; STD 4 100 ppb; STD 5 250 ppb.

In order to operate the device, its software program is turned on. The obtained values are used via a special method. Recommended reading (plasma view) for low concentrations (ppb levels) is axial. This option is also entered into the method. Sample information is created to state the locations of the samples in auto sampler. Before the calibration process, the standard of the highest concentration is viewed as a sample and peak correction is made accordingly. After the blank and standards are viewed, the calibration curve is drawn. Correlation coefficient is expected to have three or four 9's for the sensitivity of the calibration. Samples, whose flow is 1.5 ml/minute, are placed in the auto sampler. The device begins to read the sample in 45 seconds after the sample flow. It makes 3 readings for each sample and gives the result, as the average of them in terms of µg/L. Plasm speed is 17L/m. Nebulizer speed is 0.55 L/m. The washing process is carried out with 45-secondperiods.

Domestic, industrial, agricultural and chemical wastes threaten human health as well as the marine life. Toxic materials and heavy metals in fish species cause irreversible damages in neural system, muscle functions, respiration system, circulatory system, immune system and affect negatively the growth and many other functions of the organisms. The heavy metals accumulate in liver, kidney and spleen intensively. Due to the negative effects of the heavy metals as indicated above, the rates of them need to be investigated and analyzed statistically.

In this analysis that is based on environmental pollution, a descriptive analysis of variables, correlation matrix and dendogram of hierarchical cluster are investigated. Multivariable analysis exhibits interaction among variables. The variables are introduced on two-main axis. Pb, Co, Zn, Ni, Cu, V, Cr and K scatter in ±x, Mg, Cd, Al, Ca and Na scatter in ±y.

One of the sources of heavy metal pollution is also automobiles. The soil absorbs those metals spread from automobiles. This fact needs to be analyzed rigorously. The analysis reveals the correlation of the metals. For example, Na and K alkali metals have the same property with each other; Al, Mg, Cr, Ni and Cu soil alkali metals as well.

The descriptive analysis values of heavy metals in fish samples are shown in Table1. Accordingly the most potential damaging heavy metals are Pb, Cu, Cd, Mn respectively.

TABLE 1
Descriptive analysis

	N	Minimum	Maximum	Mean	Std. Deviation
Ba	36	0	1,09	0,1984	0,32728
V	36	0	0,29	0,0982	0,08092
Cr	36	0	0,74	0,2948	0,21158
Ni	36	0	5,17	0,1489	0,86040
Cu	36	0,66	12,84	3,8156	3,63103
Pb	36	0,00	,36	0,0974	0,13535
Mn	36	0,17	3,73	1,5638	1,20537
Cd	36	0	0,03	0,0029	0,00892
Co	36	0	0,12	0,0084	0,02634
Sr	36	1,00	50,60	9,8627	14,16121
Fe	36	2,20	186,21	41,9825	50,55500
Zn	36	7,33	107,20	41,8176	30,25427
Al	36	0	104,49	16,7064	26,13252
Na	36	1601,24	14618,97	5339,0807	3757,38811
K	36	4605,68	19028,21	12259,1377	4134,39235
Mg	36	459,94	2676,61	1385,3217	567,25131
Ca	36	193,02	5298,34	1843,5403	1413,30051
P	36	4722,57	12445,02	8013,1191	1850,88630

Correlations. The instant correlation coefficients of the heavy metal variables in fish samples between each other are shown in Table2.

TABLE 2
Pearson's correlation matrix for the metal concentrations

	Ba	V	Cr	Ni	Cu	Pb	Mn	Cd	Co	Sr	Fe	Zn	Al	Na	K	Mg	Ca	P
Ba	1	,410*	,288	-,106	,408*	,030	,692**	,282	-,192	,531**	-,026	,481**	,558**	,259	-,383*	,020	,880**	,045
V	,410*	1	-,087	,111	,389*	,616**	,373*	,087	,029	,586**	-,082	,182	,549**	,531**	-,257	,123	,373*	-,202
Cr	,288	-,087	1	,293	,577**	-,273	,688**	,097	,016	,406*	,709**	,632**	,405*	,546**	,232	,694**	,513**	,670**
Ni	-,106	,111	,293	1	,099	-,128	,161	-,048	,152	-,029	,348*	,273	,068	,083	,115	,287	-,043	,241
Cu	,408*	,389*	,577**	,099	1	,194	,666**	-,058	,155	,838**	,578**	,544**	,720**	,762**	-,252	,538**	,485**	,133
Pb	,030	,616**	-,273	-,128	,194	1	-,043	-,227	-,236	,479**	-,275	-,217	,311	,536**	,221	,288	,022	-,014
Mn	,692**	,373*	,688**	,161	,666**	-,043	1	,300	,086	,539**	,623**	,865**	,609**	,561**	-,167	,505**	,818**	,398*
Cd	,282	,087	,097	-,048	-,058	-,227	,300	1	-,104	-,053	-,057	,088	,220	-,033	-,302	-,125	,340*	-,069
Co	-,192	,029	,016	,152	,155	-,236	,086	-,104	1	-,139	,456**	,319	-,141	-,119	-,357*	-,229	-,238	-,247
Sr	,531**	,586**	,406*	-,029	,838**	,479**	,539**	-,053	-,139	1	,164	,270	,840**	,870**	-,222	,478**	,600**	,017
Fe	-,026	-,082	,709**	,348*	,578**	-,275	,623**	-,057	,456**	,164	1	,802**	,149	,367*	,089	,592**	,183	,502**
Zn	,481**	,182	,632**	,273	,544**	-,217	,865**	,088	,319	,270	,802**	1	,259	,338*	-,085	,459**	,618**	,465**
Al	,558**	,549**	,405*	,068	,720**	,311	,609**	,220	-,141	,840**	,149	,259	1	,737**	-,314	,357*	,590**	-,039
Na	,259	,531**	,546**	,083	,762**	,536**	,561**	-,033	-,119	,870**	,367*	,338*	,737**	1	,136	,774**	,494**	,333*
K	-,383*	-,257	,232	,115	-,252	,221	-,167	-,302	-,357*	-,222	,089	-,085	-,314	,136	1	,569**	-,209	,779**
Mg	,020	,123	,694**	,287	,538**	,288	,505**	-,125	-,229	,478**	,592**	,459**	,357*	,774**	,569**	1	,331*	,791**
Ca	,880**	,373*	,513**	-,043	,485**	,022	,818**	,340*	-,238	,600**	,183	,618**	,590**	,494**	-,209	,331*	1	,280
P	,045	-,202	,670**	,241	,133	-,014	,398*	-,069	-,247	,017	,502**	,465**	-,039	,333*	,779**	,791**	,280	1
*. Correlation is significant at the 0.05 level (2-tailed).																		
**. Correlation is significant at the 0.01 level (2-tailed).																		

TABLE 3
KMO and Bartlett's Test

Kaiser-Meyer-Olkin Measure of Sampling Adequacy.		0,606
Bartlett's Test of Sphericity	Approx. Chi-Square	931,843
	Df	153
	Sig.	0,000

KMO and Barlett's Test tables (Table3) indicate the suitability of the data for structure detection. The **Kaiser-Meyer-Olkin Measure of Sampling Adequacy** is a statistics that indicates the proportion of variance in our variables that might be caused by underlying factors. High values (close to 1,0) generally indicate that a *factor analysis* may be useful with our data. Therefore our value is greater than 0,50, the results of the *factor analysis* probably will be very useful.

Dendogram of hierarchical cluster analysis of heavy metal concentrations in fish of Istanbul's seas are shown in Figure1. Metal clusters of variables are expressed in the figure hierarchical structure between these variables. Accordingly, there are two main heaps. The first phrase is Na, P, K which are beneficial substances. When the variables are substituted into the data reduction method, three maximum eigenvalues of covariance matrix describe 71,225% of total change. The number of variables is 18.

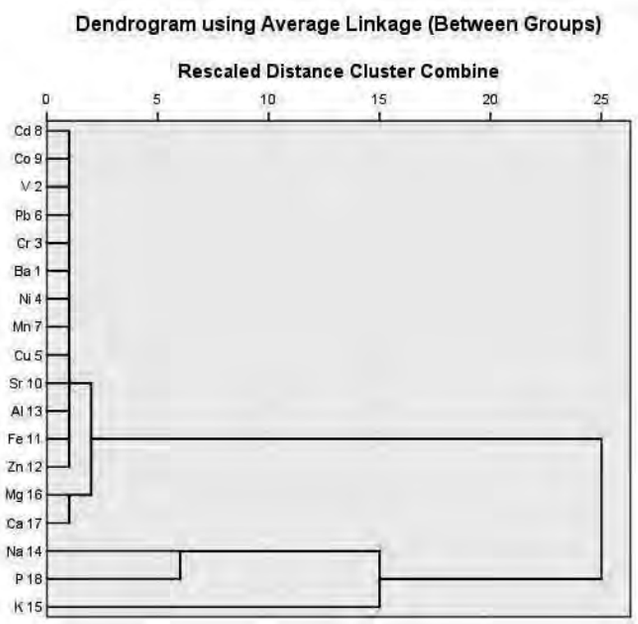

FIGURE 1
Dendogram for Variables

TABLE 4
Principal component analysis

Component	Initial Eigenvalues			Extraction Sums of Squared Loadings	
	Total	% of Variance	Cumulative %	Total	% of Variance
1	6,085	38,004	38,039	6,847	38,039
2.	3,036	18,067	56,710	3,361	18,671
3.	2,061	14,052	71,225		

The first two-main axes explain 71% of total variance:

Y_1=0,133*Ba-0,056*V+0,884*Cr+0,398*Ni+0,535*Cu-0,113*Pb+0,676*Mn-0,066*Cd+ 0,048*Co+0,298*Sr+0,837*Fe+0,744*Zn+0,246*Al+0,557*Na+0,443*K+0,863*Mg+0,405 *Ca+0,841*P

Y_2=0,746*Ba+0,743*V+0,150*Cr-0,136*Ni+0,660*Cu+0,407*Pb+0,595*Mn+0,258*Cd- 0,095*Co+0,850*Sr-0,04*Fe+0,274*Zn+0,849*Al+0,625*Na-0,537*K+0,115*Mg+0,707 *Ca-0,257*P

TABLE 5
Total variance Rotated Component Matrix[a]

	Component	
	1	2
Ba	0,133	0,746
V	-0,056	0,743
Cr	0,884	0,150
Ni	0,398	-0,136
Cu	0,535	0,660
Pb	-0,113	0,407
Mn	0,676	0,595
Cd	-0,066	0,258
Co	0,048	-0,095
Sr	0,298	0,850
Fe	0,837	-0,04
Zn	0,744	0,274
Al	0,246	0,849
Na	0,557	0,625
K	0,443	-0,537
Mg	0,863	0,115
Ca	0,405	0,707
P	0,841	-0,257
Extraction Method: Principal Component Analysis.		
Rotation Method: Varimax with Kaiser Normalization.		
a. Rotation converged in 3 iterations.		

TABLE 6
Total variance Component Transformation Matrix

Component	1	2
1	0,736	0,677
2	0,677	-0,736
Extraction Method: Principal Component Analysis.		
Rotation Method: Varimax with Kaiser Normalization.		

When the variables are rotated with Varimax method, the projection of variables lie on the main axis. According to that, two groups can be obtained from the cluster analysis. The variables are scattered along two–main axes. The first one is V, Pb, Cd, Ba, Al, Sr, Ca, Cu, Na and the second one is Mn, Zn, Mg and Cr. Co, Ni, Fe, P and K elements scatter the negative axis for stability.

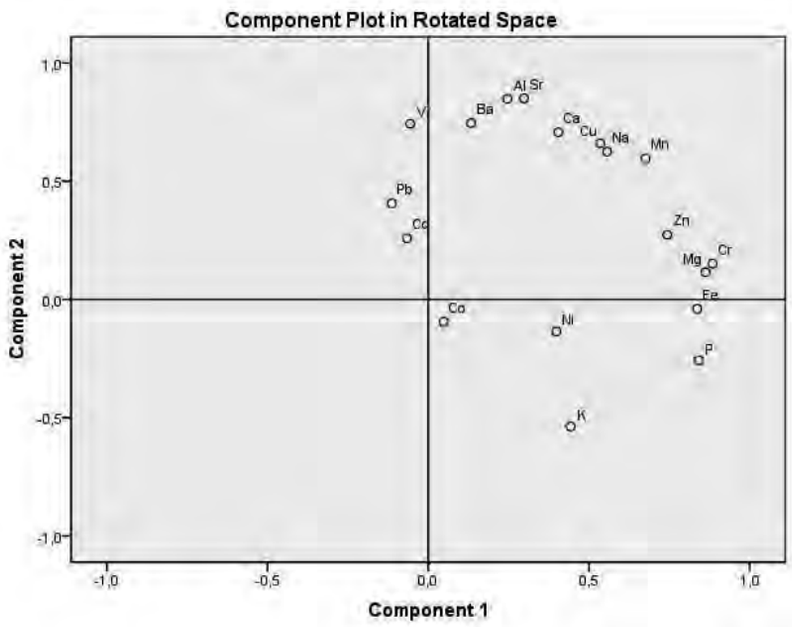

FIGURE 2
Factor Loadings for variables

CONCLUSION

This study is based on environmental pollution variables. It has yielded its statistical analysis from a descriptive analysis of variables, a correlation matrix and a dendogram of hierarchical cluster. The results of multivariable statistics are significant in that two main clusters can be observed.

The variables are introduced two-main axis in R^2 space and they are observed to lie ±x and ±y axis. Pb, Co, Zn, Ni, Cu, V, Cr and K scatter in ±x axis. Mg, Cd, Al, Ca and Na scatter in ±y. Those with the largest share of heavy metal in the fish could be identified in the factor loading of the two analyses. In the first axis the four significant elements are Cr, Mg, Fe and in the second axis they are V, Ba, Al, Sr respectively.

REFERENCES

[1] Yi, Y., Yang, Z., & Zhang, S. (2011) Ecological risk assessment of heavy metals in sediment and human health risk assessment of heavy metals in fishes in the middle and lower reaches of the Yangtze River basin. Environmental Pollution, 159(10): 2575-2585.

[2] Elnabris, K. J., Muzyed, S. K., & El-Ashgar, N. M. (2013) Heavy metal concentrations in some commercially important fishes and their contribution to heavy metals exposure in Palestinian people of Gaza Strip (Palestine). Journal of the Association of Arab Universities for Basic and Applied Sciences, 13(1): 44-51.

[3] Amundsen, P. A., Staldvik, F. J., Lukin, A. A., Kashulin, N. A., Popova, O. A., & Reshetnikov, Y. S. (1997) Heavy metal contamination in freshwater fish from the border region between Norway and Russia. Science of the Total Environment, 201(3): 211-224.

[4] Yohannes, Y. B., Ikenaka, Y., Nakayama, S. M., Saengtienchai, A., Watanabe, K., & Ishizuka, M. (2013) Organochlorine pesticides and heavy metals in fish from Lake Awassa, Ethiopia: Insights from stable isotope analysis. Chemosphere, 91(6): 857-863.

[5] Gorur, F. K., Keser, R., Akcay, N., & Dizman, S. (2012) Radioactivity and heavy metal concentrations of some commercial fish species consumed in the Black Sea Region of Turkey. Chemosphere, 87(4): 356-361.

[6] Yi, Y. J., & Zhang, S. H. (2012) The relationships between fish heavy metal concentrations and fish size in the upper and middle reach of Yangtze River. Procedia Environmental Sciences, 13: 1699-1707.

[7] Balkas, T. I., Tugrul, S., & Salihoğlu, I. (1982) Trace metal levels in fish and crustacea from northeastern Mediterranean coastal waters. Marine Environmental Research, 6(4): 281-289.

[8] Tariq, J., Jaffar, M., & Moazzam, M. (1991) Concentration correlations between major cations and heavy metals in fish from the Arabian Sea. Marine pollution bulletin, 22(11): 562-565.

[9] Giordano, R., Arata, P., Ciaralli, L., Rinaldi, S., Giani, M., Cicero, A. M., & Costantini, S. (1991) Heavy metals in mussels and fish from Italian coastal waters. Marine Pollution Bulletin, 22(1): 10-14.
[10] Schroeder HA. (1973) The trace elements and nutrition. Faber and Faber, London.
[11] Somers, E. (1974) The toxic potential of trace metals in foods. A review. Journal of Food Science, 39(2): 215-217.
[12] Gladyshev, M. I., Sushchik, N. N., Anishchenko, O. V., Makhutova, O. N., Kalachova, G. S., & Gribovskaya, I. V. (2009) Benefit-risk ratio of food fish intake as the source of essential fatty acids vs. heavy metals: A case study of Siberian grayling from the Yenisei River. Food Chemistry, 115(2): 545-550.
[13] Fairey, R., Taberski, K., Lamerdin, S., Johnson, E., Clark, R. P., Downing, J. W., Newman, J. & Petreas, M. (1997) Organochlorines and other environmental contaminants in muscle tissues of sportfish collected from San Francisco Bay. Marine Pollution Bulletin, 34(12): 1058-1071.
[14] Andres, S., Ribeyre, F., Tourencq, J. N., & Boudou, A. (2000) Interspecific comparison of cadmium and zinc contamination in the organs of four fish species along a polymetallic pollution gradient (Lot River, France). Science of the Total Environment, 248(1): 11-25.
[15] Turkmen, A., Turkmen, M., Tepe, Y., & Akyurt, I. (2005) Heavy metals in three commercially valuable fish species from Iskenderun Bay, Northern East Mediterranean Sea, Turkey. Food Chemistry, 91(1): 167-172.
[16] Turkmen, M., Turkmen, A., Tepe, Y., Tore, Y., & Ates, A. (2009) Determination of metals in fish species from Aegean and Mediterranean seas. Food Chemistry, 113(1): 233-237.
[17] Dural, M., Goksu, M. Z. L., & Ozak, A. A. (2007) Investigation of heavy metal levels in economically important fish species captured from the Tuzla lagoon. Food Chemistry, 102(1): 415-421.
[18] Uluozlu, O. D., Tuzen, M., Mendil, D., & Soylak, M. (2007) Trace metal content in nine species of fish from the Black and Aegean Seas, Turkey. Food chemistry, 104(2): 835-840.
[19] Turkmen, A., Tepe, Y., & Turkmen, M. (2008) Metal levels in tissues of the European anchovy, Engraulis encrasicolus L., 1758, and picarel, Spicara smaris L., 1758, from Black, Marmara and Aegean seas. Bulletin of environmental contamination and toxicology, 80(6): 521-525.
[20] Tepe, Y., Turkmen, M., & Turkmen, A. (2008). Assessment of heavy metals in two commercial fish species of four Turkish seas. Environmental monitoring and assessment, 146(1-3), 277-284.
[21] Canli, M., & Atli, G. (2003) The relationships between heavy metal (Cd, Cr, Cu, Fe, Pb, Zn) levels and the size of six Mediterranean fish species. Environmental pollution, 121(1): 129-136.
[22] Uysal, K., Emre, Y., & Kose, E. (2008). The determination of heavy metal accumulation ratios in muscle, skin and gills of some migratory fish species by inductively coupled plasma-optical emission spectrometry (ICP-OES) in Beymelek Lagoon (Antalya/Turkey). Microchemical Journal, 90(1): 67-70.
[23] Dalman, O., Demirak, A., & Balcı, A. (2006) Determination of heavy metals (Cd, Pb) and trace elements (Cu, Zn) in sediments and fish of the Southeastern Aegean Sea (Turkey) by atomic absorption spectrometry. Food Chemistry, 95(1): 157-162.
[24] Ozdemir, H.I. (1970) Genel Anorganik ve Teknik Kimya (General Inorganic and Technical Chemistry), Metaller Bolumu (Section of Metal). pp. 5-50 [in Turkish].
[25] Gulsoy, F., Guney, I. and Ozdamar, E. (2013) Mathematical and statistical modeling of the musical compositions. Balkan Journal of Mathematics. 1(1):35-43.
[26] Karadede-Akin, H., & Ünlü, E. (2007) Heavy metal concentrations in water, sediment, fish and some benthic organisms from Tigris River, Turkey. *Environmental Monitoring and Assessment*, *131*(1-3): 323-337.
[27] Rashed, M. N. (2001). Monitoring of environmental heavy metals in fish from Nasser Lake. Environment International, 27(1), 27-33.
[28] Vicente-Martorell, J. J., Galindo-Riaño, M. D., García-Vargas, M., & Granado-Castro, M. D. (2009). Bioavailability of heavy metals monitoring water, sediments and fish species from a polluted estuary. Journal of Hazardous Materials, 162(2), 823-836.
[28] Chi, Q. Q., Zhu, G. W., & Langdon, A. (2007). Bioaccumulation of heavy metals in fishes from Taihu Lake, China. Journal of Environmental Sciences, 19(12), 1500-1504.

Received: **12.10.2015**
Accepted: **16.01.2016**

CORRESPONDING AUTHOR

Emre Eroglu
Kirklareli University
Department of Mathematics
3900 Kirklareli – TURKEY
e-mail: emreeroglu@klu.edu.tr

by PSP Volume 25 – No. 1/ 2016, pages 300-306 Fresenius Environmental Bulletin

APPLICATION OF TREND ANALYSIS METHOD ON RAINFALL-STREAM FLOW-SUSPENDED LOAD DATAS OF WEST AND EAST BLACK SEA BASINS AND SAKARYA BASIN

Gokmen Ceribasi[1], Emrah Dogan[2]

[1]Sakarya University, Technology Faculty, Department of Civil Engineering, Sakarya, Turkey
[2]Sakarya University, Faculty of Engineering, Department of Civil Engineering, Sakarya, Turkey

ABSTRACT

In hydraulic engineering, it is of vital importance to estimate suspended load correctly in planning and projecting stream structures. On the other hand, problems increase with the effect of heating and climate changes in a globalizing world, and it is thought that the decrease of usable freshwater sources would pose a serious risk. Due to these risks, studies on the potential effect of climate change and on hydraulic time series have increased in recent years. Therefore, in this study, the trend analysis method will be applied to annual average rainfall, stream flow and suspended load of West, East Black Sea Basins and Sakarya Basin. While there was no trend in the data of most stations obtained from West Black Sea Basin, there was a decreasing trend in the data of some stations in stream flow and suspended load. While there was an increase trend in data of most stations obtained from rainfall stations for East Black Sea Basin, there was no trend in the data of some stations in stream flow and suspended load data. There was a decrease trend in data of most of the stations obtained from rainfall, stream flow and suspended load measurement stations for Sakarya Basin.

KEYWORDS:
Basin, Trend Analysis, Rainfall, Stream flow, Suspended Load.

INTRODUCTION

Dams are built on rivers for various reasons such as obtaining potable and utilizable water, and for energy generation and flood control. Therefore, solid materials such as sand, gravel, silt and clay, which are brought by rivers feeding basins of these structures fill in reservoirs, decrease their storage capacity and as a result shorten their economic life. Moreover, it causes extinction of topsoil, which is one of the most important production sources of an agricultural economy. For this reason, extinction of agricultural land brings together problems such as losing multi-purpose water structures and environmental pollution. Data about suspended loads, which are brought by rivers, are first of all used in sizing water structures such as dams, weirs and groins and calculation of dead storage. Moreover, suspended load sheds light on determination of erosion characteristics of the basin. Therefore, studies on suspended load data have become quite important [1].

On the other hand, air and water are indispensable elements of life on earth. With the effect of increasing population and difficult environmental conditions, it is one of the important issues in planning for protection and use of water, which is a restricted resource because of increasing demand. Planning and management of water resources have become quite important in parallel with increased water demand, and it has become compulsory to carry out more detailed and comprehensive studies in developing water structures. As a result of rapid development in industry, agriculture, urbanism and urban development, it should be remembered that the need for water resources would only be met by sustainable, determined environmental policies in the future. In at globalizing world, where problems increase with the effect of warming and climate changes, it is thought that a decrease in usable freshwater bodies will pose a serious problem. Due to these risks, it is seen that studies on the potential effect of climate change and on hydraulic time series have increased in recent years. These studies are generally carried out in order to find out whether there is climate change or not [1].

Therefore, in this study, the trend analysis method will be applied on annual average rainfall, stream flow and suspended load of West and East Black Sea Basins and Sakarya Basin, which carry the risk of erosion and flooding in Turkey.

MATERIALS AND METHODS

Data used in this study, including stream flow and suspended load measurements were obtained from State Hydraulic Works and rainfall measurements were obtained from State Meteorological Service [2, 3].

TREND ANALYSIS

Since hydraulic sizes have randomly changing characteristics within time, examination of continuously decreasing or increasing trends requires special methods.

Basic assumptions such as normality, linearity and independence in standard parametric tests generally cannot be attained in the data of typical surface water quality. Therefore, it is more suitable to use non-parametric tests rather than parametric tests [4-9]. These non-parametric tests are those such as Spearman's rho test and Mann-Kendall test. Consequently, these tests were used in this study.

Spearman's Rho Test. This is a quick and simple test to determine whether there is a correlation between two observation series. R_{xi}, which is a rank statistic, is determined by ordering data in increasing or decreasing order. Spearman's Rho test statistics (r_s) is calculated according to the equation below [10, 11].

$$r_s = 1 - 6\frac{\sum_{i=1}^{n}\left(R_{xi} - i\right)^2}{\left(n^3 - n\right)} \quad (1)$$

Since rs distribution will proximate to normal for n > 30, normal distribution tables are used. For this, test statistics (Z) of r_s;

$$Z = r_s\sqrt{n-1} \quad (2)$$

It is concluded that if normal distribution corresponding to α significance level which is chosen as absolute value of Z is smaller than $Z_{\alpha/2}$ then null hypothesis is accepted and it is concluded that there is no trend in time series observed; if it is bigger it is concluded that there is trend and iv Z value is positive there is an increase trend and if it is negative there is a decrease trend.

Mann-Kendall Test. Since the Mann-Kendall test is a non-parametric test, it is independent from distribution of random variable. With this test, the presence of a trend in a time series is checked with null hypothesis "H_0: no trend" [12-21]. In x_1, x_2, ... x_n time series on which the test will be applied xi, x_j pairs are divided into two groups. For i < j, if the number of the pairs $x_i < x_j$ is indicated with P and number of the pairs $x_i > x_j$ test statistics (S) are calculated by the following equation:

$$S = P - M \quad (3)$$

Kendall correlation coefficient:

$$\tau = \frac{S}{\left[n(n-1)/2\right]} \quad (4)$$

For n ≥ 10

$$\sigma_s = \sqrt{n(n-1)(2n+5)/18} \quad (5)$$

$$Z = \begin{cases} (S-1)/\sigma_s & S > 0 \\ 0 & S = 0 \\ (S+1)/\sigma_s & S < 0 \end{cases} \quad (6)$$

It is concluded that if normal distribution corresponding to α significance level, which is chosen as absolute value of Z, is smaller than $Z_{\alpha/2}$ then null hypothesis is accepted and it is concluded that there is no trend in time series observed; if it is bigger it is concluded that there is a trend and Z value is positive there is an increase trend and if it is negative there is a decrease trend [22-26].

RESULTS AND DISCUSSION

SPEARMAN'S RHO TEST AND MANN-KENDALL TEST RESULTS

Spearman's Rho test and Mann-Kendall test results of rainfall, stream flow and suspended load datas of West Black Sea Basin are given in table 1 and table 2.

TABLE 1
Spearman's Rho Test and Mann-Kendall Test Results of Stream Flow and Suspended Load Datas of West Black Sea Basin.

Year of Observation	The Station Number	The Station	Stream flow		Suspended load	
			Spearman's Rho Test (Z)	Mann-Kendall Test (Z)	Spearman's Rho Test (Z)	Mann-Kendall Test (Z)
1980-2009	1307	Devrekani Stream	**-2,03**	**-1,96**	**-2,32**	**-2,25**
1979-2009	1314	Soganli Stream	**-2,47**	**-2,19**	**-2,48**	**-2,41**
1979-2009	1332	Karasu Stream	-0,01	-0,07	-1,24	-1,36
1979-2009	1334	Bolu Stream	**-3,16**	**-3,09**	**-2,58**	**-2,65**
1979-2009	1335	Filyos Stream	-1,72	-1,53	**-2,26**	**-2,07**

TABLE 2
Spearman's Rho Test and Mann-Kendall Test Results of Rainfall Data of West Black Sea Basin.

Year of Observation	The Station Number	The Station	Spearman's Rho Test (Z)	Mann-Kendall Test (Z)
1979-2012	17020	Bartin	-0,88	-0,77
1979-2012	17022	Zonguldak	-0,70	-0,83
1979-2012	17024	Inebolu	-0,41	-0,42
1979-2012	17026	Sinop	0,94	0,95
1979-2012	17070	Bolu	1,21	1,25
1979-2012	17072	Duzce	-1,79	-1,81
1996-2012	17078	Karabuk	**-2,72**	**-3,09**
1979-2011	17602	Amasra	-0,71	-0,70
1979-2011	17606	Bozkurt	-1,78	-1,91
1980-2012	17618	Devrekani	**-2,97**	**-2,97**
1979-2011	17646	Cerkes	-1,18	-1,26

Spearman's Rho test and Mann-Kendall test results of rainfall, stream flow and suspended load datas of East Black Sea Basin are given in table 3 and table 4.

TABLE 3
Spearman's Rho test and Mann-Kendall test results of stream flow and suspended load datas of East Black Sea Basin.

Year of Observation	The Station Number	The Station	Stream flow		Suspended load	
			Spearman's Rho Test (Z)	Mann-Kendall Test (Z)	Spearman's Rho Test (Z)	Mann-Kendall Test (Z)
1988-2009	2228	Fol Stream	-1,20	-0,85	-1,88	-1,35
1988-2009	2232	Firtina Stream	1,01	1,07	1,95	1,35
1979-2009	2238	Melet Stream	-0,87	-0,85	-1,39	-1,28
1988-2009	2245	Terme Stream	-0,45	-0,51	-0,02	-0,11
1988-2009	2251	Degirmen Stream	0,77	0,51	0,02	-0,11

TABLE 4
Spearman's Rho test and Mann-Kendall test results of rainfall data of East Black Sea Basin.

Year of Observation	The Station Number	The Station	Spearman's Rho Test (Z)	Mann-Kendall Test (Z)
1979-2012	17033	Ordu	1,24	1,36
1979-2012	17034	Giresun	1,51	1,60
1979-2012	17038	Trabzon	1,09	1,16
1979-2012	17040	Rize	**2,02**	**2,00**
1979-2012	17042	Hopa	0,99	0,93
1979-2012	17088	Gumushane	1,12	1,10
1980-2011	17624	Unye	1,65	1,77
1979-2011	17626	Akcaabat	0,45	0,57
1979-2011	17628	Pazar	**2,70**	**2,65**

Spearman's Rho test and Mann-Kendall test results of rainfall, stream flow and suspended load datas of Sakarya Basin are given in table 5 and table 6.

TABLE 5
Spearman's Rho test and Mann-Kendall test results of stream flow and suspended load datas of Sakarya Basin.

Year of Observation	The Station Number	The Station	Stream flow		Suspended load	
			Spearman's Rho Test (Z)	Mann-Kendall Test (Z)	Spearman's Rho Test (Z)	Mann-Kendall Test (Z)
1979-2008	1203	Porsuk Stream	**-2,59**	**-2,68**	**-3,30**	**-3,39**
1979-2009	1233	Aladag Stream	-0,54	-0,61	0,29	0,27
1991-2009	1253	Sohu Stream	0,98	0,98	0,50	0,49
1979-2011	1257	Porsuk Stream	**-2,18**	**-2,15**	**-2,83**	**-2,96**

TABLE 6
Spearman's Rho test and Mann-Kendall test Results of Rainfall Data of Sakarya Basin.

Year of Observation	The Station Number	The Station	Spearman's Rho Test (Z)	Mann-Kendall Test (Z)
1979-2012	17069	Sakarya	**-3,15**	**-3,29**
1991-2012	17123	Eskisehir	**-2,36**	**-2,48**
1979-2012	17130	Ankara	1,26	0,92
1979-2011	17155	Kutahya	**-2,34**	**-2,34**
1979-2011	17662	Geyve	**-2,68**	**-2,31**
1991-2011	17664	Kizilcahamam	1,28	1,48
1979-2011	17680	Beypazari	-1,37	-1,41
1979-2011	17702	Bozoyuk	-1,04	-0,85
1979-2011	17726	Sivrihisar	-0,51	-0,36
1979-2011	17728	Polatli	-1,91	-1,75
1979-2011	17752	Emirdag	-1,43	-1,50

CONCLUSIONS

For West Black Sea Basin, trend analysis was applied on average stream flow and suspended load values of five stream flow and suspended load observation stations and rainfall values of 11 Meteorology Observation station. Common trend results of rainfall, stream flow and suspended load datas of West Black Sea Basin are given in Table 7.

TABLE 7
Common Trend Results of Rainfall, Stream Flow and Suspended Load Data of West Black Sea Basin.

The Station Number	The Station Name	Rainfall	Stream Flow	Suspended Load
1307 / 17618	Devrekani S. / Devrekani	Decrease Trend	Decrease Trend	Decrease Trend
1314 / 17078	Soganli S. / Karabuk	Decrease Trend	Decrease Trend	Decrease Trend
1332 / 17026	Karasu S. / Sinop	No Trend	No Trend	No Trend
1334 / 17070	Bolu S. / Bolu	No Trend	Decrease Trend	Decrease Trend
1335 / 17020	Filyos S. / Bartin	No Trend	No Trend	Decrease Trend

Golkoy Dam arranges stream flow and saves suspended load carried on the stream as dead storage, it caused a decrease trend on stream flow and suspended load. Moreover 30% of the water in the dam is used as drinking water by Bolu Municipality and the rest of the water is used for irrigation. Then, there is a result of decrease trend in stream flow of Bolu Stream.

While there is no trend in rainfall and stream flow data of Filyos stream, it is seen that there is decrease trend in suspended load. When the reason for this is analyzed, it is seen that sand and gravel pits located near Filyos stream withdraw sand and gravel from the stream. Therefore, there is a decrease trend in suspended load data of Filyos Stream.

For East Black Sea Basin, trend analysis was applied on average stream flow and suspended load values of five stream flow and suspended load observation stations and rainfall values of nine Meteorology Observation stations. Common trend results of rainfall, stream flow and suspended load data of East Black Sea Basin are given in Table 8.

TABLE 8
Common Trend Results of Rainfall, Stream Flow and Suspended Load Data of East Black Sea Basin.

The Station Number	The Station Name	Rainfall	Stream Flow	Suspended Load
2228 / 17626	Fol Stream / Akcaabat	No Trend	No Trend	No Trend
2232 / 17628	Fırtına Stream / Pazar	Increase Trend	No Trend	No Trend
2238 / 17033	Melet Stream / Ordu	No Trend	No Trend	No Trend
2245 / 17624	Terme Stream / Unye	No Trend	No Trend	No Trend
2251 / 17038	Degirmen Stream / Trabzon	No Trend	No Trend	No Trend

While there is no trend in stream flow and suspended load of Firtina River, there is an increasing trend in rainfall data. When the result is observed, Firtina Stream belongs to Rize region. The most important climactic characteristic of Rize is that it is rainy in all seasons. Therefore, Rize is the city that receives the most rain in Turkey so there is increasing trend in rainfall data of this region.

The reason why there is no trend in stream flow and suspended load of Firtina River is that there is no HES or dam on it. This stream is completely under protection and the amount which passes to stream flow from rainfall is lower. Therefore, there is no trend in stream flow and suspended load data of this stream. Moreover, since the grain diameter of suspended load transported in this region is large it is transported as bed load. DSI only measures suspended load. Therefore, since data used in the study are suspended load data, there is no trend. On the other hand, Firtina Stream, which is nearly 2 km from Ardesen, is in a convenient location in the sense of river tourism (canoe-rafting). Therefore, foreign and local sportsmen particularly like this stream. For these reasons, there is no trend in stream flow and suspended load data in this region.

For Sakarya Basin, trend analysis was applied on average stream flow and suspended load values of four stream flow and suspended load observation stations and rainfall values of 12 Meteorology Observation stations. Common trend results of rainfall, stream flow and suspended load data of Sakarya Basin are given in Table 9.

TABLE 9
Common Trend Results of Rainfall, Stream Flow and Suspended Load Data of Sakarya Basin.

The Station Number	The Station Name	Rainfall	Stream Flow	Suspended Load
1203 / 17155	Porsuk Stream / Kutahya	Decrease Trend	Decrease Trend	Decrease Trend
1233 / 17680	Aladag S. / Beypazarı	No Trend	No Trend	No Trend
1253 / 17664	Sohu S. / Kızılcahamam	No Trend	No Trend	No Trend
1257 / 1257	Sakarya River / Sakarya	Decrease Trend	Decrease Trend	Decrease Trend

When the situation in all basins is analyzed, there is a decrease trend in stream flow, suspended load and rainfall data of some basins. When general factors of this decrease are summarized;

Since buildings such as hydroelectric plants and dams located in the station region keep stream flow and suspended load, there will be a decrease trend in trend results of stream flow and suspended load data.

Climactic changes experienced in our country in recent years caused lower rainfall and higher temperatures compared to previous years. Due to this negative situation there should be a decrease trend in rainfall data of stations. Since the amount of water transported to stream flow would decrease as the rainfall decreases, there would be decrease in trend analysis results of stream flow and suspended load values.

Factories located near station regions withdraw water and suspended load from these streams. Water and suspended load withdrawn from the stream would have a great effect on the decrease trend attained as a result of trend analysis.

When all the measurements taken from these results are listed;

- Since the invaluable ecological and economic benefit of natural cycle and flow of water is essential for life on earth, water resources management of natural and artificial water areas should be planned and applied properly.
- Available resources should be used as usefully as possible.
- Protection of forests and the promotion of tree planting are two of the best efforts to be carried out in this sense. Forestation studies are the best studies to be carried out both against the effect of global warming and in protecting dam reservoirs against suspended load. Such activities should be increased.
- Another step to be taken in decreasing the effect of global warming is education. Future generations should be taught not to make excessive water demands at an early age and that it is essential to use water economically without wasting it.

REFERENCES

[1] Ocal, O, (2007), Determınatıon of Rainfall-Runoff-Sediment Transport Relationship in Watersheds by Using Artificial Neural Network Algorithm, Institute of Science, Department of Civil Engineering, Pamukkale University, Denizli, Turkey.

[2] State Hydraulic Works (DSI), (2010), Stream Flow and Sediment Station Data of West Black Sea Basin, East Black Sea Basin and Sakarya Basin.

[3] State Meteorological Service (DMI), (2013), Rainfall Station Data of West Black Sea Basin, East Black Sea Basin and Sakarya Basin.

[4] Helsel, D.R. and Hirsch, R.M, (1992), Statistical Methods in Water Resources, Techniques of Water-Resources Investigations of the United States Geological Survey, Book 4, Hydrologic Analysis and Interpretation, Chapter A3, Amsterdam.

[5] Aherne, J., Mongeon, A. and Watmough, S.A, (2010), Temporal and Spatial Trends in Precipitation Chemistry in the Georgia Basin, British Columbia, Journal of Limnology, 69, 4–10.

[6] Ceribasi, G, (2010), Estimation of Sediment Discharge Transported in Sakarya River by Using Trend Analysis Method, Institute of Science, Department of Construction, Sakarya University, Sakarya, Turkey.

[7] Feller, M.C., (2010), Trends in Precipitation and Stream Water Chemistry in East Creek Watershed in Southwestern British Columbia, 1971-2008, Journal of Limnology, 69, 77–91.

[8] Kumar, A., Chattopadhyay, C., Singh, K.N., Vennila, S. and Rao, V., (2014), Trend Analysis of Climatic Variables in Pigeonpea Growing Regions in India, Mausam, 65, 161-170.

[9] Vadadi-Fulop, C. and Hufnagel, L., (2014), Climate Change and Plankton Phenology in Freshwater: Current Trends and Future Commitments, Journal of Limnology, 73, 1–16.

[10] Buyukkaracigan, N. and Kahya, E., (1997), The Dependency Analysis of Annual Peak Flows of Streams in Konya Basin, International Conference on Water Problems in the Mediterranean Countries, Ankara, Turkey.
[11] Gumus, V., (2006), Evaluation of Firat River Basin Streamflow by Trend Analysis, Institute of Science, Department of Civil Engineering, Harran University, Sanliurfa, Turkey.
[12] Mann, H.B., (1945), Non-parametric Tests against Trend, the Econometric Society, 3, 245–259.
[13] Kendall, M.G., (1975), Rank Correlation Methods, 4th ed. Charles Griffin, London.
[14] Van Belle, G. and Hughes, J.P., (1984), Nonparametric Tests for Trend in Water Quality, Water Resources Research, 1, 127–136.
[15] Gumus, V. and Yenigun, K., (2006), Evaluation of Lower Fırat Basin Streamflow by Trend Analysis, 7th International Advances in Civil Engineering Conference, Yildiz Technical University, Istanbul, Turkey.
[16] Kalayci, S. and Kahya, E., (2006), Assessment of Streamflow Variability Modes in Turkey 1964-1994, Journal of Hydrology, 1-4, 163-177.
[17] Partal, T., Kahya, E., Seker, D. and Kabdasli, S., (2003), Precipitation Trends in the Aegean Region, International Association of Hydraulic Engineering and Research Congress, Thessaloniki, Greece.
[18] Partal, T. and Kucuk, M., (2006), Long-term Trend Analysis Using Discrete Wavelet Components of Annual Precipitations Measurements in Marmara Region (Turkey), Physics and Chemistry of the Earth, 18, 1189–1200.
[19] Fiala, T., (2008), Statistical Characteristics and Trends of Mean Annual and Monthly Discharges of Czech Rivers in the Period 1961-2005, Journal of Hydrology and Hydromechanics, 56, 133-140.
[20] Rani, B.A., Manikandan, N. and Maragatham, N., (2014), Trend Analysis of Rainfall and Frequency of Rainy Days over Coimbatore, Mausam, 65, 379-384.
[21] Remya, K., Ramachandran, A., Jayakumar, S., Kumar, D.S., Radhapriya, P. and Malin, P., (2015), Rainfall Trend Analysis of Kolli Hill, Tamil Nadu, India, Mausam, 66, 151-154.
[22] Yu, S., Zou, S. and Whittemore, D., (1993), Non-parametric Trend Analysis of Water Quality Data of Rivers in Kansas, Journal of Hydrology, 1, 61–80.
[23] Aris, P., Sophia, M. and Antonios, P., (2006), Simulation and Trend Analysis of the Water Quality Monitoring Daily Data in Nestos River Delta, Contribution to the Sustainable Management and Results for the Years 2000–2002, Environ. Monit. Assess, 1-3, 543–562.
[24] Seseogullari, B., Eris, E. and Kahya, E., (2006), Trend Analysis of Sea Levels along Turkish Coasts, Hydrology Days.
[25] Ceribasi, G., Dogan, E. and Sonmez, O., (2013), Evaluation of Sakarya River Streamflow and Sediment Transport with Rainfall Using Trend Analysis, Journal of Fresenius Environmental Bulletin, 3A, 846–852.
[26] Ceribasi, G., Dogan, E. and Sonmez, O., (2014), Evaluation of Meteorological and Hydrological Data of Sapanca Basin by Trend Analysis Method, Journal of Environmental Protection and Ecology, 2, 705–714.

Received: **03.11.2015**
Accepted: **10.12.2015**

CORRESPONDING AUTHOR

Assist. Prof. Dr. Gokmen Ceribasi
Sakarya University
Technology Faculty
Department of Civil Engineering
54187 Sakarya – TURKEY

e-mail: gceribasi@sakarya.edu.tr

by PSP Volume 25 – No. 1/ 2016, pages 307-315 Fresenius Environmental Bulletin

ESTIMATING THE SOIL REDISTRIBUTION RATES IN A SMALL AGRICULTURAL REGION (KARKIN VILLAGE) IN GEDIZ BASIN BY USING ^{137}Cs AND ^{210}Pb MEASUREMENTS

Ramazan Manav*, Görgün Ugur Aysun, Özden Banu, Arslan Fatih Dursun

Ege University, Institute of Nuclear Sciences, 35100 Bornova, İzmir, Turkey

ABSTRACT

Gediz Basin supports the considerable amount of Turkey's agricultural need and erosion have long been causing a serious problem in the basin. To evaluate the erosion rate by using ^{137}Cs and $^{210}Pb_{ex}$ measurements, bulk soil samples were collected in cultivated site from Karkın Village in Middle Gediz Basin. Soil loss rates were calculated from ^{137}Cs and ^{210}Pb inventories of the samples using the proportional and the mass balance conversion models. The activity concentrations of ^{137}Cs and ^{210}Pb were measured and their values are obtained in the ranges of 0,4 - 24 Bq kg^{-1} and 17-58 Bq kg^{-1} respectively. The ^{137}Cs and ^{210}Pb inventories of reference, erosion and deposition are obtained as follow in sequence; 3162 Bq m^{-2}, 2285 Bq m^{-2}, 6272 Bq m^{-2} and 3723 Bq m^{-2}, 2544 Bq m^{-2} and 4138 Bq m^{-2}. Soil redistribution rates, within the field, determined for ^{137}Cs and ^{210}Pb 10,8 t ha^{-1} y^{-1} and 13,07 t ha^{-1} y^{-1} and the mean erosion rates for the eroding area was obtained as 25,8 t ha^{-1} y^{-1} and 54,05 t ha^{-1} y^{-1} respectively.

Keywords:
^{210}Po, ^{210}Pb, Soil erosion, Gediz Basin

INTRODUCTION

Soil erosion is one of the main degradation processes to occur on soil, having high productive capacity, in Turkey. The semiarid climate and the irregular terrain enhance erosion in Aegean region. Extremely short duration and very high intensity rainfall regime of Gediz Basin areas is particularly conductive to erosion and it has been increasingly considered as a serious environmental problem in region. It can be figured out that soil erosion is not only a natural processes, but also it can be accelerated by human intervention through deforestation, overgrazing, and nonsustainable farming practices. Information on rates of soil loss from agricultural land must be seen as an important requirement for effective environmental management. Rates of soil loss exert a key control on crop productivity and the longer-term sustainability of the soil resource (Oldeman, 1994). Many studies were made for understanding the soil and sediment movement.

Mostly caesium-137 (^{137}Cs) and excess lead-210 ($^{210}Pb_{ex}$) fallout radionuclides are used to provide the rates of soil and sediment redistribution in recent years (Mabit, Benmansour & Walling, 2008). Porto, Walling & Capra, (2014) indicated that ^{137}Cs measurements are primarily used to generate information on mean annual erosion rates over the past ca. 50 years. It is a man-made radionuclide (half-life 30.2 years) generating from the nuclear weapon tests and nuclear accidents. ^{137}Cs, coming out with nuclear studies, penetrates to the atmosphere and then deposited to landscape and soil.

Lead-210, a naturally occurring radionuclide (half-life 22.2 years), is a product of the ^{238}U decay series, derived via a series of other short-lived radio nuclides from the decay of gaseous ^{222}Rn (half-life 3.8 days), the daughter of ^{226}Ra (half-life 1622 years). The ^{210}Pb content of soils and rocks produced by the natural in situ decay of ^{226}Ra is termed 'supported' ^{210}Pb because it is in equilibrium with its parent. However, upward diffusion of a small proportion of the ^{222}Rn produced naturally in soils and rocks releases ^{222}Rn to the atmosphere, and the subsequent fallout of ^{210}Pb provides an input to surface soils and sediments which is not in equilibrium with ^{226}Ra. Such fallout ^{210}Pb is commonly termed 'excess' or 'unsupported' ^{210}Pb (Robbins, 1978). Because of its natural origin, the deposition of fallout ^{210}Pb has been essentially constant through time. Relatively little is currently known about the global distribution of fallout ^{210}Pb, although in a review of existing data on ^{210}Pb deposition fluxes for different areas of the world, Appleby and Oldfield (1992) indicate that such fluxes are greater over the land than over the ocean and lower over the western margins of continental land masses, due to the predominant west to east trajectory of air mass movement. The same authors report an average deposition flux for the world of 118 Bq m^{-2} $year^{-1}$, with values generally lying in the range 50–150 Bq m^{-2} $year^{-1}$.

The study reported here aims to determine the soil redistribution with fallout radionuclides (^{137}Cs and ^{210}Pb) in cultivated region at Gediz Basin, Turkey. The proportional Model and mass balance models were used to quantify the erosion and deposition rates in these regions by using ^{137}Cs and $^{210}Pb_{ex}$ measurements respectively.

MATERIALS AND METHODS

GEOGRAPHICAL PROPERTIES OF STUDY AREA

The Gediz Basin is located at the Aegean Region of the western Turkey. The basin lies between northern latitudes of 38° 04' — 39° 13' and southern longitudes of 26° 42' — 29° 45'. . The cultivated study area, Karkın Village, is located in the east of the basin (Figure 1). The Gediz Basin covers 2.2% (1.721.895 hectare) of the total area of Turkey. A typical Mediterranean climate prevails in the basin and towards the insides different climatic characters are seen. Gediz basin has very rich agricultural soils formed by the Gediz River. The basin fairly productive for agriculture so various agricultural crops are grown on the alluvial soils, present between the mountains lying in the east-west direction of the Basin. Ploughed and cultivated areas comprise 37.40% of the basin. The fact that annual average of precipitation is around 450–1060 mm, and that the period of plant maturing is relatively short, (176–184 days) allows almost all cultural plants to be grown (Bolca, Saç, Çokuysal, Karalı & Ekdal (2007).

There are 14 types of soil groups in the Gediz Basin and the majors are 28,27% calcareous forest, 48,9% stony soils, complicating cultivate the soil, and 2.3% coarse textured soils, low water-holding capacity. So that 45-50 percent of basin is used for agricultural process and it supports the considerable amount of Turkey's agricultural need. Yet it has suffering from soil erosion.

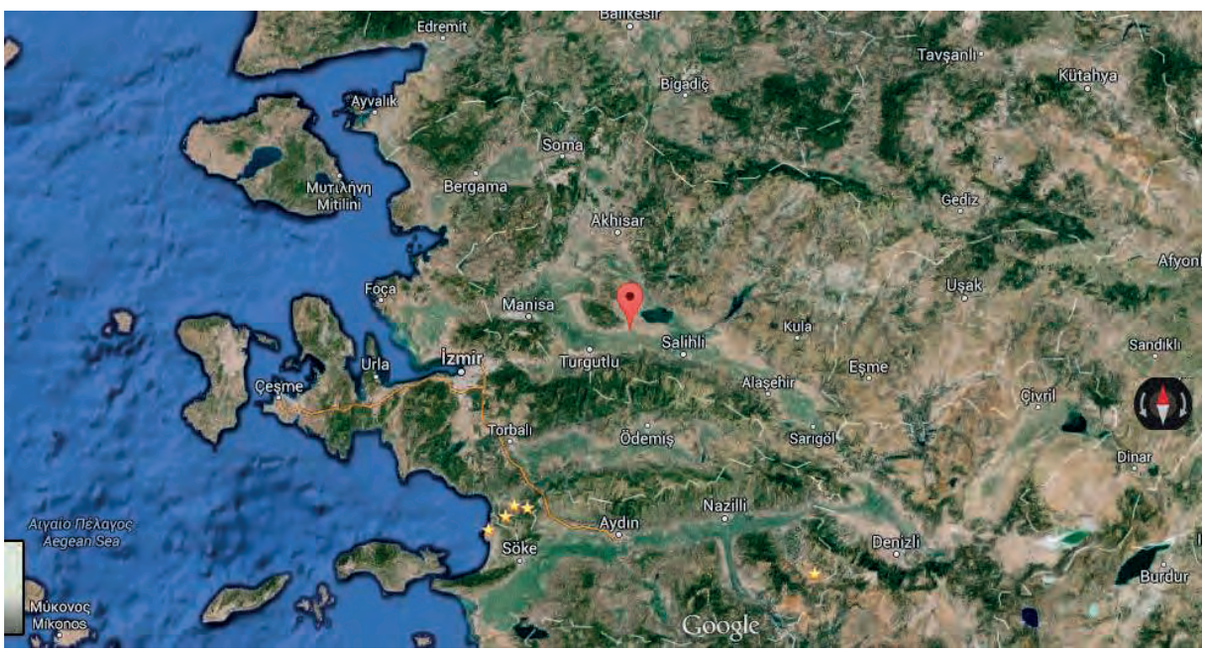

FIGURE 1
General view of the Karkın Village, Gediz Basin

Soil sampling. The sampling strategy and sampling design depend on the aim of the study and the environmental conditions (Pennock and Appleby, 2002). In this study, samplings were based on the intersections of grids with 20x30 m spacing 35 bulk soil samples were collected for cultivated region. Bulk soil samples were collected from 20x20 cm area within 25 cm depth from intersection points of the regions. The slope of area was obtained as 12% for cultivated area. The organic matter, pH, salinity, humidity and carbonate contents were determined from the bulk samples (Table 1). In addition, reference, deposition and erosion cores were sampled to

characterize the depth distribution of ^{137}Cs and ^{210}Pb concentrations.

TABLE 1
The mean values of chemical parameters in Karkın Village

Area of Karkın	Organic matter (%)	pH	Salinity (%)	Humidity (%)	Carbonate (%)
Cultivated (n=35)	1.70	7.62	0.05	8.73	11.7

n: number of samples

Reference areas were stated on uncultivated agricultural lands near the selected areas according to Zapata (2002) for core sampling. Zapata stated some basic rules for reference region and three of them as; i) The ideal reference site has experienced neither soil loss nor sediment deposition; the inventory reflects only the atmospheric inputs of the specific radionuclide and its decay through time. Level sites that do not receive flows from upslope positions are the preferred locations. ii) Protected areas such as parks, ceremonial areas, burial grounds are commonly used for reference sites although clearly some cultural sensitivity is required. and iii) The reference site should be located as close as possible to the disturbed sitesthat are to be sampled

Core samples were obtained with the 10x50x8 cm iron mold (Figure.2) and were cut into 2 cm and 5 cm increments in order to see the depth distributions of unsupported ^{210}Pb and ^{137}Cs concentrations.

FIGURE 2
The placed iron mold for core samples

LABORATORY ANALYSIS

Gamma spectrometric analysis for ^{137}Cs. The soil samples were dried at 105^0C, sieved from 600 μm, mixed, weighted and put in the Marinelli beakers (1,200 mL) with 1,500 g weight.

Tennelec/Nucleus HPGe (184 cc) planar type coaxial intrinsic germanium detector was used for direct gamma assay. 137Cs activities were measured with its 662keV emissions. Each sample was counted for 20,000 s. 137Cs standard of Amersham (Certificate no. 317776-3 of sealed radioactive sources) was used to determine the efficiency of the spectrometer.

Alpha spectrometric analysis for ^{210}Pb. Measurements of ^{210}Po were realized through its 5.30 MeV alpha particle emission, using ^{209}Po (4.88 MeV, $t_{1/2}$: 109 y) as the internal tracer. After standard addition of 0.1 Bq mL^{-1}, 1 g of each sample was completely dissolved with concentrated HNO_3 and HF under heating at 55 °C on a hot plate and evaporated to dryness. After this step, concentrated HCl was added and evaporated to dryness three times (HNO_3:HF:HCl=1:1:10 mL). Polonium was spontaneously plated on copper disks in 0.5 M HCl in the presence of ascorbic acid to reduce Fe^{+3} to Fe^{+2} (Flynn, 1968). The recovery

rates of standardized tracer for the soil samples varied from 70% to 90%. Alpha activities were measured using Ortec Octete Plus with 450 mm^2 ULTRA-AS Detectors. Concentrations of ^{210}Po in all the samples were well above the detection limit (0.0003 Bq). Sample count times were 86,400 s, with counting errors in the order of ±10% or less.

After the first deposition of ^{210}Po, the residual 0.5 M HCl was kept for one year to allow ^{210}Po in-growth from the ^{210}Pb contained in the solution to search supported ^{210}Pb in the samples. The samples were re-plated and the ^{210}Po activities were determined. Well known Bateman equations were used to obtain ^{210}Pb activity from measured ^{210}Po activity (Bateman, 1910; Cetnar, 2006). The second deposition provided information on the ^{210}Pb content of the samples and hence on the extent to which the initial ^{210}Po was supported by its grandparent.

MATHEMATICAL MODELS USED IN THE STUDY

The proportional model for ^{137}Cs. The reference inventories at the sampling area should be higher than the erosion region and higher than the deposition sites to apply the ^{137}Cs model. So it is observed that some sampling points' ^{137}Cs inventories are lower than reference inventory showing the soil loss while some points getting higher for deposition areas. The proportional model was used widely for ^{137}Cs to calculate the soil loss and deposition rate all over the world. It is based on the assumption that ^{137}Cs fallout inputs are completely mixed within the plough or cultivation layer and that soil loss is directly proportional to the reduction in the ^{137}Cs content in the soil profile (Saç, Uğur, Yener & Özden, (2008). The mean annual soil loss rate Y (t ha^{-1} y^{-1}) can be written as follows: (Walling and He 199a)

$$Y = 10dB[1 - \left(1 - \frac{X}{100}\right)^{\frac{1}{(t-1963)}}] \quad (1)$$

where
X = the percentage reduction in total ^{137}Cs inventory (defined as (Aref – A)/Aref · 100)
d = the depth of the plough or cultivation layer (m)
B = the bulk density of the soil (kg m^{-3})
t = the time elapsed since initiation of 137Cs accumulation (since 1963) (year)
Aref = the local reference inventory (Bq m^{-2})
A = the total inventory measured at the sampling point (Bq m^{-2}).

The mass balance model for ^{210}Pb. The mass balance conversion model (Walling and He, 1999b) was used to estimate the soil redistribution rates (kg/m/year) from the unsupported ^{210}Pb inventories associated with collected soil samples.

Following Walling and He the change in the activity of accumulated ^{137}Cs or $^{210}Pb_{ex}$ A(t) (Bq m^{-2}) per unit area with time t (yr) at an eroding site can be represented as:

$$A(t) = A(t_0)e^{-\int_{t_0}^{t}(PR/D+\lambda)dt'} + \int_{t_0}^{t}(1-\Gamma)I(t')e^{-(PR/D+\lambda)(t-t')}dt \quad (2)$$

where
R= mean annual erosion rate (kg m^{-2} yr^{-1})
D = mass depth representing the average plough depth (kg m^{-2})
l= decay constant for ^{137}Cs or $^{210}Pb_{ex}$ (yr^{-1})
I(t) =annual ^{137}Cs or $^{210}Pb_{ex}$ deposition flux (Bq m^{-2} yr^{-1})
Γ = proportion of the freshly deposited ^{137}Cs or $^{210}Pb_{ex}$ fallout removed by erosion before being mixed into the plough layer
P = particle size correction factor
t_0 (yr) = year when cultivation started
$A(t_0)$ (Bq m^{-2}) = $^{210}Pb_{ex}$ or ^{137}Cs inventory at t_0.

Γ can be expressed as

$$\Gamma = P\gamma(1 - e^{-R/H}) \quad (3)$$

γ is the proportion of the annual ^{137}Cs or $^{210}Pb_{ex}$ fallout susceptible to removal by erosion prior to incorporation into the soil profile by tillage and is dependent on the timing of cultivation and the local rainfall regime; H (kg/m^2) is the relaxation mass depth of the initial distribution of the fallout radionuclide in the soil profile, which can be determined experimentally for local conditions (He and Walling, 1997).

According to mass balance conversion model the following parameters were obtained from the studying area. An average plough depth (D) of 220 (kg m^{-2}) (corresponding to an average bulk density and a plough depth), a value of the relaxation mass depth (H) equal to 98.04 (kg m^{-2}) (it was derived from the graph of the lnA of ^{210}Pb of reference core vs relaxation mass depth) , a value of γ equal to 0.14 based on the relationship between the timing of cultivation and the rainfall regime of the sampling area and also ^{210}Pb decay constant 0,0311 (y^{-1}) was used. A particle size correction factor P of 1.4 was calculated by considering the enrichment of the eroded soil in fines relative to the source material. And also annual fallout ^{210}Pb deposition was determined as 116 (Bq m^{-1} $year^{-1}$).

RESULTS AND DISCUSSION

^{137}Cs AND ^{210}Pb IN CORE AND BULK SAMPLES

The results of distribution of ^{137}Cs and ^{210}Pb radionuclides in the reference are presented graphically in Figure. 3. The ^{137}Cs and ^{210}Pb concentrations were obtained between 0,4 – 24 Bq kg^{-1} and 17-58 Bq kg^{-1} respectively. It is shown in Figure 3 that the activity concentrations of radionuclide in soil decrease regularly with increasing depth on reference. This observation shows that ^{137}Cs and ^{210}Pb are deposited on the soil from the atmosphere and ^{210}Pb is able to move down to a maximum depth of about 20 cm in the soils of study points. Thus, $^{210}Pb_{ex}$ was defined as up to 20 cm and the mean $^{210}Pb_{ex}$ concentration in this region was determined 20 Bq kg^{-1}.

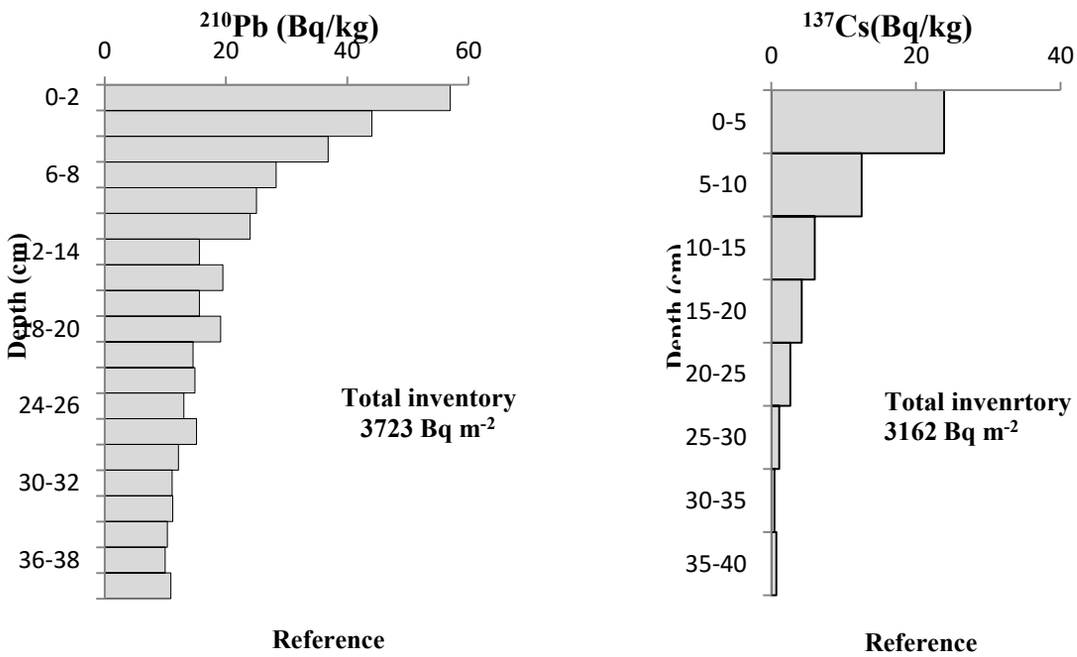

FIGURE 3
The ^{210}Pb and ^{137}Cs concentrations with depth in reference

The ^{137}Cs and ^{210}Pb concentrations of erosion and deposition side of cultivated field were showed in Figure 4 and Figure 5. The inventories of ^{210}Pb were determined as, 3723 Bq m^{-2},2544 Bq m^{-2} and 4138 Bq m^{-2} in reference, erosion and deposition respectively. Also the inventories of ^{137}Cs were determined as, 3162 Bq m^{-2},2285 Bq m^{-2} and 6272 Bq m^{-2} in reference, erosion and deposition sides. It is shown that the total inventories of the erosion regions decreasing while the deposition regions increasing according to reference region.

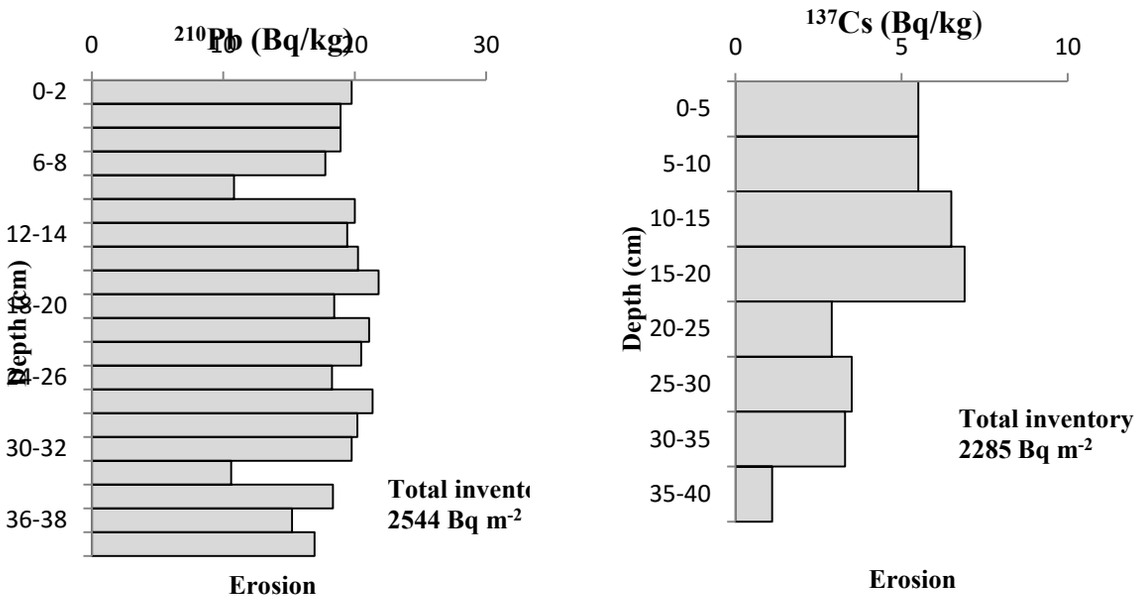

FIGURE 4
The ^{210}Pb and ^{137}Cs concentrations with depth in erosion

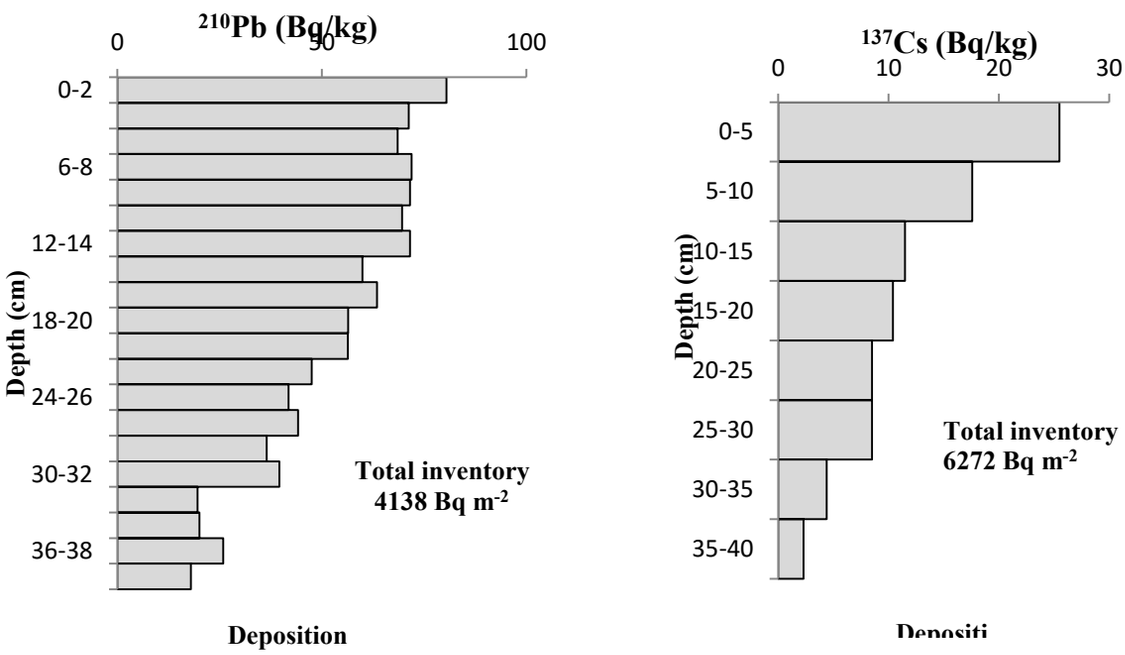

FIGURE 5
The ^{210}Pb and ^{137}Cs concentrations with depth in deposition

The inventories of ^{137}Cs and ^{210}Pb in bulk samples sites are found to vary between 178-2851 Bq m^{-2} (mean 1667 Bq m^{-2}) and 828-7395 Bq m^{-2} (mean 2759 Bq m^{-2}) respectively. The inventories spatial distributions are showed in Figure 6.

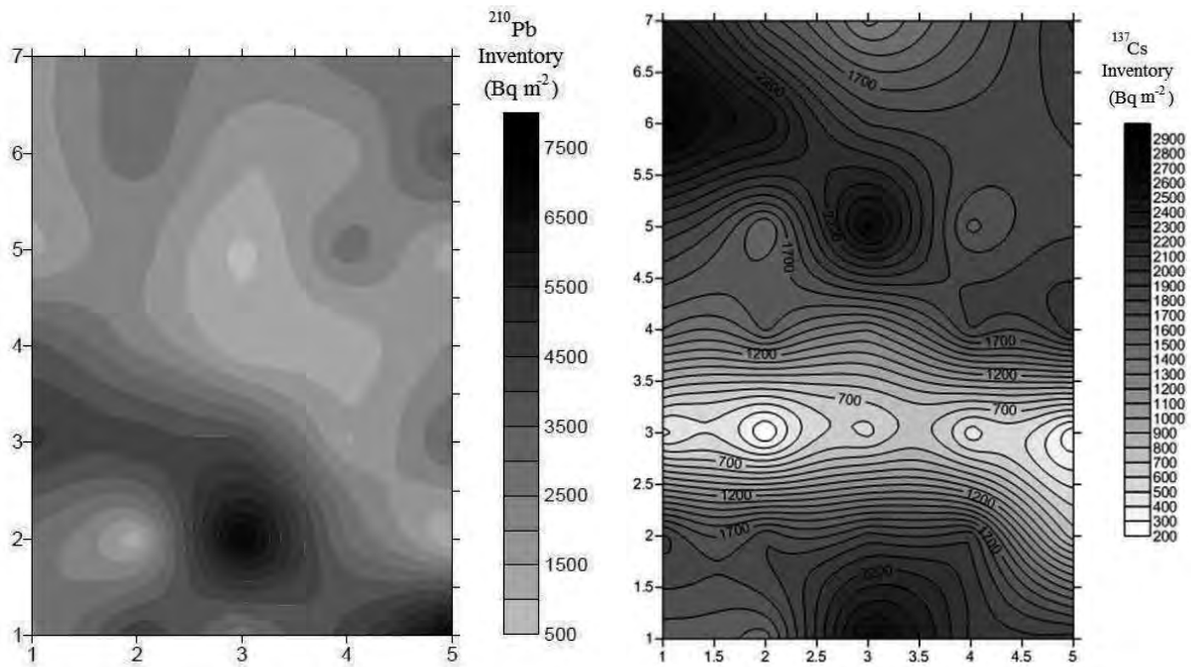

FIGURE 6
The spatial distributions of ^{210}Pb and ^{137}Cs inventories

DETERMINED EROSION AND DEPOSITION RATES

The distributions of ^{137}Cs and ^{210}Pb activities as a function of the soil depth in the reference, erosion and deposition sites were studied to acquire information on the behavior of ^{137}Cs and ^{210}Pb fallouts within the soil. The ^{137}Cs and ^{210}Pb activity concentrations in the profiles for the reference site shows a sharp decrease with increasing depth an exponential function. It is seen that the ^{137}Cs concentration was quite equally distributed throughout the plough layer (20 cm from the surface) in erosion parcel. This shows that the soil is mixed properly due to the cultivation activities in the field.

The average erosion and deposition rates in the region were determined in 35 bulk samples according to the proportional model for ^{137}Cs and the mass balance model for ^{210}Pb. The erosion rates were obtained between 5,9 ile 78,9 t ha^{-1}y^{-1} (mean 25,8 t ha^{-1}y^{-1}) while the depositions ranged from 4,1 to 16,4 t ha^{-1}y^{-1} (mean 10,8 t ha^{-1}y^{-1}) by the proportional model. In addition, the erosion and deposition rates were determined as, 1,16 - 176,89 t ha^{-1}y^{-1} (mean 54,05 t ha^{-1}y^{-1}) and 12,81-13,32 t ha^{-1}y^{-1} (mean 13,07 t ha^{-1}y^{-1}) according to the mass balance model respectively. The 2D distributions of erosion and deposition rates are presented in Figure 7.

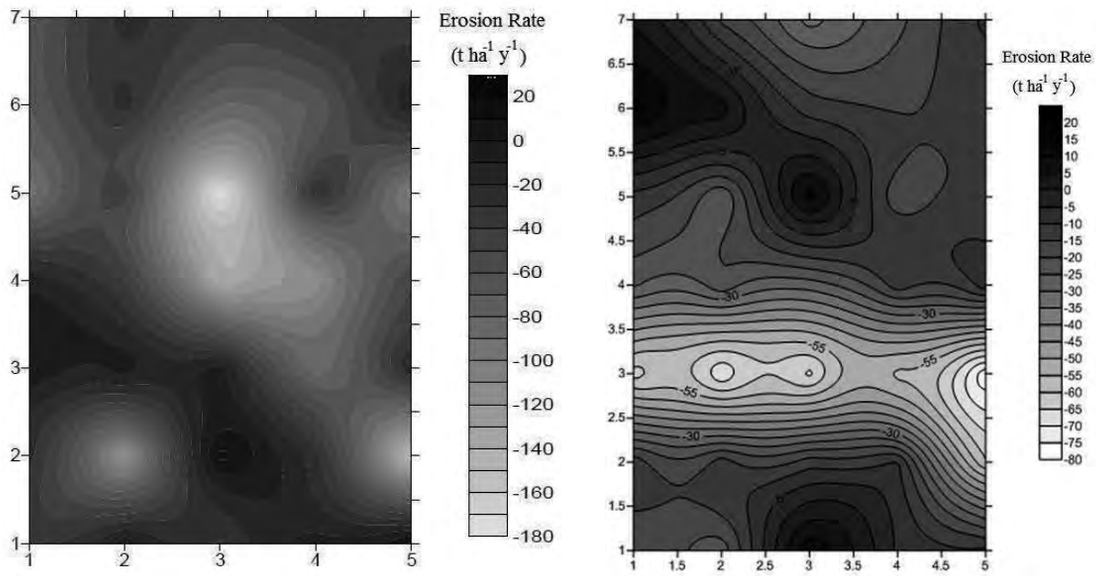

(a) (b)

FIGURE 7
The erosion rates of agricultural land according to (a) the mass balance model and (b) the proportional model

CONCLUSION

Soil redistribution rates were determined using the proportional and the mass balance models for ^{137}Cs and $^{210}Pb_{ex}$ on a cultivated slope located near the Karkın Village in Gediz Basin. The highest inventories of ^{137}Cs and $^{210}Pb_{ex}$ were observed at the bottom of the slope and the lowest ones were determined at the top of the region. By combining the estimates of soil erosion rates provided by the ^{137}Cs and $^{210}Pb_{ex}$ measurements, the mean soil loss were estimated 25,8 t $ha^{-1}y^{-1}$ and 54,05 t $ha^{-1}y^{-1}$ respectively. The estimated values are classified the studied area as risked region according to The Ministry of Forestry and Waterworks of Turkey. The soil erosion rate for the cultivated soil of Karkın showed that some farming practices, ploughing parallel to slope, should be changed to reduce the soil loss in valuable cultivated region. This study is first one to estimate the soil erosion by $^{210}Pb_{ex}$ in Gediz Basin and the further studies will be planning to do.

ACKNOWLEDGEMENTS

This work was supported by grants from The Scientific and Technical Research Council of Turkey (TÜBİTAK) contract no. 106Y054 and The Ege University Science and Technology Research Center (EB İLTEM) contract no. 2007BİL021.

REFERENCES

[1] Appleby, P. G. & Oldfield, F.0 (1992). Application of Lead-210 to sedimentation studies. In Ivanovich, M. and Harman, R. S. (ed.) Uranium-series Disequilibrium: Application to Earth, *Marine and Environmental Sciences. Clarendon Press, Oxford, UK.* pp. 731-738.

[2] Bateman, H., (1910). Solution of a system of differential equations occurring in the theory of radioactive transformations. *Proceedings of the Cambridge Philosophical Society 15*, 423–42

[3] Bolca M., Saç M.M., Çokuysal B., Karalı T. & Ekdal E. (2007). Radioactivity in soils and various foodstuffs from the Gediz River Basin of Turkey. *Radiation Measurements 42*, 263 - 270. http://dx.doi.org/ 10.1016/j.radmeas.2006.12.001

[4] Cetnar, J., (2006). General solution of Bateman equations for nuclear transmutations. Annals of Nuclear Energy 33, 640–645. http://dx.doi.org/10.1016/j.anucene.2006.02.004

[5] Flynn, W.W. (1968). The determination of low levels of polonium-210 in environmental materials. *Analytica Chimica Acta 43*, 221 - 227.

[6] He, Q., & Walling, D. E. (1997). The distribution of fallout ^{137}Cs and ^{210}Pb in undisturbed and cultivated soils. *Applied Radiation and Isotopes, 48*, 677–690. http://dx.doi.org/10.1016/S0969-8043(96)00302-8

[7] Mabit L., Benmansour M. & Walling D.E., (2008). Comparative advantages and limitations of the fallout radionuclides ^{137}Cs, $^{210}Pb_{ex}$ and ^{7}Be for assessing soil erosion and sedimentation. *Journal of Environmental Radioactivity 99*, 1799–1807. http://dx.doi.org/10.1016/j.jenvrad.2008.08.009

[8] Oldeman, L.R. (1994). The global extent of soil degradation. In: Greenland, D.J., Szabolcs, I. (ed.), Soil Resilience and Sustainable Land Use. *CAB International, Wallingford, Oxon, UK*, pp. 99–118.

[9] Pennock, D.J. & Appleby, P.G. (2002). Site selection and sampling design. In: Zapata, F. (Ed.), Handbook for the Assessment of Soil Erosion and Sedimentation Using Environmental Radionuclides. *Kluwer Academic Publishers,* pp. 15 40.

[10] Porto P., Walling D.E., Capra A., (2014). Using ^{137}Cs and $^{210}Pb_{ex}$ measurements and conventional surveys to investigate the relative contributions of interrill/rill and gully erosion to soil loss from a small cultivated catchment in Sicily. *Soil & Tillage Research 135*. 18–27. http://dx.doi.org/10.1016/j.still.2013.08.013

[11] Robbins, R.A. (1978). Geochemical and geophysical application of radioactive lead. In: Nriagu, J.O. (ed.), *The Biogeochemistry of Lead in the Environment. Elsevier, Amsterdam,* pp. 286–383.

[12] Saç M. M., Uğur A., Yener G., Özden B. (2008). Estimates of soil erosion using cesium-137 tracer models. *Environ Monit Assess 136*, 461 - 467. http://dx.doi.org/10.1007/s10661-007-9700-8

[13] Walling D.E., He Q., (1999a). Improved models for estimating soil erosion rates from Cesium-137 measurements. *J Environ Qual 28,*611–622 http://dx.doi.org/10.2134/jeq1999.00472425002800020027x

[14] Walling, D.E., He Q., (1999b). Using fallout lead-210 measurements to estimate soil erosion on cultivated land. *Soil Science Society of America Journal 63*, 1404 - 1412. http://dx.doi.org/10.2136/sssaj1999.6351404x

[15] Zapata F., (2002) Handbook for the Assessment of Soil Erosion and Sedimentation Using Environmental Radionuclides, *Kluwer Academic Publishers, Boston*.

Received: **22.06.2015**
Accepted: **06.01.2016**

CORRESPONDING AUTHOR

Manav Ramazan
Ege University
Institute of Nuclear Sciences
35100 Bornova, İzmir – Turkey

e-mail: ramazanmanav@gmail.com

by PSP Volume 25 – No. 1/ 2016, 316-324 Fresenius Environmental Bulletin

REMOVAL OF NITRATE FROM GROUND WATER BY MIEX RESINS

Cheng Liu [1,2], Lifei zhu[2], Gian zhang[2], Jie Wang[2], Yang Deng[3], Wei Chen [2*]

[1] Key Laboratory of Integrated Regulation and Resource Development Shallow Lakes (Ministry of Education) Hohai University, Jiangsu, Nanjing 210098, China.
[2] College of Environment, Hohai University, Jiangsu, Nanjing 210098, China.
[3] Department of Earth and Environmental Studies, Montclair State University, Montclair, United States

ABSTRACT

Batch experiments were used to study the adsorption characteristics of nitrate on magnetic ion exchange resins (MIEX®), the distribution of nitrate in groundwater was investigated in the meantime. In addition, the material was characterized, and the effects of coexisting anions and organic matter on the adsorption properties were determined. The results showed that the content of nitrate in Xuzhou city was about 20mg/L, especially higher than 25mg/L in rainy season. MIEX® could effectively remove nitrate from groundwater. At 288 K and 298 K, the adsorption trend was well fitted by the Langmuir isotherm. The exchange capacity of the MIEX resin was determined to be 14.62 mg-N/g, which was tested by flowing 20 mg-N/L solution. To reach the MIEX saturation adsorption, a 0.6-M NaCl solution was used to satisfy the elution. The MIEX resin dose clearly affected the nitrate adsorption, where the maximum adsorption per unit of resin volume was 10 mL-resin/L. The following major anions in order reduced the nitrate adsorption: SO_4^{2-} > CO_3^{2-} >Cl^- > HCO_3^-. However, humic acid did not have a clear effect on nitrate removal. The experimental results using ground water verified that the MIEX resin can be used as a new nitrate removal technique for water treatment.

KEYWORDS:
Nitrate, Drinking water, MIEX, Groundwater

INTRODUCTION

Groundwater is the vital water source all over the world. If pollution exists in the groundwater, then the difficulty and cost in governing these problems are challenging to solve. In particular, nitrate contamination not only affects the surface but also the groundwater, which is becoming an increasingly more important world problem[1,2]. Groundwater is being contaminated by both human and animal wastes, excessive use of chemical fertilizers and industrial wastewaters; all of which elevate nitrate concentrations[3].

This issue has been garnering more and more attention[4-7]. Excessive nitrate levels can cause several health problems. The effect of nitrate itself is described as primarily toxic. A high intake causes abdominal pains, diarrhea, vomiting, hypertension, increased infant mortality, central nervous system birth defects, diabetes, spontaneous abortions, respiratory tract infections, and changes to the immune system, which is compromised due to reactive nitrite ions via intestinal bacteria. Nitrate has been implicated in methemoglobinemia, particularly in infants less than six months of age[8,9]. Methemoglobin (MetHb) is formed when nitrite (for our purposes, formed from the endogenous bacterial conversion of nitrate from drinking water) oxidizes ferrous iron in hemoglobin (Hb) into ferric form. MetHb cannot bind with oxygen, and the condition of methemoglobinemia is characterized by cyanosis, stupor, and cerebral anoxia. Symptoms include an unusual bluish gray or brownish gray skin color, irritability, and excessive crying in children at moderate MetHb levels and drowsiness and lethargy at higher levels.

To protect consumers from the adverse effects associated with high nitrate intake, nitrate consumption should be limited, and therefore, standards have been established [10-12]. According to TSE 266, WHO, EC standards, drinking water must contains no more than 50 mg/L of nitrate, and the EPA established a maximum contaminant level of 45 mg/L. The European Community recommends levels less than 25 mg-N/L [13]

The magnetic ion exchange (MIEX®) resin, which was jointly developed by Orica Watercare, Commonwealth Scientific Industrial Research Organization and the South Australian Water Corporation, is a strong base anion exchange resin with magnetic properties that can be used to remove negatively charged materials from water [14,15].

In this paper, the adsorption properties of MIEX for nitrate removal were investigated. Column performances of the resin for nitrate removal from aqueous solutions and ground water were also studied.

MATERIALS AND METHODS

Underground water sample was taken from Xuzhou city in Jiangsu province of China.

The magnetic ion exchange resins were kindly provided by the China Agent of the Australian company Orica

Watercare. This magnetic ion exchange resin is a strong basic anion resin with a macroporous, polyacrylic matrix and is typically used with chloride as the exchangeable ion. The first advantage of the MIEX resin is the high surface area of the resin beads, which can be used to facilitate ion exchange in mixed or fluidized bed reactors at extremely low resin concentrations and short detention times. Moreover, the magnetic properties of the resin beads result in the beads forming agglomerates that settle rapidly or fluidize at high hydraulic loading rates, which results in small unit process footprints. The physical properties and specifications of the MIEX resin are given in Table 1. The functional groupings of the MIEX resin are quaternary ammonium, which has a high selectivity for nitrate.

TABLE 1
Typical physical and chemical indicators of the magnetic resin

Humidity	60-65%
Wet superficial density	Approximately 1.15 g/mL
Granulometry	Approximately 180 μm
Exchangeable ion	Cl^-
Skeleton	Polypropylene cross-linked with DVB of the macroporous type
Functional groupings	Quaternary ammonium
Pore size	Majority less than 10 nm
Limits of pH	1-14

Reagents. Humic acid, sodium sulfate, sodium nitrate, sodium carbonate, sodium chloride, sodium bicarbonate, and cellulose acetate membrane (0.45 μm) are the chemicals used in this study (analytic reagent grade) and purchased from Zhongdong Chemical Reagent Company (Nanjing, China).

Experimental apparatus and equipment. An ultraviolet spectrophotometer, coagulation test mixer, magnetic stirrer, peristaltic pump, pure water machine, ion chromatography, scanning electronic microscope, Fourier transform infrared spectrometer, specific surface area and pore size analyzer were all used in this study.

EQUILIBRIUM STUDIES

The equilibrium studies were conducted in batch mode. A fixed dosage (10 mL) of the MIEX resin was added into a set of beakers that contained 1000 mL of nitrate at different concentrations (5, 10, 15, 20, and 30 mg/L). Then, the beakers were sealed with parafilm and kept on a digital display stable temperature magnetic stirrer (78HW-1). The slurries were mixed at a constant agitation speed of 120 rpm. The aqueous samples were removed at preset time intervals, and the solid adsorbent was separated from the mixture using a 0.45-μm cellulose acetate membrane. Then, the amount of nitrate ions remaining in the filtrate was determined. To compare the equilibrium process with the initial nitrate concentrations, similar equilibrium experiments were performed at different temperatures (288 K, 289 K). In these experiments, the pH of the nitrate solution remained the same. All the experiments were performed in triplicate, and the average values are reported herein.

The Langmuir adsorption isotherm model (Eq. (1)) is valid for monolayer sorption on a surface with a finite number of identical sites and can be described by

$$Q_e = \frac{Q_0 \mathrm{b} C_e}{1 + bC_e} \quad (1)$$

where Ce is the equilibrium concentration (mg/L), Qe the amount adsorbed at equilibrium (mg/g), and Q_0 and b are the Langmuir constants related to the capacity and energy of adsorption, respectively. The Langmuir adsorption isotherm model can be rearranged as follows:

$$\frac{C_e}{Q_e} = \frac{1}{Q_0 b} + \frac{C_e}{Q_0} \quad (2)$$

The Langmuir adsorption isotherm plot and the linear plot of C_e/Q_e vs. C_e indicate the applicability of the Langmuir adsorption isotherm [14-16].

The Freundlich model, which is an indicator of the surface heterogeneity of the sorbent, is given by

$$Q_e = K_f C_e^{1/n} \quad (3)$$

The Freundlich equation can be linearized by a logarithmic transfer:

$$\log Q_e = \log K_f + \frac{1}{n} \log C_e \quad (4)$$

where Kf and 1/n are the Freundlich constants related to the adsorption capacity and adsorption intensity, respectively[14-16].

Analysis method. The solution concentration of $NO3^-$- N was determined by an ultraviolet spectrometer. The solutions of sulfate, chloride ion, carbonate ions, etc., were determined by ion chromatography. Before these ions were determined, the ion chromatography used gradient elution to remove the impurities at a fixed washing speed of 1.0 mL/min. Firstly, 30.0 mmol/L of NaOH flowed for 2 minutes. Afterwards, 5 mmol/L of NaOH flowed through the machine for 5 minutes. Finally, 30

mmol of NaOH was used to wash the chromatographic column for 3 minutes. A 1-ml insoluble sample was then obtained via a cellulose acetate membrane (0.45 μm). After filtration, the sample was poured into a chromatographic column, and a curve appeared after 10 minutes of analysis. The ion species were determined by the different retention times, and the ion concentrations were determined by the peak area.

RESULTS AND DISCUSSION

The quality of raw water. The quality of water used in the test is shown in Table 2. The water was typical nitrate-polluted groundwater, with a concentration of approximately 18 mg-N/L. Generally, the ground water hardness is higher than that of surface water, and thus, the concentration of carbonate ions and bicarbonate ions will significantly affect nitrate removal. The major organics are humus at a low concentration level, and the measured the DOC was approximately 5 mg/L.

TABLE 2
Test result of water quality

pH	Turbidity	NO_3^--N (mg/L)	SO_4^{2-} (mg/L)	Cl^- (mg/L)	CO_3^{2-} (mg/L)	HCO_3^- (mg/L)	DOC(mg/L)
7.3-7.8	0.47-0.65	17.4-29.5	50.5-62.3	25.6-35.6	-	156.8-261.5	0.6-0.8

For further investigate the variation regularity of the nitrate, the contents of nitrate in the raw water were examined monthly during the phase of 2010.1-2013.12, the results was shown in figure1.

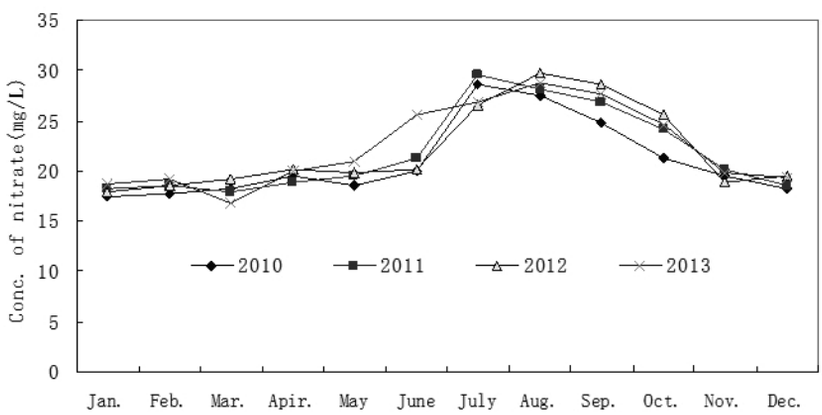

FIGURE 1
Variation of the nitrate's content in the groundwater with time

As shown in fig.1, the content of nitrate in the groundwater was mainly around 20mg/L, which was higher than the recommended value of WHO(10mg/L). In addition, the content was relatively stable for the investigated several years. However, there existed a similar variation regularity as to the month's value in one year. The content of nitrate was relatively higher in June, July, August and September than other months, the reason may lies in the derivation of nitrate in the groundwater. Xuzhou city lies in the core zone of Huang-Huai-Hai Plain, which is the typical Cultivated Region of China. Due to higher rate of fertilizer application, a mount of residual nitrogen existed in the soil. When rain fall into ground, some nitrate may dissolve into the groundwater, which cause the higher concentration of nitrate in rainy season (June, July, August and September).

Adsorption isotherm. The adsorption isotherm is a relationship curve that describes the nitrate adsorption characteristics when adsorption equilibrium is reached at a constant temperature [14-16]. The adsorption isotherm typically provides several insights into the sorption mechanism, surface properties and affinity of the adsorbent. The results of the adsorption equilibrium of nitrate for the

MIEX resin at 288 K and 298 K are given in Figure 2. The equilibrium data were fitted by the Langmuir and Freundlich isotherm models in Table 3.

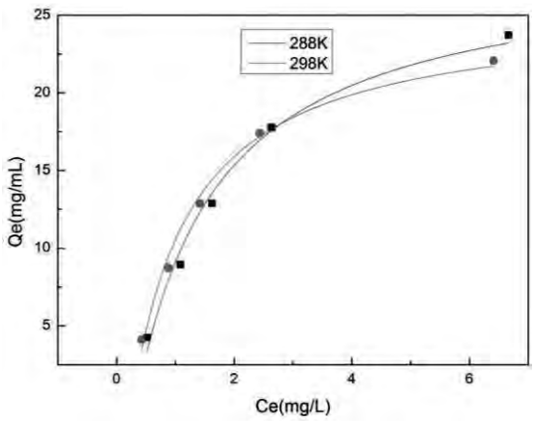

FIGURE 2
Fitted Langmuir adsorption isotherms of nitrate on the MIEX resin

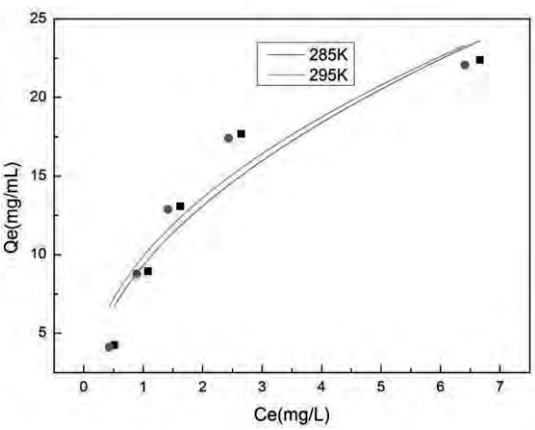

FIGURE 3
Fitted Freundlich adsorption isotherms of nitrate on the MIEX resin

TABLE 3
Constants and correlation coeficients of the Langmuir and Freundlich isotherm models

Models		Constants			R^2
Langmuir	288K	$Q_e = \frac{Q_0 b C_e}{1 + bC_e}$	Q_0=13.27 mg-N/L	b=0.64	0.985
	298K		Q_0=13.63 mg-N/L	b=0.75	0.977
Freundlich	288K	$Q_e = K_f C_e^{1/n}$	K_f=8.7	1/n=0.52	0.884
	298K		K_f=7.2	1/n=0.52	0.878

The results show that the adsorption of nitrate on the MIEX resin agreed well with the Langmuir isotherm. The

Langmuir model explains that only monolayer adsorption occurs on the surface of the MIEX resin in the process of removing nitrate.

Effect of resin dose. To determine the optimum amount of resin dosage that can completely remove nitrate from aqueous solutions, a batch-mode sorption study was performed using various amounts of resin. The prepared initial nitrate concentration was 20 mg-N/L. Figure 4 shows the removal of nitrate as a function of resin dosage. In general, an increase in resin dosage increased the percentage removal of nitrate; however, the greatest removal rate per unit of volume was obtained at a dosage of 10 mL MIEX.

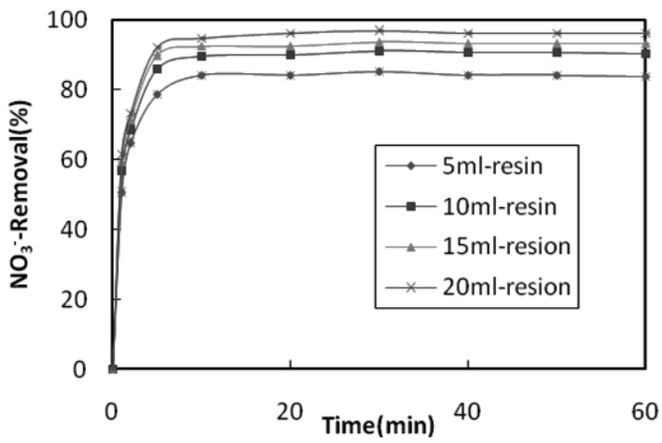

FIGURE 4
Effect of resin dose on the removal of nitrate ions from an aqueous solution.

Effect of bed volume. The preliminary column studies were prepared using a model solution of 20 mg-N/L. The solution was passed through the column at a constant speed. The breakthrough curve of nitrate obtained using the MIEX resin is given in Figure 5. Outflow was collected in a container, and after determining the volume and concentration of the solution, the exchange capacity was calculated as 12.62 mg-N/L, which agrees with the conclusion from the Langmuir isotherm.

Solutions with varying NaCl concentrations were prepared to regenerate the MIEX resin, which had been saturated with nitrate. The nitrate adsorption on the resin was in contact with various concentrations of NaCl solutions. The results are given in Figure 6. As seen in Figure 6, the elution of nitrate increased as the NaCl concentration increased; however, at a concentration greater than 0.6 M NaCl, the tendency is inconspicuous, and the achieved regeneration rate is approximately 92%.

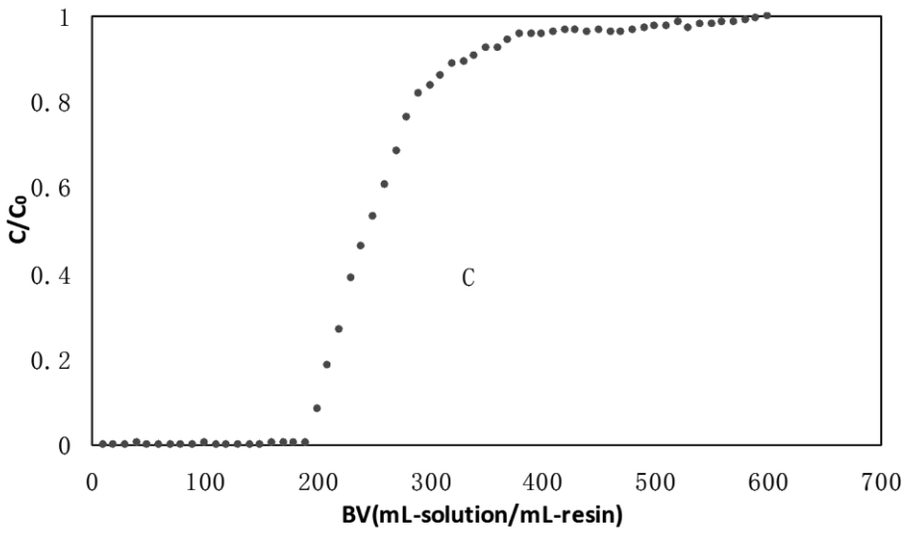

FIGURE 5
Breakthrough curve of nitrate obtained by the MIEX resin

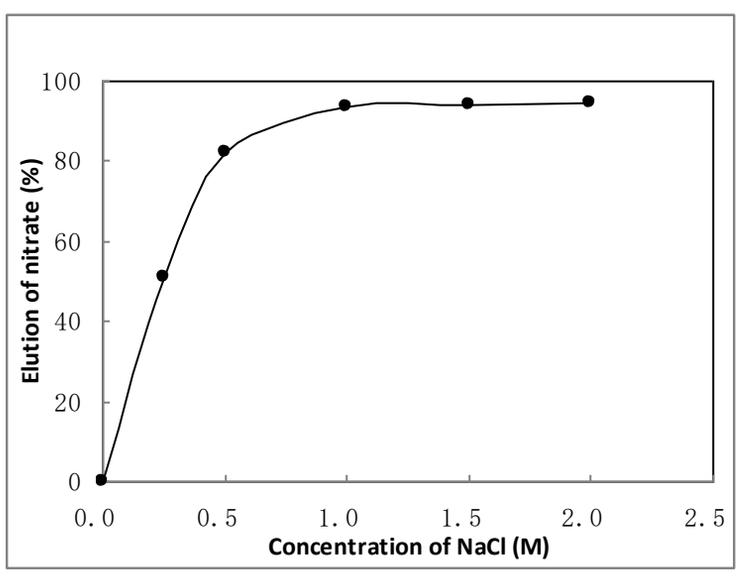

FIGURE 6
Effect of NaCl concentrations on NO3--N removal

Effect of coexisting anions. A variety of inorganic anions at high concentrations, such as sulfate, carbonate, chloridion, and bicarbonate, are often present in ground water. In this study, the effects of different anions (SO42-, CO32-, Cl- and HCO3-) on nitrate removal were investigated by varying the type of anion with the same equivalent concentration ratio to nitrate. The results are shown in Figure 7. The initial concentration of nitrate was 20 mg-N/L in all the experiments.

The two sulfate ions, the carbonate ions and the chloride and bicarbonate ions significantly affected the breakthrough curves of nitrate. Interactions between nitrate ions and the ions on the MIEX resin were hindered in the presence of coexisting anions. The breakthrough point of nitrate shifted more with the presence of sulfate ions than that in the presence of other coexisting ions at the same equivalent concentration, which is mostly related to the charges of the ion. For carbonate ions, not only to they compete with nitrate in the solution, they can also change the pH of the solution, which can affect the ability of the MIEX resin to remove nitrate. As the concentration of chloride increases, the original equilibrium is broken and

clearly shifts towards removing less nitrate. In short, the coexisting anions negatively affect the ability of the MIEX resin to remove nitrate because the exchange sites on the MIEX surface are limited, and therefore, the coexisting anions are in direct competition with the nitrate. It can also be observed in Figure 7 that the impact of each type of anion on the nitrate removal is different and can be ordered as follows: SO_4^{2-} >CO_3^{2-}>Cl^- >HCO_3^-

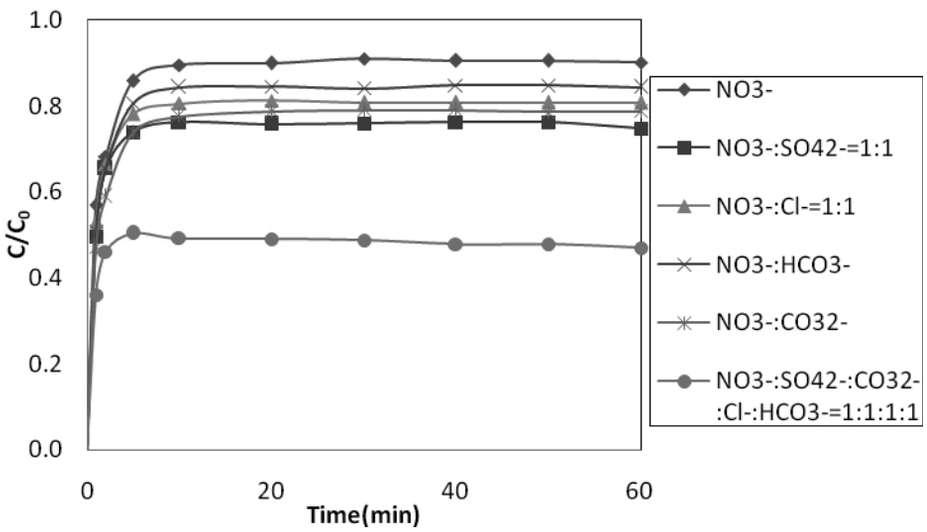

FIGURE 7
Effect of sulfate, carbonate, bicarbonate and chloride ions on NO_3^--N removal by the magnetic resin

Effect of natural organic matter. Natural organic matter (NOM) has a significant impact on water quality. Humic acid (HA) is a naturally occurring macromolecular organic matter, which is ubiquitous at low concentrations in ground water. MIEX resins have been shown to be effective for HA removal [17].

In this study, the HA concentrations of the prepared solution were 1.0, 1.5, and 2.0 mg/L. The results of the HA effect on nitrate removal are shown in Figure 8. The initial concentration of nitrate was 20 mg-N/L in all the experiments. The almost coinciding curves indicate that HA did not have a clear effect on removing nitrate compared with the coexisting anions removal by the MIEX resin. It is thus feasible that MIEX resins can be used to remove nitrate in ground water.

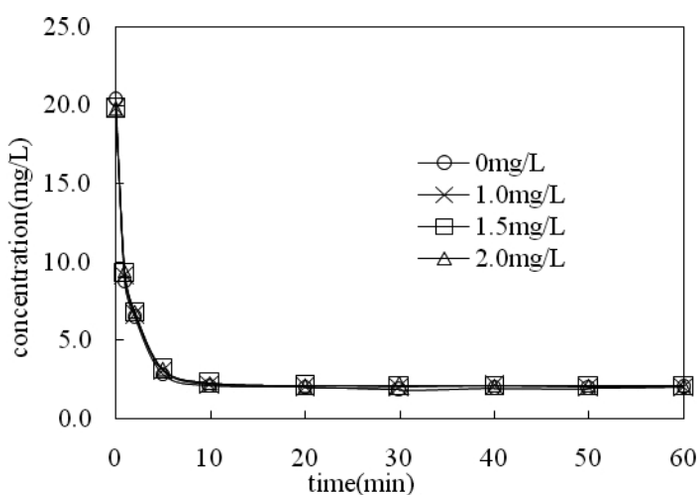

FIGURE 8
Effect of organic on NO_3^--N removal by the magnetic resin

Column removal of nitrate from ground water. The test parameters are shown in Table 4. The results of the column removal of nitrate from ground water are shown graphically in Figure 9. As seen in Figure 9, nitrate was successfully removed from ground water containing other anionic species, such as bicarbonate, chloride and sulfate ions. In the cycling test, after 9 cycles, the curve became level, where the bed volume was approximately 500BV; approximately 60% of the nitrate was removed. The outflow quality satisfies the standards for drinking water.

TABLE 4
Test parameters

Column diameter	Expansion rate	Flow	MIEX initial dosage	MIEX refresh
5 cm	100%	0.25 L/min	300 mL	15 mL/0.5 h

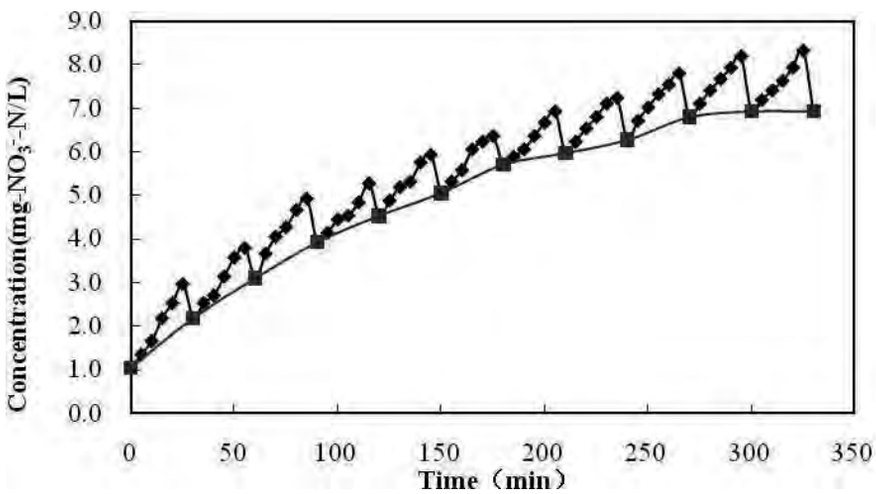

FIGURE 9
Test result of groundwater cycling

CONCLUSION

In this study, the removal of nitrate from aqueous solutions was investigated using MIEX resins. Nitrate content of groundwater in Xuzhou city was about 20mg/L, especially higher than 25mg/L in rainy season. The removal of nitrate increased as the resin dose increased. The adsorption process obeys the Langmuir isotherm. The impact of each type of anion on the nitrate removal is different with the following order: SO_4^{2-} >CO_3^{2-}>Cl^- >HCO_3^-. At low concentrations, natural organic matter has only a slight effect on nitrate removal. The specific resin, the MIEX resin, gave promising results for column-mode removal of nitrate from ground water. As a result, ground water containing a lower nitrate concentration than the permissible level for drinking water is obtained using the MIEX resin. The ion exchange process using MIEX resins can be applied more widely and economically for ground water nitrate removal.

ACKNOWLEDGMENTS

This work was supported by the National Natural Science Foundation of China (51378174, 51438006), the Project Funded by the Priority Academic Program Development of Jiangsu Higher Education Institutions.

REFERENCES

[1] Saccona. P, Leis. A, Marca. A, et al. Determination of nitrate pollution sources in the Marano Lagoon (Italy) by using a combined approach of hydrochemical and isotopic techniques. [J]. Procedia Earth and Planetary Science, 2013, (7)758-761.

[2] Kunkel R, Kreins P, Tetzlaff B. Forecasting the effects of EU policy measures on th e nitrate pollution of groundwater and surface waters [J]. Journal of Environmental Sciences 2010, 22(6) 872-877.

[3] Savci S. Investigation of effect of chemical fertilizers on environment. [J]. APCBEE Procedia, 2012, 1, 287-292.
[4] Goberna M., Podmirseg S.M., Waldhuber S. et al. Pathogenic bacteria and mineral N in soils following the land spreading of biogas digestates and fresh manure.[J] Applied Soil Ecology, 2011, (49)18-25.
[5] Milmile S. N.,.Pande J. V, Karmakar S,et al. Equilibrium isotherm and kinetic modeling of the adsorption of nitrates by anion exchange Indion NSSR resin.[J]. Desalination, 2011, 276 (1-3) 38-44.
[6] Devadas A, Vasudevan S, Epron F. Nitrate reduction in water: Influence of the addition of a second metal on the performances of the Pd/CeO_2 catalyst. [J]. Journal of Hazardous Materials, 2011,185 (2-3), 1412-1417.
[7] Rogers. K.M., Nicolini. E, Gauthier. V. Identifying source and formation altitudes of nitrates in drinking water from Réunion Island, France, using a multi-isotopic approach. [J]. Journal of Contaminant Hydrology, 2012, (138-139) 93-103.
[8] Bryan N. S., Alexander D. D., Coughlin J.R. Ingested nitrate and nitrite and stomach cancer risk: An updated review. [J] Food and Chemical Toxicology 2012, (50)3646-3665.
[9] Xu Jiang, Hao Zhiwei, Xie Chunsheng, et al. Promotion effect of Fe^{2+} and Fe_3O_4 on nitrate reduction using zero-valent iron.[J]. Desalination, 2012, 284, 9-13.
[10] Ayyasamy P. M, Rajakumar S, Sathishkumar M,et al. Nitrate removal from synthetic medium and groundwater with aquatic macrophytes[J]. Desalination, 2009,242 (1-3):286-296.
[11] Hekmatzadeh A A, Karimi-Jashani A, Talebbeydokhti N,et al. Modeling of nitrate removal for ion exchange resin in batch and fixed bed experime nts[J].Desalination,2012,284:22-31.
[12] Xiaolei Fan, Franch C., Palomares E., et al. Simulation of catalytic reduction of nitrates based on a mechanistic model.[J] Chemical Engineering Journal, 2011, (175)458-467.
[13] Bae S, Jung J, Lee W. The effect of pH and zwitterionic buffers on catalytic nitrate reduction by TiO2-supported bimetallic catalyst [J]. Chemical Engineering Journal, 2013, (232)327-337.
[14] Liu C., Chen W., Cao Z., et al. Removal of Algogenic Organic Matter by MIEX® pre-treatment and its Effect on Fouling in Ultrafiltration. Fresenius Environmental Bulletin, 2010, 19(12b): 3118-3124.
[15] Liu C., Chen W., Hou W. N, et al. Performance of MIEX Pre-treatment to treat AOM and Metabolites in Tai-hu Water Source. Fresenius Environmental Bulletin, 2011, 20(4a): 1057-1062.
[16] Lei Ding, Huiping Denga, Chao Wu. Affecting factors, equilibrium, kinetics and thermodynamics of bromide removalfrom aqueous solutions by MIEX resin [J]. Chemical Engineering Journal, 2012, (181-182) 360-370.
[17] Tang Y, Lian S, Guo H, et al. Adsorptive characteristics of perchlorate from aqueous solutions by MIEX resin [J]. Colloids and Surfaces A: Physicochem. Eng. Aspects, 2013 (417) 26-31.
[18] Nguyen T V, Zhang R, Vigneswaran S,et al. Removal of organic matter from effluents by Magnetic Ion Exchange (MIEX®)[J]. Desalination, 2011, 276:96-102.
[19] Ghouas H, Haddou B, Kameche M, et al. Extraction of humic acid by coacervate: Investigation of direct and back processes [J].Journal of Hazardous Materials, 2012, 205-206:171-178.

Received: **02.07.2015**
Accepted: **03.01.2016**

CORRESPONDING AUTHOR

Chen Wei
Hohai University
Ministry of Education
Key Laboratory of Integrated Regulation and Resource Development Shallow Lakes
1 Xikang Road
Nanjing 210098 - P. R. CHINA

e-mail: cw5826@hhu.edu.cn

by PSP Volume 25 – No. 1/ 2016, pages 325-336 Fresenius Environmental Bulletin

IRRIGATION OPTIMIZATION BY THE USE OF FUZZY LOGIC TECHNOLOGY

[1]Hussein Bizimana, [2]Muhammad Yaqub, [3]Osman Sönmez, [4]Beytullah Eren, [5]Fatma Demir

[1, 4] Sakarya University, Environmental Engineering, 54187 Serdivan/Sakarya, Turkey
[2, 3, 5] Sakarya University, Civil Engineering, 54187 Serdivan/Sakarya, Turkey

ABSTRACT

The aim of this study was to develop a Fuzzy Inference System (FIS) to optimize the water requirements as per standards for irrigation purposes.There are three major inputs in FIS including water quality, field capacity and water quantity while one output named as optimized irrigation. Firstly water quality FIS was developed by using three important such as electrical conductivity (EC), pH and sodium absorption ratio (SAR) with excellent, good, permissible and harmful membership functions for inputs and same for output. To create fuzzy inference system for water quantity, five membership functions were developed as very low, low, middle, high and very high considering the discharge of water available in the Sakarya River, Turkey and low, medium and high as fuzzy membership functions for field capacity were also developed. To complete the FIS of the study, very low, low, medium, high and very high fuzzy membership functions were developed for a fuzzy optimized irrigation as the output of the system and the main finding of the study. In this study a practical solution based on FIS is presented for Sakarya River Basin in Turkey to meet irrigation objectives locally. The findings clearly indicate that fuzzy logic method may successfully interpret complex conditionsto classify the optimized irrigation with respect to water quality, water quantity discharge and soil filed capacity. The developed fuzzy model was validated by using data collected from Pamukova, Doğançay and Adatepe three monitoring stations of Sakarya River during 1993-2013.

KEYWORDS:
Electrical conductivity (EC), Fuzzy logic, Field capacity, Irrigation, pH (Hydrogen proton concentration), SAR (Sodium Absorption Ratio), Optimization.

INTRODUCTION

Irrigation is defined as replenishment of soil water storage in plant root zone using methods other than natural methods such as precipitation [1]. Irrigation has seen its roots in the history of mankind since earliest beginning. Irrigation helps to reduce the uncertainties, particularly the climatic uncertainties in agriculture practices [2].

For example equatorial part of the world which mostly was used to have high rainfall intensities has a mean rainfall of 900 mm a year and according to projections rainfall would be of 630 mm a year which may speed up the expansion of dry area. In this regard, many plants must adapt themselves to new climate conditions and improve their management strategies of available water resource; highly water optimizing irrigation methods are required [2].

Therefore, it is necessary to implement efficient irrigation systems by using strategies of water resource to assure food safety in regions and environmental sustainability [3]. With other strategies, approximations to modeling studies happened to required and require nowadays new abstractions allowing improving our nature predictive skills and consequently striving for a sustainable development [4]. The application of system known as intelligent systems in Agricultural Sciences studies is relatively recent in comparison to other knowledge areas like electronic engineering, electric engineering, mechatronics and telecommunications.

Huang [5] insured that intelligent systems are an integration of biological structures with computing techniques. In agricultural sciences worldwide fuzzy logic is used for modeling and prediction, control, classification, fuzzy clustering, rule based inference, multisensory data fusion, optimization [6]. Finally, this work aimed to implement fuzzy logic system as a tool to evaluate the optimization of irrigation systems from a set of indicators for efficient use of water.

MATERIAL AND METHODS

This research was carried out by students from two departments, civil and environmental

engineering departments. To be able to implement the projects, some important indexes in irrigation such as: Water Quality, Field capacity, Water Quantity Discharge were studied and used for the simulated project.

Water quality. Both irrigation water quality and appropriate irrigation management are significant factors to maximize crops production. The quality of irrigation water may influence soil physical conditions as well as crops yield, although all other parameters and practices are optimal. According to American Public Health Association, irrigation water characteristics differ with the source of the water [7]. Therefore, testing of irrigation water is a critical and important parameter that must be consider before the selection of crop type and soil site [8]. The quality of some water sources may change significantly with time or during certain periods such as in dry or rainy seasons [9] so it is recommended to take more than one sample and must be analyzed, in different time periods. The parameters which determine the irrigation water quality are divided in to three categories: chemical, physical and biological. In this study, chemical properties of the irrigation water are discussed. The chemical characteristics of irrigation water refer to the content of salts in the water as well as to parameters derived from the composition of those salts in the water parameters such as EC/TDS (Electrical Conductivity/ Total Dissolved Solids), SAR (Sodium Adsorption Ratio) alkalinity i.e pH and hardness.

Field capacity. Field Capacity (FC) is the amount of water in the soil layer that can be easily used by the plant for its growth different from gravitational water and wilting point[3]. FC for irrigation is an important factor providing an idea about water requirement of soil in order to avoid over irrigation which may cause leaching and lodging of soil layers [5].

Water quantity discharge. Without a certain source of water irrigation can't be performed and if the source is with seasonal regime (means available only for some time) also irrigation performance through a year is very critical [10].It means the source of water for irrigation is very important for plants growth, their production and sustainable use of water.

Design of fuzzy inference system (fis). In case of imprecise, vague, incomplete, ambiguous or noisy input information of water sources where by global climate change nowadays it is very hard to predict with exactitude about rainfall, hence FIS is a tool that allows arriving at a conclusion in a simple way, trying to simulate expert knowledge of a human being. In this work three variables such as water quality, field capacity and water quantity were considered to develop FIS. Firstly water quality was analyzed by an environmental engineering team, keeping pH, Electrical Conductivity (EC) and Sodium Absorption Ratio (SAR) as inputs.
After the simulation and set of membership function for water quality, it was used as input along with field capacity and water quantity for the final simulation to optimize irrigation system. Membership functions of different inputs were fixed in FIS according to literature review and interview with field experts and their experiences in civil engineering based project. For this purpose, Fuzzy Logic toolbox in Matlab was used to construct FIS, wheremembership's ranges, active rules functions are chosen; likewise, response functions are analyzed and the system is verified.

Design steps. A Mamdani-type fuzzy logic system was designed based on the tool Fuzzy Logic Toolbox of Matlab to evaluate the optimization of the irrigation system according to the indexes of outputs as Water Quality (WQ), Water Quantity (WaQ) discharge and Field Capacity (FC) and the final output of the system as optimized irrigation.

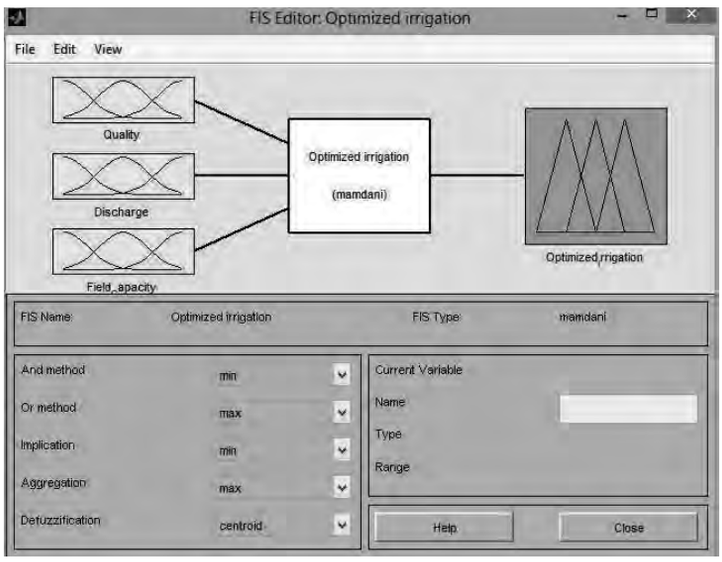

FIGURE 1
General view of the final simulation

FUZZY SIMULATION OF SYS. INPUTS

Water Quality (WQ) simulation with fuzzy logic. All the studies pertaining to assess the quality of water for irrigation consider two parameters, namely Sodium Absorption Ratio (SAR) and Electrical conductivity (EC). In this project we considered pH as a third variable to optimize the irrigation more accurately. The Water Pollution Control Regulation (WPCR) Turkey provided the standards for irrigation water quality, in which permissible limits for SAR, EC, pH and other elements are specified, and from those acceptable limits it helps to create the membership functions for our simulated Water Quality system in fuzzy logic and at the end we were able to use specified membership functions in the final fuzzy simulation which will provide us optimized irrigation.

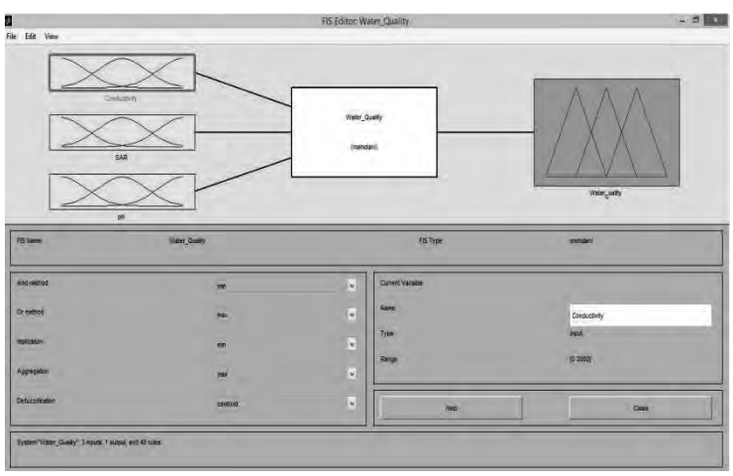

FIGURE 2
General view of a simulation for Water Quality

The membership functions are created on the basis of already done research work in this area and by consultation with our teachers. There are different parameters that are important to control the irrigation water quality and vary from place to place so, it is difficult to develop a standard model

that will be suitable for all water sources. In such circumstances it is the need of hour to develop the various models by keeping all the factors in view and fuzzy logic provide a good solution in such situations.

Electrical conductivity (EC). Salinity is a measure of the Total amount of salts in the water is known as salinity and if high than permissible range causes to reduce water availability to the crop and affect the yield. Electrical conductivity (EC) or Total Dissolved Solids (TDS) tests are two means of measuring salinity and EC is a helpful and reliable tool for the measurement of water salinity or TDS. The total amount of TDS should be used together with SAR.The properties of the soil, the ground water and the landscape interact with the salinity of the irrigation water to either increase or decrease the salinity hazard [11].The salinity is a main problem related to irrigation water quality which refers to the total amount of dissolved salts but does not indicate which salts are present. High level of salts in the irrigation water reduces water availability to the crops and causes yield reduction. Above a certain threshold, reduction in crop yield is proportional to the increase in salinity level.

The salinity effects are generally evidenced by reducing transpiration rates and proportionally related growth, and producing smaller plants. The salinity also alters the soil ability to retain nutrients, thus suppressing plant growth [12].Different crops vary in their tolerance to salinity and therefore have different thresholds and yield reduction rates [13]. The most common parameters used for determining the irrigation water quality, in relation with its salinity, are EC and TDS. In this study conductivity ranges from 479- 1208 µmho/cm.

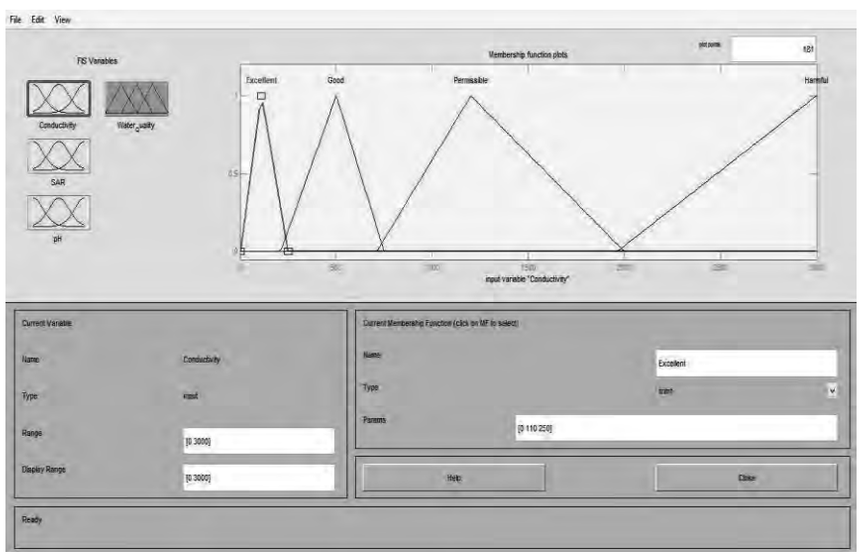

FIGURE 3
Membership functions selected for Electrical Conductivity (EC) simulation.

pH. It is an index of hydrogen ions concentration (H^+) in water and defined as –Log (H^+) and ranges from 0 to 14 where, lower than 7 is considered to be acidic and higher than 7 is considered to be basic while pH of 7.0 is considered to be neutral. In irrigation water quality could be basic that mainly affects the availability of nutrients while acidic water is also important to know how quickly irrigation is required, to keep the metals in dissolved form and make them more readily available. In irrigation process normal pH range is from 6.5 to 8.4. The pH ranges of obtained data from Sakarya River are 7.61-8.63. Unusually low pH may cause acceleration of corrosion in irrigation systems while pH above 8.5, causes to form insoluble salts of calcium and magnesium, leaving sodium as leading ion in the solution. Alkaline water intensifies solidity of soil [14].

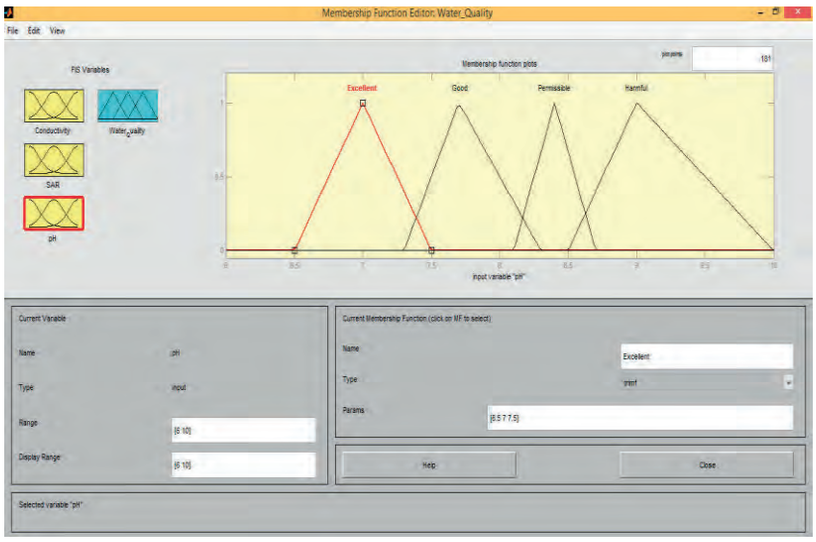

FIGURE 4
Membership functions selected for pH simulation.

Alkalinity is the measure of a water's capacity to neutralize acids (consume H+ ions), is the sum of the amounts of bicarbonates (HCO_3^-), carbonates (CO_3^{2-}) and hydroxide (OH^-) in water and is expressed as mg/l or meq/l $CaCO_3$. Alkalinity buffers the water against sudden changes in pH and if the alkalinity is too low, then any addition of acidic fertilizers will immediately lower the pH. The main characteristic of irrigation water system is alkalinity as it affects the pH of root medium not the water.

Sodium Absorption Ratio (SAR). Sodium is adsorbed and becomes attached to soil particles causes to harden and compact soil structure and increasingly impervious to water penetration. The soil salinity is a severe factor that causes various abnormal, physio-morphological and biochemical changes, delay germination, high seedling mortality, poor crop stand, stunted growth [15] as literature stated crops production is seriously affected by soil salinity [16].The breakage of soil structure is commonly caused by continuous application of high SAR water in irrigation because salts effecting osmotic relationship between the root and the soil moisture [17].The salinity level is the primary water quality parameter mostly applicable in irrigation systems because the soil structure and crop yield is affected by the salts quantity.

Direct effect of salts on plant growth may be classified into three categories: (i) a decrease in osmotic potential of the soil solution causes to reduces available water to plants, (ii) a deterioration in physical structure of soil happens due to which water permeability and soil aeration are decreased, and (iii) an increase in concentration of certain ions that have an inhibitory effect on plant metabolism [18]. Salinity is predicted from a recurrent measurement of total dissolved solids (TDS). TDS is a measure of salts present in water, counting organic and very small suspended particles [19].

Irrigation water whether of good quality or not, can have effect on plant growth, for example poor irrigation water quality with excess salt can damage plants in various ways.Water with high amount of salts can hinder the conversion of ammonium salts to nitrate by nitrifying micro-organisms in soil when used for irrigation.Furthermore, most of tomato plants are more sensitive to salt during seed germination, seedling growth and when flowering or fruiting. The seed and seedling stages are vulnerable not only because the plant structures are immature and delicate, but also because tiny roots system draw moisture and nutrients from the soil surface where salts tend to concentrate [20].

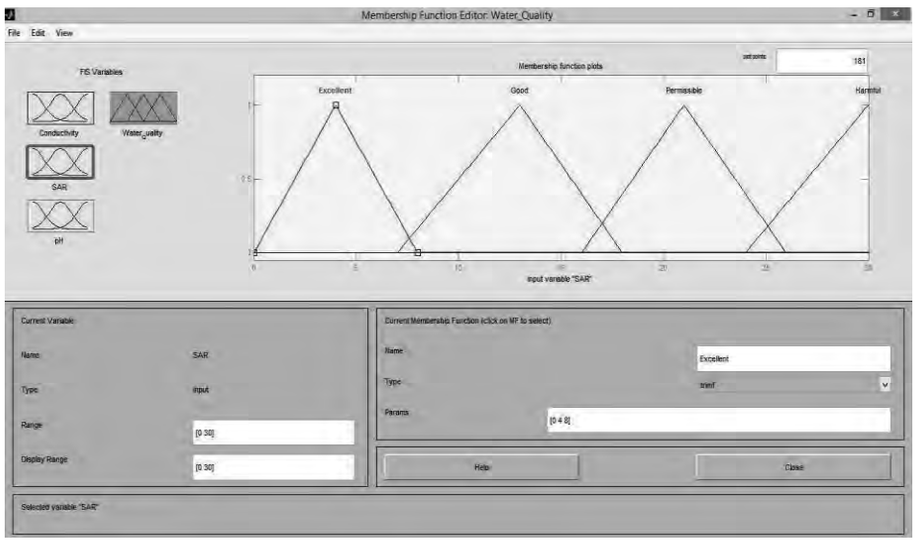

FIGURE 5
Membership functions selected for Sodium Absorption Ration (SAR) simulation.

The sodium problem is reduced if the amount of calcium plus magnesium is high as compare to sodium. This relation is called the sodium adsorption ratio (SAR) and it is a calculated value from the formula:

$$SAR = \frac{Na}{\sqrt{\frac{Ca+Mg}{2}}}$$

SAR was calculated from the data obtained from Sakarya River and found it ranges 2.35-14.50 in this study.

The combination of EC,pH and SAR as inputs in Mamdani fuzzy inference system basis on literature reviews, international and local standards, expert's advices and was found important parameters to assess the output water quantity with accuracy.

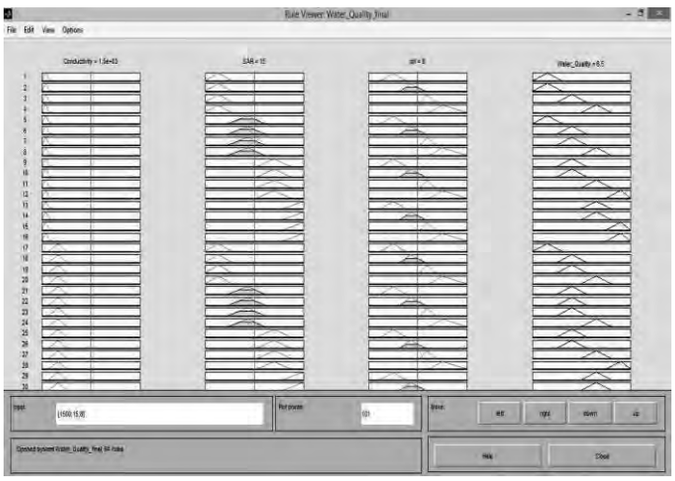

1. If (Conductivity is Excellent) and (SAR is Excellent) and (pH is Excellent) then (Water_Quality is Excellent) (1)
2. If (Conductivity is Excellent) and (SAR is Excellent) and (pH is Good) then (Water_Quality is Excellent) (1)
3. If (Conductivity is Excellent) and (SAR is Excellent) and (pH is Permissible) then (Water_Quality is Good) (1)
4. If (Conductivity is Excellent) and (SAR is Excellent) and (pH is Harmful) then (Water_Quality is Permissible) (1)
5. If (Conductivity is Excellent) and (SAR is Good) and (pH is Excellent) then (Water_Quality is Excellent) (1)
6. If (Conductivity is Excellent) and (SAR is Good) and (pH is Good) then (Water_Quality is Good) (1)
7. If (Conductivity is Excellent) and (SAR is Good) and (pH is Permissible) then (Water_Quality is Good) (1)
8. If (Conductivity is Excellent) and (SAR is Good) and (pH is Harmful) then (Water_Quality is Permissible) (1)
9. If (Conductivity is Excellent) and (SAR is Permissible) and (pH is Excellent) then (Water_Quality is Good) (1)
10. If (Conductivity is Excellent) and (SAR is Permissible) and (pH is Good) then (Water_Quality is Good) (1)
11. If (Conductivity is Excellent) and (SAR is Permissible) and (pH is Permissible) then (Water_Quality is Permissible) (1)
12. If (Conductivity is Excellent) and (SAR is Permissible) and (pH is Harmful) then (Water_Quality is Harmful) (1)
13. If (Conductivity is Excellent) and (SAR is Harmful) and (pH is Excellent) then (Water_Quality is Permissible) (1)
14. If (Conductivity is Excellent) and (SAR is Harmful) and (pH is Good) then (Water_Quality is Permissible) (1)
15. If (Conductivity is Excellent) and (SAR is Harmful) and (pH is Permissible) then (Water_Quality is Harmful) (1)
16. If (Conductivity is Excellent) and (SAR is Harmful) and (pH is Harmful) then (Water_Quality is Harmful) (1)
17. If (Conductivity is Good) and (SAR is Excellent) and (pH is Excellent) then (Water_Quality is Excellent) (1)

FIGURE 6
Water Quality Fuzzy system rules.

Field Capacity (FC) simulation with fuzzy logic. Field Capacity (FC) is the amount of water in the soil layer that can be easily used by the plant for its growth different from gravitational water and wilting point which are the amounts of water in the soil layer but which can't be used by the plant for its growth [21]. The FC for irrigation is very important because it is the one giving the idea of how much water to be added to the soil in order not to over irrigate which may cause leaching and lodging of soil layers [21]. It is measured in height inch per ha, where height inch times hectare that is 100 m^3. Hence in the simulation in order to keep the use of SI units a range from 0 to 300 cubic meters was used as FC is ranging from 0 to 300 cubic meters in crisp sets and correspond to low, middle and high in fuzzy sets.

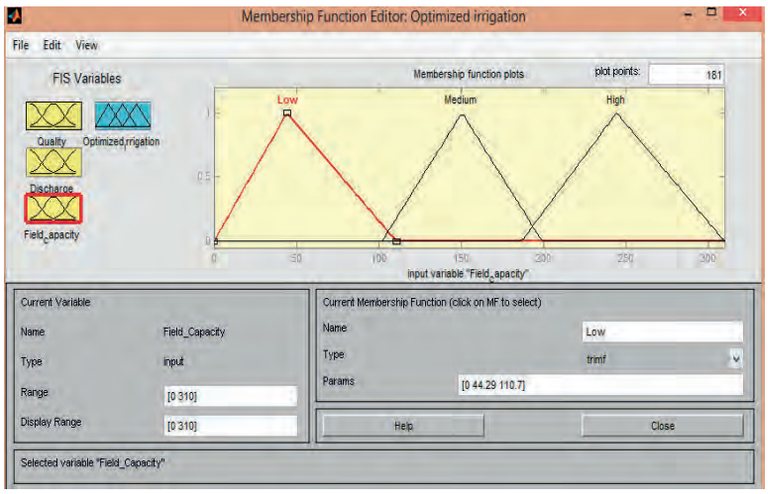

FIGURE 7
Membership functions selected for FC

Water quantity (discharge) simulation with fuzzy logic. This index gives the information on the amount of water available from the source that will be used to irrigate. If the amount is very low, low, medium, high or very high then the irrigation will be with same membership functions too .With river engineering discharge quantifyingmethods; water which is not flooding the upland of the channel have to be between 0-500 m^3/s.

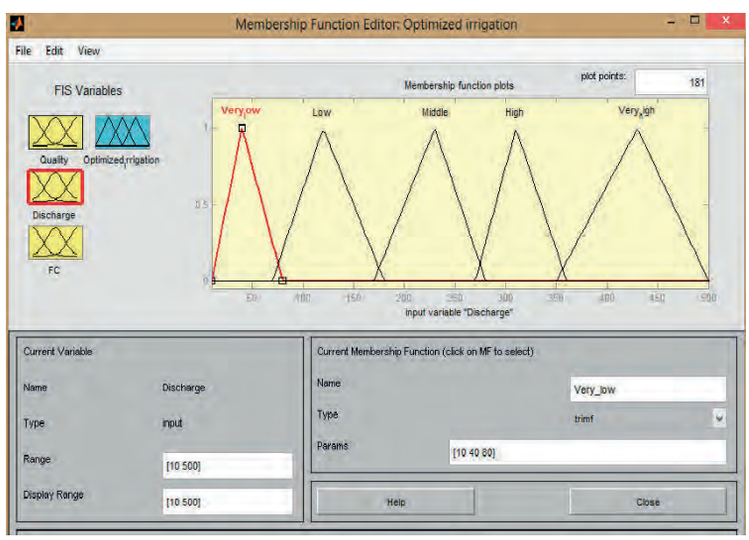

FIGURE 8
Fuzzy simulated Water Quantity

RESULTS AND DISCUSSION

MATLAB Fuzzy Inference System (FIS) was applied in present study to optimize irrigation by using three inputs and one output variable. Different membership functions were given to FIS for evaluation of results.FIS Tool of MATLAB showed precise and reliable resultsand those results will be helpful in decision making. The output of the system was the optimized irrigation, the membership functions were defined by the help of literature review and experts advices in the field. A set of 53 system rules and surface view were presented. The fuzzy simulated irrigation water

(Fig.9), FIS rules (Fig.10 and Fig.11) and the FIS rules surface review (Fig.12) are shown below.

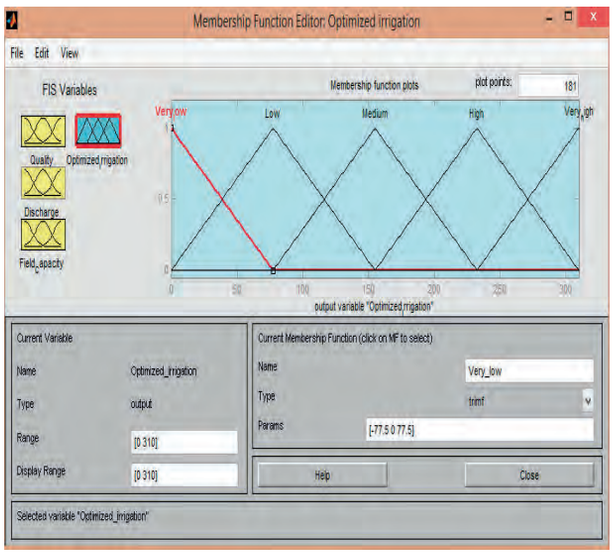

FIGURE 9
Fuzzy simulated irrigation water.

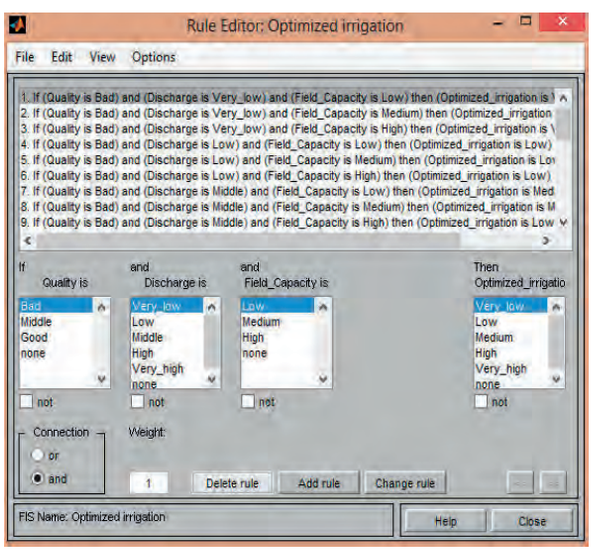

FIGURE 10
FIS rules.

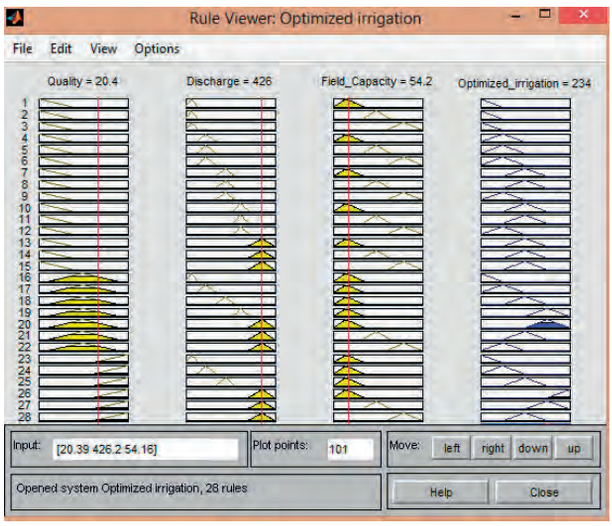

FIGURE 11
FIS and rules and output minimums

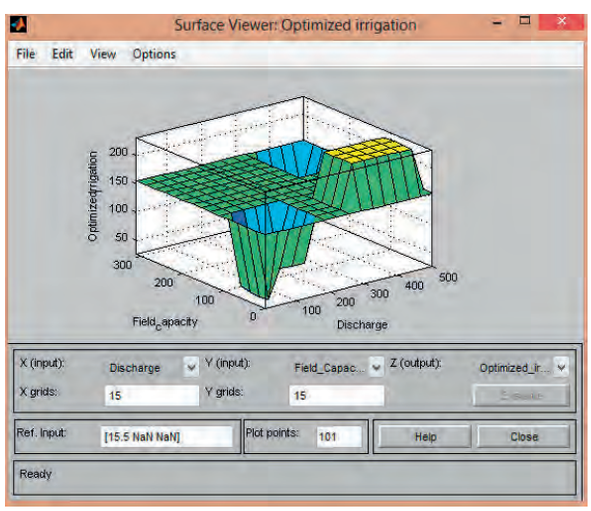

FIGURE 12
FIS rules on a surface view

DISCUSSION

An optimized irrigation system is proposed, taking into consideration indicators of optimization use of water resource and tools of intelligent systems like fuzzy logic. The results of this study showed that fuzzy set theory is more reliable and flexible option in irrigation optimization as compare to CROPWAT 8.0 and SAPWAT 8.1 because it deals with different hydrological uncertainties. It is helpful in decision making regarding irrigation optimization in vague conditions without relying on Evapotranspiration equations.

In the present study, a Fuzzy Inference System (FIS) has been developed to classify the water for irrigation purposes. The membership functions were developed for three significant parameters such as SAR, EC and pH and rules were fired to arrive at a Fuzzy Inference System for assessing irrigation water quality. In last studies initially two parameters were used to develop the fuzzy logic but in this work it was further improved by incorporating one more significant parameter namely pH. Thus, the developed fuzzy model showed more reliable results for irrigation water classification and avoided the vagueness in the decision making.

The set of indicators proposed is a basis to compare the optimization and fuzzy simulation of the irrigation systems which can help in the identification of infrastructure which can be replaced by the use of fuzzy controllers in irrigation and drainage control, detection of needs for technology transfer in research and the improvement of the system operation.

This system of fuzzy logic was implemented in order to estimate the optimization of an irrigation system based on the index of output per available Water Quality, Field Capacity and available water supply. This type of tool implemented in the irrigation sector and specifically in the evaluation of optimization of irrigation systems are innovative and could be helpful in decision making for agricultural professionals.

REFERENCES

[1] Allen, R.G., Pereira, L.S., Raes, D., and Smith, M, "Crop evapotranspiration: Guidelines for computing crop requirements", Food and Agriculture Organization (FAO), Rome, Italy, 1998.

[2] Ruiz, J. Gutiérrez, and J. Fernández, "A fuzzy controller with an optimized defuzzification algorithm," IEEE Micro, pp. 1–10, Dec. 1995

[3] Burman, R. and L.O. Pochop, 2004. Evaporation evapotranspiration and climatic data. Elsevier, Amsterdam.

[4] Ioslovich, I. P. Gutman and I. Seginer, 2006. A non linear optimal greenhouse control problem with heating and ventilation. Optimal Control Applications and Methods, 17: 157-169.

[5] P. Javadi Kia, A. Tabatabaee Far, M. Omid, R. Alimardani and L. Naderloo, "Intelligent Control Based Fuzzy Logic for Automation of Greenhouse Irrigation System and Evaluation in Relation to Conventional Systems" World Applied Sciences Journal 6 (1): pp. 16-23, 2009.

[6] Harrison, L. P., "Fundamental"s concepts and definitions relating to humidity", In Wexler, A (Editor) Humidity and moisture, Vol. 3, Reinhold Publishing Co., New York, 1963.

[7] APHA., (2005).Standard methods for examination of water and wastewater. 21st ed. American Public Health Association, Washington DC,USA

[8] Shahimasi, E and V.Kashuta., (2008).Irrigation water quality and its effects upon soil.Tirana Agricultural University,Tirana,Albania BALWOIS 2008-ohrid,Republic of Macedonia

[9] Islam, M. S. and S.Z.K.M. Shamsad,(2009).Assessment of irrigation water qualityof Bogra District in Bangladesh.Bangladesh J. Agril.Res.34(4) 597-608.

[10] Murray, F. W., "On the computation of saturation vapor pressure", J. Appl. Meteor. 6: 203-204, 1967.

[11] Peterson, H.G., (1999). Water Quality and Micro-irrigation for Horticulture http://www.safewater.org/PDFS/resourceswaterqualityinfo/Resource_Water_Qual_Facts.pdf

[12] Guodie, A. S., (1992).the human impact:man's Role in environmental change –black well publishing press,Oxford, England

[13] Bauder, T. A., R. M. Waskom and J. G. Davis (2007), Irrigation water quality criteria. Colorado State University, Us Department of Agriculture. Research Report, 7/03.

[14] Mass., (1990).Crop salt tolerance. In: Agricultural Assessment and Management Manual. K.K. Tanji (ed.). ASCE, New York. pp. 262-304. pH and Alkalinity

[15] Ahmad, M.S.A., Ashrafm, M., Ali, Q., 2010. Soil salinity as a selection pressure is a key determinant for the evolution of salt tolerance in blue panicgrass (Panicumantidotale Retz.). Flora 205, 37–45.

[16] Munns, R., 2002. Comparative physiology of salt and water stress. Plant Cell Environ. 25, 239–250.

[17] Malash, N., T.J Flowers and R. Ragab., (2005). The Effect of irrigation systems and water management practies using saline and non-saline water on tomato production. Agric. Water. Manage, 78:25-38. Department of Agriculture Engineering, University of Cape Coast, Ghana.

[18] Yeo, A.R.: Molecular biology of salt tolerance in the context of whole plant physiology. J. Exp. Bot., 49, 915-929 (1998).

[19] Grattan, S.R. and C.M. Grieve: Salinity-mineral nutrient relations in horticultural crops. Sci. Hort., 78, 127-157 (1999).

[20] Podmore, C., 2009. Irrigation salinity – causes and impacts. PRIMEFACT for profitable, adaptive and sustainable primary industries-937.October.

[21] Jensen, M.E., R.D. Burman and R.G. Allen. 1990. Evaporation and Irrigation Water Requirements. ASCE Practice No. 70. ASCE, NY, NY.

Received: **01.07.2015**
Accepted: **22.12.2015**

CORRESPONDING AUTHOR

Hussein Bizimana
Sakarya University
Civil Engineering Department
54187 Serdivan/Sakarya – TURKEY

e-mail: mutembealhussein@gmail.com

by PSP Volume 25 – No. 1/ 2016, pages 337-344 Fresenius Environmental Bulletin

BACTERIA IMMOBILIZED ON MICROPOROUS POLYURETHANE TO ENHANCE CAMPUS SEWAGE TREATMENT IN CONSTRUCTED WETLANDS MICROCOSMOS

Yuanyuan Shao[1, 2, 3], Haiyan Pei[1, 2], Wenrong Hu[1,2], Panpan Meng[1], Zheng Li[1], Yang Chen[1]

[1] School of Environmental Science and Engineering, Shandong University, 250061 Jinan, Shandong Province, China
[2] Shandong Provincial Engineering Centre on Environmental Science and Technology, 250061 Jinan, Shandong Province, China
3 School of Municipal and Environmental Engineering, Shandong Jianzhu University, 250000 Jinan, Shandong Province, China

ABSTRACT

Nutrient removal in constructed wetland (CW) microcosms planted with *Phragmites* and inoculated with microporous polyurethane immobilized with denitrifying bacteria was evaluated as a possible treatment for campus sewage. Constructed wetlands microcoms (CWMs) inoculated with bacterial suspension (S2) or bacteria immobilized on microporous polyurethane (S3) showed significant improvements in COD, total nitrogen (TN) and total phosphorus (TP) removal efficiency compared with S1 CWMs without bacteria. Microporous polyurethane immobilized denitrifying bacteria (S3 CWMs) had a lasting effects of pollutants removal. The removal efficiency of S3 was 75% for chemical oxygen demand (COD_{Cr}), 69% for total nitrogen (TN), 75% for ammonia-N (NH_4^+-N) and 78% for total phosphorus (TP). The removal of NO_3^--N reached up to 91%. The effulent concentration of TN, TP, NH_4^+-N and COD_{Cr} achieved the GB/T18921-2002 standard (China) or the GB18918-2002 standard (China) for Class I-A criteria in 5 days. Characteristics of bacteria on microporous polyurethane and immobilization methods of bacteria will be investigated in our later research. The CWs would be a cost-effective measure for pullutants removal of sewage by means of bioaugmentation.

KEYWORDS:
Constructed wetlands; campus sewage; bioaugmentation; wastewater treatment; Paenibacillus lautus CL-5; pollutants removal; denitrification

INTRODUCTION

The lack of water resources is emerging as a critical concern for the future development of China [1]. Groundwater is currently of critical shortage due to the significantly increasing usage [2]. A large number of untreated sewage directly flow into the natural rivers and lakes, cause problems including eutrophication and the generation of undesirable odors, and ultimately threaten surface and ground water quality and human health [3-4]. Campus sewage as a domestic wastewater started to be paid attention and reused after treatment in China [5]. Constructed wetlands (CWs) has proved to be a good alternative for wastewater advanced treatment with the consideration of efficiency and cost [6]. They have been designed and constructed to utilize the natural processes involving wetland plant, soil and associated microbial assemblages to assist in treating 20 different types of wastewater [7]. Pollutant removal in CWs is typically associated with specific microbial functional groups [8]. Nitrification of nitrobacteria coupled with denitrification of denitrifying bacteria is usually the most significant N removal mechanism in the CW [9].

Pollutant-degrading microorganisms are often introduced into a contaminated environment to accelerate bioremediation and meet effluent standards. Immobilized microorganism technology began to be used in wastewater treatment due to the increasingly serious water pollution problems from 1970s. Two kinds of carrier material, macroporous polyurethane and haydite, seeded with the same bacteria were used to compare the efficiency of chemical oxygen demand (CODCr) and ammonium nitrogen (NH4+-N) treatment from wastewater. The reductions in the overall NH4+-N and CODCr supported by macroporous polyurethane were higher than supported by haydite [10]. The macroporous structure of the polyurethane and its active chemical groups are suitable for the immobilization of microorganisms [11].

A denitrifying and phosphorus bacterium Paenibacillus lautus CL-5 was isolated from the sludge of the double sludge switching-sequencing batch reactor (DSSBR), with a high removal efficiency of NO3--N [12]. The objectives of this study were: (1) to investigate the treatment performance of wastewater from a university campus area using constructed wetland microcosms system; (2) to judge whether the application of immobilized bacteria on macroporous polyurethane could promote sewage treatment in constructed wetlands.

MATERIALS AND METHODS

Experimental setup and design. Constructed wetland microcosms (CWM) were designed according to a surface flow style and established under a rain shelter outdoors in March, 2014 in Shandong province, northern

China (36.65' N, 117.0' E). The climate is cold and dry during spring and winter, with wetter and warmer summers (annual precipitation of 670.7 mm, and an average temperature of 14.3 ◦C). Eighteen wetlands were constructed using circular barrel-type polyethylene containers, each of which had a surface area of 0.19 m^2 and a depth of 65 cm, with an outlet at the bottom (Fig.1).

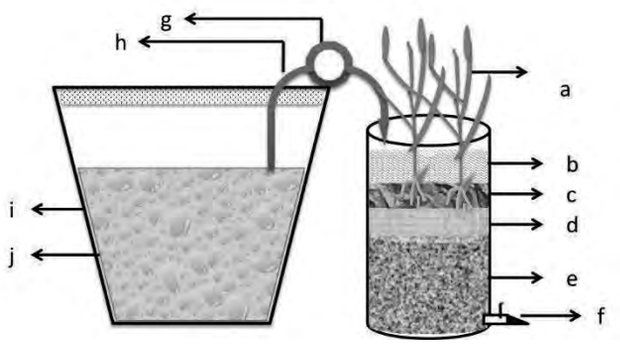

FIGURE 1
Schematic diagram of a constructed wetland microcosm (CWM)
(a: *Phragmites australis*; b: water; c: soil; d: washed sand; e: detritus; f: water outlet; g: influent pump; h: perforated PVC pipe; i: tank; j: campus sewage)

The microcosm wetland filter beds consisted of three successive layers from top to bottom with soil to a height of 10 cm, washed river sand (particle size <2 mm, mainly Si_2O_3, Al_2O_3, Fe_2O_3) to a height of 5 cm, detritus, which was used as the supporting layer, to a height of 35 cm. Water depth was kept at 15 cm above the soil surface. One vertical, perforated PVC pipe (65 cm in length and 3 cm in diameter) was inserted into the substrate in the middle of each wetland system to enable measurements of various physical and chemical parameters. Each CWM system held 15 L water when filled.

Composition of campus sewage. The raw wastewater was delivered from the sewage system of a university and contained in a tank using a wet pump to deliver. The influent was a combined wastewater, from toilets, bathrooms, etc. During the entire operation period, the characteristics of raw wastewater exhibited both diurnal and seasonal variations mainly due to infiltration to the sewage system especially in wet weather and changes in student populations during weekends and holidays. The ranges of major water quality indices were as follows: COD (chemical oxygen demand) 123-143 mg/L, NH_4^+-N (ammonia-N) 27-38.2 mg/L, TN (total nitrogen) 51.9-66.3 mg/L, TP (total phosphorus) 2.35-2.49 mg/ and NO_3^--N (nitrate-N) 4.57-4.65 mg/L.

Preparation of bacterial solution and microporous polyurethane immobilized with bacteria. *Paenibacillus lautus* CL-5 (Chinese patent ZL 201310033056.2) was isolated in the School of Environmental Science and Engineering in Shandong University and preserved in the China Center for Type Culture Collection (CCTCC) with the number of M 2012227. Enrichment medium (pH 7.2-7.4) was prepared by dissolving 10 g Tryptone, 5 g Yeast extract and 10 g NaCl in 1L of distilled water. This medium (200 mL) was autoclaved for 30 min at 121 ◦C. Two mediums were separately inoculated with 4 mL of bacterial suspension stored in the fridge. Then one medium of the two above was added several microporous polyurethane. The two mediums were incubated at 35 ◦C for 24 h in the next step. The bacterial solution was measured by Most-Probable-Number (MPN) analysis before using [13].

Experimental operation. Nine constructed wetlands microcosms were used for the sewage treatment. The following treatment designations were used: campus sewage without bacteria (1) or with bacteria solution (2) or with microporous polyurethane immobilized with bacteria (3), which resulted in the following specific treatments: S1 = *Phragmites* planted but no bacterial inoculation, S2 = *Phragmites planted* with bacterial solution inoculation, S3 = *Phragmites* planted with microporous polyurethane immobilized with bacteria.

Each group consisted of three microcosm units and three replicates. Before experiments were performed, plants were watered every 2 days by the sewage to maintain the water level at the soil surface. The water level was gradually increased to 15 cm and held at that level for 2 weeks to acclimate before the experiment started. A fill-and-draw batch mode was applied to influent from April 5 to April 30, 2014. The units were manually filled with the campus sewage from a tank containing. The water depth above the soil surface was 15 cm with 15 L sewage in total. Units were re-filled with fresh sewage immediately after drainage. Bacterial solution (150 ml) with a total bacterial population of $2.1x10^8$ cfu/ml was inoculated into

S2 microcosms. An injector (Chinese patent number ZL 20112485865.3) was used to add an equivalent volume of inoculum into the units at three different depths below the water surface (0.20 m, 0.35 m and 0.45 m). Seven microporous polyurethane immobilized with a total bacterial population of $3.2x10^8$ cfu/ml were set on the surface of soil surrounding by the plants in S3 microcosms.

Water samples were collected using a syringe 10 cm below the water surface of each unit every day to test the water quality achieved the GB/T18921-2002 standard (China) or the GB18918-2002 standard (China) for Class I-A criteria. Five days were considered as a test period. After five days, the units were manually drained through a valve at the bottom and immediately re-filled with fresh test solution. Five periods were set up during the whole experiments (Period Ⅰ, Ⅱ, Ⅲ, Ⅳ, Ⅴ). Estimated evapotranspiration was compensated for with distilled water for each wetland unit during the experiment.

Water quality monitoring. The following laboratory analyses were performed on water samples: COD_{Cr}, NH_4^+-N, TN, TP, NO_3^--N. All parameters were determined according to standard methods [14]. TN, NH_3-N and NO_3^--N were evaluated by a UV-Vis spectrophotometer (Shimadzu Instrument Co. Ltd., UV-2450, Japan). Treatment efficiency was calculated as the percentage of removal for N and P as follows: Removal efficiency (%) = (Ci − Ce)/Ci × 100 where Ci and Ce are the influent and effluent concentrations in mg/L.

RESULTS AND DISCUSSION

Removal of COD_{Cr}. In a constructed wetland system, organic matters will be absorbed by the soil and the plant growth, then broken down by the microbes through fermentation and/or respiration, and mineralized as a source of energy or assimilated into biomass [15]. Therefore, the removal efficiency of COD always gradually decreased because of adsorption saturation. As shown in Figure 2, COD_{Cr} actually had good removal effects in the three treatments (S1, S2, S3). However, COD_{Cr} removal efficiency did not present many varies during the whole persistent five periods in the control group S1 CMWs with an approximate removal efficiency of 60%. Denitrifying bacteria solution (S2) and immobilized denitrifying bacteria (S3) had obviously positive influence on COD_{Cr} removal of the campus sewage. Water flow eroded microorganism population sizes during the experiments resulting in gradually declined removal efficiency of COD_{Cr}, from the original 79% to 63% in the S2 CWMs. The effluent concentrations of COD_{Cr} were less than 30 mg/L with the removal efficiency of 76%-82% in S3 CWMs and had met local and national Chinese government standards, i.e, Class I-A criteria of GB18918-2002 (COD_{Cr} ≤50 mg/L) in the entire five periods. These observations confirmed that after 25 days, allochthonous denitrifying bacteria CL-5 isolated from sludge could still well survive in the nature. Increasing bacterial population could affect COD removal in the following ways. Firstly, bacteria consumed organic shortening the hydraulic retention time (HRT). Though organic substrates were not fully degraded, the treated sewage could meet the standard. Secondly, immobilized bacteria on microporous polyurethane could decrease the clogging possibility. This is also responsible for the decrease of COD removal efficiencies.

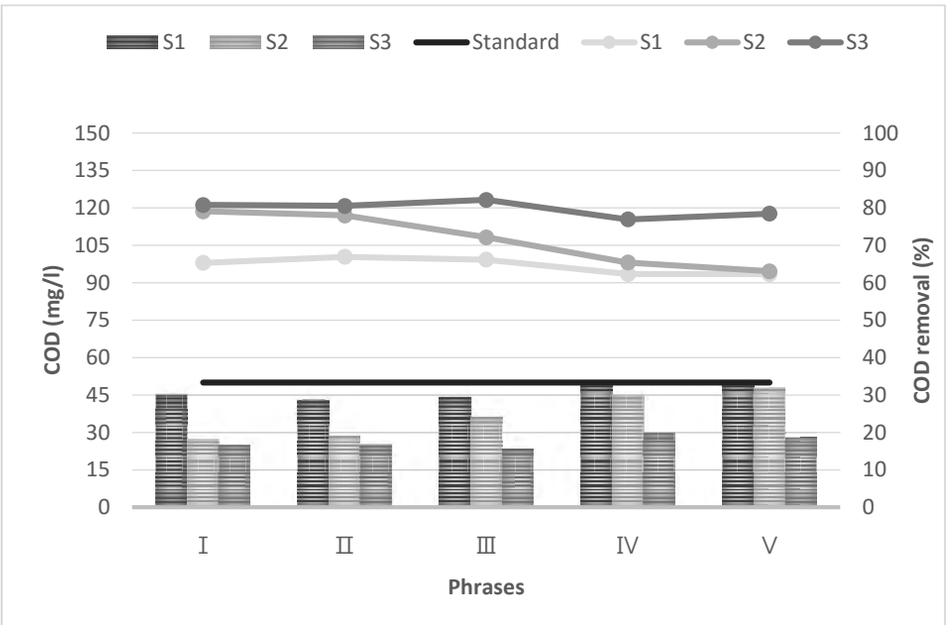

FIGURE 2
Mean chemical oxygen demand (COD_{Cr}) in the outflow of constructed wetland microcosms (CWMs) during five periods (S1: CWMs were without bacterial inoculation; S2: CWMs were inoculated with bacterial solution; S3: CWMs were inoculated with microporous polyurethane immobilized with bacteria; Standard: the GB18918-2002 standard (China) for Class I-A criteria $COD_{Cr} \leq 50$ mg/L)

Removal of TP. Phosphorus transformations in wetlands contain soil accretion, adsorption/desorption, precipitation/dissolution, plant/microbial uptake, etc. Microbial uptake is very fast, but the amount stored is very low [16]. R. Bhamidirnarri found that the mean TP removal efficiency reached to 90% when the influent TP concentration was in the range of 2.5-5.9 mg/L [17]. With respect to the TP removal, the removal efficiency was above 60% in S1 CWMs in five periods. It seems that the wetland system itself did have an effect on P removal in the current study, but the effluent TP of S1 did not meet the standard due to the high concentration of campus sewage (Fig. 3). To some extent, denitrifying bacteria (S2, S3 CWMs) presented a positive effect on P removal. The removal efficiency of TP was gradually declined, from the 80% in the first period to 70% in the fifth period of S2 CWMs. The effluent concentrations of TP were 0.23-0.48 mg/L with the removal efficiency of 78%-84% in S3 CWMs and had met the GB/T18921-2002 standard (China) (TP ≤0.5 mg/L) in the entire five periods. The uptake by microbiota (bacteria, fungi, algae, macroinvertebrates, etc.) is rapid because these organisms grow and multiply at high rates. The amount of microbial also depends on trophic status of the wetland. In less enriched sites the microbial uptake may store more phosphorus as compared to more eutrophic sites. When evaluating a wetland ecosystem to retain P, all these components should be quantified.

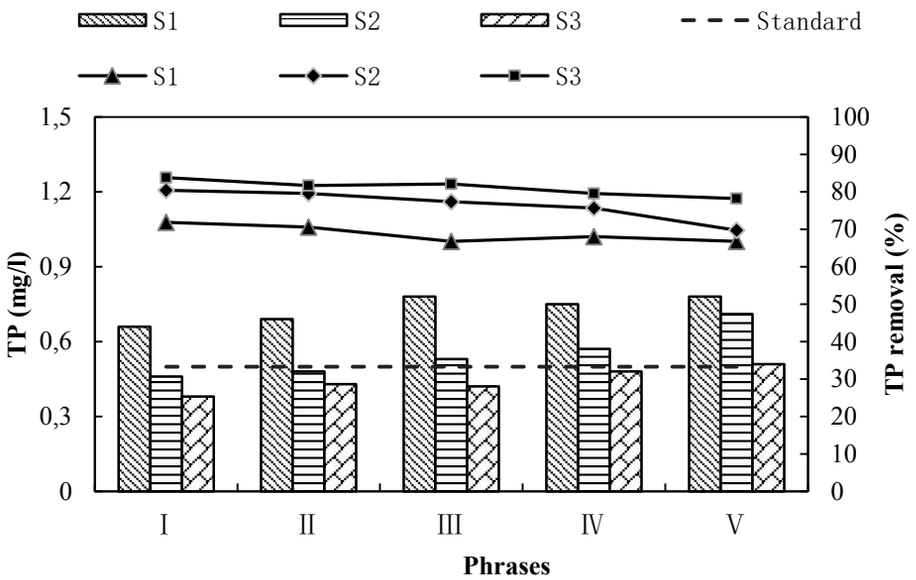

FIGURE 3
Mean total phosphorus (TP) concentration in the outflow of constructed wetland microcosms (CWMs) during five periods (S1: CWMs were without bacterial inoculation; S2: CWMs were inoculated with bacterial solution; S3: CWMs were inoculated with microporous polyurethane immobilized with bacteria; Standard: the GB/T18921-2002 standard (China) TP ≤ 0.5 mg/L)

Removal of N. Nitrogen has a complex biogeochemical cycle with multiple transformations. The most important inorganic forms of nitrogen in wetlands are NH4+-N, nitrite (NO2--N) and NO3--N. The major nitrogen transformations in wetlands are presented as volatilization, ammonification, nitrification, nitrate-ammonification, denitrification etc. All of these transformations are necessary for wetland ecosystems to function successfully. Nitrification is thought to result in the oxidation of NH3-N to NO3--N via NO2--N by autotrophic bacteria under aerobic conditions, while denitrification results in the conversion of NO2--N and NO3--N to volatile N oxides and N2 gas by denitrifying bacteria mostly under anaerobic conditions (Chang et al., 2011; Farhadian et al., 2008; Daniel et al., 2009) [18-20]. As seen in Figure 4, the mean TN (Fig. 4a), NO3--N (Fig. 4b) and NH4+-N (Fig. 4c) concentration and removal efficiency in the outflow of CWMs were shown. Varies of TN and NH4+-N were similar. As the five cycling periods were going on, the NH4+-N removal efficiency was gradually getting worse in S1 with a percentage from 72% to 63% and S2 from 61% to 54%. The effluent concentrations of NH4+-N fluctuated at 8 mg/L with the removal efficiency of 76%-82% in S3 CWMs and closed to Class I-A criteria of GB18918-2002 (NH4+-N ≤8 mg/L) in the entire five periods. The removal rates of NO3--N were in a specific range from 82% to 91% and the effluent concentrations were also kept in a certain range less than 0.8 mg/L in S3 CWMs. Wetlands internal denitrifying bacteria could create a good environment for the denitrification process. Along the experimental periods extended, NO3--N gradually increased and maintained at a higher concentration in S1 and S2 CWMs. The pattern and efficiency of TN removal were partially affected by different N species.

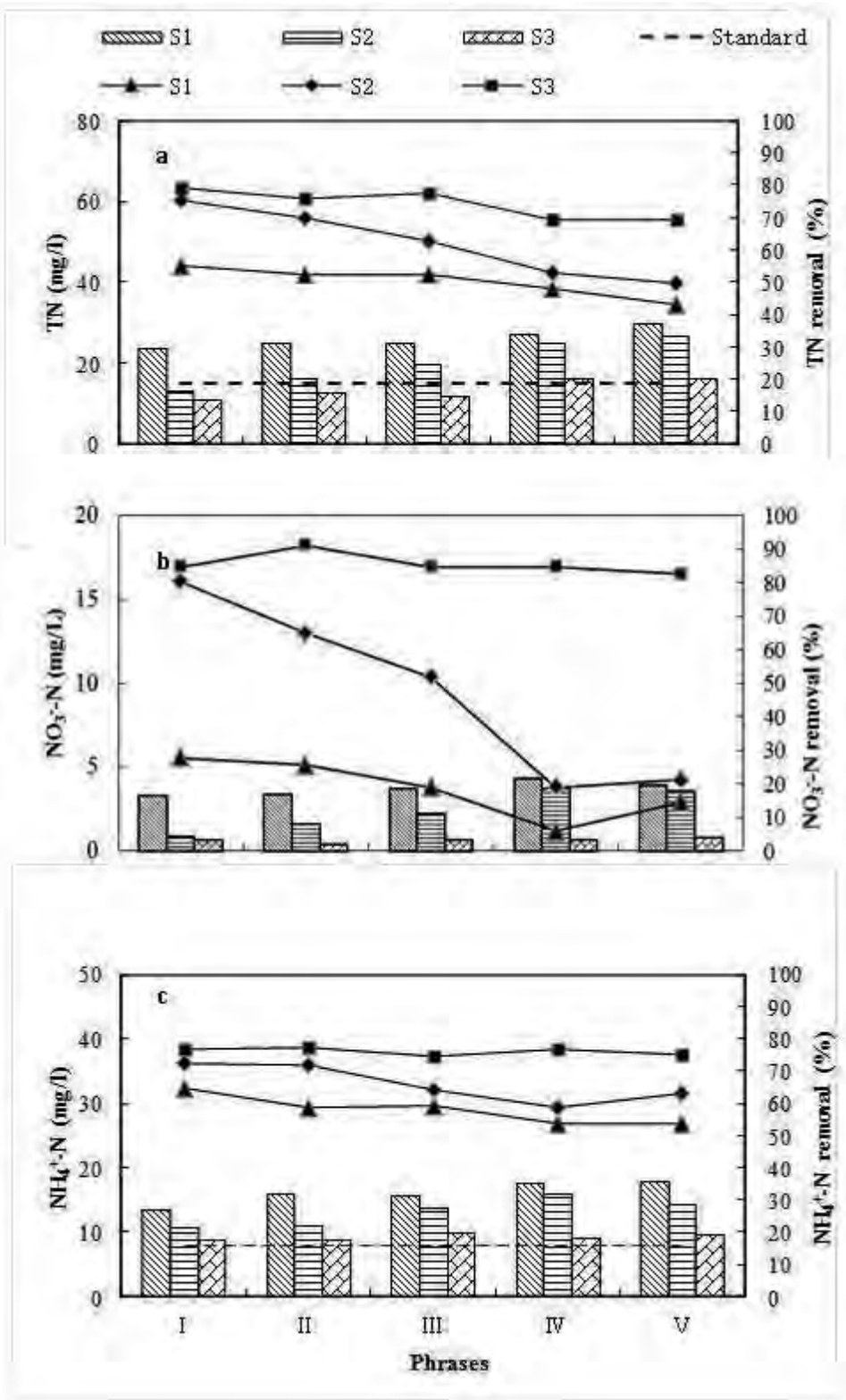

FIGURE 4
Mean total nitrogen (TN), ammonia-N (NH_4^+-N) and nitrate-N (NO_3^--N) concentration in the outflow of constructed wetland microcosms (CWMs) (S1: CWMs were without bacterial inoculation; S2: CWMs were inoculated with bacterial solution; S3: CWMs were inoculated with microporous polyurethane immobilized with bacteria)

NH_4^+-N and NO_3^--N are the dominant types of N in the campus sewage. The effluent concentrations of TN were less than 15 mg/L with the removal efficiency of 78%-84% and had met the GB/T18921-2002 standard (China) (TN ≤15 mg/L) in the previous three periods of S3 CWMs. In the later two periods, the effluent TN concentrations increased slightly. During the experiments the removal efficiency of TN gradually declined from the original 75% to 49% in the S2 CWMs, even it dropped to 43% in the S1 CWMs.

CONCLUSIONS

The experimental results can be summarized as follows: CWMs inoculated with bacteria (S2 and S3) showed significant improvements in COD_{Cr}, TN and TP removal efficiency compared with S1 CWMs without bacteria. Microporous polyurethane immobilized denitrifying bacteria (S3 CWMs) had a lasting effects of pollutants removal. The removal efficiency of S3 was 75% for COD_{Cr}, 69% for TN, 75% for NH_4^+-N and 78% for TP. The removal of NO_3^--N reached up to 91%. The effulent concentration of TN, TP, NH_4^+-N and COD_{Cr} achieved the GB/T18921-2002 standard (China) or the GB18918-2002 standard (China) for Class I-A criteria in 5 days. This study was just a starting research about whether the application of immobilized bacteria could successfully promote sewage treatment in constructed wetlands. Characteristics of bacteria on microporous polyurethane and immobilization methods of bacteria will be investigated in our later research.

ACKNOWLEDGMENTS

This research was financially supported by the Nature Science Foundation of China (51378300); Nature Science Foundation of China (50978156); Nature Science Foundation of Shandong Province (ZR2009BZ007); Key Research Foundation of Shandong Provincial Environmental protection bureau (hcyf0602) and Technology Development Projects of Shandong Province (2009GG2GC06002). The authors thank Tim A. Sheedy for revising the English in the manuscript.

REFERENCES

[1] Qian, Y., Wen, X.H., Huang, X. (2007) Development and application of some renovated technologies for municipal wastewater treatment in China. Frontiers of Environmental Science & Engineering 1(1), 1-12.

[2] Zhang, J., Huang, X., Liu, C.X., Shi, H.C., Hu, H.Y. (2005) Nitrogen removal enhanced by intermittent operation in a subsurface wastewater infiltration system. Ecological Engineering 25, 419-428.

[3] Camargo, J.A., Alonso, A. (2006) Ecological and toxicological effects of inorganic nitrogen pollution in aquatic ecosystems: a global assessment. Environment International 32, 831-849.

[4] Ding, Y., Song, X.S., Wang, Y.H., Yan, D.H. (2012) Effects of dissolved oxygen and influent COD/N ratios on nitrogen removal in horizontal subsurface flow constructed wetland. Ecological Engineering 46, 107-111.

[5] Li, H.B., Li, Y.H., Sun, T.H., Wang, X. (2012) The use of a subsurface infiltration system in treating campus sewage under variable loading rates. Ecological Engineering 38, 105-109.

[6] Truu, M., Juhanson, J. and Truu, J. (2009) Microbial biomass, activity and community composition in constructed wetlands. Science of the Total Environment 407(13), 3958-3971.

[7] Zhang, T., Xu, D., He, F., Zhang, Y.Y., Wu, Z.B. (2012) Application of constructed wetland for water pollution control in China during 1990-2010. Ecological Engineering 47, 189-197.

[8] Green, M.B. (1997) Experience with establishment and operation of reed bed treatment for small communities in the UK. Wetlands Ecology and Management 4, 147-158.

[9] Faulwetter, J.L., Gagnon, V., Sundberg, C., Chazarenc, F., Burr, M.D., Brisson, J., Camper, A.K., Stein, O.R. (2009) Microbial processes influencing performance of treatment wetlands: a review. Ecological Engineering 35, 987-1004.

[10] Jia X., Zhou L., Li Y. (2012) Comparative study of laboratory-scale biological aerated filters based on macroporous polyurethane and haydite carrier materials. Environmental Engineering Science 29 (5), 350-356.

[11] Jiang C.D., Zhi X., Fei, Q.Z. (2012) Treatment of Synthetic Wastewater in a Pre-Denitrification Biofilm Reactor Packed with Polyurethane Media. Energy Procedia 16, 1642-1649.

[12] Li, Z., Pei H.Y., Hu, W.R., Shao, Y.Y., Meng, P.P. (2013) Screening and Characterization of a New Denitrifying Phosphorus-Removal Bacterium. Fresenius Environmental Bulletin 22(10), 2809-2815.

[13] Rowe, R., Todd, R., and Waide, J. (1977) Microtechnique for Most-Probable-Number Analysis. Applied and Environmental Microbiology 33, 675-680.

[14] APHA, (1998) Standard Methods for the Examination of Wastewater, 20th ed., Washington DC. American Public Health Association.

[15] Gelsomino, A., Badalucco, L., Landi, L., Cacco, G. (2006) Soil carbon, nitrogen and phosphorus dynamics as affected by solarization alone or combined with organic amendment. Plant and Soil 279, 307-325.
[16] Vymazal J. (2007) Removal of nutrients in various types of constructed wetlands. Science of the total environment 380 (1), 48-65.
[17] Bhamidimarri, R., Bickers, P.O., Thayalakumaran, N., Hu, Z.B. (2003) Developments in Enhanced Biological Phosphorus Removal (EBPR). New Horizons in Biotechnology, 221-230.
[18] Chang, C.Y., Tanong, K., Xu, J., Shon, H. (2011) Microbial community analysis of an aerobic nitrifying–denitrifying MBR treating ABS resin wastewater. Bioresource Technology 102, 5337-5344.
[19] Daniel, L.M., Pozzi, E., Foresti, E., Chinalia, F.A. (20090 Removal of ammonium via simultaneous nitrification–denitrification nitrite-shortcut in a single packedbed batch reactor. Bioresource Technology 100, 1100-1107.
[20] Farhadian, M., Vachelard, C., Duchez, D., Larroche, C. (2008) In situ bioremediation of monoaromatic pollutants in groundwater: a review. Bioresource Technology 99, 5296-5308.

Received: **25.06.2015**
Accepted: **16.01.2016**

CORRESPONDING AUTHOR

Haiyan Pei
Shandong University
School of Environmental Science and Engineering
250061 Jinan, Shandong Province – CHINA

e-mail: haiyanhup@126.com

by PSP Volume 25 – No. 1/ 2016, pages 345-354 Fresenius Environmental Bulletin

MONITORING LAND USE/LAND COVER CHANGE AROUND A PLAIN RESERVOIR ALONG SOUTH-NORTH WATER TRANSFER PROJECT-EASTERN ROUTE, CHINA

Rui-Juan Wu and Xiu-Feng He*

School of Earth Science and Engineering, Hohai University, No. 1 Xikang Road, Gulou District, Nanjing 210098, P. R. China

ABSTRACT

The implementation of the South–North Water Transfer Project (SNWTP)-Eastern Route triggered construction of new reservoirs and expansion of old reservoirs that inevitably changed land use/land cover in surrounding areas. Taking the Shuangwangcheng (SWC) plain reservoir as a case study, this study aimed to resolve two challenges in land use/land cover change (LUCC) detection: (i) limited classification capabilities with medium-resolution remote sensing images, and (ii) the "salt and pepper" phenomenon observed in classification maps created using traditional pixel-based classification methods. The image fusion algorithm, which combined the nonsubsampled contourlet transform and generalized intensity-hue-saturation (NSCT-GIHS), and object-oriented image classification were utilized to generate high-quality classification maps. Post-classification comparisons were used to obtain LUCC patterns during five periods between 2000 and 2013. The results indicated that significant changes occurred in the SWC reservoir area, including clear increases in the reservoir, rural settlement, and canal classes, but decreases in the salt field class. LUCC was most rapid immediately before and after the SWC reservoir construction. Due to its expansion in August 2010, the SWC reservoir showed the highest land use dynamic degree (LUDD; 16.01%) between 2009 and 2011. Rural settlements increased continuously from 2003 to 2013, and had the highest LUDD (4.41%) between 2011 and 2013, reflecting population migration following the SWC reservoir construction.

KEYWORDS:
South-North Water Transfer Project; Eastern Route; reservoir; land use/ land cover change; object-oriented image classification; image fusion.

INTRODUCTION

Water resource distribution in China is uneven, with sufficient supply in Southern China but a water deficiency in Northern China [1, 2] (Figure 1). To alleviate water shortage in Northern China, the South–North Water Transfer Project (SNWTP), which includes western, central, and eastern routes, was implemented at the end of 2002. It aimed to meet a series of social, economic and environmental requirements, including domestic consumption, hydropower generation, flood prevention, and agricultural irrigation [3]. According to the project plans for the Eastern Route, a large number of reservoirs were constructed or rebuilt along rivers in order to provide a regulated water supply. Along with reservoir construction, the surrounding areas underwent land use/land cover change (LUCC), while local residents were resettled. These changes were essential to facilitate the construction of reservoirs, which were designed to play a positive role in water supply for urban living and agricultural irrigation; however, they also contributed to the deterioration of the surrounding eco-environment [3]. Therefore, there is an urgent need to identify an effective method for the timely monitoring of these changes.

Satellite remote sensing technology is a widely applied and effective tool for detecting LUCC in reservoir regions [4–7]. It has been demonstrated that the exploitation of remote sensing images with low or medium spatial resolution (e.g., Thematic Mapper (TM), Multispectral Scanner System (MSS), and Advanced Spaceborne Thermal Emission and Reflection Radiometer (ASTER) images) can provide meaningful insights into LUCC. However, it has also been shown that high spatial resolution remote sensing images are more appropriate for land use/land cover interpretation when land use types are complex [8]. Only traditional pixel-based image classification methods (e.g., supervised classification and maximum likelihood classification) are described in the literature, and these often display the "salt and pepper" phenomenon on the land use/land cover classification maps produced [8]. In order to solve these issues, this study considered two remote sensing processing approaches: image fusion and object-oriented image classification.

The purpose of this study was to develop an efficient method to investigate LUCC around the Shuangwangcheng (SWC) plain reservoir, situated along the SNWTP-Eastern Route, China. The NSCT-GIHS image fusion method, which combined the nonsubsampled contourlet transform (NSCT) and generalized intensity-hue-saturation (GIHS), the object-oriented image classification method, and manual interpretation were utilized to obtain high-quality land use/land cover classification maps. The LUCC in the SWC region was then analyzed in order to identify the driving forces behind the changes.

MATERIALS AND METHODS

Study area. The SNWTP is a national mega-project aimed at resolving the deteriorating drought problems of Northern China. The project diverts 44.8 billion m^3 of water per year from the Yangtze River to Northern China through three systems: the Western, Central, and Eastern Routes [9]. Among the three routes, the Eastern Route was the first to be built, and was put into operation in December 2002. According to the water diversion plan of the Eastern Route, water from the Yangtze River is first drawn into the Jiangdu hydro-junction, where a huge 400 m^3/s pumping station was built in the 1980s [10]. Due to the topographic difference between the Yangtze and North China plains, pumping stations are used to raise water from the Yangtze River to the Yellow River. Water is then pumped in a northward flow along the Beijing-Hangzhou Grand Canal. On reaching Shandong province, one tributary flows eastward to Weihai and Qingdao cities, while the other flows further north to Tianjin municipality (Figure 1). The Eastern Route extends ~1152 km and is equipped with 23 pumping stations that have a power generation capacity of 454 mega-watts (MW) [9]. The greatest challenge for the Eastern Route is dealing with heavily polluted waters in the Beijing-Hangzhou Grand Canal.

Shandong province is one of the water-starved provinces. In order to provide a timely supply of water during the dry season, several plain reservoirs were constructed, (e.g., the Datun Reservoir and the SWC Reservoir; Figure 1). The SWC reservoir, located in Shouguang city, is an important regulating reservoir along the SNWTP-Eastern Route, the Jiaodong Water Transfer Line, and the Water Diversion Project from the Yellow River into Qingdao. It was initially constructed in March 1972, but then further expanded in August 2010 in order to improve its water storage capacity. Today, its maximum water storage capacity is 61.5 million m^3.

Datasets. In this study, five Landsat satellite images acquired by the United States Geological Survey (USGS) on 2 May 2000, 11 May 2003, 25 April 2009, 2 June 2011, and 30 May 2013 were used. The first three images pre-date the re-building of the SWC reservoir, while the last two relate to periods of re-construction and post-completion, respectively. All images contain <0.2% cloud cover, and their similar dates of acquisition (25 April–2 June) allow for reliable comparisons of land use/land cover classes between different years. For the 2 May 2000, 11 May 2003, 25 April 2009, and 2 June 2011 images, Landsat 7 Enhanced Thematic Mapper Plus (ETM+) bands 1–4 (with 30 m spatial resolution) and 8 (with 15 m spatial resolution), representing the blue, green, red, near-infrared, and PAN bands, were used. For the 30 May 2013 image, Landsat 8 Operational Land Imager and Thermal Infrared Sensor (OLI_TIRS) bands 2–5 (with 30 m spatial resolution) and 8 (with 15 m spatial resolution), which also represent the blue, green, red, near-infrared, and PAN bands, were used.

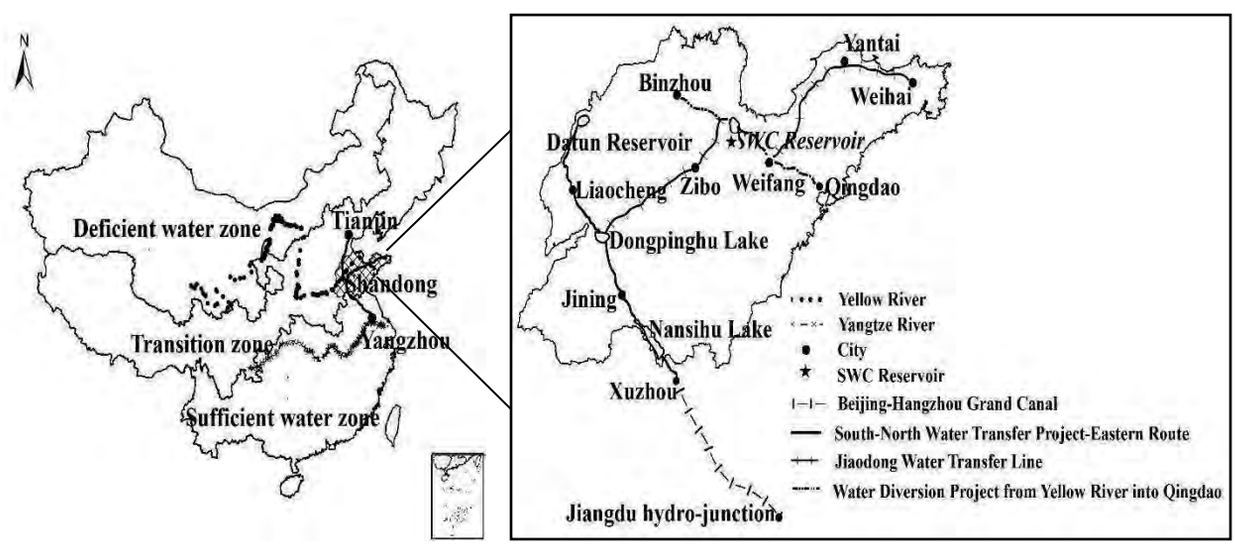

FIGURE 1
Location map of the study area.

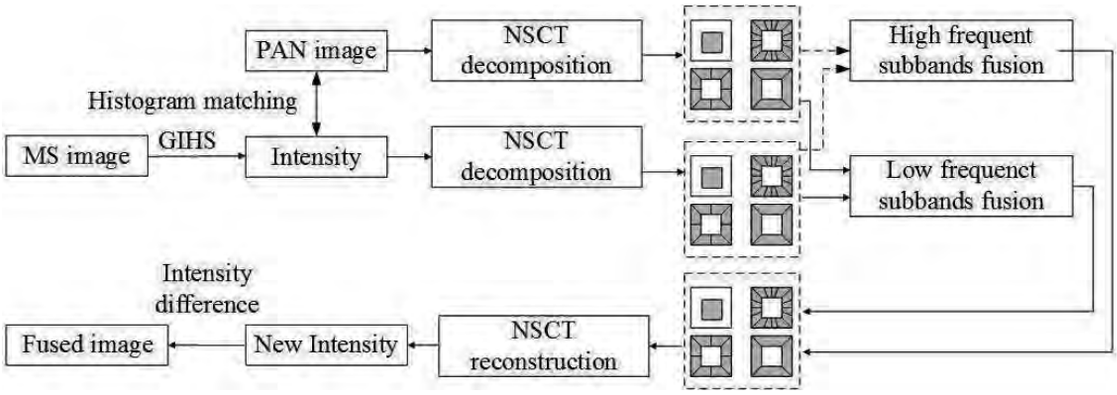

FIGURE 2
The flowchart of the image fusion method as the integration of the nonsubsampled contourlet transform and generalized intensity-hue-saturation (NSCT-GIHS).

Image preprocessing. All USGS images are pre-projected onto the Universal Transverse Mercator (UTM) coordinate system (WGS 84 datum, UTM Zone 50N), and so geometric correction was not required. However, additional image-to-image registration was needed to correctly align the multi-temporal pixel locations. Registration was performed with sub-pixel accuracy so as to avoid registration error effects impacting the quality of change detection. In addition, radiometric and atmospheric corrections are important for multi-temporal LUCC monitoring. Thus, the multi-temporal images were converted to radiance values, and then atmospheric effects were corrected using the FLAASH model, available in the ENVI software package (Exelis Visual Information Solutions Inc., Boulder, Colorado, USA).

NSCT-GIHS image fusion method. Recent studies have demonstrated that the integration of the nonsubsampled contourlet transform (NSCT) and classical fusion methods, for example, intensity-hue-saturation (IHS) and principal component analysis (PCA), can significantly reduce spectral distortion in pan-sharpened images [11]. Different from the IHS transform, the generalized intensity-hue-saturation (GIHS) transform can expand traditional RGB to IHS from three bands to more than three bands [12]. Therefore, the NSCT-GIHS image fusion method was exploited for the pan-sharpening of multispectral (MS) images composed of blue, green, red, near-infrared bands and PAN image, as shown in Figure 2. The NSCT-GIHS method was programmed using the MATLAB® 2012a software (MathWorks Inc., Nat ick, Massachusetts, USA).

Land use / land cover classification system. In general, land use/land cover classification systems are determined according to the purpose of the study and the data resource used. Numerous studies have discussed and proposed land use/land cover classification systems [13–15]. In these classification systems, one-level land cover classes include cropland, woodland, grassland, water body, building land, and others, while two-level land cover classes are subdivided according to practical conditions in the study area. According to the principles above and to the 15 m spatial resolution data used in this study, four one-level land cover classes (cropland, building land, water body, and others) and seven two-level classes (cultivated cropland, fallow cropland, rural settlement, SWC reservoir, another reservoir, canal, and salt field) were determined. Given that the SWC reservoir was the primary target, it was better to separate the SWC reservoir from other reservoirs in order to highlight its expansion and the changes to its surrounding areas.

Land use / land cover classification method. In the SWC reservoir region, fallow cropland and the reservoir embankment produced similar spectra, appearing bright white on pseudo color MS images composed of near-infrared, red and green band as RGB. Furthermore, there were slight seasonal differences between the multi-temporal datasets; therefore, a fully automatic classification method was difficult implement with accuracy. Instead, the strategy employed combined the automatic object-oriented image classification method with manual interpretation. The object-oriented image classification method, which differs from pixel-based classification methods, focused on image objects composed of homogeneous adjacent pixels. Manual interpretation was then used to extract land cover classes that the object-oriented classification method could not achieve. The object-oriented image classification method followed two steps: 1) image segmentation, in which image objects were generated, and 2) image classification, in which image objects were classified into different classes according to their spectral and spatial characteristics (e.g., color, shape, texture).

In this study, fused images composed of blue, green, red, and near-infrared bands with 15 m spatial resolution were used to perform image segmentation and classification processing. Segmentation parameters were uniformly set to scale = 10, color = 0.9, and smoothness =

50. Experimental results [16] have shown that values of 10 and 50 for scale and smoothness, respectively, are ideal segmentation parameters.

During image classification processing, segmented image objects were classified by seven land use/land cover classes. The classification procedure was mainly based on the spectral characteristics and spectral transformation features of the image objects. Through experimentation, the normalized difference vegetation index (NDVI), the brightness values of the red band, was used. The classification flowchart is shown in Figure 3.

An object-oriented image classification method based on the rule-set depicted in Figure 3 was used to extract the cultivated cropland, salt field, and canal classes. NDVI was first used to extract cultivated cropland, and was calculated as $NDVI = 100 \times (1 + \frac{NIR - R}{NIR + R})$ in order to enlarge NDVI differences, in which R is the red band of Landsat fused images, and NIR is the near-infrared band. For different date-acquired images, slight time difference can cause significant NDVI differences with regard to cultivated cropland. Manually defining fixed thresholds to extract cultivated cropland is time-consuming and therefore an automated threshold algorithm embedded in the eCognition Developer 8.7, was used instead. For the salt field and canal classes, slight time differences don not result in obvious spectral variance; therefore, fixed threshold values were set. For the fallow cropland, rural settlement, SWC reservoir, and another reservoir classes, manual interpretation was used. In particular, manual interpretation with the assistance of Google Maps place names was used to classify rural settlements. The object-oriented image classification method and manual interpretation were performed using the eCognition Developer 8.7 software (Trimble Navigation Ltd., Westminster, Colorado, USA).

Land use / land cover change detection method. Many studies have investigated LUCC using multi-temporal satellite data, including the use of the spectral variance based method [17], the cross-tabulation detection method [18], the hybrid classification method [19], visual interpretation [20–22], and post-classification comparison [23–27]. Post-classification comparison is one of the most used methods and can minimize the influence of data acquisition differences. The accuracy of the post-classification comparison method depends on classification accuracy and image recognition precision. In this study, the land use/land cover classification maps were statistically analyzed to quantify the LUCC. The change amount and change rate of land use/land cover of the five periods (2000–2003, 2003–2009, 2009–2011, 2011–2013, and 2000–2013) were obtained.In order to determine the change rate of land use/land cover within a certain period, the land use dynamic degree (LUDD) was used. The LUDD was calculated as shown in Eq. (1):

$$LUDD = \frac{(S_b - S_a)}{S_a \times T} \times 100\% \quad (1)$$

where S_b and S_a are the areas of the land use/landcover types at times b and a, respectively, and T is the cover types at times b and a, respectively, and T is the time interval between b and a.

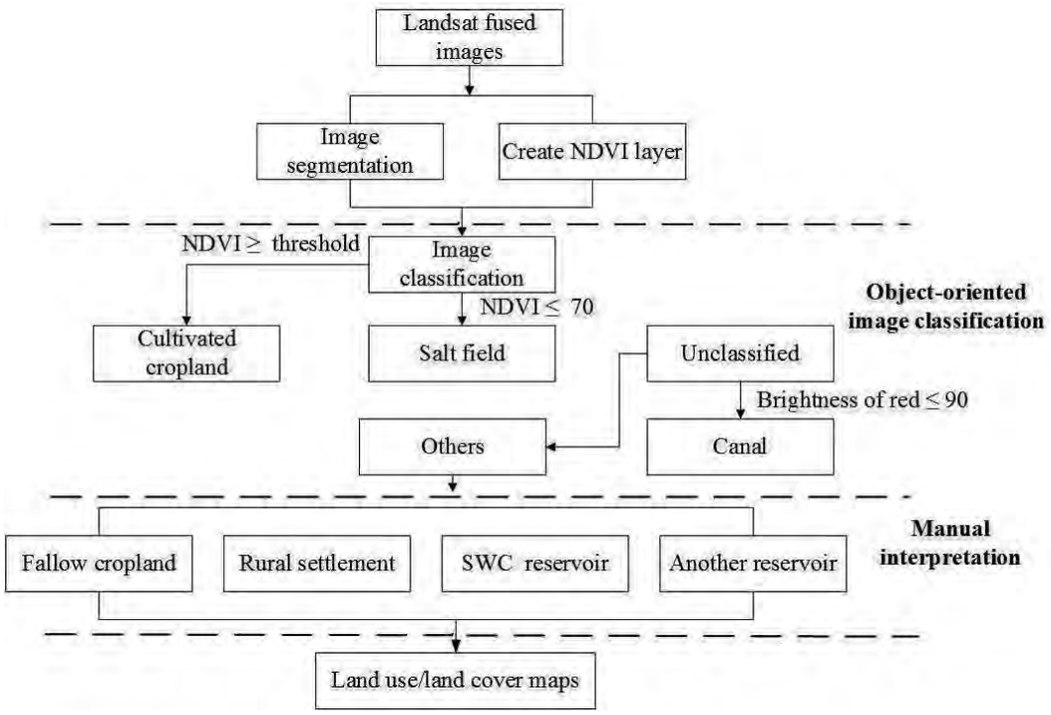

FIGURE3
The flowchart of land use / land cover classification methodology.

RESULTS AND DISCUSSION

Land use / land cover classification results. According to the methodology described in Figure 3, land use/land cover classification maps (and associated qualitative information) of the SWC reservoir region during the five different times periods were obtained using both the Landsat ETM+ and OLI_TIRS images. The results, which are shown in Figure 4, Figure 5, and Table 1, show the LUCC across the study period. In summary, the results show increases in the areas of the SWC reservoir, another reservoir, and rural settlement classes, but significant decreases in the area of the salt field class. The another reservoir class doesn't appear in the classification maps of 2000 and 2003, but appears on the maps for 2009, 2011, and 2013, and clearly relates to the increased number of reservoirs. In addition, the results clearly show a converse change trend between cultivated cropland and fallow cropland. For example, the area rates of cultivated cropland (28.30%) and fallow cropland (57.85%) in 2000 were higher and lower, respectively, than in 2003 (13.81% and 72.43%, respectively).

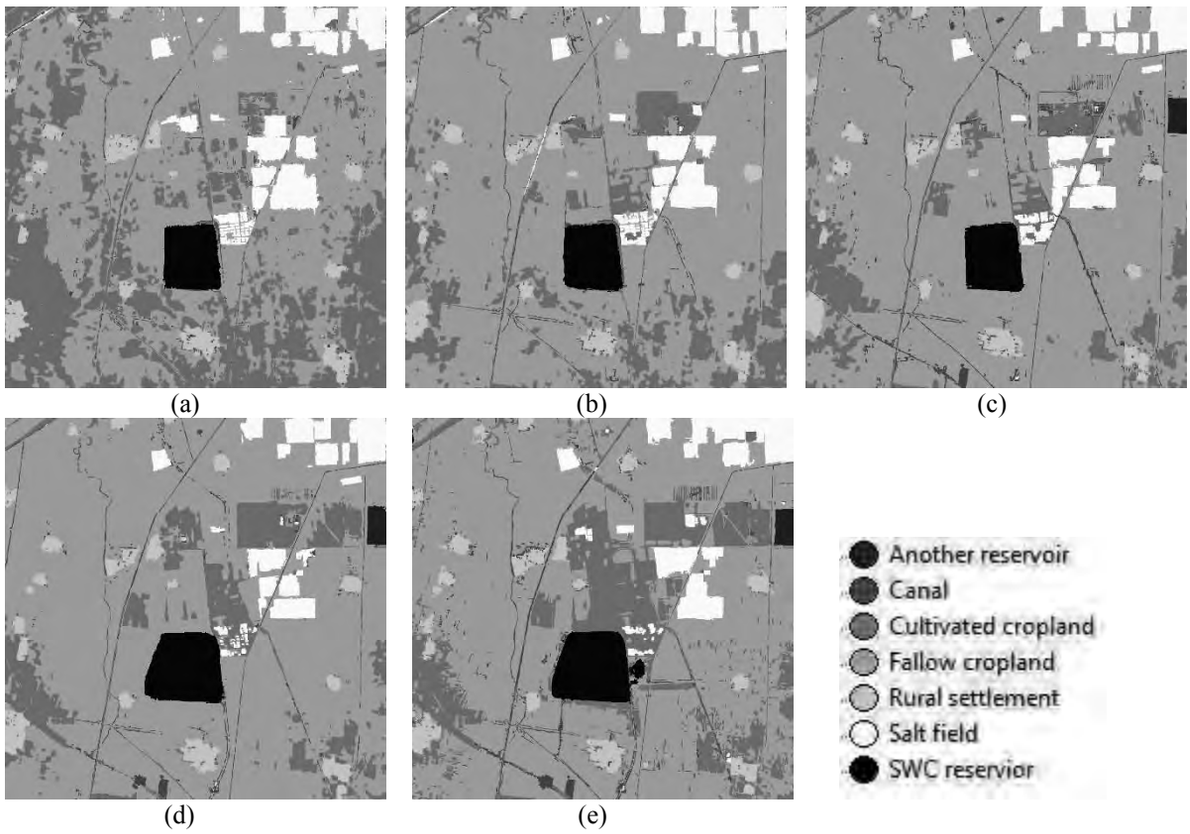

FIGURE 4
Land use and land cover (LULC) classification maps of the Shuangwangcheng reservoir region within time. (a) LULC map in 2000. (b) LULC map in 2003. (c) LULC map in 2009. (d) LULC map in 2011. (e) LULC map in 2013.

TABLE 1
Land use/land cover area in the Shuangwangcheng reservoir region from 2000 to 2013 (unit: km^2).

Land use/land covers	2000	2003	2009	2011	2013
Canal	2.26	3.09	5.74	3.47	5.16
Cultivated cropland	63.67	31.08	22.99	27.13	39.74
Fallow cropland	130.17	162.96	169.05	166.85	150.02
SWC reservoir	5.33	5.50	5.55	7.32	7.79
Another reservoir	0.00	0.00	1.04	1.04	1.04
Rural settlement	7.64	7.64	7.65	7.88	8.57
Salt field	15.93	14.71	12.99	11.31	12.68

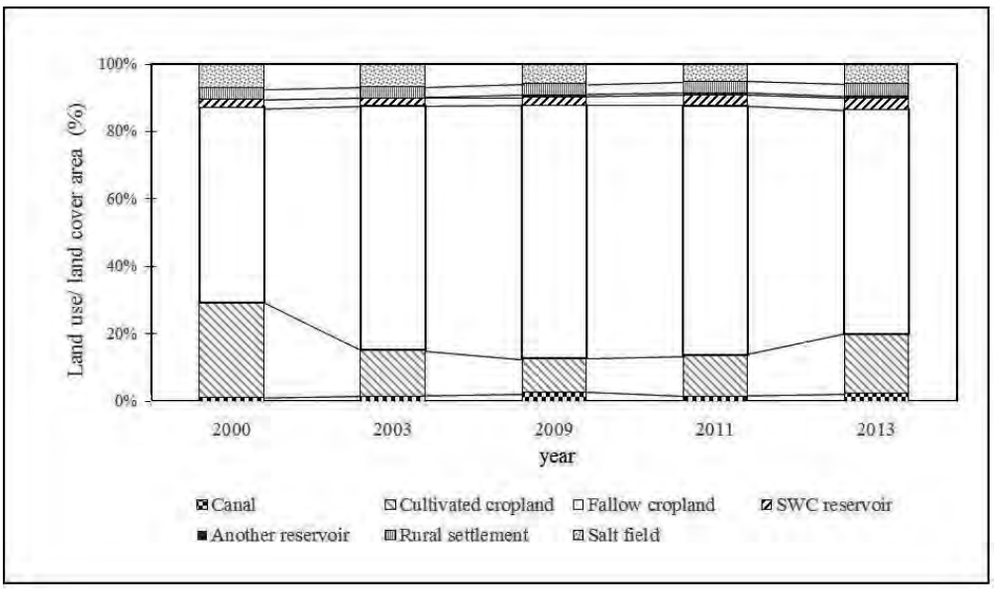

FIGURE 5
Land use/land cover area change within years (%).

Land use / land cover change. The LUCC in the SWC reservoir region across the 13-year study period are shown in Table 2 and Table 3. The area of the SWC reservoir increased from 5.33 km^2 in 2000 to 7.79 km^2 in 2013. From 2000 to 2013, the area of rural resettlements increased steadily, with 0.93 km^2 of other land use types being converted to rural settlements. The salt field area decreased by 3.25 km^2, falling from 15.93 km^2 in 2000 to 12.68 km^2 in 2013. Compared with other land cover types, cropland, including cultivated cropland and fallow cropland, show a small LUDD rate (−0.16%). For the periods 2000–2003, 2003–2009, 2011–2013, and 2000–2013, the canal area showed an increasing trend, reaching an average LUDD of 9.86% between 2000 and 2013, but there was a declining trend between 2009 and 2011. These increases were due to canal construction, connecting water sources (e.g., rivers and reservoirs) to rural settlements, croplands, etc., following the completion of two projects: the Water Diversion Project from the Yellow River into Qingdao and the SNWTP-Eastern Route. The decline between 2009 and 2011 can be explained by the planting of cropland (cultivated or fallow) along the canal lines to facilitate irrigation. Furthermore, in the land use/land cover classification processing, the cultivated cropland class was designed to be the first land use type extracted. Therefore, mixed pixels consisting of cultivated cropland and canals were initially classified as cultivated cropland because their NDVI values were greater than the user-defined threshold value. For the mixed pixels classified as cultivated cropland, it was considered an appropriate extraction and was not corrected.

For the SWC reservoir area, the change trend accelerated continuously during all periods, reaching the highest rate (16.01%) between 2009 and 2011, and exhibiting a mean LUDD of 3.55% between 2000 and 2013. These results reflect the expansion of the SWC reservoir in August 2010, which was scheduled for completion in 2013. Therefore, the area of the SWC reservoir continued to increase between 2011 and 2013, with LUDD of 3.21%.

In addition to the SWC reservoir, an additional reservoir was also completed before April 2009; therefore, the area of another reservoir class increased by 1.04 km^2 from 2003 to 2009. From 2009 to 2013, the area of another reservoir class remained unchanged.

TABLE 2
Land use/land cover change and its dynamic degree in the Shuangwangcheng reservoir region from 2000 to 2013 (area unit: km^2, LUDD unit: %).

Land cover change	2000-2003		2003-2009		2009-2011		2011-2013		2000-2013	
	Area	LUDD	Area	LUDD	Area	LUDD	Area	LUDD	Area	LUDD
Canal	0.83	12.29	2.65	14.26	-2.27	-19.75	1.68	24.25	2.90	9.86
Cultivated cropland	-32.59	-17.06	-8.09	-4.34	4.14	8.99	12.61	23.24	-23.94	-2.89
Fallow cropland	32.80	8.40	6.08	0.62	-2.20	-0.65	-16.83	-5.04	19.85	1.17
SWC reservoir	0.17	1.09	0.04	0.12	1.78	16.01	0.47	3.21	2.46	3.55
Another reservoir	0.00	N/A	1.04	N/A	0.00	0.00	0.00	0.00	1.04	N/A
Rural settlement	0.00	0.00	0.01	0.02	0.23	1.52	0.70	4.41	0.93	0.94
Salt field	-1.21	-2.54	-1.73	-1.96	-1.68	-6.46	1.37	6.06	-3.25	-1.57

Note: N/A denotes that its value can't be calculated because the denominator is zero.

TABLE 3
The land use/land cover change and its dynamic degree of cropland in the Shuangwangcheng reservoir region from 2000 to 2013.

Cropland	2000-2003	2003-2009	2009-2011	2011-2013	2000-2013
Land use/land cover change (km^2)	0.20	-2.00	1.94	-4.22	-4.08
Land use dynamic degree (%)	0.03	-0.17	0.50	-1.09	-0.16

Note: Croplands include cultivated croplands and fallow croplands.

Accordingly, the area of the rural settlement class increased continuously from 2003 to 2013, with the highest rate (4.41%) between 2011 and 2013, and a mean LUDD of 0.94% between 2000 and 2013. These results reflect population migration resulting from the construction of the SWC reservoir.

Accuracy assessment. LUCC detection accuracy fully depends on the accuracy of the land use/land cover classification, with higher classification accuracy resulting in higher LUDD accuracy. Due to the difficulty in acquiring historical land use/land cover maps, 100 random samples from the multi-temporal Landsat fused images were selected and used for manual verification with the assistance of Google Maps. The results showed that the proportion of corrected classifications was greater than 90%. In addition, the SWC reservoir was selected as the reference land cover type and the actual SWC reservoir area and the evaluated area were compared. Based on information from the relevant department, the expanded SWC reservoir is known to cover an area of 7.79 km^2, while the evaluated SWC reservoir area was also 7.79 km^2; thus, the results of this study showed 100% consistency.

CONCLUSIONS

In this study, LUCC from 2000 to 2013 in the SWC reservoir area of the SNWTP-Eastern Route, China, was evaluated using the NSCT-GIHS image fusion method and object-oriented image classification. Between 2000 and 2013, large changes occurred in the land use/land cover of the SWC reservoir area. In particular, there was an increase in the total area of reservoirs, including the SWC reservoir and another reservoir class. In addition, there was an increase in rural settlements, with LUCC changing most rapid immediately before and after the construction of the SWC reservoir. The SWC reservoir area had the highest land use dynamic rate (16.01%) between 2009 and 2011, reflecting the SWC reservoir expansion in August 2010. The area of the rural settlement class increased continuously from 2003 to 2013, reaching the highest LUDD (4.41%) between 2011 and 2013, reflecting population migration resulting from the construction of the SWC reservoir. The results also showed an increase in canals, but a decrease in salt fields from 2000 to 2013. During this time, a number of canals were constructed as a part of water transfer projects.

In Shandong Province alone, thousands of plain reservoirs along the SNWTP-Eastern Route are under-construction or in the planning stage; therefore, it is important to acknowledge the LUCC induced by plain reservoir construction. This study provides an example methodology for characterizing patterns of LUCC in plain reservoir areas. Remote sensing datasets and technology are available for advanced, yet cost effective LUCC monitoring. In particular, the image fusion and object-oriented image classification method can be utilized to achieve accurate LUCC results. The processing flow developed in this study can also be used for LUCC monitoring of urban expansion, wetland reclamation, landslide hazard, soil erosion, etc.

ACKNOWLEDGMENTS

The authors would like to thank the editor, associate editor, and the anonymous reviewers for several helpful comments and suggestions. This study is supported by National Natural Science Foundation of China (Grant No. 41274017 and 41474001), Priority Academic Program Development of Jiangsu Higher Education Institutions, the Key Laboratory of Mapping from Space, National Administration of Surveying, Mapping and Geoinformation (Grant No. K201410) and Fundamental Research Funds for the Central Universities (Grant No. 2013B27114).

REFERENCES

[1] Wang, L. S. and Ma, C. (1999) A study on the environmental geology of the Middle Route Project of the South-North Water Transfer. Engineering Geology, 51(3), 153-165.

[2] Ye, A. Z., Duan, Q. Y., Chu, W., Xu, J. and Mao, Y. N. (2014) The impact of the South-North Water Transfer Project (CTP)'s central route on groundwater table in the Hai River basin, North China. Hydrological Processes, 28(23), 5755-5768.

[3] Yang, H. and Zehnder, A. J. B. (2005) The South-North Water Transfer Project in China - an analysis of water demand uncertainty and environmental objectives in decision making. Water International, 30(3), 339-349.

[4] Musaoglu, N., Tanik, A. and Kocabas, V. (2005) Identification of land-cover changes through image processing and associated impacts on water reservoir conditions. Environmental Management, 35(2), 220-230.

[5] Rautela, P., Rakshit, R., Jha, V. K., Gupta, R. K. and Munshi, A. (2002) GIS and remote sensing-based study of the reservoir-induced land-use/land-cover changes in the catchment of Tehri dam in Garhwal Himalaya, Uttaranchal (India). Current Science, 83(3), 308-311.

[6] Cao, Y. G., Zhou, W., Wang, J. and Yuan, C. (2011) Spatial-temporal pattern and differences of land use changes in the Three Gorges reservoir area of China during 1975-2005. Journal of Mountain Science, 8(4), 551-563.

[7] Seeber, C., Hartmann, H., Xiang W. and King, L. (2010) Land use change and causes in the Xiangxi catchment, Three Gorges area derived from multispectral data. Journal of Earth Science, 21(6), 846-855.

[8] Ouyang, Z. T., Zhang, M. Q., Xie, X., Shen, Q., Guo, H. Q. and Zhao, B. (2011) A comparison of pixel-based and object-oriented approaches to VHR imagery for mapping saltmarsh plants. Ecological Informatics, 6(2), 136-146.

[9] South-to-north water diversion project, china. http://www.water-technology.net/projects/south_north.

[10] South–north water transfer project. http://en.wikipedia.org/wiki/South–North_Water_Transfer_Project.

[11] Metwalli, M. R., Nasr, A. H., Faragallah, O. S., El-Rabaie, E. M., Abbas, A. M., Alshebeili, S. A. and Abd El-Samie, F. E. (2014) Efficient pan-sharpening of satellite images with the contourlet transform. International Journal of Remote Sensing, 35(5), 1979-2002.

[12] Tu, T. M., Su, S. C., Shyu, H. C. and Huang, P. S. (2001) A new look at HIS-like image fusion methods. Information Fusion, 2(3), 177-186.

[13] Li, X. Y., Wang, Z. M., Song, K. S., Zhang, B., Liu, D. W. and Guo, Z. X. (2007) Assessment for salinized wasteland expansion and land use change using GIS and remote sensing in the west part of Northeast China. Environmental Monitoring and Assessment, 131(1-3), 421-437.

[14] Zhao, Y. L., Zhang, K., Fu, Y. C. and Zhang, H. (2012) Examining land-use/land-cover change in the lake Dianchi watershed of the Yunnan-Guizhou plateau of southwest China with remote sensing and GIS techniques: 1974-2008. International Journal of Environmental Research and Public Health, 9(11), 3843-3865.

[15] Liu, J. Y., Kuang, W. H., Zhang, Z. X., Xu, X. L., Qin, Y. W., Ning, J., Zhou, W. C., Zhang S.W., Li, R. D., Yan, C. Z., Wu, S. X., Shi, X. Z., Jiang, N., Yu, D. S., Pan, X. Z. and Chi, W. F. (2014) Spatiotemporal characteristics, patterns, and causes of land-use changes in China since the late 1980s. Journal of Geographical Sciences, 24(2), 195-210.

[16] Yang, R. M., An, R., Wang, H. L., Chen, Z. X. and Quaye-Ballard, J. (2013) Monitoring wetland changes on the source of the Three Rivers from 1990 to 2009, Qinghai, China. IEEE Journal of Selected Topics in Applied Earth Observations and Remote Sensing, 6(4), 1817-1824.

[17] Chen, J., Lu, M., Chen, X. H., Chen, J. and Chen, L. J. (2013) A spectral gradient difference based approach for land cover change detection. ISPRS Journal of Photogrammetry and Remote Sensing, 85, 1-12.

[18] Zhang, H., Zhou, L. G., Chen, M. N. and Ma, W. C. (2011) Land use dynamics of the fast-growing Shanghai Metropolis, China (1979-2008) and its implications for land use and urban planning policy. Sensors, 11(2), 1794-1809.

[19] Deng, J. S., Wang, K., Hong, Y. and Qi, J. G. (2009) Spatio-temporal dynamics and evolution of land use change and landscape pattern in response to rapid urbanization. Landscape and Urban Planning, 92(3-4), 187-198.

[20] Zhang, J. X., Liu, Z. J. and Sun, X. X. (2009) Changing landscape in the Three Gorges reservoir

area of Yangtze River from 1977 to 2005: Land use/land cover, vegetation cover changes estimated using multi-source satellite data. International Journal of Applied Earth Observation and Geoinformation, 11(6), 403-412.
[21] Naik, D. R., Bosukonda, S. and Mrutyunjayareddy, K. (2011) Reservoir impact assessment on land use/land cover and infrastructure-a case study on polavaram project. Journal of the Indian Society of Remote Sensing, 39(2), 271-278.
[22] Zhang, L., Wu, B. F., Zhu, L. and Wang, P. (2012) Patterns and driving forces of cropland changes in the Three Gorges area, China. Regional Environmental Change, 12(4), 765-776.
[23] Tarantino, C., Blonda, P. and Pasquariello, G. (2007) Remote sensed data for automatic detection of land-use changes due to human activity in support to landslide studies. Natural Hazards, 41(1), 245-267.
[24] Reis, S. (2008) Analyzing land use/land cover changes using remote sensing and GIS in Rize, North-East Turkey. Sensors, 8(10), 6188-6202.
[25] Zhou, Q. M., Li, B. L. and Chen, Y. M. (2011) Remote sensing change detection and process analysis of long-term land use change and human impacts. Ambio, 40(7), 807-818.
[26] Kumar, L. and Ghosh, M. K. (2012) Land cover change detection of Hatiya Island, Bangladesh, using remote sensing techniques. Journal of Applied Remote Sensing, 6 (1).
[27] Nigatu, W., Dick, O. B. and Tveite, H. (2014) GIS based mapping of land cover changes utilizing multi-temporal remotely sensed image data in lake Hawassa watershed, Ethiopia. Environmental Monitoring and Assessment, 186(3), 1765-1780.

Received: 23.04.2015
Revised: 31.08.2015
Accepted: 07.12.2015

CORRESPONDING AUTHOR

Xiu-Feng He
Hohai University
School of Earth Science and Engineering
No. 1 Xikang Road, Gulou District
Nanjing 210098 - P. R. CHINA

e-mail: xfhe@hhu.edu.cn; rjwu2004@hhu.edu.cn

by PSP Volume 25 – No. 1/ 2016, pages 355-364 Fresenius Environmental Bulletin

OPTIMIZATION OF BASALT FIBER IN CONCRETE COMPOSITE FOR INDUSTRIAL APPLICATION IN ESTONIA

Eyup Zorla[1], Cagatay Ipbuker[1], Volodymyr Gulik[1*], Sergei Kovaljov[2], Martti Kiisa[3], Alex Biland[4], Alan H. Tkaczyk[1]

[1] University of Tartu, Institute of Physics, Estonia
[2] OÜ Laiers Group, Tartu, Estonia
[3] TTK University of Applied Sciences, Tallinn, Estonia
[4] US Basalt Corp., Houston, USA

ABSTRACT

In this paper, the effect of basalt fiber (BF) on mechanical properties of concrete as well as the BF production in stages and the cost analysis of BF are reported. As emphasized in the recent literature, the industrial and academic world are focusing their attention and efforts towards the development of sustainable composite materials, reinforced with natural fibers, among which BF stands out for its properties. In this work, the BF production is analyzed in a perspective for development and manufacturing of BF in a country with small GDP. It is found that BF production lines could be arranged at low capital costs for any business needs. Normal strength concretes were cast with fixed water to cement ratio of 0.55 and a total of ten mixtures were prepared by incorporating different amounts and sizes of BF and steel fibers. Experimental results show that the inclusion of BF even at low contents result in an increase in the flexural strength. The cost analysis of using BF in concrete indicate that it is cheaper than using steel fiber as well as s-glass and carbon fibers. All in all, BF has all the properties that are sought by the building industry, such as moderate structural strengthening, in combination with low implementation costs, high durability, environmental friendliness, recyclability and high resistance to fire. Therefore, basalt fiber strengthening in fiber reinforced concrete systems is a very good alternative methodology.

KEYWORDS:
Basalt fiber; basalt fiber production; mechanical strength; mechanical testing; cost analysis

INTRODUCTION

Concrete is a composite material with a low tensile strength and tensile strength limit (Uygunoglu 2008, Tassew and Lubell 2014, Faiz 2013). Fibers are known to deteriorate the workability of concrete due to the fact that fibers have a larger surface area than aggregates and therefore surface coating of fibers need to adsorb a lot of water and cement paste and this process causes a loss in the viscosity of the overall composite (Dias and Thaumaturgo 2005, Chen and Liu 2005). On the other hand, the addition of fibers in the concrete mixture can considerably improve the engineering properties of concrete such as toughness, load bearing capacity upon cracking, post-cracking ductility, flexural and impact strength, rheology and durability (Mohammadi et al. 2008, Yazıcı et al. 2007, Hannant 2003, Banthia and Sappakittipakorn 2007, Felekoğlu et al. 2009). According to previous studies (Grdic et al. 2012, Horszczaruk 2005, Li et al. 2006, Yen et al. 2006, Siddique 2003, Siddique et al. 2012, Atiş 2002). The use of fibers have also some additional advantages, such as reduction in abrasive wear of concrete which is mostly affected by the aggregate properties, environmental conditions, water to cement ratio, fiber volume in the mixture, use of additives, voids, type of cement and concrete mixture proportions. Various types of fibers can be used to reinforce the cement composite products, such as steel, organic fibers, glass, asbestos and polypropylene (Hannant DJ, 2003).

Among all the currently used fibers, steel fibers stand out due to their high elastic modulus and stiffness which help improve the compressive strength of concrete. However, corrosion is a persisting problem in the use of steel fibers in concrete composite. Additionally, it has been observed that steel fibers will cause a balling effect when introduced in the mixture and workability of the concrete will be substantially decreased (Nanni A., 1991). Glass fibers are susceptible to alkaline environments, whereas the chemically inert carbon fiber has a distinct disadvantage of high cost and anisotropy. On the other hand, synthetic fibers usually have low elastic modulus and low melting point.

Basalt fiber (BF) is a good alternative to other type of fibers and offer the possibility of innovative applications in concrete composite, due to its expedient characteristics such as high elastic

modulus, thermal stability, fire with less poisonous fumes, resistance to chemical attacks, sound insulation, strength and electrical (Barashykov A.Ya.2012, Gulik and Biland 2012, Jiang et al. 2010, Artemenko 2003, Sivakumar and Santhanam 2007, Shen et al. 2008, Huang and Deng 2010, Sim et al. 2005). In addition, BF manufacturing process is similar to that of the glass fiber, but with no additives, which makes it cheaper than some of the glass fibers and a somewhat more environmentally friendly option (Deák and Czigány 2009, Lopresto et al. 2011, Borhan 2012). BF is produced in a continuous process similar in many respects to glass fiber production (Swink and Sokolinsky, 2002), which can be divided in 7 different process which are the rock preparation, melting, fiber formation, coating, winding, drying and assembling/chopping/twisting.

The credit for the BF production process has to be given to Paul Dhé, Paris, France, who in 1923 got a US patent for extruding filaments from basalt. Despite this relatively early progress towards BF production, the first continuous basalt fibers (CBF) was successfully produced in the 1960s in the U.S. and the Soviet Union (USSR). The aim behind these particular researches was mainly for military applications. Owens Corning and several other U.S. glass companies, which conducted independent R&D programs, abandoned BF programs, but CBF research had been continued in Eastern Europe. As a result the first industrial scale CBF plant was built in Ukraine in late 80s (Jigiris, 2002).

A lot of researches have been performed on BF as a strengthening material for concrete composites (Sim et al. 2005, Manikandan et al. 2012, Yeboah et al. 2012, Fiore et al. 2011). These researches are on the effect of short length BF on concrete properties. There is also an early study on the chemical durability of BF which was conducted in 1981 by Ramachandran et al.. This study can be considered as the basis on the potential of using BF in reinforced concrete. Furthermore, Zieliński and Olszewski (2005) studied the physical and mechanical properties of concrete composite reinforced with BF at 28 days and realized the optimum mixing amount of BF with cement paste. There has also been numerous studies on the relation between mixing amount of BF and the fracture toughness (Dias and Thaumaturgo, 2005), impacting behavior and damage evolution of basalt-FRC (Zhao et al., 2010) and impact behavior of BF reinforced concrete under various high strain rates (Li and Xu, 2009). There were also other studies providing the community a better knowledge of BF properties to facilitate its use in concrete composites such as the study of Brik (Brik et al. 1998, Brik VB. 1999, Brik VB. 1999) investigating the properties of BF as a replacement for steel fibers for concrete structures. Brik et al. (1998) states that BF mixes in the concrete without segregation and do not form balls such as steel fibers, therefore it is easier to handle during construction process.

In this paper, the authors investigate normal strength concrete samples with different amounts of BF. They report on the analysis of test results from an engineering standpoint to evaluate the applicability of BF in civil engineering applications. The study focuses on the floor slab with self levelling concrete construction in an industrial building with the partial use of BF as main reinforcing material in concrete. The results indicate an improved flexural strength even at low BF content. The overall results confirm the authors' claim that BF is a good alternative to other similar products, in consideration with construction of facility for producing of BF in Estonia. This study also compares the experimental results of flexural strength for steel fiber reinforced self-levelling concrete with the BF reinforced one as well as overall cost analysis for the construction of the said-object. The authors also give their unique perspective on the development and manufacturing of BF in a country with small GDP.

METHODOLOGY

Comparison of fibers as strengthening material for concrete composite. As different constructions have different properties and requirements, it has been an interesting topic to improve durability and toughness of concrete. Concrete is in essence a brittle material and tends to crack during its life span. Several types of fibers as strengthening materials to concrete are available:

- Steel fibers: there are different patterns such as straight, twisted, hooked, ringed etc. Diameter range differs from 0.25 to 0.76 mm.
- Glass fibers: Pattern is straight. Diameter range differs from 0.005 to 0,015mm.
- Natural organic and mineral fibers: Wood, cotton, bamboo and rockwool. They have variety of sizes and properties.
- Polymer fibers: There are variety of types. Cost-efficiency must be a consideration.
- Asbestos: primarily used in the early 1900s, although abandoned due to serious associated health risks.

As stated previously, various types of fibers can be added in concrete composite as strengthening materials. Among all the fibers, steel fiber is the most commonly used in the industry, as it has high elastic modulus, stiffness and its addition in the mix improves the compressive

strength and toughness of concrete. However, steel fibers are susceptible to chemical environments. In addition, Nanni A. (1991) states that adding steel fiber into the concrete composite will cause a balling effect and severely reduce the workability of concrete. Furthermore, glass fiber has high sensitivity to alkaline conditions. Carbon fiber is chemically inert and very stiff, but it has very high cost and has problems with anisotropy. Polymeric fibers on the other hand usually have low elastic modulus and melting point as well as poor bonding with inorganic matrices.

BF can be offered as a potential strengthening material in concrete composite. BF is an inorganic fiber extruded from melted basalt rock. Therefore, it can be stated that it is environmentally friendly and it can also be recycled when necessary. BF has certain disadvantages. The chemical durability of BF was first demonstrated by Ramachandran et al. in 1981. In the recent literature the study of Sim et al. (2005) stands out as a fully comprehensive study on the characteristics of BF as a strengthening material for concrete structure. Sim et al. (2005) finds that when BF is immersed into an alkali solution it loses its volume and strength (Sim et al. 2005). Sim et al. (2005) also states that BFs provide excellent fire resistance, as they keep 90% of their normal temperature strength when exposed to 600 ^{o}C over 2 hours. In addition, BFs do not produce poisonous fumes during a fire. Additionally, BFs have approximately the same specific density as concrete, therefore the distribution of BFs in the concrete matrix tends to be homogenous unlike steel and polymeric fibers (Sim et al., 2005).

Another interesting property of BF is its radiation shielding property. After further testing and thorough qualification, it may be useful to consider such composites for projects with specific operating conditions over a long period of time, such as certain components at nuclear power plants or radioactive or hazardous waste storage facilities (Gulik, V., Tkaczyk, A.H., 2014, Pavlovych V.M. et al. 2008, Ipbüker C. et al. 2015).

The overall cost of using BFs in construction projects is also of importance. Previous studies on the cost-efficiency of BF addition in concrete has shown that it may be several times cheaper than using steel fibers (Gulik and Biland, 2012).

Practical approach for the development of basalt fiber manufacturing in a country with a small Gross Domestic Product (GDP). There has been growing interest in the recent years to set up continuous BF production lines by non-core businesses or businesses with a limited budget of capital expenses. This was promoted by several factors. First, there are many companies using BFs in one form or another only for internal consumption, e.g. for improving technical or mechanical properties of their own current products. Second, purchasing fiber in bulk from major manufacturers would lead to a potential price increase for their own products. Third, there is a clear lack of flexibility for the current BFs available on the market. When a specific character property is required, fiber producer would need to alter their existing production process, such as necessity for high resistance to acids or alkalis. None of the major manufacturers of BFs can easily adapt their big ovens for a new raw material and therefore the so-called smaller producers would be forced to build their own production lines accordingly.

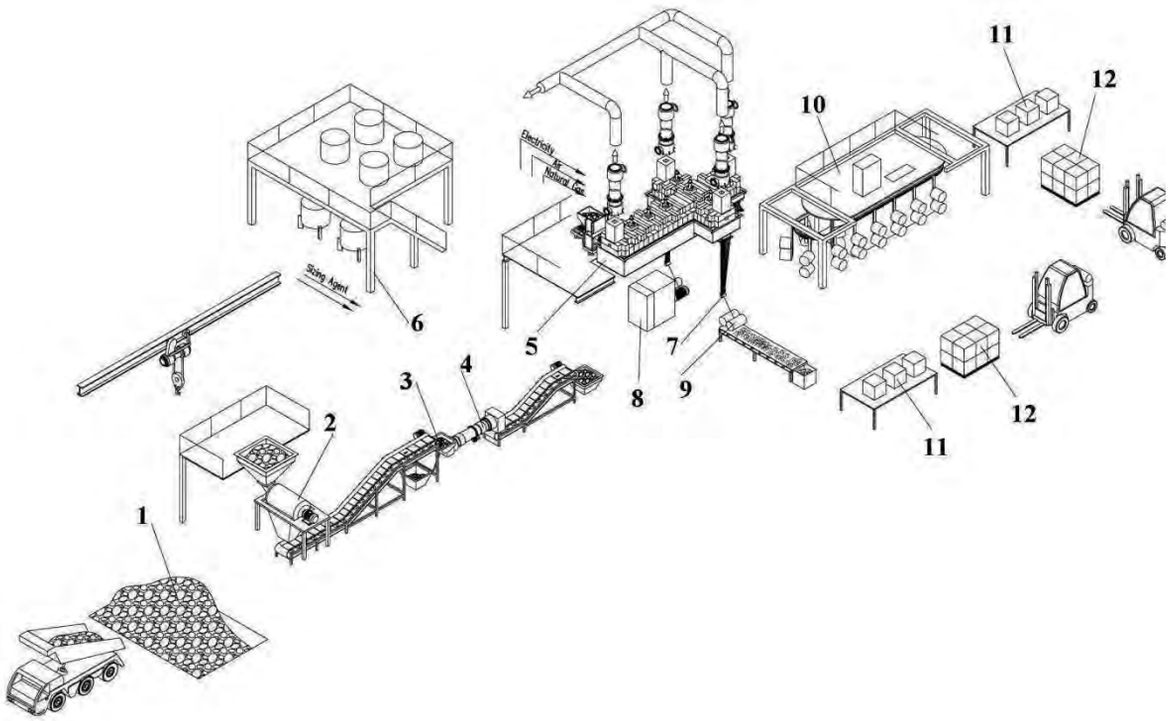

FIGURE 1
1. The simple scheme of small facility for basalt fiber producing. 1. Basalt from quarry; 2. Washing; 3. Magnetic separation; 4. Dryer; 5. Melting furnace; 6. Sizing agent storage tanks; 7. Sizing agent applicator; 8. Winder; 9. Chopper; 10. HF dryer; 11. Packing; 12. Warehouse.

Several engineering companies are specialized in designing and installing such small facilities for the production of BF. Capital costs are strongly dependent on the production capacity of the proposed equipment and can range from EUR 0.54 million to EUR 1.34 million.

Figure 1 shows an example of a relatively small production facility on a plot area of 600m^2, comprised of all the necessary components of BF production. The BF production in such a facility can be summarized as follows: Before the start of production of continuous BF, basalt gravel is crushed to the required fraction and delivered to the site for the preparation of raw materials (1). Gravel with average size of 5 to 12 mm is washed (2), then it is separated from random metallic inclusions by a magnetic separator (3), and dried in a special drying apparatus. The next step is using the crane or telpher to intermittently feed the basalt gravel into the hopper loader, which is installed above the melter. The melt from the furnace forehearth flows to the feeder by gravity, where the platinum drain tubes are located at the bottom. At this point, the melt is fed into a platinum bushing with an electro-heating through the drain tube, which helps to form a strand of thin basalt filaments. This strand then passes through the sizing applicator (7) where sizing agent is applied to the surface of basalt filaments (6). Filaments are then collected as a multifilament yarn and wound onto removable bobbins (8). Direct chopping of filament yarn by means of special chopping apparatus take place (9) directly under the platinum bushing. These wound bobbins are dried (10) and sent out for further processing. The wet chopped fibers are subject to further processing by manufacturer, e.g. preparation for further mixing with concrete composite.

This scheme has been greatly simplified and does not take into account certain specificities and the differences in existing equipment of various manufacturers, but in general the elements of production are the same, as well as the order of process.

Materials, specimen and testing procedure. The object of this study is a self-levelling floor of an industrial building, in Elva, Estonia. The slab is illustrated in Figure 2. and has the following dimensions: length = 36m; width = 17m; thickness = 6cm.

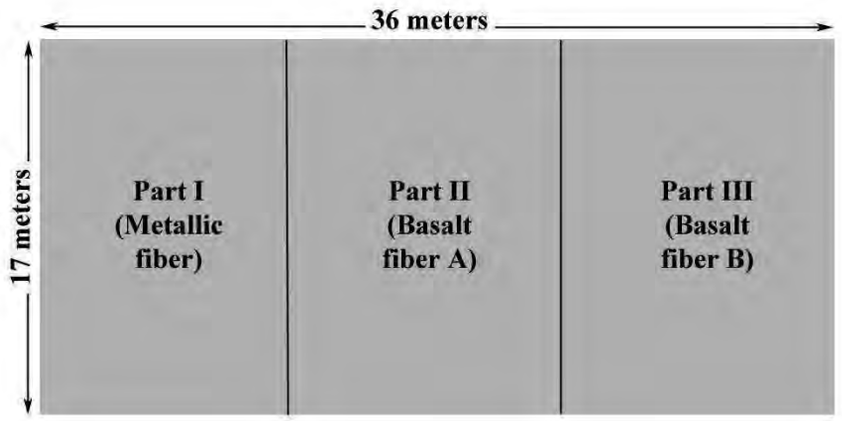

FIGURE 2
The simple scheme of building site

The materials used include limestone coarse aggregate, natural river sand, cement, chemical admixtures, BF and steel fiber. The maximum particle size for the coarse aggregate and natural river sand was 16mm and 2mm respectively. The type of cement used was rapid hardening oil-shale cement CEM II/A-T 52.5 N and its physical and mechanical properties are presented in Table 1. A setting accelerator was used to reduce the setting time, increase the early strength as well as protect the concrete from frost attack. In addition, an acrylic polymer based superplasticizer was used to reach a high level of workability. The concrete was cast with a water to cement ratio of 0.55.

TABLE 1
Physical and mechanical properties of cement.

Physical Properties	
Setting time (min)	180
Volume expansion (mm)	≤10
Specific surface (cm^2/g)	4200
Compressive strength	
1 day (MPa)	17
2 days (MPa)	31
28 days (MPa)	58

BF with a density of 2.8 g/cm^3 and a length of 12 mm was used in this study at varying content. Physical and mechanical properties of BF and steel fibers are presented in Table 2 and 3, and the chemical composition of BF is presented in Table 4.

TABLE 2
Properties of basalt fiber

length (mm)	diameter (μm)	density (g/cm^3)	Elastic Modulus (GPa)	Elongation (%)
24	13 - 20	2.8	89	3.15

TABLE 3
Properties of HE 75/50 hooked-end steel fiber* (in accordance with EN 14889-1 type 1 cold-drawn wire)

length (mm)	diameter (μm)	Tensile strength (MPa)	Bending angle	Hook depth (mm)	Hook length (mm)
50	750	1200	45°	1.8	1 - 4

* Information retrieved from ArcelorMittal

TABLE 4
Chemical composition of basalt fiber

Chemical Composition of Basalt Fiber (%)											
SiO_2	TiO_2	Al_2O_3	Fe_2O_3	MnO	MgO	CaO	Na_2O	K_2O	P_2O_5	S	Cl
49.68	2.67	15.62	11.72	0.20	4.81	8.29	4.30	1.75	0.90	0.04	0.02

As stated in Dias and Thaumaturgo (2005) study, fibers consume a fraction of water and cement paste to coat its surface area which generally increases the viscosity of the mixture, therefore it is characteristic for fibers to deteriorate the workability of concrete. In order to provide the target slump of slump class S4 (16-21cm), as designated by EN 206-1:2000, superplasticizer was used. As the use of admixtures might retard the setting time, setting accelerator was used.

The object slab was divided on three equal parts with dimensions 17m to 12m. The first part was reinforced with steel fiber, whereas the second and third parts were reinforced with BF.

Steel fibers used were hooked-end steel fibers with a wire diameter of 0.75mm (± 2.0 mm) and a length of 50mm (± 0.3 mm). The tensile strength of drawn wire is 1200 N/mm^2. The steel fibers were used as described in EN 14889-1:2006 with a dosage of 20 kg/m^3.

The dosage of BFs in second and third part of the slab were 2 and 3 kg/m^3 and they are referred to in this study as type A and type B BF respectively.

RESULTS

Experimental Results. In order to determine the effect of BF addition on flexural strength and compare it with the steel fibers, 10 prismatic specimens were cast with dimensions of 600x100x100mm. All specimens were cured in water at 20 ± 2 °C before performing hardened concrete tests.

The flexural strength of prismatic specimens as well as the concrete density estimations were determined according to EVS-EN 12390-7:2009 and EVS-EN 12390-5:2009 respectively.

The average of flexural strength values of concretes and associated densities of specimens are given in Table 5. Table 5 shows that the average flexural strength of concrete reinforced with steel fibers with a dosage of 20 kg/m^3 roughly equals to the average flexural strength of concrete reinforced with BFs with a dosage of 3 kg/m^3. However, flexural strength is observed to be improved in the case of BFs with a dosage of 2 kg/m^3. It must also be noted the highest flexural strength is observed for the sample with the highest density.

TABLE 5
The flexural strength and density characteristics of concrete samples with different types of fiber

Samples	Dimensions (mm)			Density (kg/m^3)	Force (kN)	Flexural strength(MPa)	
	length	width	height			Single	Average
HE 75/50 hooked-end steel fiber							
MF #1	598.0	106.0	106.5	2240	22.6	5.6	5.2
MF #2	598.0	103.0	107.0	2320	19.5	4.9	
MF #3	596.5	101.0	109.5	2330	20.9	5.2	
MF #4	597.0	101.0	110.0	2350	21.0	5.2	
Type A basalt fiber with a dosage of 2 kg/m^3							
BFA #1	596.5	103.0	106.5	2400	23.3	6.0	5.5
BFA #2	597.0	102.5	106.0	2320	20.3	5.3	
BFA #3	596.5	102.0	106.5	2330	20.6	5.3	
Type B basalt fiber with a dosage of 3 kg/m^3							
BFB #1	597.0	104.0	106.5	2320	20.2	5.1	5.1
BFB #2	598.0	102.0	103.0	2300	17.4	4.8	
BFB #3	596.0	104.0	107.0	2300	20.8	5.3	

the slight drop in flexural strength from fiber dosage of 2 kg/m^3 to 3 kg/m^3 is in accordance with the results of previous studies. Jiang et al. (2014) reports that when the fiber volume fraction increases from 0.3% to 0.5%, then a marginal drop in the flexural strength can be observed. Kabay (2014) also reports a similar result of 1% drop in higher amount of fibers. This drop in flexural strength with the increase of fiber content in concrete can be explained with the difficulty in dispersion of fiber in the matrix due to high volume, thus it is often indicated in the literature that there is a suitable admixture rate of BF in concrete.

Previous studies also indicate that the addition of fiber into the concrete significantly improve the flexural behavior of concrete. Song and Hwang (2004) states that the flexural strength of concrete increases considerably with the addition of steel fibers into the mix, whereas Sivakumar and Santhanam (2007) reports that the addition of 0.6 kg/m^3 of polypropylene, polyester and glass fiber improve the flexural behavior of concrete by 7.6%, 21.3% and 14.4% respectively. These results are also in accordance with the studies of Suna and Xu (2009), Felekoğlu et al. (2007) and Altun et al. (2007). Suna and Xu (2009) note that the addition of 0.9 kg/m3 polypropylene fiber results in a 14.4% increase in flexural strength. Felekoğlu et al. (2007) indicate that the addition of steel fibers with a dosage of 156 kg/m^3 improve the flexural strength by 19%. Altun et al. report that the use of steel fibers enlarge the flexural strength by 46 to 81% depending on fiber volume ratio.

Cost analysis. The cost analysis of this study is comprised of materials and labor. The cost analysis study solely focus on the construction of self-leveling floor which is divided into 3 sections, steel fiber reinforced and BF reinforced at varying dosage. The data on materials and labors for the construction of these sections gives us the opportunity to provide a comparison between two types of construction.

The amount of concrete used is 3.8 m^3. As the concrete type do not differ for the construction, it is of no use to compare it in the cost analysis. On the other hand, 1 kg of steel fiber cost 0.9€, therefore, an average of 18€ for steel fiber per cubic meter is recorded. The average cost of 1kg of BF is 5€, thus, an average of 10-15€ of BF per cubic meter is recorded. The cost of BF differs greatly depending on the producers and amount imported. This is the reason this study intends to give an overview of perspective on setting up small scale BF production facility for industrial purposes in Estonia. It is worth noting that if such a BF factory were to be constructed, the cost of BF would be reduced from 10-15€ per cubic meter to only 8-10€. It is observed that the cost of steel and BF per cubic meter also do not differ from each other on a great extent.

Consequently, an advantage in the use of BF is seen in labor savings. 30 plus man hours were required to install the formwork on the slab. However, the main difficulty in steel fiber reinforced concrete construction is the workability. More man hours are needed in order to increase the workability of concrete because getting proper distribution of fibers in the matrix is very important. Otherwise, the steel fibers tend to ball up in the matrix. This difficulty is generally overcome by feeding the fibers slowly, continuously and

uniformly into the wet mix through vibratory feeders. Water addition into the matrix can also be considered in order to improve the workability, but this eliminates the advantage of using fiber reinforcements by severely reducing the flexural strength. On the other hand, as BFs are very light, of short length, and do not form balls in the matrix, they are very easy to feed into the concrete.

All in all, it can be concluded that BF has a distinct advantage in reducing the overall construction costs, especially in terms of labor costs. However, it is also worth indicating that fiber reinforced concrete (FRC) has a generally higher cost as it employs higher cement content, which may lead to possible thermal contraction problems in the setting stage.

CONCLUSION

This study analyses the effects of BF addition in normal strength concrete in terms of flexural strength as well as the comparison of results with the usage of steel fibers. In addition, this study also informs in terms of cost analyses of employing BF and steel fibers and gives a unique perspective on setting up small scale BF production facility for industrial purposes. Experimental results have shown that the addition of BF even at low contents could provide significant contributions to concrete in terms of flexural strength. An increase in flexural strength up to 6% is observed when the dosage of BF in the mixture is 2 kg/m^3. When the BF dosage is increased to 3 kg/m^3, the flexural strength of this matrix equals to 20 kg/m^3 steel fibers in concrete.

The main conclusions of the study may be summarized as follows:

1. BF is overall a cheaper alternative to other fiber strengthening materials for concrete as it reduces the construction costs.
2. Small scale BF production facilities in Estonia will further reduce the production costs.
3. Addition of BF resulted in an improvement in flexural strength.
4. BFs can be regarded as a very good strengthening material for concrete in comparison with carbon and glass fibers, even though to some extent BFs' structural strengthening effects may be less than these two types of fibers.
5. Moderate structural strengthening, in combination with low implementation costs, with high durability, environmental friendliness, recyclability and high resistance to fire are all good characteristics that are sought by today's Building industry. Therefore, it can be concluded that BF strengthening in fiber reinforced concrete systems has the potential to become an alternative methodology.

ACKNOWLEDGMENTS

This research was supported by European Social Fund's Doctoral Studies and Internationalisation Programme DoRa, which is carried out by the Foundation Archimedes. This research was carried out with the financial support of the ERMOS programme (Co-funded by Marie Curie Actions) within the project "Development of a computational model for transmutation and minimization of nuclear waste within the scope of advanced nuclear fuel cycles" (ERMOS107). We acknowledge support from Estonian Research Council award ETF9304 and the CRDF Global and Estonian Science Foundation 2010 Energy Research Competition (CRDF-ETF II), including CRDF award ESP1-7030-TR-11 (National Science Foundation cooperative agreement OISE-9531011) and ETF award 22/2011. We appreciate the help of OÜ Laiers Group Company (Tartu, Estonia) and Rudus AS Company (Tallinn, Estonia) for useful suggestions and for materials supplied.

REFERENCES

[1] ArcelorMittal. "Technical Data Sheet Hooked-End Steel Fibers, HE 75/50." Retrieved 21.01.2016, from http://ds.arcelormittal.com/wiresolutions/steelfibres/products/hooked_end_fibres_he/language/EN.

[2] Artemenko, S. E. (2003). "Polymer composite materials made from carbon, basalt, and glass fibres. Structure and properties." Fibre Chemistry 35(3): 226-229.

[3] Atiş, C. D. (2002). "High volume fly ash abrasion resistant concrete." Journal of Materials in Civil Engineering 14(3): 274-277.

[4] Banthia N. P., Sappakittipakorn M. (2007). "Toughness enhancement in steel fiber reinforced concrete through fiber hybridization." Cement and Concrete Research 37(9): 1366-1372.

[5] Borhan T. M. (2012). "Properties of glass concrete reinforced with short basalt fibre" Materials and Design 42: 265-271.

[6] Brik V.B. (1999). "Advanced concept concrete using basalt fiber composite reinforcement." Tech Res Report submitted to NCHRP-IDEA, Project 25; 1999.

[7] Brik V.B. (1999). "Performance evaluation of basalt fibers and composite rebars as concrete

reinforcement." Tech Res Report submitted to NCHRP-IDEA, Project 45; 1999.
[8] Brik V.B., Ramakrishnan V., Tolmare N. (1998). "Performance evaluation of 3-D Basalt fibre reinforced concrete &Basalt rod reinforced concrete." IDEA Program Final Report, Contract No. NCHRP-45.
[9] Chen B., Liu J. (2005). "Contribution of hybrid fibers on the properties of the high-strength lightweight concrete having good workability." Cement and Concrete Research 35(5): 913-917.
[10] Deák T., Czigány T. (2009). "Chemical composition and mechanical properties of basalt and glass fibers: A comparison." Textile Research Journal 79(7): 645-651.
[11] Dias D. P., Thaumaturgo C. (2005). "Fracture toughness of geopolymeric concretes reinforced with basalt fibers." Cement and Concrete Composites 27(1): 49-54.
[12] Faiz S. U. A. (2013). "Review of mechanical properties of short fibre reinforced geopolymer composites." Construction and Building Materials 43: 37-49.
[13] Felekoğlu B., Tosun-Felekoğlu K., Baradan B. (2009). "Effects of fibre type and matrix structure on the mechanical performance of self-compacting micro-concrete composites." Cement and Concrete Research 39(11): 1023-1032.
[14] Felekoğlu B., Türkel S., Altuntaş Y. (2007). "Effects of steel fiber reinforcement on surface wear resistance of self-compacting repair mortars." Cement and Concrete Composites 29(5): 391-396.
[15] Fiore V., Di Bella G., Valenza A. (2011). "Glass-basalt/epoxy hybrid composites for marine applications." Materials and Design 32(4): 2091-2099.
[16] Gulik V. I., Tkaczyk A. H. (2014). "Cost optimization of ADS design: Comparative study of externally driven heterogeneous and homogeneous two-zone subcritical reactor systems." Nuclear Engineering and Design 270: 133-142.
[17] Gulik V.I., Biland A.B. (2012). "The Use of Basalt, Basalt Fibers and Modified Graphite for Nuclear Waste Repository". Proceeding of Waste Management Conference (WM2012), Phoenix, Arizona, USA.
[18] Hannant D. J. (2003). Fibre-reinforced concrete. Advanced Concrete Technology. B. S. C. J. Newman. Oxford, U.K., Elsevier: 6/1-6/17.
[19] Horszczaruk E. K. (2005). "Abrasion resistance of high-strength concrete in hydraulic structures." Wear 259(1-6): 62-69.
[20] Huang K., Deng M. (2010). "Stability of basalt fibers in alkaline solution and its effect on the mechanical property of concrete." Fuhe Cailiao Xuebao/Acta Materiae Compositae Sinica 27(1): 150-154.
[21] Ipbüker C., Nulk H., Gulik V. I., Biland A., Tkaczyk A. H. (2015). "Radiation shielding properties of a novel cement-basalt mixture for nuclear energy applications." Nuclear Engineering and Design 284: 27-37.
[22] Jiang C., McCharty T. J., Chen D., Dong Q. Q. (2010). "Influence of basalt fiber on performance of cement mortar." Key Engineering Materials 426-427: 93-96.
[23] Jigiris D.D., Mahova M.F. (2002). "The bases of producing of basalt roving and products." Teploenergetic, Kamenny Vek, Moscow, pp. 407-417 (in Russian).
[24] Li H., Zhang M., Ou J. (2006). "Abrasion resistance of concrete containing nano-particles for pavement." Wear 260(11-12): 1262-1266.
[25] Li W., Xu J. (2009). "Dynamic behavior and constitutive model of basalt fiber reinforced concrete under impact loading." Gongcheng Lixue/Engineering Mechanics 26(1): 86-91.
[26] Lopresto V., Leone C., De Iorio I. (2011). "Mechanical characterisation of basalt fibre reinforced plastic." Composites Part B: Engineering 42(4): 717-723.
[27] Manikandan V. C., Jappes J. T. W., Kumar S. M. S., Amuthakkannan P. (2012). "Investigation of the effect of surface modifications on the mechanical properties of basalt fibre reinforced polymer composites." Composites Part B: Engineering 43(2): 812-818.
[28] Mohammadi Y., Singh S. P., Kaushik S. K. (2008). "Properties of steel fibrous concrete containing mixed fibres in fresh and hardened state." Construction and Building Materials 22(5): 956-965.
[29] Nanni A. (1991). "Fatigue behaviour of steel fiber reinforced concrete." Cement and Concrete Composites 13(4): 239-245.
[30] Pavlovych V. M., Khotyayintsev V. M., Khotyayintseva O. M. (2008). "The physical basis of the fission wave reactor." Nuclear Technology and Radiation Protection 23(2): 3-15.
[31] Siddique R. (2003). "Effect of fine aggregate replacement with Class F fly ash on the abrasion resistance of concrete." Cement and Concrete Research 33(11): 1877-1881.
[32] Siddique R., Kapoor K., Kadri E. H., Bennacer R. (2012). "Effect of polyester fibres on the compressive strength and abrasion

resistance of HVFA concrete." Construction and Building Materials 29: 270-278.
[33] Sim J., Park C., Moon D. (2005). "Characteristics of basalt fiber as a strengthening material for concrete structures." Composites Part B: Engineering 36(6-7): 504-512.
[34] Sivakumar A. V. N., Santhanam M. S. (2007). "Mechanical properties of high strength concrete reinforced with metallic and non-metallic fibres." Cement and Concrete Composites 29(8): 603-608.
[35] Swink M., Sokolinsky M. (2002). "Continuous filament basalt fiber shows promise in high-temperature applications." International Fiber Journal 17(4): 52-56.
[36] Tassew S. T., Lubell A. S. (2014). "Mechanical properties of glass fiber reinforced ceramic concrete." Construction and Building Materials 51: 215-224.
[37] Uygunoğlu T. (2008). "Investigation of microstructure and flexural behavior of steel-fiber reinforced concrete." Materials and Structures/Materiaux et Constructions 41(8): 1441-1449.
[38] Yazıcı Ş., Inan G., Tabak V. (2007). "Effect of aspect ratio and volume fraction of steel fiber on the mechanical properties of SFRC." Construction and Building Materials 21(6): 1250-1253.
[39] Yeboah D., Taylor S. E., McPolin D. O., Gilfillan R. (2012). "Pull-out behaviour of axially loaded Basalt Fibre Reinforced Polymer (BFRP) rods bonded perpendicular to the grain of glulam elements." Construction and Building Materials 38(5): 962-969.
[40] Yen T., Hsu T., Liu Y., Chen S. H. (2007). "Influence of class F fly ash on the abrasion-erosion resistance of high-strength concrete." Construction and Building Materials 21(2): 458-463.
[41] Z. J. Grdić, Curcic G. A. T., Ristić N. S., Despotović I. M. (2012). "Abrasion resistance of concrete micro-reinforced with polypropylene fibers." Construction and Building Materials 27(1): 305-312.
[42] Zhao Q., Dong J., Pan H., Hao S. (2010). "Impact behavior of basalt fiber reinforced concrete." Fuhe Cailiao Xuebao/Acta Materiae Compositae Sinica 27(6): 120-125.
[43] Zieliński K., Olszewski P. (2005). "The impact of basaltic fibre on selected physical and mechanical properties of cement mortar." Betonwerk und Fertigteil-Technik/Concrete Precasting Plant and Technology 71(3): 28-33.

Received: **09.06.2015**
Accepted: **05.12.2015**

CORRESPONDING AUTHOR

Volodymyr Gulik[1]
University of Tartu
Institute of Physics
Ravila 14c - D516
50411 Tartu – Estonia

e-mail: volodymyr.gulik@gmail.com

AUTHOR INDEX

SUBJECT INDEX

FEB- GUIDE FOR AUTHORS

General

FEB accepts original papers, review articles, short communications, research abstracts from the entire sphere
of environmental-chemistry,-biology,-microbiology,- technology, -biotechnology and-management, furthermore, about residueanalysis/ and ecotoxicology of contaminants.
Acceptance or nonacceptance of a contribution will be decided, as in the case of other scientific journals, by a board of reviewers.Papers are processed with the understanding that they have not been published before (except in form of an abstract or as a part of a published lecture, review or thesis);that they are not under consideration for publication elsewhere; that their publication has been approved by all co-authors, if any, as well as-tacitly or explicitly- by the responsible authorities at the institute where the work has been carried out and that, if accepted, it will not be published elsewhere in the same form, in either the same or another language, without the consent of the copyright holders.

Language

Papers must be written in English. Spelling may eitherfollow American (Webster) or British (Oxford) usage but must be consistent. Authors who are less familiar with the English language should seek assistance from proficient colleagues in order to produce manuscripts that are grammatically and linguistically correct.

Size of manuscript

Review articles should not exceed 30 typewritten pages. In addition up to 5 figures may be included. Original papers must not exceed 14 typewritten pages. In addition up to 5 figures may be included. Short-Communications should be limited to 4 typewrittenpages plus not more than 1 illustration. Short descriptions of the authors, presentation of their groups and their research activities (with photo) should together not exceed I typewritten page.Short research abstracts should report in a few brief sentences (one-forth to one page) particularly significant findings.Short articles by relative newcomers to the chemical innovation arena highlight the key elements of their Master and PhD-works in about I page.
Book Reviews are normally written in-house, but suggestions for books to review are welcome.

Preparation of manuscript

Dear authors,
FEB is available both as printed journal and as online journal on the web. You can now e-mail your manuscripts with an attached file. Save both time and money.To avoid any problems handling your text please follow the instructions given below:
When preparing your manuscripts have the formula K/SS (Keep It Simple and Stupid) in mind.Most word processing programs such as MS-Word offera lot of features. Some of them can do serious harm to our layout. So please do not insert hyperlinks and/or automatic cross-references, tables of contents,references, footnotes, etc
1. Please use the standard format features of your word processor (such as standard.dotfor MS Word).
2. Please do not insert automatisms or secret link-ups between your text and your figures or tables. These features will drive our graphic department sometimes mad.
3. Please only use two fonts. for text or tables "Times New Roman" and for graphical presentations "Arial".
4. Stylesheets, text, tables and graphics in shade of grey
5. Turn on the automatic language detection inEnglish (American or British)
6. Please - check your files for viruses before you send them to us!!

Manuscripts should send to:parlar@wzw.tum.de
or:parlar@prt-parlar.de

Thank you very much!

STRUCTURE OF THE MANUSCRIPT

Title page: The first page of the manuscript should contain the following items in the sequence given:A concise title of the paper (no abbreviations)The names of all authors with at least one first name spelled out for every author.The names of Universities with Faculty, City and Country of all authors.

Abstracts: The second page of the manuscript should start with an abstract that summarizes briefly the contents of the paper (except short communications). Its lenght should not exceed 150-200 words. The abstract should be as informative as possible. An extended repetition of the paper's title is not considered to be an abstract.

Keywords: Below the Summary up to 6 key words have to beprovided which will assist indexers in crossindexing your article.

Introduction: This should define the problem and, if possible, the frame of existing knowledge. Please ensure that people not working in that particular field will be able to understand the intention. The word length of the introduction should be 150 to 300 words.

Materials and methods:
Please be as precise as possible to enable other scientiststo repeat the work.

Results: Only material pertinent to the subject must be included.Data must not be repeated in figures and tables.

Acknowledgements: Acknowledgements of financial support, advice orother kind of assistance should be given at the end of the text under the heading "Acknowledgements". The names of funding organisations should be written in full.

Reference: Responsibility for the accuracy of references rests with the authors. References are to be limited in number to those absolutely necessary.References should appear in numerical order in brackets and in order of their citation in the text. They should be grouped at the end of the paper in numerical order of appearance. Abbreviated titles of periodicals are to be used according to Chemical or Biological Abstracts,but names of lesser known journals should be typed in full.References should be styled and punctuated according to the following examples:

ORIGINALPAPERS:
l. Author, N.N. and Author, N.N. (Year) Full title of the article. Joumal and Volume, first and last page.

BOOK OR PROCEEDING:
2. Author, N.N. and Author, N.N. (Year) Title of the contribution.
In: Title of the book or proceeding. Volume (Edition
of klitor-s, ed-s) Publisher, City, first and last page

DOCTORALTHESIS:
3. Author, N.N. (Year) Tille of the thesis, University and
Faculty, City

UNPUBLISHED WORK:
Papers that are unpublished but have been submitted to a joumal may be cited with the joumal's name followed by "in press". However,
this practice is acceptable only if the author has at least received galley proofs of his paper. In all other cases reference must be made to”unpublished work" or "personal communication".
Discussion and Conclusion: This part should interpret the results in reference to the problem outlined in the introduction and of related
observations by the author/s or others. Implications for further studies or application may be discussed. A conclusion should be added if results and discussion are combined.

Corresponding author: The name of the corresponding author with complete postal address

Precondition for publishing:
A minimum number of 25 reprints must be ordered and prepaid.
1 - 4 pp.: 200,- EURO + postage/handling
5 - 8 pp.: 250,- EURO + postage/ handling
more than 8pp: 1.50 EURO/page x number of reprints +postage/ handling.
The prices are based upon the number of pages in our journal
layout (not on the page numbers of the submitted manuscript).
Postage/ Handling: The current freight rate is Germany 10 €,Europe 18,00 €, International 30 €.
VAT: In certain circumstances (if no VAT registration number exists) we may be obliged to charge 7% VAT on sales to other EU member countries.MESAEP and SECOTOX members get a further discountof 20% (postage/ handling full).